International Conference
“Micro- and Nanoelectronics – 2012”

Book of

ABSTRACTS

October 1st - 5th, 2012
Moscow – Zvenigorod, Russia

Russian Academy of Sciences (RAS)

Russian Foundation for Basic Research

The International Society for Optical Engineering (SPIE), Cooperating Organization

- Institute of Physics and Technology (IPT) of RAS, Moscow, Russia
- Institute of Semiconductor Physics (ISP) of Siberian Brahch of RAS, Novosibirsk, Russia
- Lomonosov Moscow State University, Moscow, Russia

International Conference "Micro- and Nanoelectronics – 2012"

ICMNE-2012

October, 1st - 5th, 2012
Moscow – Zvenigorod, Russia

Supported by:

TABLE OF CONTENTS

How to search for necessary abstract?

The sheets of paper abstracts in this issue are colored according to the day of presentation at Conference. Every Abstract has its own identification number (for instance L1-04, O1-07, P2-28 and so on), which is marked in the right bottom corner of page. This number is corresponding to the one in *Conference Programme*. If you don't know the number of paper and one of the authors of paper is known it is possible to search for necessary Abstract by *Author Index* located at the end of the *Book of Abstracts*.

Как отыскать интересующие Вас тезисы доклада?

Страница сборника, содержащая искомые тезисы доклада, имеет цвет, соответствующий дню представления доклада на Конференции. Каждый доклад имеет собственный идентификационный номер (например, L1-04, O1-07, P2-28 и т.д.), который указан в правом нижнем углу страницы. Этот номер совпадает с номером, присвоенным докладу в *Программе Конференции*. Если Вы не знаете номера доклада, но Вам известен хотя бы один из авторов, вы можете воспользоваться *Авторским Указателем*, расположенным в конце *Сборника Тезисов.*

SemiTEq technological equipment for nanoelectronics

S.I. Petrov[1], A.N. Alexeev[1], D.M. Krasovitsky[2], V.P. Chaly[2]
1. SemiTEq JSC, Saint-Petersburg, Russia, petrov@semiteq.ru. 2. Svetlana-Rost JSC, Saint-Petersburg, Russia.

SemiTEq is the Russian brand which covers wide range of HV and UHV equipment meeting all modern semiconductor technology requirements. State-of the art design of both Molecular Beam Epitaxy Systems (for growth of different material systems such as InAlGaN, InAlGaAs, wideband A2B6 etc) and Vacuum Wafer Processing Equipment lines (for electron-beam and magnetron sputtering, thermal annealing, plasma etching and deposition etc) ensure high quality of epiwafer growth and its further processing under R&D and pilot production in the field of opto-, micro- and nanoelectronics. These products are the base for fully equipped compact Nanolaboratory which intended for creating the wide range of semiconductor devices.

Complete set of Nanolab's technological equipment includes: compact MBE system STE75 in two configurations: for A3B5/A2B6 and A3N compounds; electron-beam evaporation system STE EB71; magnetron sputtering system with lock chamber; plasma etching and plasma enhanced chemical vapour deposition system (PE & PECVD) with inductive and capacitive matched plasma sources; RTA and RTP systems; complex of required analytical tools; equipment for chemical process and photolithography; basic technology processes documentation; extensive modern training program, including video-training, 3D-visualization of technological route of nanodevices manufacturing, and specialized training software.

Equipment is oriented to R&D on substrates of Ø50.8 mm with the possible to upgrade the equipment components to increase the maximum diameter of the substrates up to 100 mm. The systems are unified of substrate holders type. Systems technological reactors are equipped with viewports for maximum process visualization. Graphical interface of process control is realized to simplify the process of specialists training to perform various technological operations.

Using of complex equipment SemiTEq shown in example of a closed cycle of basic technological operations for production of high-power field microwave transistors based on gallium nitride in the "Svetlana-Rost" JSC. Basic technological operations are shown: MBE growth of heterostructures, metal deposition of contacts using electron-beam evaporation system, thermal annealing of ohmic contacts, meza-isolation plasma-chemical etching and dielectric plasma deposition. The main problems during the technological route as well as ways to solve are discussed. In particular, ways to reduce the dislocation density in the active region of the transistor heterostructures grown on the mismatched substrates are described in detail. Special attention is given to the homogeneity and reproducibility both after some manufacturing operations and applied to the end product.

Structural diagnostics, elemental and characteristic analysis of modern micro- and nanosystems using analytical SEM/FIB tools

A. Tagachenkov[1], E. Zenova[1], Y. Anufriev[1], V. Dubrovinskiy[2]
1. Institute of Nanotechnology of Microelectronics, Russian Academy of Sciences, Moscow, Russia, e-mail: hf_hf@newmail.ru. 2. JSC «NPO Sernia», Moscow, Russia, e-mail: dv@sernia.ru.

The article covers capabilities of research equipment, particularly FIB/SEM tools, and methods for analysis of integrated devices made with submicron technology. At present technological stages used for manufacturing of modern nanosystems represent a complex sequence of chemical, plasma-, photolithography and other processes. The accuracy of these operations depends on several factors, such as technological equipment, operator experience, using this equipment, development of working processes and the compatibility of all these processes. The proposed method allows us to control the quality of manufactured micro- and nanosystems at the intermediate stages, and on the stage of final product as well. In addition to that these techniques make it possible to estimate in advance the reliability of the prospect devices, developed by domestic and foreign manufactures.

The methods under subject are based on the using special sample preparation for further analyzing by means of SEM/FIB/TEM and probe microscopy. The most powerful and prospective method for the preparation and analysis of samples is promised to be using FIB/SEM tools for this purpose, particularly, Nova 600 NanoLab company FEI, designed to study the internal structure of the objects at the micro - and nanoscale, creating stereo images of samples in real time without additional software processing and providing elemental analysis.

Due to the shrinking chip geometries of technological standards in microelectronics, up to 22 nm, and variety of functional submicron devices with properties different from the standard solid-state structures, the interest in the study of electrical properties and analyzing individual elements of these devices grows up more and more. Now the main instrument for measuring and analyzing electrical properties is microprobe technology tools.

To analyze electrical parameters of small size elements in the optical microprobe system the researcher should apply technology of making diagnostic contacts in SEM/FIB microscope. Apart from that the cooperation of SEM/FIB- and microprobes technologies enhances opportunities for analyzing modern integrated devices. Particularly, it is possible to analyze nanostructures by means of electron beam induced current method.

The proposed methods for analyzing micro- and nanosystems based on SEM/FIB microscopy allow researchers to study any objects of interest in modern microelectronics.

Ultra-high resolution AFM imaging

M.G. Minin
Intertech Corporation, 119333, Moscow, Russia; minin@intertech-corp.ru, www.intertech-corp.ru

Achieving ultra-high resolution in combination with fast scanning is of primary importance for modern AFM systems. Means of lowering noise affecting the scanner and the cantilever are described in the present paper. The fundamental noise is considered to be Brownian (thermal) motion of the cantilever. It is shown that the only way to significantly decrease abovementioned noise is to make the cantilever smaller.

Experiments described in the present paper were carried out by the scientists of Asylum Research Inc. (USA) in Santa-Barbara, CA, USA.

Three different in sizes cantilevers (200 um, 40 um, 10 um) with very similar spring constant (~ 4.3 N/m) and Q-factors (~4.53) are compared. Spectrum of thermal noise is analyzed.

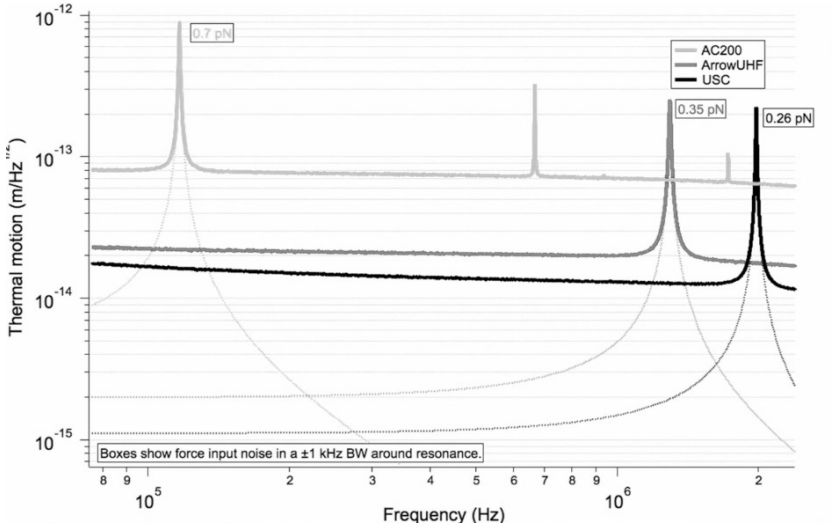

Figure 1. Thermal noise spectra in liquid.

Thermal noise values are measured in ±1 kHz BW around resonance frequency. It decreases significantly (by the factor of 3 to 5) from the biggest cantilever to the smallest one (Figure).

Atomic resolution scanning on the calcite crystal and bacretiorhodopsin is performed using the Asylum Research Cypher AFM (1) and the main instrumental aspects affecting the resolution and the speed of scanning are discussed.

1. Scheuring et al., Euro Biophysics J, DOI 10.1007/s00249-001-0197-8 (2002).

Oxford Instruments Plasma Technology equipment for the micro- and nano- engineering of materials for semiconductor, optoelectronics, MEMS and other applications

K. Kuvaev, A. Krynin
Technoinfo Limited, Moscow, konstantin@technoinfo.ru

Oxford Instruments Plasma Technology (OIPT) provides a range of high performance, flexible tools to semiconductor and electronic processing customers in both R&D and production. Today the company offers equipment and technology for Plasma Etch and Deposition, Atomic Layer Deposition, Ion Beam Etch and Deposition, Nanoscale Growth and Hydride Vapour Phase Epitaxy. With a 30-year history of high performance tools production and process development, OIPT has great experience in this area and good worldwide reputation. More than 2.500 systems were installed around the world.

Oxford Instruments has a process library of over 6,000 recipes developed in our process laboratories. Our processes are backed by process guarantees for key parameters and repeatability such as rate and uniformity to ensure rapid start-up during installation. Oxford Instruments' process tools offer a powerful range of stand-alone and clusterable process modules to enable the widest range of applications: Plasma Etch (ICP, RIE, RIE/PE, DRIE), Plasma Deposition (PECVD and ICP CVD, ALD (PE & thermal), DLC, PVD).

ALD systems have next features: Plasma and thermal ALD in one tool, possibility to be clustered to other modules using hex handler with robot and 25 wafer cassette for 4", 6" or 8" wafers, 100% conformal coatings of up to 200mm wafers handling and pieces on carrier plate.

Nanoscale features can be formed by growth techniques ('bottom up') and etching ('top down'). The NanofabTM Systems are aimed to satisfy the nanotechnology market. Nanoscale growth processes encompass: Nanotubes/nanowires, Nanoscale thin films. Nanofab700 and Nanofab800Agile: can accommodate variable sample sizes up to 200 mm wafer with excellent temperature uniformity, can provide growth of nanotubes and nanowires with a flexible temperature range up to 700°C and 800°C respectively.

Oxford Instruments' Ion Beam technology offers unique abilities in etch and deposition. OIPT Ion Beam tools have next benefits: Etch and Deposition tools, Versatile tool for a wide range of applications, Flexible system configuration to match specific process applications, easy optimisation for repeatable process results. Next processes can be started: Ion Beam Etch (IBE), Reactive Ion Beam Etch (RIBE), Chemical Assisted Ion Beam Etch (CAIBE), Ion Beam Deposition (IBD), Reactive Ion Beam Deposition (RIBD).

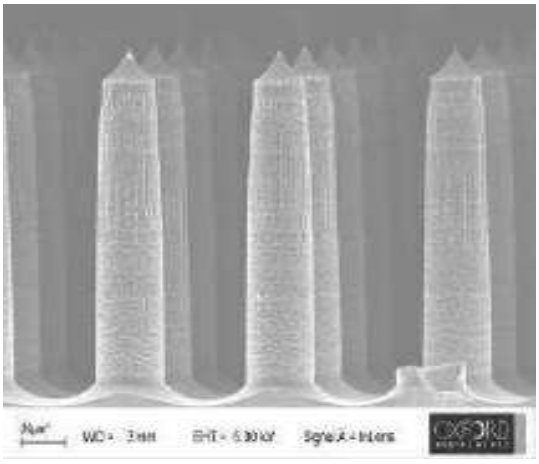

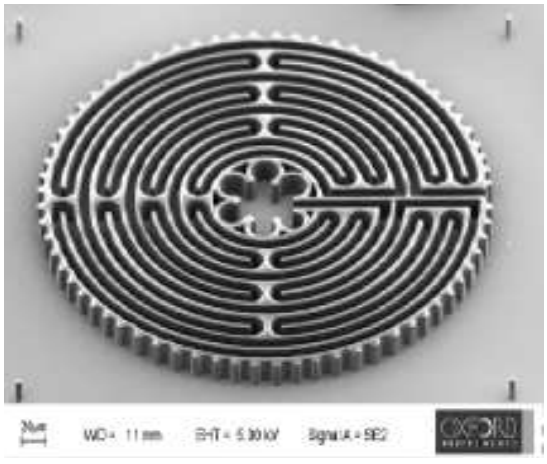

Left Image
Microneedles (Bosch-process) for Bio-medical application.
Right Image
Micro-mould (Cryo etching) for Micromachines / Actuators

Novel Vion™ Plasma FIB system for nano- and micro- electronics application by FEI Company

A. Poletaev, I. Bredikhin
Technoinfo Limited, Moscow, Russia. andreypoletaev@technoinfo.ru

FEI is a leading diversified scientific instruments company, featuring electron and ion-beam microscopes and other instruments for nanoscale applications across many industries: industrial and academic materials research, life sciences, semiconductors, data storage, natural resources and more. With a 60-year history of technological innovation and leadership, FEI has set the performance standard in transmission electron microscopes (TEM), scanning electron microscopes (SEM) and DualBeams™, which combine a SEM with a focused ion beam (FIB).

For Semiconductor, Solar and MEMS labs, and Data Storage production facilities, users can get to data faster, with the world's finest, most flexible suite of integrated imaging and analysis tools. FEI delivers superior images, faster sample preparation, more precise circuit editing and analysis resulting in faster design validation and higher throughput process development and control.

Unique PFIB Vion is the first product to incorporate plasma ion source technology in a modern ion column, gas delivery and end point detection to provide fast, efficient, cost-effective editing on advanced integrated circuits. Circuit editing allows product designers to reroute conductive pathways and test the modified circuits in hours, rather than the weeks or months that would be required to generate new masks and process new wafers. With over one microamp of beam current, it can remove material much faster (>20X) than FIBs based on liquid metal ion sources (LMISs) that typically max out at a few tens of nanoamps, while still preserving excellent milling precision and imaging resolution at low beam currents.

The Vion Plasma FIB has the ability to selectively mill areas of interest. Additionally, various gases can be introduced in the chamber which change the beam interaction and cause deposition to occur (either insulator or conductor). With the introduction of other gases, the etch rate can be selectively modified for a preference of silicon over conductor or vice versa.

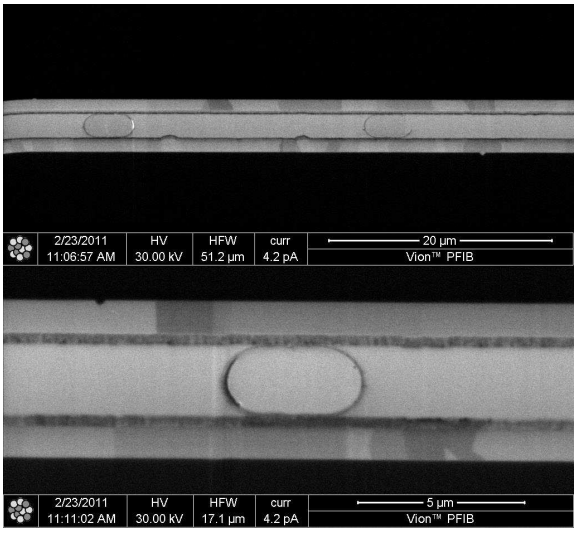

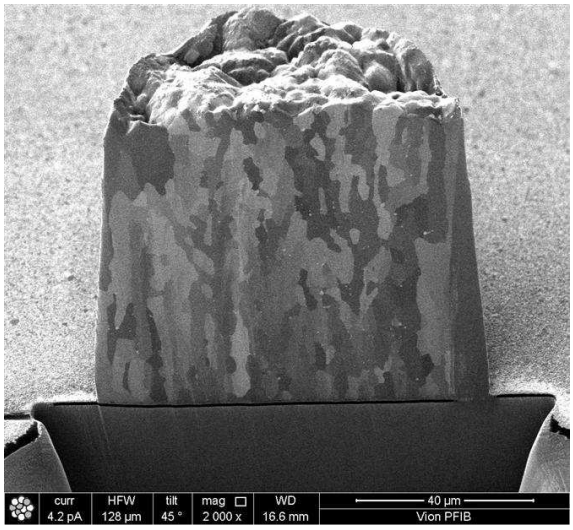

Left Image
PFIB section and image through wafer-to-wafer bond region, exposing 4 µm diameter interconnecting spheres.
Right Image
80 µm wide and 100 µm tall bump cross-sectioned with Vion in 20 minutes.

Modern semiconductor equipment for metrology and failure analysis by Hitachi High Technologies

E. Kremer
JSC InterLab, Moscow, Russia

New materials and structures in future ULSI generation

A. Orlikovsky, V. Vyurkov
Institute of Physics and Technology, Russian Academy of Sciences, Moscow, Russia, orlikovsky@ftian.ru

Silicon remains the basic material of integrated circuits. The technology node of 6 nm is anticipated in the production in 2026. For the advance into this region it is necessary to employ thin undoped (depleted) channels wrapped by gates. Just those structures allow avoiding channel doping which substantially impairs a bulk transistor performance. The fully depleted channels can be implemented on the wafer "silicon on the insulator- SOI" (IBM Corp. and STMicroelectronics) or on the bulk wafer (Intel Corp.). Nanowire transistors belong to the same paradigm. That construction of transistors provides the high ON-state current owing to ballistic transport in a channel. The OFF-state current is low as the subthreshold slope approaches its thermionic limit: 59 mV of gate voltage per decade of current at room temperature.

Possibly, in the future it would be necessary to reject also the doping of contact regions because of the fluctuations of number of impurities, which lead to the large dispersion of transistor parameters in a circuit. Therefore, Schottky Barrier Field-Effect Transistors are regarded as plausible successors. They could revert again to bulk wafers or, at least, to thick silicon body in SOI wafers.

New constructions of transistors imply also new materials: the high-conductivity materials (metals and silicides) as gates and high-k dielectrics as gate dielectrics. The germanium and A_3B_5 channels are now in the stage of research. Their application can also prolong an employment of bulk silicon wafers.

The use of new materials as a transistor channel offers new possibilities. Recently, close attention was paid to carbon nanotubes and graphene. However, the absence of the band gap in graphene and rather small band gap in semiconductor nanotubes and nanoribbons results in high OFF-state current which prevents their application in large digit circuits. Nevertheless, an application of such transistors in fast analog circuits looks as promising.

The main reason restricting the speed of processors is heating, therefore, low-power transistors are challenging. Tunnel transistors (p-n junction manipulated by a gate voltage) exhibit a subthreshold slope bigger than the thermionic limit for conventional transistors. This allows a decrease in drive voltage. However, due to low frequency of operation those transistors could hardly be used in ULSI technology.

The transistors based on novel principles of operation are intensively investigated. One impetus is to lower a switching energy. Indeed, spin precession and quantum interference require no energy at all. However, even experimental samples of those transistors demonstrate very low ON/OFF ratio. For spin transistors much stronger spin-orbit interaction is required. The high ON-current of interference transistors seemingly contradicts with high ON/OFF ratio. As for single-electron transistors based on Coulomb blockade, they have a fundamental restriction of a channel conductance limiting the frequency of corresponding digit circuits. Poor reproducibility is also an everlasting drawback of those transistors.

The problem of interconnects is critical. With decreasing thickness the conductivity of metals dramatically falls down, furthermore, the electromigration is strengthened. Carbonic materials (nanotubes and graphene) according to their physical properties can successfully replace metallic interconnects, but the technology of their formation in definite sites is not thus far developed.

For the connection between cores of a processor it is possible to use photon switches with a large bandwidth. Waveguides and modulators can be formed via silicon technology, whereas, light sources can be still manufactured on the basis of A_3B_5 compounds, although, purely silicon sources are intensively searched.

The motion of carriers in the channel of a nanotransistor is similar to the propagation of waves in the waveguide; therefore, the self-consistent solution of the Schroedinger and Poisson equations for its description is required [1]. As far as graphene transistors are concerned, the hydrodynamic approach [2] turned out to be the most acceptable for them due to extremely strong collisions between carriers.

Silicon is the most preferable material for creating solid-state quantum computers on the basis of nuclear spins of impurities, spin and orbital states of electrons in impurity atoms and in quantum dots [3]. The technology of silicon quantum computers may inherit advances in micro- and nanoelectronic technologies.

1. V. Vyurkov, I. Semenikhin, S. Filippov, A. Orlikovsky, Solid-State Electronics, **70**, pp.106–113, 2012.
2. D. Svintsov, V. Vyurkov, S. Yurchenko, V. Ryzhii, T. Otsuji, J. Appl. Phys., **111**, 083715, 2012.
3. S. Filippov, V. Vyurkov, and A. Orlikovsky, Proc. EUROSOI-2011, Granada, Spain, pp.101-102, 2011.

New devices and materials for ultra low power operation

F. Balestra
Sinano Institute, IMEP-Minatec (CNRS-Grenoble INP, UJF), France

The historic trend in micro/nano-electronics these last 40 years has been to increase both speed and density by scaling down the electronic devices, together with reduced energy dissipation per binary transition. We are facing today dramatic challenges dealing with the limits of energy consumption (static+dynamic) and heat removal, inducing fundamental tradeoffs for the future ICs. The researches on ultimate reduction of computation dissipation are strongly needed for the development of future high performance terascale integration and autonomous (nano)systems. This paper addresses the main challenges, limits and possible solutions for strongly reducing the energy per binary switching. Several paths are possible: the adiabatic logic using a slow clock, which cannot be used for high performance devices, logic stochastic resonance, feedback-controlled dynamic gate, or conventional logic with a reduction in the stored energy, therefore a decrease of device capacitance C (device integration) or applied bias V, which seems to be the most promising for future ICs.

The reduction of the stored energy in conventional logic can be done with a strong reduction in V using new physics and/or devices with sub-60mV/dec subthreshold swing S, which is the limit of MOSFETs at 300K. The main following concepts are possible: energy filtering (Tunnel FET, with MOS-NW- CNT- or Graphene, using band-to-band tunneling to filter energy distribution of electrons in the source, or NW FET with superlattice (e.g. InGaAs-InAlAs) hetererostructure in the source), internal voltage step-up (Ferroelectric gate FET, inducing a negative capacitance to amplify the change in channel potential induced by the gate), Nano-Electro-Mechanical-Structures, or Impact Ionisation MOS devices.

We will focus here on the best ones for ULSI, TFETs, using gate-controlled pin structures with carriers tunneling through the barrier and not flowing over. The most interesting structures, proposed using experiments or numerical simulations with the aim of reducing the effective mass, the bandgap and/or the tunnelling length for increasing Ion and reducing S for several decades of current, are the following: i) Bandgap reduction using Ge or III-V channel materials (operation down to 0.2V) (simul) [1], ii) InAs TFETs (SG, DG, GAA NW) with small bandgap and electron-hole effective mass, S down to 20mV/dec for 2nm nanowires or UTB double-gate TFETs (simul) [2], iii) Uniaxial and biaxial strained InAs nanowire TFET with S down to 22mV/dec and large Ion/small switching delay (simul) [3], iv) HTFET using InGaAs with thin gate oxide, high source doping leading to sub-60mV/dec (exp) [4], v) CNT tunnel FET with S=40mV/dec (exp) [5], vi) Feedback TFET with gate-controlled injection barrier leading to very small S-a few mV/dec (exp) [6], vii) Thin and Double-Gate SOI TFET with high k dielectrics, or SGOI, or GOI for higher Ion (exp) [7,8].

1. C. Hu et al, VLSI 2008, p. 14.
2. M. Luisier et al, IEEE EDL **30**, p.602, 2009.
3. F. Conzatti et al, IEDM 2011, p.95.
4. G. Dewey et al, IEDM 2011, p.785.
5. J. Appenzeller et al, Phys. Rev. Lett**. 93,** 196805, 2004.
6. F. Padilla et al, IEDM 2008, p.171.
7. K. Boucart et al, ESSDERC 2009, p.452.
8. F. Mayer et al, IEDM 2008, p.163.

SiGe and Ge: selective epitaxial growth and application in advanced MOS devices

A. Hikavyy, B. Vincent, W. Vanherle, J. Dekoster, L. Witters, H. Bender, A. Thean, R. Loo
Imec, Kapeldreef 75, B-3001 Leuven, Belgium, Andriy.Hikavyy@imec.be

Selective growth of SiGe in source/drain areas of pMOS transistors is one of the key processes allowing Si based transistors to remain at the leading edge of microelectronics. The well known use of SiGe in the Source/Drain stressors allows to boost its performance dramatically due to both: favorably strained channel and decreased S/D series resistance [1, 2]. As the scaling goes on, Ge concentration is gradually increased and for 22 nm node, built on fin FET architecture, it has reached 55% [3]. All new device concepts such as buried SiGe channel, implant free quantum wells (IFQW), tunnel FETs, relaxed or strained Ge channel devices, in one or another way, also rely on strain engineering.

Typically epi processes used in production of high end, either high performance or low voltage transistors should fulfill a number of requirements. Among them: selectivity towards oxides and nitrides used for spacers and hard masks; acceptable growth rate; suitable temperatures and minimal loading effects. If SiGe is considered, Ge concentrations span over the whole range from 0 up to pure Ge depending on application. Depending on Ge concentration the growth temperature must be carefully chosen in order to avoid elastic relaxation of the layers.

In this contribution we will first discuss a few different transistor devices architectures considered to be promising for the coming generation nodes: Implant Free Quantum Well, FinFet and strained Ge-based devices (Fig.1). Need for epitaxial growth and challenges associated with it will be outlined.

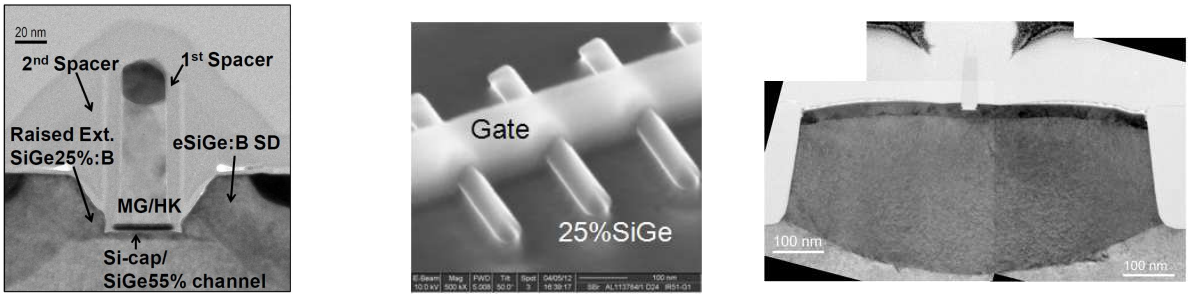

Figure 1. Transistor device concepts considered for 14 nm node and below: a) SiGe Implant Quantum Well transistor [4]; b) FinFET based transistor; c) strained Ge based transistor [5].

Next, Si surface preparation (pre-epi cleans) typically used in the semiconductor industry and difficulties observed with cleans implementation in the cases of mentioned above devices will be presented.

Selective epitaxial growth (SEG) of Si, SiGe and Ge will be further discussed in details. Difficulties associated with SEG (loading effects, facet growth, etc) will be outlined and typical applications of SEG will be shown together with available electrical results.

1. T. Ghani et al., IEDM Technical Digest., p.978, 2003.
2. P. Verheyen et al., *VLSI Technology Digest of Technical Papers*, p.194, 2005.
3. C. Auth et al., *VLSI Technology Digest of Technical Papers*, p.131, 2012.
4. S. Yamaguchi et al., IEDM Technical Digest., p.829, 2011.
5. V.Benjamin et al., to be published in Journal of Electrochemical Society.

Bumpless Interconnects Technology for Wafer-based Three-Dimensional Integration (3DI)

Takayuki Ohba
Institute of Engineering Innovation (IEI), Graduate School of Engineering, The University of Tokyo, 2-11-16 Yayoi, Bunkyo-ku, Tokyo 113-8656, ohba@sogo.t.u-tokyo.ac.jp

The key features are bumpless interconnects for the three-dimensional (3D) integration including vertical wiring without bumps for Chip-on-Wafer (COW) and Wafer-on-Wafer (WOW) as a second-generation alternative to the use of micro-bump. Wafer-based 3D technologies are the fabrication of three-dimensional structures in which any number of thinned 300 mm wafers can be stacked back-to-front realizing further large-scale devices with low cost instead of the scaling using extreme ultraviolet (EUV) lithography.
The two-dimensional (2D) scaling based on planar technology that has led the semiconductor industry so far no longer makes economic sense in many situations. For instance, the industry is facing a major turning point in how to realize the next generation of large-scale integration. In this context, 3D approaches have been proposed on the basis of next-generation 2D transistors and 3D architectures, and recent attention has focused on productivity and the costs involved in volume production. WOW is the third-generation replacement for Chip-on-Chip (COC) technology and is also applicable to wafer-based COW. Stacking at the wafer level drastically increases the processing throughput, and bumpless interconnects provide an appropriate yield using existing technology which is equivalent to or greater than that achievable with 2D scaling beyond 22 nm nodes. Also, since it is compatible with existing wafer processing facilities, transistors with three-dimensional structures can be designed in a continuous manufacturing line.
WOW is classified into two types, according to the stacking method: Thinning before Bonding and Via-Last after Bonding. The development of WOW has proceeded through four modules, classified along the process flow. The modules include a thinning module for thinning the wafer substrates in which devices are implemented, a stacking module for bonding and stacking the wafers, a vertical interconnects module for forming Cu interconnects embedded in upper and lower wafers with via-holes, and a packaging module for singulating the stacked wafers. Damascene interconnects form a so-called redistribution layer and also serve as a counter electrode for the subsequent stacked wafer.
In this presentation, the WOW technology and trends in conventional scaling compared with advanced technologies such as 3D integration (3DI) and bumpless interconnects processes, as well as the characteristics of devices after thinning the wafers to less than 10 μm and allpications including Closed-Channel-Cooling System (C^3S) will be addressed.

Acknowledgements
Author would like to thank Drs. S. Yoshimi, M. Akazawa, Y. Mizushima, N. Maeda, H. Kitada, K. Fujimoto, Y. S. Kim, and S. Kodama for their support on process integrations. This study was carried out based on the three-dimensional integration development program of the WOW alliance at the University of Tokyo, and the author thanks the more than 20 alliance members including Nagoya University, ITRI Ad-STAC (Taiwan), and the WOW Research Center Ltd. for their cooperation.

1. N. Maeda et al., Proc. Advanced Metallization Conference 2008, Eds. M. Naik, R. Shaviv, T. Yoda, and K. Ueno, Mat. Res. Soc., p. 501, 2009.
2. Y. S. Kim et al., IEEE IEDM Tech. Dig., p. 365, 2009.
3. T. Ohba et al., Microelectronic Eng., Elsevier, **87**, pp. 485-490, 2010.
4. S. Tominaga et al., Jpn. J. Appl. Phys., **49,** 05FG01, 2010,
5. T. Ohba et al., IEICE Trans. and Electronics, Electronics Soc., J**93**-C (11), pp. 464-476, 2010.
6. H. Kitada et al., Jpn. J. Appl. Phys., **50** (5), 05ED02, 2011.
7. O. Nakatsuka et al., Jpn. J. Appl. Phys., **50** (5), 05ED03, 2011.
8. D. Diehl et al., Microelectron. Eng., **92**, pp. 3-8, 2011.
9. T. Ohba, Electrochem. Soc., Trans., **34** (1), pp. 1011-1016, 2011.
10. Y. S. Kim et al., IEEE Symp. on VLSI Technol., pp. 144-145, 2011.
11. Y. Mizushima et al., Jpn. J. Appl. Phys., **51**, DOI: 10.1143/JJAP.51.05EE03, 2012,
12. T. Ohba, CSTIC2012, Electrochem. Soc. Trans. **44** (1), pp. 827-840, 2012.
13. N. Maeda et al., IEEE VLSI Symp., p. 171, 2012.

Qualification of Deep-Submicron OTP Poly-Fuse Memory

N. Belova[1], D. Allman[1], S. Tibbitts[2]

1. *ON Semiconductor, Phoenix, AZ, USA, E-mail Nadya.Strelkova@onsemi.com , Derryl.Allman@onsemi.com*
2. *Jet City Electronics Inc., Seattle, WA, USA, E-mail address steve@jetcityelectronics.com*

One-time programmable memory (OTP) belongs to the fast growing semiconductor Non-Volatile-Memory family. OTP memory has multiple applications in Consumer Electronics, Automotive, Computer, Medical, etc. industries. There are Zener-diode based, Metal-Fuse based and Poly-Fuse based OTP memory types.
We present CoSi2/P-poly-Si fuse based OTP memory qualified for the 0.25um CMOS technology. The OTP memory bit is programmed by applying electrical stress to blow a single poly fuse (poly resistor). Applied voltage across the fuse creates local heat sufficient for CoSi2 migration [1-3] and transforming the Poly-Si-crystalline structure into amorphous silicon. Amorphized Poly-Si provides high fuse resistance (~5Mohm) thus changing the memory bit state from "0" to "1". OTP retention time, critical for industrial applications, should be longer than 10 yrs at elevated temperatures 85C-125C. The fuse programming conditions were optimized in order to minimize or eliminate fuse and silicon damage, and/ or void formation (Fig.1). Electrical and physical characterization results of the OTP programming optimization are presented.
The OTP reliability tests were performed using the package level High Temperature Operating Life (HTOL) and High Temperature Storage Life (HTSL) tests per JEDEC standard. For reliability testing, the 16 Kilo-Bit Retention Vehicle was designed with the 5V OTP Memory core. 240 parts (total ~3.9MB fuse elements) were submitted per each test. The HTOL test was performed at T=125C @ Vdd=5V. Storage Life (HTSL) test was done at T=150C. Per JEDEC requirements the drift analysis was performed using functional electrical test data collected before the burn-in (HTOL/HTSL), at intermediate reading points 168h & 504h, and after 1008h burn-in. Reliability results showed robust Poly-Fuse OTP performance: all parts passed functional tests at each read point; drift test showed less than 10% fuse resistance shift at elevated temperature under dynamic electrical load.

(a) (b)

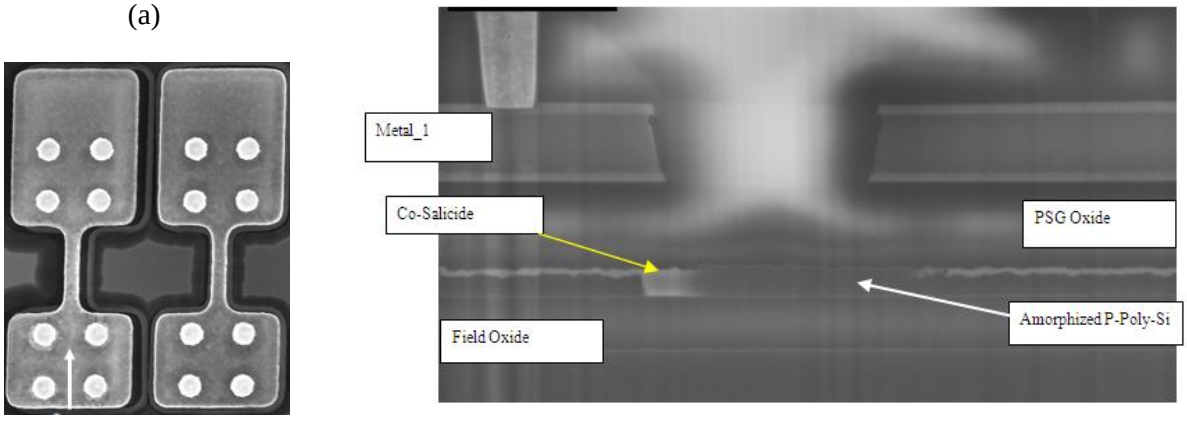

Fig.1 OTP memory bit element: Top view (a), Programmed Poly fuse cross-section (b).

1. C. Kothandaraman, Sundar K. Iyer, and Subramanian S. Iyer, "Electrically Programmable Fuse (eFUSE) Using Electromigration in Silicides", IEEE ELECTRON DEVICE LETTERS, **23**, No. 9, pp.523-525, 2002.
2. A. Ito, E. W. (Pete) George, R. K. Lowry, and H. A. Swasey "The Physics and Reliability of Fusing Polisilicon", *IEEE/IRPS*, pp.193-197, 1984.
3. R.F. Rizzolo, et. al. "IBM System z9 eFUSE applications and methodology", IBM J. RES. & DEV. **51** No. 1/2 JANUARY/MARCH, pp.65-75, 2007.

Recording of information in nanostructures of transition metal silicides

A.S. Sigov[1], B.M. Darinskiy[3], L.A. Bityutskaya[2], O.V. Ovchinnikov[2], M.S. Smirnov[2], M.V. Grechkina[2], A.P. Lazarev[3], G.A. Veligura[4], A.V. Tuchin[3], E.V. Bogatikov[3]

1. *MIREA,Moscow, Russia, E-mail: rector@mirea.ru*
2. *VSU, Voronezh, Russia, E-mail: me144@phys.vsu.ru*
3. *Rosbiokvant Ltd., Voronezh, Russia, E-mail: main@rosbiokvant.ru*
4. *Scientific research institute of electronic engineering, Voronezh, Russia, me144@phys.vsu.ru*

Realization of silicon spintronics requires new materials to provide effective injection of carriers in semiconductor spin-polarized carriers at room temperature. To ensure the effective spin injection requires a material with close to the silicon a value of lattice parameter and the Fermi velocity, and forming with it an atomically thin interface [1]. These requirements are met by some transition metal silicides. Therefore, a promising direction is to study the magnetic properties of low dimensional silicides of 3d-metals such as Ni, Co. Thick film of disilicides and monosilicides 3d-metals do not possess magnetic properties. However, in modeling the electronic structure of nanoclusters silicides of transition metals (Ni, Co, Fe, Mn) by density functional theory (approximation B3LYP, basis of 6-31 (dp) G) were detected size-effect magnetic properties due to the transition of 3d-metals from low-spin in the high-spin state near the surface of the nanostructures.

Using methods of Plasma technology were obtained self-assembled nanoclusters of Ni and Co silicides on Si (100) with a size of 20-50 nm [2]. Using magnetic force microscopy (MFM) the magnetic response of nanostructures of Ni and Co silicides at room temperature was observed.

To demonstrate the applicability of these materials for data recording was made a local magnetization by two methods: the influence of circularly polarized light and the influence of a magnetic probe of magnetic force microscope. This result is completely optical magnetization reversal of nanostructures of Ni silicides, which has magnetic properties due to the size effect was obtained for the first time.

Research changes in the state of magnetization of nanostructures of transition metal silicides carried out by repeatedly scanning a magnetic probe for SPM Solver P-47 Pro with a surface area of up to 250 x 250 nm at a distance of 10 nm. At the same time revealed a significant increase in the magnetic response in previously subjected to repeated scanning at a small distance between the probe and the sample. The experiments show the possibility of a superdense information recording systems based on Si-Ni, Si-Co nanostructures. A model of switching of the magnetization vector of isolated clusters of silicides by light was developed. Excited electronic light system undergoes a quantum transition with the change of quantum numbers s and m. From the excited state electronic system relaxes to the ground state by radiationless transition, giving the excitation energy of the phonon system without changing the magnetic number m. With further lighting of the process is repeated until not occur a remagnetization of magnetic nanoclusters. Implemented method of recording with circularly polarized light confirmed developed model of remagnetization of clusters of transition metal silicides. These results are the basis for a magnetic memory that is compatible with silicon technology.

This work was financially supported by state contract 16.513.11.3014.

1. H. Wu, P. Kratzer, H. Scheffler, Phys. Rev. B, **72**, 144425, 2005.
2. A.S. Sigov, A.V. Abramov, L.A. Bityutskaya, et al., International Conference “Micro- and nanoelectronics-2009”, Moscow-Zvenigorod, P1-13, 2009.

Study of the resistive switching mechanism in Pt/ZrO_x/HfO_2/p^{++}-Si stacks by hard X-ray photoelectron spectroscopy

Yu. Matveyev[1], A. Zenkevich[1], Yu. Lebedinskii[1], S. Thiess[2], and W. Drube[2]

1. NRNU "Moscow Engineering Physics Institute", 31, Kashirskoe chaussee, 115409, Moscow, Russia;

2. Deutsches Elektronen-Synchrotron DESY, D-22603 Hamburg, Germany

While the non-volatile memory concept exploiting the hysteretic resistance switching in transition metal oxides under an external electric field is very close to commercialization, the microscopic mechanism of the effect is still debated [1]. In particular, the role of oxygen vacancies in a metal-insulator-metal (MIM) structure based on metal oxides is not fully understood. In this contribution, we present a detailed hard X-ray photoelectron spectroscopy (HAXPES) study of the chemical and electronic structure evolution in Pt/ZrO_x/HfO_2/p^{++}-Si stacks upon different switching steps. HAXPES experiments were performed at the PETRA III storage ring at E=6 keV which enables to reach deep (up to ~20 nm) layers and thus provides an opportunity to probe the whole MIM stack with a continuous metal gate. The reversible resistive switching steps of the bi-layered ZrO_x/HfO_2 dielectric were induced by a bias applied to the stack both ex situ and in situ, and recorded in I-V characteristics (see Fig. 1). The corresponding cyclic changes of the metallic vs. oxidized component ratio in the Hf *4f* and Zr *3d* core level lines were observed in HAXPES spectra suggesting the redistribution of oxygen between HfO_{2-x} and ZrO_x (see Fig. 3). The correlated evolution of the electrical and chemical properties of Pt/ZrO_x/HfO_2/p^{++}-Si stacks corroborates the model attributing the resistive switching effect in bi-layered ZrO_x/HfO_2 dielectrics to the drift of (charged) oxygen atoms and/or vacancies at the interface (see Fig. 3).

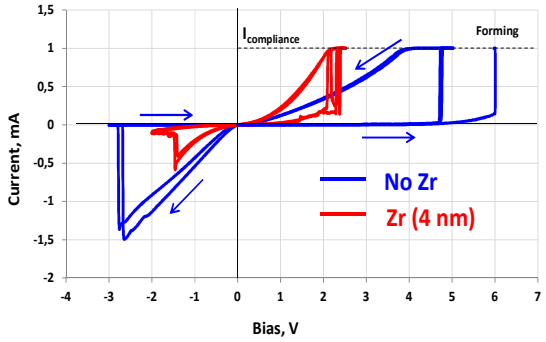

Fig. 1 I-V characteristics of Pt/HfO_2/p^{++}Si and Pt/ZrO_x/HfO_2/p^{++}Si stacks with the resistive switching behavior.

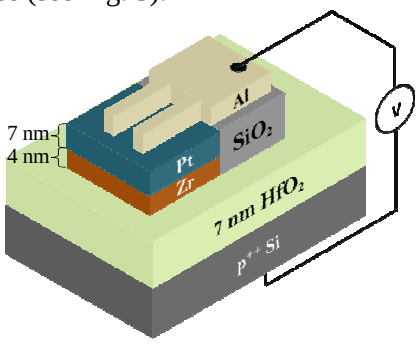

Fig. 2 The schematic structure of the sample with Pt/ ZrOx/HfO_2/p^{++}Si functional part prepared for *in situ* biasing during HAXPES analysis.

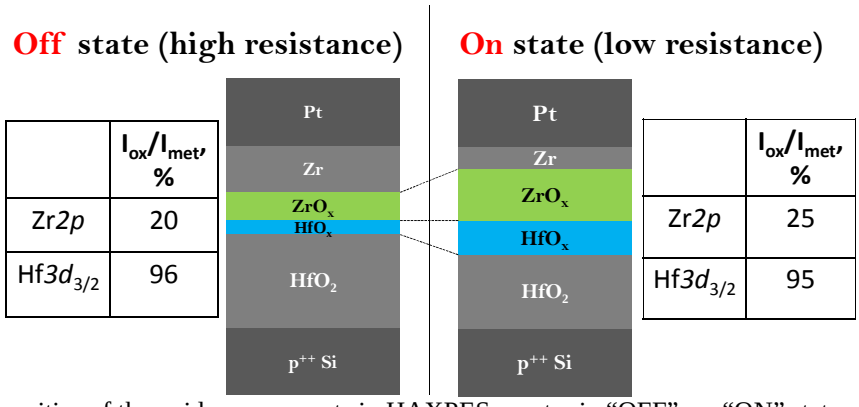

	I_{ox}/I_{met}, %
Zr*2p*	20
Hf$3d_{3/2}$	96

	I_{ox}/I_{met}, %
Zr*2p*	25
Hf$3d_{3/2}$	95

Fig. 3 Relative intensities of the oxide components in HAXPES spectra in "OFF" vs. "ON" states, and the model describing the evolution in ZrO_x/HfO_2 layer following the resistive switching step.

[1] http://www.itrs.net/Links/2011ITRS/2011Chapters/2011ERD.pdf

Switching of domains in ferroelectric domain boundary

B.M. Darinskiy[1], A.P. Lazarev[2], A.S. Sigov[3]

1. *VSU, Voronezh, Russia, E-mail: me144@phys.vsu.ru.*
2. *Rosbiokvant Ltd., Voronezh, Russia, E-mail: main@rosbiokvant.ru.*
3. *MIREA, Moscow, Russia, E-mail: rector@mirea.ru.*

At present, the possibility of creating storage devices on the basis of switching of domain in ferroelectrics is under investigation. At the same time seeks to radically increase the recording density of information, reduction of energy costs on the process of recording, storing, reading information, increasing performance and service life. To solve these problems is natural to use the ideas and approaches developed in nanophysics.

In this paper, as an active element of the memory cell is proposed to use the domain, which at confluence of circumstances is formed in a domain boundary of a ferroelectric crystal.

To study the conditions for the occurrence of such domains and their characteristics, the method is used developed in [1], which is based on Morse theory about the indexes of singular points. The process of switching the direction of rotation of the polarization vector in a domain wall can occur during thermal exposure (phase transition of first or second kind), and under the influence of an electric field. In this paper we consider a model of rotation in the domain wall under an electric field.

A determination of the equilibrium values of the components of the spontaneous polarization P_1, P_2 and coercitive field E. The state with $P_1 \neq 0, P_2 = 0$ corresponds to the ground state, state with $P_1 = 0, P_2 \neq 0$ corresponds to a metastable state. Comparison of the switching field E with the same field to switch the polarization components P_1 shows that E is much smaller than P.

Thus, applying an electric field perpendicular to the plane of the plate, you can switch the polarization vector in the domain wall. That is, for a special material is possible to develop nanoscale memory elements at the domain boundaries of nonlinear dielectrics. Because of the relatively small value of the operational fields of the proposed mechanism of memory should have an advantage compared to the same device on the domains.

This work was financially supported by state contract 16.513.11.3014.

1. B.M. Darinskii, A.A. D'yachenko, A.P. Lazarev, "Topological method of analysis in the thermodynamics of ferroelectrics", Bulletin of the Russian Academy of Sciences: Physics, **71**, pp.1388-1341, 2007.

Theoretical study of terahertz plasma instability in asymmetric double-grating-gate transistor structures

A. Satou[1], H. Shida[1], T. Otsuji[1], V.V. Popov[2]

1. Research Institute of Electrical Communication, Tohoku University, Sendai, Japan, a-satou@riec.tohoku.ac.jp. 2. Kotel'nikov Institute of Radio Engineering and Electronics (Saratov Branch), Russian Academy of Sciences, Saratov, Russia

Plasma waves in double-grating-gate (DGG) transistor structure have been researched as candidates of room-temperature operating, frequency-tunable terahertz emitters and detectors. Experimental observation of terahertz emission at room temperature by DGG transistors was reported [1, 2]. On the other hand, although there has been extensive study of the so-called Dyakonov-Shur instability in a single-gate structure driven by DC current originating from [3], plasma instability in DGG structures has not been studied theoretically except the work in [4] about the transit-time instability. In this paper, we develop a numerical model to calculate plasma spectra in asymmetric DGG and report on a novel plasma instability driven by DC current.

The asymmetric DGG structure under consideration is illustrated in Fig. 1(a). Here, we consider a AlGaAs/GaAs heterostructure two-dimensional electron gas (2DEG) with periodic boundary. Focusing on plasma waves propagating in x-direction, we use the linearized collisionless hydrodynamic equations for the electron transport in the 2DEG, as well as the Maxwell equations for the self-consistent field:

$$-i\omega\Sigma_\omega + \frac{\partial}{\partial x}(\Sigma_0 v_\omega + v_0\Sigma_\omega) = 0, \quad -i\omega v_\omega + \frac{\partial}{\partial x}(v_0 v_\omega) = -\frac{e}{m}E_\omega \qquad (1)$$

where v_0, v_ω, Σ_0, Σ_ω are steady-state/variation of the electron velocity/concentration, E_ω is the electric field which is connected self-consistently with the current $J_\omega = -e(\Sigma_0 v_\omega + v_0\Sigma_\omega)$ through the Maxwell equations. We assume the profiles of the steady-state variables as shown in Fig. 1(b). After expanding all the dependent variables in the Fourier basis, we arrive at an eigenvalue problem for the complex frequency ω and the coefficients of the current $J_{\omega k}$. We solve it numerically by truncating the matrix. Among all the eigenmodes calculated, we selected those who satisfy $\mathrm{Im}\omega > 0$, corresponding to instable modes rather than damped modes, and further selected the first instable mode having smallest frequency.

Figure 2 demonstrates the plasma growth rate ($\mathrm{Im}\omega$) and plasma frequency ($\mathrm{Re}\omega/2\pi$) of the first instable mode as a function of the maximum velocity $v_{0\max}$ (see Fig. 1(b)). Values of parameters used are seen in Fig. 2. As clearly demonstrated in Fig. 2, the instable mode exists for the velocity above 10^5 m/s, having the frequency around 2 THz, and the value of the growth rate increases as the velocity increases. This instability can be attributed to the nonuniform velocity profile in the 2DEG and, hence, to the DC current and the modulation of the concentration by gate 1 and 2.

1. T. Otsuji *et al.*, "Grating-bicoupled plasmon-resonant terahertz emitter fabricated with GaAs-based heterostructure material systems," Appl. Phys. Lett., **89**, pp.263502 1-3, 2006.
2. T. Otsuji *et al.*, "Emission of terahertz radiation from dual grating gate plasmon-resonant emitters fabricated with InGaP/InGaAs/GaAs material systems," J. Phys.: Condens. Matter, **20**, 384206 (1-11), 2008.
3. M. Dyakonov and M. Shur, "Shallow water analogy for a ballistic field effect transistor: new mechanism of plasma wave generation by dc current," Phys. Rev. Lett., **71**, pp.2466-2468, 1993.
4. V. Ryzhii *et al.*, "Mechanism of self-excitation of terahertz plasma oscillations in periodically double-gated electron channels," J. Phys.: Condens. Matter, **20**, 384207 (pp.1-6), 2008.

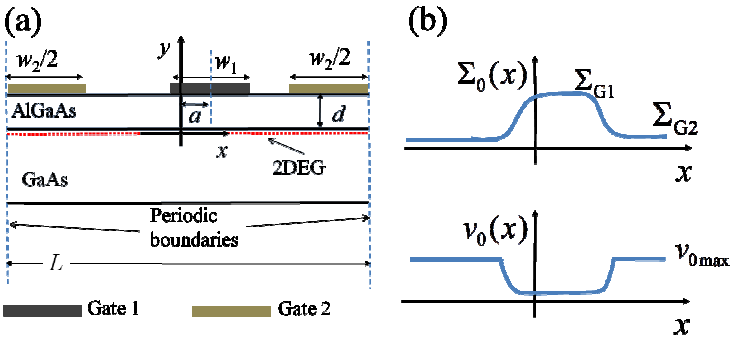

Fig 1. (a) Schematic view of the asymmetric DGG transistor structure and (b) steady-state profiles of electron concentration and velocity.

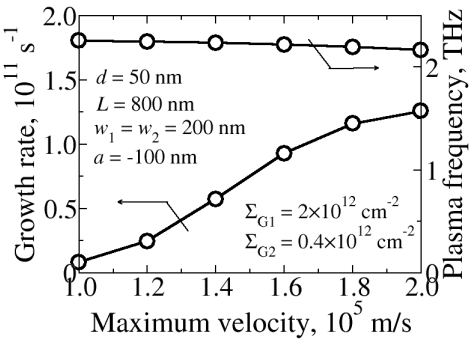

Fig 2. Growth rate and frequency of the first instable mode vs maximum velocity.

Voltage-controlled surface plasmon-polaritons in double-graphene structures

D. Svintsov[1], I. Semenikhin[1], V. Vyurkov[1], V. Ryzhii[2], T. Otsuji[2]

1. Institute of Physics and Technology, Russian Academy of Sciences, Moscow, Russia, vyurkov@ftian.ru

2. Research Institute of Electrical Communication, Tohoku University, Sendai, Japan

Plasma waves in graphene attract great interest due to their possible application in THz and infrared detectors and emitters. A number of systems for excitation of plasmons have been already studied [1], and the gated graphene structures turned out to be one of the most promising due to the voltage tunable wave dispersion [1]. However, plasmons in gated structures exhibit linear spectrum with much lower velocity than that of light, and thus cannot be effectively coupled to electromagnetic radiation. Moreover, the quality factor for such oscillations cannot exceed 10 in THz domain, even if the wave damping is caused solely by acoustic phonons [0].

This communication presents the spectra and damping of plasmon-polaritons in structures with two parallel graphene layers separated by a thin insulator (double graphene). The wave velocity and damping in those structures can be tuned by the bias voltage between layers similarly to gated graphene. Owing to the absence of metal gates, those waves are effectively coupled to the light and exhibit much smaller damping compared to that of gated plasmons.

It is demonstrated that in double graphene the propagation of two plasmon-polariton modes is possible: the first one corresponds to in-phase current oscillations in layers, while another corresponds to the counter-phase oscillations.

The damping of in-phase oscillations rapidly increases at the frequencies $\omega > 2\mu/\hbar$ (where μ is the Fermi energy) due to the interband absorption [4]. As the Fermi energy can be easily altered by the bias voltage, the proposed structures have prospects of plasmon modulators.

The wavelength of counter-phase oscillations is much smaller than that of in-phase ones. At interlayer distances of the order of 10 nm it can exceed ω / v_F, where $v_F = 10^6$ m/s is the characteristic electron velocity in graphene. At such small wavelengths the interband electron transitions are blocked due to the impossibility of energy and momentum conservation. That leads to a decrease in dynamic conductivity and an increase in wave quality factor.

The work was supported by the Russian Foundation for Basic Research (grants # 11-07-00464-a).

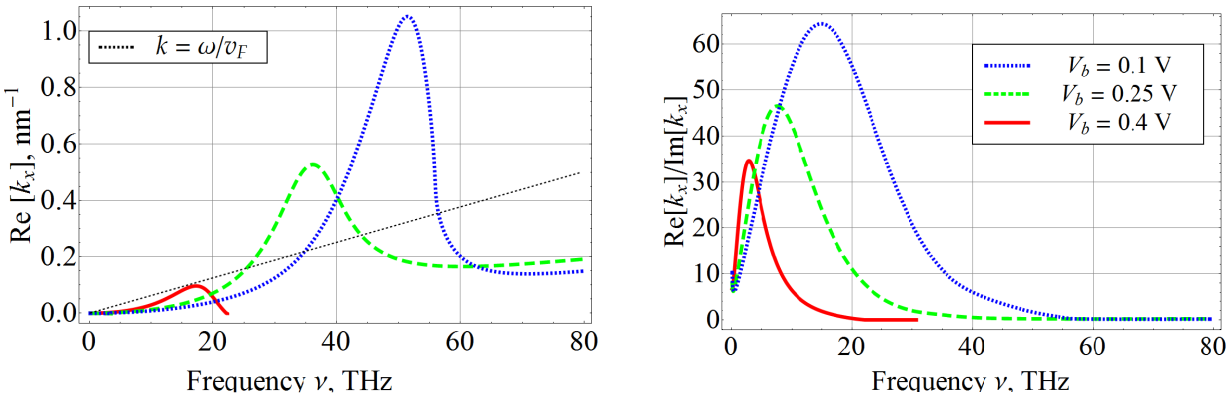

Fig. 1. Real part of wave vector of plasmon-polariton in double graphene at different bias voltages (left) and quality factor of the wave (right)

1. V. Ryzhii, A. Satou, and T. Otsuji, J. Appl. Phys., **101**, 024509, 2007.
2. D.R. Andersen, J. Opt. Soc. Am. B, **27**, 2010.
3. D. Svintsov, V. Vyurkov, S. Yurchenko, V. Ryzhii, T. Otsuji, J. Appl. Phys, **111**, 083715, 2012.
4. L.A. Falkovsky and A.A. Varlamov, Eur. Phys. J. B, **56**, pp.281-284, 2007.

Advanced impact ionization current model for MOS devices including heat effects

T. Krupkina, D. Rodionov
National Research University 'MIET'
E-mail address: denis.rodionov@gmail.com

Semiconductor technologies today allow manufacture hundreds of thousands of elements on single chip [1]. It is very important for designers to remember and understand interactions between elements via substrate during integrated circuits design cycle. MOS device interacts with substrate by drain-bulk, source-bulk capatitance and impact ionization physical phenomena. When a transistor is in the saturation mode, the internal the electric field occurs between the drain and the source. Channel electrons (for nMOS case) get high velosity and energy in electric field (such carriers call 'hot' carriers). Collisions between 'hot' electrons and lattice result electron-hole pair generation in drain depletion region [2-4]. New electrons go out to drain and new holes go out to substrate and forme substrate current Isub (fig. 1a).

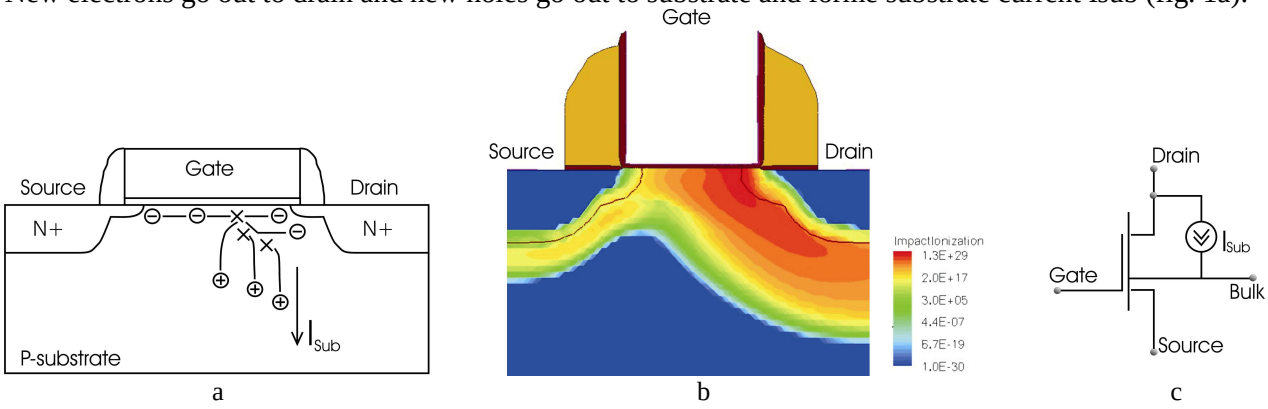

a b c

Fig. 1 Impact ionization phenomena in MOS device: phenomena structure (a), DESSIS device simulation results (b), impact ionization modeling with current generator (c).

Short channel nMOS device simulation with DESSIS software tool allows see high intensive of impact ionization under gate in drain depletion region (fig. 1b) [5]. So this physical phenomena can be modeled by current generator (fig. 1c) [6].

Moor's law gets us doubling on chip elements quantity every 18 monthes and permanent integrated elements size decrease [7]. Fast MOS device miniaturazation results in high on chip element density and high (and permanent increase) internal electric field value along the channel. High electric field value in the channel region results in high channel carriers velocity, high carrier temperature and increase lattice temperature.

IC designers still need accurate model that can consider heat effects influence on impact ionization phenomena and substrate current value. Short channel MOS device was modeled and advanced impact ionization model including temperature effects in channel region was develop.

1. R. Doering, Y. Nishi. *Handbook of Semiconductor Manufacturing Technology*. Second edition. CRC Press, 2008.
2. S. Donnay, G. Gielen. *Substrate Noise Coupling in Mixed-Signal ASICs*. Kluwert Academic Publishers, 2004.
3. E. Charbon, R. Gharpurey et al. *Substrate noise. Analysis and Optimization for IC Design*. Kluwert Academic Publishers, 2003.
4. S.M. Sze. *Physics of Semiconductor Devices.* John Willey and Sons, New York, 1981.
5. *Synopsys Sentaurus* User Manual.
6. P.R. Gray, P.J. Hurst et al. *Analysis and Design of Analog Integrated Circuits*. John Wiley & Sons, Inc., 2001.
7. International Technology Roadmap for Semiconductor. www.itrs.net

Electric instability in $GaAs/Al_xGa_{1-x}As$ superlattices with barrier layers non-transparent for tunneling

V. Gergel`[1], G.Galiev[1], E. Il`ichev[2], A. Verhovtseva[1], N. Gorshkova[1], A. Zelenyi[1], I. Altuкhov[1], S. Paprotskiy[1]

1. Kotel`nikov Institute of Radio Engineering, Russian Academy of Sciences, Moscow, Russia, vgergel@mail.ru

.

2. National Research University of Electronic Technology (MIET), Moscow, Russia

The computer simulation of conductivity of multibarrier $GaAs/Al_xGa_{1-x}As$ heterostructures on the base of quasi-hydrodynamic (thermic) model of electron drift is performed and analyzed. The basic mechanism of conductivity of superlattices studied is shown to be a thermally stimulated injection of electrons from heavily doped narrow-gap GaAs layers into undoped wide-gap AlxGa1-xAs layers at electron heating within the barrier layers. The energy balance nonlocality within an electron subsystem turns out to give rise to S-shaped current-voltage characteristics with pronounced negative differential resistance (NDR). The approximate analytical model of the S-shaped characteristics is developed. The frequency dependence of real and imaginary parts of small-signal impedance is determined [1].

The experimental samples represented 1000 μm^2mesas of structures consisted of five couples of successive layers of heavily doped $N_d = 10^{18}$ cm^{-3}) GaAs and undoped $Al_xGa_{1-x}As$ ($x = 0.3$). Time dependences of current $I(t)$ and voltage $U(t)$ were measured at room temperature at the approximate fixed-current mode. Short (1 μs) triangular voltage pulses with repetition frequency 1 to 10 Hz were used to diminish pulsed and averaged Joule heating. The current-voltage characteristics were found from instantaneous values of $I(t)$ and $U(t)$ at the same time moment.

The pronounced NDR region on the current-voltage characteristic at voltages 1 V < U< 4 V and current below 1 A was observed. The high-current part of the *I-V* curve could not be measured because of overheating sample during the voltage pulse.

The time dependences of sample temperature at experimental conditions were calculated and the ways for minimization of heating were analyzed.

This work was supported by Russian Foundation for Basic Research (RFBR): №12-07-00063, №12-07-00589.

1. V.A. Gergel', A.V. Verhovtseva, N.M. Gorshkova, and M.N. Yakupov, "Electric instability in multibarrier heterostructures: Features of the RF impedance", J. Comm. Tech. and Electronics, **57**, pp.441-444, 2012.

Ionization energy oscillations in metallic and semiconducting nanotubes of ultra small diameters

A. Ganin, E. Bormontov, L. Bitytskaya
Voronezh State University, Voronezh, Russia, E-mail address: me144@phys.vsu.ru.

Single-walled carbon nanotubes (SWNT) with ultra small diameter (0.2 – 1.2 nm) are of particular interest for investigation of properties of nanotubes of different structures. In previous work [1] it was shown, that SWNTs electronic band gap oscillates in region of ultra small diameters. Observed nonmonotonic change of band gap of SWNTs with their radius in region of ultra small diameters is a consequence of peculiar properties of diverse groups of nanomaterials such as fullerenes and other nano-sized particles. In current work we present results of ab initio calculation of impact of diameter and symmetry on bond energy and ionization energy of metallic and semiconducting nanotubes (27 tubes total) with small and ultra small diameters (ranged 0.2 – 1.2 nm).

In order to theoretically find ionization energy we have considered three methods: the Hartree – Fock method, the tight-binding method, and the density-functional method (DFT). Hartree – Fock method's scope is generally limited (as long as chemical precision is necessary) by molecules having only few chemically active electrons (so-called, “exponential wall”). In calculations carried out within the tight binding model curvature effects are being neglected, what implies essential difference between results of such calculations and experiment (for SWNTs of small and ultra small diameters). Therefore, we decided to use the Kohn – Sham method (DFT) within local-spin-density approximation and 3-21G basis. We used TubeGen 3.4 software for carbon nanotube (CNT) generation and Gaussian 03 (Windows version) for the calculation. Cylindrical unit cell of the tube was chosen. CNTs were assumed to be of infinite length. Periodic boundary conditions (PBC) were applied. Relevancy of the method and basis was verified in previous calculations for SWNTs [1], and also by comparison of the results obtained with published data of experimental and theoretical investigations [2, 3].

The dependency of the nanotubes bond energy vs. their diameter has monotonically increasing character, meaning that tubes of larger diameters tend to be more stable (in range 0.2 – 1.2 nm). Average bond energy for all tubes is 8.5 eV per atom.

As for the ionization energy, we have separated the results of the calculation into two groups according to the well-known '3k' rule: if difference of chirality indexes is a multiple of three than SWNT has metallic conductance or its band gap is zero, otherwise SWNT has semiconducting conductance [4]. We have found that ionization energy is different not only for nanotubes of different diameters but it also depends on SWNTs symmetry. For nanotubes from the first group a complex dependency of ionization energy on diameter with large-scale oscillations (of period 0.13 nm) in diameters range from 0.2 to 0.4 nm and small-scale oscillations (of period 0.10 nm) in diameters range from 0.4 to 0.7 nm have been observed. For SWNTs from the second group large-scale oscillations (of period 0.12 nm) with fading amplitude have been observed in diameters range from 0.2 to 0.7 nm. Different CNTs symmetry influences also the general character of the dependencies. Particularly, for SWNTs from the first group ionization energy grows with diameter, while for SWNTs from the second group ionization energy decreases with diameter. The largest ionization energy (for both groups) is found for nanotube with chirality indexes (0, 4) and diameter 0.31 nm and amounts to 6.11 eV.

The results obtained are considered to be a consequence of quantum size effects in region of small and ultra small diameters.

1. E. Bormontov, A. Ganin, and L. Bitytskaya, “Oscillations of electronic band gap in carbon nanotubes of small and ultra small diameters”, Izvestia vuzov, Electronica, **94**, pp.10-14, 2012 (in Russia).
2. M. Shiraishi and M. Ata, “Work function of carbon nanotubes”, Carbon, **39**, pp.1913-1917, 2001.
3. E. Bogoslavskaya and I. Bazhin, “Modeling of fracture processes of carbon nanotubes and their contacts”, Investigated in Russia, **46**, pp.532-536, 2009. http://zhurnal.ape.relarn.ru/articles/2009/046.pdf
4. R. Saito, G. Dresselhaus, and M. Dresselhaus, *Physical properties of carbon nanotubes*. Imperial College Press, Singapore, 1998.

The brain is a nanoelectronic object

I.I. Abramov
Belarusian State University of Informatics and Radioelectronics, Minsk, Belarus, E-mail: nanodev@bsuir.edu.by

It was noted that «the brain can be interpreted as an object of organic hybrid nanoelectronics created by Nature» [1]. Therefore the nearest analogue in artificial electronics is an integrated circuit (IC) of micro-and nanoelectronics.

The aim of this work is a deeper argumentation of these statements, as well as an attempt to answer the following questions: 1) Why can the brain be interpreted as an object of organic hybrid nanoelectronics? 2) How does the brain function from the point of view of a specialist in electronics? 3) Is quantum mechanics enough for description of the brain functioning, including consciousness, thought, and its other mental functions? 4) How to investigate the brain further?

The following hypotheses are formulated: 1) the hypothesis of the dominant influence of electrical processes on the brain function; 2) the hypothesis of the adequacy of quantum mechanics as a base for the study of the brain; 3) the hypothesis that rigorous mathematical simulation of the brain functioning is refered to NP class problems. The hypotheses allow satisfactorily answering these questions as shown in the paper.

In particular, it is shown that all the basic elements of neuronal sets of the brain can be considered as elements of electrical circuits, i.e. neuronal circuit (first type) is a peculiar kind of electrical circuits. Therefore the comparison of the first type circuits with ICs of micro- and nanoelectronics (second type) was made and their basic differences were determined. Thus, the neuronal circuit is firstly growing, and then possibly modified electrical circuit. In addition, this is perhaps the most important and fundamental its difference from the IC, which leads to the most significant advantages of first type circuits over the second type ones.

In accordance with the carried out analysis the hypothesis of the dominant influence of electrical processes on the functioning of the brain is stated. Chemical processes provide a supply for the electrical circuits of the brain, as well as their possible modification. First of all this is why Nature did not follow a purely «electronic way», but followed the «hybrid way», i.e. the way of elegant interaction (transformation) of electrical and chemical processes.

Thus, according to the proposed interpretation, the human brain is a set of nonlinear electrical (neuronal) circuits of the two kinds that shouldn't be modified and which should be modified. In all cases it is memory.

Since the brain is a multifunctional device the various modes of its operation are discussed in the paper. Three types of operation modes of the brain as a set of nonlinear electrical circuits are realized, namely: 1) with external influence; 2) without external influence (internal), and 3) mixed. All the individual modes of the brain, including perception, thinking, and other mental functions, are related to one of these types. It is shown that any particular operation mode of the brain is a result of the passage of an electrical signal (or signals) across a corresponding set of electrical circuits of the first type, besides basic possible operations are following: comparison, encoding, decoding, action command, modification of neuronal circuits.

Such important modes of functioning of the brain as processing of sensory information, image recognition, thinking, dreams, etc. are discussed. In particular, thought is a decoding (internal reproduction) of electrical signal (or signals) initiated by the brain itself, passing by the brains' neuronal circuits of a corresponding spatial-temporal configuration. The more complex mental processes are considered, for example, insight. Usually, however, thinking is the internal perception of the earlier coded information in the brain.

In the paper the scheme of a multilevel simulation of the brain based on the noted key ideas is presented.

The above mentioned interpretation and its consequences allow, on the one hand, to analyze the principles of the brain functioning more deeply, and, on the other − to suggest a complex approach to brain investigation, based on a multilevel simulation combined with experimental methods.

1. I.I. Abramov, "Problems and principles of physics and simulation of micro- and nanoelectronic devices. I. Basic positions", Nano- and mikrosistemnaya tekhnika, № 8, pp.34–37, 2006 (in Russian).

Boundary conditions for the contact between normal metal and multiband superconductors with unusual types of pairing

I. Devyatov, A. Burmistrova
Lomonosov Moscow State University, Skobeltsin Institute of Nuclear Physics, Moscow, Russia,
igor-devyatov@yandex.ru

Based on the equations of tight-binding model [1], boundary conditions for the contact of a normal metal and the multiband superconductors with unusual types of superconducting pairing were obtained. These boundary conditions were obtained outside of the effective mass approximation, and allows to consider as a complex nonparabolic and anisotropic spectrum of normal excitations in the superconductor and its multiband structure, and unusual types of symmetries of the superconducting order parameter. Derived boundary conditions are applied by us for the calculation of conductivities of contacts of a normal metal (or ferromagnet) with high-temperature superconducting pnictides for different angles of orientation of the boundary with respect to the crystallographic axes of the pnictides. Using these boundary conditions, the multiple Andreev reflection between two superconducting pnictides has investigated. The phase and temperature dependencies of Josephson current in heterostructures containing pnictides have calculated. The application of suggested method for calculation of electron transport in other unusual superconductors has discussed.

1. Q.-G. Zhu and H. Kroemer, “Interface connection rules for effective-mass wave functions at an abrupt heterojunction between two different semiconductors”, Phys. Rev. B, **27**, pp.3519-3527, 1983.

New method for calculation of the electron transport in heterostructures with different unusual types of superconducting pairing

A. Burmistrova, I. Devyatov
Lomonosov Moscow State University, Skobeltsin Institute of Nuclear Physics, Moscow, Russia
igor-devyatov@yandex.ru

At present time there is great interest in studying of high-temperature superconductors. The possibility of the existence in such superconductors unusual symmetry of the order parameter is considered. In high-temperature iron-based pnictides the presence of $s_{\pm}$ symmetry of the order parameter and the interorbital superconducting pairing is actively discussed. In superconducting Sr_2RuO_4 compounds as a p-wave symmetry and $p_x + ip_y$-wave symmetry of the order parameter are discussed.

These investigations suggest the presence of reliable experimental data and adequate theories of coherent transport in such structures, as it was in the investigation of $YBaCuo$ systems. In the study of superconducting pnictides and superconducting perovskites abundance of interesting experimental data contrasts with the lack of a consistent microscopic theory that adequately describes the coherent electron transport in their contacts with a normal metal or other superconductor. Difficulty of creating a consistent microscopic theory of coherent transport in structures with superconducting pnictides and perovskites is explained by their multiband structure, complicated anisotropic excitation and also by anisotropy and sign-changing of the order parameter for different directions.

Based on equations of tight-binding model, we obtained the new boundary conditions for the contact of a normal metal and the multiband superconductors with arbitrary types of superconducting pairing and complicated anisotropic excitation spectrum. In the framework of this new tight-binding approach we calculated the conductivities of the contacts between a normal metal and superconducting pnictide for different angles between crystallographic axes of the pnictide and a normal metal. We also calculated the conductivities of the contacts between a normal metal and superconducting perovskite for different misorientation angles of the interface with respect to the crystallographic axes of the superconductor. Also the temperature and phase dependencies of the Josephson current in structures with superconductors with different unusual types of pairing were calculated.

Superconducting quantum arrays as electrically small antennas

I. Soloviev[1], N. Kolotinsky[2], N. Klenov[2], A. Sharafiev[2], V. Kornev[2], and O. Mukhanov[3]
1. *Scobeltsyn Institute of Nuclear Physics, Moscow State University, Moscow, Russia, igor.soloviev@gmail.com.*
2. *Physics Department, Moscow State University, kornev@phys.msu.ru.* 3. *HYPRES, Inc., Elmsford, NY, USA, mukhanov@hypres.com*

Recent progress in communication technology has led to a concept of broadband receiving systems capable of high-performance simultaneous receiving of radio-frequency signals which can differ sharply in both amplitudes and frequency ranges. This can be achieved with the direct digitization of wideband RF signals. Only superconductor Analog-to-Digital Converters (ADC) can do this with adequate performance. Such ADCs demonstrate outstanding noise temperature, linearity and dynamic range [1]. At the same time, with the use of the superconductor ADCs, antenna and low noise amplifier both limit the overall system performance since they have higher noise temperature and lower linearity and dynamic range than the ADC. It is possible to solve this problem with the implementation of the cooled active superconductive Electrically Small Antenna and their integration with the ADCs in one cryogenic package. Such an active ESA can be designed with implementation of Superconducting Quantum Array (SQA) which is a regular two-dimensional array with the specially designed basic cells. Two promising basic cells capable of providing highly linear voltage response to magnetic component of an incident electromagnetic wave were devised and experimentally evaluated [2-3]. A prototype of the active ESA occupying area 3.3 x 3.3 mm^2 has been fabricated using Nb process with critical current density 4.5 kA/cm^2 and experimentally evaluated. The obtained results are presented and discussed in detail.

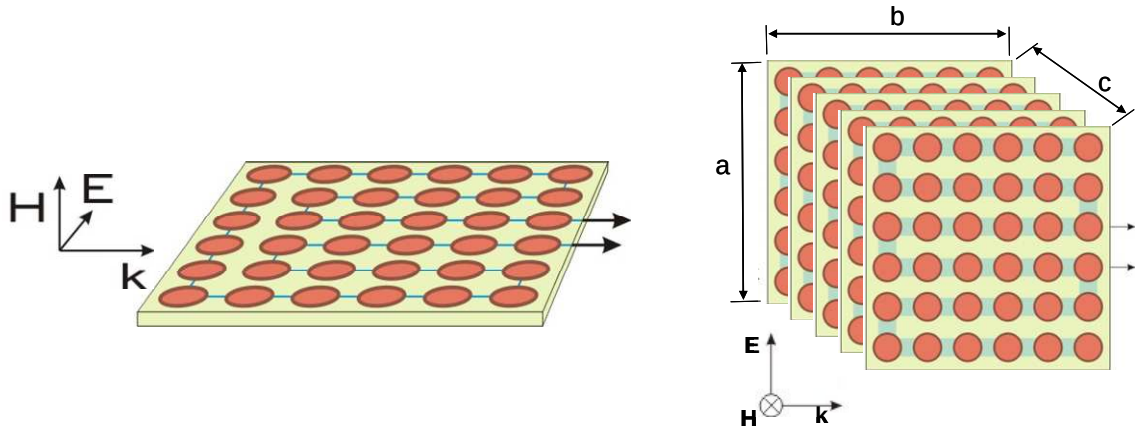

a *b*

Fig. 1. Active Electrically small Antennas (ESA) based on 2D Superconducting Quantum Array (SQA) with normal-metal connectors between the cells (a) and active ESA based on 3D SQA (b)

1. D. Gupta, A. Inamdar, D.E. Kirichenko, A.M. Kadin, and O.A. Mukhanov, "Superconductor analog-to-digital converters and their applications," Microwave Symposium Digest (MTT), IEEE MTT-S, June 2011, p.1-4, 2011.
2. V.K. Kornev, I.I. Soloviev, et al.,"Performance advantages and design issues of SQIFs for microwave applications," IEEE Trans. Appl. Supercond., **19**, pp.916-919, 2009.
3. V.K. Kornev, I.I. Soloviev, N.V. Klenov and O.A. Mukhanov, "Bi-SQUID - Novel Linearization Method for dc SQUID Voltage Response", Superconductor Science and Technology (SUST), **22**, 114011 (pp.1-6), 2009.

Combined Magnetic Field Sensor with Superconductive Magnetic Field Concentrator

L.P. Ichkitidze
National Research University of Electronic Technology "MIET", MIET, Zelenograd, Moscow, 124498 Russia
leo852@inbox.ru

Superconducting film loops are often used in magnetic field sensors (MFS) as magnetic flux transformers (MFT) and magnetic field concentrators (MFC). They are used as MFTs in MFSs, which magneto sensitive elements (MSE) are Josephson junctions (SQUID magnetometers) or Josephson area (ceramic high-temperature superconductors (HTSC)) [1]. They are also used as MFCs in MFSs, which MSE are Hall sensors or sensors on the effect of giant magnetic resistance (GMR) [2]. The combined magnetic field sensor based on the MFT (superconducting film ring) and GMR (magnetically sensitive film resistor) was considered in papers [3,4]. It was shown that the MFS efficiency increases at the optimal fragmentation of active stripe of MFTs to multiple parallel canals and slits. Canals and slits had micron or submicron sizes.

The object of this study is a magnetic field multiplication (concentration) factor F for MFC of combined MFS. This sensor consists of a MFC with a tapered active stripe and a film MSE based on GMR effect. The MSE is overlapped with the MFC active strip and is separated with an insulator film.

It is found that in the case of optimal division of the active strip (7 μm wide) of MFC into parallel branches with nanodimensional widths (90-350 nm), F increases relative to the case of the active strip prior to its division by a factor 25 to 80. For the low-temperature superconducting films (LTS), i.e., the films with small London penetration depth λ of the magnetic field (e.g., for heteroepitaxial layers of Nb, $\lambda \sim 50$ nm), the higher values of F relative to HTS films are attained (e.g., for Y-123, $\lambda \sim 200$ nm). An increase in F promotes attaining the resolution level of magnetic field ($\delta B \leq 1$ pT) at temperature ≈77 K, which is more effective that the resolution ($\delta B \sim 10$ pT) of HTS SQUID.

Analysis of the results leads to the conclusion that the fragmentation of the active strip on a small number of nanoscale chanals (3) and slits (2), i.e. topological nanostructuring of the active strip, increases the MFC multiplication factor and make it possible to achieve a larger magnetic field concentration on the magneto sensitive element in 4 times. Therefore, characteristics of magneto sensitive element are improved accordingly. The positive effect, i.e. the increase in F for the fragmentized active strips, is achieved through a more uniform distribution of current than in the solid active strip. The current density near the edges of the superconducting film reaches its maximum value, and is greatly reduced in the middle of it, therefore, there is fragmentation is less efficient. The consequence is the decrease in F, when the slits are located near the middle of the active strips.

Thus, the value of F is increased when the value λ is reduced. It means that clean LTS (e.g. niobium) materials are more efficient then granular or HTS materials (e.g. ceramics system Bi-2223) that are used in the superconducting film MFC. It should be noted when the distance to the critical temperature is increased the MFC efficiency is reduced, because the value λ is increased.

The results will be in demand in different magnetic systems and magnetic sensors, that registering ultra weak magnetic fields (≤ 10 pT): in the noninvasive biomedical diagnostics, nondestructive testing of solids, the electrical circuits in a field short circuit.

The author is grateful to Professor S.V. Selishchev for their helpful advice and support of this work.

1. M.I. Faley, U. Poppe, K. Urban, and R.L. Fagaly, "Noise analysis of DC SQUIDs with damped superconducting flux transformers", Journal of Physics: Conference Series, **234,** 042009, 2010.
2. K.H. Kuit, W. van de Camp, S. Waanders, H. Rogalla, and J. Flokstra, "Hybrid magnetometers based on a doped silicon-on-insulator Hall device and a YBa2Cu3O7−δ flux concentrator", Supercond. Sci. Technol., **22**, 114006, 2009.
3. L.P. Ichkitidze and A.N. Mironyuk, "Superconducting film flux transformer for a sensor of magnetic field", Physica C, **472**, pp.57-59, 2012.
4. L.P. Ichkitidze and A.N. Mironyuk, "Topological nanostructure superconducting film flux transformer", Nano- and Microsystem Tehknika, No. 1, pp.47-50, 2012 (in Russian).

Comparative Parameters of Superconductor-Based Sensors of Weak Magnetic Fields

L.P. Ichkitidze[1], M.L. Gavryushina[2]

1. National Research University of Electronic Technology "MIET", Zelenograd, Russia, leo852@inbox.ru. 2. Bazovye Technologii JSC, Moscow, Russia

Various sensors of the magnetic field (constant or weakly variable, frequency ≤1 kHz, range 10^{-6}÷10^{-15} T) based on superconducting materials are considered. Physical principles of operation are described for each type of sensors, and their calculated and experimental characteristics such as absolute magnetic sensitivity, relative magnetic sensitivity, magnetic-field resolution δB, magnetic flux resolution $\delta\phi$, and dynamic measurement range D_r are presented.

Special attention is paid to sensors of ultra-weak ($\leq 10^{-12}$ T) magnetic fields. It is noted that SQUID sensors based on high-temperature superconducting (HTSC) materials of the Y-Ba-Cu-O system with working temperature T_w~77 K have resolutions $\delta\phi \sim 10^{-5}$-10^{-6} ϕ_0, (where $\phi_0 \approx 2\times10^{-15}$ Wb is the magnetic flux quantum) and $\delta B \sim 10^{-13}$ T are worse than SQUID sensors based on low-temperature superconducting (LTSC) materials, for example Nb with T_w~4 K, by a factor of several times. SQUID sensors are characterized by high $D_r \geq 140$ dB. Commercial HTSC SQUID sensors have resolution $\delta B \sim 10^{-14}$ T at T_w~77 K, while LTSC SQUID sensors have resolution $\delta B \sim 10^{-15}$ T at $T_w \sim 4$ K. However, their energy resolution can attain the record low value $\sim 10^{-32}$ J/Hz [1].

Magneto-modulation sensors based on ceramic HTSC materials (particularly, in a form "Josephson medium" for the Y-Ba-Cu-O and Bi-Sr-Ca-Cu--O systems) are characterized by acceptable absolute magnetic sensitivity ($\geq 10^5$ V/T), $\delta B \geq 10^{-13}$ T and $\delta\phi \geq 10^{-4}$ ϕ_0 at $T_w \sim 77$ K, but they are considerably worse than SQUID sensors. The further improvement of technology of superconducting materials in a form "Josephson medium" and design of magnetomodulation sensors with improve their useful parameters and approach them to parameters of SQUID sensors.

Resolution $\delta B \geq 10^{-10}$ T is attained for magnetoresistive thick-film (thickness ≥ 10 μm) sensors based on ceramic HTSC materials (particularly, for the Y-Ba-Cu-O and Bi-Sr-Ca-Cu-O systems in a form "Josephson medium") at T_w~77 K. We expect to attain $\delta B \sim 10^{-11}$-10^{-12} T and D_r ~110-120 dB upon realizing the dimensional effect in this films.

When comparing magnetically sensitive characteristics of SQUID, magnetomodulation, and magnetoresistive HTSC-based sensors, we can assume that the latter sensors have advantages in regards to SQUID sensors. They are simple in fabrication, reliable in operation, and are less expensive by a factor of many times. In addition, these sensors measure the absolute magnitude of the magnetic field, while the SQUID sensors measure only its increment.

We analyzed combined sensors based on superconductor/nonsuperconductor materials, particularly HTSC/semiconductor, HTSC/materials with giant magnetic resistance (GMR), etc. Resolution $\delta B \sim 10^{-9}$ T at T_w~77 K is implemented for the combination involving the superconducting film magnetic-field concentrator (MFC) and the Hall sensor. The combination Y-Ba-Cu-O film (MFC)/CoFe film (GMR) can have $\delta B \sim 10^{-15}$ T at T_w~4 K, which is noticeably better in regard to resolution of the SQUID sensor.

According to preliminary evaluations, we can expect considerable improvement by magnetic field in the combined sensor consisting of the nanostructured superconducting film, which serves as the magnetic field concentrator, and magnetoresistive nanometer film based on the GMR effect, which serves as the magnetic sensitive element [2]. In this case, we expect resolution $\delta B \leq 10^{-15}$ T, which is comparable or better than SQUID resolution in the low-temperature region. Several tens (for example, in the magnetocardiograph) or several tens (for example, in the magnetoencephalograph) SQUID sensors are used in commercial magnetic systems. They are very fragile and expensive (price more than $1500 for each), and combined sensors will have considerable advantages in this respect. Consequently, combined sensors with nanostructured parts are promising for the development of reliable and inexpensive sensors of ultra-weak magnetic fields.

The authors are grateful to Professor S.V. Selishchev for their helpful advice and support of this work.

1.D. Robbes, "Highly sensitive magnetometers –a review", Sensors and Actuat. A, **129**, pp.86-93, 2006.

2.L.P.Ichkitidze, A.N. Mironyuk, "Superconducting film magnetic flux transformer", Patent № 2455732 RU.

A dynamic simulation model for functionally-integrated injection laser-modulator

B. Konoplev[1], E. Ryndin[2], M. Denisenko[1]
1. Taganrog Institute of Technology, Southern Federal University, Taganrog, Russia, kbg@tti.sfedu.ru.
2. Southern Scientific Center of Russian Academy of Sciences, Rostov-on-Don, Russia, rynenator@gmail.com

Injection lasers and modulators are the basic elements of integrated optical commutation systems. Functionally integrated injection lasers-modulators, which discussed in this paper, are characterized by the maximum amplitude modulation frequencies over 1 THz. Thus it can be implemented in a single technological cycle. Constructing method of these devices is presented in [1 – 3]. Such parameters as the dynamics of the space distributions of the velocity of spontaneous and stimulated radiative recombination, as well as the concentrations of electrons and holes not only in the active region but also in the peripheral regions of the laser-modulator is necessary to consider while the modeling of optoelectronic components. To solve this problem we propose a model (1) – (5) developed on the basis of a fundamental system of equations and kinetic equations of a semiconductor laser:

$$\varepsilon_0 \nabla(\varepsilon \cdot \nabla\varphi) = e(n - p - N); \tag{1}$$

$$\frac{\partial n}{\partial t} = -\nabla\left(\mu_n\left(n \cdot \nabla(\varphi + V_h) - \varphi_T \nabla n\right)\right) - (n - n_0)\left(\frac{1}{\tau_S} + \alpha \cdot n_{ph}\right); \tag{2}$$

$$\frac{\partial p}{\partial t} = -\nabla\left(\mu_p\left(p \cdot \nabla(\varphi - V_H) + \varphi_T \nabla p\right)\right) - (p - p_0)\left(\frac{1}{\tau_S} + \alpha \cdot n_{ph}\right); \tag{3}$$

$$\frac{dn_{ph}}{dt} = -\frac{n_{ph}}{\tau_f} + (n - n_0)\left(\frac{\beta}{\tau_S} + \alpha \cdot n_{ph}\right), \tag{4}$$

$$n_{ph} = 0 \ \text{ for } \ E_{F_n} - E_{F_p} < E_C - E_V . \tag{5}$$

where n – the concentration of electrons; p – the concentration of holes; N – the effective concentration of impurities; n_{ph} – the density of photons in the laser mode; φ – the electric potential; V_h – the heterostructure potential in the conduction band; V_H – the heterostructure potential in the valence band; t – the time; e – the elementary charge; ε – the permittivity of semiconductor; ε_0 – the vacuum permittivity; α – the optical gain coefficient; β – the fraction of spontaneous emission entering the lasing mode; τ_S – the spontaneous recombination lifetime of the carriers; τ_f – the photon lifetime of the cavity; μ_n, μ_p – the electrons and the holes mobilities; φ_T – the temperature potential; E_C – the bottom of the conduction band; E_V – the top of the valence band; E_{Fn}, E_{Fp} – the electron and the holes quasi Fermi levels.

Applicability of the results of numerical analysis not only of the active region of the laser-modulator, but also peripheral areas is important feature of the proposed model. However, one of the quantities in the basis of the variables of the model is the density of photons in the laser mode n_{ph}, occurring only in the active region of the laser when the current density of the pumping is sufficient. Accounting for this factor provides the condition (5).

1. B.G. Konoplev, E.A. Ryndin, M.A. Denisenko, “Integrated injection laser with rearrangement of wave function of carriers”, Vestnik Yujnogo nauchnogo centra RAS, **6**, № 3, pp.5–11, 2010 (in Russian).
2. B.G. Konoplev, E.A. Ryndin, M.A. Denisenko, “Integrated Injection Laser with Amplitude Modulation in Terahertz Band”, Abstracts of the International Conference “Micro- and nanoelectronics - 2009”. Moskow – Zvenigorod, Russia, p.O1-28, 2009.
3. B.G. Konoplev, E.A. Ryndin, M.A.Denisenko, Patent RU 2400000 C1, 2010.

Computationally Efficient Methods for Optical Simulation of Solar Cells and their Applications.

M. Zanuccoli[1], I. Semenikhin[2], V. Vyurkov[2], E. Sangiorgi[1], C. Fiegna[1]
1 ARCES-DEI University of Bologna & IUNET ,47521 Cesena (FC), Italy
2 Institute of Physics and Technology RAS, 117218 Moscow, Russia

Modeling of optoelectronic devices like solar cells requires an accurate prediction of the spatially resolved optical generation rate per unit volume and time inside the absorbing media. In low-cost photovoltaic devices the reduction of volume of the absorber material leads to a relatively limited capability to collect photons from the external source, therefore an effective way to improve the performance is the enhancement of the photon management strategy. Nanometric structures (like photonic-crystals [1] and diffraction gratings [2]) and nanorough interfaces [3] are commonly adopted in thin-film photovoltaic devices in order to enhance the absorption of photons. In addition, a growing interest in nanorod and nanowire based solar cells [4] as well as in macroporous silicon [5] for photovoltaic application has been reported. In order to solve the optical problem, a rigorous numerical solution of the Maxwell equations is required. The most common approaches to the solution of the Maxwell equations are the Finite Difference Time Domain method (FDTD) [6] and the Finite Element Method [7]. However these methods are typically cpu and memory expensive especially in solar cells modeling. On the other hand the Fourier Modal Method (FMM) [8], also known as Rigorous Coupled-Wave Analysis (RCWA) [9] is a general and accurate method based on Fourier expansion in terms of spatial harmonics of the electromagnetic field and of the permittivity which leads to a excellent trade-off between accuracy and computational resources requirements and that can be applied to a wide variety of optical problems. The new iterative methods for solving Maxwell's equations are also of great interest in this field because they allow to attain the computational complexity proportional to the total number of Fourier modes N considered in the expansion [10] instead of N^3 as in case of conventional methods like the RCWA and similar ones.

In this work a novel implementation of the iterative method is put forward. Differently from that proposed in Ref. [10], it allows for modeling of absorptive media that is crucial for solar cell simulation. The comparison with the Fourier modal method and the previously developed 2-D tools [11-12] is performed. We also present some applications of those methods to nano and microstructured solar cells. In particular, the influence of nanorough and nanoporous interfaces and of the geometrical configuration of a silicon nanorod array on the photo-generated current has been investigated.

1. R. H. Lipson, and C. Lu, Eur. J. Phys., pp. 33-48, 2009.
2. S. H. Zaidi, J. M. Gee and D. S. Ruby, Conference Record of the 28th IEEE Photovoltaic Specialists Conference, pp. 395-398, 2000.
3. J. Krc, M. Zeman, O. Kluth, F. Smole F. and M. Topic, Thin Solid Films, **426**, pp. 296-304, 2003.
4. E. C. Garnett, M.L. Brongersma, Y. Cui and M. D. McGehee, Annu. Rev. Mater. Res., **41**, 2011.
5. M. Ernst, Rolf Brendel, Solar Energy Material, **95**, pp. 1197-1202, 2011.
6. K.S. Kunz and R.J. Luebbers. The *Finite Difference Time Domain Method for Electromagnetics*, CRC Press, 1993.
7. J. M. Jin. *The Finite element method in electromagnetics*, Wiley, New York, 1993.
8. K. Knop, J. Opt. Soc. Am., **68**, pp. 1206-1210, 1978.
9. M. G. Moharam and T. K. Gaylord, J. Opt. Soc. Am., **71**, pp. 811-818, 1981.
10. A. A Shcherbakov, A. V. Tishchenko, Journal of Quantitative Spectroscopy and Radiative Transfer, **113**, pp. 158–171, 2012.
11. Semenikhin, M. Zanuccoli, M. Benzi, V. Vyurkov, E. Sangiorgi and C. Fiegna, Optical and Quantum Electronics, **44**, 3-5, pp.149-154, 2012.
12. Semenikhin, I.; Vyurkov, V.; Zanuccoli, M.; Sangiorgi, E.; Fiegna, C., 14th International Workshop on Computational Electronics (IWCE), 2010.

Optical absorption of silicon layer with incorporated nano-voids and metal nanoparticles

V. Shautsova, P. Gaiduk
Belarusian State University, Minsk, Belarus, v.shautsova@gmail.com

Light trapping structures are essential for enhancement of conversion efficiency in opto-electronic devices and photovoltaics. In the case of conventional thick silicon solar cells, surface texturing is typically used for this matter . However, texturing technique is not effective for thin-film solar cells. As alternative approach, it has recently been demonstrated that freely propagating sunlight can be concentrated into a thin semiconductor layer by metallic nanostructures that support surface plasmons [1] – coherent electron oscillations at the metal/dielectric interface. An advantage of surface plasmon excitations arises from the huge electromagnetic field enhancement near the metal surface. Therefore metal nanoparticles incorporated into a silicon layer are able to enhance optical absorption of incident photons in a surrounding semiconductor material [1,2]. Although gold and silver nanoparticles are widely used for plasmonic applications [2-4], the metals create deep recombination centers in the band gap of semiconductor which dramatically limit collection of carriers. Thus, novel materials for enhancement of light absorption and carrier generation are required.

In this work, nano-voids incorporated in highly doped silicon layers are evaluated as alternative approach. A comparative discussion of absorption efficiency of silicon layers with incorporated nanoholes and nanoparticles will be carried out in the talk.

It is well known that plasma frequency depends on the carrier concentration N in the following form

$$\omega_p = \sqrt{\frac{Ne^2}{\varepsilon_0 m^*}},$$

with e the elementary charge, m^* the effective mass of the electrons and ε_0 the electric permittivity of vacuum. A typical value of plasma frequency for noble metals is located in the visible spectral range and with higher refractive index of the medium shifts to the near-infrared part of the spectrum which is poorly absorbed by thin silicon film. Highly doped silicon however can exhibit plasma frequencies in the mid- and far-infrared spectral region. To achieve optical frequencies the carrier concentration should be as high as $5*10^{22}$ cm^{-3}, i.e., the value of approximately one electron per atom. Due to surface states, this condition might be achieved in the thin surface layer of highly doped silicon [5]. The shell of nano-void incorporated in highly degenerated silicon might be one possibility for that.

The present work proposes an approach for enhancing of the absorption of thin-film silicon solar cells using array of incorporated nano-voids which might support the excitation of localized surface plasmons at near-infrared frequencies. Using 3D full field finite difference time domain (FDTD) simulations it has been numerically demonstrated that incorporated nano-voids might result in absorption enhancement compared to those, typical for incorporated metallic nanoparticles.

1. A. Harry and A. Polman, “Plasmonics for improved photovoltaic devices”, Nat. Mater., **9**, pp.205–213, 2010.
2. S. K. Jana, A. L. Donne and S. Binetti, “Enhancement of silicon solar cell performances due to light trapping by colloidal metal nanoparticles”, J. Phys. Chem. Solids, **73**, pp. 143–147, 2011.
3. I. Diukman, L. Tzabari, N. Berkovitch, N. Tessler and M. Orenstein, “Controlling absorption enhancement in organic photovoltaic cells by patterning Au nano-disks within the active layer”, Opt. Express, **19**, pp. A64–A71, 2011.
4. C. Hägglund, M. Zach, G. Petersson and B. Kasemo, “Electromagnetic coupling of light into a silicon solar cell by nanodisk plasmons”, Appl. Phys. Lett., **92**, pp. 053110-1–053110-3, 2008.
5. L. F. Wagner and W. E. Spicer, “Observation of a Band of Silicon Surface States Containing One Electron Per Surface Atom”, Phys. Rev. Lett., **28**, pp. 1381–1384, 1972.

Simulation of resonant tunneling devices based on different materials

I.I. Abramov, N.V. Kolomejtseva, I.A. Romanova, A.G. Klimovich
Belarusian State University of Informatics and Radioelectronics, Minsk, Belarus, E-mail: nanodev@bsuir.edu.by

In the paper the nanoelectronic devices based on the resonant tunneling effect are analyzed. In particular, the current-voltage characteristics of resonant-tunneling diodes (RTD's) based on Si/Ge, Si/SiGe heterostructures and based on carbon nanotubes (CNT) are calculated using the proposed models.

The first combined two-band model [1, 2] for calculation of RTD characteristics with account of valence band influence is modified for the case of account of quantum well width deviation. The combined numerical model of RTD is based on the self-consistent solution of the Poisson and Schrödinger equations. In the paper the results of calculation according to the proposed model for double-barrier Si/Ge, Si/SiGe RTD's are obtained. The developed modified model provides a good agreement with experimental data at the room temperature.

The second and third models for calculation of RTD based on CNT are presented. The second model is a simple analytical one. The results of calculation according to this model for devices based on CNT are presented for different values of the Fermi energy level. The Fermi energy level depends on the material used for the contact system.

The third model is a self-consistent one. A comparison of the analytical model and the self-consistent one is carried out. A good agreement of calculation results was obtained only at small voltages. IV-characteristics with larger values of the peak current and peak voltages were obtained with the use of the third numerical model. Thus the second model can be only used for rapid engineering estimations of characteristics of RTD based on CNT.

All above-listed results were obtained with the use of the nanoelectronic devices simulation system NANODEV [3] on PC.

1. I.I. Abramov, N.V. Kolomejtseva, "Simulation of resonant tunneling diode based on Si/SiGe", Nano- and mikrosistemnaya tekhnika, № 11, pp.16–18, 2011 (in Russian).
2. I.I. Abramov, N.V. Kolomejtseva, I.A. Romanova, "Combained two-band models of resonant tunneling diodes", Russian Microelectronics, **41**, 2012 (in print).
3. I.I. Abramov, A.L. Baranoff, I.A. Goncharenko, N.V. Kolomejtseva, Y.L. Bely, I.Y. Shcherbakova, "A nanoelectronic device simulation software system NANODEV: New opportunities", Proc. SPIE, **7521**, 75211E (11 pp.), 2010.

ELECTRONIC STRUCTURE OF MAGNETIC NANOCLUSTERS OF COBALT AND NICKEL SILICIDES

A. TUCHIN[1], L. BITYUTSKAYA[1], A. LAZAREV[2], A. SIGOV[3]

1. *VORONEZH STATE UNIVERSITY, VORONEZH, RUSSIA, E-MAIL: ME144@PHYS.VSU.RU.*
2. *2. "ROSBIOKVANT" LTD, VORONEZH, RUSSIA. 3. MIREA, MOSCOW, RUSSIA, E-MAIL: RECTOR@MIREA.RU.*

Co and Ni silicides are widely used to form the gates and interconnects in microelectronics and are attractive materials of spintronics [1, 2]. However, the bulk phase and disilicides monosilicides are not magnetic. Seo et al. [3] experimentally found properties of ferromagnetic nanowires silicide Co. Wu et al. [1] DFT method showed the emergence of the magnetic properties of ultrathin films of MnSi and CoSi monosilicides co structure of CsCl. Of particular interest are quantum dots and clusters of silicides, since increase the surface area of silicides may lead to an increase in the magnetic moment of surface atoms of 3d-metals [2, 3]. The size, composition and coordination of the atoms in the clusters significantly affect their magnetic properties. The purpose of this paper is the quantum-chemical modeling by DFT UB3LYP approximation of the electronic structure of clusters of Co and Ni silicides, depending on the configuration of atoms and atoms of 3d-metal n from 1 to 7. The clusters with n> 2 are two configurations of Ni atoms and Co: linear and compact.

The results of total energy calculations for different values of the spin multiplicity showed that the number of atoms and their configuration in the Ni silicide clusters has little effect on the total electron spin of the ground state of the cluster S_{cl}, whose value varies between 1 and 3 for n= 1,...7. Spin of Co silicide clusters increases with increasing n and is sensitive to the configuration of atoms. The change of n from 1 to 4 leads to an increase S_{cl} 1/2 to 19/2 for the linear cluster with 1/2 to 8 for a compact. The effective magnetic moment of the linear clusters μ_{leff} silicide Co magnetic moment μ_{keff} more compact clusters. Maximum μ_{leff} = 4.66 μB / Co for n = 3, the minimum μ_{keff} = 2.24 μB / Co for n = 4. The effective magnetic moment of Ni silicide in clusters decreases with increasing n. Minimum μ_{keff} = 0.99 μB / Ni for n = 7.

Based on the calculation of binding energy in clusters of Ni and Co silicides shows that compact clusters are more stable than linear. The maximum binding energy Eb = 2.61 eV have compact clusters of Ni and Co silicide with n = 7.

Directed to change the desired properties of nanomaterials can be achieved by the introduction of impurities. The introduction of chromium can enhance the magnetic properties of thin films of cobalt silicide. We study the electronic structure of clusters and $CrNi_6Si_{20}$ $CrCo_6Si_{20}$ with a compact configuration. Replacement of cobalt chromium atom leads to a decrease in the total electron spin of the cluster to 0.5 and the binding energy of 3 meV / atom. For clusters of nickel silicide is an increase in the total electron spin of 1, the binding energy is reduced by 5 meV / atom.

The work was supported by the Federal Target Program "Research and development on priority directions of scientific-technological complex of Russia for 2007-2012", SC № 16.513.11.3014.

1. H. Wu, P. Kratzer and M. Scheffler "First-principles study of thin magnetic transition-metal silicide films on Si(001)", Phys. Rev. B., **14**, pp.144425-144437, 2005.

2. A.S. Sigov, A.P. Lazarev, L.A. Bityutskaya, et.al "Spin states of transitional metals silicides nanoclusters", NMST, **12**, pp.25-27, 2011.

3. K. Seo, S. Lee et al., "Composition-Tuned Co_nSi Nanowires: Location-Selective Simultaneous Growth along Temperature Gradient", NanoLetters, **5**, pp.1145-1150, 2009.

Dressed state amplification by a superconducting qubit

G. Oelsner[a], P. Macha[a], E. Ilichev[a], U. Huebner[a], H.-G. Meyer[a], M. Grajcar[b], O. Astafiev[c]
[a]*Institute of Photonic Technology, P.O. Box 100239, D-07702 Jena, Germany;*
[b]*Department of Experimental Physics, Comenius University, SK-84248 Bratislava, Slovakia;*
[c]*NEC Nano Electronics Research Laboratories. Tsukuba, Ibaraki, 305-8501, Japan.*

We demonstrate amplification of a microwave signal by a strongly driven two-level system. The effect known from optics as dressed-state lasing is observed with a single quantum system formed by a persistent current (flux) qubit coupled to coplanar waveguide resonator. The transmission through the resonator is enhanced when the Rabi frequency of the driven qubit is tuned into resonance with one of the resonator modes. Amplification as well as linewidth narrowing of a weak probe signal has been observed. The emission at the resonator's fundamental mode has been studied by measuring the emission spectrum. We analyzed our system and found an excellent agreement between the experimental results and the theoretical predictions obtained in the dressed state model.

Quantum correlations: entanglement and discord in the simplest physical systems

E.B. Fel'dman, E.I. Kuznetsova, M.A. Yurishchev, A.I. Zenchuk
Institute of Problems of Chemical Physics, Russian Academy of Sciences, Chernogolovka, 142432, Moscow Region, Russia, efeldman@icp.ac.ru

Quantum correlations in many-particle systems are responsible for the effective work of quantum devices (in particular quantum computers) and give them significant advantages over their classical counterparts [1]. Until recently it was supposed that entanglement is responsible for quantum correlations, and quantum devices can be created only on the basis of using materials with entangled states [1]. However, it turned out that quantum algorithms [2] which significantly outperform the classical counterparts can work using mixed separable (non-entangled) states. Furthermore, it turned out that quantum non-locality can be observed in systems without entanglement [3]. From this we can conclude that entanglement describes only a part of quantum correlations but not all of them. According to the current understanding [1], total (quantum and classical) correlations in a system are defined by the mutual information. The problem is how to separate the classical correlations from the quantum ones. This problem was solved independently by Henderson and Vedral [4] as well as Ollivier and Zurek [5]. The classical correlations in a binary system are determined by a complete set of projective measurements carried out only over one of the subsystems [4] Then a measure of quantum correlations (the quantum discord) is determined as the difference between the mutual information and its classical part minimized over all possible projective measurements [4, 5]. The quantum discord is determined completely by quantum properties of the system and equals zero for classical systems.

We consider a connection between the quantum discord and physical parameters of simple systems [6-8]. Such investigations open a direct way to experimental measurements of discord. We focus on the simplest relevant systems, such as a pair of spins $s = 1/2$ coupled by the dipole-dipole interaction (DDI) under the conditions of the multiple quantum (MQ) NMR experiment. It is shown [8] that the observable intensity of the second order MQ NMR coherence can be a witness of both entanglement and discord. There is a critical value of the intensity of the MQ NMR coherence of the second order such that the entanglement vanishes at smaller intensities. However the discord does not equal zero at an arbitrary intensity of MQ NMR coherence of the second order. We study [6] the asymmetry of the discord with respect to the subsystem picked out for the projective measurements in a two spins -1/2 particle system with DDI governed by the XY-Hamiltonian in an inhomogeneous magnetic field. The quantum discord in Heisenberg dimers is expressed [7] via the spin-spin correlation function, internal energy, specific heat, and magnetic susceptibility. We also determine the temperature dependence of the discord for a number of materials. Entanglement and the quantum discord for a couple of $s = 1/2$ spins in a nanopore filled with a gas of spin-carrying molecules (atoms) are studied. A dependence of the spin-pair entanglement on the temperature and the number of spins is obtained with the reduced density matrix which is centrosymmetric (CS). The analytic expressions for the concurrence and the geometric discord are obtained for an arbitrary 4×4 CS-matrix.

1. S.M. Aldoshin, A.I. Zenchuk, E.B. Fel'dman, M.A. Yurishchev, "On the way to creation of materials for quantum computing", Russ. Chem. Rev., **81**, pp.91-104, 2012.
2. A. Datta, A. Shaji, C.M. Caves, "Quantum discord and the power of one qubit", Phys. Rev. Lett., **100**, 050502, 2008.
3. C.H. Bennet, D.P. DiVincenzo, C.A. Fuchs, "Quantum nonlocality without entanglement", Phys. Rev. A, **59**, pp.1070-1091, 1999.
4. L. Henderson, V. Vedral, "Classical, quantum, and total correlations", J. Phys. A: Math and Gen., **34**, pp.6899-6906, 2001.
5. H. Ollivier, W.H. Zurek, "Quantum discord: a measure of the quantumness of correlations", Phys. Rev. Lett., **88**, 017901, 2001.
6. E.B. Fel'dman, A.I. Zenchuk, "Asymmetry of bipartite quantum discord", JETP Lett., **93**, pp.459-462, 2011.
7. M.A. Yurishchev, "Quantum discord in spin cluster materials", Phys. Rev. B, **84**, 024418, 2011.
8. E.I. Kuznetsova, A.I. Zenchuk, "Quantum discord versus second order MQ NMR coherence intensity in dimers", Phys. Lett. A, **376**, pp.1029-1034, 2012.

Fingerprinting based algorithms for quantum branching programs

F. Ablayev[1,2]
1. Institute for Informatics of Tatarstan Academy of Sciences, Kazan, Russia
2. Kazan Federal University, Kazan, Russia

There are many models of computation based on the quantum paradigm. Due to severe limits of existing physical implementations of quantum computer it is natural to consider the restricted models of quantum computations. During the last two decades different restricted types of quantum computation models based on Turing Machines, automata, and circuits have been considered. The one computational model we consider is based upon quantum branching programs. Two variants of quantum branching programs were introduced by Ablayev, Gainutdinova, Karpinski [1] (leveled programs), and by Nakanishi, Hamaguchi, Kashiwabara [2] (non-leveled programs). The most commonly used restricted variant of quantum branching programs is the model of Ordered Read-Once Quantum Branching Programs. This restriction implies that each input variable may be read at most once, which is the least possible for any function essentially depending on it's variables. Thus, the read-once restriction corresponds to minimizing of computational steps for quantum algorithms. For this model we develop the fingerprinting technique, which is generally used to perform space-efficient computations in randomized and quantum models of computation.

References

1. Ablayev, F., Gainutdinova, A., Karpinski, M. On computational power of quantum branching programs. In: FCT. pp.59-70 (2001), http://arxiv.org/abs/quant-ph/0302022.
2. Nakanishi, M., Hamaguchi, K., Kashiwabara, T. Ordered quantum branching programs are more powerful than ordered probabilistic branching programs under a bounded-width restriction. In: Du, D.Z., Eades, P., Estivill-Castro, V., Lin, X., Sharma, A. (eds.) Computing and Combinatorics, Lecture Notes in Computer Science, **1858**, pp.467-476, Springer Berlin. Heidelberg (2000).

Mathematical modeling of quantum noise and the quality of hardware components of quantum computers

Yu.I. Bogdanov[1], A.Yu. Chernyavskiy[1], A.S. Holevo[2],
V.F. Luckichev[1], S.A. Nuyanzin[1,3], A.A. Orlikovsky[1]

[1] Institute of Physics and Technology, Russian Academy of Sciences. [2] Steklov Mathematical Institute, Russian Academy of Sciences. [3] National Research University of Electronic Technology MIET

In the present report methods and algorithms of modeling quantum operations for quantum computer integrated circuits design are considered. We examine different ways of quantum operation descriptions, including operator-sums, unitary representations, Choi-Jamiolkowski state representations and the corresponding chi-matrices, as well as quantum system evolution operators. The results of modeling of practically important quantum gates: SQiSW (square root of i-SWAP gate), controlled-NOT (CNOT), and controlled Z-transform (CZ) subject to different decoherence mechanisms are presented. These mechanisms include analysis of depolarizing quantum noise and processes of amplitude and phase relaxation. Finally, we consider error correction of phase flip, and the tasks of creating and maintaining the entanglement, as well as its breaking for two- and multi-qubit realizations of quantum operations. Importance of the present analysis for the quality and efficiency of quantum information technologies in practical applications is discussed.

Quantum correlations (entanglement, discord), quantum phase transitions, and magnetic toroidal states in an anti-ferromagnetic XXZ chain of spins S= ½ in the presence of an inhomogeneous transverse magnetic field

A.A. Kokin
Institute of Physics and Technology, RAS, Moscow, Russia

An anti-ferromagnetic chain of $N>>1$ spins ½ with one-axis anisotropy (XXZ – model) at zero temperature and in the presence of an inhomogeneous transverse axially directed magnetic field $B(x)$ with constant gradient $\partial B(x)/\partial x$ along the length of chain has been considered.

Quantum correlations in many-spin systems are partitioned into two types. One is known as the entanglement of quantum states and other known as discord is due to the contribution of unentangled quantum states. A variety of techniques for study of this quantum correlation was discussed. The local entanglement method provides the relatively simple approach which based on the using of reduced density matrix of two neighboring spins in chain [1]. The reduced density matrix describes not only correlations and entanglement inside of the sated aside two neighboring spins, but it depends on the entanglement between the spin pair and the rest part of the chain. This relationship has to be taken in account if the ground state of all chain was found.

The results of performed investigations of entanglement and discord behavior for XXZ model near quantum phase transition in presence of magnetic field gradient are presented. Concurrence as a parameter of nondiagonal order has been also treated. Finally, the formation of magnetic toroidal states and dimerisation of the spin chain was considered.

1. S.-Q. Su at al., New J. of Phys., **8**, p.61, 2006; arXiv:quant-ph/0509070.

Quantum and classical correlations in high temperature dynamics of two coupled large spins

V.E. Zobov
L.V. Kirensky Institute of Physics, Russian Academy of Sciences, Siberian Branch, 660036, Krasnoyarsk, Russia, rsa@iph.krasn.ru

In recent years, many authors are used high temperature dynamics of nuclear spins to study quantum computing [1] and quantum correlations [2]. This system has simple interactions and can be easily controlled by nuclear magnetic resonance (NMR) techniques. In such conditions we now consider two spins coupled by a spin-spin interaction

$$H_{SS} = (J/S_2) S_{1Z} S_{2Z}$$

(S_i^α is α-components (α=X,Y,Z) of spin *i* and we assume $\hbar = 1$) and we investigate the change of quantum and classical parts of dynamic correlations versus increasing of quantum spin numbers $S_2 \geq S_1$. If $S_1 = S_2 = 1/2$, these two parts are equal at any time and any temperature [3]. On the contrary, if $S_1, S_2 \to \infty$ one expects that quantum magnetic moments transfer into classical magnetic moments [4]. In the high temperature approximation, we describe time evolutions of the system by a spin density matrix:

$$\rho(t) = \frac{1}{d_1 d_2}[1 + \frac{\beta}{2}\{S_{1+}\exp(-i\tau S_{2Z}) + S_{1-}\exp(i\tau S_{2Z}) + S_{2+}\exp(-i\tau S_{1Z}) + S_{2-}\exp(i\tau S_{1Z})\}],$$

where $S_{j\pm} = S_{jX} \pm iS_{jY}$, $\tau = tJ/S_2$, $d_j = 2S_j + 1$, and $\beta << 1$ is a polarization.

To extract classical correlations we use a positive-operator-valued measure (POVM) with measurement operators $|\theta,\varphi\rangle\langle\theta,\varphi|$, where $|\theta,\varphi\rangle$ is a spin coherent state [5] and θ, φ denote the polar and azimuth angles on Bloch sphere. (Point that POVM measurement with Gaussian photon coherent states was used to calculate Gaussian quantum discord [6].) After two-sided measurements we obtain analytic formula for the quantum part of correlations expended to the leading order in β:

$$D_{GG} = I(\rho) - J_{GG}(P_{12}) \approx (S_1)^2 B[1 - f_2(t)] + (S_2)^2 B[1 - f_1(t)] +$$
$$+ S_1 B[1 - g_2^2(t)] + S_2 B[1 - g_1^2(t)]$$

where $I(\rho)$ is the total mutual information for density matrix $\rho(t)$, $J_{GG}(P_{12})$ is the classical mutual information for the distribution function on the unit sphere

$$P_{12}(\theta_1\varphi_1\theta_2\varphi_2;t) = \langle\theta_1\varphi_1\theta_2\varphi_2|\rho(t)|\theta_1\varphi_1\theta_2\varphi_2\rangle,$$

$$B = \frac{\beta^2}{6\ln 2},\quad g_j(t) = \frac{\sin(d_j\tau/2)}{d_j\sin(\tau/2)},\quad f_j(t) = \sum_{m=0}^{m=2S_j}\binom{2S_j}{m}\left(\cos^2\frac{\tau}{2}\right)^{2S_j-m}\left(\sin^2\frac{\tau}{2}\right)^m\frac{1}{2m+1}.$$

The obtained analytic formula shows next properties of the quantum part of correlations: a time period $T = 2\pi S_2/J$, decreasing of this part ($D_{GG}/I(\rho)$) with increasing of spin quantum numbers (with transferring into classical moments) at small time, and increasing of one at the half period.

1. J.A. Jones, *Quantum Computing with NMR.* Prog. NMR. Specrosc., **59**, pp.91-120, 2011.
2. R. Auccaise, L.C. Celeri, D.O. Soares-Pinto, et al. Phys. Rev. Lett. **107**, 140403, 2011; G. Passante, O. Moussa, R Laflamme, Phys. Rev. A **85**, 032325, 2012.
3. E.I. Kuznetsova, A.I. Zenchuk, Physics Letters A, **376**, pp.1029-1034, 2012.
4. B.C. Sanders, Phys. Rev. A **40**, pp.2417-2427, 1989.
5. F.T. Arrechi, E. Courtens, R. Gilmore, and H. Thomas, Phys. Rev., **A6**, pp.2211–2237, 1972.
6. G. Adesso and A. Datta, Phys. Rev. Lett. **105**, 030501, 2010; P. Giorda and M.G.A. Paris, Phys. Rev. Lett. **105**, 020503, 2010.

QUANTUM COMPUTER ON MULTI-ATOMIC ENSEMBLES IN QUANTUM ELECTRODYNAMIC CAVITY

F.M. Ablayev[1,2], S.N. Andrianov[1,2,3], S.A. Moiseev[1,2,3], A.V. Vasiliev[1,2]
1. Institute for Informatics of Tatarstan Academy of Sciences, Kazan, Russia
2. Kazan Federal University, Kazan, Russia
3. Kazan Physical and Technical Institute, Kazan, Russia

Realization of the quantum computer on multi-atomic ensembles of Rydberg atoms was proposed in [1]. We have proposed an effective realization of a complete set of quantum gates in a solid state quantum computer based on macroscopic resonance systems – multi-atomic coherent ensembles, squids or quantum dots in microcavities contained in a common quantum electrodynamic cavity [2, 3]. Here, we use encoding of logical qubits on pairs of macroscopic two-level systems without micro-cavities (Fig. 1). Logical single-qubit gates are realized via the swapping transfer [4, 5] of single-photon excitation in the pair. In the case of two-level systems, logical two-qubit gates are realized via the unequal Lamb frequency shift of transition frequencies in the pair controlled by a third system from another pair. With the use of three-level systems, swapping in the pair is blocked by the transition of operative excitation to an additional level at the direct impact of control pair excitation.

In the proposed architecture we explicitly construct a computation of the Equality function via quantum fingerprinting technique, which is a classical task in many computational and communication scenarios. We present a step-by-step implementation of this algorithm including "low level" transfers of the qubit states from the quantum memory to the processing nodes and backwards. Finally, we estimate the optimal number of qubits stored in the memory and the number of processing nodes for implementation of the aforementioned algorithm.

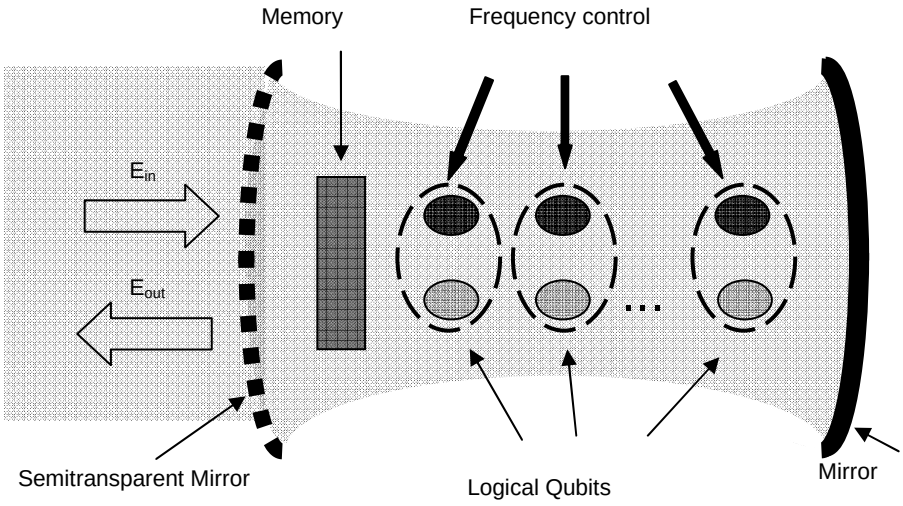

Fig. 1. Quantum computer on multi-atomic systems with logical qubit encoding

Work is supported by RFBR grants No. 10-02-01348 and 11-07-00465.

1. M. Saffman, Rev. Mod. Phys., 82, pp.2313-2363, 2010.
2. S.A. Moiseev, S.N. Andrianov, F.F. Gubaidullin, Laser Phys., 21, pp.1503-1510, 2011.
3. S.N. Andrianov and S.A. Moiseev, Opt. and spectr., 112, pp.394–400, 2012.
4. A. Imamoglu, et al., Phys. Rev. Lett., 83, pp.4204-4207, 1999.
5. N. Schuch, J. Siewert, Phys. Rev. *A*, 67, 032301 (8 pages), 2003.

Quantum addressing in photon echo based quantum random access memory

S.A. Moiseev[1,2*], and E.S. Moiseev[2]
1. Kazan Physical-technical Institute of Russian Academy of Sciences, Sibirsky Trakt 10/7, Kazan, 420029, Russia
2. Kazan Federal University, Kremlevskaya 18, Kazan, 420008, Russia
** samoi@yandex.ru*

A quantum random access memory is an important counterpart of the quantum computer [1] which is a subject of intensive theoretical [2,3] and experimental studies [4,5] aimed to the elaboration of multi-qubit quantum computing. In the last decade a large successes have been achieved in realization of the quantum memories (QMs) based on the coherent multi-atomic ensembles, where the photon echo QMs [6] have demonstrated most promising properties for efficient storage of the multi-qubit photon fields. Based on our recent approach to the photon echo QM in the optimal QED-cavity [7], we have elaborated a perfect integration of the QM into the quantum computer scheme providing thereby an effective storage and reversible transfer of the many photon qubits to the processing nodes [8]. In this letter, we propose a photon echo QM scheme in the optimal QED-cavity accompanying by an additional controlling resonant atom. The atom provides a coupling of the external waveguide modes with the single mode QED-cavity containing resonant multi-atomic ensemble that can be used for quantum storage control of the photonic qubits.

We have derived the optical quantum approach to the proposed QM scheme and found the efficient quantum storage is possible only at some special physical parameters of the atoms and the cavity. These parameters reveal two optimal matching conditions: for the coupling constants of resonant atom with the waveguide field –"g", for the resonant atom and QED-cavity mode –"p" and for the multi-atomic ensemble and QED-cavity mode – "$\Gamma=Nf^2/D$" (where "f" is an interaction constant between atom and resonant photon in the QED-cavity, "D" – is an inhomogeneous broadening of the resonant atomic transition). The first matching condition –"$p^2=\Gamma g/2$" provides the perfect storage of the photonic qubits from the waveguide mode on the atomic ensemble. Second condition "$\Gamma=g/2$" extends the effective storage to the broadband spectrum of the photon fields. It is worth noting that in comparison with recent results [8], the second matching condition can be realized at larger inhomogeneous broadening of the multi-atomic ensemble.

We have analyzed in details the spectral properties of the proposed QM scheme in terms of the possible atomic and cavity parameters where we found a complete blockade of the photon transfer (storage and retrieval) into the atomic ensemble by placing the controlling atom on third (blockade) level characterized by large enough spectral detuning from the resonant QED-cavity mode. Based on the obtained results, we have demonstrated the quantum addressing for the storage and retrieval of the photonic qubits. Here, the quantum address state is transferred to the quantum superposition of the ground and blockade states of the single atom. The address state is given by additional single photon field interacting with the atom via lambda-atomic transition in the presence of coherent laser field. Finally we have discussed possible realizations of the proposed quantum random access memory by using narrow optical waveguides coupled with high quality QED nano-cavities or superconducting planar waveguides interacting with the resonant superconducting qubits.

Financial support by grants RFBR ## 10-02-01348 and 12-02-91700 is gratefully acknowledged.

1. M.A. Nielsen and I. L. Chuang, *Quantum Computation and Quantum Information*, Cambridge University Press, Cambridge, 2000.
2. V. Giovannetti, S. Lloyd, and L. Maccone, Phys. Rev. Lett., **100**, 160501, 2008.
3. J.H. Wesenberg, et al., Phys. Rev. Lett., **103**, 070502, 2009.
4. H. Wu, et.al., Phys. Rev. Lett., **105**, 140503, 2010.
5. M. Mariantoni, et al., Science, **334**, pp.61-65, 2011.
6. S.A. Moiseev and S. Kroll., Phys. Rev. Lett., **87,** 173601, 2001.
7. S.A. Moiseev, S.N. Andrianov, and F.F. Gubaidullin, Phys. Rev. A, **82**, 022311, 2010.
8. S.A. Moiseev and S.N. Andrianov, J. Phys. B: At., Mol. & Opt. Phys., **45**, 124017, 2012.

Spatial structure of two-photon and thermal light

S.P. Kulik, S.S. Straupe, I. Bobrov
Faculty of Physics, Moscow M.V. Lomonosov State University, 119991, Moscow, Russia

The talk is devoted to the correlation properties for bipartite optical systems. In the first part we report an experimental approach to entanglement characterization in high-dimensional quantum systems using Schmidt decomposition techniques as well as physical properties of the Schmidt decomposition. A particular experiment uses spatial degrees of freedom of biphotons. We present a technique to realize projective measurements in Schmidt basis, allowing us to measure the coefficients in Schmidt decomposition and to estimate the degree of entanglement directly. Issues of modeling the spatial part of the biphoton amplitude with simple double-Gaussian functions are discussed and shown to be in a good agreement with experimental results.

The second part of the talk relates to investigation of mode structure of the thermal light beam. We apply the developed technique [1] to quasi-thermal light and discuss close analogy between quantum and classical correlations. The usual Hanbury Brown and Twiss scheme is used for revealing intensity correlations of the quasi-thermal source (rotating ground disk). After proper preparation of the thermal light beam by means of appropriate lenses and apertures we introduce the spatial light modulator (SLM) followed by a single-mode fiber in one arm of intensity interferometer followed by a single-mode fiber. The other channel of the interferometer is supplied with a single-mode fiber which might be scanned in the transverse direction(s). Switching by SLM between different Hermite-Gauss modes we check the angular correlation function in the fourth order in the field. The preliminary results show that there are no correlations ($g^{(2)}(0) \approx 1$) between orthogonal modes while choosing the same modes the corresponding meaning reaches its maximal weighted value $g^{(2)}(0) \approx 1.7$.

1. S.M. Sze. *Physics of Semiconductor Devices.* John Willey and Sons, New York, 1981.
2. J. Nishizawa and K. Suto, “Semiconductor Raman laser”, J. Appl. Phys., **51**, pp.2429-2431, 1980.
3. S.S. Straupe, D.P. Ivanov, A.A. Kalinkin, I.B. Bobrov, S.P. Kulik, “Angular Schmidt modes in spontaneous parametric down-conversion”, Phys. Rev. A, **83**, 060302(R), 2011.

Biphoton spectrum control

N. Borschevskaya[1], I. Dyakonov[1], K. Katamadze[1,2], S. Kulik[1], A. Paterova[1]

1. Moscow State University, Moscow, Russia, 2. Institute of Physics and Technology, Russian Academy of Sciences, Moscow, Russia, k.g.katamadze@gmail.com

Controlling the parameters of nonclassical fields is one of the main problems in quantum optics. Such parameters include polarization, angular and spectral distributions, correlation and time parameters, etc. Much attention is recently focused on controlling the spectrum of a biphoton field as one of the most popular representatives of the family of nonclassical fields. Control of the entanglement degree[1–3], development of coherent quantum optical tomography[4] and quantum interferometric optical lithography [5] are examples of the quantum optics and quantum information problems in which control of a biphoton field spectrum is required.

In the present work we analyze methods for controlling the spectrum of the biphoton field and for preparing the biphoton field with the broad spectrum. All methods are based on the spontaneous parametric downconversion [6], which can be phenomenologically described as a three-photon process in a medium with nonzero quadratic susceptibility $\chi^{(2)}$, where the photon of the pump splits spontaneously into two photons, called "signal" and "idle".

The simplest way to prepare the broadband biphoton field is using the thin nonlinear crystal. But there is too small process efficiency in this case, and the high pump intensity is required. So we place the nonlinear crystal inside the laser cavity to prepare broadband and high-intensity biphoton source.

Secondly, it is possible to control the biphoton field spectrum using spatially-inhomogeneous nonlinear media. We analyze the method based on the spatial modulation of the refractive indices of a nonlinear crystal. Modulation is due to the thermo-optic [7], [8] and electro-optic [9] effects.

1. G. Brida, V. Caricato, M. V. Fedorov, M. Genovese, M. Gramegna, and S.P. Kulik, "Characterization of spectral entanglement of spontaneous parametric-down conversion biphotons in femtosecond pulsed regime," EPL (Europhysics Letters), **87**, p.64003, 2009.
2. M.V. Fedorov, Y.M. Mikhailova, and P.A. Volkov, "Gaussian modelling and Schmidt modes of SPDC biphoton states," Journal of Physics B: Atomic, Molecular and Optical Physics, **42**, p.175503, 2009.
3. M.V. Fedorov, M.A. Efremov, P.A. Volkov, and J.H. Eberly, "Short-pulse or strong-field breakup processes: a route to study entangled wave packets," Journal of Physics B: Atomic, Molecular and Optical Physics, **39**, pp.S467-S483, 2006.
4. M. Nasr, B. Saleh, A. Sergienko, and M. Teich, "Demonstration of Dispersion-Canceled Quantum-Optical Coherence Tomography," Physical Review Letters, **91**, pp.083601-1-4, 2003.
5. A. Boto, P. Kok, D. Abrams, S. Braunstein, C. Williams, and J. Dowling, "Quantum interferometric optical lithography: exploiting entanglement to beat the diffraction limit," Physical Review Letters, **85**, pp.2733-2736, 2000.
6. D.N. Klyshko, *Physical Principles of Quantum Eltctronics*, Nauka, Moscow, 1986 (in Russia).
7. D.A. Kalashnikov, K.G. Katamadze, and S.P. Kulik, "Controlling the spectrum of a two-photon field: Inhomogeneous broadening due to a temperature gradient," JETP Letters, **89**, pp.224-228, 2009.
8. K.G. Katamadze and S.P. Kulik, "Control of the spectrum of the biphoton field," Journal of Experimental and Theoretical Physics, **112**, pp.20-37, 2011.
9. K.G. Katamadze, A.V. Paterova, E.G. Yakimova, K.A. Balygin, and S.P. Kulik, "Control of the Frequency Spectrum of a Biphoton Field Due to the Electro Optical Effect," JETP Letters, **94**, pp.262-265, 2011.

Quantization effects observed in asymmetric rings

V.L. Gurtovoi, A.I. Ilin, A.V. Nikulov, and V.A. Tulin
Institute of Microelectronics Technology, Russian Academy of Sciences, 142432 Chernogolovka, Moscow District, Russia. E-mail: nikulov@iptm.ru

The quantization postulated by Bohr as far back as 1913 in order to describe the stationary electron orbits in atoms is observed also in micro- and nanostructures [1-8]. The observations on the level of nanostructures quantum phenomena discovered on the atomic level provide us with ample opportunity of detailed investigations and possible application. For example, it is not feasible to make an asymmetric atom with electric contacts whereas it is perfectly possible to make an asymmetric ring with electric contacts. The energy difference between permitted states of single electron $E_{n+1}-E_n = mv_{n+1}^2/2 - mv_n^2/2 = (2n+1)\hbar^2/2mr^2$ in a ring is much smaller than in atom because its realistic radius $r \approx 500$ *nm* is much larger than the Bohr radius $r_B \approx 0.05$ *nm*. But the discreteness of the energy spectrum of a real superconducting ring with a section *s*, pairs density n_s and radius *r* may be strong as well as in atom because of the same quantum number *n* of all $N_s = s2\pi r n_s$ pairs [9]. Therefore superconducting loop is considered as artificial atom in recent publications [10,11].

Some of the investigations [1-6] of this artificial atom have corroborated the basic principles of quantum mechanics and allow to propose new type of micro- and nanodevices [3]. But results of other investigations [7,8] contradicts to the predictions of quantum mechanics. We will present in this work experimental results testify against the jump of critical current of asymmetric ring predicted by quantum mechanics at the change of the quantum number describing the angular momentum of superconducting pairs. Our investigations of asymmetric rings allow to discover that Nature wants to avoid jumps in some cases. This surprising result may have fundamental importance. Its thorough investigation may give new information about basic principles of quantum mechanics and limits of their applicability.

1. A.C. Bleszynski-Jayich, W.E. Shanks, B. Peaudecerf, E. Ginossar, F. von Oppen, L. Glazman, J.G.E. Harris, “Persistent Currents in Normal Metal Rings”, Science, **326**, pp.272-275, 2009.
2. N.C. Koshnick, H. Bluhm, M. E. Huber, K. A. Moler, “Fluctuation Superconductivity in Mesoscopic Aluminum Rings”, Science, **318**, pp.1440-1443, 2007.
3. A.A. Burlakov, V.L. Gurtovoi, A.I. Ilin, A.V. Nikulov, V.A. Tulin, “Possibility of persistent voltage observation in a system of asymmetric superconducting rings”, Phys. Lett. A, **376**, pp.2325–2329, 2012.
4. V.L. Gurtovoi, A.A. Burlakov, A.V. Nikulov, V.A. Tulin, A.A. Firsov, V.N. Antonov, R. Davis, and S. Pelling, “Multiple Current States of Two Phase-Coupled Superconducting Rings,” J. Exper. Theor. Phys., **113**, pp.678–682, 2011.
5. V.L. Gurtovoi, A.I. Ilin, A.V. Nikulov, V.A. Tulin, “Weak dissipation does not result in disappearance of persistent current”, Low Temp. Phys., **36**, pp.974-983, 2010.
6. A.A. Burlakov, V.L. Gurtovoi, S.V. Dubonos, A.V. Nikulov, and V.A. Tulin, “Little–Parks Effect in a System of Asymmetric Superconducting Rings”, JETP Lett., **86**, pp.517-521, 2007.
7. V.L. Gurtovoi, S.V. Dubonos, S.V. Karpi, A.V. Nikulov, V.A. Tulin, “Contradiction between the Results of Observations of Resistance and Critical Current Quantum Oscillations in Asymmetric Superconducting Rings”, Zh. Eksp. Teor. Fiz., **132**, pp.297–302, 2007.
8. V.L. Gurtovoi, S.V. Dubonos, A.V. Nikulov, N.N. Osipov and V.A. Tulin, “Dependence of the magnitude and direction of the persistent current on the magnetic flux in superconducting rings”, Zh. Eksp. Teor. Fiz., **132**, pp.1320-1339, 2007.
9. A.V. Nikulov, “Bohm’s quantum potential and quantum force in superconductor”, AIP Conference Proceedings, **1101** “Foundations of Probability and Physics-5”, pp.134-143, 2009.
10. O. Astafiev, A.M. Zagoskin, A.A. Abdumalikov Jr., Yu.A. Pashkin, T. Yamamoto, K. Inomata, Y. Nakamura and J.S. Tsai, “Resonance Fluorescence of a Single Artificial Atom”, Science, **327**, pp.840-843, 2010.
11. J.Q. You and F. Nori, “Atomic physics and quantum optics using superconducting circuits”, Nature, **474**, pp.589-597, 2011.

Quantum communication with Bose-Einstein condensates

A.N. Pyrkov, T. Byrnes
National Institute of Informatics, Tokyo, Japan, E-mail address: apyrkov@nii.ac.jp

In the past years, a lot of attention is focused on quantum networks [1, 2]. In the context of quantum information science [3], quantum networks have an important role both for the formal analysis and physical implementation [3] of QIP. Quantum information is generated, stored and processed in individual quantum systems (quantum nodes) and transmitted via quantum channels. In practice, the physical implementation of the nodes and channels require transport quantum states from site to site with high fidelity and distribute entanglement across the network. Thus, in accordance with [2] quantum networks can be divided into two major classes: (1) quantum communication networks for the long distance transmission of information, and (2) quantum computation networks for the distribution of quantum entanglement over large numbers of quantum memories for large-scale quantum processing. Usually photonic channels are used for transmission of quantum information. Photons can carry quantum information over long distances with almost negligible decoherence and are compatible with existing telecommunication fiber technology. The versatility of quantum networks is largely defined by the capability of the network nodes. Two well-studied approaches for quantum nodes are atomic ensembles [5] and single atoms [2]. Recently the experimental realization of an elementary quantum network of single atoms in optical cavities was presented [6].

We consider a Bose-Einstein condensate (BEC) as a node for quantum networking. Recently, two-component Bose-Einstein condensates were realized which allow us to control the BEC coherent on the Bloch sphere and spin squeezing [7-9]. Also the experimental generation of remote entanglement between a single atom inside an optical cavity and a BEC was reached [10] and photon-photon gates in BEC were introduced [11]. The framework for qubit encoding in BEC was presented [12] where the possibility of implementation of quantum algorithms on basis of BEC qubits was shown.

In this work we introduce a protocol for quantum information transfer between two BEC qubits. It is shown that fidelity of the transfer tends to 1 for big N where N is the BEC atom number. We introduce a way to produce entanglement between two almost macroscopic objects (two components BEC). This proposal is motivated by recent works [13, 14]. Thus BEC systems open up promising perspectives for building of quantum networks with possibility of deterministic transfer of quantum information.

1. H.J. Kimble, Nature, **453**, p.1023, 2008.
2. L.-M. Duan, C. Monroe, Rev. Mod. Phys., **82**, p.1209, 2010.
3. M. Nielsen, I. Chuang, *Quantum computation and quantum information* (Cambridge University Press, 2000).
4. M.D. Eisaman et al., Rev. Sci. Instrum., **82**, 071101, 2011.
5. L.-M. Duan et al., Nature, **414**, p.413, 2001.
6. S. Ritter et al., Nature, **484**, p.195, 2012.
7. M. Riedel et al., Nature, **464**, p.1170, 2010.
8. P. Bohi et al., Nature Phys., **5**, p.592, 2009.
9. Y. Colombe et al., Nature, **450**, p.272, 2007.
10. M. Lettner et al., Phys. Rev. Lett., **106**, 210503, 2011.
11. A. Rispe, B. He, and C. Simon, Phys. Rev. Lett., **107**, 043601, 2011.
12. T. Byrnes, K. Wen, and Y. Yamamoto, Phys. Rev. A, **85**, 040306(R), 2012.
13. P. Sekatski et al., arxiv: 1206.1870.
14. J. Kofler et al., arxiv: 1206.2141.

Effect of image charges on a space qubit evolution

V. Vyurkov, M. Rudenko, S. Filippov
Institute of Physics and Technology, Russian Academy of Sciences, Moscow, Russia, vyurkov@ftian.ru

Polarization of environment could be crucial for a solid-state qubit evolution. Recently, it was shown that image charges induced in metal electrodes result in decoherence due to Joule losses [1]. Here we pay attention to the coherent dynamics of space (charge) qubits affected by image (bound) charges created not only in metal electrodes but also in dielectric media, including that inside a quantum dot and outside it.

Image charges drastically differ from fixed ones. The influence of image charges on a qubit dynamics cannot be described by an introduction of any constant potential, and, therefore, that influence cannot be compensated by any constant field induced by nearby electrodes. To cope with the problem one could solve self-consistently the Schrödinger equation for electron wave function $\psi(x,t)$ and the Poisson equation for the charge distributed as $e|\psi(x,t)|^2$, where e is an electron charge. That mean-field approach is widely used for description of many-particle systems. Its applicability to a single electron in a qubit was somehow justified in [2] by a supposition that the electron in qubit moved much slower than electrons in media which give rise to its polarization. Unlike a many-particle system, the problem for a single electron has a special feature. Before substituting the potential obtained from Poisson equation into Schrödinger equation one should exclude potential produced by the electron itself. This potential can be obtained by solving Poisson equation with the same distribution of electron charge $e|\psi(x,t)|^2$ in vacuum. As the Schrödinger equation becomes non-linear, the qubit behavior becomes unusual. Here we demonstrate it for the typical qubit based on a double quantum dot (DQD). The structure is sketched in Fig. 1. For simplicity the structure is perfectly symmetric.

The electrostatic energy caused by polarization of outer space (including dielectrics and metal electrodes, if any) is equal to E_C when electron is located in one quantum dot. Evidently, E_C is proportional to squared electron charge e^2; therefore, if the electron is equally distributed between dots, the electrostatic energy turns $E_C/2$. Initially the electron is located in the first quantum dot. As soon as tunneling T is switched on, the Rabi oscillations begin. The calculated maximum probability to find the electron in the second quantum dot during Rabi oscillations for different ratio E_C/T is depicted in Fig. 2. The critical value is E_C/T=4. For greater numbers a total coherent pumping from one state to the other is impossible. In fact, this relation reminds the uncertainty principle of Heisenberg as h/T is a time of transition. In the case, the qubit possesses quite unusual states. Namely, the lowest stationary state is still symmetric due to symmetry of the structure; however, two non-stationary states with lower mean energy exist. In those states the electron occupies presumably one quantum dot. Fairly large value of E_C may also prevent from a total coherent transition of the electron from one level to the other in the same quantum dot (vertical transition) caused by a pulse of oscillating electric field. For realistic structures E_C could be hardly smaller than 0.1meV. It means that the qubit must be operated faster than 1ps with the accuracy 10^{-4} required for quantum computing. That demand is far beyond current capabilities. One way out is to employ space qubits without charge transfer [3].

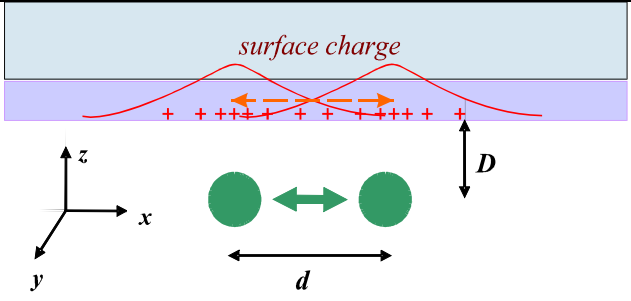

Fig. 1. Moving charge in DQD and polarization of media.

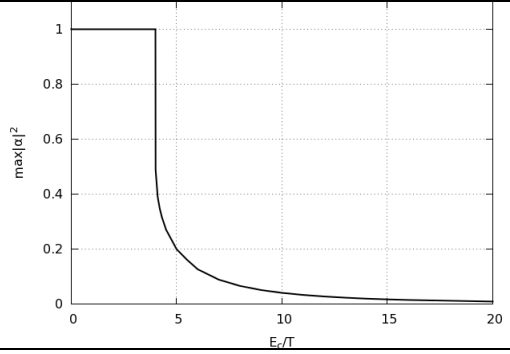

Fig. 2. Maximum probability to find the electron in the second quantum dot for different ratio E_C/T.

The work was supported via the grant 07.524.12.4019 of the Ministry of Education and Science of the Russian Federation.

1. S. Filippov, V. Vyurkov, L. Fedichkin, Physica E, **44**, pp.501-505, 2011.
2. S. Filippov, V. Vyurkov, Quantum Computers & Computing, **9**, pp.60-65, 2009.
3. V. Vyurkov, S. Filippov, and L. Gorelik, Physics Letters A, **374**, pp.3285-3291, 2010.

Graphene-based infrared and terahertz detectors: Concepts, features, and comparison

V. Ryzhii[1], T. Otsuji[1], M. Ryzhii[2], V. Mitin[3], M.S. Shur[4]
[1] *Tohoku University, Sendai, Japan v-ryzhii@riec.tohoku.ac.jp,*
[2] *University of Aizu, Aizu-Wakamatsu, Japan, m-ryzhii@u-aizu.ac.jp,*
[3] *University at Buffalo, SUNY, Buffalo, USA, vmitin@buffalo.edu,*
[4] *Rensselaer Polytechnic Institute, Troy, USA, shurm@rpi.edu*

Graphene and more complex graphene-based structures are recent additions to the carbon materials family that includes diamond, graphite, fullerenes, and carbon nanotubes. Graphene is a monolayer of carbon atoms forming a dense honeycomb two-dimensional crystal exhibiting unique energy spectrum of electrons and holes, which resembles the energy spectrum of the neutrino-antineutrino pair. The characteristic velocity of the graphene spectrum is just 300 times smaller than the speed of light. Such a spectrum has zero energy gap and enables very interesting electronic and optical properties of graphene.

Main initial hopes for future graphene applications were associated with relatively high electron and hole mobility even at room temperature (about 200,000 cm^2/Vs) and possibility to achieve ballistic electron and hole transport in micrometer-size ultra-high speed devices. Even more importantly, the gapless energy band structure of graphene (which is a substantial obstacle for applications in digital circuits) enables graphene to absorb and emit photons with rather low energies corresponding to terahertz (THz) and infrared (IR) ranges of electromagnetic spectrum. This opens up the prospects of exploiting the interband transitions for creation of novel IR and THz devices, such as lasers, photodiodes, phototransistors, mixers, and phase shifters. Owing to a rather high quantum efficiency of interband transitions in a single GL (SGL), graphene bilayers (GBLs), non-Bernal stacked (twisted) multiple graphene layers (MGLs), electrically isolated double graphene layers (DGLs), as well as graphene nanoribbons (GNRs), enables superior performance of IR and THz graphene devices.

In this presentation, the recently proposed concepts of IR and THz detectors based on SGLs, GBLs, MGLs, DGLs, and GNRs [1-3] are discussed, focusing on diode structures using interband and intraband transitions. We consider the photodetector characteristics (responsivity and dark current-limited detectivity) and analyze the physical reasons for their superiority in comparison with the other IR and THz photodetectors.

1. V. Ryzhii, M. Ryzhii, V. Mitin, and T. Otsuji, "Terahertz and infrared photodetection using p-i-n multiple-graphene structures," J. Appl. Phys., **106**, p.084512, 2009.
2. V. Ryzhii, N. Ryabova, M. Ryzhii, N.V. Baryshnikov, V.E. Karasik, and T. Otsuji, "Terahertz and infrared photodetectors based on multiple grapheme layer and nanoribbon structures," Optoelectronics Review, **20**, pp.15-21, 2012.
3. V. Ryzhii, T. Otsuji, M. Ryzhii, and M.S. Shur, "Double graphene-layer resonant terahertz detector", J. Phys. D: Appl. Phys., **45**, p.30201, 2012.

Terahertz-Wave Generation Using Graphene -toward the Creation of Graphene Injection Lasers

T. Otsuji[1], A. Satou[1], S.A. Boubanga Tombet[1], M. Ryzhii[2], V. Ryzhii[1]

1. Research Institute of Electrical Communication, Tohoku University, Sendai, Japan, E-mail address (otsuji@riec.tohoku.ac.jp). 2. Computational Nano-Electronics Laboratory, University of Aizu, Aizu-Wakamatsu, Japan, E-mail address (m-ryzhii@u-aizu.ac.jp).

Graphene, a monolayer carbon-atomic honeycomb lattice crystal, has attracted attention due to its peculiar carrier transport properties owing to the massless and gapless energy spectrum [1]. Optical and/or injection pumping of graphene can exhibit negative-dynamic conductivity in the terahertz (THz) spectral range [2, 3].

When the photogenerated electrons and holes are heated, collective excitations due to the carrier-carrier scattering take a dominant roll to perform an ultrafast carrier quasi-equilibration (see Fig. 1). Then carriers at high-energy tails of their distributions emit the optical phonons, cooling themselves and accumulating around the Dirac points (see Fig. 1). Due to a fast intraband relaxation (ps or less) and relatively slow interband recombination (>>1ps) of photoelectrons/holes, the population inversion is obtainable. We also theoretically revealed the occurrence of negative dynamic conductivity in a wide THz frequency range under a sufficiently high pumping intensity > 10^6 W/cm^2 [3, 4] (see Fig. 1). We conducted THz time domain spectroscopy for fs-laser pumped graphene samples and showed that graphene amplifies an incoming THz field [5]. When the pumping intensity weakens below 1 x 10^7 W/cm^2 threshold behavior can be seen, testifying the occurrence of amplified stimulated THz emission.

Optical pumping with rather high photon energy of the order of "~eV" significantly heats the carriers, which dramatically increases the pumping threshold, preventing from population inversion [6]. Current injection pumping is a best of solution because electrical pumping can serve any pumping energy down under the order of "meV" when a p-i-n junction is formed like semiconductor laser diodes. Dual gate structure can make a p-i-n junction in the graphene channel [3] (see Fig. 2). Waveguiding the THz emitted waves with less attenuation is another key issue (see Fig. 2). We theoretically discover the amplification of surface plasmon-polariton when traveling along the graphene-channel waveguide under population inversion [7]. These new findings can lead to creation of a new type of room-temperature operating graphene injection THz lasers.

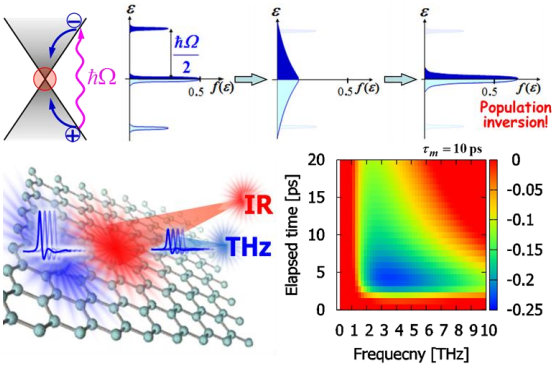

Fig. 1. Carrier dynamics and negative THz conductivity in graphene.

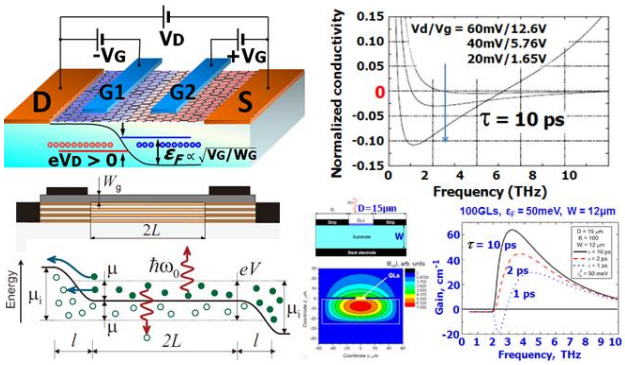

Fig. 2. Structure and gain spectral profile of a dual-gate current-injection graphene laser.

1. A. K. Geim and K. S. Novoselov, "The rise of graphene," Nat. Mater. **6**, pp. 183-191, 2007.
2. V. Ryzhii, M. Ryzhii, and T. Otsuji, "Negative dynamic conductivity of graphene with optical pumping," J. Appl. Phys. **101**, pp. 083114-1-6, 2007.
3. V. Ryzhii, M. Ryzhii, V. Mitin, and T. Otsuji, "Toward the creation of terahertz graphene injection lasers," J. Appl. Phys. **110**, pp. 094503-1-9, 2011.
4. A. Satou, T. Otsuji, and V. Ryzhii, "Theoretical study of population inversion in graphene under pulse excitation," Jpn. J. Appl. Phys. **50**, pp. 070116-1-4, 2011.
5. S. Boubanga-Tombet, S. Chan, T. Watanabe, A. Satou, V. Ryzhii, T. Otsuji, "Ultrafast carrier dynamics and terahertz emission in optically pumped graphene at room temperature," Phys. Rev. B **85**, pp. 035443-1-6, 2012.
6. V. Ryzhii, M. Ryzhii, V. Mitin, A. Satou, and T. Otsuji, "Effect of heating and cooling of photogenerated electron-hole plasma in optically pumped graphene on population inversion," Jpn. J. Appl. Phys. **50**, pp. 094001-1-9, 2011.
7. A.A. Dubinov, Y.V. Aleshkin, V. Mitin, T. Otsuji, V. Ryzhii, "Terahertz surface plasmons in optically pumped graphene structures," J. Phys.: Condens. Matter **23**, pp. 145302-1-8, 2011.

Perspective applications for 3C-SiC on silicon technology

Francesca Iacopi[1], Li Wang[1], Glenn Walker[1], Leonie Hold[1],
Ben Cunning[1], Jisheng Han[1], Philip Tanner[1], Alan Iacopi[1], Sima Dimitrijev[1]
Queensland Micro and Nanotechnology Facility, Griffith University, Australia, f.iacopi@griffith.edu.au

Silicon carbide (SiC) has the potential to unlock technology behind a vast range of energy efficient smart devices, ranging from power electronics to optoelectronics and harsh environment sensors. However, so far the interest in SiC has mainly regarded a niche (intermediate voltage devices) in the power electronics area [1], and it has only been marginally considered for MEMS fabrication [2]. The main reason for the limited introduction of SiC –based technologies is the scarce availability and high cost of the SiC bulk material [3].

This limitation can be circumvented by growing epitaxial 3C-SiC films on silicon surfaces. However, there are considerable challenges in growing good quality SiC on silicon, due to a 20% lattice misfit and the additional mismatch in coefficient of thermal expansion. These issues lead to a large number of epitaxial defects and usually high residual tensile stresses (occasionally originating cracks in the films), limiting their extent of application. The most likely defects to appear in epitaxial SiC on Si are stacking faults, as they have extremely low nucleation energy. Stacking faults are likely to originate electrically active states within the bandgap of the SiC, influencing the electronic properties of the films [4].

The Queensland Microtechnology Facility at Griffith has developed a solid knowledge and control of epitaxial growth of 3C-SiC films on Silicon [5]. Moderate film growth temperature (1000˚C), capabilities for doping, oxidation and growth on large area substrates (shortly up to 300mm wafers) in a clean room environment, makes this a suitable technology for large -scale fabrication. Moreover, the low deposition temperature and the specific epitaxial growth process allows to obtain SiC films with intrinsic stress as low as 300-100MPa.

Although the electronic properties are still hindered by extensive stacking faults, such films can be either used for leveraging SiC on Si – based applications, such as bio- and harsh- environment sensors [6], or as intermediate layer for enabling the deposition of high –quality III-V nitrides [7] and graphene [8] on Silicon.

3C-SiC films possess intermediate lattice properties between Silicon and relevant III-N such as GaN and AlN. When 3C-SiC films are deposited onto Si(111) surfaces as intermediate layer, the lattice mismatch of GaN is reduced from more than 20% down to 3-4%. III-N films on SiC/Si would enable low cost production of high –efficiency optoelectronics (GaN –based blue LEDs and UV photodetectors). Additionally, SiC(111) surfaces are also optimal for the synthesis of high- quality graphene over large area Si wafers [9].

Mono-crystalline 3C-SiC films on Si are an ideal material for MEMS. On the one hand, they intrinsically possess outstanding properties for use in harsh environments: high temperature and chemical resistance, excellent mechanical properties (E=400GPa, H=25-30GPa, high wear and fracture resistance), in addition to piezo-resistive behaviour. On the other hand, 3C-SiC on Si enables the use of conventional Si micromachining, relieving MEMS costs and manufacturing hurdles. MEMS building blocks such as diaphragms and cantilevers or double –clamped beams based on 3C-SiC on Si were fabricated with sizes ranging from hundreds of μm up to mm. Quasi –static and dynamic mechanical testing methods are used to identify the influence of parameters like film stress, geometry, thickness and density of defects.

1. P. Friedrichs, Physica Status Solidi **245** (1232-1238) (2008).
2. A. B. Horsfall N. G. Wright, K. Vassilevski, Materials Today **11** (2008).
3. J. Pezoldt and O. Ambacher V. Cimalla, Journal of Physics D: Applied physics **40**, 6386 (2007).
4. H. Iwata U. Lindefelt, S. Oberg, P. R. Briddon, Physical Review B **67**, 155204 (2003).
5. L.Wang, S.Dimitrijev, J.Han, P.Tanner, A.Iacopi, L.Hold, B.Harrison Thin Solid Films **519**, 6443 (2011).
6. D.J. Young, J. Du, C. A. Zorman, W. H. Ko, IEEE Sensors Journal **4** (2004).
7. H. Fujimori Y. Abe, A. Watanabe, N. Ohmori, J. Komiyama, S. Suzuki, H. Nakanishi, T. Egawa, Journal of Crystal Growth **318**, 460 (2011).
8. A. Kahouli A. Ouerghi, D.Lucot, M.Portail, L.Travers, J.Gierak, J.Penuelas, P.Jegou, A.Shukla, T.Chassagne, M.Zielinski, Applied Physics Letters **96** (2010).
9. V. Russo R. Parisi, A. Fedorov, F. Iacopi, C.S. Casari, A. Li Bassi, G.J. Norga, in *44th workshop on Dynamical Phenomena in Low-Dimensional Systems* (Erice, Italy, 2008)

Carbone nanotubes and nanostructures - multifunctional materials for emission electronics

Yu.V. Gulyaev
Kotel'nikov Institute of Radio Engineering and Electronics, RAS, Moscow, Russia

Research activity in field of Projection XEUV Lithography in IPM RAS

N.N. Salashchenko, N.I. Chkhalo
Institute for Physics of Microstructures, RAS, Nizhniy Novgorod, Russia

Next Generation Lithography – fundamental problems

S.I. Zaitsev
IMT RAS, Chernogolovka, Russia, e-mail: zaitsev@iptm.ru

The empirical regularity first formulated by Moore, by the efforts seem primarily of Intel, has been elevated to the rank of a "law". There is a fundamental physical limit of the current optical lithography based on 193nm light source it is a quarter wavelength. This limitation can be bypassed by exposure in the immersion fluid. Double patterning is planned to use for further progress. However, during more than ten past years an active search for technologies that could replace the modern photolithography has been performing. The technologies have a special name «next generation lithography» (NGL).

It is believed that the most mature pretendent is technology of extreme ultraviolet lithography (EUVL). However, along with it other approaches are seriously considering and developing. This report examines these, so called, alternative technologies. The technologies are based on the use of electron beams, and also they are called as technologies of direct drawing or maskless lithography. Now there are quite a few projects:

- Multi- beam lithography **MAPPER**, the company Mapper
- reflectance electron lithography, **REBL**, the company KLA-Tencor
- a multi-beam projection lithography, **PML2**, IMS Nanofabrication Company
- **MultiShaped Beam**, the company VISTEC
- **Multi Column E-beam**, the company ADVANTEST
- the system of projection cells, **CellProjection System**
- complementary electron lithography, **Complimentary EBL**, Japan
- autoemission electron lithography, **SelfEmission Litho**, company CRESTEC

Extremely tough competition claims arising from the modern photolithography are imposed on all the next-generation technologies. Such is, for example, the requirement for performance of 100 wafers per hour at a cost of 30-50 million dollars per setup.

The report briefly describes the technologies, analyzes the claimed potentials. In general, all the technologies demonstrate high resolution, or clearly demonstrate the possibility of achieving. However, the main difficulty of the direct drawing technologies is the need to satisfy two mutually exclusive requirements - high-resolution at high throuput. Performance can be improved by increasing the current, but it inevitably increases the diameter of the beam and decreases the resolution due to the next fundamental restriction caused by Coulomb interaction. Therefore, all the technology of direct drawing considers creating a multi-cathode (columns) systems to overcome these difficulties. And even when considering a multi-cathode system requirements for current and stability of a single electron source are extremely high.

In the report selection criteria for the EB next-generation technologies are derived from the competitive requirements, one of them is absence of so called “crossover” in electron optics. From the criteria one should come to pessimistic conclusion that in spite of the promises and plans, hardly any of the announced projects will reach potential to replace the current lithography in 2015. The most promising, if not the only project is the project MAPPER, which the report describes in details.

It is dicussed in the report additionally that the nearest fundamental problem which definitely will seriosely restrict possibilities of the next generation lithography is equilibrium fluctuations. The fluctuations are fundamental consiquence of statictical mechanics. It is explained that at decreasing critical dimension below 16nm statictcal noise of electron current results to fluctuations in dose of exposed elements what is incresed by resiste contrast. The level of resulting errors becomes unapproprited.

Thus, the most likely consequence is the conclusion that the existing technology of EB maskless lithography can not provide progress in following Moore's Law.

NANOMAKER - the electron lithography tool for ultimate resolution

B.N. Gaifullin[1], I.S. Stepanov[1], A.A. Svintsov[2], S.I. Zaitsev[2]
[1]Interface Ltd, Moscow, Russia, [2]IMT RAS, Chernogolovka, Russia, e-mail: zaitsev@iptm.ru

The two key and non-breaking technologies:
-electron-beam lithography (for making masks) and
-optical lithography (for mass, industrial production with the use of the masks) constitute the basis of modern micro-and nano-electronics. However, electron-beam lithography is certainly more important, because it is universal. It is used in mass production, not only for mass making, but also directly in the production of limited-edition products. In addition, advanced research and development are made using only the electron-beam lithography. In this case the electron-beam lithography provides the major means of nanostructuring and due to its versatility is significantly ahead of other well-known lithography, for example, ion-beam lithography or lithography based on scanning probes.

Electron-beam lithography allows structuring with the utmost accuracy of 5-10nm in the squares above 100x100mm^2.

The report will focus on describing the achievements of electron-beam lithography of ultimate resolution achieved in IPTM Academy of Sciences. In particular, the hardware-software system NanoMaker (www.nanomaker.com) will be presented. The basic physical and instrumentation limitations such as proximity effect, static and dynamic distortions of electron columns with a focused electron beam leading to a decrease in the accuracy of electron-beam lithography will be discribed. The technical solutions implemented in NanoMaker for compensation and correction of the sources for accuracy and resolution losses in modern electron lithography will be presented. One of the important achievements is the system's ability to provide NanoMaker writing in a large field with a good steaching without the use of expensive laser table. Features of NanoMaker will be compared with similar systems capabilities that are available on the market. Examples of using electron-beam lithography with high resolution will be shown

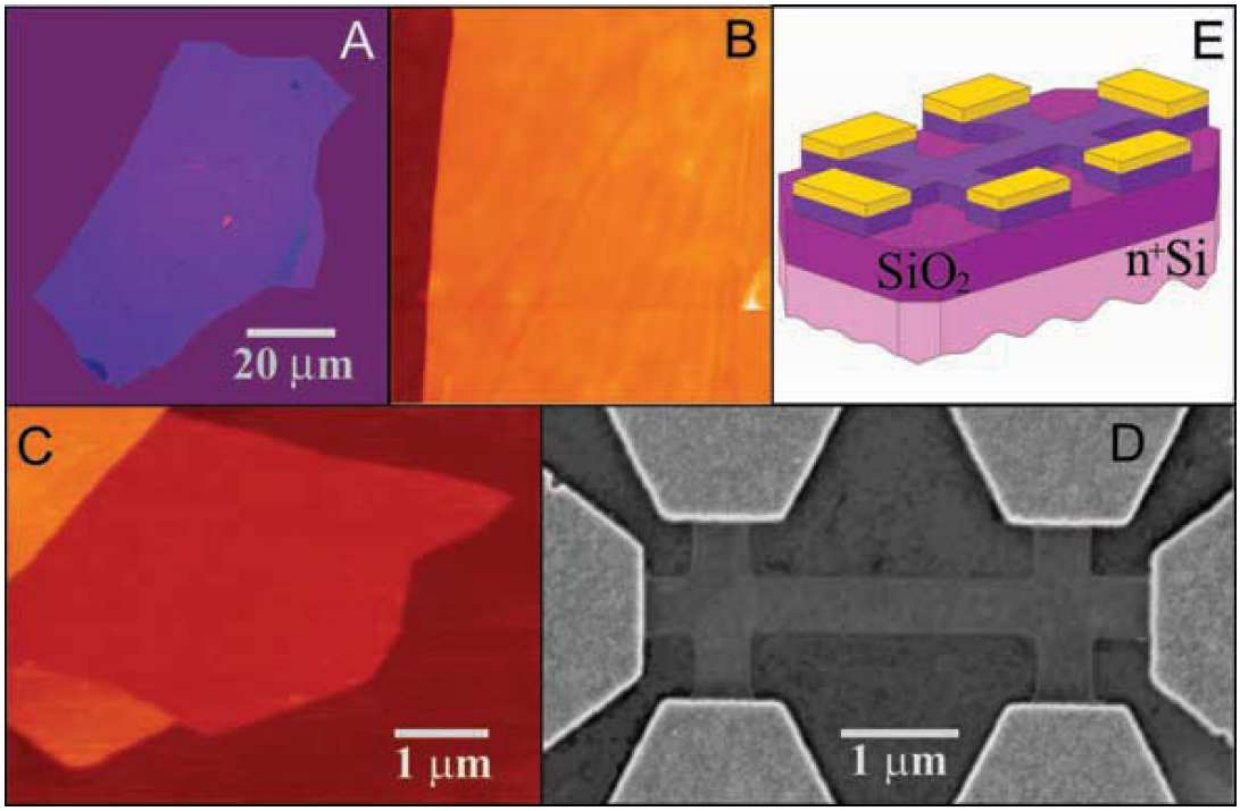

On the thermodynamics of antiferromagnetic nanoparticles and macroscopic quantum effects observed by Mössbauer spectroscopy

M.A. Chuev
Institute of Physics and Technology, Russian Academy of Sciences, Moscow, Russia, E-mail: chuev@ftian.ru

A great progress in applications of modern materials containing nano-sized magnetic particles or clusters in different branches of nanotechnology is primarily due to a number of specific structural, magnetic and thermodynamic properties of these materials found within long-term fundamental studies. However, the principle question of the effect of the magnetic nature of particles on their properties remains actually open to a large extent since the widely studied and obvious effect in the field is only superparamagnetism of ferromagnetic (FM) particles. The physical ideas for understanding magnetic properties of antiferromagnetic (AFM) nanoparticles on a phenomenological level have been suggested by Néel in terms of uncompensated magnetic moments on two magnetic sublattices and superantiferromagnetism [1]. Several models incorporating the uncompensated moment for describing magnetization curves of AFM particles have been developed, which are actually reduced, from the thermodynamic viewpoint, only to modifications of the Langevin function whereas the ground AFM state is treated in a rather simplified manner [2]. However, the ground state for AFM nanoparticles should be much more complicated as compared to that for a bulk sample and FM nanoparticles, which is evidenced from the atomic-scale magnetic modeling [3] that in its turn is hardly possible to be used for analyzing experimental data in practice due to computational expenses. Meanwhile, the same Néel's idea of the uncompensated moment has been widely explored in studies of macroscopic quantum phenomena in small AFM particles [4], but again within a simplified treatment of the ground and lowest-lying states in the large spin approximation. Generally speaking, in spite of the right physical meaning of the Néel's idea [1], it has also played a negative role because the behavior of ideal (compensated) AFM nanoparticles has not been seriously considered so far, that in its turn has restricted the development of a general theory.

In the present contribution I will discuss a quantum-mechanical model for describing thermodynamic properties of an ensemble of ideal and "uncompensated" AFM nanoparticles with axial magnetic anisotropy in the first approximation of slowly relaxing macrospins of magnetic sublattices [5]. This model clarifies principally the difference in thermodynamic behavior of FM and AFM particles revealed in spectroscopic measurements. In particular, one can now qualitatively describe specific (non-superparamagnetic) temperature evolution of the ^{57}Fe Mössbauer spectra of AFM nanoparticles, which has been often observed for almost half a century and looks like a quantum superposition of well-resolved magnetic hyperfine structure and single line (or quadrupolar doublet of lines) with the temperature-dependent partial spectral areas [6, 7]. This approach can be easily generalized for describing ferrimagnetic nanoparticles as well as magnetic relaxation processes [8], which would allow one to take directly into account the magnetic nature inherent to the particles in analyzing and re-evaluating a large amount of experimental data collected so far.

This work is financially supported by the Russian Foundation for Basic Research.

1. L. Néel, "Superantiferromagnetism in small particles", C. R. Acad. Sciences, **253**, pp.203-208, 1961.
2. C. Gilles, et al., "Magnetic hysteresis and superantiferromagnetism in ferritin nanoparticles", J. Magn. Magn. Mater., **241**, pp.430-440, 2002.
3. R.H. Kodama and A.E. Berkowitz,"Atomic-scale magnetic modeling of oxide nanoparticles", Phys. Rev. B, **59**, pp.6321-6336, 1999.
4. Y.-H. Nie, et al., "Macroscopic quantum coherence in small antiferromagnetic particles and quantum interference effects", Physica B, **270**, pp.95-103, 1999.
5. M.A. Chuev, "On the thermodynamics of antiferromagnetic nanoparticles by example of Mössbauer spectroscopy", JETP Lett., **95**, pp.295-301, 2012.
6. W. Kündig, et al., "Some properties of supported small α-Fe_2O_3 particles determined with the Mössbauer effect", Phys. Rev., **142**, pp.327-333, 1966.
7. I.P. Suzdalev, et al. "Magnetic phase transitions in nanostructures with different cluster orderings", Nanotechnologies in Russia, **4**, 467-474, 2009.
8. M.A. Chuev, "Multilevel relaxation model for describing the Mössbauer spectra of nanoparticles in a magnetic field", JETP, **114**, pp.609-630, 2012.

Characterization of nanoparticles in a media using multilevel models of magnetic dynamics

I. Mischenko[1], M. Chuev[1], V. Cherepanov[2], M. Polikarpov[2], V. Panchenko[2]
1. Institute of Physics and Technology, Russian Academy of Sciences, Moscow, Russia.
2. National Research Centre "Kurchatov Institute", Moscow, Russia. E-mail: IlyaMischenko@rambler.ru

The most informative techniques to study the structural, magnetic and thermodynamic properties of magnetic nanomaterials seem to be the conventional magnetization measurements and Mössbauer spectroscopy. The combination of those two methods can supply full set of practically important characteristics inherent to the magnetic nanoparticles into various environment, in particular those delivered in a body [1, 2]. In order to reliably decompose the experimental data into partial contributions of nanoparticles and their surrounding we have used multilevel models of magnetic dynamics [3-6]. The specialty of these models consists in explicit accounting the small size of the particles which results in comparable values of the particle magnetic anisotropy energy and the thermal fluctuations and so the significant role of relaxation processes in the observable effects. These models form the unified theoretical basis for interpreting large amount of non-equilibrium magnetic and Mössbauer measurements. This work demonstrates the advantages of the approach by the example of studying nanoparticles injected into mice.

Investigation of mice organs at different times after nanoparticles injection by Mössbauer spectroscopy obviously demonstrates along with erosion of iron-contain particles accumulation of ferritin-like protein in living tissues. A conventional analysis of such spectra and their decomposition into partial components is based on a formal consideration of continuous hyperfine field distributions at iron nucleus. But it results in only qualitative treatment of the spectra. In order to extract quantitative information about characteristics of the studied samples we used self-consistent fitting procedure based on the relaxation model of the magnetic dynamics. Thus, we managed to match the large set of the experimental data, particularly, the evolution of Mössbauer spectral form with temperature and external magnetic field as well as the magnetization curves.

The method allowed us to reliably evaluate changes in the nanoparticles parameters and numerically characterized the conversion of the iron to paramagnetic ferritin-like forms in animals' organs in the course of time. In particular, we have estimated iron concentrations in both chemical phases and sizes of the residual particles at different stages of biodegradation. Actually, the approach allows one to quantitatively characterize biodistribution and metabolism of magnetic nanoparticles injected into a body.

Improvement of the stated method consists in development more detailed models for describing nanoparticles of various magnetic natures (ferro-, antiferro- and ferrimagnetism) [7]. Though magnetization and Mössbauer curves for particles of different magnetic types often are similar the mechanisms of their formation are essentially different and their precise calculation requires specific schemes for each sort of magnetic structure. Implementation of this program shall result in data analysis procedure for magnetic and Mössbauer measurements of single-domain particles of almost every kind.

Support by Russian Foundation for Basic Research is acknowledged.

1. M.A. Chuev et al., "Interpretation of the Mössbauer spectra of the magnetic nanoparticles in mouse spleen", AIP Conf. Proc., **1311**, pp.322-328, 2010.
2. I. Mischenko, M. Chuev, "Biotransformation and metabolism of magnetic nanoparticles in an organism from Mössbauer spectroscopy", J. Phys.: Conf. Series, **345**, 012026 (8), 2012.
3. M.A.Chuev, J.Hesse, "Nanomagnetism - extension of the Stoner-Wohlfarth model within Neel's ideas and useful plots", In: *Magnetic Properties of Solids*, K.B. Tamayo, Nova Science, New York, 2009, pp.1-104.
4. M.A. Chuev, "Non-Langevin high-temperature magnetization of nanoparticles in a weak magnetic field", JETP, **108**, pp.249-259, 2009.
5. M.A. Chuev, "Multi-level relaxation model for describing the Mössbauer spectra of single-domain particles in the presence of quadrupolar hyperfine interaction", J. Phys.: Condens. Matter, **23**, 426003 (11), 2011.
6. M.A. Chuev, "Multilevel relaxation model for describing the Mössbauer spectra of nanoparticles in a magnetic field", JETP, **114**, pp.609-630, 2012.
7. M.A. Chuev, "On the thermodynamics of antiferromagnetic nanoparticles by example of Mössbauer spectroscopy", JETP Letters, **95**, pp.295-301, 2012.

The effect of technological factors on micromagnetic states of magnetic nanostructures

O.S. Trushin[1], V.V. Naumov[1], V.F. Bochkarev[1], N. Barabanova[2], V.A. Paporkov[2]
1. Yaroslavl Branch of the Institute of Physics and Technology, RAS, Yaroslavl, Russia, otrushin@gmail.com. 2. Yaroslavl State University, Yaroslavl, Russia

Multilayer magnetic nanostructures play an important role in modern spintronics. Due to Giant Magnetoresitive effect (GMR) they find wide range of applications in technology, such as magnetic field sensors and MRAM cells [1,2]. However achievement of high performance parameters (such as GMR ratio) put strict requirements on the technology of multilayer structure deposition [3].
Typical magnetoresitive structure is a spin valve, which consists of several magnetic and nonmagnetic layers with nanometer range thickness. In this work we perform systematic experimental and theoretical study of the effect of technological factors (such as growth conditions and presence of structure imperfections) on micromagnetic states of spin valve structures. Spin valve structures with given layer composition: $Ta(5nm)/Fe_{50}Mn_{50}(10nm)/Py(4nm)/Co(1nm)/Cu(2.5nm)/Co(1nm)/Py(4nm)/Ta(5nm)/SiO_2/Si(100)$
were grown by magnetron sputtering using standard industrial equipment TETRA SCR-650 (Alcatel). By varying technological parameters (such as growth rate, temperature of substrate and others) optimal conditions were choosen for well reproducible fabricating samples with GMR ration equial to 3.3 % at room temperatire. Micromagnetic states of as deposited samples during magnetic reversal were studied using Kerr effect microscope (Evico). Visualization of the domain structure during magnetic transitions and magnetic reversal loop helps to characterize the magnetic layers and quality of the nonmagnetic spacer (Fig.1).

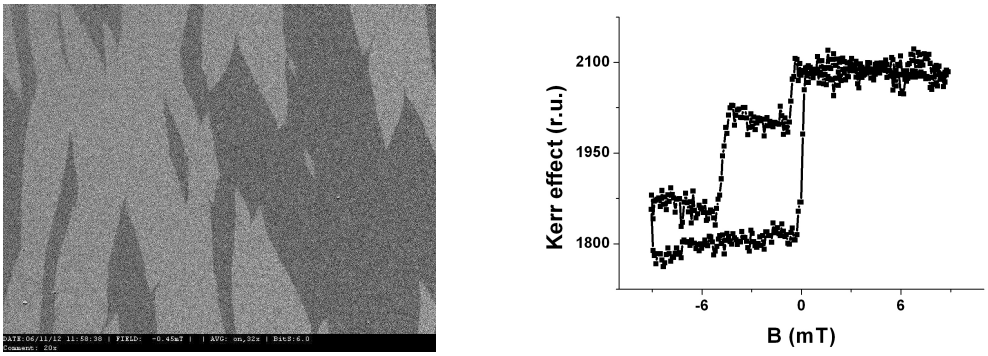

Fig.1 Domain structure of spin-valve during magnetic transitions and the corresponding magnetic reversal loop obtained using the Kerr effect microscope.

To study the effect of technological imperfections on the characteristics of magnetic nanostructures in more details we also performed micromagnetic simulations of spin-valves having different defects in layers using home made program package MICROMAG. In particular, presence of pinholes in spacer layer may create ferromagnetic connections between layers and lead to worsening functional characteristics. Another important factor is substrate roughness. The waving interface leads to additional magnetic interactions between the ferromagnetic layers (Neel effect). Our simulations showed clear trend in changing shape of magnetic reversal loop of spin-valve with increasing ferromagnetic connection through pinholes and with increasing amplitude of interface waving. Thus analysis of magnetic reversal loops of spin-valve structures may be used for diagnostics of different imperfections in structure and help in optimization of the technology.
This work has been supported by the program for fundamental research at the division of nanotechnology and informatics of RAS.

1. S. Tumanski *Thin film magnetoresistive sensor*s, IOP publishing Ltd., Bristol, 2001.
2. D.D. Tang and Y-J. Lee. Magnetic memory (Fundamentals and Technology), Cambridge University Press, UK, 2010.
3. R. Coehorn “Giant magnetoresistance and magnetic interactions in exchange-biased spin-valves”, in *Handbook of magnetic materials*, Vol. **15**, Elsevier Science, Amsterdam, 2003.

Magnetoresistance of Multilayer Ferromagnetic Nanoparticles

S.N. Vdovichev, B.A. Gribkov, S.A. Gusev, A.Yu. Klimov, V.L. Mironov, I.M. Nefedov, V.V. Rogov, A.A. Fraerman, and I.A. Shereshevskii

Institute for Physics of Microstructures, Russian Academy of Sciences, Nizhniy Novgorod, Russia,
E-mail andr@ipm.sci.nnov.ru

The transport characteristics of multilayer ferromagnetic systems are significantly affected by the distribution of the magnetization over the layers. This forms the basis for their application in information storage and processing devices. Structures with a noncollinear distribution of the magnetization with coupled spin and orbital degrees of freedom are currently of special interest. Noncollinear states can manifest in multilayer ferromagnetic nanoparticles due to the magnetostatic interactions between the layers. The stability of these states is determined by the particle shapes. For simplicity, we consider three magnetic discs separated by insulating spacers. The distribution of the magnetization in each disc is assumed to be uniform. The magnetostatic interaction between the layers is of the long - range antiferromagnetic character and the theory [1,2] predicts a helical ground state of the system. The distribution of the magnetization over multilayer particles, including three ferromagnetic layers separated by insulating spacers, was studied experimentally [3]. Experimental data on the magnetic state of these particles are obtained by measuring their magnetoresistance. Figure 1 shows the scheme of the multilayer magnetic particle embedded into a thin film electrode system in order to connect it to the measurement circuit.

For the case of the zero applied field, it is shown that a multilayer particle with easy plane magnetic anisotropy is a noncollinear helical state. With the growth of the particle anisotropy, the canted phases will be unstable and the magnetic field dependence of the resistance will exhibit the features corresponding to the transitions between the collinear phases. With this in mind, using electron lithography we prepared multilayer particles CoFe(10 nm)/AlO_x(2 nm)/CoFe(5 nm)/AlO_x(2 nm)/CoFe(10 nm) with lateral sizes of 100nm × 200 nm. Fig. 2 shows the relative resistance change for this sample as a function of the magnetic field applied along the long axis of the particle. Indeed, we observe resistance jumps that correspond to the transitions between the collinear states indicated in the Fig.2.

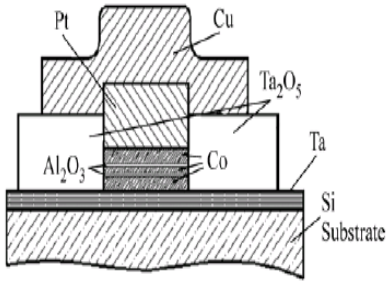

Fig. 1

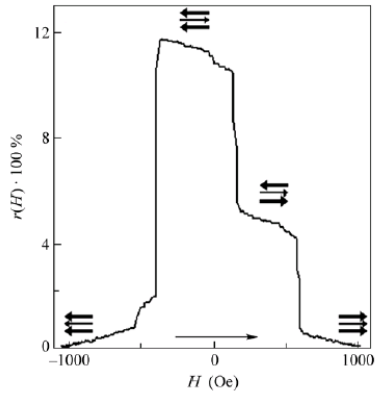

Fig.2

Possibilities of applications of these results in information storage and processing devices are discussed.

This work was supported by the Russian Foundation for Basic Research (Projects No. 11-02-00434 and No. 11-02-00589) and Presidium of RAS in the program of basic researches "Fundamental principles of technology of nanostructures and nanomaterials".

1. A.A. Fraerman, B.A. Gribkov, S.A. Gusev, et al., J. Appl. Phys., **103**, 073916, 2008.
2. K.R. Mukhamatchin and A.A. Fraerman, JETP Lett., **93**, p.716, 2011.
3. S.N. Vdovichev, B.A. Gribkov, S.A. Gusev, et al, JETP Lett., **94**, p.386, 2011.

Magnetic logical cells based on domain wall pinning effects in ferromagnetic nanowire-nanoparticles systems

V.L. Mironov, O.L. Ermolaeva, E.V.Skorohodov, A.Yu. Klimov
Institute for Physics of Microstructures, Russian Academy of Sciences, Nizhniy Novgorod, Russia,
E-mail mironov@ipm.sci.nnov.ru

The field-driven motion and pinning of domain walls (DWs) in ferromagnetic nanowires (NWs) are the subjects of intensive research motivated by promising applications for the development of magnetic logic and data storage systems [1]. The operation of DW based systems requires the controlled DW pinning-depinning for organization of logical calculations, preservation from accidental data erasing and to save the results of intermediate computations. In our work, we consider a DW pinning control in a combined system consisting of a planar ferromagnetic NW and two elongated ferromagnetic nanoparticles (NPs), which is based on the effective change of the stray field in NP subsystem. The application of these NW-NP systems to create a magnetic logic cells (MLCs) is decussed.

We considered two systems with different NP configurations (see fig. 1). The low-coercive circular pad N is used for the nucleation of domains with opposite orientation, while the NPs are used as a magnetic gate for the field-controlled DW pinning-depinning. The magnetization reversal of NW in an external magnetic field occurs via DW nucleation at the left end and subsequent movement to the right free end. The theoretical estimations and micromagnetic simulations have showed that in dependence on relative orientation of magnetic moments in NW and NPs subsystem there are two variants of DW pinning connected with a potential barrier or a potential well caused by magnetostatic interaction between the DW and local NPs stray field. We propose the prototype logical cells based on considered NW-NPs systems and discuss the algorithm of external magnetic field commutation and independent switching of NPs moments that permits the realization of logical operations.

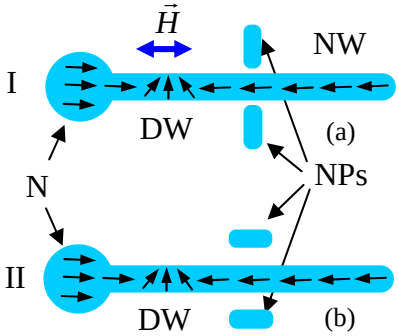

Fig. 1. Schematic drawing of field-driven NW-NP systems.

In particular, it is shown that for the system I presented in fig. 1a the magnitude of potential barrier is equal to the depth of potential well. This system can be considered as a prototype of MLC, which realizes the “exclusive disjunction” logical operation (so-called XOR) [2].

In contrast with system I, in system II the magnitude of the pinning potential barrier is twice smaller than the depth of the potential well. This enables the realization of two different logical operations on the same logical element. If the operating magnetic field is less than the depinning field for the potential barrier, this system performs the XOR operation. On the other hand, if the operating magnetic field is more than the depinning field for the potential barrier, but less than the depinning field of the potential well, this system performs the simple OR operation.

The system I was investigated experimentally by magnetic force microscopy methods [2]. For the $Co_{60}Fe_{40}$ based NW-NPs system consisting of $100 \times 2800 \times 20$ nm nanowire with 200 nm in diameter nucleating part and $200 \times 100 \times 20$ nm nanoparticles gate (with 100 nm NW-NP separation) the nucleating field 300 Oe and depinning field 560 Oe were registered.

The authors are very thankful to S.A. Gusev, S.N. Vdovichev, and V.V. Rogov for assistance in samples preparation and to B.A. Gribkov and A.A. Fraerman for the very fruitful discussions.

This work was supported by the Russian Foundation for Basic Research (Projects No. 11-02-00434 and No. 11-02-00589) and Presidium of RAS in the program of basic researches "Fundamental principles of technology of nanostructures and nanomaterials".

1. D.A. Allwood, G. Xiong, C.C. Faulkner, D. Atkinson, D. Petit, R.P. Cowburn, “Magnetic domain-wall logic”, Science, **309**, pp.1688-1692, 2005.
2. V.L. Mironov, O.L. Ermolaeva, E.V. Skorohodov, A.Yu. Klimov, “Field-controlled domain wall pinning-depinning effects in ferromagnetic nanowire-nanoislands system”, Phys. Rev. B, **85**, 144418 (pp.1-9), 2012.

Field-induced transitions in ferrimagnetic chain of spins: stability of ferromagnetic and antiferromagnetic phases

M. Kostyuchenko
Yaroslavl State Technical University, Yaroslavl, Russia, mkspin@mail.ru.

Physical properties of nanostructures (magnetic multilayers, chains of atoms, magnetic molecular nanoclusters, etc.) are studied intensively at present time. Great interest in studying of nanostructures is not only due to their importance to theoretical science, but also to promising perspectives of their practical application in development of new types of devices and fundamentally new computing machines – quantum computers. Importance of studying transitions induced by magnetic field consists in the fact they are effective means of control of the main state of magnetic structures.

This paper covers studying of field-induced transitions in ferrimagnetic chain of spins. Solving this problem by analytic methods is reduced to the problem of minimization of nonlinear functional of N variables and it is very hard, therefore there relatively few studies that covers effect of finite size by analytic methods [1–3]. Main method of calculation of critical fields for such systems is numeric procedure [4–6], but none of mentioned studies has developed a reliable universal method.

This work presents employment of new technique: a method of finite-difference equations [7]. Given method is applied to this task for the first time. It enabled to study stability of ferromagnetic and antiferromagnetic phases for ferrimagnetic chain that consists of even number of spins. Universality of method of finite-difference equations consists in the fact that for every chain of spins of even length analytical relations between critical fields and number of spins are obtained.

1. A.K. Zvezdin, S.N. Utochkin, “About processes of the magnetization and mechanism of kinetic anomalies in magnetic nanostructures”, JETP Letters, **57**, pp.418-423, 1993.
2. A.K. Zvezdin, V.V. Kostyuchenko, “Phase transitions in the anisotropic magnetic multilayers”, Solid State Phenomena, **39**, pp.178-180, 1997.
3. A.L. Dantas, A.S. Carrico, “Surface-induced low-field instability of antiferromagnetic multilayers”, Phys. Rev. B, **59**, pp.1223-1231, 1999.
4. M. Amato, M.G. Pini, A. Rettori, “Optimization study of the nanostructure of hard/soft magnetic multilayers”, Phys. Rev. B, **60,** pp.3414-3420, 1999.
5. U.K. Robler, A.N. Bogdanov, “Magnetic phases and reorientation transitions in antiferromagnetically coupled multilayers”, Phys. Rev. B, **69**, 184420, 2004.
6. D.L. Mills, “Phase transitions in magnetic multilayers: statics and dynamics”, J. Magn. Magn. Mater., **198-199,** pp.334-337, 1999.
7. V.V. Kostyuchenko, “ *Field-induced transitions in magnetic nanostructures and molecular magnets. Thesis for degree of doctor of physical and mathematical sciences*”, Moscow, 2009 (in Russian)

Quantum information and spectroscopy of cold Rydberg atoms

I.I. Ryabtsev, I.I. Beterov, D.B. Tretyakov, V.M. Entin, and E.A. Yakshina
Institute of Semiconductor Physics, Pr. Lavrentyeva 13, 630090 Novosibirsk, Russia, E-mail: ryabtsev@isp.nsc.ru

Highly excited Rydberg atoms have many unique properties compared to low-excited atoms: large electron orbit radius, large dipole moments of transitions between neighboring states, strong long-range interactions, long radiative lifetimes, huge polarizabilities, etc. [1-3]. Laser and microwave spectroscopy of Rydberg atoms can reveal these properties by observing the quantum interference, dephasing, shifts or broadenings of various resonances in single Rydberg atoms. Single Rydberg atoms are detected using the selective field ionization technique. Control of long-range interactions between Rydberg atoms by laser and microwave radiations, as well as by external electric and magnetic fields, forms the basis for quantum information processing with neutral trapped atoms.

Rydberg atoms are therefore a promising approach to quantum information processing with neutral atoms because of the low decoherence rate of Rydberg states, possibility of fast MHz rate gates using dipole-dipole interaction, and the potential for scalability to large numbers of qubits in optical lattices [1-3]. Experimental techniques of laser cooling and trapping of atoms and high precision spectroscopy allow confining and manipulating single atoms in the optical dipole traps and optical lattices. Entangled states can be generated using temporary excitation of ground-state atoms to a strongly interacting Rydberg state or using interaction-induced changes in the spectra of collective excitations of an ensemble of Rydberg atoms (dipole blockade effect).

In this report we will review the recent experimental advances towards quantum information processing with Rydberg atoms. We will also present our related experimental and theoretical results on laser and microwave spectroscopy cold Rb Rydberg atoms in a magneto-optical trap and on dipole-dipole interaction between a few cold rubidium Rydberg atoms confined in a small laser excitation volume [4-7]. The new ideas on deterministic single-atom loading of optical lattices using dipole blockade with chirped laser pulses [8] and on Doppler- and recoil-free laser excitation of Rydberg states via three-photon transitions [9] will be discussed in the context of quantum information processing with neutral atoms.

This work was supported by RFBR (Grant Nos. 10-02-00133 and 12-02-92606), by the Russian Academy of Sciences, by the Presidential Grants Nos. MK-3727.2011.2 and MK-7060.2012.2, by the Dynasty Foundation, and by the EU FP7 IRSES Project "COLIMA".

1. I.I. Ryabtsev et al., J. Phys. B, **38**, p.S421, 2005.
2. M. Saffman et al., Rev. Mod. Phys., **82**, p.2313, 2010.
3. D. Comparat et al., J. Opt. Soc. Am. B, **27**, p.A208, 2010.
4. I.I. Ryabtsev et al., Phys. Rev. Lett., **104**, p.073003, 2010.
5. I.I. Ryabtsev et al., Phys. Rev. A, **82**, p.053409, 2010
6. I.I. Beterov et al., Russian Microelectronics, **40**, p.237, 2011.
7. D.B. Tretyakov et al., JETP, **114**, p.14, 2012.
8. I.I. Beterov et al., Phys. Rev. A, **84**, p.023413, 2011.
9. I.I. Ryabtsev et al., Phys. Rev. A, **84**, p.053409, 2011.

Creating a single-atom array for quantum computation using Rydberg blockade in an atomic ensemble

D.B. Tretyakov, I.I. Beterov, V.M. Entin, E.A. Yakshina, and I.I. Ryabtsev
Institute of Semiconductor Physics, Pr. Lavrentyeva 13, 630090 Novosibirsk, Russia, E-mail: dtret@isp.nsc.ru

Single neutral atoms confined in an array of optical dipole traps are promising candidates to implement quantum bits [1]. Two-qubit gates can be implemented using a temporary excitation of chosen atoms to high energy Rydberg states by a short laser pulse. Atoms in Rydberg states have unique properties compared to low-excited atoms [2]. Their long radiative lifetimes provide coherence preservation during two-qubit gate execution time. Large dipole moments of transitions between neighboring Rydberg states allow the atoms to couple via strong dipole-dipole interaction.

However, deterministic loading of single atom in each optical dipole trap of the array remains a difficult problem so far. When these traps are loaded from a cold atom cloud, the number of atoms in each trap is random. To load a single atom in each trap, it was proposed to exploit a dipole blockade effect at the laser excitation of mesoscopic ensembles [3]. Effect of the dipole blockade appears as selective excitation of one-atom collective Rydberg states of an atomic ensemble by narrow-band laser radiation, while an excitation of other collective Rydberg states is completely or partially suppressed because of their energy shifts due to dipole-dipole interaction [4]. The mean interatomic distance in the optical dipole trap lies in the micron range. Therefore, the atoms can exhibit strong dipole-dipole interaction at their excitation to Rydberg states and a dipole blockade regime can be implemented. In the full blockade regime the full population inversion between collective ground state and one-atom collective Rydberg states of an atomic ensemble can be achieved by applying a laser pulse. The amplitude and duration of this laser pulse, however, depend on the number of atoms in the ensemble. Therefore, in order to excite only one atom from whole ensemble, the number of atoms in the ensemble must be known. In the case of the array of optical dipole traps loaded from a cold atom cloud the number of atoms in each trap is unknown.

We propose to use adiabatic passage in the conditions of the full Rydberg blockade to overcome the dependence of the laser exciting pulse parameters on the number of interacting atoms [5]. We have found that deterministic excitation of a single Rydberg atom can be implemented with high efficiency using an excitation by linearly chirped laser pulse or stimulated Raman adiabatic passage in mesoscopic ensembles with unknown number of atoms. These methods with removing ground-state atoms by an additional laser pulse allow for high-fidelity single-atom loading in optical dipole traps.

This work was supported by RFBR (Grant Nos. 10-02-00133 and 12-02-92606), by the Russian Academy of Sciences, by the Presidential Grants Nos. MK-3727.2011.2 and MK-7060.2012.2, by the Dynasty Foundation, and by the EU FP7 IRSES Project "COLIMA".

1. M. Saffman et al., “Quantum information with Rydberg atoms”, Rev. Mod. Phys., **82**, pp.2313-2363, 2010.
2. T.F. Gallagher, “Rydberg atoms”, Cambridge University Press, 1994.
3. M. Saffman et al., “Creating single-atom and single-photon sources from entangled atomic ensembles”, Phys. Rev. A, **66**, 065403, 2002.
4. M.D. Lukin, “Dipole Blockade and Quantum Information Processing in Mesoscopic Atomic Ensembles”, Phys. Rev. Lett., **87**, 037901, 2001.
5. I.I. Beterov et al., “Deterministic single-atom excitation via adiabatic passage and Rydberg blockade”, Phys. Rev. A, **84**, 023413, 2011.

Integrated diamond nanostructures for quantum informatics

V.P. Popov[1], L.N. Safronov[1], V.A. Antonov[1], S.N. Podlesnyi[1], A.V. Shishaev[1], I.I. Ryabtsev[1], N. Kupriyanov[2], Yu.N. Pal'yanov[2]

5. Rzhanov Institute of Semiconductor Physics, Russian Academy of Sciences, Novosibirsk, Russia, E-mail address popov@isp.nsc.ru. 2. Sobolev Institute of Geology and Mineralogy, SB RAS Novosibirsk, Russia

A set of unique properties of semiconducting diamond remains unrealized due to a number of outstanding problems in materials science: graphitization layers implanted by ions; the lack of annealing the defects and diffusion of impurities up to temperatures of 1200^{o}C, and their compensation by deep levels due to formation of thermo-stable defect centers with vacancies, own interstitial atoms and impurity atoms. In addition to the problems, some defects such as NV centers have useful properties.

In particular, due to the large relaxation time of spin states for electrons and nuclei at room temperature, NV centers are considered potentially the most prospective platform for implementation of quantum information processes (QIP) in solid state devices [1]. Electronic and optical properties of NV centers depend on elastic, electric and magnetic fields, allowing to create a stable, high sensitive sensors for these fields. Individual NV centers, located at the spearhead of the cantilever, provide measurement of electric and magnetic fields with atomic resolution. Magnetic dipole interaction between closely spaced NV centers implements them entangled quantum state in the QIP and the nuclear spin of the nucleus of nitrogen atom allows to record and store the quantum information in dynamic quantum memory cell [2].

Required properties of NV centers are observed only in the negative charge state (NV^-), which is realized in the bulk of diamond at the certain concentration of nitrogen atoms in the lattice sides or inside the charge space away from the surface where they are neutral due to Fermi level pinning. [3].

The aim of this work was the search the processes enabling to put NV-centers managed by electric fields in the NV^- state and the concentration inside the local volume of semiconductor diamond. Tens nanometer thick layers of diamond with NV-center concentration (1-100) x10^{18}cm^{-3} were created using N^+ ion implantation and annealing at high pressure-temperature (HPHT: 4-8 GPa, 1200-1600^{o}C), or in a vacuum (VPHT). Electric field for charge control of NV-centers was generated inside thin film layers (30-300 nm) separated from (111) surface of synthetic diamond plates, using buried semi-transparent multigraphene layers with sheet resistance 1 mOhm/qua to 1 kOhm/qua, as electrodes or contacts for p-n junctions [4]. Manufactured, measured and analyzed multiple types of the structures by optical and electrical methods are compared as a promising elemental base for future devices in quantum informatics.

1. M.V.G. Dutt, L. Childress, L. Jiang, E. Togan, J. Maze, F. Jelezko, A.S. Zibrov, P.R. Hemmer, and M.D. Lukin, "Quantum register based on individual electronic and nuclear spin qubits in diamond", Science, **316**, pp.1312-1316, 2007.

2. J.H. Shim, I. Niemeyer, J. Zhang, D. Suter, "Robust Dynamical Decoupling for Arbitrary Quantum States of a Single NV Center in Diamond", arXiv:1205.6938.

3. P. Siyushev, H. Pinto, A. Gali, F. Jelezko, J. Wrachtrup, "Low Temperature Studies of Charge Dynamics of Nitrogen-Vacancy Defect in Diamond"; arXiv:1204.4898.

4. V.P. Popov, L.N. Safronov, O.V. Naumova, D.V. Nikolaev, I.V. Kupriyanov, Yu.N. Palyanov. "Conductive layers in diamond formed by hydrogen ion implantation and annealing", Nuclear Instruments and Methods in Physics Research B, **282**, pp.100–107, 2012.

Color centers in nanodiamonds of different origin

I.I. Vlasov[1], V.G. Ralchenko[1], O. Shenderova[2], A.A. Shiryaev[3], A.A. Khomich[1], V.S. Sedov[1], M.S. Komlenok[1] , V. S. Pavelyev[4,5] , K. N. Tukmakov[5] , S. Turner[6], F. Jelezko[7], J. Wrachtrup[8], V.I. Konov[1]

[1] *General Physics Institute RAS, Moscow, Russia, vlasov@nsc.gpi.ru*
[2] *International Technology Centre, Raleigh, USA*
[3] *Institute of Physical Chemistry RAS, Russia*
[4]*Image Processing Systems Institute RAS, Samara, Russia*
[5]*Samara State Aerospace University, Samara, Russia*
[6] *EMAT, University of Antwerp, Antwerpen, Belgium*
[7]*Institute for Quantum Optics, Ulm University, Ulm, Germany*
[8]*Physical Institute and research center SCOPE, Stuttart University, Stuttgart, Germany*

For the last decade an interest to the luminescent nanodiamond (ND) has multiply increased. This is explained by promising results on use of luminescent NDs as a source of a single-photon emission for quantum information technologies [1] and, alternatively, as a bright light source applicable for biolableling.[2] The brightest color centers used for a production of the luminescent nanodiamond are nitrogen-vacancy (NV) and silicon-vacancy (SiV) centers. The development of luminescent NDs has mostly focused on a use of high-pressure high-temperature (HPHT) diamonds containing NV color centers. An "indirect" production of the luminescent NDs is used for this purpose, i.e. micron-scale diamond crystals are synthesized fist, and then are milled down to required nano-sizes. An intensity of NV luminescence in ND particles is controlled by pos-synthesis treatments of the HPHT diamond crystals.

Photoluminescent properties of the color centers in nanodiamond (ND) materials of different origin, namely, in ND produced by CVD technique, detonation ND, and ND extracted from meteorite have been studied in this work. Thermodynamic and photo stability of the SiV centers formed in 5-nm crystallites of CVD diamond was demonstrated [3]. It was shown that a density of NV centers in detonation nanodiamond particles can be controlled through a proper selection of the carbon precursor material [4]. For the first time we have found that isolated meteoritic diamond nanoparticles of molecular size (2 nm) are capable of housing photo-stable SiV centers [5]. Examples of photonic structures based on luminescent CVD diamond films patterned with laser and focused ion beam are demonstrated.

This work was supported by Russian Ministry of Education and Science under the Contract no. P925, RFBR grant no. 12-02-90820, and the grant of Presidium of RAN "Innovation and Development Program".

[1] J. Tisler, G. Balasubramanian, B. Naydenov, R. Kolesov, B. Grotz, R. Reuter, J.-P. Boudou, P. A. Curmi, M. Sennour, A. Thorel, M. Borsch, K. Aulenbacher, R. Erdmann, P. R. Hemmer, F. Jelezko, J.Wrachtrup, "Fluorescence and Spin Properties of Defects in Single Digit Nanodiamonds", ACS Nano**, 3**, pp.1959-1965, 2009.

[2] A.M. Schrand, S.C. Hens, and O.A. Shenderova, *Critical Reviews in Solid State and Materials Sciences*, **34**, pp.18–74, 2009.

[3] I.I. Vlasov, *et al.*, "Nanodiamond Photoemitters Based on Strong Narrow-Band Luminescence from Silicon-Vacancy Defects" Adv. Mater. **21**, pp.808-812, 2009.

[4] O.A. Shenderova et al., "Nitrogen Control in Nanodiamond Produced by Detonation Shock-Wave-Assisted Synthesis" J. Phys. Chem. C, **115**, pp.14014-14020, 2011.

[5] A.A. Shiryaev, A.V. Fisenko, I.I. Vlasov, L.F. Semjonova, P. Nagel, S. Schuppler, "Spectroscopic study of impurities and associated defects in nanodiamonds from Efremovka (CV3) and Orgueil (CI) meteorites", Geochimica et Cosmochimica Acta, **75**, pp.3155–3165, 2011.

Quantum register based on structured diamond waveguide with NV centers

A.V. Tsukanov, I.Yu. Kateev, A.A. Orlikovsky
Institute of Physics and Technology, Russian Academy of Science, Moscow, Russia, ikateyev@mail.ru

We propose a scheme of quantum information processing with NV-centers embedded inside a diamond nanostructure (fig. 1). A single NV-center placed in the cavity plays a role of an electron spin qubit which evolution is controlled by microwave pulses. Besides, it couples to the cavity field via optical photon exchange. In their turn, neighbor cavities are coupled to each other through the photon hopping to form a bus waveguide mode. This waveguide mode overlaps with all the NV-centers. Entanglement between distant centers is organized by an appropriate tuning of their optical frequencies relative to the waveguide frequency via electrostatic control without lasers. We describe the controlled-Z operation that is by one order of magnitude faster than in off-resonant laser-assisted schemes proposed earlier. Spectral characteristics of the one-dimensional chain of microdisks are calculated by means of numerical modeling, using the approach analogous to the tight-binding approximation in the solid-state physics. The data obtained allow to optimize the geometry of the microdisk array for the effective implementation of quantum operations.

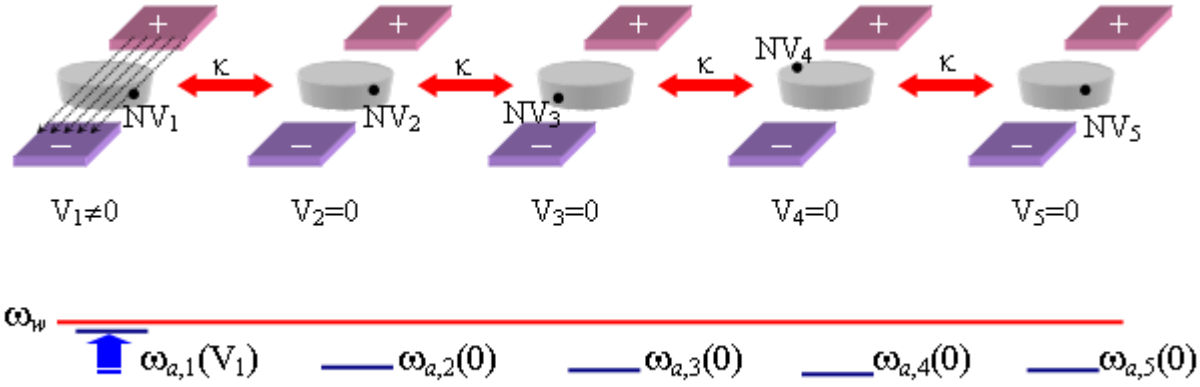

Fig. 1. Scheme of a five qubits quantum register based on a quasi-linear photonic nanostructure consisting of diamond disk resonators connected through photon hopping κ. Each cavity contains the NV-center encoding quantum information into the electronic spin states. The optical transition frequencies $\omega_{a,k}$ of the centers are controlled by an electric field generated by a system of gates. Each gate are supplied by the bias voltage V_k (k = 1 - 5). A diagram of the alignment of the first center frequency into the resonance of the waveguide mode ω_w is shown on the bottom.

Charge pumping with Coulomb blockade devices

Yu.A. Pashkin
Physics Department, Lancaster University, United Kingdom,
NEC Smart Energy Research Laboratories and RIKEN Advanced Science Institute, Tsukuba, Japan
E-mail: ypashkin@mail.ru

Coulomb blockade devices offer a possibility to control charge transfer at the level of elementary charge *e*. Since late 80s several charge pumping schemes have been proposed and demonstrated experimentally. Surprisingly, a simple charge pumping device based on a SINIS type single-electron transistor was overlooked. After the demonstration of its operation principle in 2008 by the group of Aalto University (AU), researches from AU and NEC Lab in Tsukuba are trying to develop a dc current source with an output current of up to 1 nA and a relative uncertainty of 10^{-6}. In my presentation, I will describe the latest results on this.

I will also present some data on coherent Cooper pair pumping with a SISIS type single-electron transistor using nonadiabatic gate control.

Quantum Discord in Materials with Electron and Nuclear Spins

M.A. Yurishchev
Institute of Problems of Chemical Physics of the Russian Academy of Sciences, Chernogolovka, Moscow Region, 142432 Russia, E-mail address: yur@itp.ac.ru

It is discussed the total purely quantum information correlation (discord) in spin systems with Heisenberg exchange and magnetic dipole-dipole interactions [1, 2]. The relations between quantum discord Q and magnetic susceptibility and heat capacity are found. This allows one to measure indirectly the discord through calorimetric and magneto-metric measurements. Using the available experimental data, we found the discord versus temperature T and external magnetic field for a number of solids containing electron and nuclear spin dimers. A typical example is given in Fig. 1. It is established that the quantum correlations by high temperatures tend to zero according to the law $1/T^2$.

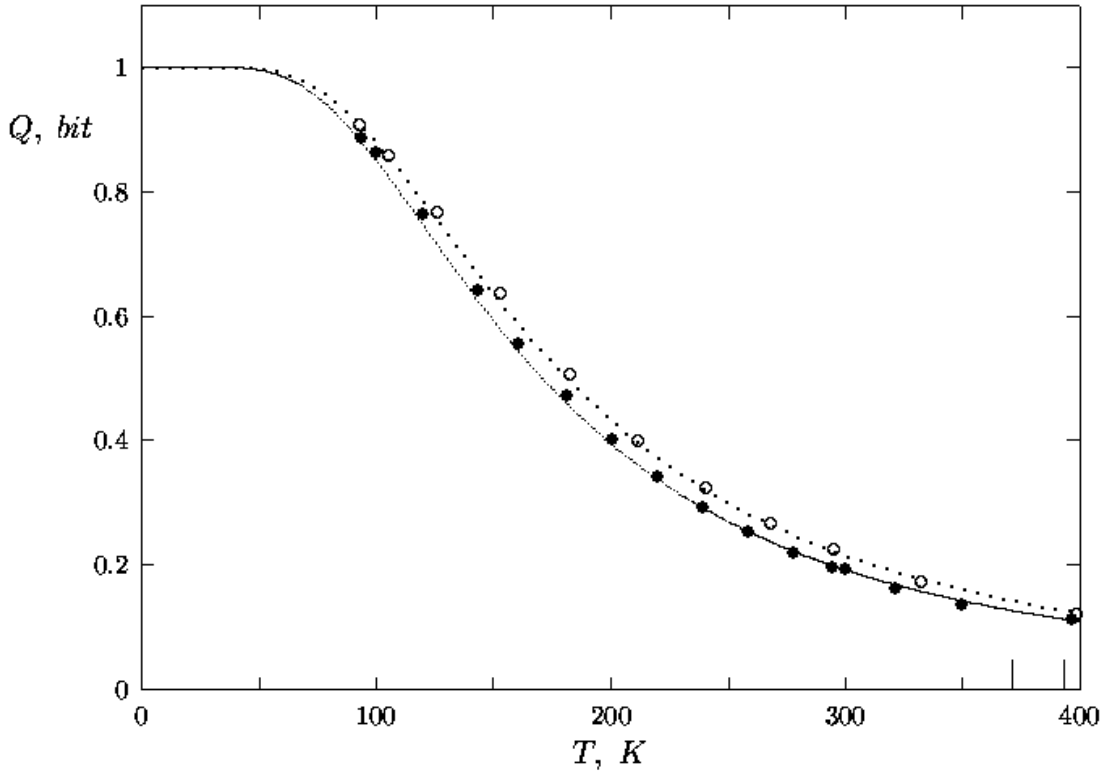

Fig. 1. Experimental data (circles) and theoretical dependences (lines) for the thermal quantum discord vs temperature in the hydrated (black circles and solid line) and anhydrous (open circles and dotted line) copper (II) acetates.

1. M.A.Yurishchev, "Quantum discord in spin cluster materials", Phys. Rev. B, **84**, pp.024418-1–024418-7, 2011
2. E.I. Kuznetsova and M.A. Yurishchev, "Quantum discord in spin systems with dipole-dipole interaction" (to be published)

On the time-optimal implementation of quantum Fourier transformation for qudits represented by quadrupole nucleus

V.P. Shauro, V.E. Zobov
L. V. Kirensky Institute of Physics, Siberian Branch of Russian Academy of Sciences,Krasnoyarsk, Russia, rsa@iph.krasn.ru

The problem of time-optimal realization of quantum gates at different quantum systems is investigated actively now. This issue studied quite extensively in the literature for systems of multiple qubits, both analytically and numerically, but such studies for more complex *d*-levels elements (qudits) are almost not performed [1]. For example, it is shown in [2] for quantum circuits consisting of *k* qubits ($d = 2^k$) that for QFT gate the minimal time $T_{\min}$ increases proportionally to the number k ($T_{\min} \sim \log d$). Witch nature of this dependence in case of qudits will be of interest to evaluate the perspectives for practical applications of qudits in quantum computing and quantum communication. In this regard, the present work is devoted to the numerical evaluation of $T_{\min}$ for the QFT gate for qudits with different $d=2I+1$ on the example of quadrupole nucleus with spin $I > 1/2$.

Let us consider the spin I in a static magnetic field B_0 along the z axis and controlled by optimized RF pulse with the frequency $\omega_{rf} = \omega_0$, where $\omega_0 = \gamma B_0$ is a Larmor frequency of spin. In the reference frame rotating with frequency ω_{rf}, the total spin Hamiltonian of the our model has the form [1]:

$$H(t) = (\omega_{rf} - \omega_0)I_z + q(I_z^2 - I(I+1)/3) + u_x(t)I_x + u_y(t)I_y . \quad (1)$$

Here I_α is the spin projection operator on the α axis, q is a constant of the quadrupole interaction of the nucleus with the gradient of the axially symmetric crystal field, $u_\alpha(t)$ is the projection of the control RF field γB_{rf} on the α axis. For QFT gate, given by the matrix F [1-3], it is necessary to find a form of RF pulse (i.e. $u_\alpha(t)$ parameters) that minimizes the gate error Δ:

$$\Delta = 1 - \left| Tr\left(F^+ U(T)\right)\right|^2 / Tr^2(\mathbf{1}), \qquad U(T) = \hat{T}\exp\left(-i\int_0^T H(t)dt\right). \quad (2)$$

Here $U(T)$ is the evolution operator of the system during the time T, 1 is a unit operator and $\hat{T}$ is the time-ordering operator. The calculation of $u_\alpha(t)$ was performed numerically using the Krotov algorithm as in [4].

Performing the calculation for different times T, from the dependence of Δ on T [1-3] we can estimate the minimum time $T_{\min}$ required for the implementation of the QFT gate for the appropriate spin. However, in the determination of gate error (2) we ignore the global phase of gate, which is known to has a significant effect on the minimum time of implementation [2, 3]. Thus, for different initial conditions in the algorithm we obtain solutions with different gate error depending on the global phase of obtained gate. To distinguish among these solutions the desired one, i.e. with minimal time for a given error, by analogy with [2] we performed from 10 to 50 calculations with a random initial pulse for several values of time T, and one solution was chosen with the smallest error. From the obtained data it is possible to estimate the value of $T_{\min}$ for a given error threshold, for example, $\Delta < 10^{-5}$. For a more accurate estimate the dependence of Δ on T was built according the PFT technique of [3]. As a result, we obtain estimates of $T_{\min}$ for d from 3 to 8.

An interesting result is that the dependence of $T_{\min}$ on d is different for even and odd values of d. In this regard, the available data are not sufficient to conclusively determine the character of these dependences.

1. V.E. Zobov, V.P. Shauro, "On Time-Optimal NMR Control of States of Qutrits Represented by Quadrupole Nuclei with the Spin I = 1", JETP, **113**, pp.181-191, 2011.
2. T. Schulte-Herbrüggen, A. Spörl, N. Khaneja, S.J. Glaser, "Optimal control-based efficient synthesis of building blocks of quantum algorithms: A perspective from network complexity towards time complexity", Phys. Rev. A, **72**, p.042331, 2005.
3. K. Moore, C. Brif, M. Grace et al., "Exploring the trade-off between fidelity- and time-optimal control of quantum unitary transformations", ArXiv:quant-ph/1112.0333v1, 2011.
4. I. Maximov, Z. Tošner, N. Nielsen, "Optimal control design of NMR and dynamic nuclear polarization experiments using monotonically convergent algorithms", J. Chem. Phys., **128**, p.184505, 2008.

A spin chain under the pulse conditions as a quantum data channel

M.M. Kutcherov
Institute of Space and Information Technology, Siberian Federal University, 660074, Krasnoyarsk, Russia, MKucherov@sfu-kras.ru

The quantum channel consists of N spin-½ particles sitting at sites 1 to N of a one-dimensional lattice and interacting through the Hamiltonian

$$H = H_{\text{int}} + H_Z = -\frac{1}{2} D \sum_{l=1}^{N-1} \left(\sigma_l^1 \sigma_{l+1}^1 + \sigma_l^2 \sigma_{l+1}^2 + \Delta \sigma_l^3 \sigma_{l+1}^3 \right) - \frac{1}{2} B_m \sum_{l=1}^{N} \sigma_l^3 ,$$

where $J > 0$ is the strength of the exchange interaction, Δ – anisotropy of the system, and $\Delta = -2$ for the secular part of nuclear spin-spin interaction ($\Delta = 0$ for the isotropic XY model). The maximal concurrence C_r (measure of entanglement) after a $(\pi/2)_y$ pulse between two spins sitting on sites i and j, with $|i - j| = r$, reads [1–2, cf. 3]

$$C_r = \max\{0, C_r', C_r''\}, \; C_r' = \tfrac{1}{2}\left(K_r^{22} + K_r^{33} - \sqrt{\left(1 + K_r^{11}\right)^2 - \left(K_i^1 + K_j^1\right)^2} \right), \; C_r'' = \tfrac{1}{2}\left(K_i^1 + K_j^1 + K_r^{11} - 1\right),$$

with correlation functions $K_{ij}^{\eta\eta} = \left\langle \sigma_i^\eta \sigma_j^\eta \right\rangle$, and spin expectation values $K_\eta = \left\langle \sigma_i^\eta \right\rangle$. The term C' is related to the probability for the two considered spins to be in the antiparallel Bell state, and C'' − in parallel Bell state [4]. These results are eventually a consequence of the fact that the dynamical effect of the additional coupling term ($\Delta \neq 0$) is equivalent to that of an overall uniform magnetic field, applied to every spin but for the ones at end-points; which implies that the dynamics still remains restricted to the zero- and single-excitation sectors of the total Hilbert space. When calculating the spectra of correlation functions (spin expectation values) we take into account longitudinal interactions. In the series of transverse interactions we discard the terms in which they lead to a change in z-components, while retain the terms in which transverse interactions lead to correlations between the x-components of neighboring spins. While being in a certain point the transverse component is rotated in a constant field.

Now we concentrate on the transport of quantum correlations across a spin chain. We consider quantum states which can be assigned to individual spectral lines, corresponding to transitions between energy levels. Then one has to use an extra qubit called an "observer" qubit. The Hilbert space of $2m$ neighboring spins has a basis labeled by the 2^{2m} bit strings: $\left| b_{-m} ... b_{-1} b_1 ... b_m \right\rangle, b_j \in \{0,1\}$. The observer qubit I_0 serves for preparation of the pure factor state $I_{0z} I_{\pm 1}^{\alpha/\beta} I_{\pm 2}^{\alpha/\beta} ... I_{\pm m}^{\alpha/\beta}$, where the single-spin eigenfunctions are $\alpha = \left|1/2\right\rangle \equiv 0$ and $\beta = \left|-1/2\right\rangle \equiv 1$. Such a NMR spectral implementation of a quantum computer in liquids was demonstrated [5]. In this case, the array of spins can be modeled by differential equations for quantum coherences:

$$i \frac{d}{dt} \mathbf{x}(t) = \mathbf{v}(\mathbf{x}),$$

where $\mathbf{v}(\mathbf{x}) = (v_{-m}(\mathbf{x}), \ldots, v_m(\mathbf{x}))$ – vector of functions that characterize dynamics, and the initial state $\mathbf{x}(0)$ corresponds to a superposition of all 2^{2m} bit strings. Thus it becomes possible to calculate point-to-point polarization transfer. The ability to increase magnetization via transport of quantum correlations across a spin chain is exciting, since it does not require macroscopic transport of the polarization. It should be possible to polarize a sample more rapidly by transferring spin polarization through entangled quantum correlations. We just mention that the models that have been considered can be experimentally realized in different ways, ranging to atoms loaded into one-dimensional optical lattices that are able to simulate spin Hamiltonians with a very high degree of accuracy [6].

7. U. Glaser, H. Büttner, and H. Fehske, Phys. Rev. A, **68**, 032318, 2003.
8. L. Amico, A. Osterloh, F. Plastina, R. Fazio, and G. Massimo Palma, Phys. Rev. A, **69**, 022304, 2004.
9. M. Kutcherov, *Quantum Informatics 2007*, Proceedings of the Society of Photo-Optical Instrumentation Engineers (SPIE) / Ed. by Ozhigov Yu.I., **7023**, 70230E, 2008.
10. A. Fubini, T. Roscilde, V. Tognetti, et al., Eur. Phys. J. D, **38**, p.563, 2006.
11. R. Das, A. Kumar, J. Chem. Phys., **121**, p.7601, 2004.
12. I. Bloch, J. Dalibard, and W. Zwerger, Rev. Mod. Phys., **80**, p.885, 2008.

A unitary invariant measure of quantum correlations

A.I. Zenchuk
Institute of Problems of Chemical Physics, Russian Academy of Sciences,
Chernogolovka, Moscow reg. 142432, E-mail address: zenchuk@itp.ac.ru

The quantum correlations are known to be responsible for advantages of quantum devises in comparison with their classical counterparts. However, it is still not completely understood what kind of quantum correlations is important. The quantum discord [1, 2] introduced as an alternative (with respect to the entanglement) measure of quantum correlations possesses some disadvantages. For instance, it depends on the subsystem taken for the projective measurements [3]. This is a motivation to introduce a measure of quantum correlations [4], which takes into account correlations in all possible bi-partite decompositions of the given quantum system considered in all possible basis. In result, this measure is invariant with respect to the unitary transformations of the whole system. As a consequence, (i) it is completely defined by the eigenvalues λ_i of the density matrix and (ii) this measure does not evolve. We refer to this measure as the unitary invariant discord. In addition we introduce a modified version of the unitary invariant discord, which is simpler for calculation. The case of two spin-1/2 particles is considered in details. In particular, it is shown that the unitary invariant discord takes its maximal value for a pure state. A geometric measure for the unitary invariant discord is introduced and its simple analytical formula is derived for system of arbitrary number N of spin-1/2 particles:

$$Q = \frac{2^N \sum_{i=1}^{2^N} \lambda_i^2 - 1}{2^N - 1}$$

This simple formula allows one to consider this measure as a witness of quantum correlations. The relation of the unitary invariant discord with the quantum state transfer along the spin chain is considered. We also compare the modified SU(4)-invariant discord with the geometric measure of SU(4)-invariant discord of the two-qubit system in the thermal equilibrium state governed by different Hamiltonians.

1. L. Henderson, V. Vedral, “Classical, quantum, and total correlations”, J. Phys.A: Math and Gen., **34**, pp.6899-6906, 2001.
2. H. Ollivier, W.H. Zurek, “Quantum discord: a measure of the quantumness of correlations”, Phys. Rev. Lett., **88**, 017901, 2001.
3. E.B. Fel’dman, A.I. Zenchuk, “Asymmetry of bipartite quantum discord”, JETP Lett., **93**, pp.459-462, 2011.
4. A.I. Zenchuk, Quantum Inf Process, DOI 10.1007/s11128-011-0319-x.

Quantum correlations in a nanopore filled with a gas of spin-carrying molecules (atoms) in a strong magnetic field

E.B. Fel'dman, E.I. Kuznetsova, M.A. Yurishchev
Institute of Problems of Chemical Physics of the Russian Academy of Sciences, Chernogolovka, Moscow Region, 142432 Russia, E-mail address: kuznets@icp.ac.ru

Entanglement and quantum discord for a pair of nuclear spins $s = 1/2$ in a nanopore filled with a gas of spin-carrying molecules (atoms) are studied [1]. The correlation functions describing dynamics of dipolar coupled spins in a nanopore are found. The dependence of spin-pair entanglement on the temperature and the number of spins is obtained from the reduced density matrix, which is centrosymmetric (CS) [2]. An analytic expression for the concurrence [3] is obtained for an arbitrary CS density matrix. It is shown that the quantum discord [4, 5] as a measure of quantum correlations attains a significant value at low temperatures. It is also shown [1] that the discord in the considered model has a "flickering" character and disappears periodically in the course of the time evolution of the system. The geometric discord [6] is studied for arbitrary 4×4 CS density matrices.

1. E.B. Fel'dman, E.I. Kuznetsova, M.A. Yurishchev, "Quantum Correlations in a System of Nuclear $s = 1/2$ Spins in a Strong Magnetic Field", Phys. Rev. A (in press).
2. J. Weaver, "Centrosymmetric (cross-symmetric) matrices, their basic properties, eigenvalues, and eigenvectors", Amer. Math. Monthly, **92**, p.711, 1985.
3. W.K. Wootters, "Entanglement of Formation of an Arbitrary State of Two Qubits", Phys. Rev. Lett., **80**, p.2245, 1998.
4. L. Henderson, V. Vedral, "Classical, Quantum and Total Correlations", J. Phys. A: Math. Gen., **34**, p.6899, 2001.
5. H. Ollivier, W.H. Zurek, "Quantum discord: A Measure of the Quantumness of Correlations", Phys. Rev. Lett., **88**, 017901, 2001.
6. B. Dakic, V. Vedral, and C. Brukner, "Necessary and Sufficient Condition for Nonzero Quantum Discord", Phys. Rev. Lett., **105**, 190502, 2010.

Random telegraph noise diagnostics of nanowire SOI MOSFETs

A.N. Nazarov[1], I. Ferain[2], R. Yu[2], A. Kranti[2], P. Razavi[2]

1. *Institute of Semiconductor Physics, 41 Prospect Nauki, 03028, Kyiv, Ukraine, nazarov@lab15kiev.ua*
2. *Tyndall National Institute, Cork, Ireland, isabelle.ferain@tyndall.ie*

In nanowire MOSFETs dielectric/semiconductor interface affects very strongly on electrical properties of the devices such as mobility, channel current fluctuations and others. In these devises charge trapping in single trap located near the interface results in strong changing of channel current and initiation of random telegraph noise (RTN) in the drain current. Study of RTN drain current amplitude (DCA) and combination of the RTN DCA vs. gate voltage (V_G) characteristic with I_D-V_G one allow us to characterize quality of interfaces of studied devices and extract field effect mobility of charge carriers without knowledge of gate dielectric capacitance, which is not measurable value in such devices. Thus the paper considers a RTN in nanowire multigate (MuG) SOI MOSFETs fabricated as a standard inversion mode (IM) device and a new promising junctionless (JL) device [1].

Multigate silicon NW n-type MOSFETs with pi-gate architecture were fabricated on UNIBOND® silicon-on-insulator wafers (see Fig. 1a and 1b). The width and thickness of the devices is near 10 nm and the gate length is 1 μm. The gate oxide and buried oxide (BOX) thickness are 7 nm and 340 nm correspondingly. The JL MOSFET has uniform n-type doping concentration of $1x10^{19}$ cm^{-3} in the source, drain and channel regions (Fig. 1c). "Standard" IM pi-gate MOSFET have the same dimensions as the JL devices but have a p-type channel doping concentration of $2x10^{18}$ cm^{-3} and an n-type doping concentration of $1x10^{20}$ cm^{-3} in the source and drain regions (Fig. 1d). The JL MOSFETs have a P^+-polysilicon gate electrode and the IM devices have an N^+- polysilicon gate.

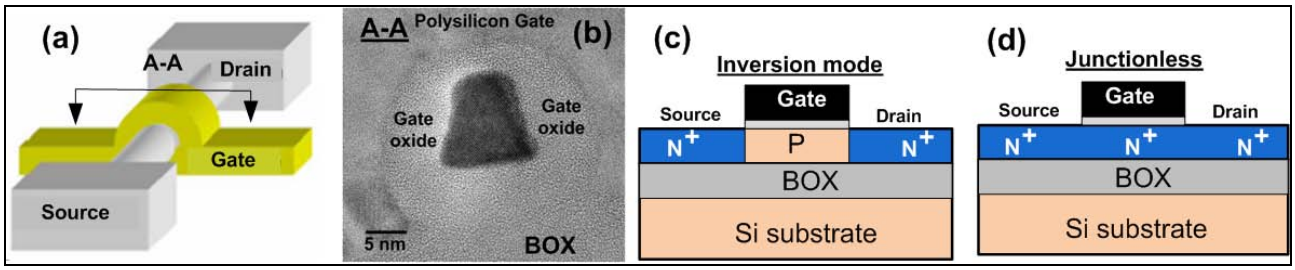

Fig. 1. Schematic view of architecture of the MOSFETs (a) and HRTEM photograph of the A-A section of the device (b). Schematic view of doping in the inversion-mode (c) and junctionless (d) n-channel devices.

The RTN both in IM and JL MOSFETs was measured at gate voltage values significantly higher than the threshold voltage (V_{TH}). The RTN DCA, the average capture time ($<\tau_c>$) of traps and average emission time ($<\tau_e>$) from traps versus gate voltage, drain voltage and temperature were studied. Considerable smaller emission time and relative amplitude of RTN were observed in JL devices than in IM MOSFETs. The inverse relationship of the relative amplitude of the RTN and the applied gate voltage both for IM and JL devices was demonstrated which suggests that the RTN appears in the JL MOSFET when V_G is high enough to form an accumulation layer at the SiO_2-Si interface. The measurements show that JL nanowire devices reveal considerable smaller relative RTN DCA and number of RT signals than IM nanowire MOSFETs. This is associated with location of main charge carriers inside of the Si nanowire and their weak interaction with the gate dielectric/Si layer interface.

Measurement of the $<\tau_c>$ and $<\tau_e>$ in dependence on gate voltage allows us to estimate the energetic and geometrical location of the trap levels responsible for the charge trapping and creation the RTN in the gate oxide, which was E_C-E_T = 3.05 eV in SiO_2 band gap for the JL device and 2 nm and 2.9 nm from SiO_2-Si interface for IM and JL devices, respectively.

The method of field effect mobility extraction with taking into account parasitic resistance of the source and drain regions is discussed both for IM and JL MOSFETs.

1. C. W. Lee, A. Afzalian, N. Dehdashti Akhavan, et al., "Junctionless multigate field-effect transistor", Appl. Phys. Lett., **94**, pp. 053511, 2009.

SOI structure with Si-nanoclusters embedded in the oxide layer prepared by low-dose co-implantation

V. Litovchenko, B. Romanyuk, V. Melnik, O. Oberemok, V. Popov, A. Sarikov
V. Lashkarev Institute of Semiconductor Physics, NAS of Ukraine, Kiev, Ukraine, lvg@isp.kiev.ua

One of the most developed technology for the fabrication of the important in microelectronics layered structures "semiconductor on insulator" (SOI) is the SIMOX procedure, which includes high voltage and high dose oxygen implantation. The disadvantages of this technique are its complexity, high cost, use of complicated annealing steps etc.

We have proposed earlier a new implementation of this technique, which provides due to the co-implantation of oxygen and carbon (or other small size ions, such as N, Al etc.) a substantial decrease in the dose and the energy of oxygen ions due to some physical effects: 1) redistribution of implanted oxygen in deeper or more shallow "skin" region of the front side semiconductor region; 2) condensation of oxygen atoms in the vacancy enriched layer created by carbon and hence the decrease of oxygen doses, which are critical for the creation of high quality SiO_2 dielectric. We call this procedure enhanced inner-Si stimulated oxidation (ESO). In this way, a good quality stoichiometrical SiO_2 layers with a thickness of 100 to 400 Å and Si upper film of the same or higher thicknesses could be obtained.

In this presentation we propose the new procedure to that discussed above. Namely, we create the oxygen enriched layer with oxygen deficiency comparing to perfect SiO_2 formation. The mass spectroscopy and Auger depth analysis demonstrate the oxygen redistribution to the layer of C localization (and to vacancy enriched layer too). TEM and AFM investigations as well as measurements of photoluminescence (PL) spectra show the formation of Si nanoclusters distributed by the programmed way in different depths. The details of technology are presented below.

P-type Si (100) samples, ρ=10 Ohm·cm, were implanted with O^+ at the energy of 125-150 keV and doses of $(1\text{-}3)\cdot10^{17}$ cm^{-3}. Then samples were implanted with C^+ at the energy of $(0.3\text{-}1)\cdot10^3$ keV and doses of $(0.2\text{-}1)\cdot10^{16}$ cm^{-2}. The furnace and radiation annealing (RTA) were realized at temperatures of 1050-1200°C in Ar atmosphere.

Measurements of PL spectra as well as impurity depth distribution by mass-spectrometry, C(V), and X-ray spectroscopy (to reveal mechanical stresses) have been performed.

PL spectra demonstrate the following peculiarities: 1) appearance of narrow peak in the UV region. We attribute this peak to the C-containing complexes of carbo-oxysilicides SiO_xC_y; 2) IR peak, which is mainly determined by non- compensated dangling bonds on the surface and in the bulk of crystalline Si nanoclusters i. e. "defect" radiative centers; 3) the most distinguished is the peak in the middle-energy region known to correspond to the "intrinsic" recombination mechanism in irradiated nanosized Si, in first approximation depending on the thickness *d* as

$$E_R = E_{go} + \Delta E = E_{go} + L/(d - d_0)^2 \qquad (1)$$

From (1) the size of Si nanoclusters, its dependence on the C^+ dose, and dose dependence of PL intensity can be estimated. The received values are in accordance with direct TEM data.

In conclusion we summarize:

4. ESO technology is capable to create SOI structures in economical regimes with control of the thicknesses of Si and SiO_2 layers and providing high quality of layers and interfaces, as well as high intensity of intrinsic PL.
5. Obtained Si nanoclusters have smaller sizes and size dispersion, and improved structure (as proved by the X-ray investigations, measurements of PL spectra etc.) as compared to the conventional technique.
6. The technology is energy and time saving. The mechanism behind the technology was discussed in the framework of the model of C catalytic stimulation, in which the carbon atoms enhance oxidation and collection of Si atoms in nanoclusters with subsequent crystallization of Si during annealing.

Quantum noise in field-effect nanotransistors

V. Vyurkov, S. Filippov, I. Semenikhin, A. Orlikovsky
Institute of Physics and Technology, Russian Academy of Sciences, Moscow, Russia, vyurkov@ftian.ru

Current noise is one of the major characteristics of a transistor required for its practical application. Along with the shot noise and the Johnson–Nyquist noise well-known far before, an especial quantum excess noise was revealed in nanotransistors at zero temperature T=0 [1]. Lately, a general expression to calculate the current noise for an arbitrary temperature and a voltage was derived [2]. That expression could be used in the same simulation of a field-effect transistor based on the Landauer-Buttiker approach.

The general idea of derivation was guided by the current theory of quantum measurements. Indeed, the source and drain contacts measure the state of an electron in the channel. The wave function could collapse in one contact or in another, contributing or not contributing to the current. The calculation of quantum noise allows for the Fermi-Dirac statistics, transmission coefficients, and the Pauli exclusion principle. Just that principle establishes the statistical correlations between the source and drain contacts absent in classical description. For zero bias the resultant expression gives rise to the Johnson–Nyquist noise in quantum limit. This noise is also roughly proportional to the temperature. For a non-zero drain bias there is a blend of the Johnson–Nyquist noise and the shot noise (including the excess quantum noise).

The goal of present communication is to reveal how random impurities in the channel affect the noise. In Figs. 1 and 2 there are depicted the current and the renormalized noise $I_n^2 / e\Delta\nu$, where $\Delta\nu$ is a bandwidth. Upper curves correspond to classical regime as the lower ones correspond to quantum regime. In Fig. 1 a single random impurity was inserted in the channel as well as in Fig. 2 there were two of them. To avoid misunderstanding it should be noted that a positively charged impurity shifts the threshold voltage, therefore, all currents in Fig. 2 are greater compared to that in Fig. 1.

In classical regime the transmission coefficient can acquire only two values: 0 and 1, and the Pauli exclusion principle is ignored. The thermal (Johnson–Nyquist) noise is clearly visible at zero drain voltage. For higher drain voltage the current and renormalized shot noise coincide for classical calculations. In the quantum limit they diverge. Comparison of curves results in the estimation of the mean quantum transmission coefficient for conducting electrons which turns out to be about 0.7 for the sample structure.

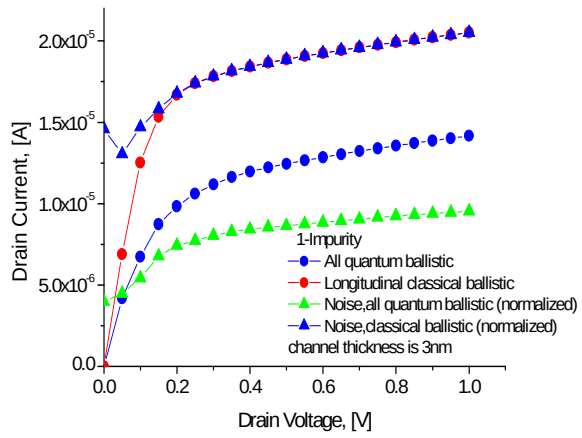

Fig. 1. Classical ballistic current and renormalized classical noise (upper lines), quantum ballistic current and renormalized quantum noise (lower lines) for one random impurity in the channel.

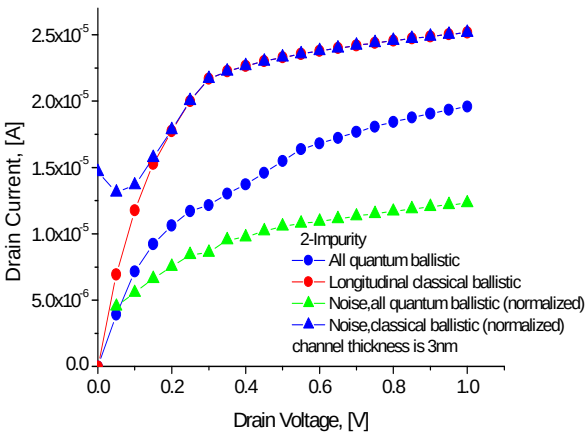

Fig. 2. The same as in Fig. 1 for two random impurities in the channel.

The work was supported by the Russian Foundation for Basic Research (grants # 11-07-00464-a and #12-07-90011-Bel_a).

1. G. B. Lesovik, JETP Lett., **49**, p.594, 1989.
2. V. Vyurkov, I. Semenikhin, S. Filippov, A. Orlikovsky, Solid-State Electronics, **70**, pp.106–113, 2012.

Revision of interface coupling in ultra-thin body SOI MOSFETs

T. Rudenko[1], A. Nazarov[1], V. Kilchytska[2], and D. Flandre[2]
1. Institute of Semiconductor Physics, National Academy of Sciences of Ukraine, Kyiv, Ukraine; tamara@lab15.kiev.ua
2. ICTEAM Institute, Université catholique de Louvain, 1348 Louvain-la-Neuve

The fully depleted (FD) ultra-thin-body (UTB) SOI MOSFET with low-doped or undoped channel is presently considered as one of the best candidates for nano-scaled CMOS technologies [1]. A fundamental property of any FD SOI MOSFET, affecting the device characteristics, is the effect of the charge coupling between the front and back SOI interfaces [2]. The interface coupling is also widely used for characterization purposes. Besides, the interface coupling lies at the basis of the back-gate controlled schemes. Thus an adequate understanding of the behavior of the interface coupling in UTB SOI MOSFETs is of crucial importance. The main manifestation of the interface coupling in a FD SOI MOSFET is the modulation of the threshold voltage at one gate by the opposite gate bias, which is usually described by the classical Lim-Fossum model [2]. According to this model, the threshold voltage in a FD SOI MOSFET varies linearly on the back-gate gate as long as the back silicon film interface is depleted and saturates with strong accumulation or inversion at the back interface. In accordance to the Lim-Fossum model, the slope of the linear region of the coupling curves is determined by the structure capacitances, and thus it is frequently used for the evaluation of the silicon film thickness. Several publications reported the deviations from the Lim-Fossum model in the case of UTB SOI MOSFETs [3],

For better understanding the behavior of interface coupling in UTB SOI MOSFETs, in this work we revise the classical Lim-Fossum model [2], using 1-D numerical simulations in both classical and quantum-mechanical modes and their comparison with experimental data. It is demonstrated that the behavior of interface coupling in UTB SOI MOSFETs has two distinctions from the Lim-Fossum model. The first is an increased threshold voltage shift with opposite gate bias (*i.e.*, an increased slope of the coupling curves), which originates mainly from the field-induced quantum-mechanical (QM) effects. This QM effect is caused by the variation of the electric field in the Si film at threshold, resulting in the variation of the electrical confinement. It is well-marked even in rather thick-film (>10 nm) SOI devices, whose threshold voltage is usually considered to be unaffected by quantization effects, though it is stronger for thinner films. The second is significant extending of the linear region of the coupling curve compared to the Lim-Fossum model. It is demonstrated that there are three factors contributing to this effect. The first consists in the fact that the surface potential at threshold conditions in thin-film moderately or low-doped SOI MOSFETs significantly exceeds $2\varphi_F$ (where φ_F is the Fermi potential in the semiconductor body), and, in addition, it increases with opposite gate bias. The second (coupled to the first) is that the accumulation surface potential needed for stabilization of the potential and carrier distributions in the silicon film (which means interface de-coupling and saturation of the coupling curve) significantly differs from the conventionally assumed 0 V. The third factor contributing to the extended range of the linear region of coupling curves in UTB SOI MOS is related to QM effects. These findings should be taken into account in the analysis, characterization and modeling of advanced UTB SOI MOSFETs. Taking into consideration the foregoing findings, a revised analytical model of interface coupling valid for UTB SOI MOSFETs is derived. The presented model is validated by numerical simulations and experimental results.

This work is supported in part by National Academy of Science of Ukraine in the framework of the project No. 39-02-12/1.

1. H-S.P. Wong, D.J. Frank, P.M. Solomon, “Device design considerations for double-gate, ground-plane, and single-gated ultra-thin SOI MOSFET's at the 25 nm channel length generation”, IEDM Tech. Dig., pp. 407-410, 1998
2. H.K. Lim, J. G. Fossum, “Threshold voltage of thin-film silicon-on-insulator (SOI) MOSFETs”, IEEE Trans. Electron Dev. **30**, pp. 1244-1251, 1983
3. S. Eminente, S. Cristoloveanu, R. Clerc, A. Ohata, G. Ghibaudo, “Ultra-thin fully-depleted SOI MOSFETs: special charge properties and coupling effects”, Sol. State El., **51**, pp.239-244, 2007

Noise characteristics of nanoscaled SOI MOSFETs

N. Lukyanchikova[1], N. Garbar[1], V. Kudina[1], A. Smolanka[1], E. Simoen[2], C. Claeys[2,3]
1. V. Lashkaryov Institute of Semiconductor Physics, National Academy of Science of Ukraine, Kiev, Ukraine, kudinavaleriya@isp.kiev.ua. 2. Imec, Leuven, Belgium. 3. KU Leuven, Leuven, Belgium

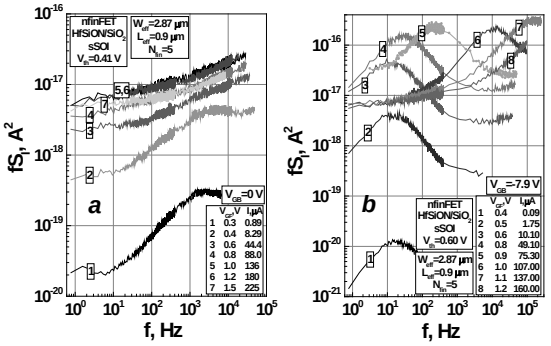

Fig. 1. Noise spectra $[f \times S_I(f)]$ for sSOI HfSiON-*n*finFET, measured for V_{GF}=*var* and V_{GB}=0 V (a) and V_{GB}=-7.9 V (b); V_{th} is the threshold voltage.

The low-frequency noise performance of advanced SOI tri-gate Metal-Oxide-Semiconductor Field-Effect-Transistors (finFETs) with $HfSiON/SiO_2$ (equivalent oxide thickness t_{EOT}=1.5 nm) and HfO_2/SiO_2 (t_{EOT}=1.9 nm) gate dielectrics are investigated in linear operation at front interface (drain voltage V_{DS}=25 mV) for back-gate voltage V_{GB}=0 V or in accumulation $V_{GB}=(V_{GB})_{acc}$. The influences of the gate stack material, stressor technique (biaxial sSOI and uniaxial CESL) and fin length L_{eff} and width W_{eff} on noise characteristics are revealed. The procedure of finFET parameters evaluation based on noise study is developed.

Fig. 1a shows the noise spectra $S_I(f)$ multiplied by the frequency f of a sSOI $HfSiON/SiO_2$-*n*finFET measured for different front gate voltages V_{GF} at V_{GB}=0 V. It was found that the demonstrated shape of noise spectra for which $S_I(f) \sim 1/f^{\gamma}$, where γ=(0.7 – 1), is typical for all finFETs investigated. The analysis showed that the $1/f^{\gamma}$ noise discussed is of the McWhorter type [1], which ascribed fluctuations to the exchange of free charge carriers in the channel with traps in the gate oxide. Evaluated trap concentrations N_{ot} appear to decrease typically with increasing distance x from the Si/SiO_2 interface (Fig. 2); moreover, it was found that the dependencies $N_{ot}(x)$ are influenced by the gate dielectric material (curves 1 and 4), stressor techniques (curves 1 and 2) and channel width (curves 2 and 3).

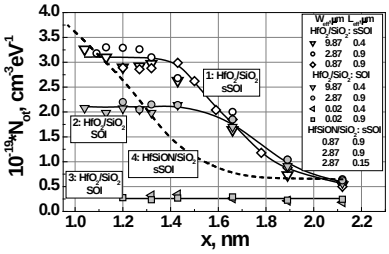

Fig. 2. Distribution $N_{ot}(x)$ for the sSOI (1,4) and SOI (2,3) HfSiON-(4) and HfO_2-*n*finFETs (1,2) of $W_{eff} \geq 0.87$ μm (1,2,4) and HfO_2-*n*finFETs of W_{eff}=0.02 μm (3).

Fig. 1b shows noise spectra $[f \times S_I(f)]$ measured when the accumulated back-gate voltage is applied which is found to be typical for all finFETs studied. Two types of Lorentzian components for which $S_I(f)=S_I(0)/[1+(2\pi f\tau)^2]$, where $S_I(0)$ is the Lorentzian plateau, $\tau=(2\pi f_0)^{-1}$ is a time constant, f_0 is turn-over frequency, are revealed: 1. Back-gate-induced (BGI) Lorentzians [2] are observed when the front interface is biased in depletion/weak inversion; their noise plateau $[S_I(0)]_{BGI}$ increases with increasing V_{GF} while $\tau_{BGI} \neq \tau_{BGI}(V_{GF})$ (curves 1-3); 2. Linear kink effect (LKE) Lorentzians [2] are found when the front interface is biased in strong inversion; their parameters $[S_I(0)]_{LKE}$ and τ_{LKE} decrease with increasing V_{GF} (curves 4-8). The analysis of the observed Lorentzians allowed to develop the procedure to determine the following values: 1. electron-valence-band tunneling current densities j_{EVB} flowing through the front gate oxide (Fig. 3, SEG means Selective Epitaxial Grown source/drain regions, $m' \approx 1$); 2. body-source capacitance $(C_{eq}/m'\beta^2)$, where β is the body factor (Fig. 4); 3. mobility of free carriers in the channel. The influences of dielectric type and strain in the channel are also analyzed (Fig. 3 and 4).

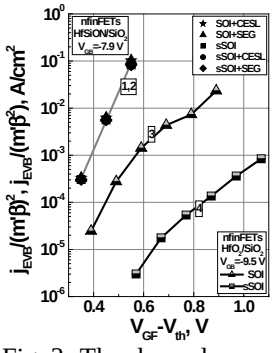

Fig. 3. The dependences of $[j_{EVB}/(m'\beta)^2]$ and $[j_{EVB}/m'\beta^2]$ on $(V_{GF}-V_{th})$ for SOI (1,3) and sSOI (2,4) HfSiON- (1,2) and HfO_2-*n*finFETs (3,4), respectively.

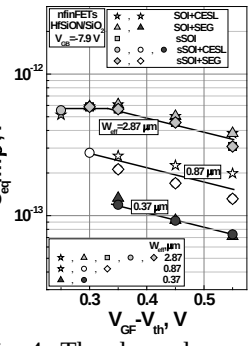

Fig. 4. The dependences of $(C_{eq}/m'\beta^2)$ on $(V_{GF}-V_{th})$, evaluated for HfSiON-*n*finFETs.

1. E. Simoen, C. Claeys, "On the flicker noise in submicron silicon MOSFETs", Solid-State Electron, **43**, pp. 865–882, 1999

2. N. Lukyanchikova, N. Garbar, A. Smolanka, M. Lokshin, E. Simoen, C. Claeys, "Origin of the front-back-gate coupling in partially depleted and fully depleted silicon-on-insulator metal-oxide-semiconductor field-effect transistors with accumulated back gate", J. Appl. Phys., **98**, pp. 114506–114506-11, 2005

Threshold voltage of advanced MOSFETs: Physical criteria and experimental extraction methods

T. Rudenko[1], A. Nazarov[1], V. Kilchytska[2], and D. Flandre[2]
1. Institute of Semiconductor Physics, National Academy of Sciences of Ukraine, Kyiv, Ukraine; tamara@lab15.kiev.ua
2. ICTEAM Institute, Université catholique de Louvain, 1348 Louvain-la-Neuve

The threshold voltage (V_{TH}) is a fundamental parameter for any MOSFET, characterizing the transition from weak to strong inversion, *i.e.*, from the exponential to linear charge control regimes. Thus accurate and reliable determination of the V_{TH} value is very important for CMOS design and modeling, and becomes increasingly important as the gate oxide thickness as well as power supply voltage scale down. Traditionally, the threshold voltage of a MOSFET has been defined as gate voltage needed to provide the critical surface potential equal to twice the Fermi potential in the semiconductor body. However, this V_{TH} criterion is inadequate in the modern MOSFETs featuring ultra-thin or high-*k* gate dielectrics [1], and it is meaningless in the case of advanced silicon-on-insulator (SOI) MOSFETs with undoped silicon body [2]. Thus a variety of different threshold criteria have been proposed for these devices [1], [2]. As a result, the V_{TH} value turns out dependent on the particular V_{TH} criterion [2]. Presently there are many V_{TH} determination methods, which differ by the underlying V_{TH} criteria, extraction procedures and sensitivity to parasitic effects. Thus it is highly desirable to have a clear physical understanding of these methods.

In this work, we review the existing V_{TH} criteria and demonstrate that, in case of nano-scale MOSFETs with ultra-thin gate dielectrics or/and undoped SOI thin body, featuring gradual transition between weak and strong inversion, the most physically adequate V_{TH} criteria are: (i) the maximum of the second derivative of the inversion charge with respect to the gate voltage (d^2Q_{inv}/dV_g^2), corresponding to the inflection point in the rate of the inversion charge growth, and (ii) the equality between the drift and diffusion drain current (I_D) components, $I_{diff}=I_{drift}$. The experimental methods for the V_{TH} extraction based on these criteria are examined. Particular attention is given to the recently proposed method, using the transconductance-to current ratio (g_m/I_D), in which V_{TH} is evaluated from the gate voltage of the minimum of the $d(g_m/I_D)/dV_g$ versus gate voltage function [3]. Using analytical modeling, it is shown that the V_{TH} criterion of the $d(g_m/I_D)/dV_g$ method is the maximum of d^2Q_{inv}/dV_g^2, just as of the popular transconductance change method, in which V_{TH} is defined from the position of the maximum of the transconductance derivative ($dg_m/dV_g \equiv d^2I_d/dV_g^2$) [4]. However, though dg_m/dV_g and $d(g_m/I_D)/dV_g$ methods rely on the same V_{TH} criterion, they feature different sensitivity to the mobility variation with gate voltage and drain voltage value. With analytical modeling and experimental data for advanced SOI FinFETs and ultra-thin-body SOI MOSFETs, it is demonstrated that the $d(g_m/I_D)/dV_g$ method is much less sensitive to the V_g-dependent mobility and drain voltage value, and thus is more reliable than the dg_m/dV_g method. Furthermore, it is found that at the point of the minimum of $d(g_m/I_d)/dV_g$, at vanishingly small drain voltage and ideal MOSFET operation, the value of g_m/I_d is equal to 2/3 of its maximum value. This can be used as alternative quick method for the V_{TH} extraction corresponding to the criterion of the maximum of d^2Q_{inv}/dV_g^2. At the same time, at the condition $I_{diff}=I_{drift}$, the ratio of g_m/I_d to its maximum value is found to be 1/2. The difference between the two V_{TH} extractions in the ideal MOSFET is estimated to be ~1.2 kT/q. However, such V_{TH} extractions are possible only when the $g_m/I_d(V_g)$ curve has a clearly defined plateau in the range of the maximum, whereas it is frequently distorted, for example, due to gate-induced drain leakage current, short-channel effects, or V_g-dependent mobility. Thus the $d(g_m/I_d)/dV_g$ method seems to be more preferable.

This work is supported in part by National Academy of Science of Ukraine in the framework of the project No. 39-02-12/1.

1. C.-H. Shih, J.-S. Wang, "Threshold voltage of ultrathin gate-insulator MOSFETs", IEEE Electron Dev. Lett., **30,** pp. 278-280, 2009
2. F.J. Garcıa Sanchez, A. Ortiz-Conde, J. Muci, "Understanding threshold voltage in undoped-body MOSFETs: An appraisal of various criteria", Microelectronics Reliability, **46**, pp.731–742, 2006
3. D. Flandre, V. Kilchytska, T. Rudenko "g_m/I_d method for threshold voltage extraction applicable in advanced MOSFETs with non-linear behavior above threshold", IEEE El. Dev. Lett., **31**, pp.930-932, 2010
4. H.S. Wong, M.H. White, T. J. Krutsick, R.V. Booth, "Modeling of transconductance degradation and extraction of threshold voltage in thin oxide MOSFET", Solid-State Electron., **30**, pp. 953-968, 1987.

Electrical Characterization of High-k Gate Dielectrics for Future CMOS Technology

Y.Y. Gomeniuk[1,*], Y.V. Gomeniuk[1], A.N. Nazarov[1], I.P. Tyagulskii[1], V.S. Lysenko[1], K. Cherkaoui[2], S. Monaghan[2] and P. K. Hurley[2]

1. *Lashkaryov Institute of Semiconductor Physics, NAS of Ukraine, Kyiv, Ukraine, * ygomeniuk@gmail.com*
2. *Tyndall National Institute, University College Cork, Lee Maltings, Prospect Row Cork, Ireland*

Searching for ultrathin gate dielectric materials is one of the major challenges associated with further downscaling in CMOS technology. High-κ dielectrics can be grown thicker providing the same EOT and significantly reduced gate leakage currents. However, high-κ materials often suffer from the charge trapping and poor electrical quality of the dielectric-semiconductor interface [1, 2]. Transition metal and rare-earth metal oxides have been considered as perspective materials to replace SiO_2 for future CMOS.

We present the results of electrical characterization for high-κ dielectrics, including Hf, Gd and Nd oxides, ternary compounds ($LaLuO_3$) and silicate ($LaSiO_x$), epitaxially grown on Si substrates. Al, NiSi, TiAlN, TiN, Pt used as top metal gate of MOS stacks. Both *p*- and *n*-MOSFETs with high-κ gate oxide were fabricated on UTB SIMOX SOI wafers (t_{BOX}=150 nm). The channel length and width were 1 μm and 50 μm, respectively.

The conductance-frequency (*G*-*ω*) measurements allow to determine the interface state density (D_{it}) using the classical approach of Nicollian and Goetzberger [3]. In the case of leaky dielectric layers, the results of both capacitance-voltage (*C*-*V*) and *G*-*ω* measurements require correction, as described in [4]. Fig. 1 shows the D_{it} distribution over Si bandgap for *n*- and *p*-type samples with 10 nm $LaSiO_x$ dielectric layer. The D_{it} distribution near the edges of bandgap was obtained using Gray-Brown technique [5].

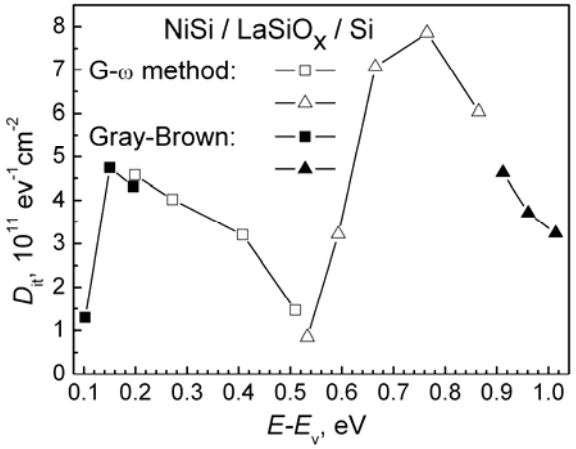

Fig. 1. D_{it} distribution over the Si band gap determined by *G*-*ω* and Gray-Brown methods.

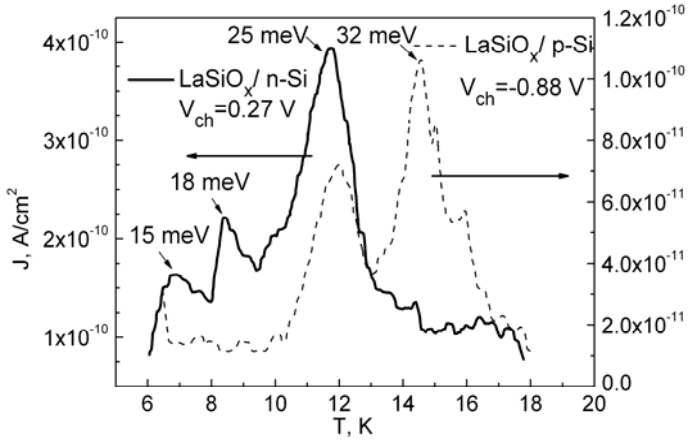

Fig. 2. Low-temperature thermally stimulated current (TSC) spectra after filling the electron (solid) and hole (dash) traps.

The TSC spectra (Fig.2) revealed the presence of shallow electron and hole traps with activation energies ranging from 15 to 32 meV near the silicon conduction and valence band edges. The concentration of traps is 2.6×10^{11} cm^{-2} for the electron traps and 4.7×10^{10} cm^{-2} for the hole traps.

SOI MOSFETs with $LaLuO_3$ (20 nm thick) gate oxide demonstrated feasibility of $LaLuO_3$/TiN gate stack. The subthreshold slope of 100 mV/dec for *p*-MOSFET and 90 mV/dec for *n*-MOSFET was obtained.

1. H. Wong, H. Iwai, "On the scaling issues and high-κ replacement of ultrathin gate dielectrics for nanoscale MOS transistors", Microelectronic Engineering, **83**, pp. 1867-1904, 2006

2. O. Engström, B. Raessi, S. Hall, O. Buiu, M.C. Lemme et al., "Navigation aids in the search for future high-κ dielectrics: physical and electrical trends", Solid-State Electronics, **51**, pp. 622-626, 2007

3. E.H. Nicollian and A. Goetzberger, "MOS conductance technique for measuring surface state parameters", Appl. Phys. Lett., **7**, pp. 216-219, 1965

4. Y. Gomeniuk, A. Nazarov, Ya. Vovk, Yi Lu, O. Buiu, S. Hall, J.K. Efavi, M.C. Lemme, "Low-temperature conductance measurements of surface states in HfO_2-Si structures with different gate materials", Mat. Sci. in Semicond. Processing, **9**, pp. 980-984, 2006

5. P. V. Gray and D. M. Brown, "Density of SiO_2-Si interface states", Appl. Phys. Lett., **8**, pp. 31-33, 1966

The mobility models for TCAD simulation of extremely thin nanoscale SOI MOSFETs

Y. Chaplygin, A. Krasjukov, T. Krupkina, I. Titova
National Research University of Electronic Technology, Moscow, Russia, ieem@miee.ru

Problems with the further miniaturization of the basic element of silicon electronics, the bulk MOS transistor, make it preferable to use the fully depleted SOI MOSFET with ultra-thin bodies. The advantages of such structures are the control of short-channel effects and the reduction of the mobility degradation in the case of an undoped channel. Thus, the long-term use of SOI MOSFETs is expected not only as elements of special integrated circuits suitable for operation in extreme environment, but also as the main element of mainstream semiconductor products. Analysis of the characteristics of SOI MOSFETs as a key element of various types of integrated circuits can be successfully performed by using an environment of virtual manufacturing, namely, TCAD Synopsys software platforms [1], under the condition of the selection and calibration of the appropriate models. One of the most important parameters in these structures is the carrier mobility in the channel within extremely thin Si layer.

However, the transition to nanoscale transistors using the traditional route of process-device simulation becomes problematic. In particular, it does not take into account the roughness of the interface Si/SiO_2, which leads to inaccuracies in the assessing the dependence of the mobility of the charge density in the channel [2]. For SOI MOS structures formed in extremely thin films, the contribution of this error may be significant, especially under condition of the high field saturation. The features of the choice of mobility models for the simulation of SOI MOSFETs structures with undoped silicon as the active region were analyzed. The electrical characteristics of the extremely thin SOI MOSFETs structure (pic.1) were simulated with Synopsys Sentaurus Device tool using the hydrodynamic model. The simulated structure includes an intrinsic SOI body with thickness 8.6 nm, SiON gate oxide with thickness 1.1 nm and $\varepsilon = 4.8$. The effective channel length is 38 nm. Experimentally determined series resistance of source/drain regions [3] were used during the device simulation. The analysis showed that the main factors controlling the mobility are the surface contribution due to acoustic phonon scattering and surface roughness scattering. More fine adjustment was carried out using the energy relaxation time τ_{ec} (pic.1,b) according to the high field mobility degradation by the Meinerzhagen-Engl model.

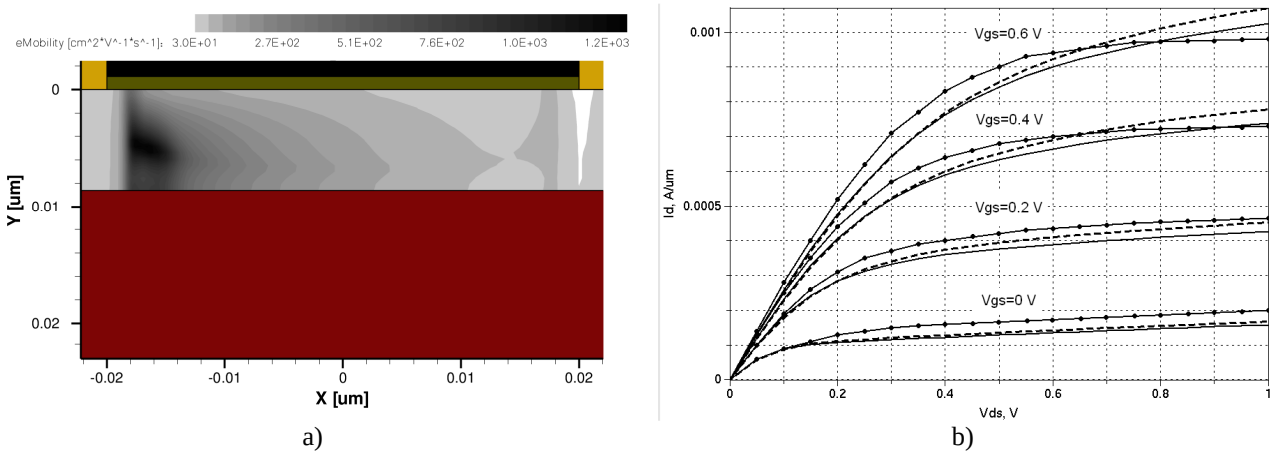

a) b)

Fig. 1 The results of extremely thin SOI MOSFET TCAD simulation: a – the 2D distribution of electron mobility at Vgs=0.6 V, Vds=1.0 V; b - I-V characteristics (•—• experiment [3], — τ_{ec}=0.2 ps, --- τ_{ec}=0.15 ps)

1. http://www.synopsys.com
2. T. Krupkina, D. Rodionov, I. Titova, A. Shvetz, "An account of the Si/SiO_2 interface roughness for simulation of nanoscale MOS transistors", Proc. Int. Conf. “Opto-, nanoelectronics, nanotechnology and Microsystems”, Ulyanovsk, 2011, pp.454-455.
3. Y. Liu, M. Luisier, A. Majumdar, D. Antoniadis, M. Lundstrom, “On the interpretation of ballistic injection velocity in deeply scaled MOSFETs”, IEEE Trans. on Electron Devices, **59**, pp.994-1001, 2012.

SOI CMOS RadHard SRAM 256K, 1M, and 4M

N. Alieva[1], A. Belous[1], V. Bondarenko[2], L. Dolgyi[2], E. Lozitskyi[1], S. Soroka[1], G. Usov[1], A. Turzevich[1], S. Shvedov[1]

6. "Integral" Join Stock Company, Minsk, Belarus, E-mail address: office@bms.by 2. Belarussian State University of Informatics and Radioelectronics, Minsk, Belarus, E-mail address: vitaly@bsuir.edu.by

CMOS static random access memory (SRAM) is a field of industrial interest for "Integral" Join Stock Company. Bulk silicon wafers are used by "Integral" to fabricate CMOS SRAM for civilian applications. To produce CMOS SRAM for military and aerospace applications it is reasonable to use Silicon-On-Insulator (SOI) structures instead of bulk silicon wafers. SOI structures together with special schematic designs and technological solutions provide high information capability and radiation hardness of CMOS SRAM. "Integral" developed RadHard CMOS SRAM for aerospace and military systems requiring reliable high performance solutions for radiation intense environments.

In this paper the main efforts of "Integral" on the way from the applied research to industrial production of RadHard SOI CMOS SRAM 256K, 1M and 4M are presented and discussed.

To produce RadHard CMOS SRAM 256K, 1M and 4M we use commercial SIMOX and Unibond SOI structures and specially designed 0.8 µm, 0.5 µm and 0.35 µm technological processes. Memory cell of SRAM consists of six MOS transistors and a lightly doped drain structure is used for improved short channel reliability. To provide high radiation hardness a number of schematic designs and technological solutions are used: (a) introducing of resistor-capacity circuits in memory cells; (b) topological symmetry of memory cells; (c) applying of potentials to the walls of MOS transistors and substrate of SOI structure; (d) introducing of highly doped regions to prevent inversion in p-type walls; (e) doping engineering of silicon at the interface with silicon oxide, etc. Family of RadHard CMOS SRAM offers the performance, weight and size needed in critical aerospace and military missions. The designed topologies of memory cells of RadHard SOI CMOS SRAM are protected by certificates of Russian Federation. All memory products are certificated and passed special radiation tests. The SOI CMOS SRAM will not latch up due to any of the radiation exposure conditions (presented in the table) when applied under recommended operating conditions.

Main parameters of RadHard SOI CMOS SRAM products of "Integral"

Parameters	SOI CMOS SRAM products		
	256K (32Kbit x 8)	1M (128Kbit x 8)	4M (512Kbit x 8)
Die size, mm	9 x 8.5	9.5 x 9.5	14 x 11
SRAM cell size, µm	11 x 18	6.2 x 9.7	5 x 8
Voltage, V	5.0	5.0/ 3.3	3.3
SEU, errors/bit-day	10^{-10}	10^{-10}	10^{-10}
Total dose, Rad(Si)	10^{6}	10^{6}	10^{6}
Neutron hardness, cm^{-2}	10^{14}	10^{14}	10^{14}
Dose rate survivability, Rad(Si)/s	10^{12}	10^{12}	10^{12}

RadHard SOI CMOS SRAM products of "Integral" Joint Stock Company offer high levels of integration, performance, low power dissipation and will be available for sell at the end of 2012 (http://www.integral.by).

Carrier mobility in SOI layers with bonded interface

O.V. Naumova, B.I. Fomin, V.P. Popov
Institute of Semiconductor Physics, Russian Academy of Sciences, Novosibirsk, Russia, naumova@isp.nsc.ru

Silicon on insulator (SOI) is well-known material system for high-speed electronics and for advanced Si devices. Silicon strips or nanowires (NWs) fabricated by lateral structuring of the top silicon layer can be used as a metal-oxide-semiconductor field-effect transistor body with alternative designs of multiple-channel and multiple-gate transistors, single-electron transistors with side gates (made in the same silicon layer in which the transistor body was formed). SOI nanowires with free surface and with ohmic contacts on their ends can be used as highly effective field-effect sensing elements, etc.

Silicon layer may has two interfaces with dielectrics in these structures: (1) the bonding interface; (2) the interface formed by thermal oxidation. A set of factors determines the electric properties of devices based on Si nanolayers: states at the Si/SiO_2 interfaces, properties of dielectrics, properties of the initial Si, methods of nanostructuring of SOI layers and so on. In this report we will focus on a comparing of currier mobility near the thermal and the bonded Si/SiO_2 interfaces.

To minimize the density of electron traps for Si/buried oxide system the SOI wafers were prepared using a technology similar to Smart Cut, the differences being as follows: (1) unlike in a Smart Cut process, the buried oxide was not implanted with hydrogen and (2) the interface between the buried oxide (BOX) and the top Si layer was the bonded interface (the last means that the BOX near the top Si layer has structure like one for bulk-SiO_2). To minimize the mechanical stress and density of carrier traps for top SiO_2/Si interface, the nitrogen was introduced during the oxide growth. Different SOI transistors with free surface or top gate on the surface were used for electric characterization of the systems evaluated via current-voltage measurements.

Systematic studies of the currier mobility into the SOI layers were carried out depending on 1) the properties of the initial Si (Cz, Fz), 2) the Si layer thickness (400-8 nm), and 3) surface states (free or proceeded and gate-controlled).

The obtain results allowed to determine the dominant mechanism of carrier scattering by varying the above factors, identify ways to increase the charge carriers mobility in structures up to the values of bulk-Si (~1500 cm^2V^{-1} s^{-1} and ~2700 cm^2V^{-1} s^{-1} for electrons at 300 K and 78 K correspondingly). It was found that for the "ideal" state of interfaces, the mobility of electrons depends only on the properties of the initial Si and varies depending on the excess charge carriers by a power law with n=-0.3 for Cz-Si and n=-0,6 for Fz-Si.

This work was partly supported by RFBR under Project No 12-02-90443-Ukr_a.

Current state and new prospects of semiconductor infrared photoelectronics

V. Ponomarenko[1,2], A. Filachev[1]

1. R&P Association "Orion", Moscow, Russia, E-mail: orion@orion-ir.ru. 2. MIPT, Dolgoprudny, Russia

The paper discusses condition and results of development in a number of basic technologies of infrared photoelectronics: semiconductor photosensitive materials, solid-state photo converters for IR and UV regions of the electromagnetic radiation, multispectral and fast response devices, metamaterials and nanotechnology for creation of new types of optoelectronic devices.

We describe the current state of semiconductor material science for photoelectronics. The prospects for the development of molecular beam and MOS-hydride technology for manufacturing the most important photosensitive materials - CdHgTe, InSb, InGaAs, GaAlN, GaAsP, GaInN, etc.

It is shown the main tendencies of development of solid-state photoconvertors based on $In_xGa_{1-x}As$ and $Cd_xHg_{1-x}Te$ solid solutions for "non-thermal" spectral region of night airglow 1-2 μm. The results of researches of matrix focal plane arrays based on $In_{053}Ga_{047}As$/InP are described.

The paper discusses the results of development of "staring" and TDI focal plane arrays based on $Cd_{02}Hg_{08}Te$ and InSb for spectral regions 8-12 and 3-5 μm with 2x96, 4x288, 6x576, 320x256, 384x288 formats, digital imaging systems, and also imaging modules on their basis.

The prospects for the production of fast response focal plane arrays, including those for 3D-images in thermal imaging and active-pulsed optical-electronic systems and results of pin-and avalanche photodiodes based on Si, InGaAs/InP and CdHgTe are described.

It is presented results of development of multispectral photodetectors (MPD) for the spectral regions of 1-3, 3-5 and 8-12 μm, including monolithic two-spectral 2×2×288 matrix based on CdHgTe.

The properties of UV photodetectors based on GaP, GaAs, GaP_xAs_{1-x} for ranges 0.2-0.51, 0.25-0.90, 0.25-0.68 μm are described.

Silicon Nanowire Field Effect Transistor With Highly Doped Leads

S. Amitonov[1], D. Presnov[1,2], K. Rudenko[3], V. Rudakov[3], V. Krupenin[1]

1. Laboratory of Cryoelectronics, Moscow State University, 119991 Moscow, Russia , amitonov@physics.msu.ru.

2. Nuclear Physics Institute, Moscow State University, 119991 Moscow, Russia, denis.presnov@phys.msu.ru.

3. Institute of Physics and Technology RAS, 117218, Moscow, Russia.

Silicon nanowire field effect transistor (NWFET) is a promising electric field/charge sensor. Sensitivity of nanowire-based sensor could be just a factor of 20–30 away from the record sensitivity for state-of-the-art single-electron transistors operating below 4 K [1] while its operating temperature is noticeably higher and fabrication is much more easier. To demonstrate record sensitivity length Thomas-Fermi length of screening should be similar to the nanowire diameter. It means for silicon nanowire diameter 100 nm at 300 K dopant concentration should be ~10^{15} cm^{-3}. At the same time source and drain regions should be highly doped to reduce sensor resistivity, noise level and produce good silicon-metalization interface.

Here we report about simple fabrication of a silicon NWFET with highly doped source and drain regions. We used SOI wafers with device (top) layer 110 nm and dopant (boron) concentration ~10^{15} cm^{-3}. After Arsenic ion implantation (dose $1.25 \cdot 10^{15}$ cm^{-2}) and rapid thermal annealing we get nonuniform dopant concentration ~10^{21} at the layer surface and less than 10^{18} at the depth of 50 nm. To produce silicon NWFET we used electron beam lithography, e-gun Al evaporation and reactive ion etching. This structure didn't demonstrate field effect as highly doped silicon layer were degenerated to metallic conduction. Than all the structure except silicon nanowire was masked and top highly doped layer was anisotropically etched away in plasma at the same conditions initial reactive ion etching were produced till the beginning of transistor effect. Measurements of the transistors were carried out at temperatures of 300 K, 77 K and 4.2 K with a homemade measuring system.

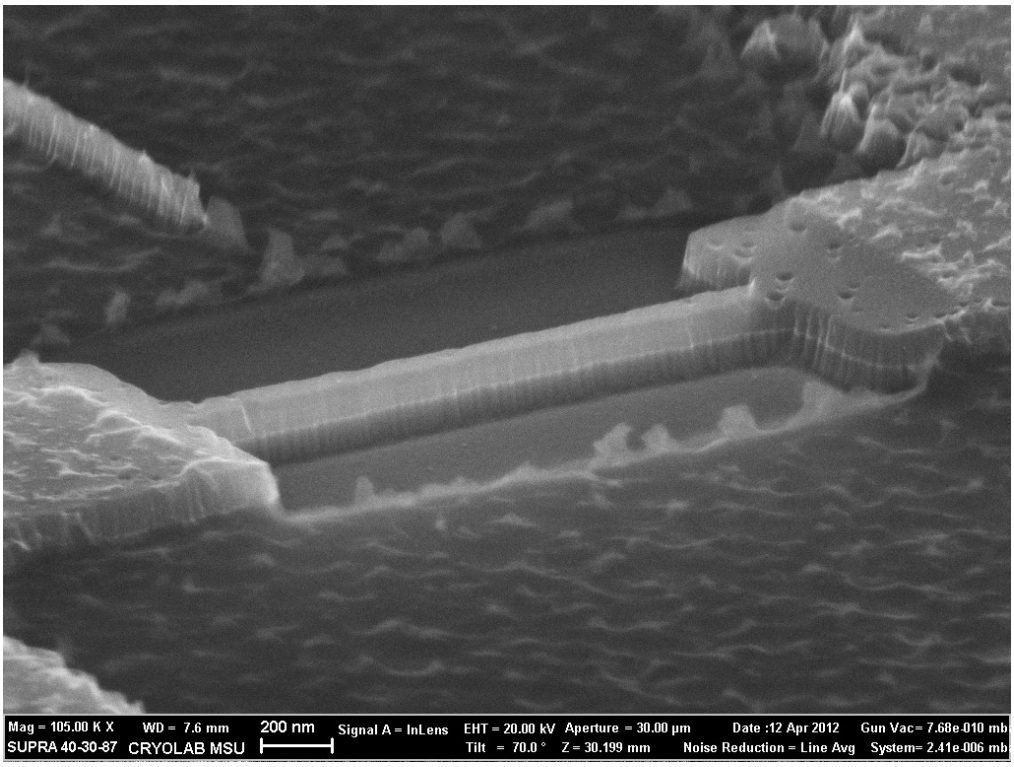

Fig. 1: Silicon nanowire field effect transistor with highly doped leads

1. J. Salfi, I. G. Savelyev, M. Blumin , S. V. Nair & H. E. Ruda, "Direct observation of single-charge-detection capability of nanowire field-effect transistors", *Nature Nanotech,* **5**, 737–741 (2010).

Electronic band alignment and electron transport in Cr/$BaTiO_3$/Pt ferroelectric tunnel junctions

A. Zenkevich[1], M. Minnekaev[1], Yu. Matveyev[1], Yu. Lebedinskii[1], K. Bulakh[2], A. Chouprik[2], A. Baturin[2], S. Thiess[3] and W. Drube[3]

1. National Research Nuclear University "Moscow Engineering Physics Institute", Moscow, Russia, avzenkevich@mephi.ru. 2. Moscow Institute of Physics and Technology, Dolgoprudny, Russia, baturin@mail.mipt.ru. 3. Deutsches Elektronen-Synchrotron DESY, Hamburg, Germany, wolfgang.drube@desy.de

The non-volatile memory concept of ferroelectric tunnel junctions (FTJ) takes advantage of an ultrathin ferroelectric (FE) layer as the barrier material between two metal electrodes, where the tunneling electroresistance is controlled by flipping the FE polarization and hence the electronic potential profile across the FTJ [1, 2]. In this work, we investigate the electronic and electrical properties of epitaxial single-crystalline $BaTiO_3$/Pt heterostructures grown on a MgO(100) substrate by pulsed laser deposition [3] with a Cr top electrode. Hard X-ray photoemission spectroscopy at E=6 keV is used to determine the electronic band alignment at the interfaces. The $BaTiO_3$ valence band offset (VBO) with respect to the Fermi level of the Pt (Cr) bottom (top) electrode is found VBO = 2.6 (2.9) eV. Assuming the previously reported band gap E_g = 4.3 eV for ultrathin $BaTiO_3$ [3], the conduction band offset is 1.7 (1.4) eV. The effect of a nm thick MgO marker layer on the band line-up at the $BaTiO_3$/Pt interface is also investigated enabling to reconstruct the band alignment diagram in the $BaTiO_3$/MgO/Pt system. The ferroelectricity of ultrathin epitaxial $BaTiO_3$ layers is confirmed by piezo-response force microscopy. The effect of the $BaTiO_3$ polarization reversal on the tunneling current is demonstrated on Au/Cr/$BaTiO_3$(4 nm)/Pt FTJ with a sub-μm Au/Cr top electrode. The tunneling electroresistance ≈10 is calculated from the I-V curves.

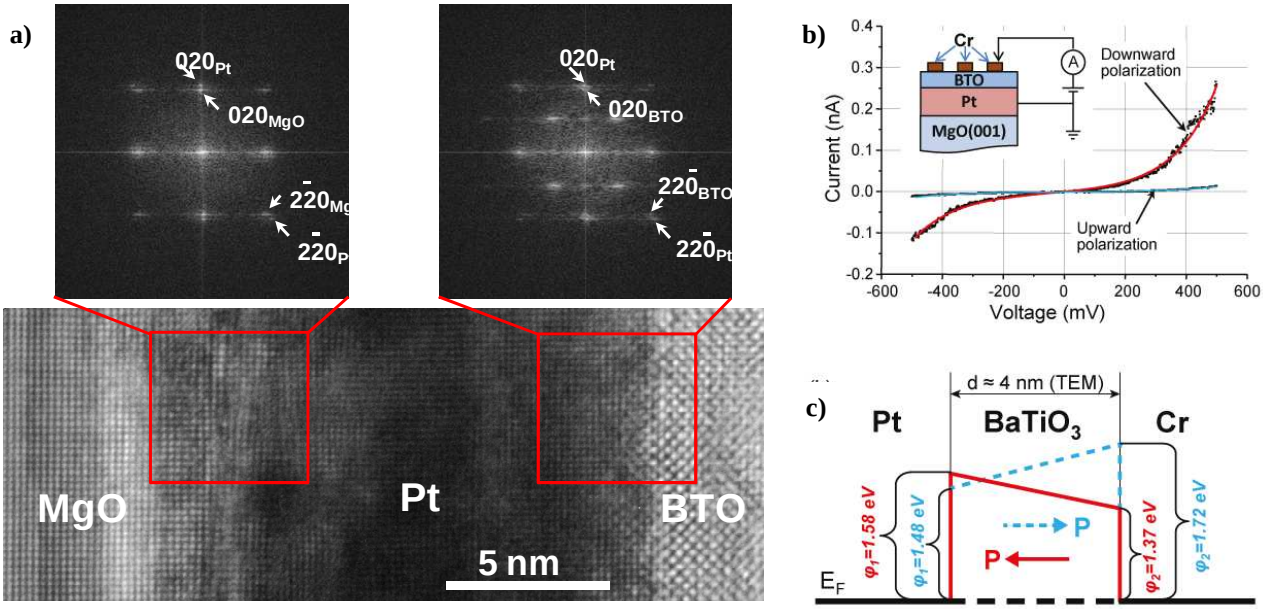

Fig. 2. a) HRTEM bright-field image of PLD grown $BaTiO_3$/Pt/MgO(100) structure and FFT images taken from Pt/MgO and BTO/Pt interfaces; b) Experimental I-V characteristics (dots) recorded on the Au/Cr/$BaTiO_3$(4 nm)/Pt tunnel junction for opposite polarization orientations and the fits (lines) with the model of tunneling through a trapezoidal barrier; c) The obtained electric potential profiles across the Cr/$BaTiO_3$/Pt junction for both ferroelectric polarization orientations.

1. E. Tsymbal and H. Kohlstedt, "Tunneling Across a Ferroelectric", Science, **313**, pp.181-184, 2006.
2. V. Garcia, S. Fusil, K. Bouzehouane, et al., "Giant tunnel electroresistance for non-destructive readout of ferroelectric states", Nature, **460**, pp.81-84, 2009.
3. A. Zenkevich, M. Minnekaev, Yu. Lebedinskii, et al., "Pulsed laser deposition of ultrathin $BaTiO_3$/Fe bi-layers: Structural characterization and piezoelectric response", Thin Solid Films, **520**, pp.4586-4589, 2012.

A Gold Free Fully Copper Metalized GaAs pHEMT for the High Frequency Applications

E. Erofeev[1], V. Kagadei[1], A. Kazimirov[2]
1. Research and Production Company "Micran", Tomsk, Russia, erofeev@micran.ru
2. Scientific Research Institute of Electrical Communication Systems, Tomsk, Russia, smart300389@mail.ru

Copper metallization has extensively used in the silicon integrated circuit technology since IBM announced its success in silicon very large scale integration process. The advantages of copper metallization for Si technology include lower resistivity and high electromigration resistance. Even though the use of copper as metallization metal has become very popular in Si devices, there were very few reports devoted to copper metallization of GaAs devices [1] – [2]. The using copper as the metallization metal instead of gold in GaAs technology has several advantages such as lower resistivity, higher thermal conductivity, and lower cost. If Cu replaces Au as the metallization metal for the HEMTs, then the resulting improvement in the electrical conductivity can increase the transmission speed of circuits. At other hand, the combination of the superior electrical and optical performance of GaAs with mature silicon technology has been very attractive for the semiconductor industry. The successful epitaxy of the III-V compound semiconductors on Si wafers reduces substrate and processing cost for III-V semiconductor manufacturing. All of them open the door to significantly less expensive optical communications, high-frequency radio devices and high-speed microprocessor-based subsystems.

The purposes of the present work are to develop and produce fully copper metalized pHEMT with Cu/Ge based ohmic contacts and Ti/Mo/Cu 150 nm T-gate and to investigate the DC and RF parameters of fabricated Cu-metalized GaAs pHEMT.

The fully Cu-metalized GaAs pHEMT was formed on the AlGaAs/InGaAs/GaAs structures. After mesa isolation the source and drain Cu/Ge ohmic contacts were formed using the lift-off method. Annealing was performed in a N_2 environment at 400 ^oC for 3 min. 150 nm Ti/Mo/Cu T-shape gates were fabricated by e-beam nanolithography Raith-150^{TWO} using a tri-layer resist stack of 950PMMA/LOR5B/495PMMA and 30 keV electron beam energy (fig.1). The device DC properties were measured with Tektronix 370A. The microwave S-parameter measurement has been carried out by using ZVA-40 network analyzer.

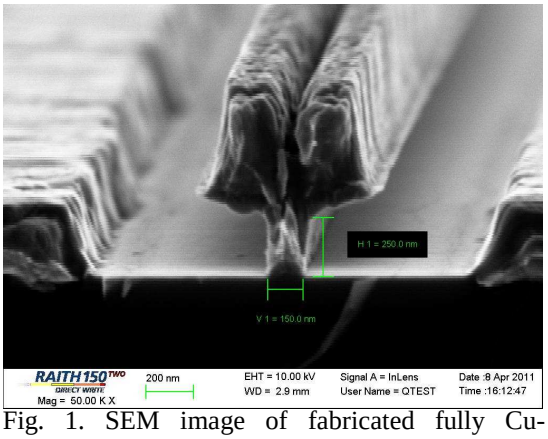

Fig. 1. SEM image of fabricated fully Cu-metalized pHEMT with 150 nm Ti/Mo/Cu T-gate.

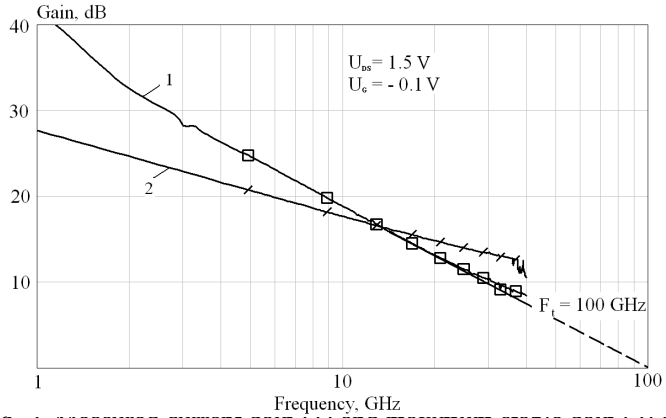

Fig. 2. Measured current gain (1) and maximum stable gain (2) as a function of frequency of fabricated Cu-based GaAs pHEMT.

The fabricated Cu-metalized pHEMT has a maximum drain current of 400 mA/mm, off-state gate-drain breakdown of 7 V and a transconductance peak of 440 mS/mm at V_{DS} = 1.5 V. The maximum stable gain value was about 18.8 dB at frequency 10 GHz. The current gain cut-off frequency of the copper metalized device is about 100 GHz at V_{ds} = 1.5 V and maximum frequency of oscillations is beyond 100 GHz (fig.2).

1. C.Y. Chen, E.Y Chang, L. Chang, and S.H. Chen, "Backside copper metallization of GaAs MESFETs", Electronics Lett., **36**, pp.1318-1319, 2000.
2. H.C. Chang, E.Y. Chang, Y.C. Lien, L.H. Chu, S.W. Chang, "Use of WN_X as the diffusion barrier for copper air bridged low noise GaAs pHEMT", Electronics Lett., **39**, pp.1763-1765, 2003.

Measurement of thickness of a layer of natural silicon oxide being on a test relief pitch structure, created on a substrate of monocrystalline silicon

M.N. Filippov[a,b,c], V.P. Gavrilenko[a,c], A.A. Kuzin[a,c], A.Yu. Kuzin[c], A.A. Kuzmin[a,c], V.B. Mityukhlyaev[a], A.V. Rakov[a], P.A. Todua[a,c], A.V. Zablotskiy[a,c]

[a]*Center for Surface and Vacuum Research, 40 Novatorov Street, Moscow, Russia 119421;*

[b]*N.S. Kurnakov Institute of General and Inorganic Chemistry 31 Leninskiy Prospect, Moscow, Russia 199991;*

[c]*National Research University "Moscow Institute of Physics and Technology", 9 Institutskii per., Dolgoprudny, Moscow Region, Russia, 141700.*

In this work, we have measured the thickness of a layer of natural silicon oxide being on a silicon relief structure, created on a substrate of monocrystalline silicon. The structure represents a set of the elements (protrusions) with a trapezoidal profile and a pitch (distance between two adjacent protrusions) of 2 microns. On one chip, the protrusions with the upper base of about 100 nm and of about 10 nm are presented. The angle of inclination of sidewalls of the trapezoidal protrusions with respect to its base is equal to 54.7°. Formation of natural silicon oxide occurred at room temperature. We measured the thickness of a layer of natural silicon oxide, using a high-resolution transmission electron microscopy. For such measurements, we used the known separation between the {111} lattice planes. We found that the thickness of a layer of natural silicon oxide depends both on the size of the upper base of the protrusion, and the size of the profile of the bottom between two adjacent protrusions. The minimum thickness of natural oxide of silicon (of about 2.4 nm) occurs in the center of this bottom, and at the edges of this bottom the thickness increases to 5 nm.

Characterization of graphene layers grown using Ni/a-SiC bi-layer as a precursor

A.V. Vasin[1], S.A. Gordienko[1], P.M. Lytvyn[1], V.V. Strelchuk[1], A.S. Nikolaenko[1], A.N. Nazarov[1], A.V. Rusavsky[1], V.S. Lysenko[1], V. Popov[2]

1. Lashkaryov Institute of Semiconductor Physics, NAS of Ukraine, Kiev, 03028 Ukraine. 2. Institute of Rzhanov Institute of Semiconductor Physics, Siberian Branch of RAS, Novosibirsk, Russia.

Graphene layers were synthesized by vacuum thermal annealing of the thin film "sandwich" Ni/a-SiC bi-layer deposited on SiO_2/Si wafer by magnetron sputtering technique. First step of the fabrication procedure was deposition of amorphous SiC film with thickness of about 50 nm on SiO_2/Si wafer by radio frequency magnetron sputtering of SiC target in argon atmosphere. On the second step Ni film of 500 nm was deposited on the top of a-SiC layer by direct current magnetron sputtering of Ni target. Finally, Ni/a-SiC/SiO_2/Si multilayer structure was then annealed in nitrogen flow at atmospheric pressure for 30 seconds or in vacuum 10^{-4} torr at temperature range 750-1150 ^{0}C for 5 minutes. At elevated temperature thin a-SiC layer is dissolved in nickel resulting in formation of nickel silicide and interstitial carbon. After cooling down carbon is precipitated on the surface of Ni film and in the bottom interface Ni/SiO_2. The effect of annealing temperature and heating rate on the formation of carbon layers were studied. It was shown that carbon layers were formed both on the top of Ni film and on the interface Ni/SiO_2 in case of vacuum annealing. In case of pulse annealing in nitrogen flow graphite-like amorphous carbon thin layer is formed only in the interface Ni/SiO_2. Graphene flakes were formed on the top of Ni surface when applying 5 minutes vacuum annealing at temperature 750-850 ^{0}C, while amorphous carbon layer was formed on the interface Ni/SiO_2. Carbon layers have been characterized by Raman scattering, atom force and Kelvin probe force microscopy.

Lateral size of graphene flake was estimated to be about tens of microns while thickness estimated by Raman scattering varied from one to few layers. Lateral size of the flakes depended on annealing temperature and temperature growth rate. Comparison of graphenes synthesized in our lab with that provided commercially CVD graphenes on nickel showd quite similar surface morphological features and Raman scattering spectra. Thus, synthesis of the graphene by thermal treatment of Ni/a-SiC bi-layer is suggested as an alternative to common CVD deposition method.

Atom force microscopy (AFM) was not able to detect the thickness of graphene flakes in regime of surface topology examination due to large roughness of Ni surface. Employment of Kelvin probe force microscopy (KPFM) demonstrated clear correlation of surface potential and graphene flakes visible by optical microscopy. The value of the contrast of surface potential correlated with number of grapheme layers measured by Raman scattering. Moreover, KPFM allowed detecting graphene layer even in case of absence of optical contrast from single graphene layer on nickel surface. Thus KPFM is demonstrated to be an effective instrument for examination of graphene topology on rough surfaces.

Characterization of Semiconductor Heterostrucrures using Dynamic Secondary Ion Mass Spectrometry

B. Ber [1,2], A. Merkulov [3]

1. A.F. Ioffe Physical-Technical Institute, Russian Academy of Sciences, St Petersburg, Russia, boris.ber@mail.ioffe.ru, 2. The Center of Multi-User Equipment "Material Science and Characterization for Advanced Technologies", St Petersburg, Russia, 3. CAMECA SAS, Gennevilliers, Cedex, France, Alexandre.Merkulov@ametek.com

Dynamic Secondary Ion Mass Spectrometry (D-SIMS) is a well approved surface analysis technique. By now D-SIMS is used for over forty years. Its development was mainly fueled by semiconductor industry, where it is one of the key characterization technique used for R&D, for monitoring of technological processes during production (in-line D-SIMS), for reengineering, and for failure analysis.

In the field of the physics of semiconductor devices D-SIMS analysis is one of the most important characterization techniques, too. The importance of SIMS is motivated by the following characteristics of this technique. SIMS can be used to measure all elements in the Periodic Table and their isotopes. SIMS has a high trace sensitivity down to ppb levels, which makes possible to measure intentional and unintentional doping in semiconductor structures. SIMS is capable to perform accurate in-depth profiling of multilayered heterostructures and ultra-shallow implanted structures with nanometer depth resolution. Valuable information about two-dimensional distribution of elements can be obtained by SIMS imaging. SIMS in-depth profiling and imaging may be combined to yield three-dimensional SIMS chemical maps of materials and heterostructures.

In this presentation basic phenomenon of SIMS process is described, and the issue of SIMS quantification for selectively doped compound semiconductor structures is addressed. The technique of in-depth SIMS analysis, its strengths and limitations are considered focusing on the challenge of accurate analysis of near-surface and interface regions. The information of state-of-the art tools for D-SIMS analysis of nano-scaled semiconductor heterostructures is presented.

The case studies shown illustrate the application of D-SIMS at low impact energy to the in-depth characterization of modern III-V, III-N, and Si-SiGe heterostructures and structures with ultra-shallow junctions. Fundamental and instrumental effects limiting the depth resolution, the sensitivity and the accuracy of SIMS analysis are discussed.

Determination of the state of non-volatile memory cell with the floating gate by using scanning probe microscopy

D. Hanzii[2], E. Kelm[1], N. Luapunov[1], R. Milovanov[1], G. Molodcova[1], M. Yanul[2], D. Zubov[1]
1. Institute of Nanotechnology of Microelectronics, Russian Academy of Science, Russia, 119991 Moscow, Leninsky Prospekt, 32A, Zone "B", office 107, kelm87@yandex.ru. 2. NT-MDT, Building 100, Zelenograd, Moscow 124482, Russia, spm@ntmdt.ru.

During a failure analysis of integrated circuits, containing non-volatile memory, it is often necessary to determine its contents. Standard memory reading procedures often are not applicable. This work discusses approaches to determining the state of non-volatile memory cell with the floating gate by using scanning probe microscopy.

The state of non-volatile memory cell with floating gate (FG) is defined by the presence or absence in him of the electric charge. Logical “one” (1b) usually corresponds to a cell without electrical charge, and a logical "zero" (0b) - with the charge in the FG. Thus, the measurement of charges in FG of cells gives the possibility to determine the content of memory.

Issues of sample preparation and methodology of measurement are demonstrated on single-chip “MICROCHIP” microcontrollers, with EPROM (PIC12C508) and flash-EEPROM (PIC16F876A) memory.

To verify the results of determination the state of non-volatile memory cells is necessary to know, how the geometric position of the cell corresponds to the address of bit. For this investigation we used the method of local erasing cell by the electron beam [1].

Memory cells of PIC12C508 were programmed two by two, and cells PIC16F876A - in groups of four, to simplify further analysis (figure 1a).

In our work we investigated two ways of sample preparation. The first way (PIC12C508) has three steps: geometric measurements of chip, mechanical backside polishing of a die up to a thickness of 5-10 microns, and chemical etching in TMAH (Tetramethylammonium hydroxide). The second way has also three steps: IC decapsulation with fuming acid, mountain of die on a silicon substrate in recess with depth 100 microns, and backside polishing of die up to 50-200 nanometers.

To investigate the FG charges was used the method of contact scanning capacitance microscopy (CSCM). As the probe signal is used a signal at a frequency of 10 MHz and the amplitude of 0.1-1 V. The best contrast of the FG charges was obtained in the memory area where the thickness of the silicon substrate over the FG was about 100 nm. The picture of the FG charge distribution fully corresponds of the geometrical arrangement of the recorded address bits (figure 1b).

It should be noted, that the second way of sample preparation is more complicated and requires more time, however, allows to remove substrate of chip a more planar and, as a consequence, to get a picture of the charge distribution on a larger area of memory. The magnitude of the contrast of charge distribution on the surface is also higher in the samples, performed by the second method.

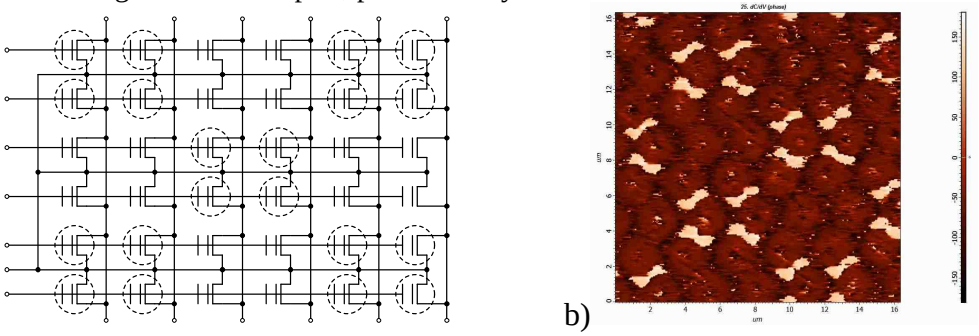

Figure 1. a – location of the recorded memory cells, b – CSCM image of charge distribution on the surface.

1. Thong John T.L. "Electron Beam Testing Technology", Plenum Press, New York, 1993.

Mechanisms of image formation in SEM

Yu.V. Larionov, Yu.A. Novikov
A.M. Prokhorov General Physics Institute, Russian Academy of Sciences, Moscow, Russia, nya@kapella.gpi.ru

Scanning electron microscopes (SEM) are used in micro- and nanoelectronics for visualization of relief structures and for measurement of its linear sizes. Special micro and nanorelief test objects were fabricated and calibration methods for low and high voltage SEMs, working in a mode of collecting slow secondary electrons, were developed for it. However, SEM image formed in any of these modes do not map a relief structure correctly. One should have comprehension of image formation mechanisms and its correct use in any SEM mode for correct structure profile reconstruction and linear size measurement. There are three modes for it: the low voltage mode (where primary electrons have energy less than 2 keV) and the two high voltage modes (primary electrons have energy more than 2 keV). In one of them SEM detector collects backscattered electrons (BSE), in another it collects slow secondary electrons (SSE). Results of investigation of image formation mechanisms in these modes are presented in the paper for spatial homogeneous relief structures.

SEM image signal V_{LE} at the low voltage mode can be expressed as:

$$V_{LE}(t) \sim \iint I(x,y)\left|\mathbf{grad}(S(x,y))\right| F(x,y,t)\,dx\,dy\,,$$

where $S(x,y)$ is a surface relief function along x and y axes, $F(x,y,t)$ is a function of electron density distribution in a probe, $I(x,y)$ is a function of electron emission of the surface, t is the scanning coordinate.
The SEM image signal V_{BSE} at the BSE mode can be covered with use of two mechanisms:

$$V_{BSE}(t) = I_1 \iint I(x,y)S(x,y)F(x,y,t)\,dx\,dy - I_2 \iint I(x,y)S(x,y)F_{BSE}(x,y,t)\,dx\,dy\,,$$

where $F_{BSE}(x,y,t)$ is a function of electron density distribution at effective depth of backscattering, I_1 и I_2 – are emission contributions of these mechanisms. An experimental evidence of possibility of this description is presented in [1]. An experimental division of these mechanism contributions is demonstrated in the paper.
It has been revealed that there is possibility of an experimental selection of two mechanisms of signal formation at SSE mode. In one of these mechanisms signal formation is similar to one used for a low voltage SEM. Another mechanism maps effect of backscattered electrons that reach the surface of the sample and generate SSE. Thus, SSE signal V_{SSE} can be expressed as:

$$V_{SSE}(t) = I_{LE}V_{LE}(t) + I_{BSE}V_{BSE}(t),$$

where $V_{LE}(x)$ is the low voltage mode signal, $V_{BSE}(t)$ is the BSE signal, I_{LE} and I_{BSE} are emission contributions of these mechanisms. An experimental division of the mechanism contributions is demonstrated in the paper.

Analytic expressions of signal amplitude for every image formation mechanism are developed for structures with trapezoid profile.

The work was supported by RFBR grant (the project No. 11-08-01217).

1. Yu.A. Novikov, “Mechanisms of SEM image formation in a mode of collection of backscattered electrons”, 24 Russian Conference on Electron Microscopy, Russia, Abstracts of Papers, pp.300-301, 2012.

Virtual scanning electron microscope

Yu.V. Larionov, Yu.A. Novikov
A.M. Prokhorov General Physics Institute, Russian Academy of Sciences, Moscow, Russia, nya@kapella.gpi.ru

Growth of micro and nanoelectronics is intimately associated with visualization of micro and nanostructures and with measurements of linear sizes of visualized structures. The best method to achieve these goals is use of scanning electron microscope (SEM). However, reconstruction of a structure profile based of its image is an incorrect task. One of proof methods of solution correctness of the incorrect task may be a program that computes a structure image in the form analogous to the corresponding SEM image (output data) using for it input data associated with profile and sizes of the model structure analogous to a real structure. This program can be named virtual scanning electron microscope (VSEM).

VSEM can be made by two methods. The first is an imitation in VSEM of scattering processes going in a sample under the action of the SEM probe. The next method is simulation (modeling) of an image with use of an equation that connects input and output parameters (without imitation process).

Main shortcomings of the first method are a long time needed for computing an image with use of a PC (in some cases about one year) and a small amount of real independed random numbers generated by a computer program for imitation of random processes for all acts of electron scattering during formation of the structure image. Thus an attempt of realizing VSEM by the first method often completes in a computer program that models only a videosignal from the sample instead of its image.

As a result of experimental and theoretical investigations, a semi empirical model of image formation is proposed for low and high voltage SEMs working at second electron (SE) and backscattered electron (BSE) emission modes. This model can be used for relief structures with the trapezoid profile. Analytic formulae of SE and BSE videosignals amplitude have been brought into being. The program for computing SE and BSE images (the VSEM) is developed on the base of a semi empirical model.

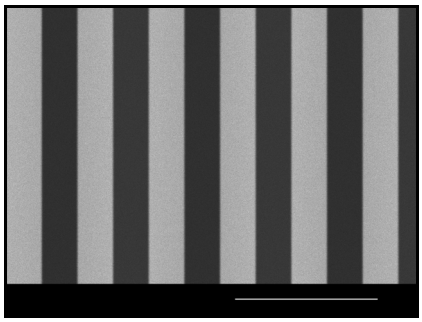

Figure 1

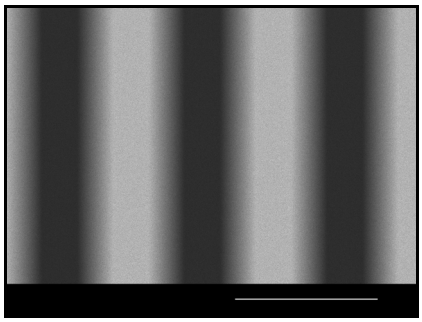

Figure 2

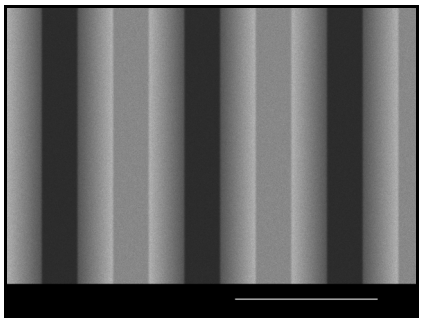

Figure 3

Figures 1 – 3 shows images of a periodic structure analogous to the test structure MShPS-2.0Si [1] with a trapezoid profile, computed with aid of VSEM. A pitch of the structure is 2000 nm, a width of the protruded upper base is 500 nm and a probe diameter in the model is 30 nm. The Fig. 1 shows the image that is computed for a low voltage SEM, the images at Fig. 2, Fig. 3 are computed for a high voltage SEM working at a SE (Fig. 2) and at a BSE (Fig. 3) modes. Elapsed time for computing the image with a sizes 1280×960 pixels is about 8 minutes for Fig. 1, Fig. 3 and about 6 minutes for a Fig. 2, frequency of the computer is being 2.2 GHg.

Results of an application of VSEM for measurements of structures with sizes in the nanometer diapason and a calibration of the SEM with its use are presented in the report.

The work was supported partially by RFBR grant (the project No. 11-08-01217).

1. Ch.P. Volk, E.S. Gornev, Yu.A. Novikov, Yu.V. Ozerin, Yu.I. Plotnikov, A.M. Prokhorov, A.V. Rakov, “Linear Standard for SEM-AFM Microelectronics Dimensional Metrology in the Range 0.01-100 μm”, Russian Microelectronics, **31**, pp.207-223, 2002.

Formation mechanism and properties of Ge quasicrystalline nanoclusters in SiO_x matrix

Yu.N. Kozyrev[1], M.Yu.Rubezhanska[1], V.S.Lysenko[2], S.V.Kondratenko[3], V.P.Kladko[2], Yu.V.Gomeniuk[2], Ye.Ye. Melnichuk[3]

1. O.O. Chuiko Institute of Surface Chemistry,17 Generala Naumova St., 03164, Kyiv, Ukraine, kozyrev@iop.kiev.ua. 2. Institute of Semiconductor Physics, 41 Prospect Nauki, 03028, Kyiv, Ukraine, nazarov51@yahoo.com. *3. Taras Shevchenko National University of Kyiv, 64 Volodymyrs'ka St., 01601, Kyiv, Ukraine,* kondr@univ.kiev.ua

Germanium nanoclusters grown on/in silicon have been successfully applied in new nanoelectronic, optoelectronic and memory devices due to quantum confinement effect and possibility of integration within Si-based technology [1]. Heterostructures with epitaxial Ge nanoclusters isolated from Si substrate by ultrathin silicon oxide layer, would be practically promising due to their nanoscale size, tunability and high density. The interest in opto-electronic and solar cells application stems from observation of infrared photoluminescence and photoconductivity caused by optical transitions via confined states of Ge nanoislands [2].

Germanium nanoclusters are grown by a molecular-beam epitaxy technique on chemically oxidized Si(100) surface at 700ºC. A standard chemical pre-epitaxial treatment gives the formation of a 2 nm thick SiO_2 layer on the substrate. Atomic force microscopy showed that deposition of germanium onto the SiO_x film results in formation of nanoclusters with the hemispherical top surface about 1.5-2 nm in height and the diameter of ~ 16 nm with average surface distribution density of ~ 5×10^{11} cm^{-2}. The base of nanoislands is almost circular.

X-ray diffraction and photocurrent spectroscopy demonstrate that the nanoclusters have the local structure of body-centred-tetragonal Ge, which exhibit an optical adsorption edge at 0.48 eV at 50 K. Deposition of silicon on surface with Ge nanoclusters leads to surface reconstruction and formation of polycrystalline diamond-like Si coverage, while nanoclusters core becomes tetragonal SiGe alloy. Possible mechanisms for such nanocluster formation in SiO_x matrix are discussed. Transmission electron microscopy (TEM) measurements of the experimental samples confirm that the Si substrate show almost no influence on Ge nanocluster formation, which are divided from the substrate by a thin SiO_x layer (the thickness about 2 nm) in which nucleation centres originate (fig. 1). As Ge epitaxy goes on, the closest to nucleation centres Si-O chemical bonds are destroyed and Ge atoms occupy O positions creation atom arrangement in tetragonal crystalline structure. The usual diamond-like crystal structure of Ge nanoclusters appears to be completely absent due to isolation from Si(100) substrate. Further deposition of silicon on the surface with Ge nanoclusters leads to the surface reconstruction and formation of polycrystalline diamond-like Si coverage, while nanoclusters core becomes tetragonal SiGe alloy. Intrinsic absorption edge for nanoclusters with silicon coverage is shifted to 0.73 eV due to Si-Ge intermixing.

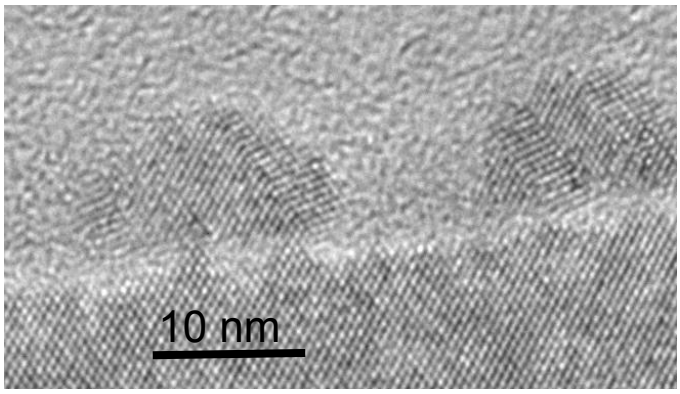

Fig. 1. TEM images of hemispherical Ge nanoclustrers formed on SiO_x thin layer and then covered with Si.

1. K. Brunner, „Si/Ge nanostructures", Rep. Prog. Phys., **65**, pp. 27-35, 2002

2. V.S. Lysenko, Yu.V. Gomeniuk, V.V. Strelchuk, S.V. Kondratenko, O.V. Vakulenko, Yu.N. Kozyrev, M.Yu. Rubezhanska, „Carrier transfer effect on transport in p-i-n structures with Ge quantum dots", Phys. Rev. B., **86**, pp. 115425-115434, 2011

Photoluminescence of Si layers on grown SiO_2 and optical resonant structures

A.A. Shklyaev[1, 2], D.V. Gulyaev[1], D.E. Utkin[1], A.V. Tsarev[1], A.V. Dvurechenskii[1], A.V.Latyshev[1,2]

1. A.V. Rzhanov Institute of Semiconductor Physics, Siberian Branch of Russian Academy of Sciences, Novosibirsk 630090, Russia, E-mail: shklyaev@isp.nsc.ru. 2. Novosibirsk State University, Novosibirsk 630090, Russia

The isotropic character of the spontaneous luminescence significantly reduces its external quantum efficiency. The increase in the quantum yield of luminescence can be achieved by providing the conditions for the directional emission and for the emission at selective wavelengths. These are realized by the fabrication of optical resonant structures, such as photonic crystal nanocavities on thin layers or distributed Bragg reflector cavities and disk resonators with periodic modulation of the form, for which thick layers are used.

Crystalline silicon has low light emission efficiency due to its indirect optical band gap structure which can be modified by introducing dislocations. Dislocated silicon enables to emit light in the 1.2-1.6 μm wavelength range due to the optical transitions via dislocation-induced deep levels in the Si band gap [1]. It has been recently shown that a high concentration of dislocations can be formed during Si growth on the oxidized Si surfaces [2], as well as in Si layers grown by molecular-beam epitaxy on the surface of SiO_2 films [3]. This technique provides the fabrication of silicon-on-isolator structures which are required for the preparation of the optical resonant structures.

It is shown here that Si layers grown on SiO_2 at temperatures between 430 and 550 °C by molecular-beam epitaxy and annealed at high temperatures emit a photoluminescence (PL) peak in the 1.4 - 1.7 μm range. The use of 1 nm Ge coverage on SiO_2, prior to the Si deposition, leads to an increase in the PL intensity. The Ge coverage also provides an increase in the average size of microcrystals in Si layers. Thick Si layers (~5 μm) exhibit resonant PL peaks in a broad spectral region from 1.2 to 1.7 μm, as shown in Fig. 1(a) and (b). Two-dimensional photonic crystals with nanocarvities, such as shown in Fig. 2, are fabricated on the basis of the Si layers grown on SiO_2 films and their light emission properties are studied.

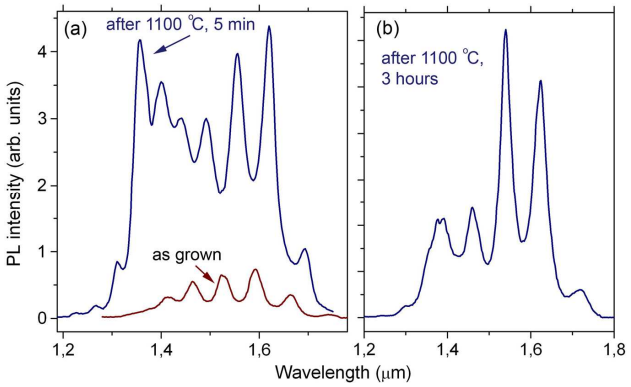

Fig. 1. PL spectra after the growth and annealing.

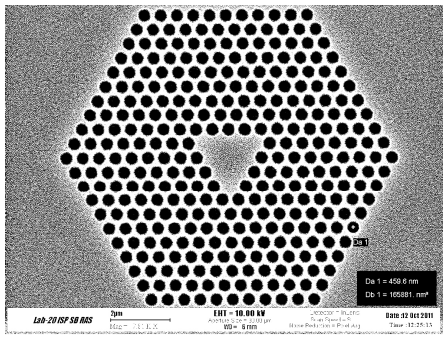

Fig. 2. REM image of the photonic crystal.

The obtained results show that the Si layers prepared on SiO_2 under certain conditions are promising for the fabrication of light emitters using optical resonant cavity structures.

1. N.A. Drozdov, A.A. Patrin and V.D. Tkachev, “Recombination radiation on dislocations in silicon”, JETP Lett., **23**, pp.597-599, 1976.
2. A.A. Shklyaev and M. Ichikawa, “Extremely dense arrays of germanium and silicon nanostructures” Physics – Uspekhi, **51**, pp.133-161, 2008.
3. A.A. Shklyaev, A.S. Kozhukhov, V.A. Armbrister, and D.V. Gulyaev, "Surface morphology of Si layers grown on SiO_2”, Appl. Surf. Sci., pp.1-5, available online 20 May 2012.
4. A.A. Shklyaev, D.V. Gulyaev, K.S. Zhuravlev, A.V. Latyshev, V.A. Armbrister, A.V. Dvurechenskii, “Resonant photoluminescence of Si layers grown on SiO_2”, Opt. Commun., submitted.

Influence of metamorphic buffer design on electrophysical and structural properties of MHEMT nanoheterostructures $In_{0.7}Al_{0.3}As/In_{0.7}Ga_{0.3}As/In_{0.7}Al_{0.3}As/GaAs$

S.S. Pushkarev[1, 2], G.B. Galiev[1], E.A. Klimov[1], D.V. Lavrukhin[1], I.S. Vasil'evskii[2], R.M. Imamov[3], I.A. Subbotin[3], O.M. Zhigalina[3], V.G. Zhigalina[3], P.A. Buffat[4], B. Dwir[4], E.I. Suvorova[3, 4]

[1] *Institute of Ultrahigh Frequency Semiconductor Electronics, RAS, 117105, Moscow, Russia*

[2] *National Nuclear Research University "MEPHI", 115409 Moscow, Russia*

[3] *A.V. Shubnikov Institute of Crystallography of Russian Academy of Sciences, 119333 Moscow, Russia*

[4] *Ecole Polytechnique Fédérale de Lausanne, CH-1015 Lausanne, Switzerland*

The goal of the present work is to investigate the influence of metamorphic buffer design on electrophysical and structural properties of the metamorphic HEMT nanoheterostructures on GaAs substrate with δ-Si doped quantum well $In_{0.7}Al_{0.7}As/In_{0.7}Ga_{0.7}As/In_{0.7}Al_{0.7}As$. The essence of metamorphic technology lies in the growing of thick layer with graded compound between substrate and active region. That layer called metamorphic buffer (MB) harmonises substrate and active region in terms of lattice parameter. Metamorphic buffers $In_xAl_{1-x}As$ ($x = 0.05 \rightarrow 0.70$) with linear or step-graded increment of In concentration (x) were used; in addition, linear MBs contain 5-period or 30-period strained superlattices $In_{(x+\Delta x)}Al_{1-(x+\Delta x)}As/In_{(x-\Delta x)}Ga_{1-(x-\Delta x)}As$ ($\Delta x \sim 0.07–0.08$) or interior inverse steps. Inverse step is a thin layer with less lattice parameter, and consequently, with less In concentration compared with the underlying part of MB, $\Delta x \sim 0.03–0.05$. The active region of all the HEMT nanoheterostructures is grown by the same manner.

Simple linear MB (sample 829) is shown to have tendency toward disastrous relaxation through twinning due to nonoptimal growth regime. The introduction of 5-period strained superlattices (sample 830) is shown to prevent such relaxation and to enhance the electrophysical and structural properties of MHEMT nanoheterostructures. The interior inverse steps in MB (sample 842) are demonstrated to be less effective for threading dislocation filtering than the 5-period strain superlattices (sample 830) that are less effective than the 30-period strained superlattices (sample 888). In particular, the STEM images showed that 5-period strain superlattices inserted into the metamorphic buffer are efficient enough to bend over the threading dislocations and to prevent their penetration into the upper layers, but interfaces of the superlattices themselves serve as a source to new dislocations (pointed out by arrows in fig.). Elongation of MB from 1.2 to 1.5 mkm (samples 830 and 835 respectively) did not improve either electrophysical properties or surface roughness. Step-graded MB (sample 889) permitted the minimal surface roughness with rather high electron mobility. Samples were investigated by the Hall effect, XRD, AFM, TEM, and photoluminescence.

Table. Electron mobility μ_e, sheet electron concentration n_S, and root mean square surface roughness (RMSSR) of investigated samples.

№	μ_e, см^2/(В·с)		n_S, см$^{-2}$		RMSSR, nm
	300 K	77 K	300 K	77 K	
829	1550	1930	1.29	1.23	23
830	10500	33300	1.45	1.38	7
835	10600	34300	1.32	1.26	8
842	8700	22800	1.84	1.76	14
888	11900	47200	1.56	1.45	8
889	11700	44900	1.49	1.41	6

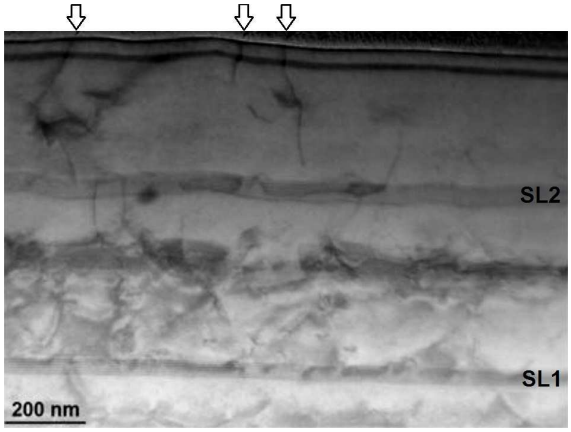

Fig. STEM image of cross-section of sample 830.

This work is supported by the Ministry of Education and Science of the Russian Federation under contracts No 14.740.11.0869 and No 16.513.11.3113, by a Grant of the Russian Foundation for Basic Research 11-07-00050. Authors acknowledge the support and help of Dr. Jean-Daniel Ganiere and Mrs. Danièle Laub. They are deeply indebted to the Centre Interdisciplinaire de Microscopie Electronique (EPFL) for making available its electron microscopes, software and sample preparation means.

GaN layers with low dislocation density and high electron mobility grown by high-temperature ammonia-MBE

S.I. Petrov[1], A.N. Alexeev[1], D.M. Krasovitsky[2], V.P. Chaly[2], V.V. Mamaev[1]
1. SemiTEq JSC, Saint-Petersburg, Russia, petrov@semiteq.ru 2. Svetlana-Rost JSC, Saint-Petersburg, Russia

One of the main problems in manufacturing of GaN-based devices up to date is the lack of low cost, lattice-matched substrates. In spite of using special procedures at the initial growth stage, heteroepitaxy of III-Nitrides on mismatched substrates usually yields high dislocation density, in the range of 10^9-10^{10} cm^{-2} for MBE and 10^7 cm^{-2} for MOCVD using ELOG, which affect the device quality and reliability. Moreover, typical growth temperatures in MBE are much lower as compared with MOCVD. It leads to insufficient surface mobility of adatoms, worse coalescence of nucleation blocks on initial growth stage, and, as a result, to high dislocation density which limits carrier mobility. Typical values of room temperature electron mobility in GaN grown on sapphire using different buffer layers (usually rather thin GaN, AlGaN or AlN layers) are in the range 250-350 $cm^2/V{\cdot}s$ for MBE and 500-700 $cm^2/V{\cdot}s$ for MOCVD. Higher mobility value (560 $cm^2/V{\cdot}s$) has been achieved in GaN grown by MBE on sapphire, using the AlN buffer layer deposited by magnetron sputtering [1]. One of the best reported values of electron mobility in GaN grown by MOCVD is 900 $cm^2/V{\cdot}s$ [2]. Recently high value of electron mobility above 1100 cm2/V.s has been achieved in MBE GaN films grown on low dislocation density GaN MOCVD templates [3].

In this paper we demonstrate low-dislocation-density and high-electron-mobility GaN layers grown by ammonia-MBE on c-Al_2O_3 under the ultimate for MBE growth temperature as high as TS = 1150 ºC. It became possible using a special MBE system STE3N manufactured by SemiTEq (Russia). The buffer layer sequence from c-sapphire substrate involved a 200-nm-thick AlN layer (TS=1100-1150ºC), AlGaN/AlN superlattice (SL), and $Al_xGa_{1-x}N$ (x = 0.1-0.3) transition layers (900-920 ºC). The scanning transmission electron microscopy (STEM) study showed gradual decrease of threading dislocation density from (2-4)$\times10^{10}$ cm^{-2} in AlN to (4-6)$\times10^9$ cm^{-2} in $Al_{0.1}Ga_{0.9}N$ grown after SL (Fig. 1). Finally, the dislocation density in the top GaN active layer was reduced down to (9-10)$\times10^8$ cm^{-2} that comparable with MOCVD GaN grown on sapphire and several times lower than in conventional NH3-MBE. Detailed study by TEM allowed separate evaluation of the density of screw (~2×10^8 cm^{-2}), edge (~4×10^8 cm^{-2}), and mixed (~4×10^8 cm^{-2}) dislocations in the top GaN layer. The improvement of structural quality resulted in substantial increase in electron mobility which reached the maximum value 600-650 cm^2/Vs in a 1.5-µm-thick GaN top layer lightly doped with silicon up to n = (3-5)$\times10^{16}$ cm^{-3}, that corresponds to a good quality MOCVD GaN. The experimental values of mobility and dislocation density are in good agreement with calculations [4].

Employing such a GaN layer in a double heterostructure (DH) with the cap $Al_xGa_{1-x}N$ barrier layer of variable composition (x = 0.25-0.4) allows to change the electron sheet density and mobility in a two dimensional electron gas (2DEG) in the range of 1300-1700 $cm^2/V{\cdot}s$ and (1.0-1.8)$\times10^{13}$ cm^{-2}, respectively, providing control of a 2DEG channel sheet resistance in the range of 230-400 Ω/□. Application of this technology and DH design for growing on SiC substrates enabled one to manufacture a DHFET with a gate length of 0.5 µm for 0.03-4.0 GHz extra-broadband power amplifiers having Pout=2.5 W, gain 17-25 dB and efficiency 30%. During aging tests all the devices have shown reliable operation for more than 3500 hours under 85 °C. These device parameters confirm the high quality of the heterostructure and chosen technological and design approaches.

1. J.B. Webb, H. Tang, J.A. Bardwell, S. Moisa, C. Peters, T. MacElwee, “Defect reduction in GaN epilayers and HFET structures grown on (0 0 0 1) sapphire by ammonia MBE”, J. Cryst. Growth, **230**, pp.584-589, 2001.
2. S.Nakamura, T.Mukai, M.Senoh, “In sifu monitoring and Hall measurements of GaN grown with GaN buffer layers”, J. Appl. Phys., **71**, pp.5543-5549, 1992.
3. G. Koblmüller, F. Wu, T. Mates, J.S. Speck, S. Fernández-Garrido, E. Calleja, “High electron mobility GaN grown under N-rich conditions by plasma assisted molecular beam epitaxy”, Appl. Phys. Lett., **91**, pp.221905-1-3, 2007.
4. Ng Hock M., Doppalapudi Dharanipal, Moustakas Theodore D., Weimann N. G., Eastman Lester F., “The role of dislocation scattering in n-type GaN films”, Appl. Phys. Lett., **73**, pp.821-823, 1998.

Formation, optical, electrical and thermoelectrical properties of silicon nanocomposites with embedded Mg_2Si nanocrystallites

K.N. Galkin[1], S.V. Vavanova[1], N.G. Galkin[1], R. Kudrawiec[2], E. Zielony[2], J. Misiewicz[2]

1. *Institute of Automation and Control Processes, Far Eastern Branch, Russian Academy of Sciences, Vladivostok, Russia, galkinkn@iacp.dvo.ru . 2. Institute of Physics, Wroclaw University of Technology, Wroclaw, Poland.*

Magnesium silicide (Mg_2Si) as a narrow band semiconductor (Eg =0.78 eV) [1] having the large thermoelectric power coefficient was considered as perspective material for the creation of thermoelectric converters on the base of silicon planar technology. However the complexities in the growth of heteroepitaxial films of semiconductor silicides on silicon (the different symmetry of crystalline lattices of silicides and silicon, distinctions in parameters of their lattices and non-possibility to obtain heterojunctions without linear and point defects) considerably decreased an interest of scientists to bulk silicides and their heteroepitaxial films on silicon substrates in the beginning of 21st century. Nevertheless, investigations in the field of semiconductor silicides in the first decade of 21st century were transferred in the region of systems with low dimensionality, including nanowires and nanocrystallites (NCs) of semiconductor silicides on and in a silicon.

Procedures of Mg_2Si island formation on the Si(111) substrate, growth conditions and deposition rates of silicon and magnesium have been early described in the article [2]. Multilayer samples with buried Mg_2Si nanocrystallites (referred to as silicon nanocomposites) were formed by multiple repetition of the first step growth process (silicide island formation and silicon cap growth). Doping process of Mg_2Si NCs in silicon cap layer was performed in two steps. The first one is formation of Sb, Al or Ag ordered surface phase. On the second step the silicide nanoislands were formed with following Si cap growth.

During growth of silicon nanocomposites we cannot increase the MBE growth temperature of silicon substrate higher than 150 ^{o}C, because at higher temperatures the Mg_2Si NCs is destroyed and magnesium desorbed from substrate. Grown silicon nanocomposites are polycrystalline by optical, Raman and topography data. Silicon nanocomposites (doped or not) grown on p-type Si(111) with 45 Ω*cm substrate are characterized by smaller values of resistance in the range of 35-270 K in comparison with clean silicon substrate. Thus, the reduction of resistivity in grown samples is observed either at the expense of increase in the carrier concentration (doping by Ag or Al atoms) in the silicon nanocomposite layer, or at the expense of increases in it carrier mobility due to change of carrier scattering conditions. But for silicon nanocomposites grown on n-type Si(111) substrate the resistance is higher than for clean Si substrate in the temperature range of 50 – 250 K. It not depends on the doping by Sb atoms during the NCs formation in Si lattice. So, we propose that conductivity of substrate conserves the higher mobility of electrons than in the silicon nanocomposites layer after doping process. The sample with two layers of Mg_2Si NCs on p-type Si is characterized by bigger values of Seebeck coefficient (53 μV/K and -130 μV/K) in comparison with a substrate. It`s caused by generation of carriers in Mg_2Si NCs and their injections in the silicon cap layer. Hence, the significant growth of Seebeck coefficient at temperatures bigger 420 K is caused by generation of carriers in Mg_2Si NCs and only electrons from Mg_2Si NCs inject in a silicon cap layer across Mg_2Si-p NC/Si-p heterojunction. When Mg_2Si NCs were formed in n-type Si substrate and covered by n-type silicon cap layer with and without Sb doping of Mg_2Si NCs a negative Seebeck coefficient was registered in the all temperature range used. The non-doped Si-n/Mg_2Si/Si-n nanocomposite displays the decrease of Seebeck coefficient module (with negative sigh value) with the temperature increase. But silicon nanocomposite layer doped by Sb atoms changes the behavior, and module of Seebeck coefficient increases with the substrate temperature increase.

This work is financially supported by RFBR Grants No. 11-02-98511-r-vostok_a, No. 12-02-31236_mol_a and by young scientist grants of President of Russian Federation: MK-3225.2011.8.

1. M.Y. Au-Yang, M.L. Cohen, “Electronic structure and optical properties of Mg_2Si, Mg_2Ge and Mg_2Sn”, Phys. Rev., **178(3)**, pp.1358-1364, 1969

2. N.G. Galkin, D.L. Goroshko, K.N. Galkin, et al., “Silicide nanostructured multilayers in monocrystalline silicon matrix: growth, structure and properties”, Rare Metals, **28**, Spec. Issue, pp.585-588, 2009

Laser pulse crystallization and optical properties of Si/SiO_2 and Si/Si_3N_4 multilayer nano-heterostructures

V.A. Volodin[1,2], S.A. Arzhannikova[1,2], A.A. Gismatulin[1,2], G.N. Kamaev[1,2], A.H. Antonenko[1,2], S.G. Cherkova[1,2], S.A. Kochubei[1], A.A. Popov[3], H. Rinnert[4], and M. Vergnat[4]

1. Institute of Semiconductor Physics, Russian Academy of Sciences, Lavrent'eva ave., 13, 630090, Novosibirsk, Russia, E-mail address: volodin@isp.nsc.ru. 2. Novosibirsk State University, Pirogova street, 2, 630090, Novosibirsk, Russia. 3. Yaroslavl Department of IPT RAS, University ave., 21, Yaroslavl, Russia. 4. Institut Jean Lamour UMR CNRS 7198 - Nancy Université - UPV Metz, Faculté des Sciences et Technologies, B.P. 70239, 54506 Vandœuvre-lès-Nancy Cedex, France.

Interest to dielectric films containing many periodical layers of Si nanoclusters or Si quantum wells is growing due to their perspectives of practical application. The most important application areas are silicon-based optoelectronic devices, non-volatile memory, and tandem solar cells based on lateral Si/SiO_2 quantum well heterostructures [1]. For many purposes, the Si/Si_3N_4 heterostructures are more preferable because of relatively low band gap in silicon nitride compared with silicon dioxide. The formation of such heterostructures, its crystallization and its optical properties are topics in current research. The laser induced crystallization has several advantages comparing to furnace annealing [2]. This work is devoted to development of laser assisted crystallization of Si/SiO_2 and Si/Si_3N_4 based multi-layer nano-heterostructures.

The multilayer Si/Si_3N_4 nano-heterostructures were deposited using low frequency plasma enhanced chemical vapor deposition technique on crystalline Si (100) and glass substrates. Its contain up to 9 periodic layers with 3 nm Si_3N_4 and 3 nm SiN_x with x varied from 1 down to zero. The multilayer Si/SiO_2 nano-heterostructures were deposited on Si and glass substrates. First, a-Si:H layer with thickness of 20 nm was deposited. Afterwards the part of amorphous silicon layer was processed by plasma enhanced oxidation, so that the thickness of the remainder of the α-Si:H after that was about 7 nm. These alternative procedures (depositions and plasma enhanced oxidation) are repeated as many times as the planned periods. Thus, a structure containing 6 layers of α-Si:H with thickness of 7 nm, inserted between the layers of SiO_2 with thickness 13 nm has been created. The nanosecond pulse XeCl laser with wavelength of 308 nm and pulse duration of 10 ns was used for laser treatments. Raman spectroscopy technique was used to identify the structure (amorphous or crystalline) of Si in the as-deposited and pulse laser annealed structures. Ellipsometry and photoluminescence (PL) spectroscopy were used for study of optical properties.

Raman data show that as-deposited structures contain amorphous hydrogenated Si. For multilayer Si/Si_3N_4 nano-heterostructures laser treatments lead to crystallization of the silicon layers or silicon clusters. The treatments with laser fluence from 200 to 300 mJ/cm^2 and from 1 up to 8 shots were used. The average sizes of Si nanocrystals (NCs) were estimated from Raman data, the sizes were about 4-5 nanometers. In the PL spectra of laser treated multilayer Si/Si_3N_4 nano-heterostructures appear peaks with maxima at 750-800 nm. The PL signal can be caused optical transitions in Si NCs, energy levels are shifted due to quantum-size effects, see review [3] and references in there. In the case of the multilayer Si/SiO_2 nano-heterostructures the laser fluences needed for its crystallization were found. But, for multilayer a-Si/SiO_2 nanostructures, the threshold for crystallization was very close to threshold of laser ablation. As it was shown from Raman spectroscopy data, using one-step pulse laser treatments one can get only partial crystallization. Presumably, it is due to high hydrogen concentration in these as-deposited films. From Raman data it was observed that as-deposited structures contain mostly $Si-H_2$ bonds. According to our estimates, atomic concentration of hydrogen reach up to 40 %, and this is enough for blistering (and film breakaway) during pulse laser treatments. It was also observed, that after laser treatments with fluence lower than ablation threshold, the most part of hydrogen abandon the film, but this can leads to appearance of tensile mechanical stresses in structures. Anyway, the developed approach can be applied for crystallization of many-layer Si based structures on non-refractive substrates.

The work is supported by Federal Program for 2009-2013 years, contract number P1283.

1. R. Rölver, B. Berghoff, D.L. Bätzner, B. Spangenberg, and H. Kurz, Appl. Phys. Lett., **92**, 212108, 2008.
2. V.A.Volodin, M.D.Efremov, V.A.Gritsenko, S.A.Kochubei. Appl. Phys. Lett., **73**, p.1212, 1998.
3. E.G. Barbaglovanni, D.J. Lockwood, P.J. Simpson, and L.V. Goncharova. J. Appl. Phys., **111**, 034307, 2012.

Fundamentals and applications of Plasma ALD in nanoelectronics

C. Hodson[1], T. Sharp[1], A. Peter[1]

1. *Oxford Instruments Plasma Technology, chris.hodson@oxinst.com*

Atomic Layer Deposition (ALD) has established itself as the deposition technique of choice for ultra thin, controlled, conformal, pin-hole free coatings. In an age of nanotechnology advances ALD is an ideal tool for depositing on nanoscale features.
The desirable properties of films deposited by ALD are derived from sequential self limiting surface reactions. In plasma ALD processes the reactant introduced in the second of the two ALD half reactions is used to generate a plasma; such as O_2 for oxides and some pure metals, H_2 for metals, N_2/H_2 for nitrides. The use of excited plasma species, as opposed to pure thermal energy, offers several advantages such as lower processing temperatures, higher quality films, reduced nucleation delay, control of stoichiometry and phase.
The use of plasma in ALD also has several potential drawbacks including plasma damage to the substrate and limits to the highest aspect ratio feature which can be coated. It is therefore vital to choose the correct plasma conditions for the material and desired application.

In this paper the fundamental principles of plasma ALD will be discussed in terms of reaction mechanisms and plasma conditions and their influence on the properties of the films deposited. Firstly the reaction mechanism for the ideal Al_2O_3 ALD process will be discussed. In situ diagnostic techniques such as ellipsometry, mass spectrometry and optical emission spectroscopy have shown the thermal process using H_2O as the co-reactant generates mostly CH_4 as a by-product but the more reactive O_2 plasma species generate CO and CO_2 as the principal by-products [1], [2].

It is well known that achieving low oxygen content in nitride films by ALD is not straight forward. The use of a plasma can significantly reduce the amount of oxygen under like for like conditions, for example it was found that a HfN film using NH_3 as the co-reactant had 20 at. % of oxygen when the reaction took place purely with thermal energy, however when RF power was added to the NH_3 exposure to strike a plasma the oxygen content was reduced to less than 2%.
The level of impurities such as oxygen, carbon and chlorine can directly influence properties of the film such as the resistivity; figure 1 shows low resistivites of less than 200μΩcm can be achieved for TiN by plasma ALD at just 350°C deposition temperature whereas the corresponding thermally deposited films would be several hundred degrees hotter.

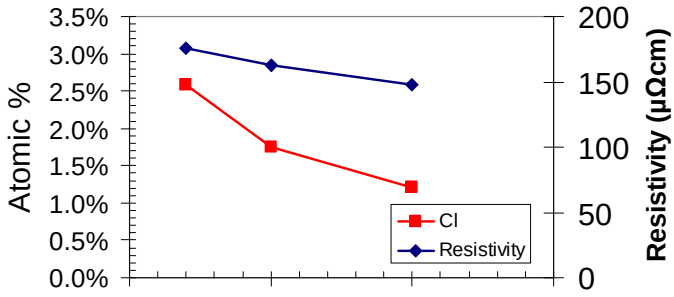

Figure 1, chlorine impurity and resistivity of TiN versus plasma exposure time at 350°C deposition temperature.

The exact composition of the plasma can directly influence the materials properties for example in the deposition of titanium nitride thermal ALD and plasma ALD using N_2 plasmas produce the resistive Ta_3N_5 phase, whereas a pure H_2 plasma will produce the cubic TaN phase which is conductive. It is not only the plasma gases that can influence the material properties but also the radical densities and ion energies play a significant role, as shown by Profit et al [3] these can influence film stress, density and crystallinity.
The properties of the films described above will be referenced against their applications in nano-electronics.

1. Heil *et al*., Appl. Phys. Lett. **89**, 131505 (2006).
2. Langereis *et al*., Appl. Phys. Lett. **92**, 231904 (2008)
3. Profijt et al, JES **158**, G88 (2011).

Applications of Plasma Immersion Ion Implantation for advanced micro/nano electronics: Challenges and case samples using IBS PULSION® Tool

F. Torregrosa[1], J. Duchaine[1], S. Spiegel[1], G. Borvon[1], F. Milesi[2], K. Hassouni[3], K. Maury[3]

1. IBS, ZI Peynier Rousset, Rue G. Imbert Prolongée, F-13790 Peynier, France, E-mail: frank.torregrosa@ion-beam-services.fr

2. CEA-Leti MINATEC Campus, 17 rue des Martyrs, 38054 Grenoble Cedex 9, France, E-mail: frederic.milesi@cea.fr

3. Laboratoire des Sciences des Procédés et des Matériaux, LSPM, CNRS-UPR3407 Université Paris 13, 99 Avenue J. B. Clément, 93430 Villetaneuse, France, E-mail: hassouni@lspm.cnrs.fr

For approximately 15 years, the development of new architectures of semiconductor devices pushes the limits of ion implantation technology. For doping applications the depth to implant is more and more shallow but the sheet resistance is asked to be reduced needing complicated "cocktail implantations". For some application doses tend to increase reaching sometime 1E17/cm² (material modification or poly-counter doping). On the industrial point of view, substrate diameter went from 150 mm to 300 mm and now 450 mm but in the same time throughput of implantation tools was asked to increase.

Thanks to its ability to implant high doses at low energies while keeping high productivity, even on large substrates, Plasma Immersion Ion Implantation (PIII) or Plasma Doping Technology has been introduced in semi-conductor production since 2005. First limited to poly counter-doping, this technology has recently seen a broadening of its potential applications and compete sometime with EPI.

After having presented the challenges needed to be solved to have PIII technology accepted in advanced semiconductor applications, we will present an overview of the work done using our PIII tool named PULSION®. First, basic phenomena taking place in the process chamber and explaining unique characteristics of plasma doped layers will be discussed and illustrated thanks to a deep modelisation of the tool. Then an overview of some applications on advanced devices will be presented: USJ doping for FD-SOI application, 3D doping for Trigate CMOS, Si Nanocrystal synthesis for Flash memories and formation of nanocavities for gettering.

Comparative Investigation of Ultra-shallow Boron Implantation into Bulk Silicon and SOI Structures by PIII technique

A. Miakonkikh[1], K. Rudenko[1], V. Rudakov[2], A. Orlikovsky[1]

1. Institute of Physics and Technology, Russian Academy of Sciences, Moscow, Russia, miakonkikh@ftian.ru

2. Yaroslavl Branch of Institute of Physics and Technology, Russian Academy of Sciences, Yaroslavl, Russia

Scaling of IC's nanotransistors to sub-32 nm nodes suggests the implementation of thin SOI-based MOSFETs with thin and undoped channels. The source, drain, and extensions regions requires extremely high doping of 5-20 nm layers with steep concentration profiles in order to avoid the side doping of channel and the insulating BOX layer. Another problem is strict limitation on silicon surface erosion during implantation process which shouldn't exceed 0.5-1 nm. Obviously, those problems are most difficult for p^+ doping with Boron. Plasma immersion ion implantation technique seems to be promising method for ultrashallow high dose doping with high performance. The present study is the development of works on bulk Silicon PIII doping [1] and focuses on above problems when PIII processing of SOI structures.

Experimental process flow has included the steps of amorphization of ultrathin layer by PIII of He ions (D = 1-5x10^{16} cm^{-2}, E_i = 1-3 keV), the PIII boron doping from BF_3 plasma (D = 1-4×10^{15} cm^{-2}, E_i = 0.2-0.7 keV) with or without gas-carrier, and RTA activation of implanted layer by Silicon re-crystallization.

It was founded significant difference in the amorphization processes in Si caused by heavy and light mass ions. The He^+ ions amorphization excludes the surface erosion and shows the complicate structures of amorphized layer. Overdosing at amorphization step can produce the nano-porous Si layer under dense a-Si affecting on resulting Boron profile after RTA. Excess over optimal ion energies results in damages at Si/BOX interface and influences on re-crystallizing of Si defects during RTA and final electrical activation of Boron impurity.

Combination of the gas-source of doping ions (BF_3) and gas-carrier (He) in plasma produce changes in relative content of ions and neutral species including chemically active F*. This effect allows to rule the side etching of surface during plasma doping step. The erosion of Si is suppressed and the upper limit of Boron concentration rising as shows by experiments.

Excess of vacancies in a-Si produced by He^+ implantation provides of effective formation of B-V clusters. As was found, the non-trivial behavior of those vacancy clusters during RTA in ultra-shallow layers close to surface could be used for Boron profile sharpening and point defect engineering in implanted layer.

Formed implanted structures were investigated by TEM, high resolution optical interferometry/microscopy, spectral ellipsometry, SIMS, and four probe techniques. The concentration profiles of Boron in SOI and bulk Si are presented in Fig. 1 and Fig.2, respectively.

Optimized regimes allows to obtain highly doped p^+ layers (up to 10^{21} cm^{-3} of boron) with thickness of 10-25 nm and slope of concentration profile 7-8 nm per decade after RTA. The sheet resistance is 1-2 kOhm/□ for sub-20 nm implanted layers in SOI.

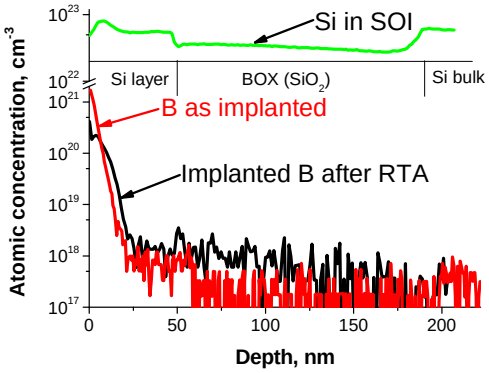

Fig. 1. Doping profile in SOI structure after PIII and RTA

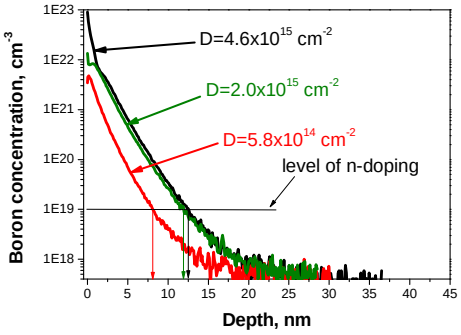

Fig. 2. Doping profiles of Boron in bulk n-Si. E_{ion}=200 eV

It was found in case of SOI doping the sheet resistance is very sensitive energy of PAI ions, whereas in case of bulk silicon doping energy of implantation was less critical. It can be explained by the role of EOR defects at the Si/BOX interface and peculiarities of subsequent RTA processing.

The work was supported by Russian Foundation for Basic Research (grant # 12-07-00745-a).

1. V. Lukichev, K. Rudenko, A. Orlikovsky, A. Lomov. Proc. of 2nd International Workshop "Plasma Etch and Strip in Microelectronics" (PESM-2009), Leuven, Belgium 2009.

Etching characteristics of GaAs in CCl_2F_2/Ar inductively coupled plasma

D.B. Murin, V.I. Svettsov, A.M. Efremov, A.E. Leventsov
Ivanovo State University of Chemical Technology, Ivanovo, Russia;
efremov@isuct.ru, svetsov@isuct.ru, dim86@mail.ru

GaAs is one of the most promising materials in modern micro- and nanoelectronic's technology. The reason is a combination of such GaAs properties as the large band gap (1.42 eV) and high charge carrier mobility (8500 cm^2/Vs) that allows one to create both high-frequency and photoelectric devices.

Currently, the patterning of the GaAs structures is provided by "dry" (plasma-assisted) technologies with the chlorine-containing gases and gas mixtures. The widely used gases are Cl_2 and BCl_3 while the inductively coupled plasma (ICP) systems are the dominant equipment type. The aims of this work were to investigate the GaAs etching kinetics in the CCl_2F_2/Ar ICP as well as to analyze the ability of optical emission spectroscopy (OES) for the etching kinetics control.

The experiments were carries out in the ICP etching reactor Platran 100 HT with a magnetic plasma confinement. The plasma was excited at 13.56 MHz. The process conditions were: gas pressure (p) of 0.1–100 mTorr, input power (W) of 500–1300 W, sample temperature (T_s) of 20–300 ^{0}C. The 50/ 50 CCl_2F_2/Ar mixing ratio was set by adjusting partial flow rates of pure gases. The GaAs samples were the fragments of polished GaAs wafer with a average size of ~ 1 cm^2. The samples were placed on the bottom electrode and negatively biased by another 13.56 MHz rf generator. The bias power (W_{dc}) was varied in the range of 0–200 W. The GaAs etching rate was calculated through the mass loss after the fixed etching time of 5 min.

Figure 1 shows the kinetic curves for GaAs plasma etching at different biasing regimes. It can be seen that for the non-zero bias the kinetic curves are quite close to direct proportionality. This allows one to assume the steady-state etching regime as well as the first kinetic order of chemical reaction between plasma active species and GaAs surface. The fact the GaAs etching rate is negligibly small at W_{dc} = 0 (i.e. when the ion bombardment energy is determined by the floating potential only) points out on the ion-assisted mechanism of the etching process. The assumption that the GaAs etching process is limited by ion-surface interaction kinetics is also confirmed by the data of Fig. 2. Really, as follows from the general plasma chemistry analysis for many molecular gases, the decreasing GaAs etching rate with increasing gas pressure is in good agreement with the change of both ion flux and energy, but contradicts with the behaviors of neutral fluxes.

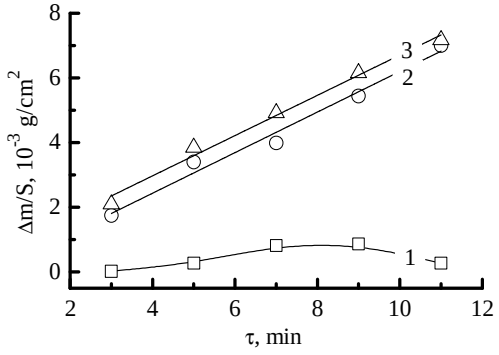

Fig. 1 GaAs mass loss as a function of etching time at W_{dc} = 0 W (1), W_{dc} = 100 W (2) and W_{dc} = 200 W (3). The other process conditions are W = 1150 W and T_s = 100 ºC.

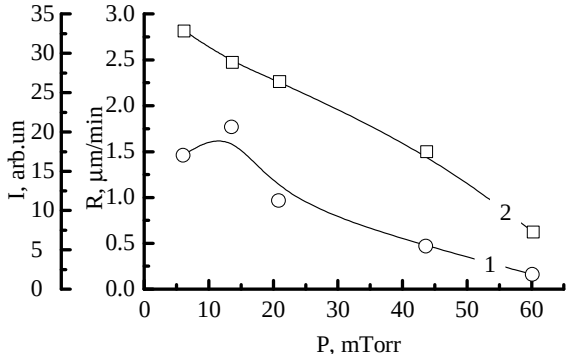

Fig. 2 GaAs etching rate (1) and Ga 417.21 nm emission intensity (2) as a function of gas pressure at W_{dc} = 200 W. The other conditions correspond to Fig. 1.

The OES measurements during the GaAs etching process showed the presence of emission lines and bands of As (228.77, 234.98 nm), Ga (294.41, 403.36, 417.21 nm) and GaCl (248.3, 251.95 nm). Assuming low excitation potential for Ga 417.21 nm line, it can be assumed that the excitation rate coefficient is low sensitive to the change of plasma parameters, and the behavior of emission intensity reflects the change of Ga density in a gas phase. Therefore, the OES data also point out on decreasing GaAs etching rate with increasing gas pressure. A not bad correlation between curves 1 and 2 in Fig. 2 opens the way for the OES-based *in situ* control of the GaAs plasma etching process.

The effects of additive gases (Ar, N_2, H_2, Cl_2, O_2) on HCl plasma parameters and composition

A. Efremov, A. Yudina, A. Davlyatshina, V. Svettsov
Ivanovo State University of Chemistry & Technology, Ivanovo, Russia, efremov@isuct.ru

The binary gas mixtures consisting of chemically active (halogen-containing) gas and noble or molecular additive gas are the widely used systems for plasma-assisted patterning of both metal and semiconductor layers in modern micro- and nano- electronics technology. The main advantage such systems is that the gas mixing ratio gives an additional tool to adjust plasma parameters and composition and thus, to optimize the etch result.

Recently, the HCl-based plasmas attract the attention due to some evident advantages over the Cl_2. Since the HCl shows much lower dissociation degrees than that for Cl_2 under the same operating conditions, the highly anisotropic etching is expected for the materials which are traditionally patterned in the chlorine-containing plasmas, and namely for the A^2B^3 and A^3B^5 group semiconductors and metals Al, Cu, Pt, Au, etc. However, the development and optimization of the etch process using the HCl-based gas mixtures is retarded by the insufficient knowledge how the additive gas influences both plasma parameters and densities of active species.

In this work we carried out the study of plasma parameters and active species kinetics in HCl/X (X= Ar, N_2, H_2, Cl_2, O_2) dc glow discharges (p = 20–300 Pa, i = 3–30 mA) using the 0-dimensional steady-state self-consistent model. The set of equations included: 1) Boltzmann kinetic equation; 2) plasma conductivity equation; 3) balance equations for neutral and charged particles; 4) quasi-neutrality conditions for densities of charged particles as well as for their fluxes to the reactor wall. The output parameters were the steady-state reduced electric field strength (E/N), electron energy distribution function (EEDF), mean electron energy and drift rate, transport and kinetic coefficients of neutral and charged species, their volume-average densities and fluxes. In order to provide the adequacy criteria for the model, the plasma diagnostics by double Langmuir probes and optical emission spectroscopy was performed.

The results can be summarized as follows:

1) The dilution of HCl by the electropositive additives (Ar, N_2, H_2) leads to decreasing E/N and to increasing electron density (n_e). This is because of decreasing both electron attachment frequency (due to decreasing HCl density) and diffusion decay frequency (due to the change of the diffusion regime with decreasing plasma electronegativity). The deformation of EEDF does not correspond to the behavior of E/N and is accompanied by increasing both fraction of high-energy electrons and electron mean energy. The reason is the lowered electron energy loss in the range of 3–10 eV due to higher excitation and ionization thresholds for additive gases compared with the HCl. A simultaneous increase in the HCl dissociation rate coefficient and the electron density provide the increasing HCl dissociation degree and the slower-than-linear fall of the Cl atom density as a function of the additive gas fraction. All mentioned effects are weakened in the sequence of Ar–N_2–H_2. The specific feature of the HCl-Ar plasma is the increasing ion flux while the rest additives results in near-to-constant ion flux.

2) The dilution of HCl by the electronegative additives (Cl_2, O_2) leads to the much weaker changes in EEDF (due to the quite close excitation and ionization thresholds for both main and additive gas) and charged species balance (due to the electron attachment to both Cl_2 and O_2 molecules). The addition of Cl_2 results in slightly increasing E/N, near-to-constant n_e and decreasing ion flux. Even the 20% Cl_2 reduces both H_2 and H densities by two orders of magnitude (due to the fast interaction of $Cl_2 + H \rightarrow HCl + Cl$) while the Cl atom density increases monotonically toward Cl_2-rich gas mixtures. The last effect is connected with the lower dissociation threshold and thus, higher dissociation rate coefficient for Cl_2 molecules. The addition of O_2 to HCl at p = const results in slightly decreasing E/N (due to lower attachment rate for O_2 compared with that for HCl) as well as in different n_e behaviors in lower and higher pressure regions. The Cl atom density exhibits a weak maximum (by 1.4 times compared with pure HCl plasma) at about 25% O_2 as well as changes insufficiently in the range of 0–50% O_2. This is because of additional formation of Cl atoms in atom-molecular reactions such as $HCl + O \rightarrow OH + Cl$, $HCl + O(1d) \rightarrow OH + Cl$ and $HCl + OH \rightarrow Cl + H_2O$. The total ion flux decreases with increasing O_2 mixing ratio.

The conductive layers on the base of multiwalled carbon nanotubes

L.P. Ichkitidze[1], B.M. Putrya[1], S.V. Selishchev[1], E.V. Blagov[2], A.A. Pavlov[2], V.A. Galperin[3], E.P. Kitsyuk[3], Yu.P. Shaman[3]

1. National Research University of Electronic Technology "MIET", MIET, Zelenograd, Moscow, 124498 Russia, leo852@inbox.ru. 2. Institute of Nanotechnology of Microelectronics, RAS, Moscow, 119991 Russia. 3. Scientific-Manufacturing Complex "Technological Centre", MIET, Zelenograd, Moscow, 124498 Russia.

Specific conductivity σ of micron- and submicron-size composite nanomaterial layers based on carboxymethyl cellulose CMC (as a matrix) and multiwalled carbon nanotubes MWCNT (as a filler) has been researched. An ultra dispersive suspension has been applied on different surfaces (cover glass, aluminium foil, polyimide and polyester sheets, cotton fabric, and shop paper) by silkscreen process.

Samples prepared on the basis of CMC without MWCNT and samples based on CMC and carbon-black K-354 were check samples. Preparation modes of dispersal suspensions with CMC+MWCNT and CMC+carbon-black K-354 were the same. Solution with 4% CMC and suspensions CMC+MWCNT and CMC+carbon black K-354 to obtain layers were disposed on substrates by silkscreen process. Substrate surfaces to improve layer adhesion were preprocessed by hydrogen peroxide. Thus prepared samples have been dried at the temperature 30 ^{o}C during ~ 60 hours.

Prepared samples corresponded layers with shape of square topology with lateral length 15 mm. In certain cases thick layers with thickness $\geq$ 50 μm were moved off from rough substrate surface by mechanical effect of scalpel tip. Generally these layers were used for measuring of material density.

Layer thicknesses were measured by different methods: hydrostatic weighing; interferometric method; micrometrical method. A relative error didn't transcend 10-15% from mean value in all cases. Electrical measures were realized by two-probe and four-probe methods. In the first method resistance was measured by contacts pressed on opposite sides of square (shape of the layer). This method allowed to test conductivity $\sigma_{\square}$ adduced on the square of the surface. The second method of measuring was realized in a "source of current" mode; in provided to define bulk specific conductivity σ subject to geometric sizes of the layer. In both methods specific conductivity was calculated from values of resistance and geometrical size of samples.

Volumes σ of samples after anneal at temperature 470 K during 30 minutes are presented. Reference values of conductivity increased in 3-5 times for samples on soft substrates; reference values of conductivity increased by a factor of ten for samples on cover glass. The highest values of conductivity $\sigma_{\square}$ adduced on the square of the surface was $\sigma_{\square} \approx 0.02 \div 0.7$ S/m. The specific conductivity ($\sigma \sim 0.01$ S/m) for check samples without MWCNT and with carbon black K-354 ($\sigma \sim 0.1$ S/m) was less in 4-5 times, than for layers based on MWCNT – $\sigma \sim 40\,000$ S/m. A conductivity variation was being observed with change of temperature for all the samples, ie samples had a semiconductor-type of conductivity. The degraded researches for numerous bendings of samples on soft layers shown that there was no significant change of conductivity. For example, bending on 180° with bending radius ~ 1 mm and frequency 100 times of samples disposed on shop paper and cotton fabric changed conductivity on ±20 % in comparison with reference values. Layers didn't peel off and split after numerous bendings.

The values $\sigma \sim 40\,000$ S/m for samples CMC+MWCNT are comparable with the conductivity (σ~10 000-50 000 S/m) tissuelike layers (so-called "buckypaper") based on the MWCNT [1], but much less than the calculated values $\sigma \geq 1\,000\,000$ S/m for individual single-walled carbon nanotubes.

Thus examined composite material has high specific conductivity and good adhesion on soft substrates. In addition material is very promissory for different applications, such as: membrane production for nanosized particles and materials for flexible electronics; security of electronic circuits and biological objects from electromagnetic radiation; elastomers and voltage-sensing device production, etc.

The work was partially funded by Ministry of Education and Science of the Russian Federation (state contract № 16.426.11.0043, September 12, 2011).

1. E.D. Laird, W. Wang, S. Cheng, B. Li, V. Presser, B. Dyatkin, Yu. Gogotsi, and C.Y. Li, "Polymer Single Crystal-Decorated Superhydrophobic Buckypaper with Controlled Wetting and Conductivity", ACS Nano, **6**, pp.1204-1213, 2012.

Investigation of nucleation and field emission characteristics of carbon nanowalls grown on porous silicon

S. Evlashin,Y. Mankelevich, A. Pilevskii, V. Borisov, P. Shevnin, A. Stepanov, N. Suetin, A. Rakhimov

Skobeltsyn Institute of Nuclear Physics, Moscow, Russia, E-mail address: stevlashin@gmail.com

In the last decades scientific attention was focused on carbon structures as a possible candidate for implementation in electronics devices. Graphene is a unique material becoming popular since 2004. Transistors, supercapacitors, Li-ion batteries, various sensors, film emission devises, and other devices are produced using carbon-based materials. In this work we investigate the nucleation of carbon nanowalls (CNWs) on porous silicon and their field emission characteristics. CNWs consist of graphene planes and the typical size of these structures is few μm in width and length and tens of nanometers in thickness. Also, these structures contain nanotubes that are formed from the nanowalls.

CNWs can be synthesized on different surfaces using seedings, mechanical polishing, and catalysts. These structures have good field emission characteristics and long lifetime.

Porous silicon was produced using photoelectrochemical methods. N-type Si (100) and p-type Si (100) with resistivity of 4.5 and 3 Ω cm, respectively, were used as substrates. The mixture of $HF:C_2H_5OH:H_2O$ in different proportions was used as a solution. Etching time varied from 10 to 100 minutes (resulting to various pore depths, which increase with the etching time). Temperature varied from 27 °C to 45 °C. N- and p-type of silicon have different structures after photoelectochemical etching. In the case of n-type silicon the created pores were up to 100 μm in depth and few microns in width. In the case of p-type silicon micron size column like structures were produced.

CNWs were grown on porous silicon in DC PECVD chamber in atmosphere of CH_4 and H_2 without additional treatment of the porous silicon surface. Growth time was 40 min. In the case of n-type silicon carbon films grow from the pore top to the bottom (see Fig 1 a)-d)). In the case of p-type silicon carbon films cover the column structures (see Fig. 1 e)-b)).

Field emission measurement was performed on hand made equipment at 10^{-7} Torr. The distance between cathode and anode was 150 μm. The emission characteristics show that with increased etching time the quantity of emission centers and the number of nucleation centers increases; the J-E curves shift to the left and the threshold decreases. The average threshold was 3 V/μm. The achieved current density was 6 A/cm^2.

The experimental setup and its parameters are thoroughly described in [1].

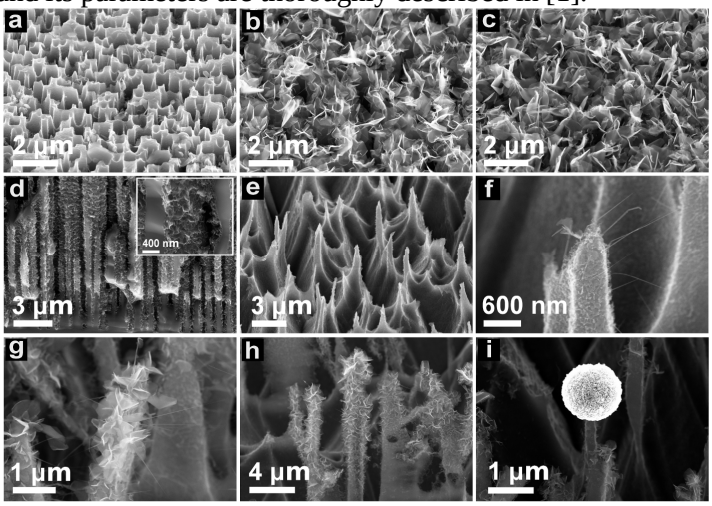

FIG. 1. SEM images of the films after photoelectochemical etching and carbon deposition in dc discharge PECVD reactor. n-type silicon—(a) etching time: 11 min, (b) etching time: 30 min, (c) etching time: 90 min, (d) cross view images at 45 tilt. p-type silicon—(e), (f) etching time: 11 min, (g), (h) etching time: 25 min, (i) formation of nanocrystalline diamond ball.

1. S. Evlashin, Yu. Mankelevich, V. Borisov, A. Pilevskii, A. Stepanov, V. Krivchenko, N. Suetin, A. Rakhimov, “Emission properties of carbon nanowalls on porous silicon”, J. Vac. Sci. Technol. B, **30**, 021801, 2012.

Properties of thin HfO_2 gate dielectric formed by Plasma ALD process

A. Miakonkikh, A. Rogozhin, K. Rudenko, and A. Orlikovsky
Institute of Physics and Technology, Russian Academy of Sciences, Moscow, Russia, miakonkikh@ftian.ru

Decrease of the gate dielectric electrical thickness providing physical thickness which is enough for suppressing tunneling current lead to implementation of high-k metal oxides as the gate dielectric, for example HfO_2 [1]. Homogeneity and electrical properties of these thin HfO_2 layers are of great importance for transistors qualities. Perspective FinFET transistors will definitely need gate dielectric deposition technology with high degree of conformity. ALD allows to produce ultrathin films with atomic level control of film thickness (only monatomic layer is deposited in each step of process), and excellent conformal coverage.

We present in this paper the results of atomic layer deposition (ALD) of high-k dielectric (HfO_2). Subsequent spectral ellipsometry measurements showed thickness uniformity of 1.5% over 100 mm wafer, and good wafer-to-wafer reproducibility. Optical constants of oxide were also measured and were shown to be in excellent agreement with reference values.

The oxide layer was formed by ALD FlexAl system (Oxford Instruments) system. Woolam Co. M-2000x ellipsometer, and Keithley 4200 SCS were used for measurements and analysis of optical and electrical properties of produced films.

The films were deposited in plasma assisted ALD process with TEMAH ($Hf(N(C_2H_5)(CH_3))_4$) as metal precursor and O_2 as non-metal plasma precursor. This process is truly self limited and hence process dependence on external parameters (stage temperature, duration of the process, pressure) is flat in wide interval. That provides “process window”, in which stable and reproducible film properties can be achieved.

Ellipsometry of 47 nm thick hafnium oxide shows n=2.27 @ λ=280 nm and n=2.05 @ λ=500 nm which is in perfect agreement with the results of previous studies [2].

CV and IV characteristics of formed gate structures were measured. They are presented on fig. 1. Obtained capacitance values correspond to dielectric constant 25.2. Leakage current values obtained at gate voltage of 1V do not exceed 0.16A/cm^2. Interface state density was also measured.

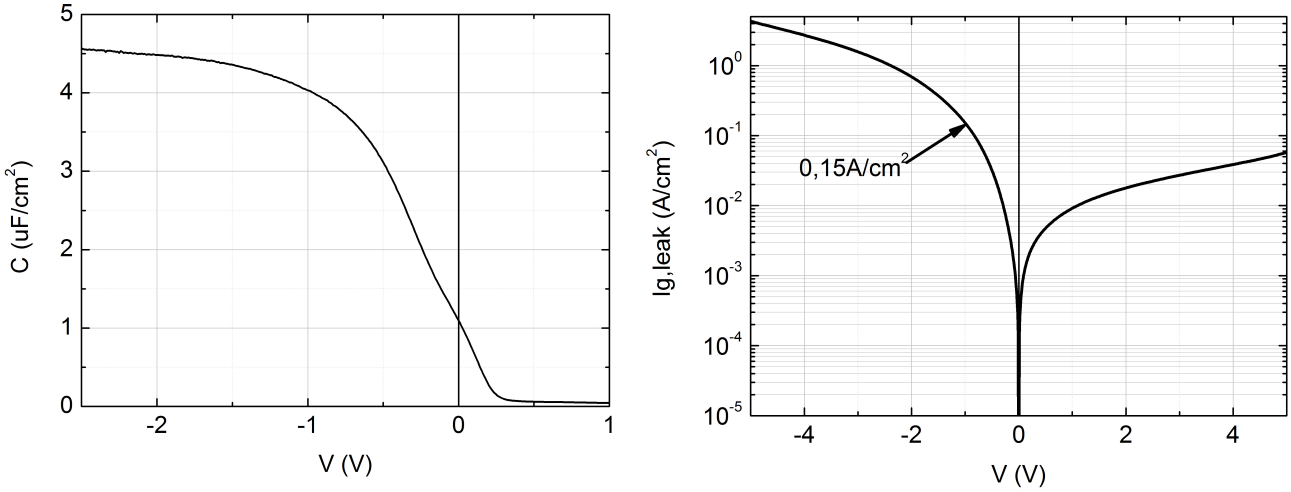

Fig. 1. CV and IV characteristics of formed gate structures.

1. J.H. Choi, Y. Mao, J.P. Chang, “Development of hafnium based high-k materials. A review”, Materials Science and Engineering, **R 72**, pp.97–136, 2011.
2. R. Rammula, J. Aarik, H. Mandar, P. Ritslaid, V. Sammelselg, “Atomic layer deposition of HfO_2: Effect of structure development on growth rate, morphology and optical properties of thin films”, Appl. Surf. Sci., **257**, pp.1043–1052, 2010.

Effect of nanodimensional polyethylenimine layer on surface potential barriers of hybrid structures based on silicon single crystal

I.V. Malyar, D.A. Gorin, S.V. Stetsyura
Saratov State University, Saratov, Russia, imalyar@yandex.ru

The recent progress of nanotechnologies gives rise to new investigations of semiconductor surface properties and thin films. The semiconductor surfaces properties crucially affect both the electric and physicochemical properties [1]. In the first case it significantly influences the characteristics of metal-insulator-semiconductor (MIS) structures, in the other one it is critical for different sensors based on field-effect [2]. The thin organic monolayers, in particular polyelectolytes, could be used for a control and adjusting of surfaces properties [3]. Such thin films have many advantages: the plenty of materials, thickness (monolayer thickness), stable and well-known simple technology (layer-by-layer electrostatic assembly), cost. Polyelectrolyte coatings can provide a high charge density that can be adjusted by changing the chemical composition and environmental parameters [4].

In this work we focused on polyethylenimine (PEI) layer influence on surface energetic characteristics of silicon single crystals as band bending, the Fermi level position, electron affinity and work function. These parameters were defined by different non-contact techniques due to artifacts of contact between metal and organic layers. Therefore we used surface photovoltage measurements and tunnel I-V curves. Different approaches were used to extract the different potential barriers from tunnel I-V curves of hybrid structures based on silicon. We estimated equilibrium tunnel barrier (which is equal to half-sum of metal and semiconductor work functions) and barrier height (which is equal the difference between metal work function and the electron affinity of semiconductor) from experiments. In addition, we characterized prepared hybrid structures using Auger electron spectroscopy (AES), ellipsometry and atomic-force microscopy (AFM), which allows one to establish the correlation between energetic and topological characteristics and parameters of organic layer.

It was revealed, that PEI deposition differently affects the surface properties of silicon single crystal versus silicon substrates conductivity type and roughness. In particular, it increases barrier height for *n*-type and decreases for *p*-type. On contrary, PEI deposition decreases the surface band bending for *n*-type (the difference between bottom of conduction band in the bulk and the surface) and increases it for *p*-type (the difference between top of valence band in the bulk and the surface). Such behavior is not usual and explanation is not obvious. We assume that electrons from the semiconductor space charge region are preferably captured to acceptor traps created by cationic polyelectrolyte on silicon surface. The behavior of the other energetic characteristics demonstrates the independence of conductivity types.

It was established that silicon substrates roughness doesn't change the behavior of changes due to PEI deposition, but influence to its magnitude. The surface roughness caused the additional surface inhomogeneities and, surface states, which essentially affects the surface potentials. But electron affinity changes after the PEI deposition are independent on roughness.

We also investigate the influence of free charge carriers concentration to PEI adsorption. We changed the charge carriers concentration by super-bandgap illumination. It was revealed that illumination generating non-equilibrium charge carriers in silicon surface layer, which affects the surface potentials barriers, charge and adsorption properties. The different effect of illumination on mentioned parameters for *n*- and *p*-type substrates was observed: increasing for *n*-type and decreasing for *p*-type.

In addition, we established the linearly dependence of some surface potential barrier changes on the molecule concentration of PEI deposited onto silicon by means of AES. All results were interpreted using band diagrams which considerate the changes of all potential barriers.

This work was financially supported in part by RFBR-project 11-08-12058-ofi-m-2011.

1. *Handbook of Semiconductor Manufacturing Technology*. ed. Y. Nishi, R. Doering . CRC Press; 2000.
2. S.M. Sze. *Physics of Semiconductor Devices.* John Willey and Sons, New York, 1981.
3. D.A. Gorin, A.M. Yashchenok, A.O. Manturov, T.A. Kolesnikova, H. Möhwald, "Effect of Layer-by-Layer Electrostatic Assemblies on the Surface Potential and Current Voltage Characteristic of Metal-Insulator-Semiconductor Structures", Langmuir, **25**, pp.12529-12534, 2009.
4. G.A. Ozin, A.C. Arsenault, *Nanochemistry. A chemical approach to nanomaterials*. The Royal Society of Chemistry, Cambridge, 2005.

Possible Influence of Nanoobjects on Properties of Nanomaterials

S.P. Timoshenkov, I.M. Britkov, O.M. Britkov, S. Evstafiev, A.S. Timoshenkov,
B.M. Simonov, E.P. Prokopev
Federal State Budgetary Institution of Higher Education "National Research University "MIET", Zelenograd, Russia,
E-mail address: epprokopiev@mail.ru

Within the limits of ideal model of property of nanomaterials in many respects are defined by joint action of the skeleton connected among themselves of nanoparticles, volume of an atmosphere of the empty space consisting of various objects of nanoemptiness (free volumes of vacancies and their complexes, pores, emptiness, etc.), and interfaces between a skeleton of nanoparticles and emptiness [1-4]. Properties of technically important materials at an atomic level are caused by generation of own Frenkel pairs (atoms and vacancies). These atoms and vacancies during work of materials in turn cooperate among themselves in rather complex image therefore defects or complexes of defects of complex structure which finally can serve as sources of dispositions are created, broken areas (BA) and pores. Protection of the basic operational characteristics of nanomaterials on visible is connected with necessity of presence for a material of certain traps of such atoms and vacancies. In volume of nanomaterials as traps own atoms and vacancies, pores, emptiness can serve, to vacancy, etc. of nanometer sizes, forming "empty" space in a material. This empty space of nanomaterials in essence is its internal atmosphere containing besides atoms and molecules of a terrestrial atmosphere own atoms, and also vacancies and their complexes in interfaces areas which are being thermal balance with a surface of nanoparticles. Owing to extremely high speeds of diffusion processes on a surface of nanoparticles in nanomaterials self-curing of mechanical and radiating infringements of a solid-state skeleton of nanoparticles while in service can undoubtedly take place. Thus within the limits of more real representations about a structure of borders of the section possessing raised energy because of presence of dispositions directly in borders has undressed and not compensated of pressure in threefold joints these representations about self-curing look even more convincing. Really, fields with distant action of forces of pressure of nonequilibrium borders of section are characterized of tensor deformations which components inside of grain of a material are proportional $r^{-1/2}$ (r - the distance up to border of grain). At this floor of pressure leads to occurrence of elastic distortions of a crystal lattice which size is maximal near to border of section [1]. This circumstance undoubtedly promotes increase in speed of diffusion and thermal processes that is caused by higher dynamic mobility of atoms of interfaces. In this connection within the limits of theoretical representations of self-organizing the hypothesis about high operational characteristics of nanomaterials, explaining on the basis of synergetic approaches [5] high operational characteristics of nanomaterials on the basis of silicon is put forward.

1. A.I. Gusev. *Nanomaterials, nanostructures, nanotechnologies*. Moscow, Fizmatgiz, 2005. 416 p.
2. E.P. Prokopev. "Synergetic approaches to problems of evolution of properties of materials and nanomaterials on the basis of silicon". *Book of Abstracts*. 3rd Chaotic Modeling and Simulation International Conference, 1-4 June 2010, Chania, Crete, Greece. pp.63-64. (see: http://www.cmsim.info/images/Book_of_AbstractsCHAOS2010a.doc)
3. E.P.Prokopev. "About gettering and synergistic approaches to the problem of silicon. Review". (in Russian) 1D = 1258787370. Science Online Library Portalus: http://www.portalus.ru/modules/science/data/files/prokopiev/Prokopiev-Getter-2009.doc
4. E.P. Prokopev. "Gettering and synergistic approaches to the problem of silicon. Review". St. Petersburg Journal of Electronics. 2009. № 3-4. P.28-46 (in Russian).
5. Yu.A. Chaplygin, V.I. Grafutin, E.P. Svetlov-Prokopiev, S.P. Timoshenkov. "Positronics and Nanotechnologies: Possibilities of Studying Nano-objects in Technically Important Materials and Nanomaterials". In book: *Advances in Nanotechnology*. Vol. 1. Editors: E.J. Chen and N. Peng. Nova Science Publishers, Binding: Hardcover, 2010. pp.191-208.

The physical and technological problems in design of pressure sensors with nano-scale piezoresistors

I. Neizvestnyi[1], G. Kamaev[1], V. Gridchin[2], and A. Cherkaev[2]

[1]*A.V. Rzhanov Institute of Semiconductor Physics SB RAS, 630090 Novosibirsk, Russia, e-mail: neizv@isp.nsc.ru;*
[2]*Novosibirsk State Technical University, pr. K. Marksa 20, 630092 Novosibirsk, Russia;*

Changing of piezoresistance coefficients with decreasing of working elements size has made it possible to suppose that the sensivity of piezoresistor increases under the transition to the nanoscale region [1]. Indeed, in a set of works it has been found that the piezoresistors sensibility really depends on cross-sectional dimensions of the sensor element [2, 3]. Manufacturing of individual pressure sensor with nano-wire piezoresistors includes such aspects as: 1) Development of technological operations for 3D formation of micro- and nano-piezoresistor structures. To produce such structures, an electron-beam and ion-beam lithography in combination with plasma-chemical etching and the double-sided lithography have been used for membrane formation with sensor location in area with a maximal mechanical stress (Fig. 1). 2) Development of methods for measuring the parameters of nano-wire piezoresistors and test structures and the investigation of their electrical characteristics. The transition from "micro-" to "nano-" parts of piezoresistor leads to a redistribution of the current density and the additional contribution to the total resistance. But the main thing is that temperature dependence of the resistance of "micro" and "nano" parts are quite different and they should be distinguished from general characteristics of the strain gauge. Experience shows that for the p^+-diffused silicon piezoresistors containing submicron (nano-sized) components, the reduction of the nano-wires cross-sectional size leads to a decrease in the temperature resistance coefficient [4]. It is shown also that the pressure sensors with nano-wire piezoresistors should have a fundamentally different topological layout that will provide the increase in their sensitivity by 30-50%.

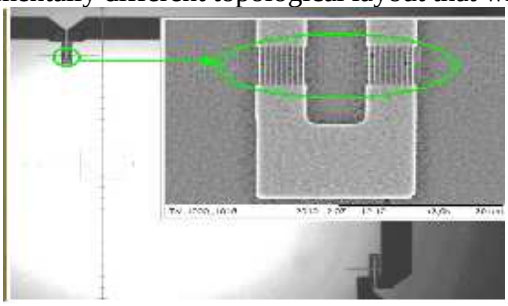

Fig. 1. The submicron set in the piezoresistor.

1. T. Toriyama, Y. Tanimoto, S. Sagiyama, “Single crystalline silicon nanowire piezoresistor for mechanical sensors”, J. Microelectromech. S., **11**, pp.605-611, 2002.
2. R. He, P. Yang, “Giant piezoresistance effect in silicon nanowires”, Nature Nanotechnology Lett., **1**, pp.42-46, Oct. 2006.
3. T. Barwicz, L. Klein, S.T. Koester, H. Hamann, “Silicon nanowire piezoresistance. Impact of surface crystallographic orientation”, Appl. Phys. Lett., **97**, 023110 (pp.1-3), 2010.
4. V.A. Gridchin, A.S. Cherkaev, M.A. Chebanov, V.B. Zinov’ev, I.G. Neizvestnyi, and G.N. Kamaev, “The influence of the sizes of the cross section of mesapiezoresistors on their characteristics”, Russian Microelectronics, **40**, pp.78-86, 2011.

Design and fabrication of piezoelectric MEMS

S. Timoshenkov, V. Vodopyanov, N. Korobova
National Research University of Electronic Technology, Department of Microelectronics, Moscow, Russia,
E-mail address:Korobova3@mail.ru

The high electro-mechanical coupling factors of PZT have made it an ideal material for use in sensors and actuators. Since thin films also exhibit these properties, they are ideally suited for applications in integrated transducers. In recent years, a new technology has emerged which allows the fabrication of integrated circuits with some type of mechanical motion built into them. These devices are called micro-electromechanical systems (MEMS) and have possible applications in devices ranging from optical shutters to air and liquid micro valves, and surface acoustic wave devices [1]. Since PZT films have the ability to transform electrical signals to mechanical motion and can be etched in the same way as conventional silicon based films, they are well suited for application in this type of device.

This paper presents short information about preparation and properties of ferroelectric films recently performed by our group. The work was carried out as direct continuation of our investigations in the field of the film preparation peculiarities and their physico-chemical properties. It is necessary to note that traditionally considerable attention was paid to the techniques for preparation of the precursor solutions containing all the elements of the future oxide composition. The reliability of the paper results is determined by the reproducibility of the object characteristics and using the metrological certified measuring equipment.

The preparation behavior of Lead Zirconate Titanate (PZT) composite films comprised of Si, SiO_2, Pt, PZT and Pt for MEMS applications was investigated. The choice of precursors can affect the microstructures and properties of the product, so in this paper we compared the crystallization behavior of PZT films derived from different precursors, stressing the influence of experiment conditions. In recent years, various methods of fabrication of PZT thick films have been proposed. However, these methods have low compatibility with conventional IC/MEMS processes or cannot obtain enough large actuator forces. The present paper proposes a simple fabrication technique of high quality PZT thick films by electrophoretic deposition method. Dense PZT films were prepared by electrophoretic deposition method (EPD), using commercial powder PZT precursor and metal alkoxide components for the same composition. EPD method is based on the principle that ceramic powders suspended in a liquid vehicle attain a surface charge. The charged particles will move under the influence of an electric field and deposit on an electrode. In general, the use of EPD for ceramic forming offers certain advantages such as short deposition time, and the ability to form a wide variety of shapes [3]. Transition metal alkoxides are very reactive and experience hydrolysis and condensation rapidly when electrophoretic deposition was carried out in air. The water content of the solution affects critically the rate of hydrolysis relative to condensation. The hydrolysis and polycondensation of metal alkoxide precursors yield an initial formation of “fractal” clusters, which upon reaching a critical size begin to form a continuous network or skeleton via cluster-cluster aggregation near the cathode-substrate. It has been found, that PZT films were crack-free and have good morphology with perfect perovskite structure and excellent piezoelectric properties. Ferroelectric hysteresis loops were measured, and the remnant polarization (P_r) of the PZT films was about 30mC/cm^2 and the coercive field (EC) was about 20kV/cm. In the radio-frequency (RF) region, the dielectric constant was about 400 and the dielectric loss is less than 0.01.

1. S. Timoshenkov, “Elements of micromechanical systems, implemented on composite structures”, Micro System Technology, N4, pp.22-25, 2002.
2. N. Korobova, Sh. Sarsembinov, “Introduction to the material science”, Almaty: KazNU, 2011, 473 pp. (in Russian)

New electronic system converter linear acceleration with custom output characteristics

S. Timoshenkov, A. Timoshenkov, A. Shalimov
National Research University of Electronic Technology, Microelectronics Dept., Zelenograd, Moscow, Russian Federation spt@miee.ru

Currently, there are a wide variety of MEMS devices: micro mirror, linear acceleration transducers (accelerometers), the angular velocity sensors (gyroscopes), pressure sensors, and others. Operation principle of these devices is different, but they all share the microsystems technology and sensor preparation methods. Special class of inertial sensors, namely, linear acceleration transducers (LAT) is allocated among the many MEMS devices.

The paper objective was to discuss preparation possibility of a linear acceleration transducer on the basis of the compensation circuitry. To achieve this goal it was necessary to solve some of the following tasks: explore the issues of building countervailing accelerometers; to develop an algorithm on the basis of existing methods for frequency determining with FPGA firmware program; develop the necessary software; model developed program; prepare test procedure to determine the basic parameters of the developed accelerometer; test similar schemes in order to compare the developed model and its analogues.

The electronic circuit of compensating accelerometer has been developed. It was shown that solving problem leads to the circuit creation which idea was so simple. It has been noted that deviation of the rotor sensing element (SE) from the starting position was done when acceleration directed along the sensitive axis of the accelerometer. It was resulting in a change in the SE equivalent capacity. Generators that were implemented under the scheme of asymmetrical multivibrator have been built in such way that the accelerometer SE acted as frequency of the driving capacitor. When acceleration appeared then changing capacity of the SE has involved a change in the frequency of generated signal. Next, the signal frequency was measured using the FPGA and the subsequent mathematical treatment. The generated output signal is a PWM FPGA - signal, which was then filtered, amplified and fed to the special plate of SE, forming thus a closed loop feedback. These generators were built around the classic multivibrator scheme. The only difference was being that the additional analog switch has been introduced to bring the signal generator level to acceptable FPGA input levels. Block diagram of signal processing unit on FPGA had two functionally counter: the input and the reference frequency. The measuring cycle began with the purification of all counters. Then both counters run on the front of the signal input frequency. Both counters were stopped when counter input frequency has been overflowed. Each of the counters formed a ready signal to the measurement when the measurement value of the counter input signal became equal to 31. The signals were formed after the capture readiness transfer counters in the appropriate registers. These signals were the start signals of the counting rate in identical units of calculation. The calculation of input signals frequency has been done in the calculation blocks. After the calculation the ready signal was formed by calculating the tone. After that, the frequencies were moved to the formation block of PWM - signal. This block was selected according to mathematical processing algorithm, and the PWM signal has been formed. Input meter block was designed to count the number of reference frequency pulses, which run out in 32 pulses frequency measuring.

It was shown that a number of basic parameters of developed LAT are either on par with similar or better than them. This allows us to talk about the viability and practical relevance of the work. Complex of scientific tasks to implement the compensating capacitive accelerometer has been decided. Designated approach provides great opportunities. In the future, the scheme can also be implemented in a solid cover with the sensing element and, therefore, to achieve dramatic downsizing accelerometer as a whole. This makes it possible to talk about the prospects of the work undertaken in order to use developed accelerometer in various fields of modern technology. Proposed electronic circuit and algorithm can significantly improve the main parameters of linear acceleration transducer in comparison with analogues.

Resonance properties of multilayer metallic nanocantilevers

I. Uvarov, V. Naumov, I. Amirov
Yaroslavl branch of the Institute of Physics and Technology, Institution of Russian Academy of Sciences, Yaroslavl, Russia, ilnik88@mail.ru

A cantilever is the key element of nano- and microelectromechanical switches, transistors, memory elements and other micro- and nanoelectromechanical devices [1, 2]. Number of switching cycles, reliability of micro- and nanomechanical devices is defined by the material properties and resonance characteristics of the cantilever. In this paper the study of resonance properties of three-layer metallic (Cr/Al/Cr and Ti/Al/Ti) nanocantilevers is presented. The thickness of metal layers was 5/30/5 nm, respectively. Thin Cr and Ti layers allowed changing the structure of basic Al layer, the surface morphology and the elastic properties of nanocantilever. Fabricated nanocantilevers (Fig. 1) had a length of 10 to 100 μm and width of 2 to 10 μm.
Nanocantilevers were fabricated using contact photolithography. After formation of cantilever pattern in photoresist mask three layers of metal (Cr/Al/Cr or Ti/Al/Ti) were sputtered. Then the lift-off process was performed and cantilevers were released by etching of sacrificial poly-Si layer in SF_6 plasma.
Cantilever vibrations were excited by an electrostatic method, registration of motion was performed by the laser beam deflection method. The resonant frequencies of cantilevers were determined from the resonant curves (Fig. 2).

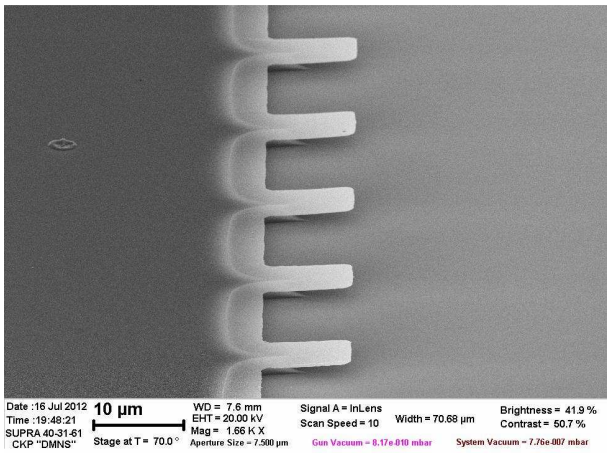

Fig. 1. SEM-image of nanocantilevers.

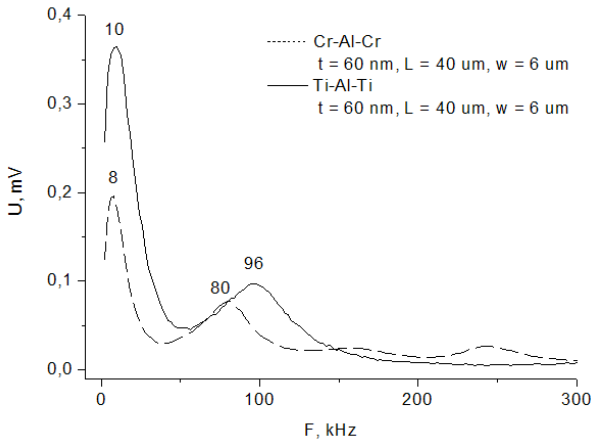

Fig.2. Resonant curves of nanocantilevers.

Dependencies of resonant frequencies on cantilever length and width were experimentally obtained. Resonant curves and the resonant frequencies of Cr/Al/Cr and Ti/Al/Ti cantilevers differed slightly, although the morphology of cantilever surface and Young's modulus of Ti and Cr were different. The comparison of experimental data with theoretical calculations according to the classical Euler-Bernoulli beam theory [3] was performed. The experimentally obtained values of the resonant frequencies were lower than theoretical predictions. It may be caused by geometrical defects arising in the fabrication process (undercut, non-ideal clamping shape of cantilevers [4], etc.), as well as the size effect that occurs in sufficiently thin films.
This work was supported by FSC "Micro- and Nanostructures Diagnosis" and RFBR grant # 10-07-00447-a.

1. S.W. Lee, S.J. Park, E.E.B. Campbell et al., “A fast and low-power microelectromechanical system-based non-volatile memory device”, Nat. Commun., **2**, p.1227, 2011.
2. Y. Loh, H.D. Espinosa, “Nanoelectromechanical contact switches”, Nat. Nanotechnol., **7**, pp.283-295, 2012.
3. R. Sandberg, W. Svendsen, K. Molhave et al., “Temperature and pressure dependence of resonance in multi-layer microcantilevers”, J. Micromech. Microeng., **15**, pp.1454-1458, 2005.
4. S. Guillon, D. Saya, L. Mazenq, “Effect of non-ideal clamping shape on the resonance frequencies of silicon nanocantilevers”, Nanotechnology, **22**, 245501, 2011.

Modeling of two-axis micromechanical gyroscope-accelerometer

I.E. Lysenko
Taganrog Institute of Technology – Southern Federal University, Taganrog, Russia, igor@fep.tti.sfedu.ru

Actual problem is to work out approaches to construction of functionally integrated micromechanical gyroscopes and accelerometers providing measurement of angular speeds and linear accelerations on several axis of sensitivity, possessing high degree of integration and allowing to lower masses characteristics of microsystems, at the expense of reduction of the substrate area used under placing of each integrated sensor. In designs of gyroscopes and accelerometers similar constructive elements are applied, therefore the same schemes of construction can be applied to their working out [1-4].

The developed integrated micromechanical gyroscope-accelerometer of the LL-type contains two inertial masses fixed on a substrate by means of a system of the springy torsions [5].

To ensure the independence of primary and secondary vibration of the inertial mass has been used principle of micromechanical gyroscopes LL-type configuration of the elastic suspension – ISOD (Inside Sense Outside Drive) [2, 6].

A gyroscope-accelerometer model of motion is developed:

$$\begin{cases} (m_n + m_m)\left[\ddot{y} - \left(\Omega_x^2 + \Omega_z^2\right)y - \Omega_x \dot{z}\right] - m_m\left[\Omega_x \dot{z}_m + \Omega_z \dot{x}_m\right] = -k_y y - \beta_y \dot{y} + F_y \pm F_{el}; \\ (m_n + m_m)\left[\ddot{z} - \Omega_x^2 z + \Omega_x \dot{y}\right] - m_m\left[\ddot{z}_m + \Omega_x \Omega_z x_m - \Omega_x^2 z_m\right] = -k_z z - \beta_z \dot{z} + F_z; \end{cases} \quad (1)$$

$$\begin{cases} m_m\left[\ddot{x}_m + \Omega_z\left[\Omega_x (z + z_m) - \dot{y} - \Omega_z x_m\right]\right] = -k_{xm} x_m - \beta_{xm} \dot{x}_m + F_{xm}; \\ m_m\left[\ddot{z} + \ddot{z}_m + \Omega_x\left[\dot{y} + \Omega_z x_m - \Omega_x (z + z_m)\right]\right] = -k_{zm} z_m - \beta_{zm} \dot{z}_m + F_{zm}. \end{cases} \quad (2)$$

where $m_п$, m_m – masses of the moveable electrodes and the inertial masses; k_y, k_z, k_{xm}, k_{zm} – suspension stiffness; β_y, β_z, β_{xm}, β_{zm} – damping factors; y, z, x_m, z_m – displacements; Ω_x, Ω_z – angular speeds; F_{el} – electrostatic force; F_y, F_z, F_{xm}, F_{zm} – inertial forces.

In deriving the model of the gyroscope-accelerometer the following assumptions were made: springy elements of the moveable electrodes and the inertial masses suspension have a finite stiffness in bending relative to the axes X, Y, Z.

The numerical modeling of the gyroscope-accelerometer in the ANSYS was executed. Results of modelling are processed in the program MATLAB. The obtained modeling results can be used in the design of two-axis micromechanical gyroscopes-accelerometers.

The research is carried out under financial support of the Ministry of education and science of Russia (project №301.38.06.51).

1. V. Raspopov. *Micromechanical devices*. Mashinostroenie, Moscow, 2007 (in Russian).
2. V.D. Verner, P.P. Malcev, A.A. Reznev, A.N. Saurov, Yu.A. Chaplygin, Modern tendencies in development of microsystem technique // Nano- and microsystem technique, **8**, pp.2-6, 2008 (in Russian).
3. M. Palaniapan. *Integrated surface micromachined frame microgyroscopes*. University of California, Berkeley, 2002.
4. I. Lysenko, B. Konoplev, “3D micromachined gyroscope”, Proceeding of the International Conference “Micro- and nanoelectronics – 2003” (ICMNE-2003), p.O3-76, 2003.
5. I.E. Lysenko. *Integrated micromachined gyroscope*. Patent №2293337 RU, 2007.
6. I.E. Lysenko, “Design method of micromachined gyroscope-accelerometer LL-type”, News of SFedU. Technical sciences, **1**, pp.117-123, 2009 (in Russian).

Matrix propulsion microthruster for nanosatelites

V. Bondarenko[1], K. Dobrego[2], L. Dolgyi[1], A. Klushko[1], E.Chubenko[1], S. Futko[2]
1. Belarusian State University of Informatics and Radioelectronics, Minsk, Belarus, E-mail address: vitaly@bsuir.edu.by 2. A.V. Luikov Heat and Mass Transfer Institute, National Academy of Sciences of Belarus, Minsk, Belarus, E-mail address: foutko@itmo.by

In the present work we reported on matrix propulsion microthrusters for high-accuracy position control of nanosatelites (mass < 10 kg).
Matrix propulsion microthrusters have been fabricated and tested. As seen from Figure 1, the microthruster consists of 25(5x5) combustion chambers containing propellant; a middle matrix of 25 ignitors made in silicon wafer with thin silicon burst membranes and heating resistors; and a matrix of 25 nozzles. All elements of microthruster are made of silicon by using MEMS technology. A propellant based on glicidil-azide-polymer (GAP) is loaded into each individually sealed combustion chamber. When the resistor of ignitor is heated, the propellant ignites, raising the pressure in the chamber and rupturing the membrane. An impulse is imparted as the high pressure fluid expelled from the chamber through the nozzle. Initial tests, using nanocomposite mixtures based on GAP as the propellant [1, 2] have produced several 10^{-3} Newton×second of impulse. The matrix propulsion microthrusters offer new possibilities of nanosatelite-keeping capabilities, potentially at lower cost.

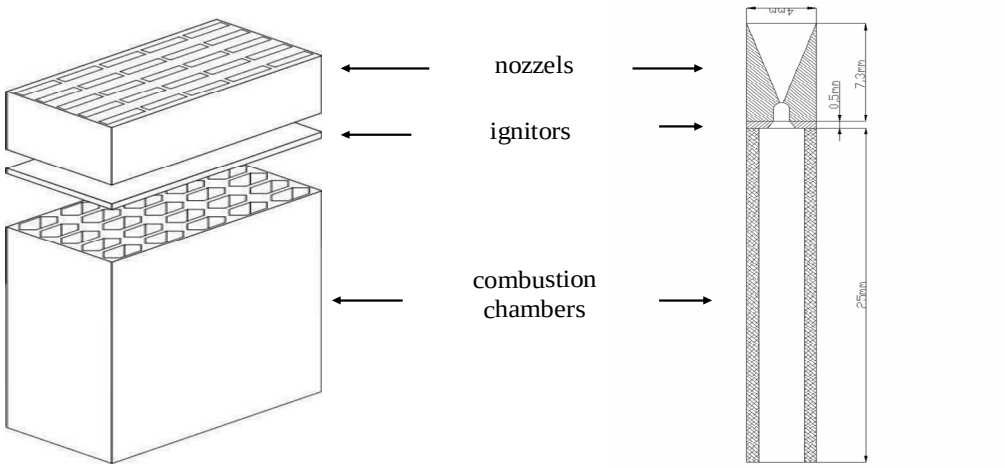

Figure 1. Schematic of matrix propulsion microthruster.

This research was financially supported by Grant 2.2.3 of the Union State Scientific Program “Nanotechnology-SG”.

S. Fut’ko, E. Ermolaeva, K. Dobrego, V. Bondarenko, L. Dolgyi, “Thermodynamic analysis of solid-fluid mixtures glycidil azide polymer (GAP)/RDX for mini-engines of a microelectromechanical systems”, J. Engineering Physics and Thermophysics, **84**, pp.1068-1073, 2011.
S. Fut’ko, E. Ermolaeva, K. Dobrego, V. Bondarenko, L. Dolgyi, “Macrokinetic calculation of the ignition of a solid-fuel charge of mixtures glycidil azide polymer in the mini-engine of a microelectromechanical systems”, J. Engineering Physics and Thermophysics, **84**, pp.1304-1310, 2011.

Formation of Nanoscale Structures by Inductively Coupled Plasma Etching

C. Welch
Oxford Instruments Plasma Technology, Bristol, UK, E-mail address colin.welch@oxinst.com

Patterning of films and substrates has long been required in the fabrication of devices for information and communication technology (memories, novel semiconductor and optoelectronic devices, displays and quantum computing), as well as other areas of technology such as medical and energy [1]. Overwhelmingly, the most popular method of patterning for devices is by the selective removal of solid material through a mask (usually photoresist) [2]. This of course is etching. The performance of devices has been steadily improving with decreasing feature size, such that now, in many technology areas the devices may be described as nanoscale i.e. one or more critical dimension of the device is within the range 1nm to 100nm.

The classic example is in etching steps required for monolithic integrated circuit fabrication (such as Complementary-Metal-Oxide Silicon (CMOS) transistor chips) with feature sizes on the micron scale and now much less. Etching for such microelectronics evolved from wet chemistry in the 1960s and 70s (usable down to about 5µm dimensions) to dry etching with parallel plate plasma systems (Reactive Ion Etching, RIE) usable down to 0.1µm or less in favourable cases and finally, since roughly the early 1990s to dry etching with high density plasma (HDP) systems, especially inductively coupled plasma (ICP) taking us below 100nm into nanoscale dimensions. Indeed CMOS technology has long since progressed into the nanoscale: The International Technology Roadmap for Semiconductors (ITRS) 2011 update indicates this occurred in about 2003 when considering half pitch gate widths for flash or DRAM technology [3].

This paper will focus on the top down technique of ICP etching for the nanoscale. The increased difficulties of nanoscale etching will be described. However it will be shown and discussed that ICP technology is well able to cope with the higher end of the nanoscale: from 100nm down to about 40nm is relatively easy with current ICP technology. It is the ability of ICP to operate at low pressure yet with high plasma density and low (controllable) DC bias that helps greatly compared to simple RIE, and, though continual feature size reduction is increasingly challenging, improvements to the ICP technology as well as improvements in masking are enabling sub-10nm features to be reached [4]. Nanoscale ICP etching results will be illustrated in the area of nano-imprint technology and in a range of various materials and technologies. The results are all achieved in Oxford Instruments ICP tools, demonstrating a strong capability in nanoscale etching.

1. See: http://en.wikipedia.org/wiki/List_of_nanotechnology_applications
2. G.S. Oehrlein, R.J. Phaneuf and D.B. Graves, Plasma-polymer interactions: A review of progress in understanding polymer resist mask durability during plasma etching for nanoscale fabrication, J. Vac. Sci. Technol. B, **29(1)**, 2011.
3. See: http://www.itrs.net/reports.html
4. C. Peroz, S. Dhuey, M. Cornet, M. Vogler, D. Olynick and S Cabrini, Single digit nanofabrication by step-and-repeat nanoimprint lithography, Nanotechnology, **23**, 015305, 2012.

Plasma etching of silicon for MEMS and optical applications: comparison of RIE, Bosch and cryogenic processes

I. Amirov[1], V. Lukichev[1], V. Yunkin[2]

1. Institute of Physics and Technology of Russian Academy of Sciences, Moscow, Russia. E-mail: lukichev@ftian.ru

2. Institute of Microelectronics Technology of Russian Academy of Sciences, Chernogolovka, Russia.

Micro-electro-mechanical systems (MEMS) are of interest for industry and science. Single microlenses (refractive and diffractive) and integrated micro-lens arrays provide interesting applications for various fields such as photonics, x-ray microscopy and imaging, LCDs, etc.

Plasma etching of silicon is a key technology in fabricating MEMS and optical devices. We compare three leading processes for deep plasma etching of silicon: reactive ion etching (RIE), the Bosch and cryogenically cooled processes.

We present main differences in plasma parameters and performance between RIE, Bosch and cryo processes, and review the advantages and drawbacks of them for various applications.

Finally, we demonstrate some MEMS and optical devices designed, developed and fabricated in Russian Academy of Sciences.

Low-temperature synthesis of carbon nanotubes by plasma enhanced chemical vapor deposition

V.A. Galperin, A.A. Pavlov, Yu.P. Shaman, A.A. Shamanaev, S.N. Skorik
Scientific-Manufacturing Complex "Technological Centre", Moscow, Russia, e-mail: artemiy.shamanaev@gmail.com

The sizes, highest mechanical, electrical, electromechanical, and thermal properties over a wide temperature range determine the perspective applications of the carbon nanotubes (CNT) in the micro- and nanoelectromechanical systems. A successful use of CNTs in functional elements of devices in some cases requires to develop a low-temperature synthesis of CNTs ($T < 600$ ºC).

The influences of the adhesive layer and the catalyst film on the growth of CNT arrays were investigated to decrease the process temperature. As the adhesive layer on the surface of the substrate were deposited Al, Al_2O_3, SiO_2, Ta, Cu, Ti, and TiN, also as catalysts for CNT growth were used Ni or FeNiCo films, deposited on the adhesive layer.

The carbon nanotubes synthesis is based on the plasma enhanced chemical vapor deposition method. The samples were annealed by oxygen before the CNT synthesis. Studies have shown that the use of an adhesive layer of Ti, as well as the Ni film catalyst can decrease the temperature of the substrate up to 350 ºC.

1. M. Meyyappan, L. Delzeit, A. Cassell, and D. Hash, "Carbon nanotube growth by PECVD: a review", Plasma Sources Sci. Technol., 12, pp.205-216, 2003.
2. S.V. Bulyarskii, O.V. Pyatilova, A.V. Tsygantsov, A.S. Basaev, V.A. Galperin, A.A. Pavlov, and Yu.P. Shaman, "Thermodynamics of the formation of catalyst clusters for carbon nanotube growth", Semiconductors, 44, pp.1718-1722, 2010.

Photovoltaic properties of porous-Si:He/Si structure produced by plasma immersion ion implantation

A. Rogozhin, A. Miakonkikh, and K. Rudenko
Institute of Physics and Technology, Russian Academy of Sciences, Moscow, Russia, rogozhin@ftian.ru

As known high dose He-implantation can dramatically affect Si properties. Basically it changes crystalline structure of silicon producing layers of amorphous, nanoporous, disordered and defected silicon. Among others the optical properties of the semiconductor can be considerably changed. Because of direct band structure of nano-porous Si and its higher band gap energy (~1.8eV) [1] amorphized Si:He (a-Si:He) could be more attractive for optical applications like photo detectors and solar cells.

Plasma immersion ion implantation (PIII) has a number of advantages compared with beam-line implantation. It allows to achieve doses up to $10^{17}cm^{-2}$ in time of several seconds, has scalability up to 500 mm and produce implantation of high conformity which is important for structures with complicated surface design. The structures a-Si:He/c-Si had electroluminescence spectrum within the wavelength range 400-800 nm [2], which covers about 80% of energy of solar radiation spectrum. This raises interest to investigation of a-Si:He/Si structures solar cell application.

In this study a structure made by PIII of He^+ into boron-doped p-type Si(100) with resistivity of 12 Ohm·cm is presented. Formation process consisted of cleaning wafers, implantation, thermal annealing, and deposition of back contact and transparent top contact.

The layer of native SiO_2 was removed by $HF:H_2O$ (6:50) preliminary rinsing for 5 min. He^+ energy in implantation process varied from 1 to 5 keV. It produced Si amorphization for depth of about 100-200 nm. Implanted ion doses was in the range $5\cdot10^{16}$-$2\cdot10^{17}cm^{-2}$, which forms layer of nano-porous silicon. Thickness of modified layer was calculated with a free software TRIM and measured by spectral ellipsometry. After annealing at 600ºC for 60 min the semi-transparent gold layer (~200Å) for photo-current collection was deposited. Top Ni electrode was formed by magnetron sputtering through mask with subsequent annealing. Area of transparent section of the devices was equal to $0.5cm^2$.

Electrical characteristics of these devices was measured and analyzed. Dark current-voltage and capacitance-voltage characteristics were measured. As it was estimated from the assumed energy band structures, the devices show diode-type characteristics with relatively high reverse current (~100 uA/cm^2 at −10 Volts). Light characteristics were obtained under radiation of the 20W-halogen lamp at constant energy flux, showing photovoltaic effect. The ways for optimization of photovoltaic parameters has been targeted.

Part of this work was supported by Russian Ministry of Education and Science. For experiments the equipment of Micro- and Nanostructure Diagnostics Center was used.

1. F.P. Romstad, E. Veje, “Experimental determination of the electrical band-gap energy of porous silicon and the band offsets at the porous silicon/crystalline silicon heterojunction”, Phys. Rev. B, **55**, pp.5220-5225, 1997.
2. P.R. Desautels, M.P. Bradley, J.T. Steenkamp, and J. Mantyka, “Electroluminescence in plasma ion implanted silicon”, Phys. Status Solidi (a), **206**, pp.985-988, 2009.

On a way to fabrication technology of ultra thin Si on sapphire

V. Chernysh[1], A. Shemukhin[2], Yu. Balakshin[1], N. Egorov[3], V. Goncharov[3], S. Golubkov[3], A. Sidorov[3], B. Malukov[3], V. Statsenko[4], V. Chumak[4]

1. Faculty of Physics, Moscow State University, Moscow, Russia, chernysh@phys.msu.ru. 2. Institute of Nuclear Physics, Moscow State University, Moscow, Russia. 3. Research Institute of Material Science and Technology, Zelenograd, Russia. 4. Epiel Joint Stock Company, Zelenograd, Russia.

The idea of silicon on sapphire (SOS) technology was invented in the early 60-th of the last century. SOS structure is fabricated by deposition of silicon film onto (1102) plane of sapphire wafer. Main advantages of such approach are possibility to develop radiation resistant electronic devices operating at high frequency (up to 12GHz) and consuming low power.

A serious problem appeared under realisation of this technology. It was found that a strongly defect layer with a thickness about 100 nm was formed at silicon–sapphire interface due to lattice unconformity between the crystal lattice of Al_2O_3 and the Si crystal lattice. To overcome the problem a process called as solid phase epitaxial regrowth (SPER) was suggested [1]. During the last decade, Peregrine Semiconductor Company successfully used this technology for production of the 0.50μm and the 0.25μm SOS wafers.

Though researches in the field of production of ultra thin SOS structures were carried out since the beginning of the 80th years of the last century (see, for example, [2-5]), parameters of implantation and annealing processes are not optimized still.

Therefore in the present work searches of optimum conditions of SPER technology were continued. First of all the main attention was given to reveal an optimum temperature and a dose of Si^+ ion implantation. In addition, the energy of implanting ions varied in these experiments.

Implantation experiments carried out on the accelerating complex created on the basis of the implanter HVVE-500 (“High Voltage Engineering Europe"). Energy of implanted Si^+ ions varied from 140 up to 230 keV. SOS structures with thickness about 300 nm produced by Epiel Joint Stock Company were investigated before and after ion implantation and also after recrystallization annealing by using RBS with 1,5 MeV He^+ ions. X-ray analysis was also applied for the analysis of the Si film crystalline structure. SIMS analysis was used to investigate the interface layer between Si film and Al_2O_3 wafer. Surface topography of the Si film was controlled at all stages by using scanning electron and atomic force microscopy. The regrowth annealing was performed in nitrogen or oxygen atmosphere at temperatures 500-1000° C.

The obtained results are discussed in the report. The carried-out researches allowed to make a conclusion on mechanisms SPER and to define implantation conditions at which significant improvement of crystal structure of the silicon film is observed.

1. S.S. Lau, et al. Applied Physics Letters, **34**, pp.76-78, 1979.
2. T. Nakamura, H. Matsuhashi, Y. Nagatomo. Oki Technical Rev., **71**, p.66, 2004.
3. I. Golecki, R.L. Madox, and K.M.Slica, J. Electron. Mater., **13**, p.373, 1984.
4. Q.Wang, Y Zan, J Wang, Y Yu, Materials Science and Engineering B, **29**, pp.43-46, 1995.
5. P.A. Alexandrov, K.D. Demakov, S.G. Shemardov, Yu.Yu. Kuznetsov, Semicoductors, **44**, pp.1433-1435, 2010.

Nonlinear waves and structures induced by ion bombardment of solids

S. Krivelevich[1], D. Korshunova[2], N. Pron[2]

1.Yaroslavl branch of the Institute of Physics and Technology, Russian Academy of Sciences, Yaroslavl, Russia, s.krivelevich@mail.ru. 2. Yaroslavl State University. PG Demidova, Yaroslavl, Russia, dasha_zor@mail.ru

Modern manufacturing technologies widely use treatment of various materials by ion beams. One of the most common tools in micro-and nanoelectronics is ion implantation. It allows introducing a certain amount of impurities with high accuracy for a given depth that can provide controlled local modifications of the properties of the material. Using ion implantation also makes it possible to synthesize buried layers with specified properties [1]. In this work presents the results of the study of processes occurring in solids under the influence of ion fluxes and processes occurring at the stage of postimplantation treatments.

The response of the system exposed to the ion beam is nonlinear and it is accompanied by significant changes in the properties of the material and the formation of different structures. The changes are observed not only in the layer, which is directly exposed, but also at depths, in some cases by orders of magnitude greater than the thickness of this layer [2]. There are several types of structures in the layer directly exposed to, and beyond. For example, well known are formed on the surface of the ripple structures [3]. The variety of forming structures, suggests that the processes initiated by exposure fluxes of ions to the solid surface, are show a number of physical mechanisms. Many of these mechanisms are currently not well studied.

Description of the processes accompanying ion implantation is complicated by the fact that real solids contain significant amounts of impurities and structural defects. External action also leads to the appearance of defects and heat fluxes directed into the depth of the irradiated material. In this regard, the behavior of multivariable heterogeneous open gradient systems was analyzed. We propose a method to describe the evolution of such systems in the framework of the Ginzburg-Landau equation. It is shown that the description of n-parametric system can be implemented using n independent nonlinear equations.

Found that one of the main mechanisms leading to the modification of the properties of the irradiated material far beyond run of the primary particles, is the mechanism of wave excitation flip. The spread of such a wave is not necessarily accompanied by mass transfer from the surface into the depths of the crystal, but may be accompanied by a redistribution of impurity atoms and intrinsic point defects

It is shown experimentally that by irradiation with argon ions of two-layer system of nickel-aluminum in the surface layer of intermetallic compounds are formed. The thickness of the intermetallic layer substantially exceeds the projected range of ions. The thickness of the layer and its composition are practically independent of the ion current density and temperature of the sample. These are determined the dose of implantation. This confirms the theoretical conclusions of the work.

On the basis of theoretical studies provided a method of formation by ion implantation of buried silicate layers of complex composition. The method is based on the sequential implantation into silicon ions of oxygen and glass-forming element is compatible with silicon. The processes of formation of the layers investigated with theoretical and experimental methods. It is shown that the hidden silicate layers are formed within a few minutes during heat treatment in the temperature range 1000-1050 °C

1. Z. Lizong, L. Diantong, W. Zhonglie, Z. Bei, P.L.F. Hemment, “SOI structures produced by oxygen ion implantation and their annealing behavior”, Nucl. Instr. Meth., B, **55**, pp.754-757, 1991.
2. D.I. Tetelbaum, E.V. Kurilchik, N.D. Latisheva, “Long-range effect at low-dose ion electron irradiation of metals”, Nucl. Instr. Meth. B, **127/128,** pp.153-156, 1997.
3. R.M. Bradley, J.E. Harper, “Theory of ripple topography induced by ion bombardment”, J. Vac. Sci. Technol. A, **6**, pp.2390-2395, 1988.

Entanglement in a system of harmonic oscillators

Y. Ozhigov
Moscow State University of M.V.Lomonosov, Insitute of Physics and Technology RAS (FTIAN)
e-mail: ozhigov@cs.msu.su

We consider the system of interacting harminic oscillators of close masses and establish the rough estimation of their degree of entanglement in ground state and few excited states. It was found that already ground state is entangled, and the entanglement of excited states depends of their modes and oscillators positions. The case where this system is conformed and included into the three dimension space is also considered.

1. K.C. Lee et al., *Entangling macroscopic diamonds at room temperature*, Science, **334**, pp.1253-1256, 2011.
2. R. Feynman et al., *Quantum mechanics in path integrals*. McGrew Hill Company, NY, 1966.
3. Y. Ozhigov, *Constructive physics*, Nova Science Publ., 2011.

The strong influence of weak observers on the electron dynamics in large coupled quantum dots clusters

L. Fedichkin[1,2,3]

1. Institute of Physics and Technology, Russian Academy of Sciences, Moscow, Russia.
2. Moscow Institute of Physics and Technology, Dolgoprudny, Russia, leonid@phystech.edu.
3. NIX, Moscow, Russia, leonid@nix.ru.

The electron transport in the array of coupled semiconductor quantum dots is considered. Since low temperatures conditions are assumed therefore thermal activated behavior of electron jumps between dots is suppressed and coherent tunneling is dominated. The interaction with outer electrons and acoustic phonons is taken into account. Analytical expressions for the electron density matrix are derived for both very weak and very strong coupling with observer-environment. The temporal dynamics results obtained reveal phase-transition features as strength of interaction with the environment gradually increases. The sharp transition between quantum and classical behavior of the same structure with only slightly different parameters provides an opportunity to combine easily elements with quantum evolution and their classical controllers on one chip.

Analysis of quantum processes: methods and results

A.Yu. Chernyavskiy[1,2]

1. *Institute of Physics and Technology, Russian Academy of Sciences, Moscow, Russia*
2. *Moscow State University, Moscow, Russia*

It's well known that an ideal quantum gate is described by a unitary transform. However, real gates are always noisy and we need to use the formalism of quantum processes (quantum operations) instead of unitary operators. Quantum processes can be described equivalently by different mathematical objects. We use Kraus operators, Choi-Jamiolkowski relative states and the evolution matrix formalism. Choi-Jamiolkowski isomorphism unambiguously associates the quantum process E with the density matrix $\rho = E \otimes I \,|\Phi\rangle\langle\Phi|$, where $|\Phi\rangle = 1/\sqrt{d}\sum_{i=1}^{d} |i\rangle\otimes|i\rangle$ is the maximally entangled state and I is the identity operation. This correspondence allows using the apparatus of density matrix analysis for quantum operations. For example, we can use fidelity to analyze an accuracy of quantum processes. In addition, we can use different measures of entanglement to analyze an entanglement of quantum processes and quantum noise.

Different quantum gates, which are important for quantum computers, are considered: CNOT, SQiSW, Toffoli, CZ. These gates are modeled under the condition of amplitude and phase relaxation. Modeled gates are analyzed in terms of Choi-Jamiolkowski isomorphism, including the analysis of entanglement dynamics during the action of gate Hamiltonian. We use the negativity and the distance to PPT-states, which is calculated by convex optimization, as entanglement measures.

Moreover, the question of the entanglement of the noise in quantum gates is discussed to quantum error correction.

1. Yu.I. Bogdanov, A.Yu. Chernyavskiy, A.S. Holevo, V.F. Luckichev1, S.A. Nuyanzin, A.A. Orlikovsky, "Mathematical modeling of quantum noise and the quality of hardware components of quantum computers.", Trudy FTIAN, 2012 (in Russian); arXiv:1207.3313 [quant-ph]
2. J. Cirac, W. D¨ur, B. Kraus, M. Lewenstein, "Entangling operations and their implementation using a small amount of entanglement", Physical Review Letters, **86**, pp.544–547, 2001.
3. A.S. Holevo, V. Giovannetti, "Quantum channels and their entropic characteristics", Rep. Prog. Phys., **75**, 046001, 2012; arXiv:1202.6480 [quant-ph].

Entanglement-annihilating quantum dynamical processes

S.N. Filippov[1,2]

1. *Institute of Physics and Technology of the Russian Academy of Sciences, Moscow, Russia*
2. *Moscow Institute of Physics and Technology, Dolgoprudny, Moscow Region, Russia*

E-mail address: sergey.filippov@phystech.edu

The most general description of quantum dynamical processes is based on the concept of completely positive trace-preserving maps also called quantum channels. This report deals with local two-qubit channels of the form $\mathrm{E}_1 \otimes \mathrm{E}_2$, where E_1 and E_2 are channels acting on individual qubits. Local channel is an appropriate model for describing the evolution of two qubits in experiments, where both of them have been prepared by a single source, then separated in space, and affected by individual environments (e.g., two electrons in quantum dots or nanowires). The originally entangled two-qubit system will become less entangled or disentangled at all due to the interaction of qubits with individual environments (see Fig. 1). We find parameters of channels E_1 and E_2 under which the entanglement can or cannot be preserved.

We will refer to the local two-qubit channel $\mathrm{E}_1 \otimes \mathrm{E}_2$ as *entanglement-annihilating* (EA) if the output state $\rho_{out} := \mathrm{E}_1 \otimes \mathrm{E}_2[\rho_{in}]$ is separable for all two-qubit input states ρ_{in} [1]. In contrast to this notion, a channel E is called *entanglement-breaking* (EB) if the state $\rho_{out}^{+anc} := \mathrm{E} \otimes \mathrm{I}_{anc}[\rho_{in}^{+anc}]$ is separable for any ancillary system. In particular, the local two-qubit channel $\mathrm{E}_1 \otimes \mathrm{E}_2$ is EB if and only if E_1 and E_2 are both EB.

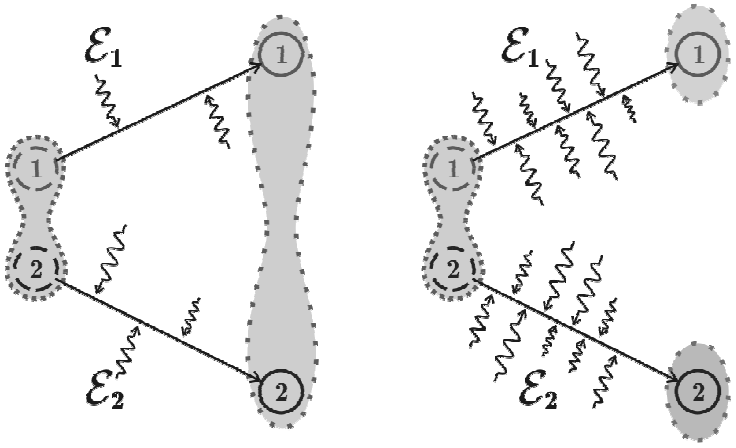

Figure 1. An initially entangled state can remain entangled at low level of quantum noise (left). In case of a strong quantum noise the entanglement can be destroyed for *any* initial state (right, EA-channel $\mathrm{E}_1 \otimes \mathrm{E}_2$).

We start with the instructive example of depolarizing qubit channels $\mathrm{E}_i[X] = q_i X + (1-q_i)tr[X]\frac{1}{2}I$, $-\frac{1}{3} \le q_i \le 1$, $i = 1,2$. The channel $\mathrm{E}_1 \otimes \mathrm{E}_2$ is shown to be EA whenever $q_1 q_2 \le \frac{1}{3}$ [2]. On the contrary, such a two-qubit channel is EB if simultaneously $q_1 \le \frac{1}{3}$ and $q_2 \le \frac{1}{3}$. This example clearly demonstrates that EA-property imposes much stronger limitations on entanglement-assisted applications then EB-property.

We provide a detailed characterization of annihilation of entanglement for a variety of channels including depolarizing, unital, (generalized) amplitude-damping, and extremal channels [2]. We also consider the convexity structure of local EA qubit channels and introduce a concept of EA duality.

Finally, the developed formalism is extended to the dynamics of multipartite systems ($\mathrm{E}_1 \otimes \mathrm{E}_2 \otimes ... \otimes \mathrm{E}_n$) and Gaussian (continuous-variable) states, which is of great interest for on-chip quantum optics experiments.

1. L. Moravčíková and M. Ziman, "Entanglement-annihilating and entanglement-breaking channels", J. Phys. A: Math. Theor., **43**, 275306, 2010.
2. S.N. Filippov, T. Rybar, M. Ziman, "Local two-qubit entanglement-annihilating channels", Phys. Rev. A, **85**, 012303, 2012.

Euclidean qubits versus conventional quantum circuits

A.Yu. Vlasov[1, 2]
1. Federal Radiology Center, IRH, St.-Petersburg, Russia, E-mail: qubeat@mail.ru
2. A. Friedmann Laboratory for Theoretical Physics, St.-Petersburg, Russia

Quantum circuits with conventional qubits are represented by complex vector spaces with Hermitian scalar product often denoted as $\langle \boldsymbol{a}|\boldsymbol{b}\rangle$ in Dirac notation [1]. Alternative models with real vector spaces and Euclidean scalar product also may be considered [2]. A reduced example of such *Euclidean qubit* with 2D real space is also known as *rebit* [3]. An extended model with 4D-real vector space is also useful, because the space corresponds to 2D complex vector space of conventional qubit. The 4D real space also corresponds to quaternions **H** and the system may be called H-*qubit* [2]. Yet, such a model [2] has some difference with usual qubit described by Bloch sphere $\mathbf{S}^2$, because scalar products are not the same in both cases and states of H-qubit are vectors with unit norm in 4D Euclidean space and belong to *glome* (hypersphere) $\mathbf{S}^3$.

Formally, H-qubit is an analogue of usual qubit up to surplus information about phase. The difference is clearer for *n*-qubits case described by tensor product of *n* 2D complex spaces. It has dimension 2^n as complex space and corresponds to real vector space with dimension $2\cdot 2^n = 2^{n+1}$, but tensor product of *n* 4D real spaces for *n* H-qubits has dimension $4^n = 2^{2n}$ and for $n > 1$ the dimension is bigger.

Euclidean qubits were considered in [2] as illustrative examples of simplification of error correction codes for such systems, e.g. simple repetitive code with *three* H-qubits *does* exist. In usual case quantum error correction codes may not use less than five qubits [1], but three H-qubits are represented by 64-dimensional real space versus 32-dimensional complex space for five qubits. Yet, physical implementation of H-qubits is rather uncertain. An example with four-component Majorana spinor was used in [2] and recently the Majorana ideas attracted more attention [4].

However, considered model should not be confused with alternative approach to fault tolerant quantum computation connected with topological properties of anions [5] despite of similarity in terminology. In fact, both interpretations of term “Majorana fermion” are discussed in [4], but analogues of H-qubit model are not affected there at all. Yet, the possibility of less direct relation between the models should not be neglected.

The presented work is mainly devoted to related pair of theoretical questions. The physical implementations of H-qubits are still not clear and too difficult nowadays, so the modeling of a system with *n* H-qubits by 2*n* qubits is discussed. Such a model also may be formulated without exhaustive use of quaternionic notation [2] as an introduction to the subject with traditional language of the quantum information science.

On the other hand, it is shown, that any quantum network with *n* qubits may be modeled by system with *n* H-qubits, yet such representation is not unique for $n > 1$. Due to such a property any quantum algorithm may be implemented by circuit with H-qubits and it justifies search for future practical applications.

1. M.A. Nielsen and I.L. Chuang. *Quantum Computation and Quantum Information*. Cambridge University Press, Cambridge, 2000.
2. A.Yu. Vlasov, “Error correction with Euclidean qubits”, Quantum Computers and Computing, **2**, pp.68-78, 2001; arXiv:quant-ph/9911074, 1999.
3. C.M. Caves, C.A. Fuchs, and P. Rungta, “Entanglement of formation of an arbitrary state of two rebits”, Found. Phys. Lett., **14**, pp.199-212, 2001.
4. F. Wilczek, “Majorana returns”, Nature Physics, **5**, pp.614-618, 2009.
5. C. Nayak, S.H. Simon, A. Stern, M. Freedman, and S.D. Sarma, “Non-Abelian anyons and topological quantum computation”, Rev. Mod. Phys., **80**, pp.1083-1159, 2008.

On the validity of neoclassical theory of the Compton effect for revision and reformulation of the standard quantum mechanics interpretation

V.V. Aristov
Institute of Microelectronics Technology and High Purity Materials, Russian Academy of Sciences, Chernogolovka, Russia, aristov@iptm.ru

In the report, we discuss alternatives to the standard interpretation of the Compton effect. It is demonstrated, both coherent and incoherent x-ray scattering can be explained within the neoclassical theory limits. It predicts all x-ray spectra features are consequences of matter structure, but not of field quantization. Adherents of modern interpretation QM completeness claim, that there are no alternative theories, and no possible to describe the experiment with results that differ from predicted in the «Copenhagen interpretation» of quantum theory. Nevertheless, attempts of creation alternative to modern QM were undertaken repeatedly [1,2]. Last years in a number of works we showed, such experiments well known, and are carried out already throughout 100 years [3,4,5], such are research of the Bragg and incoherent (Compton) scattering of hard x-ray radiation and Doppler (inverse Compton) effect of laser beam scattering on relativistic electrons.
The Compton effect is considered till now as the main argument in favor of photon concept in QM. Electromagnetic radiation is absorbed and radiated by atoms by fixed portions - quanta, but statement that light not only stored in atoms, but also extends and reradiates by electrons also in the portions, follows only from Debye and Compton interpretation of Compton effect: “Only a comedy of errors and historical accidents led to its [photon] popularity among physicist” [6]. During the long period, using, according to Jaynes, “the technology of QM like that of epicycles, has run far ahead of real understanding” [7], experimental results on incoherent scattering of x-ray radiation have been «built in» the accepted concept. Thus to an incorrectness of use of Bragg scattering intensity measurements for interpretations and calculations of incoherent spectra and Rayleigh scattering it was not paid attention. Apparently, only belief in validity of photon Compton effect explanation has not allowed to recognize, that inverse Smith - Purcell effect proves the wave nature of interaction of a free electron with an electromagnetic wave, and to understand, that Cerenkov and Doppler effects are not quantum (according to Skobel’tsyn, the quantum theory of this effects is not experimentally confirmed and contradicts relativistic mechanics requirements [8]). It is possible to claim, available experimental date it is enough, at least, to doubt correctness of the standard interpretation of the Compton effect. Revision of the Compton effect theory not only leads to verification some QM conclusions, but also reveals new possibilities of matter structure research. New possibilities arise at creation of the general theory of x-ray radiation scattering by crystals. New Compton effect interpretation can have especially big influence on development of elementary particles physics, hot plasma physics, quantum computer science

1. A. Khrennikov “Detection Model Based on Representation of Quantum Particles by Classical Random Fields: Born’s Rule and Beyond”, Found. Phys., **39**, pp.997-1022, 2009.
2. Memorandum of European Concerted Research COST Action MP1006: Fundamental Problems in Quantum Physics, Brussels, 2010.
3. V.V. Aristov, “Scattering of an Electromagnetic Wave on a Free Electron in the Semiclassical Approximation”, Doklady Physics, **54**, 4, pp.187-189, 2009.
4. V.V. Aristov, “Neoclassical Theory of X-Ray Scattering by Electrons”, *Electromagnetic Radiation*, ed. S.O. Bashir, pp.107-136, InTech, Croatia, 2012.
5. V.V. Aristov, “Neoclassical Theory of scattering”, *Nanophysics and Nanoelectronics*, XVI International symposium, 2, pp. 530-533, N.-Novgorod, 2012.
6. W.E. Lamb, “Antiphoton”, Appl. Phys. B., **60**, pp.77-84, 1994.
7. E.T. Jaynes, “Scattering of light by free electrons”, *The Electron-1990*, ed. by A. Weingartshofer, Kluwer Academic Publisher, Holland, 1990.
8. D.V. Skobel’tsyn, “Paradoxes of the quantum theory of the Vavilov-Cerenkov and Doppler effects”, Sov. Phys. Usp., **20**, pp.528-545, 1977.

Why quantum computing can be real only in multiple universes

V.V. Aristov and A.V. Nikulov
Institute of Microelectronics Technology, Russian Academy of Sciences, 142432 Chernogolovka, Moscow District, Russia. E-mail: nikulov@iptm.ru

The idea of the quantum computer was invented as a way to experimentally test the "Many Universes Theory" of quantum physics - the idea that when a particle changes, it changes into all possible forms, across multiple universes [1]. The author of the idea of the universal quantum computer, David Deutsch explains in his book [2] why, for example, Shor's algorithm can be realized only in multiple universes. Therefore it is needed first to prove unequivocally the real existence of other worlds before to make quantum computer and quantum bits. But authors of numerous publications about quantum computer and quantum bits seem to do not trouble themselves the necessity of such a proof. Apparently these authors, in defiance of Deutsch, are sure that the quantum computer can be real in our customary reality of the single universe. We will show that this groundless confidence is a consequence of a misunderstanding of the orthodox quantum mechanics.

Deutsch notes that the orthodox description, for example, of the double-slit interference experiment is deceptive because it implies an influence of the mind of the observer on quantum phenomena. The role of the 'observer' was admitted by creators of quantum theory, both adherents, Heisenberg, Dirac, Pauli, and opponents, Einstein, Schrodinger, of the positivistic quantum mechanics. The Einstein's remark "I like to think that the moon is there even if I don't look at it" expresses clearly his refusal of the psychology in physical theory. The many-worlds interpretation was proposed by Everett [3] in order to remove this psychology from quantum mechanics. But most physicists do not even hear about these problems of quantum mechanics. Their attitude of mind may be expressed with a Bell's remark [4] about [5]: "*This paper is distinguished especially by its robust common sense. The author has no patience with "…such mind-boggling fantasies as the many world interpretation...". He dismisses out of hand the notion of von Neumann, Pauli, Wigner - that 'measurement' might be complete only in the mind of the observer*". This robust common sense, supported by "*good books*" [4] on quantum mechanics, for example [6], prevents to understand the true sense of the EPR correlation [7] (determined by Schrodinger as *"entanglement of our knowledge*" [8]) and that the numerous publications about quantum computation and quantum bits are false.

The number of independent variables γ_i increases exponentially $g_N = 2^N - 1$ with the number N of quantum bits in a quantum system

$$\psi = \gamma_1|\uparrow\uparrow\uparrow\ldots\uparrow> + \gamma_2|\uparrow\uparrow\uparrow\ldots\downarrow> + \ldots + \gamma_{gN-1}|\downarrow\downarrow\downarrow\ldots\uparrow> + \gamma_{gN}|\downarrow\downarrow\downarrow\ldots\downarrow> \quad (1)$$

because of the EPR correlation. But according to the orthodox quantum mechanics the variables γ_i describe an interaction between the quantum system and the mind of the observer. Any operation of qubit gates must include an influence of the mind of the observer on the quantum system. In defiance of the groundless confidence of numerous authors this operation can not be real because of the non-locality of the EPR correlation, see Bell's work about this [9].

1. *Q. Norton, The Father of Quantum Computing,*
http://www.wired.com/science/discoveries/news/2007/02/72734?currentPage=all.
2. D. Deutsch, *The Fabric of Reality*. Penguin, 1998.
3. H. Everett, "Relative state formulation in quantum mechanics", Rev. Mod. Phys., **29**, pp.454-462, 1957.
4. J.S. Bell, "Against 'measurement'", Physics World, pp.33-40, August 1990.
5. N.G. van Kampen, "Ten theorems about quantum mechanical measurements", Physica A, **153**, pp.97-113, 1988.
6. L.D. Landau, E.M. Lifshitz, *Quantum Mechanics: Non-Relativistic Theory*. Vol. 3, Third Edition, Elsevier Science, Oxford, 1977.
7. A. Einstein, B. Podolsky, and N. Rosen "Can Quantum-Mechanical Description of Physical Reality Be Considered Complete?" Phys. Rev., **47**, pp.777-780, 1935.
8. C. Brukner, M. Zukowski, A. Zeilinger, "The essence of entanglement", E-print arXiv: quant-ph/0106119.
9. J.S. Bell, *Speakable and Unspeakable in Quantum Mechanics. Collected Papers on Quantum Philosophy*. Cambridge University Press, Cambridge, 2004.

Simulations of adiabatic and nonadiabatic chemical reactions in condensed media

K. Arakelov
Moscow State University, Moscow, Russia, karakelov@mail.ru

Algorithms of simulation of adiabatic and nonadiabatic chemical reactions in condensed media have been developed. The time behavior of the newly introduced collective coordinate of media has been studied for a model reaction of electron excitation of a single active particle. Theoretical justification of the algorithms has been stated. The dependency of correlation functions of the collective coordinate of media on temperature has been studied numerically. The dependency of reaction rate on temperature has been numerically calculated based on the algorithms developed. A certain correspondence between the calculated rate-temperature curve and simple formulas of chemical kinetics has been shown.

Quantum implication and strategies for multi-agent models

A.A Ezhov, A.G. Khromov, S.S. Terentyeva
Science Research Center of Russian Federation Troitsk Institute for Innovation and Fusion Research, city district Troitsk, Moscow, Russia, liner@triniti.ru

Implication is one of the fundamental logical functions. It plays a key role in such applied field as mathematical psychology, e.g. in the reflexive control theory developed by Lefebvre [1]. Recently, it has been demonstrated that implication can be related to the method of simulated annealing [2] and also to multi-agent models of unequal societies [3, 4]. In the last case this function describes both the basic agent strategies and their interactions. The use of classical implication can, nevertheless, restrict model properties because model agents behave "too rationally". For example for some models of wealth distribution not purely rational but rather irrational behavior can be responsible for observable dependencies [5]. Really, it is well known that generalization to a quantum domain can lead to new abilities in the fields of computation, information transmission, game theory, etc. There are also many attempts to use the quantum probability theory as a mathematical framework for cognitive modeling [6]. Focusing on the multi-agent models of unequal societies we introduce agents which are able to use some quantum strategies instead of classical ones. With this goal we propose some quantum generalization of the classical implication function. The generalization is based on a plausible modification of the circuit representation of the implication gate. It is also argued why this modification is the only one possible with due regard to some plausible restrictions to the agent behavior. Note, that it is rather problematic to introduce quantum implication in the frame of quantum logic, but our goal is just opposite: to propose strategies which lie beyond the logic itself. We demonstrate the plausibility and benefits of this quantum implication, e.g. its quite reasonable relation to the quantum simulated annealing. We derive quantum rules for the interacting agents of two types introduced earlier in [3, 4] (they obey two quantum-like statistics) and show that the statistics of fully connected agents – intermediate statistics of γ-ons corresponding to $\gamma = \pm ½$ – resembles the statistics of agents which explore classical rules but which have random interaction network. The comparison with the classical model is presented as well.

1. V.A. Lefebvre. *Algebra of conscience*. Kluwer Acad. Publ. Dordrecht, Boston, London, 2001.
2. A.A. Ezhov, A.V. Bur'yanitsa, S.S. Terentyeva, A.S. Khvalina, "Econophysics and the search of a model of economic agent". *Econophysics*, MEPhI, Moscow, 529, 2007 (in Russian).
3. A.A. Ezhov and A.Yu. Khrennikov, "Agents with left and right dominant hemispheres and quantum statistics", Phys. Rev. E, **71**, pp.016128:1-8, 2005.
4. A.A. Ezhov, A.Yu. Khrennikov, and S.S. Terentyeva, "Indication of a possible symmetry and its breaking in a many agent model obeying quantum statistics", Phys. Rev. E, **77**, pp.031126:1-12, 2008.
5. M.A. Fuentes, M. Kuperman, J.R. Iglesias, "Living in an Irrational Society: Wealth Distribution with Correlations between Risk and Expected Profits", Physica A, **371**, pp.112-117, 2006.
6. J. R. Busemeyer, P. Bruza, *Quantum models of cognition and decision making*. Cambridge University Press: Cambridge, UK., 2011.

A universal model for single-electron device simulation

I.I. Abramov, A.L. Baranoff, I.A. Romanova, I.Y. Shcherbakova
Belarusian State University of Informatics and Radioelectronics, Minsk, Belarus, E-mail: nanodev@bsuir.edu.by

Recently single-electron tunneling devices are considered to be promising candidates for basic elements of future low power solid-state electronics. Due to the complexity of physical processes and manufacture technologies involved, many efforts have been invested into modeling and simulation.

The priory trends of single-electron device models modification are [1]: 1) derivation of more accurate equations for tunneling rate; 2) account of various parasitic effects; 3) account of spatial quantization.

Accounting of spatial quantization is becoming the more important the smaller are dimensions of the device. However there are contradictory viewpoints in literature. From the one hand according to some expectations [1] it is enough to use a master equation in most cases for metal single-electron structures when electron energy quantization inside the conducting islands is ignored. From the other hand experimental results demonstrate substantial influence of energy states discretization even for metal single-electron structures with small islands sizes (< 10 nm). These devices are designed for room temperature operation, so they are of special interest for researchers.

The developed model for single-electron device simulation with accounting of spatial quantization inside islands and its application opportunities for simulation of various structures are described in the paper. Usefulness of this type of model is demonstrated by IV-characteristics calculation of metal, composite, semiconductor, and organic devices.

The developed model [2] is based on the self-consistent numerical solution of the Poisson equation in 2-D case

$$\nabla \varepsilon \nabla \phi(x, y) = -q_M , \qquad (1)$$

where ε is the dielectric constant (permittivity)); ϕ is the electrostatic potential; x, y are coordinates; q_M is the volume charge density which includes the density of charge carriers q_t directly involved in tunneling and the back-ground-charge density q_0. Charge in dielectric is ignored.

Monte-Carlo method or master equation can be used for IV-characteristics calculation. The following approximations are used while solving the Schrödinger equation: 1) of the quantum well of the infinite depth; 2) of the rectangular quantum well of a finite depth; 3) of the parabolic quantum well. These approximations enhance the investigations' opportunities and increase the models' efficiency. The first modification of the model requires the least processing time.

The programs, implementing the suggested model, were included into the simulation system of nanoelectronic devices NANODEV [2] developed for personal computers.

According to the classification [3] there are four types of single-electron transistors: metal, semiconductor, composite, and organic ones. The developed model makes it possible to simulate devices of all four abovementioned types, and enables to achieve the good agreement of simulation results with experimental data.

1. I.I. Abramov, "Problems and principles of physics and simulation of micro- and nanoelectronic devices. VI. Single-electron devices", Nano- and mikrosistemnaya teknika, № 7, pp.10–24, 2007 (in Russian).
2. I.I. Abramov, A.L. Baranoff, I.A. Goncharenko, N.V. Kolomejtseva, Y.L. Bely, I.Y. Shcherbakova, "A nanoelectronic device simulation software system NANODEV: New opportunities", Proc. SPIE, **7521**, 75211E (11 p.), 2010.
3. I.I. Abramov, E.G. Novik, "Classification of single-electron devices", Fiz. Tekh. Poluprovodn., **33**, pp.1388–1394, 1999 (in Russian).

Monte Carlo simulation of charge carrier transport in deep submicron Si MOSFET

A.V. Borzdov[1], V.M. Borzdov[1], D.V. Pozdnyakov[1], D.S. Speransky[1]
V.V. V'yurkov[2], A.A. Orlikovsky[2]
1. Belarusian State University, Minsk, Belarus, borzdov@bsu.by
2. Institute of physics and technology, Russian Academy of Sciences, Moscow, Russia

The problem of computer simulation of nanoscale semiconductor electron devices, such as deep submicron MOSFETs, still has got many problems to be resolved. One of the most powerful submicron MOSFET simulation methods is ensemble Monte Carlo procedure. This method allows different complicated physical processes to be included into simulation [1–3].

In present study the Monte Carlo simulation of charge transport in 50 nm channel length silicon MOSFET is performed. Charge transport includes the simulation of both electron and hole gases since in presence of high electric fields and impact ionization the application of quasi-equilibrium model of hole gas is questionable. The electric charge carrier transport is simulated within the effective mass framework. Electron transport simulation in conduction band of silicon includes *X* and *L* valleys with account of nonparabolicity. The main scattering processes for electrons are intravalley and intervalley acoustic and optic phonon scattering, plasmon scattering, ionized impurity scattering and impact ionization process [1–5]. The hole transport model includes anisotropy and nonparabolicity of the valence band. The degeneracy is also taken into account, so that the hole transport is considered in heavy, light and split-off bands [6]. Scattering mechanisms for holes are inelastic optical and acoustic phonon, and ionized impurity scattering [7, 8].

It is known that in numerical simulations of integrated circuit elements with the reduction of their dimensions, particularly MOSFETs, an account of impact ionization process is essential. The latter is caused by the fact that in presence of high electric field strengths the rate of impact ionization in such elements can be comparable or even greater than the rates of other considered scattering processes. In this connection the results of calculation of various parameters characterizing charge carrier transport in the deep submicron MOSFET with consideration of all the peculiarities of impact ionization process in such a device are presented in our paper.

1. M.V. Fischetti, S.E. Laux, “Monte Carlo analysis of electron transport in small semiconductor devices including band structure and space-charge effects”, Phys. Rev. B, **38**, pp.9721–9745, 1988.
2. C. Jacoboni, P. Lugly. *The Monte Carlo Method for Semiconductor Device Simulation*. Springer-Verlag, Wien – New York, 1989.
3. V.M. Borzdov, O.G. Zhevnyak, F.F. Komarov, V.O. Galenchik. *The Monte Carlo Simulation of Integrated Electronics Device Structures*. BSU, Minsk, 2007 (in Russian).
4. E. Pop, R.W. Dutton, K.E. Goodson, “Analytic band Monte Carlo model for electron transport in Si including acoustic and optical phonon dispersion”, J. Appl. Phys., **96**, pp.4998–5005, 2004.
5. D.V. Pozdnyakov, A.V. Borzdov, V.M. Borzdov, “The Monte Carlo of current-voltage characteristics of short-channel Si-MOSFET”, Proc. 21st Int. Crimean Conf. “Microwave & Telecommunication Technology”, **2**, pp.808–809, 2011.
6. S. Rodriguez-Bolivar, F.M. Gomez-Campos, J.E. Carceller, “Simple analytical valence band structure including warping and nonparabolicity to investigate hole transport in Si and Ge”, Semicond. Sci. Technol., **20**, pp.16–22, 2005.
7. S. Rodriguez-Bolivar, F.M. Gomez-Campos, F. Gamiz, J.E. Carceller, “Implications of nonparabolicity, warping, and inelastic phonon scattering on hole transport in pure Si and Ge within the effective mass framework”, J. Appl. Phys., **97**, pp.013702-1–10, 2005.
8. F.M. Gomez-Campos, S. Rodriguez-Bolivar, J.E. Carceller, “An efficient Monte Carlo procedure for studying hole transport in doped semiconductors”, J. Comp. Electron., **3**, pp.329–332, 2004.

Thermal simulating of thin-film SOI MOSFET

Yu. Chaplygin, A. Krasukov, E. Artamonova
National Research University of Electronic Technology (MIET) Moscow, Russia, artamonova@org.miet.ru

The relevance of thermal effects in device design increases during device scaling. Increasing power dissipation translates into larger heat generation and rising temperatures. The self-heating effects in silicon-on-insulator (SOI) CMOS devices become even more significant due to the low thermal conductivity of the buried-oxide layer, leading to the essential rise of temperature under nominal operation conditions. In addition, in thin-film SOI MOSFETs thermal conductivity is degraded due to phonon boundary scattering at the silicon-oxide interface that reduces the phonon mean free path and therefore the mobility of charge carriers. For these reasons, the impact of self-heating on the SOI MOSFETs has been carefully investigated both experimentally and by device simulation [1]-[2].

The most common approach for modeling the heat transport based on the Fourier's law of heat diffusion:

$$c * \frac{dT}{dt} - \nabla(\kappa \nabla T)) = H \qquad (1)$$

Where *c* and *k* are the heat capacity per unit volume and the thermal conductivity respectively, and *H* is the heat-generation rate per unit volume.

For the thin-film SOI MOSFETs the thermal conductivity can be written as:

$$k = c * \upsilon * l_S \qquad (2)$$

where l_S is the phonon mean free path, and υ is the average phonon velocity.

The effect of phonon boundary scattering at the silicon-oxide interface can be included by assuming that phonon boundary scattering mean free is equal to the silicon film thickness $l_{BS} = T_{SI}$ [3]. In this case, the overall mean free path can be calculated with the Mathiessen rule $l_S^{-1} = l_{S-bulk}^{-1} + l_{BS}^{-1}$, where l_{S-bulk} is the phonon mean free path for bulk silicon.

The electrothermal analysis of 50-nm SOI MOSFET shown on Fig. 1 has been performed using the TCAD simulator [4]. The next thermal boundary conditions are set: lumped thermal resistances R_{TB} varied from 10^{-4} to 10^{-1} K*cm^2/W connect the device bulk terminal to a 300 K isothermal boundary condition, the source, gate and drain terminals are set to 300 K isothermal boundary conditions.

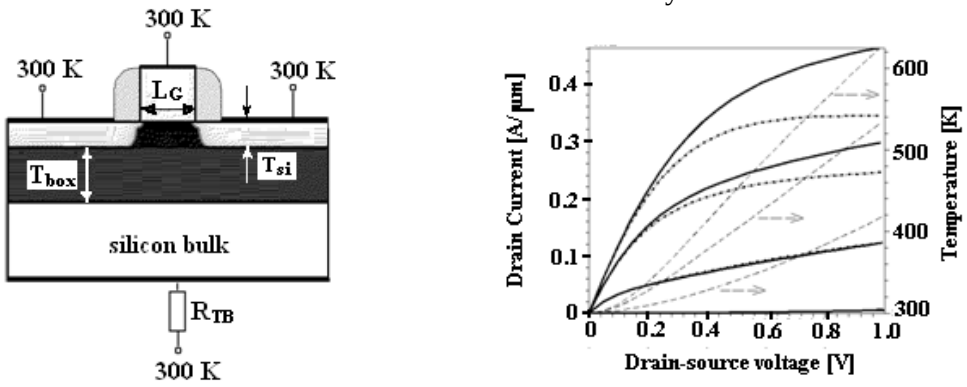

Fig.1 (Left fig.) 2D sketch of the simulated SOI MOSFET: T_{box}=150 nm, L_G=50 nm, T_{si}=50 nm;
(right fig.) output characteristics of 50-nm SOI MOSFET with R_{TB}=10^{-4} (solid lines) and 10^{-1} (dot-dashed lines) at gate-source voltage varied from 0.1 to 1.2 V; channel temperature rise (long-dashed lines).

1. C. Fiegna, Y.Yang, E. Sangiorgi, A.G. O'Neill, "Analysis of Self-Heating Effects in Ultrathin-Body SOI MOSFETs by Device Simulation", IEEE Transactions on Electron Devices, **55**, pp. 233 – 244, 2008.
2. B.M. Tenbroek, M.S.L. Lee, W. Redman-White, R.J.T. Bunyan, and M.J. Uren, "Self-heating effects in SOI MOSFET's and their measurement by small signal conductance techniques", IEEE Transactions on Electron Devices, **43**, pp.2240–2248, 1996.
3. E. Pop, R. Dutton, and K. Goodson, "Thermal analysis of ultra-thin body device scaling", Electron Device Meeting, pp.883–884, 2003.
4. http://www.synopsys.com/Tools/TCAD.

Ultimate sub-threshold slope of Schottky Barrier Field-Effect Transistors

Ye. Chaplygin, D. Svintsov, V. Vyurkov, A. Orlikovsky
Institute of Physics and Technology, Russian Academy of Sciences, Moscow, Russia, vyurkov@ftian.ru

Silicon persists to be the basic material of integrated circuits. A minimal pattern size of 6 nm is anticipated in the production in 2026. For the advance into this area it would be necessary to reject also the doping of contact regions because of fluctuations of number of impurities, which lead to the large dispersion of transistor parameters in a circuit. Schottky Barrier Field-Effect Transistors (SB FETs) are regarded as plausible successors. Moreover, they could revert again to bulk wafers or, at least, to thick silicon body in silicon-on-insulator wafers.

In this communication we argue that the sub-threshold slope of SB FETs cannot exceed $(60\text{mV/dec})^{-1}$ at room temperature. This is just a limit for usual MOSFETs which operation is based upon thermoemission current. The conclusion could be surprising as a tunnel current itself can possess any slope with respect to gate voltage operating over the potential barrier. But, at the moment, the tunnel current could be very small, at least, in comparison with thermoemission current.

In Fig. 1 two states of SB FET are depicted, the arrows designate the corresponding current. In ON-state there is tunneling into conduction band from the Fermi level in metal. In OFF-state only thermally activated electrons can tunnel into the channel. In general, the injection current could be evaluated as a product of two exponents: the Fermi distribution function rapidly (exponentially) decreases with growing electron energy, whereas the tunnel probability exponentially increases. The interplay of those exponents allows an employment of a saddle-point approximation to estimate the current. Eventually, one arrives at the limit of $(60\text{mV/dec})^{-1}$ at room temperature. The same limit is also inherent to the extreme implementation of a SB FET when a gate operates over a direct tunneling between source and drain through the ultra-short channel (< 5nm). Our conclusion regarding a limiting slope is valid for any construction of SB FET, although there are several possibilities to augment the current, for instance, to merge source/drain contacts into the substrate or to use sharp contacts.

The results of more thorough simulations are shown in Fig. 2. The sub-threshold slope is quite sensitive to a spacer length. For 3nm spacer it achieves its limit, meanwhile, for 7nm spacer it is already thrice less.

For reliable digit circuit operation the ratio I_{ON}/I_{OFF} of 10^4 is sufficient. This means that the gate voltage 0.24V is enough for the slope equal to $(60\text{mV/dec})^{-1}$.

Tunnel transistors (p-n junction manipulated by a gate voltage) exhibit a subthreshold slope higher than above limit. This is because those transistors include a tunnel contact of two semiconductors, unlike to SB FETs which include a contact of metal with semiconductor. Nevertheless, because of low frequency tunnel transistors could hardly be used in ULSI technology, but, possibly, in quite slow remote electronic devices.

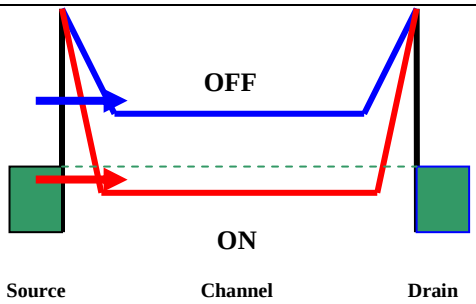

Fig. 1. Band diagram of a SB FET in OFF and ON state.

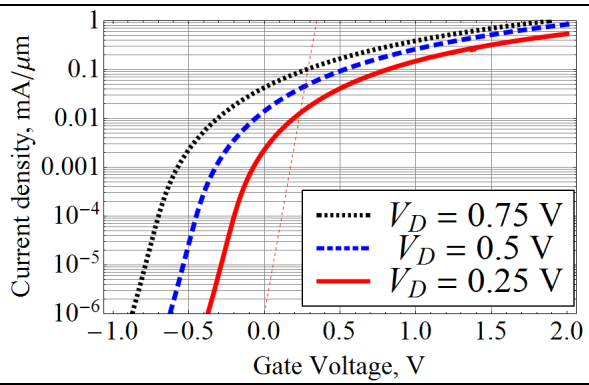

Fig. 2. Current vs. gate voltage for different drain voltage: 3nm spacer. Thin line indicates 60mV/dec slope.

The work was supported via the grant # 07.524.12.4019 of the Ministry of Education and Science of the Russian Federation.

Transient processes in the resonant tunneling diode, taking into account the electron-electron interaction

V. Elesin[1], I. Kateyev[2], A. Sukochev[1]

1. National Research Nuclear University, Moscow, Russia, aysukochev@gmail.com. 2. Institute of Physics and Technology, Russian Academy of Science, Moscow, Russia, ikateyev@mail.ru

Transient processes in the resonant-tunneling diode (RTD) without electron-electron interaction have been studied recently [1]. Using non-stationary correct boundary conditions it has been shown theoretically and numerically, that a time dependence of a current through the structure has the form of damping oscillations. The oscillation period is equal to a difference between the electron energy and the energy of the resonant level in a quantum well. The damping rate of oscillations is about the resonant level electron lifetime $2\pi\hbar / \Gamma$ (Γ – a resonant level width) in the quantum well.

In this work the transient processes in RTD are investigated taking into account strong electron-electron interaction with use of the numerical solution of the time-dependent Schrödinger equation. The electron-electron interaction is treated in a framework of the Hartree-Fock approximation. The current is calculated for two cases: an instantaneous switching of the applied bias on a value ΔV and a switching on of an electron flow. The transition from a large current state into a small current state is calculated in a presence of a hysteresis. The transition behavior is examined and its termination time is found. It is shown, that electron-electron interaction slows down a convergence of the current toward its new stationary value. When switching from the large current state into the small current state the damped oscillations starts after a threshold time t_{tr} (fig. 1). This time decreases linearly with increasing of the electron-electron interaction (fig. 2). However, the main features of transients in RTD preserve.

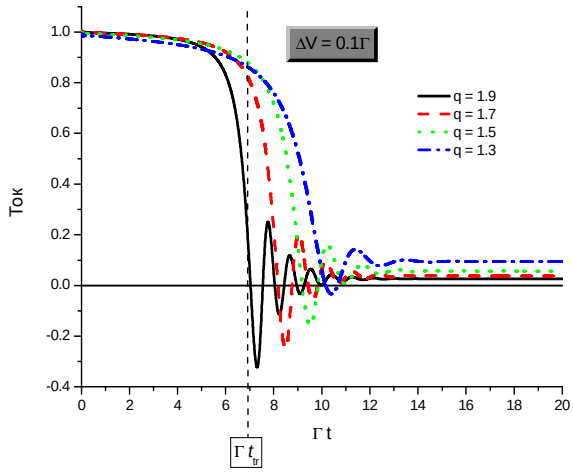

Figure 1. A time dependence of the current for different values of electron-electron interaction.

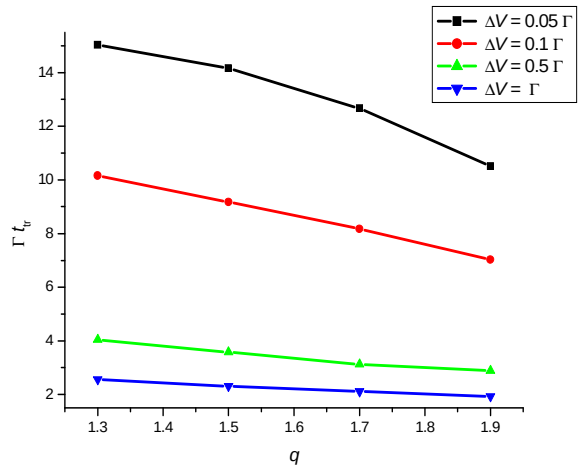

Figure 2. The dependence of t_{tr} on a strength of the electron-electron interaction q^2.

1. V.F. Elesin, I.Yu. Kateev, M.A. Remnev, M.N. Strikhanov, and A.Yu. Sukochev, “Theory of nonstationary processes in a resonant-tunneling diode”, Nuclear Physics and Engineering, **2**, pp.460-471, 2011.

Effect of emitter spacer level of resonant tunneling diode on I-V curves

V. Elesin, M. Remnev

National Nuclear Research University "MEPhI", Moscow, Russia, maremnev@mephi.ru

Resonant tunneling diodes (RTD) are fastest active semiconductor devices. They can be used as generators of the electromagnetic radiation and can be used in super-fast logical devices of nano- and microelectronics. However, characteristics of the devices are still not insufficient to use in the industry.

The spacer layers were originally grown between doping contacts and the active area (quantum well and barriers) of the device to prevent the transfer of impurities into the active area. It had been found that they essentially influenced the device characteristics. Moreover, the influence was complex. So any experimental studies showed that the peak current decreased with increasing of the spacer size [1]. But others showed that the peak current increased at first and then decreases [2].

The goal of present work was investigation of the spacer emitter level size effect on the peak current of resonant tunneling diode by means of calculations.

We used one dimensional Schrodinger equation with a coherent approximation, i. e. there was not the electron-phonon scattering. The distribution of electrons was monoenergetic. In issue [3] we got I-V curves for different sizes of the emitter and collector spacers. It was found that the peak current of I-V curves behaved in periodic manner, depending on the size of the emitter spacer (dash curve on the fig. 1). It had the pronounced maximums. Thereby there was ability to essentially increase the peak current by means of a tune of the emitter spacer size. It was suggested that the maximums were related to the level of the emitter spacer.

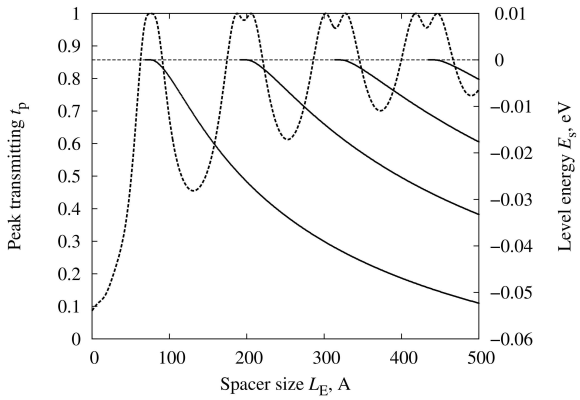

Figure 1. The peaks current and the level energy as the emitter spacer size.

In this work we showed that the maximums appeared when the emitter spacer level aligned with the resonant level of the quantum well.

Figure 1 shows the energies of emitter spacer levels as increasing the spacer size by the solid line. When the peak current depicted the dash line has a maximum the energy of the emitter spacer crosses the zero energy. Then the energy decreases as increase the spacer size. On other hand the bias corresponds to the peak voltage and the energy of the resonant level of the quantum well is close to zero. When a new maximum appears the energy of a new emitter spacer level coincides with the energy of the resonant level.

In addition the influence of the electron-electron interaction on the peak current had been investigated by means of the local interaction approximation. There were two peak currents if the interaction was intense. The first one was the direct bias and the second one was reverse bias. It was shown when the bias was direct the interaction didn't almost affect on the dependence of the peak current on the emitter spacer size. But the interaction decreased the peak current when the bias was reverse.

Thereby we showed the dependence of the peak current on the emitter spacer size had periodical pronounced maximums and it was related with the emitter spacer level. It qualitatively explains contradictions of the experiments, i. e. the peak current of RTD can increase as increase the emitter spacer size and one can decrease.

1. Z. Yang et al., "Influence of space layer thickness on the current-voltage characteristics of pseudomorphic AlAs/$In_{0.53}Ga_{0.47}As$/InAs", Chinese Physics B, **17**, pp.1472–1474, 2008.

2. T. Daniels-Race and S.Yu, "Effect of spacer layer thickness on tunneling characteristics in asymmetric AlAs/GaAs/AlAs double barrier structures", Solid-State Electronics, **38**, pp.1347–1349, 1995.

3. M.A. Remnev, I.Yu. Kateev, and V.F. Elesin, "Effect of spacer layers on current-voltage characteristics of resonant-tunneling diode", Semiconductors, **44**, pp.1034-1039, 2010.

Gold nanoparticle single-electron transistor simulation

Y.S. Gerasimov, V.V. Shorokhov, E.S. Soldatov, O.V. Snigirev
Faculty of Physics, Moscow State University, Moscow, Russia, ys.gerasimov@physics.msu.ru

The problem of selecting appropriate molecular objects is of significant practical importance for creating nanoscale molecular electronic devices [1]. Discrete structure of nanoobjects' energy spectra influences transport characteristics (IV-curves, stability diagram) of molecular single-electron transistor [2]. The study of this influence will give opportunity to make the object selection using predetermined eligible current-voltage characteristics. Investigation of the molecular spectra connection to voltage-current characteristics features is associated with high computational complexity in the study of the energy spectra of large molecules (more than 200 atoms). For this reason the problem of parameterization of the energy spectra of molecular objects (molecules, nanoparticles, nanograins) arises. The solution of the problem allows to reduce significantly the amount of direct quantum-chemical calculations of such spectra. The main goal here is to represent energy levels of a spectrum as a function of the additional electric charge of a molecular object.

In the present work charge energy properties of gold nanoparticles of different sizes and their isomeric configurations are investigated for single-electron systems. The considered particles are surrounded by the shell of ligands, where a ligand is a dodecanthiol molecule $SCH_2(CH_2)_{10}CH_3$.

Single-particle spectra of gold nanoparticles Au_NL_M were calculated by means of quantum-chemical methods for the cases of $1 \le N \le 33$ and $1 \le M \le 12$, where N – the number of atoms, M – the number of ligands. Significant influence of the ligands on the electric capacitive parameters of gold nanoparticles and its energy spectra structure is revealed.

Thus the possibility of using a simple parametric model of the formation of single-particle nanoobject's energy spectra depending on their electric charge and spin multiplicity was shown for the problem assigned.

Parametrization of the obtained gold nanoparticles energy spectra let us to construct spectra model for small particles ($N < 155$), and for the gold nanoparticles size of 2, 3, and 5 nm. Such relatively large nanoparticles were previously unavailable for the full quantum-chemical calculations of the energy characteristics required for the subsequent simulation of electron transport through them. Here transport characteristics of single-electron transistor based on gold nanoparticles were simulated at N = 13 (particle size 0.8 nm) and N = 27 and for the number of ligands M = {0;2;4;12}. Similarly, the calculations for gold nanoparticles of larger sizes were made.

As a result the new approach for simulating of electron transport on the basis of the energy spectra model for nanoobjects is presented in this work. It enables one to build adequate spectra of molecules consisting of more than 50 atoms parametrically and significantly reduces quantity of necessary quantum-chemical calculations of the properties up to two or three states of the molecule. The obtained peculiarities of energy molecular spectra in the future will significantly simplify the solution of problems associated with the modeling and study of electron transport in molecular systems.

This work has been supported by RFBR (Pr. No. 12-07-00816-a, 10-07-00712-a), Federal Target Program "Scientific and scientific-pedagogical personnel of innovative Russia" in 2009 - 2013 years (Pr. No. 14.740.11.0389, 16.740.11.0020, 14.740.11.0370) and Federal Target Programme "Research and Development in Priority Fields of S&T Complex of Russia for 2007-2013" (Pr. No. 16.513.11.3063).

1. K. Likharev, "Single-electron devices and their applications", Proc. IEEE, **87**, pp.606-632, 1999.
2. V.V. Shorokhov, P. Johansson, E.S. Soldatov, "Simulation of characteristics of a molecular single-electron tunneling transistor with a discrete energy spectrum of the central electrode", J. Appl. Phys., **91**, pp.3049-3053, 2002.
3. Y.S. Gerasimov, V.V. Shorokhov, E.S. Soldatov, O.V. Snigirev, "Calculation of the characteristics of electron transport through molecular clusters", Proc. SPIE., **7521**, p.75210U, 2009.

TCAD analysis of self heating effects in bulk silicon and SOI n-MOSFETs

K. Petrosyants[1], E. Orekhov[2], I. Kharitonov[1], D. Popov[1]
1. Moscow State Institute of Electronics and Mathematics (Technical University), 3, B. Tryokhsvyatitelskiy side-street, Moscow 109028, Russia, E-mail: eande@miem.edu.ru
2. Institute for Design Problems in Microelectronics of Russian Academy of Sciences, 3, Sovetskaya Street, Zelenograd, Moscow 124365, Russian Federation, E-mail: e.orekhov@miem.edu.ru

Introduction. SOI (silicon-on-insulator) CMOS technology are promising new possibilities for LSI and VLSI radiation hard applications in space, military and other special systems. The advantages of SOI are well known: very good individual electrical isolation of devices, low levels of leakage current, freedom from latch-up, higher packing density, reduced junction capacitance. However, due to buried silicon dioxide layer with low thermal conductivity heat, generated in active silicon layer of the SOI transistor, cannot be efficiently dissipated. This causes an increase in device operational temperature and affects several important parameters of transistor such as threshold voltage, channel mobility and carrier saturation velocity [1].
The goal of this study was to analyze self-heating effects in n-channel bulk silicon and fully depleted SOI MOS transistors.
MOSFETs structures with the gate sizes W/L=0.4/0.1 um and 3 nm gate oxide thickness for bulk silicon an SOI devices were analyzed. For SOI MOSFET the thickness of active silicon layer were 40 nm and thickness of buried oxide layer were 100 nm. MOSFETs structures were isolated with shallow trench isolation.
Simulation of bulk silicon and SOI n-channel 3D MOSFETs with hydrodynamic transport model accounting for lattice heating, with 1.2 V bias at gate and drain was performed. Surface temperature map of SOI n-MOSFET with W/L=0.4/0.1 um (a) and bulk silicon MOSFET with W/L=0.4/0.1 (b) is depicted on fig. 1. Additionally 2D simulation of self heating effects in SOI n-channel MOSFET with W/L=1/0.1 um with thickness of active silicon layer varying from 20 nm to 100 nm were done.

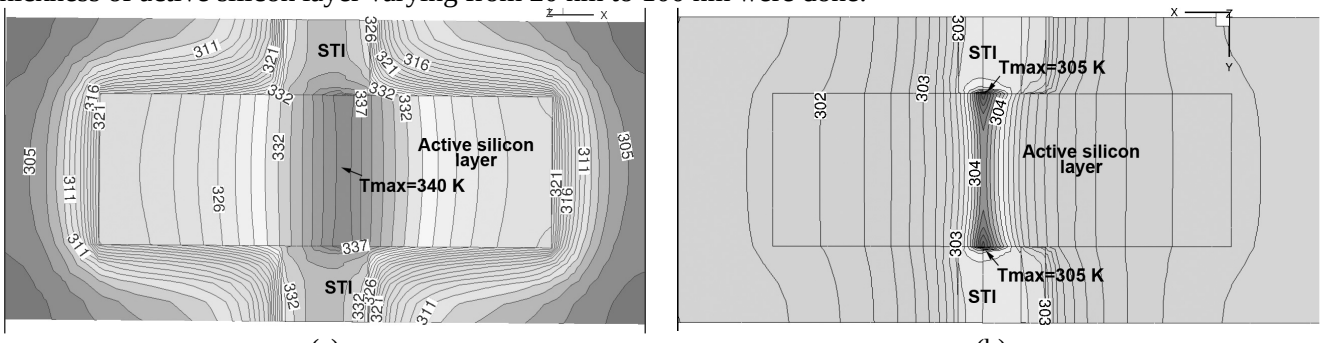

(a) (b)

Fig. 1. 3D device simulation results: surface lattice temperature map of SOI n-MOSFET with W/L=0.4/0.1 um (a) and bulk silicon MOSFET with W/L=0.4/0.1 (b) with 1.2 V bias at gate and drain electrodes.

Results and conclusions. 1) Comparison of maximum lattice temperature (T_{max}) of n-channel bulk silicon and fully depleted SOI MOSFETs was presented. T_{max} for the bulk MOSFET is 305 K and most heated regions of device are in the drain pn-junction near the STI sidewalls. T_{max} for SOI MOSFET is 340 K and most heated device region is the drain pn-junction with almost uniform temperature distribution along the channel width. 2) Analysis of active silicon thickness variation in SOI MOSFET was performed. For the thinnest 20 nm active silicon layer T_{max}=355 K with 15% decrease in transconductance compare to bulk device and T_{max}=334 K and 10% decrease in transconductance for 100 nm thickness of active silicon layer. The simulation results are in good agreement with the results presented in [2].

1. B.M. Tenbroek, M.S.L. Lee, W. Redman-White, J.T. Bunyan, and M.J. Uren, "Impact of Self-Heating and Thermal Coupling on Analog Circuits in SOI CMOS", IEEE J. Solid-State Circuits, **33**, pp.1037-1045, 1998.
2. K. Etessam-Yazdani, R. Hussin, M. Asheghi, "Impact of Scaling on Thermal Behavior of Silicon-on-Insulator Transistors", Proc. ITHERM '06, pp.1257-1264, 2006.

Terahertz oscillations from nanowires

A. Pilgun[1], V. Vyurkov[1], L. Fedichkin[1,2], V. Borzdov[3], A. Orlikovsky[1]
1. Institute of Physics and Technology, Russian Academy of Sciences, Moscow, Russia, vyurkov@ftian.ru
2. Computer company NIX, Moscow, Russia
3. Belarus State University, Minsk, Belarus

Terahertz frequencies of electromagnetic waves stay challenging for decades. This is reasoned by important areas of application such as telecommunication, investigation and operation on chemical and biological objects. Nevertheless, there are still no sources and detectors meeting practical requirements.

One of the proposals of teraherz generation was put forward in 1994 [1]. The main idea was to implement the well known transit-time diode in a low-dimensional structure, namely, that consisting of quantum wires. The planar construction allows a high frequency output because of a rather small capacitance. Moreover, the quantum wires are beneficial with respect to small dispersion of transit-times of carriers. The original proposal dealt with quantum wires cut out of a two-dimensional electron gas in A_3B_5 heterostructure by split-gate potential. However, for practical application that structure was quite embarrassing. The time has passed and the technology has gone far ahead. There are new candidates, for instance, carbon nanotubes and silicon nanowires. The latter seem more realistic at the moment. The structure could be inserted into a coplanar waveguide to transmit oscillations to an antenna. On the whole, all components of the device could be integrated into silicon technology.

The structure for simulation consists of a silicon nanowire placed between two contacts (Fig. 1). Here only the first step towards simulation of THz generation is fulfilled. We demonstrate a possibility of negative conductance at THz frequencies. The wire length is 300nm, its cross-section is 2nmx10nm. Such a small thickness results in a single mode regime. Ballistic Monte-Carlo technique is used for simulation. Steady V_0 and alternating V voltages are applied to contacts. The field along the wire corresponds to that between the plates of a coplanar capacitor. To calculate an alternating current in the outer circuit the Shockley-Ramo theorem was employed. In fact, it means that all carriers moving between contacts induce a current in outer circuit due to image charges in contacts. The leading harmonics was extracted with the help of Fourier analysis and then a complex conductance was obtained.

Some of the results of simulation are presented in Fig. 2. The conductance σ is referenced to the conductance quantum $\sigma=2e^2/h$. The best condition for generation is: Re σ <0, Im σ =0, which corresponds to the situation when the alternating current is exactly opposite to the alternating voltage. The parameters of generation providing the best concordance with a wave-guide could be estimated as: a relative negative conductance is 0.025, an alternating voltage is 1/4 of the steady one, an efficiency of generation is about 1%.

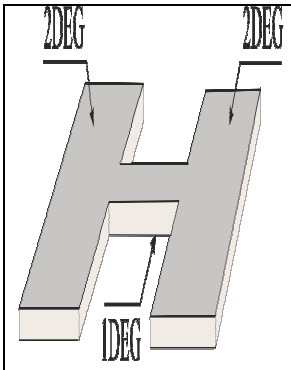

Fig. 1. A nanowire between two contacts.

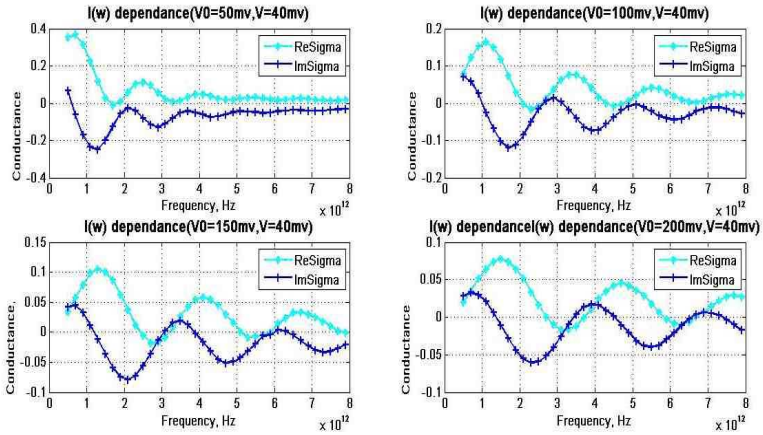

Fig. 2. Real and imaginary parts of relative conductance vs. frequency: V is an alternating bias, V0 is a steady bias.

The work was supported by the Russian Foundation for Basic Research (grants # 11-07-00464-a and #12-07-90011-Bel_a).

1. L. Fedichkin and V.V'yurkov, Appl. Phys. Lett., **64**, p.25352, 1994.

Modeling Low-Voltage Nanometer Merged MOS Devices

V. Rakitin
Scientific Research Physical Problem Institute named after F.V. Lukin, Moscow, rakitin@niifp.ru

Many technological and constructive methods are used to reduce the relative size of MOS devices and the supply voltage [1]. The new types of transistors were offered and are already used: SOI CMOS, multi-gate (MG MOS, FINFET), nanowire (NW MOS) [2], with Schottky contacts (SB MOS) [3], with tunnels sources [TFET] [4] and others. Different modes of operation are also used: subthreshold, with direct shift of the substrate, with adaptive shift, with the dynamic change of power, etc.
A merged MOS transistor (M-MOS) [5] is an inverting gate and by combining the active areas of the n-MOS and p-MOS takes a minimum space. The combined drains and/or sources can be formed using p-n junctions (Fig. 1), Schottky contacts, tunneling contacts.

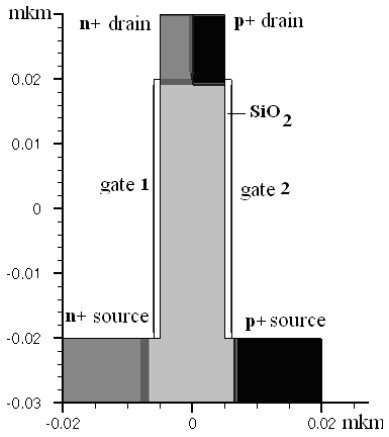

Fig. 1. A model M-MOS transistor.

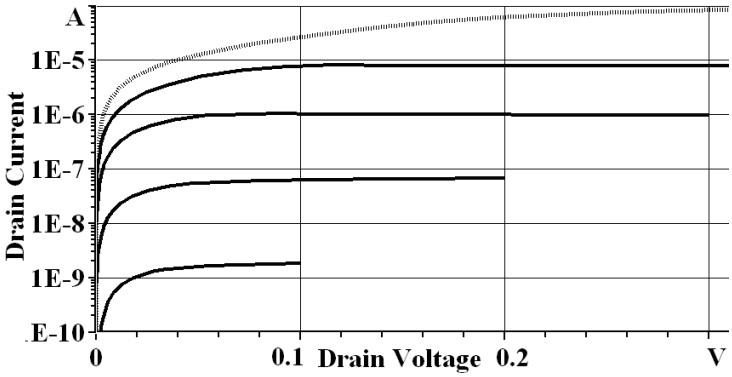

Fig. 2. Output V/I characteristic of a M-MOS.

Simulating an M-MOS with nanometer sizes (as at Fig. 1) were carried out with the program DESSIS of the package ISE TCAD. The background concentration of the impurities in the body was taken equal to $1 \cdot 10^{13}$ cm^{-3}. Arsenic and boron, with a concentration of $1 \cdot 10^{19}$ cm^{-3} were used as dopants. In the case of contacts Schottky the work function of the metal was specified. The recombination of carriers by the Shockley-Reed-Hal mechanism with the minority carrier life-time of 10 μs and with the surface recombination rate of 10^3 cm/s was taken in account. The geometrical dimensions, electro-physical parameters, and electric modes were varied. In the modeling process the basic static characteristics, the small signal parameters, and transient and frequency responses were calculated and analyzed.
Typical output characteristics of a M-MOS at the supply voltages from 0.1 to 0.4 V are shown at Fig. 2. From the transfer characteristics one can conclude that the M-MOS provide the voltage gain of more than 10, and up to 100 for a more complicated construction.
The simulation has confirmed that a multi-gate M-MOS provides realization of complex logical functions. The simulation has also indicated performance of nanometer logic M-MOSs in a wide range of the supply voltages. In such a case, the clock speed exceeds 10 GHz with the supply voltage of 0.6 V and falls down to 10 MHz at the supply voltage of 0.1 V.
In our opinion M-MOSs are suitable to construct compact low-voltage integrated devices.

1. S. Hanson et al., "Ultra-low-voltage, minimum-energy CMOS", IBM J. R&D, **50**, pp.469-490, 2006.
2. J. Appenzeller et al., "Toward Nanowire Electronics", IEEE Trans. ED, **55**, pp.2827-2845, 2008.
3. J. Larson et al., "Overview and Status of Metal S/D Schottky-Barrier MOSFET Technology", IEEE Trans. ED, **53**, pp.1048-1058, 2006.
4. A. Seabaugh et al., "Low-Voltage Tunnel Transistors for CMOS", Proc. IEEE, **98**, pp.2095-2110, 2010.
5. V. Rakitin, "Modeling of VLSI elements on MV-MOS transistors", Russ. Micr., **25**, pp.101-104, 1996.

Nonlinear model of the LDMOS transistor for RF power amplifier with output power 30 Watt in the frequency range 1.20 - 1.32 GHz

E.M. Savchenko[1,2], A.S. Budyakov[1,3], A.D. Pershin[1,2], S.M. Romanovsky[1]
1. FSUE "S&PE "Pulsar", Moscow, designcenter@pulsarnpp.ru,
2. MSTU MIREA, Moscow, 3. MSTU N.E. Baumana, Moscow

RF LDMOS transistors are widely used in communication and radar systems. They have an advantage in the absence of a positive thermal feedback in comparison with silicon bipolar RF transistors [1, 2]. Development of a simplified model for high-power RF LDMOS transistors without loss of accuracy in modeling is important task for computer-aided design (CAD) of RF power amplifiers.

The main objective of this work is to create a relatively simple nonlinear model of the high-power RF LDMOS transistor 2P983A for building matching networks in the frequency range 1.20-1.32 GHz. Transistor must provide the output power more than 30 W and a gain of at least 9 dB when operating in pulsed mode with a duty cycle of Q = 100 and pulse duration τ_i=30 us in the entire operating frequency range.

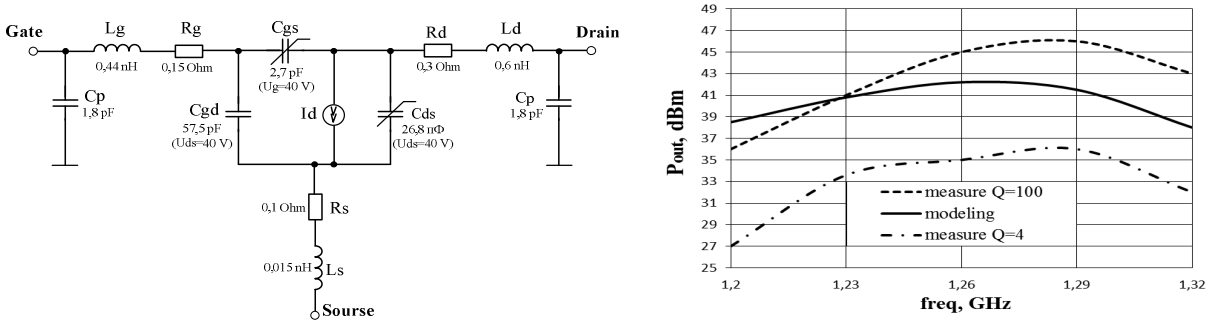

a) b)

Fig. 1 The equivalent circuit of a nonlinear high-power RF LDMOS transistor (a), modeling results and results of measurements output power versus frequency (b) (P_{in}=3 W, U_{ds}=40 V, τ_i=30 us)

The nonlinear model of a high-power RF LDMOS transistor was created in Agilent ADS 2011.10 with SDDP (Symbolically Defined Devices Ports), which provides a mapping of current and voltage between terminals [3]. The basis of the model is equivalent circuit of the transistor with a nonlinear current source (I_c) and nonlinear capacitance (drain-source - C_{ds} and gate-drain - C_{gd}) - in Fig. 1a. Parameters of the model were extracted using measurements of pulsed current-voltage characteristics (DC), capacitance-voltage characteristics (CV) and S-parameters.

In Agilent ADS 2011.10 matching networks were constructed with nonlinear model for a high-power RF LDMOS transistor in the frequency range 1.20-1.32 GHz. The input matching circuit was designed using the S-parameters for providing a minimum reflection coefficient. The output matching circuit was constructed with load-pull analysis. The results of measurements and modeling of the output power versus frequency for the power amplifier, designed with a nonlinear model are shown in Fig. 1b.

There are many models of compact LDMOS transistor (RF LDMOS, HiSIM_HV, etc.). All this complex models require a large number of extraction procedures and optimizing the model parameters (model HiSIM_HV of more than 200). Ease of parameters extraction is the advantage of this model, thus reducing the requirements for measuring equipment and the timing of creation. The developed model allows to design of RF power amplifiers, operating in pulsed mode with a high porosity (over 90), which allows to ignore the effect of self-heating.

1. A.G. Vasiliev, "Highly-integrated components for RF, power and photoelectronics. FSUE "S&PE "Pulsar" in the high-tech market", Electronics: Science, Technology, Business, No. 3, pp.70-75, 2008 (in Russian).
2. S. Didelev, "High-power LDMOS-transistors: advantages and main applications", Components & Technologies, No. 2, pp.22-26, 2002 (in Russian).
3. A.A. Barov, Y.N. Bidnenko, A.V. Kondratenko, "Extraction on non-linear model for GaAs pHEMT", Reports of Tomsk University of Control Systems and Radioelectronics, No.2, pp.137-139, 2010 (in Russian).

Modeling of the silicon complementary bipolar technology process with germanium implantation

E.M. Savchenko[1,2], D.G. Drozdov[1]
1. FSUE "S&PE "Pulsar", Moscow, designcenter@pulsarnpp.ru,
2. MSTU MIREA, Moscow

Creating of high-performance mixed signal integrated circuits (ICs) demand using of high-speed complementary bipolar transistors. In such ICs silicon-germanium technology (SiGe) are widely used.

The majority of modern technology processes applied processes of epitaxial growth of the base region. Earlier, opportunity of the creation of base npn-transistor by ion implantation of germanium was shown [1, 2]. The main advantage of the method is its compatibility with the self-alignment technology. However, insertion of defects during implantation can significantly decrease the amplifier properties of transistors. Such changes are more critical for the pnp-transistor, which have the worst values of the parameters due of physical features. Thus it is interesting to investigate the technique applied to complementary bipolar transistors with high static and dynamic parameters with account of the occurrence of defects by the technology computer-aided design. To investigate the process Sentaurus TCAD (in particular the DIOS module [3]) was used.

The germanium insertion in transistor is performed on the stage of active region formation of the base. To create germanium mole fraction greater than 0.1 the implantation with dose of more than 1000 μC/cm^2 should be used, annealing of germanium is performed simultaneously with annealing of the emitter.

Characteristics of transistors were calculated varying the dose of germanium the range of 1000-3500 μC/cm^2. The result of modeling showed that the collector current of pnp-transistor with germanium implantation of 1000 μC/cm^2 increases in more than 2 times, compared to the undoped case. However, dose increasing more than to 3000 μC/cm^2 leads to significant decrease of the Earley voltage and change of gain dependence at high currents. The results suggest that the technology can be used for increased transistors currents and for the symmetry of complementary bipolar transistors by optimizing only the pnp-transistor. Figure 1 shows the calculation results of input and output current-voltage characteristics of bipolar transistors, besides only pnp-transistor was implanted of germanium (dose Q = 1600 μC/cm^2, energy E = 100 keV).

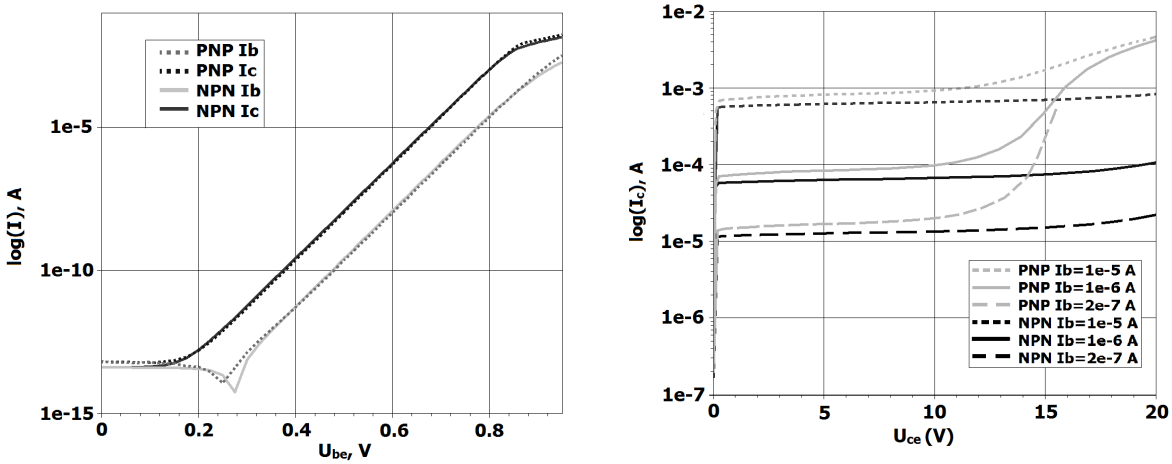

Figure 1. Input and output current-voltage characteristics of complementary bipolar transistors

1. S. Lombardo et al., "Si/Ge_xSi_{1-x} Heterojunction Bipolar Transistors with the Ge_xSi_{1-x} Base Formed by Ge Ion Implantation in Si", IEEE Electron Device Letters, **17**, pp.485-487, 1996.
2. K.C. Liu et al. "A Deep Submicron $Si_{1-x}Ge_x$ /Si Vertical PMOSFET Fabricated by Ge Ion Implantation", IEEE Electron Device Letters, **19**, pp.13-15, 1998.
3. R. Kinder, F. Schwierz, P. Beno, J. Gebner, "Simulation of boron diffusion in Si and strained SiGe layers", Microelectronics Journal, **38**, pp.576–582, 2007.

Tunnel graphene field-effect transistor

D. Svintsov[1], V. Vyurkov[1], A. Burenkov[2], R. Oechsner[2], V. Lukichev[1], and A. Orlikovsky[1]
1. Institute of Physics and Technology, Russian Academy of Sciences, Moscow, Russia, vyurkov@ftian.ru
2. Fraunhofer Institute of Integrated Systems and Device Technology, Erlangen, Germany

The absence of bandgap is the main obstacle to the inclusion of graphene-based transistors into digital circuits. Recently vertical graphene tunneling field-effect transistors were reported [1]. There the gate voltage operates over tunneling between two graphene sheets separated by a dielectric (boron nitride). The gate voltage mainly affects the Fermi energy in nearby graphene layer. Its influence on the tunnel barrier shape is negligible because of screening. Consequently, the high ON/OFF ratio contradicts with the high ON-current, whereas for digit circuits both parameters are crucial.

Here we pay attention to the lateral tunneling graphene transistor [2]. It has a semiconductor (dielectric) tunneling gap below the gate (Fig. 1). In general features the operation of the transistor resembles that of Schottky Barrier Field-Effect Transistor. To some extent, the construction is similar to that of 3D-Transistors in the new generation of Intel Inc. In the proposed transistor the gate voltage efficiently controls both the Fermi energy and the potential barrier shape. This results in the high on-state current inherent to graphene channels and low off-state current inherent to semiconductor channels. The subthreshold slope can approach the thermoemission limit of (59 mV/dec)$^{-1}$ at room temperature. Worth noting in the tunneling gap any dielectric with the bandgap smaller than that of gate dielectric could be substituted instead of silicon.

The calculated dependence of the current vs. gate voltage exhibits a high subthreshold slope (Fig. 2), meanwhile, the dependence of the current vs. drain voltage demonstrates a quite distinct saturation.

For novel generations of integrated circuits the problem of interconnects looks like critical. With decreasing thickness the conductivity of metals dramatically falls down, furthermore, the electromigration is strengthened. Potentially, carbonic materials (nanotubes and graphene) according to their physical properties can successfully replace metallic interconnects. In response to those trends in the present communication we propose to put graphene instead of all metal parts (source, drain, and gate) in the construction (Fig. 2).

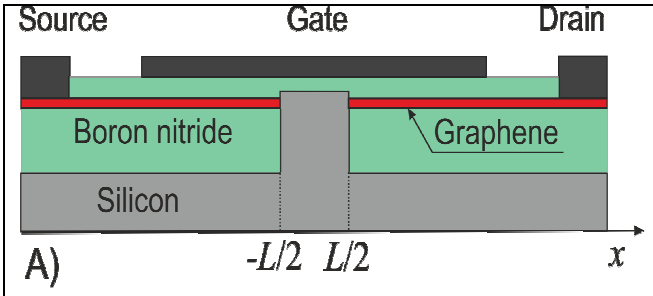

Fig. 1. Schematic view of the lateral graphene tunnel transistor.

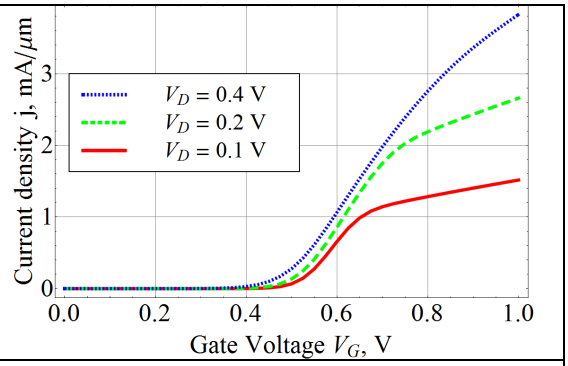

Fig. 2. Current density vs. gate voltage for different drain voltage V_D.

The work was supported by the Russian Foundation for Basic Research (grant 11-07-00464-a) and also by the grant of EU-RU.NET.

1. L. Britnell et al., Science, **335**, p.947, 2012.
2. D. Svintsov, V. Vyurkov, A. Burenkov, R. Oechsner, V. Lukichev, A. Orlikovsky, Semiconductors, to be published.

Numerical model of parallel nano-FET on Coulomb blockade in M_{55} "magic" crystals

V.A. Zhukov[1], V.G. Maslov[2], N.T. Bagraev[3]

1. St. Petersburg Institute of Information Science and Automation, Russian Academy of Sciences, St. Petersburg, Russia, E-mail address: valery.zhukov2@gmail.com. 2. St. Petersburg National Research University of Information Technologies, Mechanics and Optics, St. Petersburg, Russia,

3. Ioffe Physical Technical institute, Russian Academy of Sciences, St. Petersburg, Russia

In the last decade by the methods of colloid chemistry and liquid chromatography the so-called "magic" noble metal nanocrystals Au_{55}, Pt_{55}, Ir_{55}, Ag_{55}, Rh_{55}, Pd_{55}, Cu_{55} were obtained [1]. They have a cube-octahedron shape and size of about 1.5 nm. As shown by quantum-chemical calculations [2], the difference between the energy levels of HOMO for the neutral "magic" nanocrystals and their anions for the elements of this group is of about 1 ÷ 2 eV. The energy difference between the HOMO and LUMO levels for anions of nanocrystals is of about 0.5 eV. This allows building the single-electron nanotransistors on a "magic" nanocrystals of the above listed elements working at room temperature, as opposed to transistors considered in [3]. In order to achieve gains in the charge K_q of values greater than 1 and gains in the power K_w of values greater than 1, such single-electron transistors have been shown to be connected in a parallel structure with a large (about 100) number of identical elements [2]. Here we present the findings that the number of such single-electron elements should be about 2500 for to obtain both a sufficient gain greater than 1 and the speed in the range 0.1 ÷ 1 THz. Since the "magic" nanocrystals are capped to be stabilized with ligand shell of mercaptopropionic acid, with a thickness of ~ 0.7 nm, they can form a plane square super lattice with a surface density of ~ 0.25 nm^{-2} [4]. Therefore, the resulting nanotransistor will occupy the area of 100x100 nm^2. We found that the only material for source electrode and for control electrode of such transistor, having a metallic conductivity, chemical potential close to the energy of the anions of "magic" nanocrystals, and not prone to oxidation in air, is a newly synthesized bilayer graphene [5]. And the only insulator material with a constant layer thickness and a sufficient band gap, satisfying our problem, is a newly synthesized fluorographene [6].

It is shown that at the difference of potentials between source and drain in 2 V and at the gate potential of 0.5 V the similar nanotransistor will have a gains in power K_w and charge K_q of ~ 3 and ~ 3.5, respectively, and speed in the range of 0.1 ÷ 1 THz, depending on the choice of element for the above listed series of "magic" nanocrystals.

1. J.P. Wilcoxon and B.L. Abrams, “Synthesis, structure and properties of metal nanoclusters”, Chem. Soc. Rev., **35**. pp.1162–1194, 2006.
2. V.A. Zhukov, V.G. Maslov, “Current–Voltage Characteristic and the Spectrum Width of Electrons Tunneling through W–WO_2–(Au_{55})–Al_2O_3–Al and Nd–Nd_2O_3–(Au_{147})–Nd_2O_3–Nd Nanosandwiches. Part II: Construction and Analysis of 1D Models for 3D Nanosandwiches”, Russian Microelectronics, **41**, pp.191-199, 2012.
3. K.K. Likharev, “Single Electron Devices and their Applications”, Proc. IEEE, **87**, pp.606-632, 1999.
4. G. Schmid and U. Simon “Gold nanoparticles: assembly and electrical properties in 1-3 dimensions”, Chem. Commun., pp.697-710, 2005.
5. Y. Zhang, Tsung-Ta Tang, C. Girit, Z. Hao, M. C. Martin, A. Zettl, M. F. Crommie, Y. R. Shen & F. Wang", Direct observation of a widely tunable bandgap in bilayer graphene". Nature Letters, **459**, pp.820-823, 2009.
6. R. R. Nair, W. Ren, R. Jalil, I. Riaz, V.G. Kravets, L. Britnell, P. Blake, F. Schedin, A.S. Mayorov, Sh.Yuan, M.I. Katsnelson, Cheng Hui-Ming, W. Strupinski, L.G. Bulusheva, A.V. Okotrub, V. Grigorieva, A.N. Grigorenko, K.S. Novoselov, and A. K. Geim, "Fluorographene: A Two- Dimensional Counterpart of Teflon", Small, **6,** pp.2877–2884, 2010. www.small-journal.com

A model to describe the hump-like feature observed in the accumulation branch of *CV*-characteristics of MOS capacitors with oxide-hosted Si nanoparticles

V. Stuchinsky, G. Kamaev, M. Efremov, S. Arzhannikova
Institute of Semiconductor Physics, Russian Academy of Sciences, Novosibirsk, Russia, stuchin@isp.nsc.ru

Charge transport in dielectrics with semiconductor nanoparticles is a matter of interest for creating favorable conditions for efficient electroluminescence in film structures, for development of multi-bit flash memory cells, etc. In this connection, in our report we present a simple model clarifying the formation of a hump-like feature observed in the accumulation branch of *CV*-characteristics of MOS capacitors with oxide-hosted Si nanoparticles [1]. According to experimental observations, within the above-mentioned feature the MOS capacitance C can be well in excess of the capacitance C_a of an ideal MOS capacitor (without oxide-hosted Si nanoparticles). Generally, the model arises on adoption of the following assumptions: (i) in a biased MOS capacitor, tunneling injection of charge carriers (electrons and/or holes) from one or both contacts into the oxide takes place (for the sake of definiteness, in a particular version of the model we consider an MOS capacitor prepared on a *p*-Si substrate with holes being injected from the accumulation layer of *p*-Si into oxide-hosted Si nanocrystals (nc's)); (ii) the hole transport through the oxide proceeds along linear nc chains in a self-consistent manner with the establishment of local electric field in the oxide; (iii) in the nc chains, tunnel barriers are statistically scattered in terms of their widths, so that the widest tunneling gap presents a 'bottleneck' for the hole current. In an nc chain, the involvement of a 'bottleneck' promotes accumulation of a positive charge Q_s in the oxide, the charge being predominantly concentrated at the edge of the bottleneck from the side of the semiconductor; it is the small ac variation of Q_s that leads to the increase of C in excess of C_a. The properties of the proposed model can be elucidated considering already a simplest case in which each nc chain involves just one Si nanocrystal located, in accordance with the above-formulated assumptions, closer to the semiconductor. On increasing the dc voltage U applied to the MOS capacitor, the nc-trapped charge Q_s first grows in value together with the injection current; the increased charge Q_s results in that an additionally applied bias voltage ΔU now starts dropping predominantly across the gap between the nc layer and the metal, with the formation of a characteristic kink of electrical potential inside the oxide. As the field in the latter gap increases, the tunneling barrier there finally becomes triangular, and the rate of tunneling emission of nc-trapped holes into the metal increases sharply, making the charge Q_s rapidly decrease in value. Afterwards, further incremental voltage changes ΔU will predominantly drop across the gap in between the injecting contact and the nc layer. An analysis of the electrical state of MOS capacitor can be performed by solving a nonlinear equation system comprising the continuity equation for the electric current and the condition of field matching across the nc layer. After the dc quantities of the MOS capacitor are found, ac quantities can be determined by solving the linearized equation system. Finally, the capacitance C can be calculated by assessing the total current (hole current + displacement current) in any cross-section inside the oxide. The calculations show that, at a sufficiently low measurement frequency, a hump-like feature with two capacitance maxima appears in the accumulation branch of the *CV*-curve. In between the two peaks, the capacitance C decreases to C_a; the latter occurs when the charge $Q_s(U)$ reaches its highest. At high bias voltages U the capacitance C saturates at the same value C_a. Data illustrating the typical shape of frequency-dependent *CV*-characteristics of MOS capacitors with oxide-hosted Si nanocrystals and the structure of the total alternating current in the tunneling gaps of the double-barrier structure are presented. Experimentally, a feature with two capacitance peaks closely resembling calculated data was previously observed in [1] while measuring *CV*-characteristics of MOS capacitors with oxide-hosted *a*-Si nanoclusters (except that the injecting contact in [1] was the contact with the metal, and the injected charge carriers were electrons). The approach described above can be easily extended so that to enable analysis of more evolved tunneling configurations formed by Si nanoparticles in SiO_2 films. A joint analysis of data obtained in measurements and calculations may prove useful in electrical characterization of nanostructured dielectrics.

1. S.A. Arzhannikova, M.D. Efremov, G.N. Kamaev, D.V. Marin, V.A. Volodin, and A.A. Voshchenkov. "Charge transport through SiO_x films with Si nanoclusters", *Proc. of the VI Intern. Conference "Amorphous and Microcrystalline Semiconductors"*, pp.162-163, Polytechnical University, St.-Petersburg, 2008 (in Russian).

MCT photodiodes spectral response

K.O. Boltar[1,2], A.V. Nikonov[1,2], N.I. Iakovleva[1]
1. State Scientific Center of Russian Federation "RD&P Center ORION", Moscow, Russia, orion@orion-ir.ru
2. Moscow Institute of Physics and Technology, Moscow, Russia, info@mipt.ru

Heteroepitaxial structures mercury cadmium telluride ($Hg_{1-x}Cd_xTe$) is the ideal choice for producing large infrared focal-plane arrays (FPA) for different spectral regions due to the ability to adjust the band gap by varying the cadmium mole concentration for IR applications [1]. Grown both by molecular beam epitaxy (MBE) and liquid phase epitaxy (LPE) [2] high quality heteroepitaxial structures based on HgCdTe alloy including structures with variband layers and buffer layers nearby surface and wafer interface to decrease surface recombination have been produced. One-dimensional model of photodiode with sharp *p-n* junction is used to determine the quantum efficiency and diffusion current of small n^+-*p* junctions on the basis of HgCdTe heteroepitaxial structures (Fig. 1). Sharp p-n junction is irradiated from p-type region side, and the structure is divided into three parts: quasi-neutral p-type region ($0, x_p$), a space-charge depletion region ($x_p<x<x_n$) around metallurgical junction and quasi-neutral n-type region (x_n, L), where L is the length of p-n junction in x direction, x_j –metallurgical junction depth. The model of quantum efficiency has been calculated on the basis of time-independent continuity equation for minority carriers with the boundary conditions taking into account the surface recombination on substrate-MCT epilayer interface and Boltzmann distribution in depletion region. Additionally theoretical dependences of spectrum absorption coefficient on MCT composition and wavelength have been analyzed.

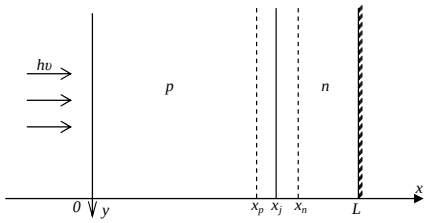

Fig. 1. One-dimensional model of photodiode with sharp p-n junction

Thus, photodiode quantum efficiency is defined as

$$\eta = hcJ_{ph}(V_a)/qI_0(\lambda)\lambda \quad (1)$$

where $J_{ph}(V_A)$ – photocurrent due to incident radiation with density $I_0(\lambda)$ at $x=0$; c – speed of light; h – Planck's constant; $I_0(\lambda)$ – irradiation density at λ wavelength on semiconductor surface.

Total current density of sharp p-n junction is determined as a sum of currents in p-type, n-type regions and depletion region

$$J_{ph} = J_{n,ph}(x_p)+J_{DR,ph}+J_{p,ph}(x_n) \quad (2)$$

Current density is directly proportional to irradiation $I_0(\lambda)$ incident on p-type region surface of photodiode (x=0). Therefore total quantum efficiency of photodiode with sharp p-n junction is equal to:

$$\eta = J_{ph}hc/qI_0(\lambda)\lambda = \eta_n+\eta_{DR}+\eta_p \quad (3)$$

where quantum efficiency in all basic regions is determined by expressions from paper [3].

The photodiode current density is determined taking into consideration spectrum absorption coefficient in the epilayer, the influence of epilayer width, composition depth variation, diffusion length of minority charge carriers, surface recombination on MCT epilayer interfaces, photodiode voltage, and reflection on vacuum/substrate, substrate/epilayer, epilayer/vacuum surfaces.

Considering an influence of the quasi-neutral p-type region, a space-charge region and quasi-neutral n-type region on the total quantum efficiency, numerical simulation of spectral response for MCT photodiode based on n^+-*p* junction versus some parameters of heteroepitaxial structures (composition, diffusion length, diffusion coefficient of minority carries, and surface recombination) have been carried out. We have used the numerical simulation of spectral response characteristics for photodiodes quantum efficiency estimation, MCT epilayers initial characteristics definition and technology improvement recommendations.

1. K.O. Boltar, I.D. Burlakov, A.M. Filachev, E.A. Klimanov, V.P. Ponomarenko, V.N. Solyakov, V.I. Stafeev, "Single and Matrix HgCdTe Photovoltaic Detectors", Optical Memory and Neural Networks (Information Optics), **16**, pp.234-247, 2007.
2. V.S. Varavin, Yu.G. Sidorov, S.A. Dvoretskii, "Molecular-beam epitaxy of mercury-cadmium telluride solid solutions on alternative substrates", Semiconductors, **35**, pp.1045-1053, 2001.
3. P. Jespers, F. van de Wiele, M.H. White. *Solid State Imaging*, Springer, New York, 1976.

Changing of magnetic properties in magneto-photonic crystals by light influence

D.E. Afanas'eva[1], A.N. Kuprianov[2], A.V. Paporkov[1], A.V. Prokaznikov[1,2]

1. Yaroslavl State University, Institute of Semiconductor Physics, Yaroslavl, Russia, E-mail pva@univ.uniyar.ac.ru,

2. Yaroslavl Branch of the Institute of Physics and Technology, Russia, E-mail prokaznikov@mail.ru

In this work the results of investigations of collective effects for magneto-optical properties of 2D photonic crystals are presented. The samples being investigated were boron doped wafers on which a 2D stricture was formed that looks like regular rows of columns with a square cross section and covered on the top by a cobalt nano-layer which was placed on a chromium film with the thickness of some tens of nanometers. The investigations have revealed the presence of quasi-periodical variations of magnetic properties of the system by interaction with an electro-magnetic radiation. Oscillations discovered on angle dependences of the transverse magneto-optical Kerr effect were connected with resonant conditions fulfillment when in the magnetic film a standing electro-magnetic wave was formed what results in spin flip in the system and thus its magnetic properties changing. The results of TMOKE investigations are presented on Figs. 1, 2.

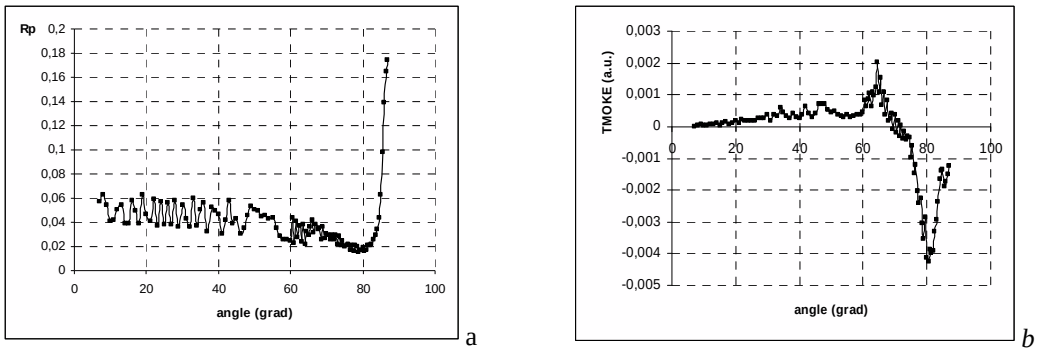

Fig. 1. Dependence of reflection coefficient R_p in diffraction maximum of the order of (0,0) on the incident angle when the incident surface is perpendicular to squares sides in cross sections of columns (a), angle dependence for TMOKE for the same configuration (b).

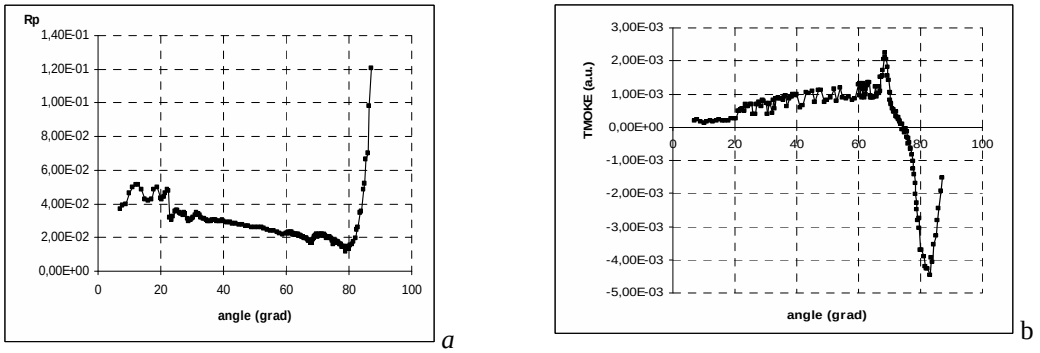

Fig. 2. Dependence of reflection coefficient R_p in diffraction maximum of the order of (0,0) on the incident angle when the incident surface is perpendicular to square diagonals in cross sections of columns (a), angle dependence for TMOKE for the same configuration (b).

The practical application of these investigations is based on the fact that the structures analogous to investigated ones were used in [1] to create terabit memory.

J.K.W. Yang, Y. Chen, T. Huang, H. Duan, N. Thiyagarajah, K.H. Hui, S.H. Leong, V. Ng. "Fabrication and characterization bit patterned media beyond 1.5 Terabit/in^2", Nanotechnology, **22**, 385301, 2011.

Comparative study of ultrathin Co films grown by ion-plasma and magnetron sputtering

V.F. Bochkarev[1], O.S. Trushin[1], V.V. Naumov[1], S.V. Vasiliev[2] and V.A. Paporkov[2]
1. Yaroslavl Branch of the Institute of Physics and Technology of RAS, Yaroslavl, Russia, otrushin@gmail.com
2. Yaroslavl State University, Yaroslavl, Russia

Magnetic multilayer nanostructure is of perspective material for spintronic applications [1, 2]. Such nanostructures show giant magnetic resistivity effect [3]. Development of cost effective and reliable technology for magnetic layers of high quality fabrication is of important direction for research. Standard way of magnetic multilayer formation is magnetron sputtering deposition. Yet another alternative method for growing multilayer films is ion-plasma sputtering. The purpose of this work was to check possibility of using ion-plasma method for fabrication of magneto-resistive structures. The most important ingredients of magneto-resistive structures are ultrathin magnetic layers (Co, Py and others). In this work we performed comparative study of ultrathin Co films grown by ion-plasma and magnetron sputtering.

As an example of magnetron sputtering tool we used standard industrial installation TETRA SCR-600 (produced by Alcatel) equipped with 4 targets for simultaneous deposition of four different materials in single vacuum cycle. Ion-plasma sputtering was done using home made installation (plasma discharge by triod scheme) having 4 targets. We performed two sets of experiments systematically comparing thin Co films produced by those two methods.

In the first set of experiments we were growing Co films on NaCl layer. By dissolving NaCl layer it was possible to separate Co thin film and place it onto Cu gratings for subsequent Transmission Electron Microscopy study of its crystal structure. In Fig.1 we present TEM images and corresponding electron diffraction patters for Co films deposited by two alternative methods.

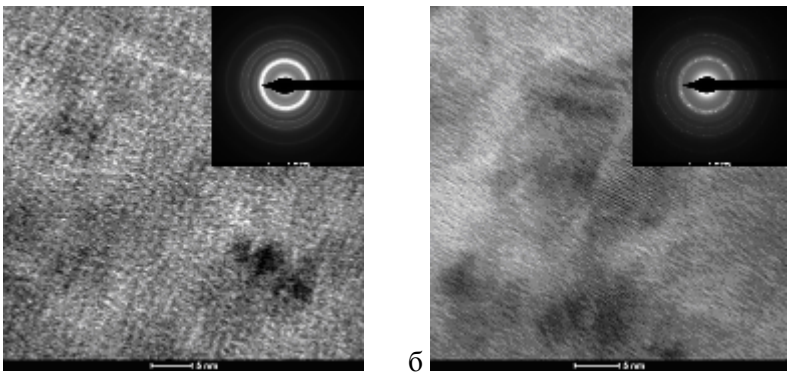

Fig.1 Transmission electron microscopy images (electron diffraction patterns on the insets) taken for two different Co films: а) ion-plasma sputtering, б) magnetron sputtering

From analysis of TEM data we conclude that ion-plasma film has less developed crystal structure (considerable fraction of amorphous phase) in comparison to magnetron film. Electron diffraction patters show presence of CoO in the ion-plasma film.

In the second set of experiments we studied physical properties of thin Co films grown on Si(100) substrate with Ta buffer layer. We measured sheet resistivity, AMR effect and magnetic reversal loop for Co films deposited by two alternative methods. In summary, we checked possibility to use ion-plasma method for ultrathin Co film deposition for magnetic multilayer fabrication. We performed a systematic comparison of as grown films with the films grown using standard magnetron sputtering. The results showed principal possibility of growing good quality magnetic films by ion-plasma method under condition of further work on improving technology.

1. S. Tumanski *Thin magnetoresistive sensor*s, IOP publishing Ltd., Bristol, 2001.
2. R. Coehorn “Giant magnetoresistance and magnetic interactions in exchange-biased spin-valves”, in *Handbook of magnetic materials*, Vol. **15**, Elsevier Science, Amsterdam, 2003.

Fabrication of epitaxial tunnel magnetic junctions Fe/MgO/Fe(001) using pulse laser deposition

A. Chernikh, V. Vinnechenko, L. Fomin, I. Malikov, and G. Mikhailov
Institute of Microelectronics Technology and High Purity Materials RAS, 6, Academician Ossipyan str, Chernogolovka, Moscow Region, 142432, Russia, E-mail address: mikhailo@iptm.ru

Single-crystalline tunnel magnetic junctions (TMJ) Fe/MgO/Fe (001) attract much scientific and application interests after discovery of giant (till 600% at room temperature) coherent tunnel magnetic resistance (TMR) effect in recent years. Investigations concentrated on the growth of heteroepitaxial multilayered structure Fe/MgO/Fe with a high quality layers interface, including interface crystalline structure, composition and interface roughness, are still of great attention. Depending on the methods involved in technology the treatments during epitaxial TMJ fabrication may influence on the interlayer composition and structure that cause a modification both of TMR and volt-current characteristics of TMJs.

Developed technological road map is desired for fabrication heteroepitaxial TMJs Fe-MgO-Fe(001) with lateral sizes 300 - 3000 nm, interface roughness below 1 nm and a tunneling dielectric layer width 1-5 nm. Fabrication of TMJs is based on the subtractive technology with use of electron lithography and ion etching of preliminary grown heteroepitaxial multilayered film Fe-MgO-Fe (001) or Fe-MgO(001) by pulse laser deposition (PLD) (second harmonic of Nd pulse laser with 540 nm wave length), followed by growth of upper epitaxial electrode by PLD or electron beam deposition (EBD). Magnesium oxide growth is performed by evaporation of magnesium target in the presence of molecular oxygen.

The technological steps for functional epitaxial TMJ Fe-MgO-Fe(001) fabrication are the following:

- growth of multilayered heteroepitaxial film Fe-MgO (1-5 nm) -Fe(001) on r-plane sapphire with W(001) or MgO(001) seed layers, covered by strong magnet layer of Co and passivated layer of Ta;
- microstructurization of low electrode and vertical multilayered tunneling structures;
- local deposition of isolating layeres;
- metallization for lower and upper electrodes.

Volt-current characteristics of TMJs measured at room and liquid nitrogen temperatures showed that tunneling properties of the junctions are strongly influenced by the plasma generated during laser ablation of the target. Tunneling resistance of TMJs with upper electrode grown by PLD are up to three order lower than that of TMJs with upper electrode grown by EBD. Exactly for latter TMJs, the product of tunneling resistance on TMJ's area is in agreement with well-known published data for definite tunneling MgO width. For TMJ's completely grown by PLD and possessed low tunneling resistance we observed tree types of tunneling-resistance temperature dependence. The first one is typical for high quality TMJ and demonstrates small (10%) increase of tunneling resistance at lower temperature. The second one is of a metallic type temperature dependence, and third one is a strong temperature activated dependence with the tunneling resistance rise in tenth times at liquid nitrogen temperature. We supposed that during upper electrode growth using PLD the high energy ions generated by laser oblation of the target impact a tunneling dielectric layer caused appearance of the energy levels in its energy gap. This leads to decreasing both the effective width and the tunneling potential. Despite it may be the origin of negative influence on the quality of TMJs, PLD technique may be used for controllable decrease of the tunneling resistance keeping the TMR effect on the appropriate level.

Experimental observation and simulation of a spin-polarized current effect on magnetic structure of epitaxial Fe (001) quadratic microstructures

L.A. Fomin, I.V. Malikov, K.M. Kalach, S.V. Pyatkin, G.M. Mikhailov

Institute of Microelectronics Technology and High Purity Materials, RAS, 6, Academician Ossipyan str, Chernogolovka, Moscow Region, 142432, Russia, E-mail address: fomin@iptm.ru

At present, the spin-polarized current driven domain wall motion in ferromagnetic nanostructures is of great scientific interest. Spin-polarized current of high density ~ 10^7 - 10^8 A/cm^2, passes through a ferromagnetic nanostructure can change its magnetization, causing the motion of domain walls in accordance with the theory of Slonczewski and Berger [1, 2]. In this paper, magnetic force microscopy (MFM) and micromagnetic calculations have been used to study the effect of spin polarized current on the magnetic

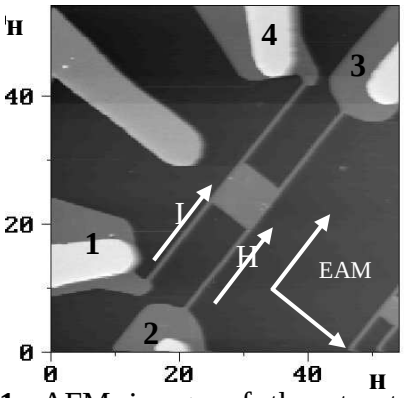

Fig. 1. AFM image of the structure. The arrows indicate the direction of current I, magnetic field H and the easy axis of magnetization.

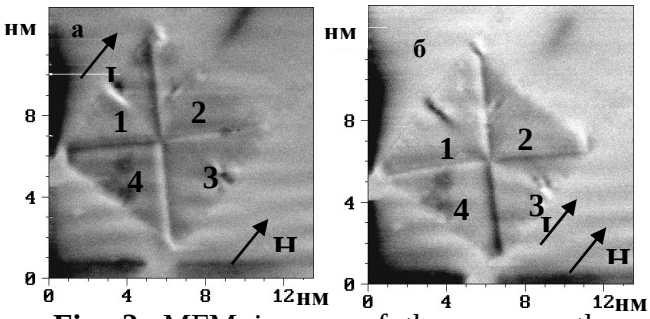

Fig. 2. MFM images of the, square, the numerals show the domain numbers: a) after the current supply to contacts 1 - 4 and b) after the current supply to contacts 2 - 3. The arrows indicate the direction of the current and the external magnetic field.

states in epitaxial Fe (001) microstructures shaped as the 8x8 μm square and connected to the four 0.5 μm wide and 20 μm long stripes at the corners of the square. The ends of the strips were attached to the external electrical contacts. The square and stripes were oriented along one of two in-plane axes of easy magnetization. In zero magnetic field, the strips are in the single-domain state, and the square is divided on to four equal triangular domains. After applying the magnetic field along the strip and after its removing the magnetization direction in the strips remains. It was observed experimentally that the current flowing through the contacts 1 and 4 (fig. 1), contributes to the orientation of the magnetization vector in the domain 1 along the field direction, but in the opposite direction in the domain 3 (fig. 2a). Passage of current through the contacts 2 and 3 contributes to the orientation of the moments in the domain 3 along the direction of the field, but in the opposite direction in the domain 1 (fig. 2b). Thus, the effect of spin polarized current on the magnetic structure of the square was observed. Micromagnetic calculations of these structures were carried out using OOMMF [3]. Simulations of MFM images using the results of the micromagnetic calculations were performed. The calculations confirmed the results of the experiment.

1. J.C. Slonczewski, “Current-driven excitation of magnetic multilayer”, J. Magn. Magn. Mater. **159**, pp.L1-L3, 1996.
2. L. Berger, “Emission of spin waves by a magnetic multilayer traversed by a current”, Phys. Rev. B, **54**, pp.9353-9358, 1996.
3. http://math.nist.gov/oommf/

Size and magnetic anisotropy effect of micromagnetic states in rectangular epitaxial Fe (011) microstructures

L.A. Fomin, I.V. Malikov, S.V. Pyatkin, G.M. Mikhailov

Institute of Microelectronics Technology and High Purity Materials, RAS, 6, Academician Ossipyan str, Chernogolovka, Moscow Region, 142432, Russia, E-mail address: fomin@iptm.ru

Ferromagnetic micro-and nanostructures are widely used in microelectronic devices as the memory elements and the read heads [1, 2]. Efficiency of their application depends on the magnetic structure and the switching fields, which are the function of their shape, size, magnetic anisotropy and magnetic prehistory of the sample. In particular, it is desired to realize a single-domain state with a rectangular hysteresis loop in

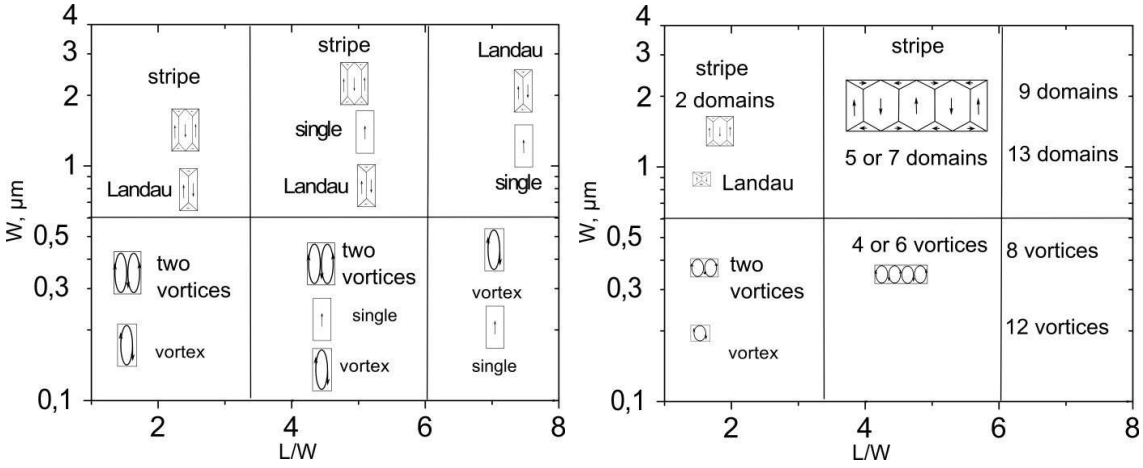

Fig. 1. Diagrams of micromagnetic states of rectangular microstructures versus widths and aspect ratios of them. The long sides of the rectangles are parallel to the easy axis of magnetization (a) and perpendicular to it (b).

samples.

In this paper, the magnetic states in epitaxial rectangular microstructures made from epitaxial Fe (011) films grown on R-plane sapphire with a Mo seed layer were investigated using magnetic force microscopy (MFM) and micromagnetic calculations [3].

The widths of the rectangles ranged between 0.3 and 8.0 μm. Aspect ratios of rectangles (length to width ratio) were 2, 4, 6, 8, respectively. The long axes of the rectangles were oriented both parallel and perpendicular to the easy magnetization axis. The film thickness was 60 nm. It was found that rectangles with the long axis perpendicular to the easy magnetization demonstrated the strip-domain structure axis in the whole range of sizes. Width of the stripe domain is independent of the aspect ratio (AR) and increases with the rectangular width as a square root. For rectangles, oriented parallel to the easy magnetization axis there are found three types of magnetic structures. Two of them included the multidomain states (Stripe-domain structure and the Landau structure) while the other one did the quasi-single-domain state. Width of the stripe domain did not depend on the width of the structure and AR. We observed transition from a stripe-domain structure to the Landau structure and further to the quasi-single-domain state with AR. The values of AR, at which these transitions occur, depend on the length of the rectangle. Based on performed study the MFM images were interpreted and micromagnetic state diagrams were drawn.

1. G.A. Prinz, "Magnetoelectronics", Science, **282**, pp.1660-1663, 1998.
2. S.A. Wolf, et al., "Spintronics: A Spin-Based Electronics Vision for the Future", Science, **294**, pp.1488–1495, 2001.
3. http://math.nist.gov/oommf/

Epitaxial film growth for Fe_3O_4 / MgO / Fe (001) tunnel magnetic junctions fabrication

I.V. Malikov, V.Yu. Vinnichenko, L.A. Fomin, G.M. Mikhailov
Institute of Microelectronics Technology and High Purity Materials, RAS, 6, Academician Ossipyan str, Chernogolovka, Moscow Region, 142432, Russia, E-mail address: malikov@iptm.ru

Spin-polarized transport in nanostructures is at present considered to be one of promising phenomena for the development of a novel class of devises. Half-metallic materials, such as CrO_2, $La_{0.7}Sr_{0.3}MnO_3$ (LSMO), and Fe_3O_4 are highly attractive for spintronics applications because of their high spin polarization. Among these materials, magnetite (Fe_3O_4) is superior to others because of its high Curie temperature (T_c) of 858 K, which is crucial for thermal stability in device applications. In addition, magnetite has proven to be a ferromagnetic material with a high spin polarization (ca. 100%) at the Fermi level, which results in a metallic minority spin channel and a semiconductor majority spin channel. Magnetite crystal structure is highly compatible with many other materials and this fact is attractive for creation of multilevel structures, such as tunnel structures for an example.

In this work, epitaxial magnetite films were grown by laser evaporation of Fe target in oxygen atmosphere on sapphire substrates A (0001) and R (-1012) with epitaxial MgO (5-10 nm) seed layer. Growth rate is 5-20 nm/min. MgO was deposited by reactive electron-beam evaporation of MgO or reactive laser ablation of Mg target. Magnetite films stable growth with sheet resistance close to the bulk material is at oxygen pressures $3x10^{-7}$ - $7x10^{-7}$ Pa. Oxygen pressure increasing and decreasing from these values leads to complete Fe oxidation with formation of Fe_2O_3 or not complete Fe oxidation. Temperature dependences of resistance and surface roughness are controversial. Improvement of the film resistance with the growth temperature deteriorates the film surface morphology. Magnetite films grown on MgO (001) seed layer on R sapphire surface has a resistance optimal minimum at the temperature about 400 ^oC according with the start of the reaction of Fe_3O_4 and MgO at 440 ^oC (known from literature). To overcome this contradiction magnetite films were grown at low temperatures and then were annealed at higher temperatures.

X-ray measurements suggest good crystal quality of grown films. Pole figures of magnetite films grown on C-sapphire revealed a strong six-fold symmetry of (111) orientation. Pole figures of magnetite films grown on R-sapphire substrate with MgO seed layer revealed (001) orientation. In the second case multilevel epitaxy of Fe, MgO and magnetite films were examined. All films are mutually epitaxial. However, they demonstrate inclination epitaxy, as each layer crystallographic normal creates some small angle about 3-4^o relatively underlayered crystallographic film normal. Tilt angles between (004) direction of magnetite film and R-sapphire substrate are about 7^o and 14^o for epitaxial structures R-sapphire/MgO (5 nm)/Fe_3O_4 and R- sapphire/MgO (5 nm)/Fe (20 nm)/MgO (2 nm)/Fe_3O_4, respectively.

This procedure gives a possibility to produce epitaxial magnetite films with low surface roughness, film resistance closed to the bulk material, sharp Verwey transition and low magnetite film magnetoresistance, and thus produced magnetite films are suitable for fabrication of multilayered heteroepitaxial structures on single crystalline sapphire substrates. Technological path for vertical structure fabrication includes electron-beam lithography to develop a nanomask on the top of sandwich Fe/MgO/Fe3O4 (001) film and subsequent ion etching. Then deposition of thick isolating dielectric film and fabrication of upper metallic electrode on the top of structure were accomplished. During technology development, the different technological approaches were investigated to fabricate epitaxial Fe_3O_4 / MgO / Fe (001) tunnel magnetic junctions with improved parameters.

Development technology of creation sensor nanomaterials based on ZnO

O.A. Ageev, E.G Zamburg, Z.E. Vakulov, A.V. Shumov, D.E. Vakulov, M.N. Ivonin, V.V. Ptashnik

Taganrog Institute of Technology, Southern Federal University, Taganrog, Russia, zamburg.evgeniy@gmail.com.

At present actual problem is creating sensors for nanosensing and nanosystem technology based on materials with unique properties. Due to the fact that ZnO has a gas– and photosensitivity, piezo – and pyro effects, biological compatibility – it is a promising material for development of devices for nanosensing materials based on ZnO [1].

The purpose was to develop technology for gas– and photosensitive materials based on ZnO for nanosensing devices by pulsed laser deposition. For this were conducted theoretical and experimental studies of modes of obtained materials based on ZnO. Developed the design of experimental samples of the gas sensors and photosensitive elements and investigated parameters of the resulting structures.

During investigation the technology of producing nanocrystalline films, horizontal-aligned nanowires, and hybrid nanostructures based on carbon nanotubes and ZnO have been developed. The method of stabilizing the electrical properties of nanostructed films of ZnO has been developed. Also experimental models of gas sensors and radiation detectors based on nanocrystalline films of ZnO have been designed and manufactured. Horizontal–aligned ZnO nanowires about which have a little information have been growth. Also hybrid nanostructures based on carbon nanotubes and ZnO, have been obtained. A method of stabilizing the electrical properties of nanostructured films of ZnO was developed, which was not previously described in papers. Also experimental models of gas sensors and detectors of radiation with huge sensitivity, based on ZnO nanostructured films have been developed.

Figure 1 shown growth horizontal–aligned ZnO nanowires (Fig. 1a), hybrid nanostructures based on carbon nanotubes and ZnO (Fig. 1b) and nanostructured films of ZnO (Fig. 1c).

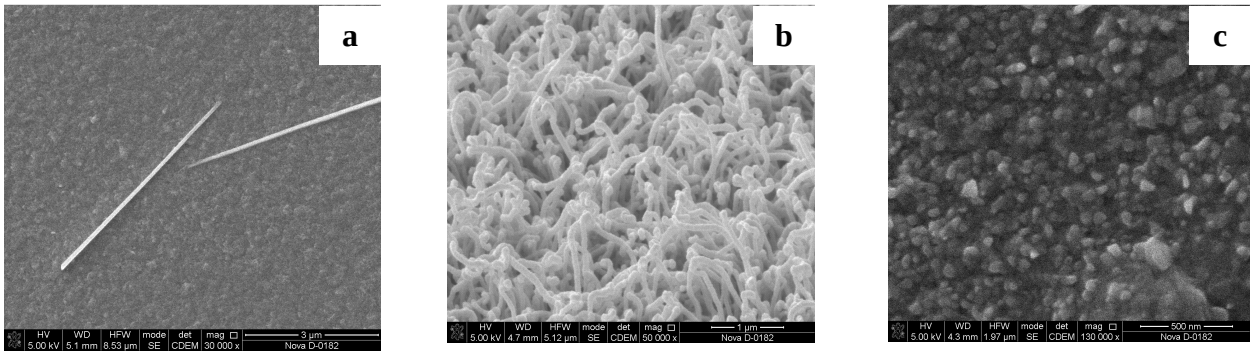

Figure 1 – SEM images of horizontal–aligned ZnO nanowires (a); hybrid nanostructures based on carbon nanotubes and ZnO (b); nanostructured films of ZnO (c)

It was fond maximum response at 10 ppm NO_2 achieved when measuring voltage was 2 V. Thus, the problems were solved restricting the using ZnO in nanosensing devices.Sensing element had maximum sensitivity (600 %) at 10 ppm NO_2. The structure has photo sensitivity 400 % at operation voltage 1V. During performance researching of obtain nanocrystalline ZnO films and nanostructures in a wide range of electrical and morphological parameters have been done. The possibility of nanocrystalline ZnO films with controlled grain size, morphology, resistivity, mobility and electron concentration have been shown. The technology of gas-sensitive materials based on nanocrystalline ZnO films has been developed.

The obtained results obtained can be used to develop design and technology of environmental monitoring systems elements, solar cells, UV radiation detectors, microelectromechanical systems and components of nanosensing [2].

1. H. Morkoc, U. Ozgur, "*Zinc Oxide. Fundamentals, Material,s and Device Technology*", pp.1-490, WILEY-VCH Verlag GmbH & Co, Weinheim, 2009.

2. E.G. Zamburg, A.V. Mikhailichenko, V.V. Ptashnik, "*Electrophisical properties ZnO and VOx films formed by pulsed laser deposition*", Southern Federal Universities' news, Technical sciences, No. 4, pp.134–141, 2011 (in Russian).

Specificity of the synthesis of carbon nanotubes using the combined catalyst

S. Basaev, V.A. Galperin, A.A. Pavlov, Yu.P. Shaman, A.A. Shamanaev
Scientific-Manufacturing Complex "Technological Centre", Moscow, Russia e-mail: artemiy.shamanaev@gmail.com

It is known that the growth of carbon nanotubes depends largely on the conditions of formation of clusters, catalysts, materials, and dimensions that determine quality and characteristics of future carbon nanotubes. Processes for the synthesis of CNT arrays, depending on the technology on which the clusters of a catalyst are formed, can be divided into two types: i) Synthesis with a localized catalyst and ii) synthesis using the injected catalyst.

The paper presents research results of a new process of synthesis of arrays of carbon nanotubes using the combined catalyst, which combines the advantages of the synthesis of carbon nanotubes as localized, and injected with a catalyst. Combined catalyst is a system consisting of an organometallic compound (injected) and its decomposition catalyst (localized).

Due to optimal synthesis parameters such as temperature, flow rate of reagent, the concentration and the type of organometallic compound, and the composition of the catalyst film, a new method of synthesis of arrays of carbon nanotubes (CNT) of a given topology is developed. We studied influence of the size effects of topological elements on the characteristics of arrays of carbon nanotubes. The results of statistical analysis and research by transmission and scanning electron microscopy are shown.

1. S.V. Bulyarskii, O.V. Pyatilova, A.V. Tsygantsov, A.S. Basaev, V.A. Galperin, A.A. Pavlov, and Yu.P. Shaman, "Thermodynamics of the formation of catalyst clusters for carbon nanotube growth", Semiconductors, **44**, pp.1718-1722, 2010.

2. A.S. Basaev, E.V. Blagov, V.A. Galperin, A.A. Pavlov, U.P. Shaman, A.A. Shamanaev, S.V. Shamanaev, and A.S. Prihodko, "Specificities of Growth of Topological Arrays of Carbon Nanotubes", Nanotechnologies in Russia, **7**, Nos.1-2, pp.22-27, 2012.

Method of fabricating nanopores in silicon wafer via P^+ and O_2^+ Co-implantation and non-isothermal annealing

Yu.I. Denisenko
Yaroslavl Branch of the Institute of Physics and Technology, Institution of Russian Academy of Sciences,
E-mail: den-yur55@mail.ru

An important problem of semiconductor material science is obtaining new materials and, based on them, microstructures with specified electrical and physical properties. The necessary variety of the properties can be reached through introducing of specific defects, phase and structural inhomogeneities into the semiconductor substrate in required quantities and at the desired depth. The intense interest in defect engineering is fabricating solid state nanopores (or nanocavities) without the use of electrochemical processes. For example, nanoporous layer in silicon can be created in a two-stage process: production of He bubbles by implantation with doses $(0.8 \div 15)\cdot 10^{16}$ He^+/cm^{-2} and removal of the gas from the bubbles by annealing at temperatures above 700 ^{0}C [1]. Another approach to formation of the layers with hollow nanospheres is attributed to the Kirkendall effect in the planar layered structure of $Ni/Ni_2Si/Si$ [2]. The control of those open volume defects allows performing important functions in device microstructures: effective sinks for metal ions, deep level defects for life-time monitoring in power devices, compensators of stresses on the border of heterostructures, centers of luminescence, etc.

The aim of the present work is further development of engineering of porous layers in silicon. Suggested the overall porosity of silicon can be increased by the way of bulk diffusion of excess vacancies generated during annealing of the specially prepared silicon-based substrates, placed in non-isothermal reactor. The initial substrates of (100)-oriented silicon are developed by using high-dose implantation of phosphorus and oxygen into silicon substrate. In the presence of ∇ T, the conditions for division of point defects fluxes are created, in which the direct recombination between vacancies and interstitials became difficult, at the same time, indirect recombination through recombination centers is possible. This increases the chemical potential of vacancies, thus, increasing probability the appearance of viable nucleus for pores formation. Thus, the emerged buried oxide layer (BOX) effectively “isolates” an influence of irradiative vacancy-type defects (near surface) from excess interstitials region (near 2 R_p). In this case, at sufficiently low thermal budget of non-isothermal annealing, the BOX is protected as a barrier from recombination of vacancies on the substrate surface, while provides the phosphorus diffusion deep into the substrate. Experimentally has been investigated the initiating of pores formation during annealing (1100 ^{0}C, 5 minutes) at the presence of the axial temperature gradient of 70 K/cm in case of one of two directions. During subsequent isothermal annealing (1150 ^{0}C, 1 ÷ 4 hours) in conventional isothermal furnace, on “cold” side of the substrate the arising nucleuses got their development to nanopores. A regular structure of 3D open-volume defects on the cleaved side of the specimen is observed. On "hot" side of the substrate, a plastic flow of surface material takes place via dislocations movement along the slip systems <110>/{111}. With annealing time, corresponding stresses lead to the formation of microcracks. In the control samples after isochronous isothermal annealing in the same temperature range, formation of pores or microcracks was not observed. Corresponding SEM images of the cleaved structures are presented.

1. V. Rainery, M. Saggio, E. Rimini, “Voids in silicon by He implantation: From basic to applications”, J. Mater. Res. **15**, pp.1449-1476, 2000.
2. K.N. Tu, U. Gusele, “Hollow nanostructures based on the Kirkendall effect: Design and stability considerations”, Appl. Phys. Lett., **86**, 093111, 2005.

Investigation of dependence of morphology and fractal characteristics of porous silicon on anodizing conditions

D. Gaev[1], A. Boyko[2], S. Timoshenkov[2]
1. Kabardino-Balkarian State University, Nalchik, Russia, dahir@mail.ru . 2. National Research University of Electronic Technology, Moscow, Russia, ant_nico@mail.ru, spt@miee.ru

Though the prospects of practical use of porous silicon have been studied in different branches of science and technology there are no industrial of manufacturing products on it basis. To some extent the situation can be explained by the facts that there are no technologies of creating structures on the basis of porous silicon that exclude temporary instability of structure properties. Due to this further improvement of techniques providing fabrication of porous silicon with the definite set of functional properties is of both scientific and practical importance.

Within the framework of this research there were carried out experimental studies of morphology and fractal characteristics of porous silicon in connection with anodizing conditions. In the experiment we use the wafers of n-type single-crystal (100) oriented silicon; anodizing solution was a mixture of 40% hydrofluoric acid and 96% ethanol. The process was carried out in one-chamber electrochemical cell of vertical type with the use of reticular platinum electrode. In the process of fabricating of experimental structures there was used anodizing at direct and alternating current without external illumination and with continuous electrolyte stirring. After this the specimens were thoroughly washed in deionized water and dried in vacuum chamber at room temperature. We estimated the thickness of the porous layer by its end view. The error of the thickness layer estimation didn't exceed 10%. The porosity value of specimens was measured using gravimetric technique and the error in the porosity value was 20-25%.

Experimental porous structures received under different current conditions and electrolyte concentrations were investigated with the use of light, atomic-force and electron microscopy. The majority of samples can be characterized by complex globular structure morphology at all the levels of structural hierarchy. Thus it was the fractal method that was used for the quantitative analysis of morphological of porous layers. The surface fractal dimensions were calculated by "perimeter-square" method in accordance with the procedure recommended in works [1-3]. For each sample we processed 90 contour cross-section images of porous layer. The calculations showed that fractal dimensions of the porous layer surface range from 2.4 to 2.6 that proves the complex self-organization process of pore-formation and developed surface of porous layer. We also found out the correlation between the fractal surface properties and the conditions of porous layer formation. It is shown, that fractal dimension depends on the anodizing current.

We also investigated the photoluminescence of structures based on porous silicon. Analysis of luminescence spectra revealed their relationship with the fractal dimension of porous layers. It is shown that with increasing the fractal dimension the peak of the luminescence spectrum was shifted to shorter wavelengths of radiation. This pattern indicates the sensitivity of characteristics of fractality to the dimensions of interporous crystal phase of porous silicon.

So we can conclude that the investigation results prove the possibility of efficient use of fractal approach for the analysis of morphological and functional properties of porous silicon.

1. P.A. Shilyaev, D.A. Pavlov, A.F. Khokhlov, "Computational methods for fractal dimension of SPM images", Microsystem Technics, **3**, **pp**.35-38, 2004 (in Russian).

2. P. Bieganski, E. Dobierzewska-Mozrzymas, M. Newelski, E. Pieciul, "Fractal dimension of discontinuous copper films", Vacuum, **46**, pp.513-516, 1995.

3. P.A. Arutinov, A.L. Tolstikhina, V.N. Demidov, "A system of parameters for analysis of microrelief roughness in SPM", Plant Laboratory, **65**, pp.27-37, 1999 (in Russian).

The study of water suspensions of nanomaterials containing carbon nanotubes

L.P. Ichkitidze*[1], S.V. Selishchev[1], E.V. Blagov[2],
V.A. Galperin[3], Y.P. Shaman[3], L.V. Tabulina[4], B.G. Shulitski[4]

1. National Research University of Electronic Technology "MIET", MIET, Zelenograd, Moscow, 124498 Russia, leo852@inbox.ru. 2. Institute of Nanotechnology of Microelectronics, RAS, Moscow, 119991 Russia. 3. Scientific-Manufacturing Complex "Technological Centre", MIET, Zelenograd, Moscow, 124498 Russia. 4. Belarusian State University of Informatics and Radioelectronics, Minsk, Belarus

High mechanical properties (the tensile strength of ~30-40 MPa and the hardness of ~ 300-400 MPa) were achieved for nanomaterials with a matrix containing bovine serum albumin (BSA) and multiwall carbon nanotubes (MWCNTs) [1]. In this work, we investigated the ultra-water suspensions and three-dimensional nanomaterials based on BSA and MWCNT. Nanomaterials were prepared from aqueous suspensions with functionalized or nonfunctionalized MWNTs by nano- and laser techniques. The bimetallic catalyst Fe-Mo/MgO was used to obtain MWCNTs. MWCNTs were synthesized at 900 ^{o}C for 40 minutes in the Ar/CH_4 flow. After the synthesis, the material was subjected to multistage chemical processing resulted in MWCNTs covered with functional groups that contribute to the formation of a stable aqueous suspension of functionalized MWCNTs. During performing the acidic treatment, carboxyl (O=C-OH), carbonyl (C=O), and aldehyde groups (O=C-H), which prevent the coagulation of MWCNTs in the solution and increase the stability of $MWCNT_f$s in water, are formed.

Control measurements were performed for the samples, which contained carbon black K-354 instead of MWNTs. As part of a suspension the albumin concentration in the suspension was always 25 wt % BSA, while the concentration of MWNTs and carbon black K-354 were varied in a range of 0-0.04 wt %. The prepared suspensions were irradiated with a laser with a wavelength of 970 nm in different radiation modes (pulsed and continuous) at various power and exposure time. All the samples, including control ones, were prepared and analyzed under identical conditions.

It is found that in the wavelength range of 400-1000, the optical density ***D*** and absorption coefficient ***k*** considerably varies with time (up to 300 hours) for the suspensions with nonfunctionalized MWNTs. The value of ***D*** initially increases and reaches the maximum, and then it decreases monotonically and asymptotically approaches a constant value. At the same time, ***D*** and ***k***_are not varied in time for the suspension with functionalized MWCNTs, but for the suspension with particles of carbon black ***D*** decreases continuously. Our explanation of the experimental results are based on the following principles: in suspensions with nonfunctionalized MWNTs, the particles have tendency to aggregate in clusters, the size of which gradually increases with time., Suspensions become inhomogeneous, and their optical properties thus change. In suspensions with functionalized MWNTs, the particles are not merged, and suspension remain ultradispersed and homogeneous, and their optical properties do not change with time, while in suspensions with carbon black particles, sedimentation at the bottom occurs. The experimental results are qualitatively described by the modified expressions of the Bouguer-Lambert-Beer for heterogeneous media. Quantitative values of the optical density and absorption coefficient suspensions of functionalized MWNTs are higher by a factor of several times than the values of ***D*** and of ***k*** in suspensions of nonfunctionalized MWNTs or carbon black.

The maximum hardness of ~ 350 MPa for nanomaterials is achieved for samples with non-functionalized MWNTs, while the hardness of nanomaterials with functionalized MWNTs lower (~ 220 MPa), and they are relatively homogeneous. Nanomaterials with functionalized MWNTs can be used in various applications, where high mechanical and optical properties of absorbing coatings are required, particularly, for receivers of thermal radiation.

This work is partially supported by the Ministry of Education of the Russian Federation (state contract no. 16.426.11.0043, September 12, 2011).

1. L.I. Ichkitidze, T.S. Ryndina, S.V. Selishchev, et al., "The bulk composite nanomaterial based on the protein and carbon nanotubes", Nano- and microsystemnaia tehnika, № 3, pp.13-19, 2012 (in Russian).

Features of nanostructures formed in solid substrates

E. Il'ichev, A. Kozlitin, D. Migunov, O. Sakharov, A. Trifonov, G. Petruchin, G. Richkov
Scientific Research Institute of Physical Problems named after F.V.Lukin, Moscow, Russia;
e-mail: admin@niifp.ru

Appeal of using the arrays of nanoscale tips in the development of high-current field-emission cathodes for microwave power devices results from the capability of electric field peaking in the tip neighborhood. In spite of high strength and the possibilities of self-organization the carbon nanostructures (CNS) did not demonstrate desired results due to principally significant value of the aspect ratio dispersion within a tip array on film and quite low yield limit of the nanoscale drop catalyst material in their base. Using the CNS array films as an active field-emission medium for integrated emission circuit production is not efficient also because of technological reasons which allow implementation of CNS arrays at the final stage of IC formation only. Hence the search for self-organization methods of forming the arrays of nanoscale objects immediately from solid films is a topic of great application importance.

In the paper results of investigations of nanoscale objects formed using nanostructure array self-organization process directly on both silicon wafer and polycrystalline diamond film are presented. The latter structure is of particular interest due to the negative electron affinity of some diamond crystal faces. The samples were investigated using Tecnai 20 S-Twin transmission electron microscope (TEM) (FEI, The Netherlands) equipped with EDAX X-ray energy-dispersive spectrometer (XEDS).

The nanoscale objects created on silicon wafers represent some regular nanoscale cones having their height of 1…2 μm and their base diameter of 100…500 nm depending on technological regimes of forming. The character of contrast on the TEM images indicates the cones have their bulk structure.

The X-ray analysis shows the cones are continuous-solid, consisting of silicon. The nanoscale tips (~20 nm) of some cones have metal inclusions (nickel), which rising is explainable with technological reasons. Diffraction pattern of cone structures and silicon wafer are quite similar that means they have the same crystallographic orientation.

The nanoscale objects formed on polycrystalline diamond films resemble cones vaguely. Their lateral size and height have significant dispersion. In wide range of their shapes a "bottlelike" structure is dominating one, and some sharp tip cones occur more rarely. According to the data of electron micro-diffraction the material of cones appears to be the polycrystalline diamond of ~0,3…1 μm crystallites. Frequently the cones are shaped with two large diamond crystals and quite often comprise a lot of twinning grains.

XEDS mapping the elements in the "bottlelike" cones shows their vertex looks like a regular carbon cylinder and its bottle shape is configured with a coat consisting of Al, Si and iron oxide mainly, that is explainable with the formation method used.

Carbon nanotubes-silicon composite material as anode structure in lithium batteries

E.P. Kitsyuk[1], V.A. Galperin[1], Y.P. Shaman[1], D.G. Gromov[2], A.M. Skundin[3], E.K. Tuseeva[3]

1. Scientific-Manufacturing Complex "Technological Centre", Moscow, 124498, Russia, E-mail hedgeshot@gmail.com. 2. National Research University of Electronic Technology, Moscow, 124498, Russia. 3. A.N. Frumkin Institute of Physical Chemistry and Electrochemistry RAS, Moscow, 119071, Russia.

Studies on anode materials aiming to improving their capacity and cyclability are one of the most important ways to increase characteristics of Li batteries. Si-CNT composite structures have received much attention as a promising material for anode structure owing to impressive theoretical capacity of silicon (4200 mA*h/g). However, Li insertion and extraction from Si leading to large volume change (over 300%) and crumbling of active material [1]. To avoid this problem and increase cycling stability, a composite anode material of multi-wall carbon nanotubes coated by silicon layer was prepared.

Multi-wall carbon nanotubes were directly grown on stainless steel substrate by PE-CVD method. After that silicon was sputtered on the substrates with MWCNT by magnetron system. SEM showed that nanotubes on the top part of MWCNT structure were fully enveloped by silicon and their diameter was increased to 500-600 nm.

Due to flexibility and alone-standing preparation MWCNT have ability to buffer the volume changes of silicon. Also MWCNT was used as an electroconductor, that allows do without binder and conductive dopants [2, 3]. As current collector was used steel substrate.

Thus, prepared structure demonstrates capacity of 3800 mA*h/g at first cycles. Capacity slowly decreases to 1500 mA*h/g after more than 100 cycles at high charge/discharge rate 0.7C. For studying the process of degradation of Si-CNT composite, after short cycling another anode with the same structure was seen by SEM. It showed that silicon layer was not corrupted at all, but has specific changes in its surface. These changes can be attributed to flexibility of substrate, pressure in process of assembling of test cell, and forming of solid-electrolyte interface.

Developed method of formation nanostructured composite is simple and efficient, and compatible with standard planar silicon technology. Designed anode structure is perspective approach to address the issues associated with the large volume changes. Structure, obtained by this technology, has reduced total weight because binder and conductive dopants are not required, increased capacity. They can find application in fabrication of ultrathin high capacity batteries for portable electronic applications.

1. P.-C. Chen, J. Xu, H. Chen, and C. Zhou, Nano Res., **4**, pp.290–296, 2011.
2. W. Wang and P.N. Kumta, Nanostructured Hybrid Silicon, ACS Nano, **4**, No.4, pp.2233–2241, 2010.
3. Y. Zhang, X.G. Zhang, H.L. Zhang, Z.G. Zhao, F. Li, C. Liu, H.M. Cheng, Electrochimica Acta, **51**, pp.4994–5000, 2006.

Formation of nanoelectrodes for high temperature single-electron sensors

A. Parshintsev, E. Soldatov
Department of Physics, Moscow State University, Russia, parshincev@physics.msu.ru

Contemporary microelectronics is very close to the limits of miniaturization of traditional electronic components. In this regard, special attention is paid to promising alternative approaches to their creation. The creation of molecular transistor, that is capable to operate in single-electron regime at room temperature, is an example of such approach [1]. This is very important for many applications, especially for chemical and biosensors [2].

The basis of the molecular transistor is a system of thin film metal electrodes separated by a gap. The gap size should be less than a few nanometers. The creation of molecular transistor electrodes with a gap between them less than a few nanometers is one of the main problems. This problem cannot be solved using traditional electron beam lithography (EBL). Currently, the most promising solution is the use of the electromigration [3]. Electrodes separated by a gap less than 2-3 nanometers can be obtained using electromigration. Thin (less than 20 nm) and narrow (less than 90 nm) nanowire is needed to provide controllable electromigration process. However, the adhesion between the nanowire and the substrate shouldn't be too strong to provide the electromigration but it should be enough to provide lithography operations. In this work the technique of electrodes formation of single electron transistor suitable for high temperature single electron sensors satisfying these conditions is described.

For the preparation of nanowire samples suitable for electromigration a layer of SiO_2 was evaporated on a standard Si wafer of 80 mm diameter to make an insulating layer on a substrate using Leybold Z400. Then a scriber was used to make chips with dimensions of 10×10 mm^2. Contact pads (to connect measuring equipment to the chip) and thin film metal (gold) electrodes (to connect nanowires to the pads) were built using photo - lithography. Nanowires for electromigration were built in the center of the chip (region of 80×80 μm^2) using EBL. To provide the appropriate adhesion between the substrate and nanowires thin Al_2O_3 layer was used. All metal and Al_2O_3 layers were evaporated using Leybold L560. As a result, samples containing 16 nanowires on each chip with width in range of 60-80 nm and resistance of a few kOhm were obtained. Such properties provides optimal regime for electromigration and proves the appropriate quality of films.

Thus, the technique of the creation of single-electron high temperature molecular transistor electrodes was developed. Such electrodes are appropriate to the creation of high temperature single electron transistor with an island of 2-3 nm size. Optimal parameters for thin and narrow metal nanowires were defined. Samples of nanowires that provide obtaining of sub-5 nm gaps between electrodes were made.

This work was supported by RFBR (projects 12-07-00816-a, 10-07-00712-a), Federal Target Program "Scientific and teaching specialists of innovative Russia for 2009-13" (contracts 02.740.11.0229,14.740.11.0389, 16.740.11.0020, 14.740.11.0370).

1. K.K. Likharev, Proc. IEEE **87**, p.606, 1999.
2. H. Zhang, R. Barsotti, F. Stellacci and J. Thong, Small **5**, p.2797, 2009.
3. H. Park, A.K.L. Lim, A.P. Alivisatos, J. Park, P.L. McEuen, Appl. Phys. Lett., **75**, pp.301-303, 1999.

Research of resolution of masking layers of the molybdenum structured on technologies of laser thermochemical record

S. Poletaev[1,2], O. Moiseev[2]

1. S.P. Korolyov Samara State Aerospace University (National Research University), Samara, Russia, sergpolet@gmail.com. 2. Image Processing Systems Institute of the RAS, Samara, Russia, moiseev@smr.ru

Plasma or "dry" etching is applied to the solution of a wide class of tasks on relief formation in the field of microelectronics and diffraction optics. Optoelectronics, microwave technology, microelectromechanical devices (MEMS), capillary chips, diffraction lattices and sensors of various types here belong [1].

One of the important stages of technology of plasma etching is application of the resistant masking layers, capable to provide necessary depth of formed structures. Besides, for production of the diffraction lattices working in an ultra-violet range of lengths of waves, the size of structures less than 0,6 microns is necessary. One of ways for formation of topology of an element is laser thermochemical record on thin films of chrome [2]. But this technology in standard execution provides the size of an element not less than 0,7 - 0,8 microns for length of a wave of the recorder of 488 nanometers. Therefore there is a problem consisting in overcoming of this barrier.

In the real work masking layers of molybdenum about possibility of achievement of the size of an element, comparable with a diffraction limit in a half of length of a wave (0,25 microns) are investigated at laser record. The method of plasma etching was made structures with the size of an element of 0,25-0,3 microns (fig. 1) and the depth exceeding 100 nanometers.

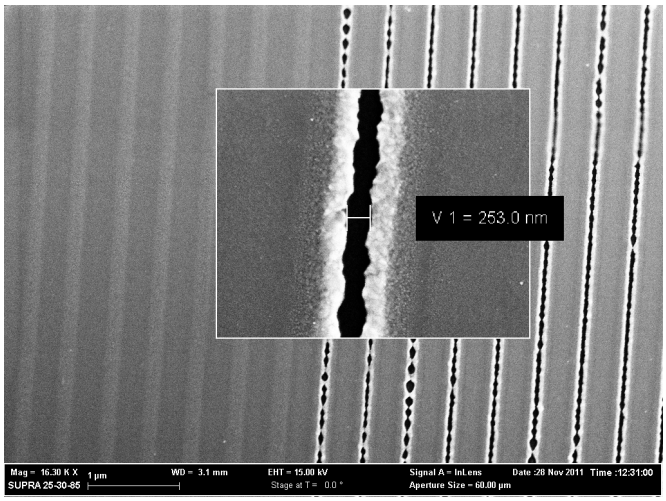

Fig. 1. SEM a picture of a surface of a film of molybdenum after laser record.

Then researches on thinner films of molybdenum were carried out. As a result the structure with the sizes of elements closed to 100 nanometer on a film in thickness about 25 nanometers was turned out. Here for receiving more authentic results further researches are conducted.

The created microstructures can find application in such areas as optoelectronics, the microwave the technician and diffraction optics for ultra-violet radiation.

1. D.A. Zeze, R.D. Forrest, J.D Carey, D.C. Cox, I.D. Robertson, B.L Weiss, S.R.P. Silva, **"**Reactive ion etching of quartz and Pyrex for microelectronic application", J. Appl. Phys., **92**, pp.3624-3629, 2002.
2. V.P. Veyko, A.G. Poleshchuk, A.R.Sametov, E.A.Shakhno, M.V. Yarchuk, "Research of spatial permission of laser thermochemical technology of record of diffraction structures", Quantum Electronics, **41**, pp.631-636, 2011.

Formation of CNT Ordered Array, as source of electrons.

A. Shuliatyev, D. Gromov, A. Zaycev, A. Shamanaev
National Research University of Electronic Technology, Russia
email: ashuliatyev@gmail.com

One dimentional structure, which is described in width number of publications, is very important now. They have amazing properties. It can be used in different places : opto- and nano electronics, microelectromechanical system and etc. Such structures as nanowires or nanotubes exhibit excellent field emission properties. Each carbon atom, in carbon nanotubes(CNT), is bound to three other carbon atoms by a (covalent) sp2 bond. As a result, the activation energy for surface migration of the emitter atoms is much larger than for a tungsten electron source. Therefore, the tip can withstand the extremely strong fields (several V nm^{-1}) needed for field emission. Also, CNT has high aspect ratio and low work function. They could be applied potentially as electron sources in various vacuum electronic applications: integrated vacuum microelectronics, energy saving light sources, planar displays.

There are some methods of establishment ordered nanostructure. For example: method of fragmentation of metal nanolattices [1], method, which used porous anodic alumina [2] and etc. We are developing the method based on nanoimprint-lithography, CVD and PECVD. This method includes: nanoimprint-lithography, sputtering of thin adhesion layer and catalyst layer, removing of the resistive layer and growing of carbon nanotubes. Structure, which we get, has ordered array with CNT on each locals areas catalysts.

1 Qiangfei Xia, Stephen Y Chou, “The fabrication of periodic metal nanodot arrays through pulsed laser melting induced fragmentation of metal nanogratings”, Nanotechnology, 20, p. 285310, 2009.

2 Chakarvarty S.K., Vetter J. A review // Radiation Measurements .29. № 2.,1998

Fabrication of integrated electrodes of molecular transistor electrodes by lithographic techniques and electromigration

A.S. Stepanov[1], E.S. Soldatov[2], O.V. Snigirev[2]

1. Skobeltsyn Institute of Nuclear Physics, M.V. Lomonosov Moscow State University, Moscow, Russia, stepanov@cryolab.ru; 2. Department of Physics, M.V. Lomonosov Moscow State University, Moscow, Russia, esold@phys.msu.ru

This year Intel introduced the 22 nm technology of integrated circuit production. Production of circuits with 14 nm technology is planned for the near future. However, the prospects for further development are not clear until now. There are several candidates for using in next-generation chips. Modern transistors can be based on graphene monolayer or single nanotube. The effect of single electron tunneling through the structure is one of another perspective effect too [1]. This effect was demonstrated previously with the STM tip at room temperature [2]. However, the practical use of it is possible only if it will have a planar implementation. In this paper the method of creating a prototype of single-electron transistor which can operate at room temperature was demonstrated. This method involves the using of lithographic techniques for creation an integrated system of transistors electrodes, and the using of electromigration effect for the formation of nanometer gap between the source and drain electrodes.

The proposed lithographic technique for electrodes creation includes several stages. At the first stage a dielectric SiO_2 layer of 400 nm thick were formed on the samples. Then the rough lead-in electrodes were deposited by using of UV lithography through the polymer mask (5 μm width, 50 nm thickness). After that the layer of Al was deposited through the polymer mask which was previously exposed in a scanning electron microscope. This Al layer can be used as gate electrode of the transistor. Aluminum is chosen because of its good oxidizing ability and sufficient adhesion to the surface of SiO_2. In the same process the Al layer was covered by 10 nm thick Al_2O_3 film which was sputtered by an electron beam. Suspended polymer mask technique allowed us to deposit this oxide layer by using “two-shadow” technique. It helps to provide an isolation of the Al film edges. After that Au strips were formed on the top of Al_2O_3 layer (thickness of 20 nm and a width of 50 nm) by the using e-beam lithography. At the last stage the gold strips lying in the center of chip were connected to the rough lead-in electrodes of the sample. So, a lithographic part of the creation of an integrated system of transistor electrodes were finished.

Achieving the required width of the gap (~ 3 nm) between the source-drain electrodes cannot be done by lithographic techniques. For this purpose we used the effect of electromigration of gold atoms in thin film. We built the setup which includes A/D and D/A boards NI PCI-6229, NI PCI-6509 and PC with RTOS Pharlab OS. We developed algorithm of control software which provides controllable rupture of the gold film. The voltage applied to the gold strip was increased step-by-step and its resistance was measured. Voltage was reset and the process was repeated from the first step if resistance exceeds a specified threshold value. When the resistance of the gold strip reached a value of 2 - 3 KOhm external voltage was completely switched-off, and formation of 2 - 3 nm gap were occurred under the influence of stress in the film (self-breaking). This technique of electromigration of gold film allows us to obtain gap of less than 5 nm in 75% of cases.

The developed techniques of lithography and electromigration allow us to create a complete integrated system of the transistor electrodes. For the testing the suitability of the proposed techniques deposition of quantum dot between the electrodes (gold nanoparticles with a diameter of 3 nm) was carried out and the characteristics of the electron transport of the system were measured. It has shown a single-electron character of the conductivity at room temperature. This demonstrates the perspective of the proposed methods in an experimental study of single-electron transistors.

This work was supported by RFBR (project № 12-07-00816-a, 10-07-00712-a) and under the Federal Target Program "Scientific and scientific-pedagogical personnel of innovative Russia" for 2009 - 2013 (state contracts № 02.740. 11.0229, 14.740.11.0389, 16.740.11.0020, 14.740.11.0370).

1. D.V. Averin, K.K. Likharev, *Mesoscopic Phenomena in Solids*, Elsevier, Amsterdam, 1991.
2. E.S. Soldatov, V.V. Khanin, A.S. Trifonov, S.P. Gubin, et al., JETP Lett, **64**, p.510, 1996.

Narrowing of nanogaps for purpose of molecular single-electronics

I.V. Sapkov, E.S. Soldatov
Department of Physics, Moscow State University, Russia, E-mail: esold@phys.msu.ru

Molecular single-electronics may be the next step in the development of modern nanoelectronics. This is due to miniaturization of element base which is described in well-known Moore`s Law [1] and leads us sooner or later to the element`s size of the order of a few nanometers. Molecular electronics proposes to use natural object for the nanometer-scale - a molecule (or a cluster). Note that such objects placed between conducting electrodes can be natural or, potentially, artificially created, that is, having the specified properties.

The development of these single-molecule test structures in the future will allow to build a hybrid micro / nanoelectronic memory devices (hybrid-CMOS, CMOL) [2] with higher recording densities than are currently available, and a new generation of neural networks. Besides that, the systems of this kind are now engaged in the research fields of spintronics [3] and electro-optics [4].

We have proposed and developed a method of implementation the nanotransistors with extremely small (2-5 nm) gap between the electrodes by means of deposition of additional metal on the electrode-workpiece. The efficiency of narrowing of the gap between source and drain-electrodes (as a result of additional deposition of metal film on the preformed gap) was 50-70% of the deposited film thickness.

The technology for implementation of electrode-workpiece with the gap`s size of about 30 nm by electron-beam lithography and two-layer polymer mask is developed. A careful selection of layer thicknesses of the polymer mask, exposure dose, development time and the type of developer provide gaps of 20-30 nm wide.

The method of wet etching of the substrate in a 6% solution of hydrofluoric acid buffered with hydrofluoride of ammonium was used. The method proved its efficiency and allowed to make samples with suspended electrodes. The depth of the silicon oxide etching under the electrodes was order of 80 nm. The rate of silicon oxide etching was about 2.7 + \ - 0.2 nm / sec.

For implementation of finished electrodes of nanotransistor with required values of gaps (2-5 nm) additional deposition technique of the metal film on a wide gap was developed. At the same time for additional metal deposition on nanostructure the reliable method of positioning and formation was developed. As a result this method provided both a necessary restriction of a nanogap and self-alignment of control electrode of the transistor (the gate) with reliable isolation of all three electrodes of nanotransistor located in the sub-5 nm range.

Method of single-electron nanotransistors implementation suitable for use at high temperatures (300 K) was developed. This allows the creation of highly sensitive sensors for use in research purposes in the fields of physics, chemistry, medicine, and the creation of a new generation of nanoelectronic devices with improved performance for systems of medical diagnostics and security. The feature of the developed technique is usage of standard microelectronic manufacturing operations, which opens up the possibility of serial implementation of complex integrated nanoelectronic single-electron systems / devices.

This work was supported by RFBR (projects № 12-07-00816-a, 10-07-00712-a) and Federal Program “Kadry” on 2009-2013 years (state contracts № 02.740.11.0229, 14.740.11.0389, 16.740.11.0020, 14.740.11.0370).

1. G.E. Moore, "Cramming more components onto integrated circuits", Electronics Magazine, **4,** 1965.
2. K.K. Likharev, “Nano and Giga Challenges in Microelectronics”, Editor J. Greer, pp. 27–68, Elsevier, Amsterdam, 2003.
3. A.R. Rocha e*t al.*, “Towards molecular spintronics”, Nature Materials, **4**, pp.335-339, 2005.
4. C.W. Marquardt *et al.*, “Electroluminescence from a single nanotube–molecule–nanotube junction”, Nature Nanotechnology, **5**, pp.863–867, 2010.

Electron multiplier on diamond-coated silicon membrane

E.A. Il'ichev, A.E. Kuleshov, N.K. Matveeva, G.N. Petrukhin, R.M. Nabiev, and G.S. Rychkov
F.V. Lukin State Research Institute of Physical Problems, Zelenograd, Moscow, 124460 Russia
E-mail: polt@niifp.ru

Diamond membranes are capable of amplifying electron flux, but membranes with dimensions exceeding 10 mm^2 are subject to deformation and sagging. In order to avoid this, it is suggested to build electron flux amplifier on a silicon grating coated with a diamond film. The possibility of using these gratings instead of microchannel plates is discussed, in particular, in cases where this grating directly plays the role of X-ray, UV, or proton detector.

We developed a technology of electron flux amplifiers based on diamond-coated silicon gratings (DCSGs) with the holes representing EMC [1] cells. The process of DCSG fabrication involves the following main technological stages (Fig. 1):

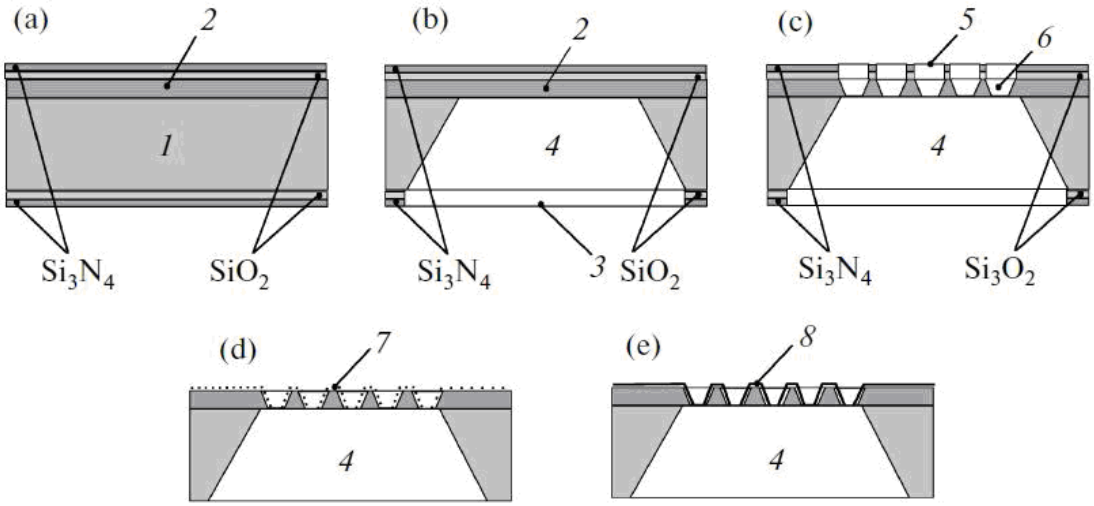

Fig. 1. Schematic diagram of DCSG technology: (a) formation of highly doped silicon layer *2* on substrate *1* and deposition of SiO_2 and Si_3N_4 layers; (b) formation of cavity *4* through window *3* in SiO_2 and Si_3N_4 layers; (c) formation of holes *6* in membrane *2* through windows *5*; (d) seeding diamond *7*; (e) growth of polycrystalline diamond film *8*.

In modern electro-optical converters (e.g., IR viewers), the presence of heavy ions sharply decreases the useful yield and the working life of devices, which usually does not exceed 1000 h (maximum working life was reported to reach 10000 h). Together with residual gases, ions are generated due to the electron and ion bombardment of the MCP surface. In DCSGs, the membrane and EMC surface is covered with diamond, which sharply decreases the probability for carbon atoms to be knocked out from the surface.

The action of X-rays, UV radiation, and protons on the diamond film covering the EMC walls leads to secondary electron emission. Thus, the amplifier of these radiations can directly ensure the position-sensitive detection with the subsequent amplification of secondary electrons.

Thus, we have considered the technology of electron flux amplifiers based on diamond-coated silicon gratings. Good prospects of this technology have been demonstrated, although some estimations (concerning maximum DCSG dimensions, cost of production, minimum EMC cell size, etc.) have to be refined.

1. E.A. Il'ichev, A.E. Kuleshov, E.A. Poltoratskii, and G.S. Rychkov, "Electron multiplier concentrator on the base of polycrystalline diamond film", Diamond and Related Materials, **20**, pp.23-25, 2011.

Mechanism of sensitivity of a three-collector magnetotransistor

V.V. Amelichev, A.A. Cheremisinov, S.A. Polomoshnov, R.D. Tikhonov
SMC "TECHNOLOGICAL CENTRE" MIET, CheremisinovAA@gmail.com

The mechanism of sensitivity of a three-collector magnetotransistor with the base in a well which serves as the third collector is investigated [1]. The device has the name 3CBMTBW. For the first time it is shown that a small rate of surface recombination and an extraction of the injected electrons pn-junction base-well allow to receive high sensitivity on voltage to 11 V/T because of effect of a magnetic field deviation in one party of two streams of the injected carriers of the charge proceeding through the base and through the junction base-well.

Sensitivity was measured in a constant magnetic field of a solenoid with the magnetic induction of B = 5 mT. Differential absolute sensitivity on voltage was determined by a formula

$$S_{DA}{}^{V} = [U_{C2}(B) - U_{C2}(0) - U_{C1}(B) + U_{C1}(0)] / B$$

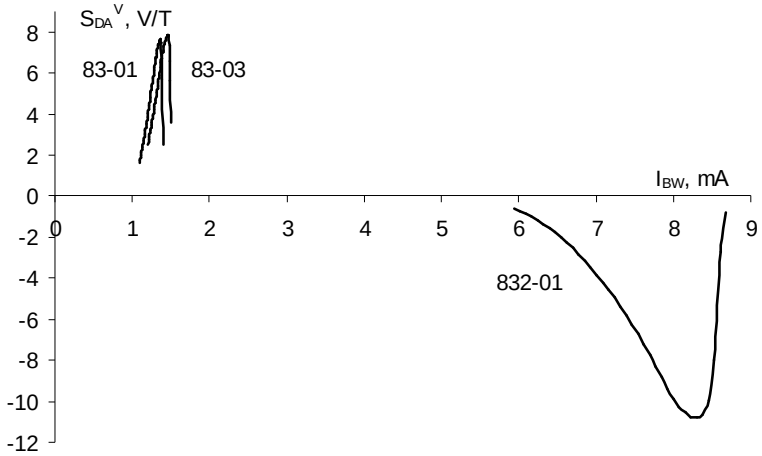

Fig. 1. Dependency of sensitivity on voltage for samples BMT on the bias current of the base and the well I_{BW}.

Features of characteristics are defined by the current distribution. The big current of the electrons injected from the emitter extracted in the pn-junction base-well and in the magnetic field deviates in relation to measuring collectors in the same party with the current, proceeding directly through the base. This gives a big change of the current of the measuring collectors.

Magnetotransistor 3CBMTBW with a small rate of surface recombination on the junction of the silicon – dioxide of silicon and with an extraction of the injected electrons remote from the surface pn-junction base-well allows to receive high sensitivity 11 V/T at the expense of effect of a deviation of the magnetic field in one party of two streams of carriers of the charge proceeding from the emitter to collectors is directed through the base and through the junction base-well.

Magnetotransistor parameters 3CBMTBW are higher in comparison with SSIMT transistors [2].

The work is carried out with a financial support of the Ministry of Education and Science of the Russian Federation within FTsP «Researches and development in the priority directions of development of a scientific and technological complex of Russia for 2008-2015» (Group of companies No. 16.513.11.3001) and Grant President MK-6977.2012.8.

1. A. Kozlov, Yu. Parmenov, R. Tikhonov, "Experimental research of the Magnetotransistor in a double well", Report P1-23 of ICMNE-2009.
2. L.J. Ristic, H.P. Baltes, T. Smy, I. Filanovsky, "Suppressed Sidewall Injection Magnetotransistor with Focused Emitter Injection and Carrier Double Deflection", IEEE Electron Devices Letters, **9**, pp.395-397, 1987.

The observation of conduction quantization of metallic nanojunctions at normal conditions

L. Fedichkin[1,2,3], A. Borisov[2], M. Chernyshev[2], V. Rubaev[2]

1. Institute of Physics and Technology, Russian Academy of Sciences, Moscow, Russia, leonidf@gmail.com .

2. NIX., Moscow, Russia, leonid@nix.ru .

3. Moscow Institute of Physics and Technology, Dolgoprudny, Moscow region, Russia, leonid@phystech.edu

The dynamics of electrical conductance between metallic contacts being mechanically gradually displaced from each other provides sensitive tool to metal surface characterization [1]. At certain conditions it enables also the fundamental study of quantum behavior of electron transport [2] revealing itself in particular in conductance quantization of nanojunction [3,4]. This report presents recent experiments [5] with mechanically controlled molybdenum contacts. We demonstrate that electron transport through molybdenum nanojunction manifests the features of ballistic and quantum motion even in air atmosphere under normal pressure and room temperature. The conduction histogram in Fig. 1, with the pronounced peak corresponding to one conduction quantum and the minimum corresponding to one and a half conduction quantum, is in nice agreement with theory. The ability to observe quantization peak proves persuasively the validity ballistic and quantum description of electron evolution at least at scales corresponding to nanojunction sizes.

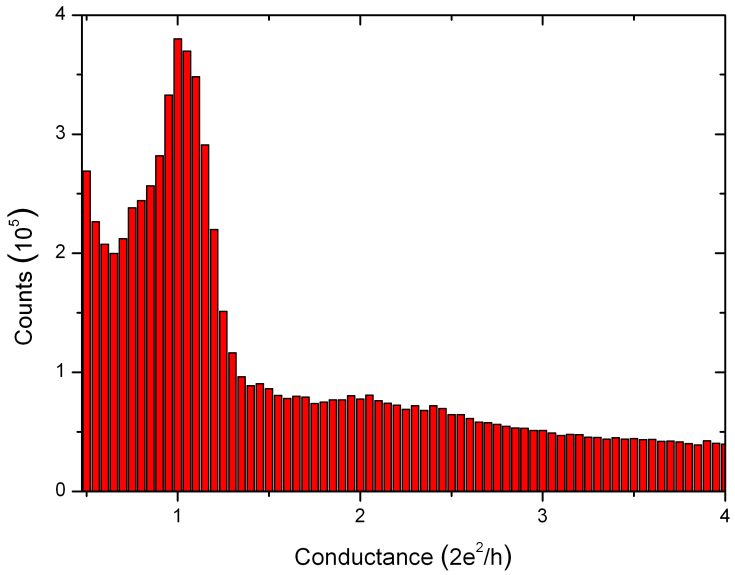

Figure 1. Conduction histogram. Number of events of nanojunction conductance value within +/- 0.025 conduction quantum from the central value of conductance versus conductance.

1. Yu.V. Sharvin, Zh. Eksp. Teor. Fiz., **21**, p.655, 1965.

2. F. Manders, A.K. Geim, and J.C. Maan, Physica B: Condensed Matter, **294–295**, p.332, 2001.

3. D.A. Wharam, T.J. Thornton, R. Newbury, M. Pepper, H. Ahmed, J.E.F. Frost, D.G. Hasko, D.C. Peacock, D.A. Ritchie, and G.A.C. Jones, J. Phys. C, **21**, p.209, 1988.

4. B.J. van Wees, H. van Houten, C.W.J. Beenakker, J.G. Williamson, D. van der Marel, and C.T. Foxon, Phys. Rev. Lett., **60**, p.848, 1988.

5. L. Fedichkin, A. Borisov, A. Konin, R. Petrukhnenko, M. Chernyshev, and V. Rubaev, Russian Microelectronics, **41**, pp.1-4, 2012.

The novel THz generation and detection possibilities of resonant-tunneling based semiconductor multiple-quantum well nanostructures

A.L. Karuzskii, V.V. Kapaev, V.N. Murzin, Yu.A. Mityagin, S.A. Savinov, A.V. Perestoronin, A.M. Tshovrebov, N.A. Volchkov, I.P. Kazakov, V.I. Egorkin, S.S. Shmelev
P. N. Lebedev Physical Institute of Russian Academy of Sciences, Moscow, Russia, E-mail address karuz@sci.lebedev.ru

The novel perspectives in THz are bound up with nanotechnology and quantum effects such as resonant tunneling, characterized by very short transient times (less than 1 ps) comparable with the fastest response of superconducting devices [1, 2]. It has been shown recently that resonant tunneling diodes (RTD) efficacy can be strongly increased with use of more complicated triple-barrier RTD structures due to interaction of electronic states in neighbour quantum wells [3-5]. These hopeful results look very promising but have been obtained in frames of an approximate quantum theory consideration.

In the present work we bring up the results of high-frequency properties of RTD investigation on the base of theoretical quantum model of resonant tunneling under external electromagnetic field using numerical solution of time-dependent Schrödinger equation with open-system boundary conditions. Applying this model the high-frequency response in resonant tunneling double-barrier (DBRTS) and triple-barrier (TBRTS) structures is analyzed for structures with different barriers of finite height and width in wide frequency range from low frequency side of gigahertz frequencies (classical amplification mechanism) up to terahertz frequencies, where high-frequency response mechanism is determined by theoretically predicted "quantum amplification regime" promising a cardinal increase of gain and efficiency of RTD at this frequency area as a result of photon-assisted character of tunneling phenomenon. We present the parsed analysis of high-frequency response regularities in RTD in depend on frequency, electron energy, structural parameters etc in both cases of monoenergetic and Fermi types of emitter electrons distributions taking into account the influence of DC bias voltage on electronic wave functions and energies states.

One of principal disadvantages of low DBRTS efficiency in THz range as shown is an occurrence of symmetry of high-frequency responses determined by injected electrons with higher or lower than resonant level energies that results to the decrease of total summary response because of a cancellation of amplification and absorption processes. In case of TBRTS the presence of additional resonant level destroys the response symmetry. The energy level in the first well becomes to be privileged that results to selective narrow-band amplification at frequency equal to the energy spacing between levels in neighbour quantum wells. The revealed phenomenon results in selecting of only a rather small portion of emitter electrons in TBRTS that actively interact with external THz electromagnetic field (energy filtration effect). Both of these circumstances promote realization in TBRTS the selective narrow-band high-frequency tuning amplification effect at terahertz frequencies by changing of applied bias voltage, that really open marvelous perspectives for engineering and development of novel high-performant generator, detector and other types units for subterahertz and terahertz frequency range.

The experimental results of research of DBRTS and TBRTS high-frequency response and effects of distortions in the DC current-voltage characteristics of DBRTS and TBRTS due to an applied gigahertz and subterahertz electromagnetic field with the use of BWT and IMPATT oscillators are presented. The investigations were performed in the frequency range from 100 GHz up to sub-THz for GaAs/AlAs and $In_{0.53}Ga_{0.47}As$/AlAs/InP samples of DBRTS and TBRTS heterostructures. The findings revealed the possibilities for the effective applications of DBRTS and TBRTS heterostructures as a basis for sensitive sub-THz and THz detectors.

This research was supported by Ministry ES of RF, by Grants RFBR (#11-02-01182, #11-02-12133), by Grants RAS (#24, IV.12 and III.7).

1. S. Suzuki et al., Appl. Phys. Lett., **97**, pp.242102-1–242102-3, 2010.
2. M. Feiginov et al., Appl. Phys. Lett., **99**, pp.233506-1–233506-3, 2011.
3. V.F. Elesin, JETP, **89**, pp.377-383, 1999; JETP, **100**, pp.116-125, 2005.
4. O.A. Klimenko, N.V. Dyakonova, W. Knap et al., Bull. Lebedev Phys. Inst., **36** (1), pp.14-20; **36** (1), pp.21-28, 2009.
5. S.A. Savinov, V.N. Murzin, JETP Letters, **93**, pp.155-160, 2011.

Suspended Silicon Single-Electron Transistor.

V. Krupenin[1], D. Presnov[1,2], S. Amitonov[1], K. Rudenko[3], V. Rudakov[3]
1. Laboratory of Cryoelectronics, Moscow State University, 119991 Moscow, Russia , vladimir.krupenin@phys.msu.ru
2. Nuclear Physics Institute, Moscow State University, 119991 Moscow, Russia, denis.presnov@phys.msu.ru.
3. Institute of Physics and Technology RAS, 117218, Moscow, Russia.

Single-Electron transistor (SET) is a promising application as an electric charge sensor. It's ultimate sensitivity can be closely achieved to the quantum limit [1]. The silicon–based nanostructures now are in a great attention due to the material mechanical solidity and simpler fabrication technology. The very important factor is higher operating temperatures at the same sizes of structure elements. In the extreme case only one atom of the dopant can be used as a core element of the structure [2]. All above enable quite convenient installation of the SET device on a cantilever tip of scanning probe microscope as field/charge sensor.

In this work we introduce fabrication and investigation of a single-electron transistor based on highly doped silicon on insulator material (SOI). We used Soitec UNIBOND® SOI wafers with top and buried oxide layer thickness of 55/145 nm and originally dopant (boron) concentration ~10^{15} cm^{-3}. After As ion implantation (dose $1.25 \cdot 10^{15}$ cm^{-2}) and rapid thermal annealing we have got nonuniform dopant concentration ~10^{21} at the layer surface and less than 10^{18} at the depth more then 50 nm. To produce SOI SET the electron beam lithography and anisotropic reactive ion etching like in previous work was used [3]. Future device size reduction carried out by the help of fluoric isotropic ion etching. To prevent the contact electrodes from degradation, the resist mask with an open windows around the SET area was used. There were several steps of etching with the test measurements between to achieve the clear single-electron behavior. The devices, locally suspended in the same area, looks more promising in terms of size reduction uniformity, removing bottom SOI layer with low dopant concentration, and probably also in terms of noise reduction [1].

Measurements of the transistors were carried out at temperatures of 77 K and 4.2 K. The devices demonstrate stable coulomb blockade and modulation curves at 4.2 K. Future investigations are in progress.

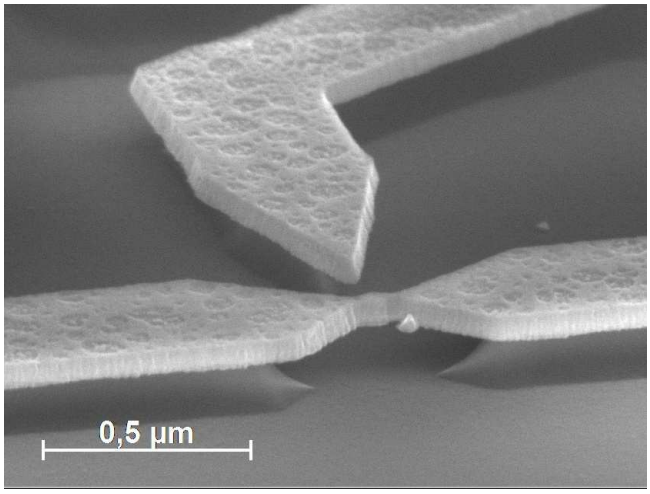

Fig.1: Suspended Single-Electron transistor fabricated from highly doped SOI.

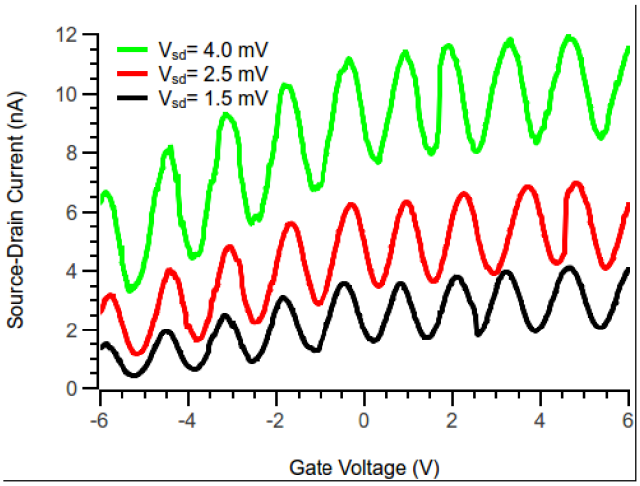

Fig.2: Typical modulation curves of SOI SETs measured at 4.2 K.

1. V.A. Krupenin, D.E. Presnov, A.B. Zorin and J. Niemeyer, “Aluminum single electron transistors with islands isolated from a substrate”, J. Low Temp. Phys., **118 (5/6)**, pp.287-296, 2000.
2. V.N. Golovach, X. Jehl, M. Houzet, M. Pierre, B. Roche, M. Sanquer, and L.I. Glazman, “Single-dopant resonance in a single-electron transistor”, Phys.Rev.B **83**, pp.075401-(1-4), 2011.
3. D.E. Presnov, V.S. Vlasenko, S.V. Amitonov, V.A. Krupenin, “Highly doped SOI based single-electron transistor: noise characteristics and charge sensitivity”, Abstracts of Invited Lectures and Contributed Papers of The International Conference “Micro- and nanoelectronics – 2009” (ICMNE-2009), Zvenigorod, Moscow region, Russia, P1-02, 5-9 October, 2009.

Optimization of topological parameters of triode with cold cathode based on ordered array of (9, 9) carbon nanotubes with open ends

D.V. Pozdnyakov[1], A.V. Borzdov[1], V.M. Borzdov[1], V.A. Labunov[2]
1. Belarusian State University, Minsk, Belarus, pozdnyakov@bsu.by
2. Belarusian State University of Informatics and Radioelectronics, Minsk, Belarus, labunov@its.bsuir.edu.by

The topological parameters of triode with cold cathode and control grid based on the ordered array of (9, 9) single-wall metallic carbon nanotubes with open ends have been optimized for the case of room temperature. It was supposed that cathode's nanotubes were placed on substrate with metallic type of conductivity in square grid-type order, and grid's nanotubes were spanned amid cathode's nanotubes like a net.

The distance between the nanotubes S has been optimized. The optimization procedure is based on search of the maximum of triode differential transconductance value along with the minimum of triode self-capacitance value under the following conditions: the height of nanotubes H, the distance L between the ends of nanotubes and the anode as well as the distance D between the control grid and the cathode are equal to 100 nm; the cathode potential φ_C is equal to 0; the control grid potential φ_G and the anode potential φ_A are equal to 12 V; the power dissipated by the anode does not exceed 1 MW/m^2. It is ascertained that the optimum distance between the nanotubes S_{opt} is equal to 82 nm.

Experimental and theoretical study of nanowire FET based on SOI

I.I. Soloviev[1], I.A. Devyatov [1], P.A. Krutitskiy[2], S.V. Amitonov[3], D.E. Presnov[3], V.A. Krupenin[3]
1. D.V. Skobeltsyn Institute of Nuclear Physics, Moscow State University, Moscow, Russia, isol@phys.msu.ru.
2. M.V. Keldish Institute of Applied Mathematics, Moscow, Russia 3. Physics Faculty, Moscow State University, Moscow, Russia.

Over the last decade the semiconductor nanowire field effect transistors (NWFETs) were extensively studied experimentally and theoretically. Large surface to volume ratio of the nanowire allows achieving the record sensitivities, e.g. 40 $(e/Hz)^{-0.5}$ [1] at 25 *K* (*e* is electron charge) that is orders of magnitude greater than the ones of conventional FET and nanomechanical systems. Opposed to highly sensitive single-electron transistors [2] NWFETs could be easy operated at room temperature that expands the area of its application.

In the work of Lieber's group [3] local Si bioprobe fabricated using VLS growing method was demonstrated. This probe was used for intracellular electrical recording from beating cardiomyocytes. Sensitivity to pH of the bioprobe was near the Nernstian limit 59 mV/pH. One year earlier this group reported about investigation of traditional planar Si biosensor with sensitivity of 30 mV/pH [4] that is more typical for silicon ion selective field-effect transistors [5]. It was shown that charge sensitivity of the sensor in sub-threshold regime is about tens of *e*. Despite the outstanding results of the works [3, 4] it can be noted that the used fabrication methods are incompatible with traditional semiconductor electronics fabrication technique.

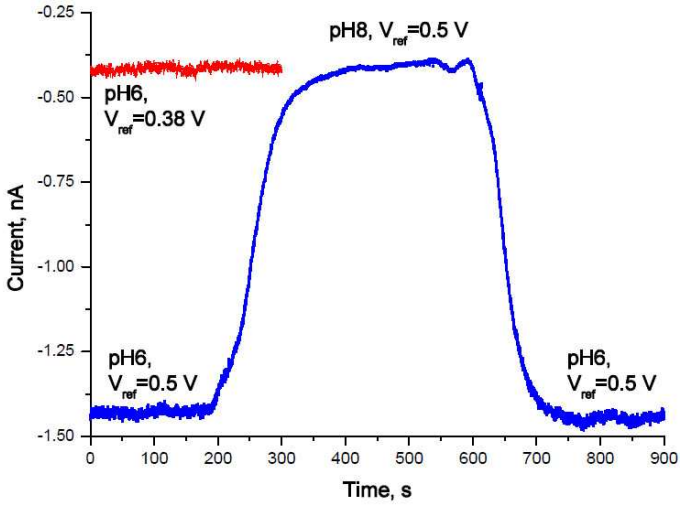

Fig 1. Si NWFET response to change in buffer solution pH. According sensitivity is 59 mV/pH.

We fabricated Si NWFET using standard semiconductor electronics fabrication technology starting from SOI wafer. Results of pH measurements in liquids showed that sensitivity of our sensor is also close to the Nernstian limit 59 mV/pH (see Fig. 1) which can be compared to the better samples fabricated using VLS growing mechanism. It was shown theoretically that our simplified technology for fabrication of contacts to NW that implies Schottky barrier formation in the contact area does not affect noise spectral density of current flowing in NW channel. At the same time the technology allows to eliminate excessive steps of doping with subsequent activation. Using theoretical model of investigated device we estimated modulation of NW channel surface charge according to observed change in conductance during pH measurements. This estimation showed that for sub-threshold regime the charge sensitivity of our sensor is of an order of 1 *e*. This means that characteristics of devices fabricated using top-down approach can be quite comparable or even better than the ones fabricated by bottom-up a method that is very promising from the point of view of further steps to mass production of such devices.

We thank M.Yu. Kuprianov, and A.V. Semenov for fruitful discussions.
The work was supported by RFBR projects 11-02-12122-ofi_m, 11-07-00748 and Project of Russian Ministry of Science, grant # 16.513.11.3063.

1. J. Salfi, I.G. Savelyev, M. Blumin et al., Nature Nanotehnology, **5**, p.737, 2010.
2. H. Brenning, S. Kafanov, T. Duty et al., J. Appl. Phys., **100**, 114321, 2006.
3. B. Tian, T. Cohen-Karni, Q. Qing, et al., Science, **39**, p.830, 2011.
4. X.P.A Gao, G. Zheng, Ch.M. Lieber, Nano Lett., **10**, p.547, 2010.
5. R.E.G. van Hal, J.C.T. Eijkel, P. Bergveld, Sens. Act. B, **24-25**, p.201, 1995.

Instability-driven terahertz emission and injection locking behavior in an asymmetric dual-grating-gate HEMT with a vertical cavity structure

T. Watanabe, T. Fukushima, Y. Kurita, A. Satou, T. Otsuji
Research Institute of Electrical Communication, Tohoku University, Sendai, Japan, watanabe@riec.tohoku.ac.jp

Two dimensional plasmons (2DPs) in high electron mobility transistors (HEMTs) have attracted much attention due to their nature of promoting emission/detection of electromagnetic radiation in the terahertz (THz) range [1-3]. The authors have developed THz radiation sources made with the authors' original dual-grating-gate (DGG) structures in the HEMT. So far a broadband THz emission has been obtained reflecting multimode of coherent/incoherent plasmons [2]. To realize coherent monochromatic THz emission we investigate the possibility of injection locked oscillation to the difference THz frequency component of photomixed dual CW laser irradiation and to the instability-driven self-oscillation modes. By irradiating dual CW laser with different frequency Δf the radiation power at the Δf component increases, attracting the surrounding frequency components although complete injection locking was not obtained [3].
We newly introduce an asymmetric DGG (A-DGG) structure [4] and try the injection locking operation. Numerical analysis revealed that the A-DGG structure drastically enhances the responsivity to the THz irradiation as well as the instability of the 2D plasmon resonance by 4 orders of magnitude (Fig. 1) [4]. The device consists of an A-DGG HEMT with a high-Q vertical cavity consisting of an Au mirror on the optically polished back surface of the substrate and ITO THz mirror on top and has a nice Q factor with finess values ranging from 20 to 60. We first observed its free-running emission spectra using Fourier transform infrared spectroscopy (Fig. 2). The gate bias V_{g1} for the narrower grating fingers is set at 0 V whereas that for the wider ones V_{g2} is varied from 0 V to −0.55 V (approaching the pinch off). With decreasing V_{g2} in negative the confinement of the 2DPs is reinforced, promoting the plasma instability under DC drain biased conditions. We confirmed clear asymptotic behavior of injection locking at 3.54 THz which is estimated to be the third harmonic 2DP mode. The frequency synchronization and the injection locking will be further accelerated by injecting the photomixed dual CW laser radiation.

[1] M. Dyakonov and M. Shur, "Detection, mixing, and frequency multiplication of terahertz radiation by two dimensional electronic fluid," IEEE Trans. Electron Devices, **43**, pp.380-387, 1996.
[2] T. Otsuji, Y. M. Meziani et al., "Emission of terahertz radiation from dual-grating-gates plasmon-resonant emitters fabricated with InGaP/InGaAs/GaAs material systems," J. Phys.: Condens. Matters **20**, 384206, 2008.
[3] T. Watanabe et al.," Terahertz injection locked oscillation in plasmon-resonant transistors," MOC'11 17th Microoptics Conference Digest, D2, 2011.
[4] V. V. Popov et al., "Plasmonic terahertz detection by a double-grating-gate field-effect transistor structure with an asymmetric unit cell," Appl. Phys. Lett. **99**, 243504, 2011.

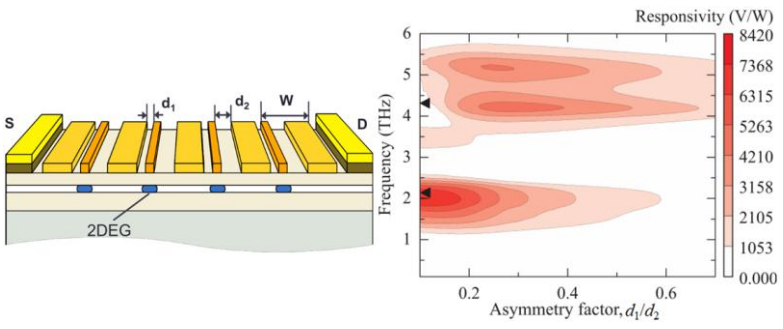

Fig. 1. Device structure of the asymmetric dual-gragting-gate (A-DGG) HEMT (left) and enhancement of the responsivity as a function of the asymmetric facter d_1/d_2, the ratio of the distances between G_1 and G_2 (right).

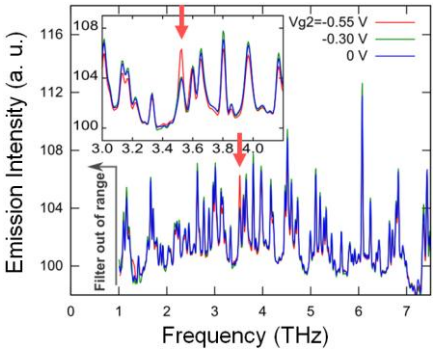

Fig. 2 Emission spectra of the A-DGG HEMT as a function of the bias for G_2. The biases for Drain and G_1 were fixed to 2 V and 0 V, respectively.

Formation of 3D high aspect ratio micro- and nanostructures in Si by plasma etching and thermal oxidation

I. Amirov[1], V. Lukichev[2], M. Izyumov[1], E. Zhikharev[2], V. Kal'nov[2].
1. Yaroslavl Branch of the Institute of Physics and Technology, RAS, Yaroslavl, Russia.
2. Institute of Physics and Technology, RAS, Moscow, Russia.

We consider etching of high aspect ratio (HAR) trenches (A = 8) and single Si pillars (A = 23) (Fig. 1) in ICP plasma C_4F_8/SF_6. Aspect ratio dependent etching (ARDE) effect and ion scattering from side walls influence on a profile shape of HAR are discussed.

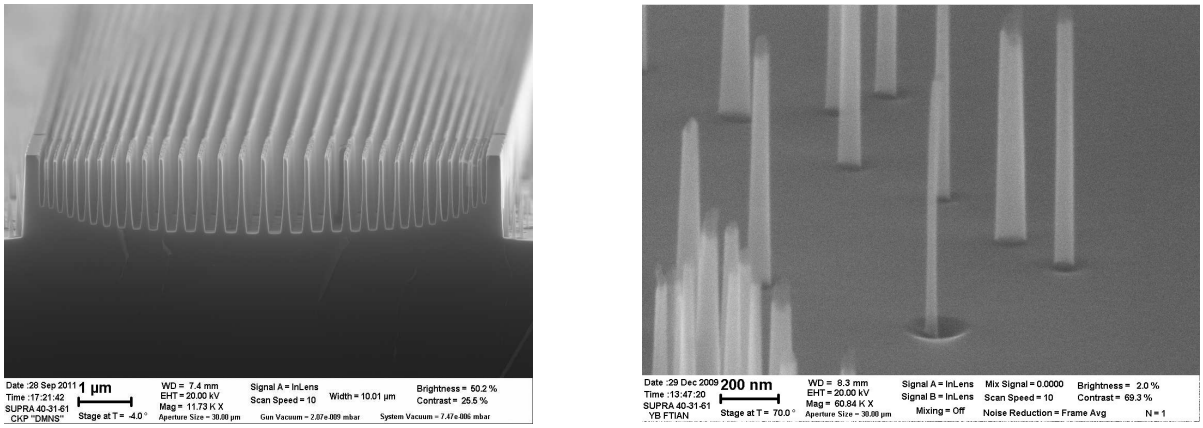

(a) (b)

Fig. 1. SEM micrograph of HAR trench (a) and single nano-pillar (b) structures.

With the use of ARDE effect and eventual thermal oxidation one can produce elements for micro- and nano-optics (micro-lens).
We present examples of suspended silicon microstructures and hollow 3D ones with SiO_2 walls.

Kinetic characteristic of electron impact processes in BCl_3

A. Efremov , V. Plotnikov, V. Svettsov
Ivanovo State University of Chemistry & Technology, Ivanovo, Russia, efremov@isuct.ru

Recently, the BCl_3-based plasmas are widely used in micro- and nanoelectronics technologies for the dry patterning of oxide materials or materials covered by the native oxides. Chemically, this works through the action of unsaturated BCl_x radicals which are able to destruct the oxide bonds and to hold the oxygen in a form of BCl_xO_y compounds. However, though the practical use of the BCl_3-based plasmas has evident perspectives, the development and optimization of the etching process is retarded by the insufficient knowledge on the plasma chemistry in this system.

Plasma modeling is an effective tool to analyze plasma chemistry as well as to obtain the information on plasma parameters and densities of plasma active species. The accuracy of modeling depends on the quality of the input data set, and the question of the principal importance is the list of the electron impact processes included in the model and their kinetic characteristics.

The goals of this work were to compose the full list of electron impact processes for BCl_3 molecule, to optimize the corresponding cross-section set using the comparison of model-predicted and measured electron gas characteristics (drift rate, attachment and ionization coefficients) as well as to analyze the contribution of various processes into the formation-decay kinetics for plasma active species. For this purpose, we used the 0-dimensional steady-state plasma model based on the Boltzmann kinetic equation. The Boltzmann kinetic equation was solved using the finite-deference conservative scheme without accounting for both electron-electron collisions and the second-order impacts. The accuracy of solution was controlled through the electron energy balance. In order to obtain the steady-state reduced electric field strength (E/N) and the densities of charged species, the self-consistent modeling algorithm was applied. Here, the Boltzmann equation was combined with the plasma conductivity equation for the conditions of the dc glow discharge, kinetic equation for negative ions and quasi-neutrality conditions for densities of charged particles as well as for their fluxes to the reactor wall. As the self-consistency criterion, we used the formation-decay balance for electrons with the approximation of "effective" diffusion coefficient.

Table 1 shows the list of inelastic processes with corresponding threshold energies which have the principal influence on electron energy distribution function (EEDF) and related plasma parameters.

Table 1

R1	$BCl_3 + e \rightarrow BCl_3(V1,2) + e$	0.06 eV	R6	$BCl_3 + e \rightarrow BCl_2 + Cl^-$	-
R2	$BCl_3 + e \rightarrow BCl_3(V3) + e$	0.15 eV	R7	$BCl_3 + e \rightarrow BCl_3^+ + 2e$	12.0 eV
R3	$BCl_3 + e \rightarrow BCl_3(V4) + e$	0.03 eV	R8	$BCl_3 + e \rightarrow BCl_2^+ + Cl + 2e$	13.2 eV
R4	$BCl_3 + e \rightarrow BCl_2 + Cl + e$	4.6 eV	R9	$BCl_3 + e \rightarrow BCl^+ + Cl_2 + 2e$	19.2 eV
R5	$BCl_3 + e \rightarrow BCl + Cl_2 + e$	5.7 eV	R10	$BCl_3 + e \rightarrow BCl_2 + Cl^+ + 2e$	17.1 eV

It was found that the basic set of cross-section from Ref. [1] provides a satisfactory agreement between calculated and measured electron drift rate and attachment rate coefficient. For the $E/N = 10^{-16}$–5×10^{-15} Vcm^2 the dominant electron energy loss comes from R1–R3 because of much higher cross-sections compared with the rest processes. However, for $E/N > 5\times10^{-15}$ Vcm^2 the contributions of R4 and R5 in the medium part of EEDF became to be noticeable. The much lower energy losses for R6–R10 allow one to assume the EEDF to be independent on the electron formation-decay kinetics in bulk plasma. The rate coefficients for R4 and R5 were found to be quite close, so that one can expect a close generation rate for BCl_2, BCl and Cl species. Therefore, the repeatedly reported fact that [Cl] > [BCl_2] > [BCl] is probably provided by various decay kinetics (various sticking coefficients and recombination probabilities) for mentioned species.

Among R7–R10, the highest rate coefficient is for R8 because of higher process cross-section compared with R7 (~6×10^{-16} and 1.5×10^{-16} cm^2 at 30 eV, respectively). This explains the numerous results of BCl_3 plasma diagnostics where the BCl_2^+ ion was found to be the dominant positively charged particle. The steady-state E/Ns in BCl_3 are comparable with those in Cl_2 plasma under the same operating conditions. The reason is the threshold-less dissociative attachment of electrons to both molecules.

1. L. G. Christophorou and J. K. Olthoff, "Electron interactions with BCl_3", J. Phys. Chem. Ref. Data, **31**, pp.971-988, 2002.

Plasma emission spectra in CCl_2F_2/Ar gas mixtures

D.B. Murin, V.I. Svettsov, A.M. Efremov, A.E. Leventsov
Ivanovo State University of Chemical Technology, Ivanovo, Russia
efremov@isuct.ru, svetsov@isuct.ru, dim86@mail.ru

The mixtures of chlorine-containing chemically active gases (Cl_2, BCl_3, HCl, CCl_2F_2) with inert gases (Ar, He) are widely used in "dry" etching technologies for patterning of metals and semiconductor layers in integrated electronic device structures. All these gases produce Cl atoms during their dissociation in plasma, and the Cl atoms form the volatile compounds with many materials used in the micro- and nanoelectronics technology. The optimization of the plasma etching processes needs to find an optimum yield of chlorine atoms and thus, to provide an optimum combination of chemical and physical etching pathways. To solve this problem, the optical emission spectroscopy (OES) is applied frequently.

The aim of this work was to investigate the emission spectra of CCl_2F_2/Ar as well as to analyze the correlations between emission intensities and densities of plasma active species.

The experiments were carries out in the ICP etching reactor Platran 100 HT with a magnetic plasma confinement. The plasma was excited at 13.56 MHz. The process conditions were: gas pressure (p) of 0.1–100 mTorr, input power (W) of 500–1300 W, sample temperature (T_s) of 20–300 ^{0}C. The CCl_2F_2/Ar mixing ratios were set by adjusting partial flow rates of pure gases. The OES measurements were carried out using the grid spectrometer AvaSpec in the wavelength range 200–1000 nm. The emission was taken by the waveguide through the wall side viewport on the reactor chamber.

Experiments showed that the emission spectrum of CCl2F2/Ar plasma contains both atomic and molecular components. The most intensive maximums with no overlapping with their neighborhood are Cl (438.99, 452.6, 725.67, 837.82 nm), C (247.62 nm), F (685.48, 703.76 nm), Ar (811.76, 912.26 nm) and band: Cl_2 (256.4 nm), CCl (277.78, 278.46 nm). Fig. 1 and 2 show the dependence of the intensities of the emission lines of atomic chlorine and chlorine molecules, and the bands of the radical CCl on the RF power and gas flow rate.

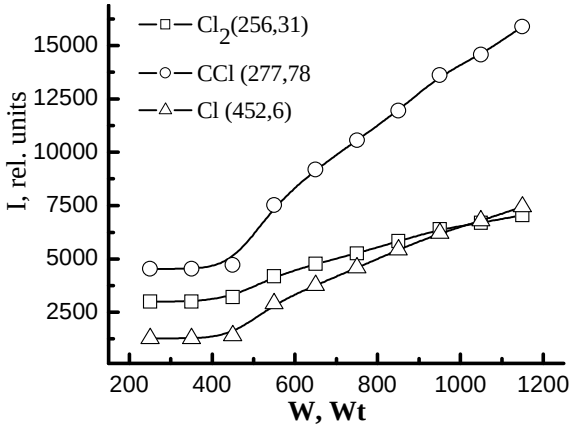

Fig. 1: Dependence of radiation intensity on the power deposition, a mixture of refrigerant R-12 to argon (U_{dc} = 200 Wt, total gas pressure of 2.4 mTorr)

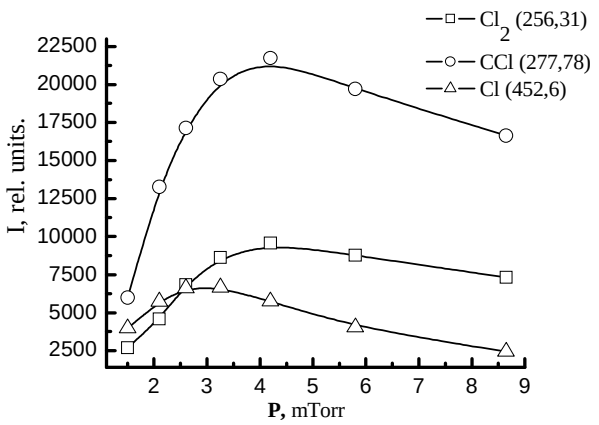

Fig. 2: Dependence of the intensity of radiation from the and gas pressure, a mixture of refrigerant R-12 to argon (W = 1150 Wt, U_{dc} = 200 Wt, the ratio of gases 50/50%)

Intensity of lines and bands of chlorine-containing components, and, consequently, their relative concentration increases with increasing of power and does not depend on the bias voltage. Effect of pressure and gas flow rate on the radiation intensity is characterized by peaks at 3 - 5 mTorr and gas flow rates of 60 - 100 cm^3/min, this is due to the fact that at low pressures the dominant factor is the increase in concentration of parent molecules, and at high pressures becomes a major factor in loss of the electron density and, consequently, decrease the rate constant of the excitation process.

Poly- and nanocrystalline silicon films formed by PECVD for micro- and nanodevices

E. Gusev, R. Velichko
Taganrog Institute of Technology – Southern Federal University, Taganrog, Russia, eyugusev@gmail.com

A polycrystalline silicon is now days widely used to construct modern micro- and nanodevices, solar cells as well as MEMS and NEMS [1]. This material has been being used in technological and sacrificial layers. One of the polycrystalline silicon obtaining methods is PECVD as a whole [1].
The present research work introduces the conditions of polycrystalline silicon layers manufacturing which is giving us the ability to obtain polycrystalline silicon films with the crystalline size (grain size) from 100 nm to 250 nm as well as nanocrystalline phase with the crystal size from 40 nm to 100 nm.
Plasma chemical polycrystalline silicon deposition was performed in accordance with a monosilane restore reaction in argon environment. The process took place in the camera at pressure of 1-2 Torr, the Ar and SiH_4 flow was kept at 450 and 50 sccm respectively, the process temperature varied from 823 K to 973 K, at power supply from 20 to 40 W [2]. The layer thickness obtained was observed to be within the range from 750 nm to 1000 nm at the deposition rate on the of order 100 nm/min.
By means of reflection high-energy electron diffraction (RHEED) it was found and indentified the existence of amorphous, nano- and polycrystalline structure of layers obtained (Fig.1). The existence of the above mentioned phases was proved by ellipsometry (the refractive index value was estimated to be within the range from 3.5 to 5.2). It was clearly established that the structure of films obtained changes with temperature increase in the following way: amorphous phase – nanocrystalline phase (813 K) – polycrystalline phase (883 K).
The grain size and the root-mean square (RMS) roughness were determined by atomic-force microscopy (AFM). Fig.2 shows the polycrystalline silicon film image. AFM data analysis clearly showed the grain size increased three times with the temperature increase from 773 K to 973 K, while the RMS roughness increased by 1.4 %. The grain size and RMS roughness increased by 8.5% and two times respectively with the pressure increase from 1 to 2 Torr. The prolongation of the process from 10 to 20 minutes also tends to increase the grain size and RMS roughness values by 14.6% and 20% respectively.
Thus the grain size and RMS roughness of the surface of the samples obtained were determined to be within 40 – 250 nm and 0.5 – 4 nm respectively. Deposition conditions of poly- and nanocrystalline silicon films with the grain size of order 100 nm and RMS roughness of 3.5 nm were obtained and are challenging for MEMS and NEMS device construction and manufacturing.

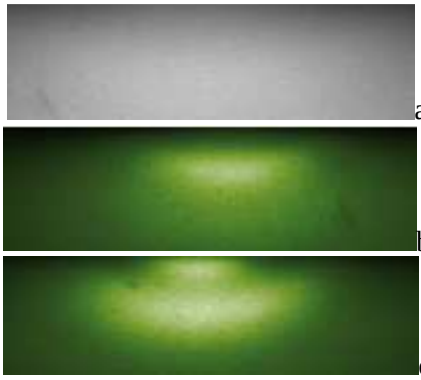

Figure 1 – RHEED images of the silicon films a) amorphous; b) nano-; c) polycrystalline

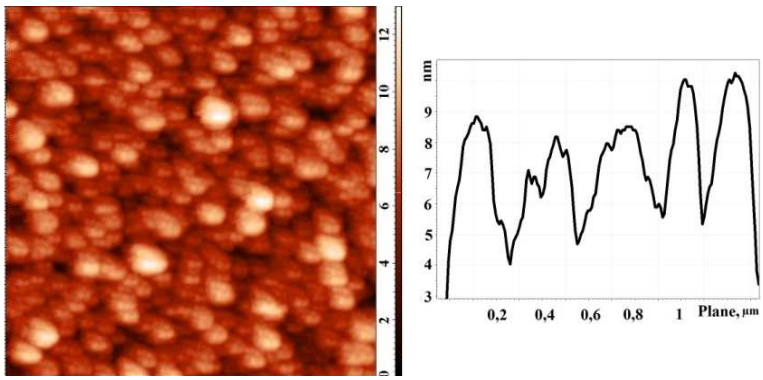

Figure 2 – AFM images (left, 2x2 µm) of polycrystalline film

1. P.J. French, “Polysilicon: a versatile material for Microsystems”, Sensors and actuators A: Physical, **99**, pp.3-12, 2002.
2. R.V. Velichko, V.A. Gamaleev, A.S. Mikhno, “The investigation of PECVD conditions for polysilicon film obtaining for micro- and nanoelectronic devices”, V.V. Titov ed., pp.178–179, SSC RAS Publishers, Rostov-on-Don, 2012 (in Russian)

Etching characteristics and mechanisms of Mo and Al_2O_3 thin films in inductively coupled $Cl_2/O_2/Ar$ plasmas

K.-H. Kwon[1)], K. Kim[2)], Y.-H. Ham[1)], A. Efremov[3)]
[1)]*Korea University, Chungnam, Korea, kwonkh@korea.ac.kr, hamcos@paran.com*
[2)]*Sogang University, Seoul 121-742, Korea, kimks@sogang.ac.kr*
[3)]*Ivanovo State University of Chemistry & Technology, Ivanovo, Russia, efremov@isuct.ru*

Recently, many new materials have been used in micro- and nano-electronics technology as substitutes for conventional materials, and have achieved improved device characteristics. Particularly, the Al_2O_3 is the promising material to be used as the gate dielectric instead of SiO_2 while the Mo is an appropriate electrode material, which can be easily combined with Al_2O_3. Thus, the optimization of the dry etching process for both Mo and Al_2O_3 thin films is important in achieving accurate pattern transfer and stable device parameters. However, the task of optimization cannot be solved without the knowledge on the process mechanism.

The gas mixtures composed from the chemically active (halogen-containing) gas and noble or molecular additive gas are the widely used systems for plasma-assisted patterning of both metal and semiconductor layers. The main advantage such systems is that the gas mixing ratio gives an additional tool to adjust plasma parameters and composition and thus, to optimize the etch result.

The main goal of this work was to analyze the influence of $Cl_2/O_2/Ar$ mixing ratio on etching characteristics of Mo and Al_2O_3 thin films in order to determine the etching mechanism as well as to find an optimal process conditions.

Mo thin film with a thickness of ~150 nm was deposited on the Si (111) substrate by RF magnetron sputtering. The Al_2O_3 films with a thickness of ~170 nm were also grown on the Si (111) substrate by the PEALD method using H_2O and $Al(CH_3)_3$ as the working gases. The experiments were carried out in a planar inductively-coupled 13.56 MHz plasma reactor. The process conditions were: gas pressure (p) of 6 mTorr, input ICP power (W) of 700 W and bias power (W_{dc}) of 200 W. The initial gas mixture compositions were set by adjusting the partial gas flow rate of the components within p = const. Langmuir probe diagnostics provided the data on electron temperature (T_e), ion current density (J_i) and total positive ion density (n_+). In order to determine the densities and fluxes of plasma active species, the simplified global (zero-dimensional) plasma model operating with volume-averaged plasma parameters and a Maxwellian approximation for the electron energy distribution function was applied. The model directly involved the experimental data on T_e and n_+ as input parameters.

It was found that the dilution of Cl_2 by Ar without the oxygen results in similar non-monotonic behaviors of both Mo and Al_2O_3 etching rates. The Mo etching rate maximum is ~160 nm/min and is located at 50-60% Ar. The Al_2O_3 etching rate maximum is ~27 nm/min and corresponds to 20-40% Ar. In both cases, a more than twofold increase in the etching rate compared with pure Cl_2 plasma takes place. The model-based analysis of etching kinetics allows one to conclude that the etching process occurs in a transitional regime of ion-assisted chemical reaction (no direct correlation with the behaviors of both Cl atom and ion fluxes is obtained) while the non-monotonic etch rates result from the concurrence of decreasing Cl atom flux and increasing ion energy flux. The last accelerates the ion-stimulated desorption of reaction products and rapidly increases the fraction of free surface acceptable for chemical reaction.

The addition of O_2 to the Cl_2/Ar gas mixture causes again the non-monotonic Mo etching rate while the Al_2O_3 etching rate decreases monotonically. Accordingly, the maximum Mo/Al_2O_3 etching selectivity of ~35-37 is obtained at 40% O_2. Plasma modeling showed that the fluxes of Cl atoms and positive ions on the etched surface change monotonically in one and the same direction. Therefore, the non-monotonic Mo etching rate can be connected only with the changes in the heterogeneous etching chemistry, and namely, with the change in the reaction probability. The reasonable assumption is an increase in the reaction probability with increasing O_2 mixing ratio due to the formation of high volatile Mo oxy-chlorides. In the framework of this assumption, the non-monotonic Mo etching rate results from the concurrence of increasing reaction probability and decreasing flux of Cl atoms. Therefore, the addition of O_2 influences the Mo etching mechanism only and serves for increasing Mo/Al_2O_3 etching selectivity.

Instrumented wafer as a Langmuir multiprobe tool for lateral plasma homogeneity measurements in processing plasma reactors

A. Miakonkikh, S. Lisovsky, M. Rudenko, K. Rudenko
Institute of Physics and Technology, Russian Academy of Sciences, Moscow, Russia, miakonkikh@ftian.ru

Introduction of new materials, processes, and process gases, as well as tightening of requirements, and tendency to use wafers of high diameter lead to constant efforts in field of improving existing plasma sources and designing of new types. Homogeneity of process parameters (e.g. plasma particles densities, electron temperature, etching rate etc.) is one of the most critical requirements to commercial plasma tools. The problem is complicated because the homogeneity as well as other parameters of the discharge depends on pressure, gas, and applied power. This means that fast, nonperturbative and reliable methods of diagnostics of the process homogeneity are still to be developed. Common constructions of reactors are hardly allows any spatial-resolved methods of generally used diagnostics. Recently adopted for processing reactors method of emission plasma tomography [1] still needs two optical windows with perpendicular orientation, which not always in hand. Though usual Langmuir probe method is suitable for measurements of local parameters (electron temperature, density of electrons and ions, plasma potential), its positioning over wafer area is barely possible. Another problem arising in processing plasmas is contamination of probe surface with dielectric films.

Recently developed technique of Dynamic Langmuir probe allows programmable cleaning of probe surface with flow of positive ions during measurement cycle [2]. The same electronic equipment and modified program could be used for realization of instrumented wafer technique of Langmuir measurements of plasma homogeneity in wafer region of reactor.

In the present work we present Langmuir multiprobe for spatially resolved measurement of electron and ion concentration, electron temperature and space potential in wafer treatment area of reactor. Multiprobe is a round fiber-glass plastic plate with round copper electrodes produced by standard printed circuit boards technology. It is placed on wafer holder during experiment, with electrodes connected to multichannel IV-curve measuring circuit of our own construction. Surface of electrodes is covered by nickel to prevent sputtering and contamination of reactor. Conductive wires between probe and connector is protected by polyimide. Special measures were taken in order to insure thermostability and high tolerance of probe to plasma treatment. Direct measurements showed that temperature of plate do not exceed 100C during 5 minutes process with applied power of 600 W.

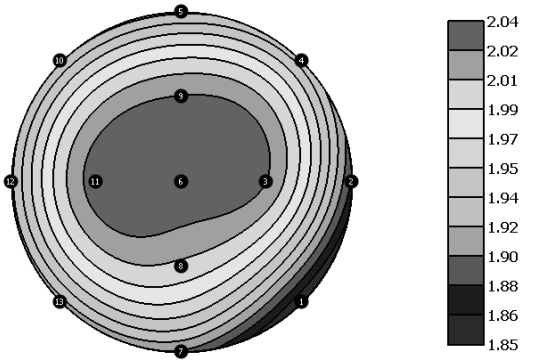

Fig. 1. Lateral distribution of plasma density in reactor for He plasma at 500 W, 7 mTorr (10^{12} cm^{-3}).

Test measurements were performed in our plasma implantation reactor in Ar and He plasmas. To check sensitivity of method to perturbations we also measured homogeneity of plasma produced with modified (asymmetric magnet confinement system) and asymmetric gas supply. Experiment shows higher degree of homogeneity for Ar plasma, and strong adverse effect of reactor asymmetry for homogeneity. Theoretical calculations prove plane probe theory to be adequate to the case. Issue of probe contamination with oxide film leading to current decay was correctly addressed by in situ probe cleaning procedure by accelerated positive ion flow.

1. K.V. Rudenko, A.V. Fadeev, A.A. Orlikovsky, K.A. Valiev, "Tomographic reconstruction of space plasma inhomogeneities", Proc. of SPIE, **5401**, pp.79-85, 2004.
2. A. Miakonkikh, K. Rudenko, "Measurement of polymerizing fluorocarbon plasma parameters", Proceedings of SPIE, **6260**, 62600A, 2006.

Method of saturable absorber fabrication by PECVD of carbon nanostructures on optical fibers

A.E. Mironov, S.V. Dubkov, D.G. Gromov
National Research University of Electronic Technology, Moscow, Russia
E-mail address: mironov.mae@gmail.com, sv.dubkov@gmail.com, gromadima@gmail.com

Recent years witnessed great interest in studying carbonic nanomaterials, i.e. nanotubes, fullerenes and diamond-like films, due to their high application potentiality. These nanomaterials feature unique structural, mechanical and electric characteristics. Chemical vapor deposition (CVD) is the most common synthetic procedure of carbonic nanostructures owing to its simplicity and economic benefits in the process of carbonic nanostructures synthesis. Usage of plasma during chemical vapor deposition (PECVD) makes it possible to decompose carbon-bearing substances and to lower the temperature of synthesis of carbon-bearing nanostructures.

One of the interesting features of carbon nanostructures is that they can act as passive Saturable Absorber (SA). A saturable absorber is a nonlinear optical material that becomes more transparent as the intensity of light falling upon it increases. Passive saturable absorbers can be integrated into laser systems to provide mode-locking and into fiberoptic systems for passive optical regeneration. Such lasers operate with short pulses about pico- and femtoseconds and have a lot of applications in micromachining, medicine. The traditional saturable absorber is a multilayer semiconductor structure that requires expensive equipment for fabrication to reduce the device's saturation recovery time from the nanosecond to the more practical picosecond range.

Recently it has been showed that carbon nanostructures offer several key advantages such as: ultra-fast recovery time (<1ps), polarization insensitivity, high optical damage threshold, mechanical and environmental robustness and chemical stability.

Some recent papers represent several technologies that allow the fabrication of mode-locked fiber lasers using carbon nanostructures as SA. For example, in [1] authors fabricated thin polyvinyl alcohol films containing carbon nanotubes and placed them between two FC/APC fiber connectors. In [2] authors proposed a method for the integration of graphene and carbon nanotubes into a fiber ferrule using an optical deposition technique allowing to deposit nanostructures directly on the core of a fiber edge and in tapered fibers.

In this paper we represent low temperature PECVD method of carbon nanotubes and carbon tubular structures deposition on the tip of the optical fiber. Before the PECVD process optical fiber was cleaved at zero angle. For nanotubes formation we used a catalyst layer of Ni with thickness of several nanometers and carbon tubular structures were deposited directly on the cleaved fiber using the method that we mentioned in our previous work [3]. In both of this processes we used CO+H2 gas mixture and temperatures lower than 400°C. After the deposition samples were tested using a broadband erbium light source and IR optical spectrum analyzer. Measurements showed that samples have absorption peak at spectral range near 1500 nm which corresponds to erbium doped fiber spectrum. For obtaining saturable absorption the thickness of our samples still should be adjusted corresponding to the pump source power.

1. S.M. Kobtsev, S.V. Kukarin, Y.S. Fedotov, “Mode-locked Yb-fiber laser with saturable absorber based on carbon nanotubes”, Laser Physics, **21**, pp.283-286, 2010.
2. A. Martinez, K. Fuse, Bo Xu, S. Yamashita, “Optical deposition of graphene and carbon nanotubes in a fiber ferrule for passive mode-locked lasing”, Optics Express, **18**, pp.23054-23061, 2010.
3. S.V Dubkov., S.A. Gavrilov, D.G. Gromov, G.A. Krasulin, “Low-Temperature Process of the Formation of Tubular and Graphene Carbon Structures”, Semiconductors, **45**, pp.1705–1708, 2011.

Plasma molding in deep silicon reactive ion etching

O. Morozov
Institute of Physics and Technology RAS, Yaroslavl branch, Russia, moleg1967@yandex.ru, 150007

In the time multiplexed deep silicon etching (TMDE) for a microelectromechanical system (MEMS), the typical etch depths are in the range of 10–500 um. Lateral sizes of etched features can vary from submicron size to millimeters. When the substrate surface contains geometrical features like deep cavity the plasma-sheath boundary will try to wrap around the contour of the cavity. This is called plasma molding. The resulting curved electric field lines can alter the oncoming ion trajectories, greatly influencing the ion impact angle. The important length scales that control behavior are the plasma-sheath thickness and the lateral sizes and depth of the cavity [1, 2].

This work presents experimental study of the plasma molding effect on etched trench tilt. Silicon etching was carried out with ICP TMDE etcher. SiO_2 and Cr layers were used as the self-aligned etching masks (fig. 1a.) The deep cavities with widths from 200 um to few millimeters were etched using Cr/SiO_2 masks (fig. 1b). The cavities depth varies from 50 um up to 1500 um. The array of narrow trenches was etched through patterned SiO_2/Cr mask (fig. 1c). Trenches slope angles were studied as function of the depth and the lateral size of cavities and distance from the corner of the cavity step.

For cavity lateral size of 3000 um and more the tilted trenches at the corner of the cavity step are observed (fig. 2). The tilts of the trenches reach its maximum at corner of the cavity step and tend to vertical across the distance of few millimeters. The grater cavity depth the more trenches slope. Experimental trench slope angle and calculated from simulation data on ion impact angle [1] are in good agreement under certain value of the plasma-sheath thickness. The plasma-sheath thickness was determined by fitting theoretical and experimental data. Narrow trenches are vertical independent of cavity depth if the cavity lateral size is 200 um. But the narrow trenches have asymmetrical bottom profile similar to shown in figure 2. Distortion of symmetry of ion angular distribution function is most likely to be the cause of this asymmetry.

Plasma molding can lead to undesirable distortions of the etched structures geometry. On the other hand the presented scheme for etching silicon trenches at an angle gives new opportunity for sophisticated MEMS design.

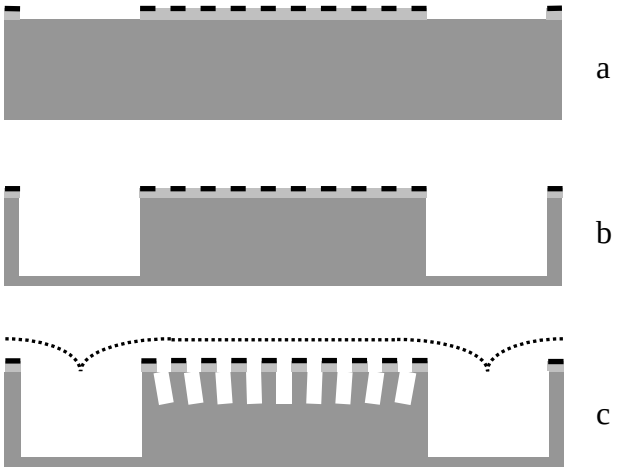

Fig. 1 Experimental process flow. In c) dashed line denotes curved plasma sheath boundary.

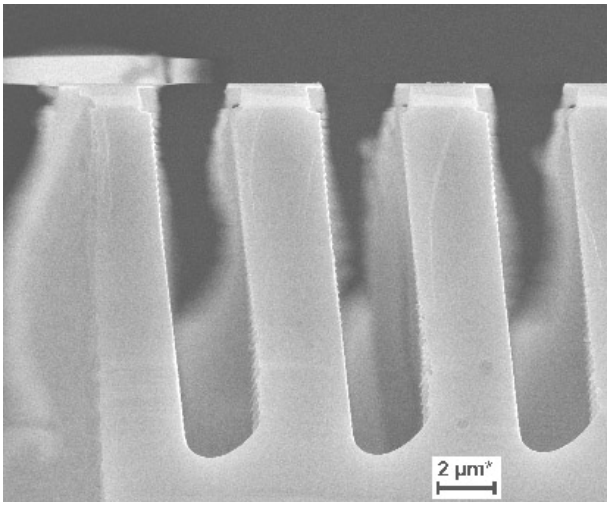

Fig.2 SEM micrograph of etched narrow trenches at the upper right hand corner of the cavity. The cavity depth was 205 um. The slope angle is 84°.

1. D. Kim and D.J. Economou, "Plasma molding over surface topography: simulation of ion flow, and energy and angular distributions over steps in RF high-density plasmas", IEEE Transactions on Plasma Science, **30**, pp.2048-2058, 2002.

2. D. Kim and D.J. Economou, "Plasma molding over deep trenches and the resulting ion and energetic neutral distributions", J. Vac. Sci. Technol. B, **21**, pp.1248-1253, 2003.

Investigation of plasma etching of Si and SiO_2 through electron resist ZEP-7000

Yu. Shikolenko[1], A. Antonovich[1], D. Lapin[1], V. Lukichev[1,2]
1. MSTU MIREA, Moscow, Russia.
2. Institute of Physics and Technology, RAS, Moscow, Russia

Plasma etching of nanometer sized features in Si and SiO_2 is of great importance for IC's fabrication. We explored electron beam lithography (RAITH-150) for producing 100-nanometer width equal spaced strips in electron resist ZEP-7000 spinned on Si and SiO_2 (Fig. 1). That type of resist is more plasma resistant than conventional PMMA.

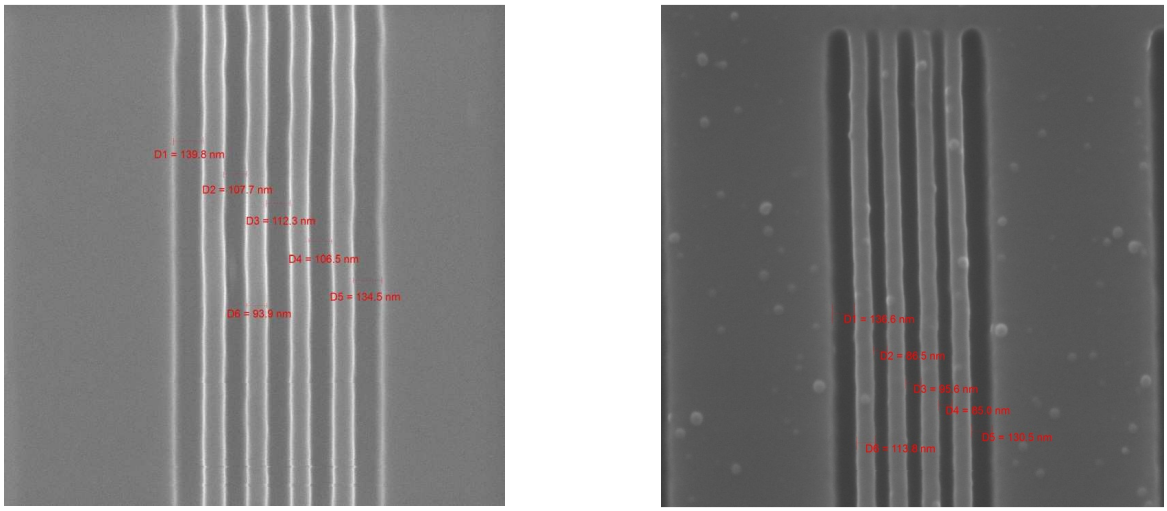

(a) (b)

Fig. 1. Developed ZEP-7000 on Si (a) and SiO_2 (b). Resist thickness 100 nm.

Those samples were etched in PlasmaLab-100 (Oxford Instr.) with SF_6/O_2 mixture (50/5 sccm) at pressures 30 – 80 mTorr for 30 s (Fig. 2).

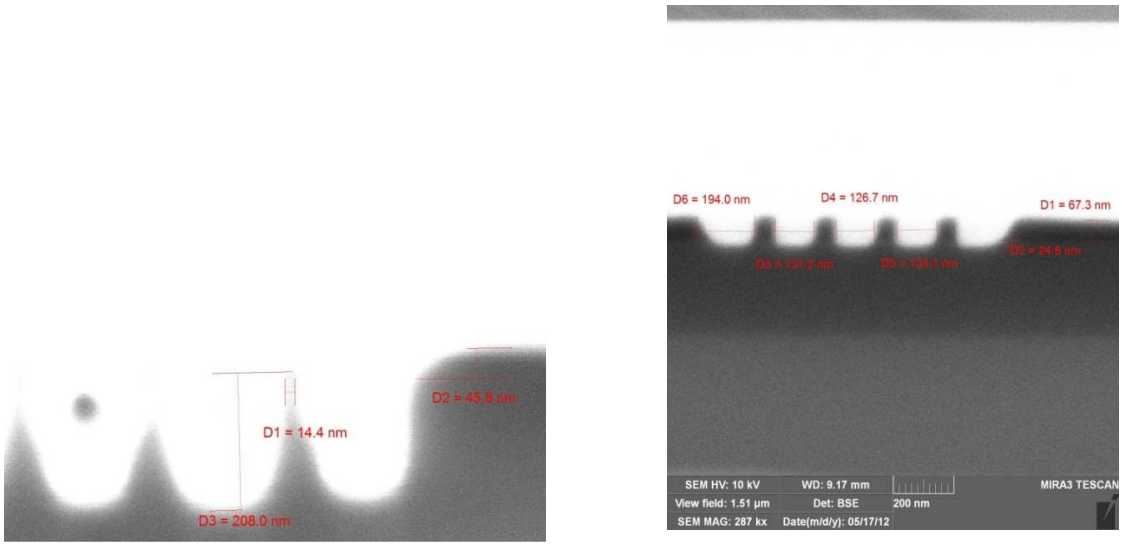

(a) (b)

Fig. 2. Cross section of etched samples on Si (a) and SiO_2 (b).

As a result etch parameters should be optimized, and work is in progress.

Determination of alloy composition in $Ge_xSi_{1-x}/SiO_2/Si$ microstructures

B.Ya. Ber, E.I. Belyakova, D.Yu. Kazanzev, L.S. Kostina, A.N.Smirnov, N.M. Shmidt
Ioffe Physical Technical Institute, Russian Academy of Sciences Petersburg, Russia Natalia.Shmidt@mail.ioffe.ru

Determination of alloy composition in individual layers in complex semiconductor structures is essential for the calibration of growth or annealing processes and control of the electrical and optical properties of the devices based on these structures. Microstructures $Ge_x Si_{1-x}/SiO_2/Si$ (SiGe-on-insulator, SGOI) are presently used to fabricate field-effect transistors (FET). One of the issues is to increase the Ge concentration on the surface of $Ge_x Si_{1-x}$ alloy, which is important to significantly improve FET parameters [1]. Express control of alloy composition and Ge profiling along rather thick (10 μm) $Ge_x Si_{1-x}$ layers after growth or annealing process is essential to achieve this task. The majority of the traditional methods allow one to examine Ge distribution in thin films (< 1000 nm), with the etching process being used to examine Ge distribution for thick films [2]. In this paper Raman spectroscopy with high resolution on split of microstructures was used for express control of $Ge_x Si_{1-x}$ alloy composition.

Two sets of SGOI microstructures under study were obtained via direct wafer bonding (DWB) of oxidized n-Si (111) wafers with $Ge_x Si_{1-x}$ (x = 3 and 6 at% of Ge) wafers, the latter were thinned up to 10 μ after DWB [3]. To increase Ge concentration on the surface of $Ge_x Si_{1-x}$, the annealing process was applied using Raman spectroscopy for express control of $Ge_x Si_{1-x}$ alloy composition. The Raman measurements were carried out using lines from an Ar^+ laser and a triple monochromator with a diode array detector. The incident excitation was focused through and the scattering light was collected by a microscope. The laser spot on split of microstructures with the line width of less than 1μm and the length of about 1 millimeter as well as the spot transference along the split were realized. To determine $Ge_x Si_{1-x}$ alloy composition, the first-order Raman spectrum was studied. It contains the three strong first-order lines due to nearest neighboring Ge-Ge (288.44cm^{-1}), Ge-Si (406.64 cm^{-1}), and Si-Si (520.0 cm^{-1}) atomic vibrations. According J.C.Tsang [2], the Si-Si phonon frequency, $\omega_{Si}(x)$ depends on x as in the following formula:

$$\omega_{Si}(x) = 520.0 - 68x \qquad (1)$$

Thus, the $Ge_x Si_{1-x}$ composition was determined from the equation (1) and Raman shift of the Si-Si phonon frequency at several points along the split of SGOI microstructures from both sets before and after different conditions of annealing process. The measurements of Raman shift at each spot were carried out automatically for several minutes on Jobin -Yvon Hariba T 64000 installation. The results of express Ge profiling were verified by means of Secondary-Ion Mass Spectrometry (SIMS) on IMS 4F CAMEC installation with several steps of 2 μm depth etching. Both methods have demonstrated good correlation of data on $Ge_x Si_{1-x}$ alloy composition on the surface and at different depths. As a result, the express Ge profiling along the split of SGOI microstructures allows to find the optimal annealing conditions and obtain SGOI microstructures with $Ge_x Si_{1-x}$ alloy (for the first set x = 8.4 at% on the surface and x = 6.5 at% at the depth; for the second set x= at.5.4 at% on the surface and x = 3.4 at% at the depth) rather fast. Moreover the express control of alloy composition along the split of microstructures can be used to study the internal boundaries.

1. Z.-Y. Cheng, M.T. Currie, C.W. Leitz *et al..*, **"**Electron Mobility Enhancement in Strained-Si n-MOSFETs Fabricated on SiGe-on-Insulator (SGOI) Substrate", IEEE Electron Dev. Lett., **22**, pp.321-323, 2001.
2. J.C. Tsang, P.M. Mooney, *et al*., "Measurements of alloy composition and strain in thin $Ge_x Si_{1-x}$ layers", J. Appl. Phys., **75**, pp.8098-8108, 1994.
3. I.V. Grekhov; L.S. Kostina; T.S. Argunova, *et al*., "Structural and electrical properties of SGOI substrates fabricated by direct bonding", Semiconductors, **44**, pp.1101-1105, 2010.

Monitoring of resonant-tunneling diode growth by reflectance anisotropy spectroscopy

I.P. Kazakov
P.N. Lebedev Physical Institute of Russian Academy of Sciences, Moscow, Russia,
E-mail address: ipkazakov@yandex.ru

Optical reflectance observation methods, in particular, reflectance anisotropy spectroscopy (RAS), have been widely used in resent years for in situ real time analysis of the heterostructures growth. In the technology of MBE, RAS is a good supplement to widely used RHEED due to the following benefits: submonolayer sensitivity to chemical bonds, non-destructive effects on the surface, large depth-sensing, electromagnetic immunity. In the present work, the possibility of growth *in situ* monitoring was studied for heterostructures with ultrathin films (few monolayers thick), such as the resonant-tunneling diode (RTD).

Heterostructures for RTD with the AlAs 2.3 nm/GaAs 4.0 nm/AlAs 2.0 nm active zone were grown by MBE. Various stages of RTD heterostructures growth were studied by RAS *in situ* (EpiRAS IR TT spectrometer). Time dependences of reflectance anisotropy for 500 nm and 950 nm light waves and RAS spectra in the range 500 – 1000 nm were analyzed. Obtained dependences clearly indicated different processes occurring on heterostructures surface during growth: oxide desorption, surface reconstruction transition, changes of surface roughness.

Figure shows the difference RAS spectrum obtained by subtracting the spectrum taken *in situ* before the formation of the active region of RTD and immediately after it growing at a substrate temperature of 600 °C.

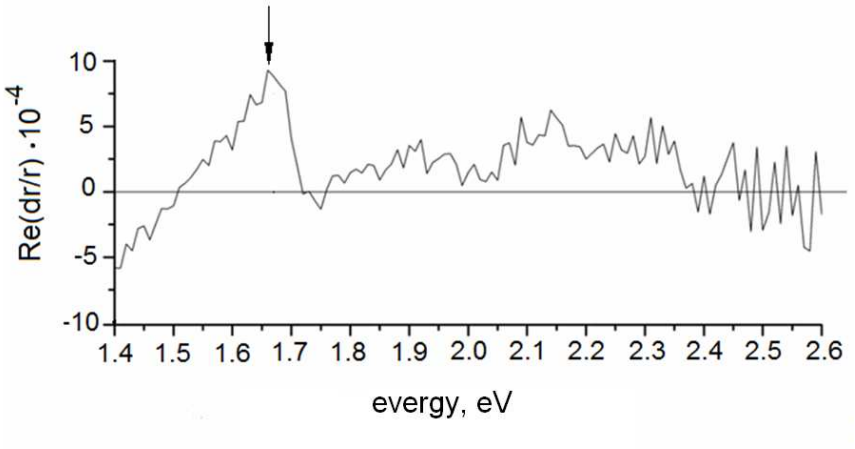

It is seen that in the 1.7 eV the difference spectrum has a feature that can be interpreted as the result of the appearance of the active region of RTD. Position of the spectral features shifts in energy, depending on the width of the QW. The amplitude of the features reflects the value of the anisotropy, which is defined by different structure of the direct and inverse heterointerfaces and their quality. This kind of spectrum will help to make the necessary conclusions about the quality of the heterostructures. It is very important that this information comes directly in the MBE process.

The research was supported by Ministry of Education and Science of RF - State Contract №16.513.11.3079, RFBR grants № 11-02-00432-a, № 11-02-12133-ofi-m.

Quality control of SOS structures by means of surface photovoltage

S.V. Kozlov[1], V.M. Maslovsky[2]

1. The company OJSC "Angstrem", Zelenograd, Russia, E-mail address nelidovec@mail.ru. 2. The company OJSC "Angstrem-M", Zelenograd, Russia, E-mail address acdmaslovsky@mail.ru.

A non-invasive method of monitoring the quality of the structures silicon on sapphire (SOS) is developed. For this, the surface structure of the CND illuminated by rectangular pulses of UV radiation is recorded in digital form the signal surface photovoltage (SPV), using a non-contact capacitive electrode. The pulse duration of exposure should be substantially longer than the leading edge of the signal and the time between pulses should be longer the trailing edge.

To correct the registration of the amplitude and shape of the pulse time constant of the PPE measuring circuit must be greater than the total duration of this pulse. At high intensity pulses of infrared radiation (~ 50 mW/cm^2 or more) sets the saturation regime, when the quasi-stationary value of SPV is almost identical with the surface potential. This makes it possible to use direct oscillographic signal SPV to determine this parameter.

The paper presents a block diagram of apparatus for signal detection, and various types of SPV signal with SOS structures (fig. A).

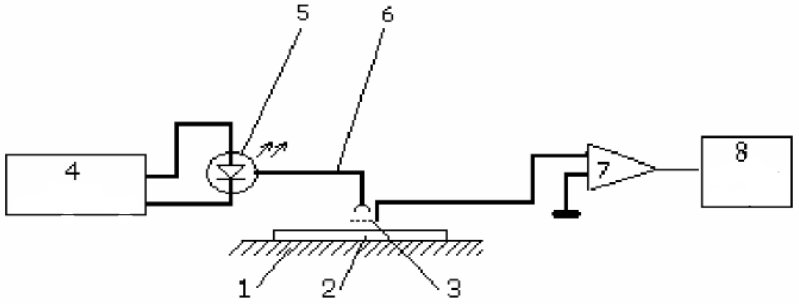

Fig. A. Block diagram of apparatus for recording signals SPV 1 - Table 2 -semiconductor wafers, 3 - transparent capacitive electrode, 4 - pulse generator; 5 - Laser LED 6 - the fiber, 7 - high impedance instrumentation amplifier, 8 - digital oscilloscope.

It was established experimentally that the leakage current structures are correlated with the magnitude of SPV (fig. B).

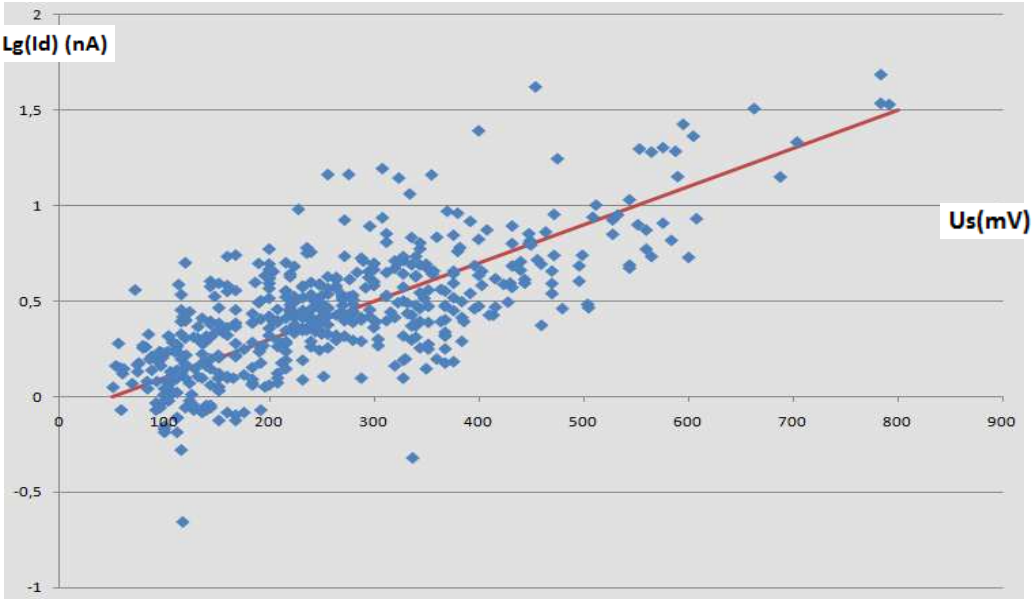

Effective probe for scanning electron microscope

Yu.V. Larionov, Yu.A. Novikov
A.M. Prokhorov General Physics Institute, Russian Academy of Sciences, Moscow, Russia, nya@kapella.gpi.ru

Scanning electron microscope (SEM) is widely used for visual inspection of micro and nanostructures and for its linear measurements. Parameters of an electron probe such as primary electron energy, probe size, angles of divergence and convergence, probe focus depth and others are main characteristics of a SEM. However, values of these parameters are not sufficient for the correct interpretation of a SEM image to conduct measurements due to existence of secondary electrons (SE) that are emitted by a sample surface and are collected to form a sample image. The SEs are generated by primary and backscattered electrons (BSE). Thus it is necessary to use for modeling effective probe (EP) and its effective parameters instead of one formed only by primary electrons.

One can represent an electron density distribution in the EP as a sum of the two distributions namely a narrow and a wide ones. A qualitative picture of a distribution is showed at Fig. 1. The narrow part of the EP distribution and its parameters are associated with primary electrons (the curve *1* at Fig. 1). The wide part of the distribution (the curve *2* at Fig. 1) and its parameters are associated with backscattered electrons. The dash lines at Fig. 1, Fig. 2 represent the null level of these density distributions.

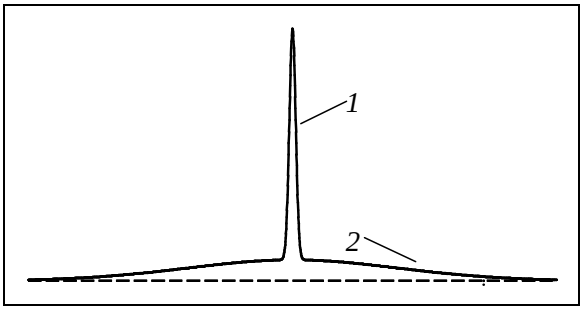

Figure 1

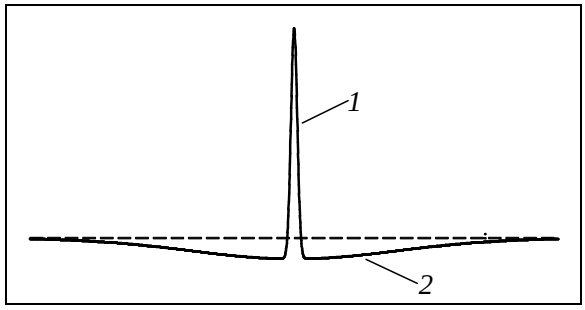

Figure 2

During a long time, an analysis of images formed by different SEMs working in SE and BSE regimes has been conducting at GPI RAS. The images were formed by electrons with energy from 300 eV to 30 keV and with a probe diameter from 10 to 300 nm from relief structures with the trapezoid profile etched in a homogeneous substrate [1].

An analysis of information brought to a conclusion that an agreement between computed and experimental videosignals is not achieved when a probe electron distribution is the one showed at Fig. 1. For achievement of this agreement one need to use the next form of a probe electron distribution (see Fig. 2):

$$\boldsymbol{F_{EF}(x,y) = I_1 F(x,y) - I_2 F_{BSE}(x,y)},$$

where $\boldsymbol{F(x,y)}$ is a function of an electron density distribution of a SEM probe, $\boldsymbol{F_{BSE}(x,y)}$ – is a function of an electron density distribution of a probe located at the effective depth of backscattering. $\boldsymbol{I_1}$ and $\boldsymbol{I_2}$ are the contributions of each of density distribution in the total EP density distribution, which are depended on primary electrons energy and from an object material. The EP density distribution can allows to achieve an agreement of experimental and computed signals almost for most analyzed cases. Causes of the density distribution with negative level values and its physical meaning are discussed in the paper.

The work was supported by RFBR grant (the project No. 11-08-01217).

2. Ch.P. Volk, E.S. Gornev, Yu.A. Novikov, Yu.V. Ozerin, Yu.I. Plotnikov, A.M. Prokhorov, A.V. Rakov, “Linear Standard for SEM-AFM Microelectronics Dimensional Metrology in the Range 0.01-100 μm”, Russian Microelectronics, **31**, pp.207-223, 2002.

Distortion of relief profile of a test object with nanometer sizes due to contamination in SEM

Yu.V. Larionov, Yu.A. Novikov
A.M. Prokhorov General Physics Institute, Russian Academy of Sciences, Moscow, Russia, luv@kapella.gpi.ru

Linear standards for SEM are subjected to prolonged and repeated effects of electron beam in the same site that results in formation of contamination film on the surface of relief structures in the site. With the passage of time, ~~a~~ film thickness can became comparable with the linear standard geometric parameters in the nanometer range and exceeds limits of a permissible error of these parameters. Because of this, the hottest task is selection of the optimal regime of standard application in SEM associated with the minimum changes of initial geometric parameters of a relief structure. The aim of the paper is revealing distortions of structure relief a test object (similar to the linear standard structure relief) due to contamination in the scanned region and selection of an area with the minimal distortions.

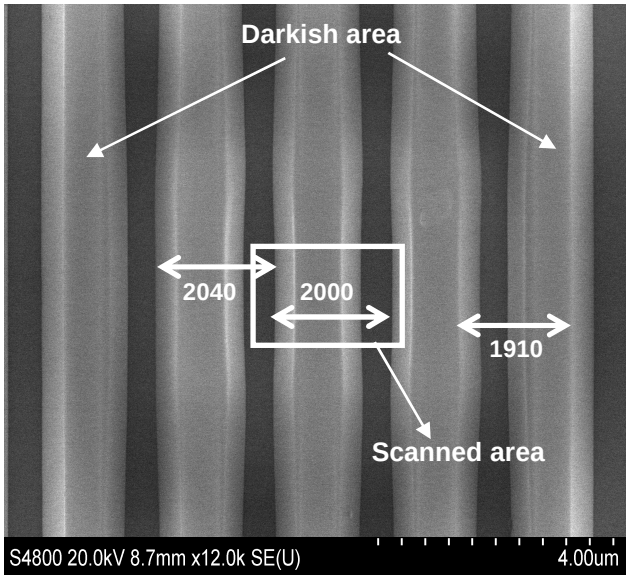

Figure

The figure shows the image (at TSE emission mode) of a test object region (similar to the linear standard [1] with the trapezoid profile) after it has been scanned in a SEM JSM-6460 during about one hour at a current about 2 nA in the television mode. Sizes of the scanned area are 1.5×2 μm^2 (indicated by the white frame in the Fig.). Overall sizes of the distorted area (is not shown at the Fig.) are 20×12 μm^2. The darkish area in the ring form (see the Fig.) is an inner part of the overall distortion area with the outer boundary which is comparable-sized with the same for contamination ring at a non-relief surface 5.5×7 μm^2. The nominal value of a period of the grating is 2000 nm. The measured values of some pitches in and near the scanned area are represented in the Fig.). As one can see, some pitches of the grating are changed due to contamination.

The non-uniform character of contamination around the scanned area capable to change a pitch between relief structures is described and explained in the paper. It depends on disposition of relief structures on the surface of a standard. This character of contamination must be taken into account at repeated measurements of geometric parameters of a standard in the selected site and at elaboration of a linear standard with some measurable structures in one chip.

It has been found that the minimum distortion of a structure profile due to contamination was in the scanned area, the maximum distortion of the one was discovered in the darkish area (see Fig.). Tolerable distortions of a structure relief in the scanned area appear as a result of exposure by relatively small doses and are associated with conform changes of an initial trapezoid profile [1] when width of its slope base projections is kept constant. A tolerable scans number of a selected site depends on the degree of contamination of a linear standard before scanning, a scan mode and a SEM type.

With increasing of exposure dose non-conform distortions of a structure profile appears. In the above-cited site (see the Fig.) a width of upper and down bases of trapezoid increases of 170 ± 5 nm (standard uncertainty) and respectively of 85 ± 10 nm. In this case, a width of slope base projections decreases of 42 ± 10 nm. As a result, a metrological quality of a standard in the selected site disrupts. One needs to select a new site of the standard for measurements or to remove the contamination film from the surface of used site.

3. Ch.P. Volk, E.S. Gornev, Yu.A. Novikov, Yu.V. Ozerin, Yu.I. Plotnikov, A.M. Prokhorov, A.V. Rakov, “Linear Standard for SEM-AFM Microelectronics Dimensional Metrology in the Range 0.01-100 μm”, Russian Microelectronics, **31**, pp.207-223, 2002.

An improved detection of the locally doped semiconductor regions with the scanning electron microscope

N.A. Orlikovsky[1], E.I. Rau[2], A.M. Tagachenkov[3], I.P. Vasyuk[4]

1. Institute of Physics and Technology Russian Academy of Sciences, Moscow, Russia;
2. Moscow state university Physical department, Moscow, Russia; rau@phys.msu.ru
3. Institute of Nanotechnology and Microelectronics Russian Academy of Sciences, Moscow, Russia;
4. Kharkov National University, Kharkov, Ukraine.

Since the time of the development of the first model of the scanning electron microtomograph in the scanning electron microscope (SEM) based on the toroidal spectrometer [1], a need has emerged for its new analytical and diagnostic possibilities in the microelectronic area. In recent years the problem of definition of dopant distribution in the scanning electron microscope has become a topic of interest [2]. There is a high need in nondestructive contactless and quantitative two-dimensional dopant profiling of modern large-scale semiconductor devices. The SEM with the adapted electron spectrometer has emerged to satisfy this need whereby it is possible to detect different energies of a filtered secondary electron (SE) signal and imaging with high contrast of the p-type and n-type doped regions.

Fig.1 shows the image of the n-type Si-crystal with the p-type local doping (implanted B) levels 10^{19} cm^{-3}. In the standard SEM with the Thornly-Everhart SE detector the contrast between n- and p- areas is very low (Fig.1, a) whereas in the SE-filtered mode the contrast reaches 40% (Fig.1, b). The p-type regions show bright contrast relatively to the n-type regions. Highly doped areas show more contrast than lightly doped areas. The spatial resolution of this technique is limited by the Debye length and the sensitivity to dopant levels is of the first order.

Another possibility to visualize the dopant distribution in semiconductor is the detection of the surface electron-beam induced voltage (SEBIV) signal in the SEM [3]. A principal application of the SEBIV-mode is to image and assess the uniformity and quality of the implanted regions which is shown on the Fig.1 (c) with the bright area representing the p-type implants, and the dark one represents the n-type Si substrate. Inhomogeneities on the border of ion-implanted area were visualized.

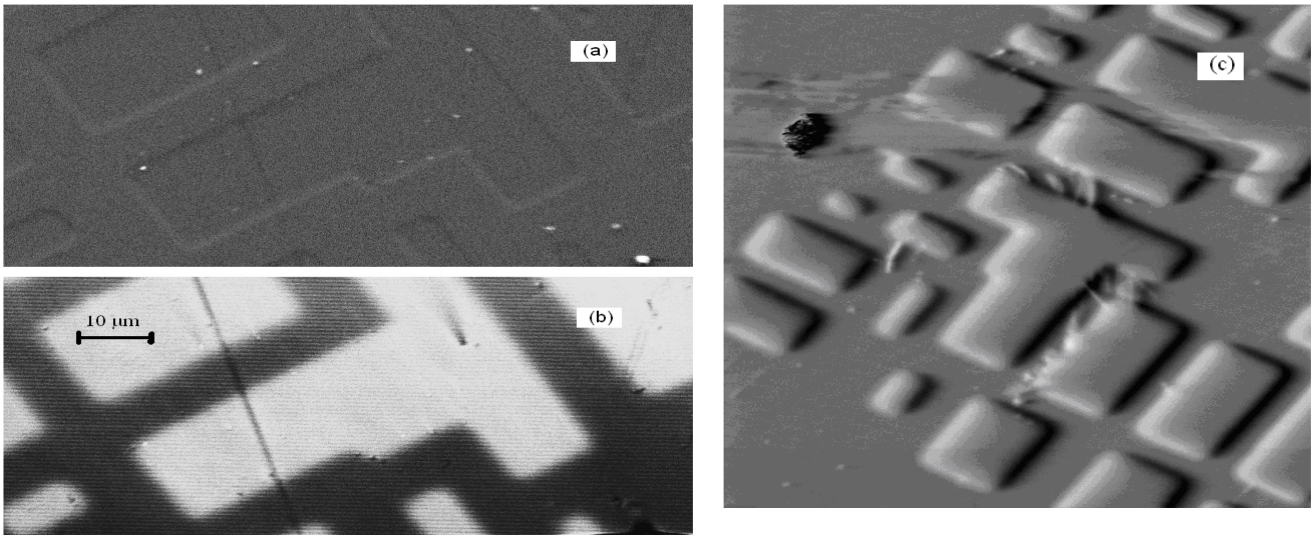

Fig.1. Images of locally doped Si crystal: in the SE standard mode (a), by the means of the spectrometer (b), and in the SEBIV-mode (c). Bright and dark regions correspond respectively to the p-type and n-type silicon

1. E.I. Rau, V.N.E. Robinson, “An annular toroidal backscattered electron energy analyzer for use in SEM”, Scanning, **18**, pp.556-561, 1996.
2. S.L. Elliott, R.F. Broom, C.J. Humphreys, “Dopant profiling with the scanning electron microscope – a study of Si”, J. Appl. Phys., **91,** pp.9116-9122, 2002.
3. E.I. Rau E.I., A.N. Zhukov, E.B. Yakimov, “Application of surface electron beam induced voltage method for the contactless characterization of semiconductor structures”, Solid State Phenom., **63**, pp.327-332, 1998.

The development of method for measuring of current density distribution in micro- and nanosystems

I. Rudnev, A. Podlivaev, S. Pokrovskiy, A. Menushenkov
National Nuclear Research University, "MEPHI", Moscow, Russia, E-mail address sergeypokrovskii@gmail.com

The analysis of different methods of measurements of current density distribution in micro- and nanosystems is presented. It is shown that high spatial resolution and good sensitivity to the magnetic field are achieved by using a magnetic force microscope (MFM). The reconstruction algorithm of current distribution from the measured MFM signal is proposed and discussed.

One of the important problems is the problem of obtaining quantitative characterization of magnetic imaging, which is closely related to the calibration of the effective parameters of the magnetic probe. Another important task is to get the MFM quality magnetic images. This problem is closely connected with the problem of the influence of defects on the magnetization characteristics of the cantilever. In the industrially produced cantilever the thickness of the magnetic needle generally covers ranges from 50 to 100 nm. Since the desired signal decreases sharply with increasing the distance from the surface of the magnetic coating of the sample, the main contribution to the signal of the MSM gives just the tip of the needle.

We have proposed the method for calibrating the magnetic-force microscope to measure the magnetic field and its derivatives on the basis of conductive bridges having the width from 200 nm to 1 micron. In addition, the numerical algorithm has been developed for solving the inverse problem of the Biot-Savart-Laplace equation to recover the spatial distribution of current in planar micro-and nanosystems.

Realization of the proposed approach allows to make qualitative and quantitative measurements of the magnetic fields of various structures and to investigate electric current flow processes in nanosystems. The developed method and a device based on it can be used in various fields of science, engineering, and technology. In particular, studies of the effects of electromigration and associated erosion of thin films, the study of current flow in nanochannels of modern nanoelectronics, redistribution of current in the pinch, the study of the anisotropy of current flow in the different structures for the solution of problems of spintronics, superconductivity can be carried out.

1. Ch. Jooss et al., Rep. Prog. Phys., **65**, p.651, 2002.
2. D.M. Feldmann, “Resolution two-dimensional currents in superconductors from a two-dimensional magnetic field measurement by the method of regularization”, Phys. Rev. B, **69**. pp.144515-144528, 2004.

Determination of the content in $Al_xGa_{1-x}As$ alloys by secondary ion mass spectrometry

V.V. Saraykin[1], I.S. Vasil'evskii[2], A.N. Vinichenko[2], K.D. Scherbachev[3]

1. Scientific Research Institute of Physical Problems named after F.V.Lukin, Moscow, Russia 124460, Moscow, Zelenograd, 4806 street, 6, e-mail: vvsaraykin@yandex.ru, 2. National Research Nuclear University «MEPhI»115409, Moscow, Kashirskoye ave., 31, e-mail: ivasilevskii@mail.ru, 3. National University of Science and Technology «MISiS», «Material science and Metallurgy» Center, 119049, Moscow, Leninskiy ave., 4, e-mail: kirill.shcherbachev@misis.ru

Ternary semiconductor compounds are the basis for the layer arrangement of the P-HEMT $Al_xGa_{1-x}As/In_yGa_{1-y}As/Al_xGa_{1-x}As$ high electron mobility heterostructures, which are commonly used in microwave electronics. $Al_xGa_{1-x}As$ layers serve as the barriers for the $In_yGa_{1-y}As$ quantum well and also as the layers where donor doping is placed. So the increase of AlAs fraction *x* leads to deeper quantum well and reduces the gate leakage. To the other hand, while *x*>24% DX-centers Si_{AlGaAs} become the traps for the electron and thus affect the transistor performance. Such parasitic effects arise as I-V hysteresis, thermal and light sensitivity. Also there is a technological aspect, because the upper contact $n^+GaAs(Si)$ layer might be removed by selective etching in the gate recess, and $Al_xGa_{1-x}As$ provides good selectivity for *x* = 22-24%. So the technology control and probing of $Al_xGa_{1-x}As$ layers are very important issues for P-HEMT technology. Secondary Ion Mass Spectroscopy (SIMS) became one of the most factual among the analytics techniques because of the unique potential in layers content profiling.

But the quantitative composition measurements are significantly affected by pronounced matrix effect, i.e. the strong dependence of secondary ion current on the surrounding matrix composition. One of the approaches to solve this problem is cluster $CsAl^+$,$CsGa^+$ ions yield registration for Cs beam etching mode [1, 2]. As Cesium possess the small ionization energy (3.89 eV), the ionization probability of this complex ions is mainly connected to electron loss of Cs atom, rather than for Al or Ga ionization (~ 6.0 eV). The difference of $CsAl^+$ and $CsGa^+$ complex ionization is much lower than that for Al^+ and Ga^+ single ions. For this etching regime by Cs^+ ions the surface is covered by deposited Cs sublayer, assisted in the complex ion yield. The $Al_xGa_{1-x}As$ composition can be determined in this case in the proportional approach:

$$x=I(CsAl^+)/ \{I(CsAl^+)+ I(CsGa^+)\}$$

The goal of the current study is the determination of accuracy of the $Al_xGa_{1-x}As$ content by the complex ion yield technique. The series of experimental samples was grown by molecular beam epitaxy with the different AlAs content (from 0.17 to 0.32) and uniform profile.

The layer composition was determined before the growth by Al and Ga flux pressures and controlled by Al and Ga cell temperatures. The two types of the samples were investigated - with thin and with thick $Al_xGa_{1-x}As$ layer, respectively. The samples with thick $Al_xGa_{1-x}As$ were used for composition profile uniformity study in the dependence of technological parameters. After the growth real composition was checked by triple crystal X-ray diffraction (XRD) by the fine structure around (004) reflection. The samples with thin (less than 100 nm) $Al_xGa_{1-x}As$ and short-period AlAs/GaAs superlattice the composition and thickness of the layers was calculated from pendulum oscillations and additional peaks. Photoluminescence (PL) spectroscopy was used to observe interband optical transitions in the samples at 77 K.

The dependence of registered current ratio on the analysis parameters was studied. The comparison of SIMS composition data to XRD and PL showed a good correspondence but had some peculiarities. The best fit was found for thick sample with the highest profile uniformity.

The examined SIMS technique with complex ion yield registration allows the quantitative study of $Al_xGa_{1-x}As$ layers for modern heterostructures profiling.

The work is partially supported by the Project of Russian Ministry of Education and Science # 16.648.12.3005.

1. Yu. Kudriavtsev, S. Gallardo, et al., Surf. Interface Anal., **43**, p.1277, 2011.
2. WWW.EAGLABS.COM, Application note AN372, 2007.

Atomic force microscopy for line edge roughness measurements

A. Sosnina, A. Miakonkikh, and A. Rogozhin
Institute of Physics and Technology, Russian Academy of Sciences, Moscow, Russia, rogozhin@ftian.ru

It is known that the influence of line edge roughness (LER), formed during lithography and plasma etching processes, on the MOSFET characteristics becomes more critical with downscaling of the device [1]. This is because LER and line width roughness do not scale down with the dimensions of the devices. High values of LER can lead to increase of current leakage and voltage fluctuations and hence cause impact on circuit performance and yield [2]. However the gate LER is hard to measure by conventional tools. Therefore reliable LER metrology approach is required.
In this work samples with lines in photoresist with different parameters were formed. Some samples were processed in ICP plasmas of He or Ne. The LER of lines were measured by atomic force microscopy (AFM) and critical dimension scanning electron microscopy (CD-SEM). Comparison of CD-SEM and AFM for LER measurements was made. The impact of the shape of AFM's tip on surface image was estimated. Also the influence of plasma treatments on LER was investigated.

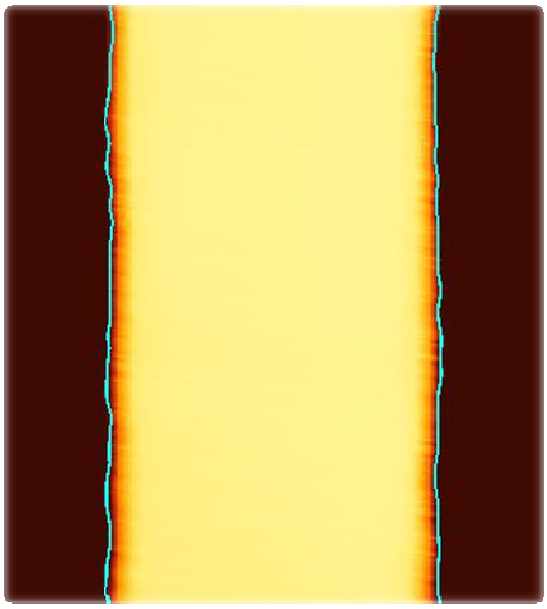

Fig. 1. AFM image of photoresist line with highlighted edge.

1. A. Asenov, S. Kaya, A.R. Brown, "Intrinsic parameter fluctuations in decananometer MOSFETs introduced by gate line edge roughness", IEEE Trans. on Electron Devices, **50**, pp.1254-1260, 2003.
2. Y. Ban, S. Sundareswaren, R. Panda, D.Z. Pan, "Electrical impact of line-edge roughness on sub-45nm node standard cell", Proceedings of the SPIE, **7275**, 727518 (pp.1-10), 2009.

Josephson φ-device based on complex nanostructures with normal metal/ferromagnet bilayer

S.V. Bakurskiy[1,2], N.V. Klenov[1], T.Yu. Karminskaya[2], A.A. Golubov[3], M.Yu. Kupriyanov[2]
1. Faculty of Physics, Moscow State University, Moscow, Russia
2. Institute of Nuclear Physics, Moscow State University, Moscow, Russia
3. Faculty of Science and Technology, University of Twente, Enschede, Netherlands

The φ-junction is the Josephson device with nontrivial ground state phase ($0 < \varphi_g < \pi$). It provides a lot of possible applications starting from double-well potential formation in quantum detectors and silent qubits, development of metamaterials and ending with self-biasing one-photon detectors.
However, φ-junction is unavailable on the base of conventional Josephson structures due to inappropriate shape of current phase relations (CPR) in them. To avoid this restriction it was proposed to use arrays of parallel 0 and π junctions[1] or SFS junctions with step-like ferromagnetic interlayer[2]. Unfortunately, these devices haven't been fabricated experimentally yet.
In this work we have demonstrated that the structures composed from longitudinally oriented normal and ferromagnet films in the weak link region can be used as reliable φ-device. To prove it, in the frame of Usadel equations we solved two dimensional boundary problem for different geometries of the structures and found analytical criteria of φ-state existence. In case of the ramp type S-FN-S structure (Fig.1a) these criteria have form of the limitations on geometrical and material parameters

$$1.00 < \sqrt{\frac{H}{2\pi T_C}\frac{L}{\xi_F}} < 2.52, \qquad (1)$$

$$0.12 < \frac{\gamma_{BF}}{2}\sqrt{\frac{H}{\pi T_C}}\frac{d_N}{d_F} < 0.2, \qquad (2)$$

where H – exchange field, T_C – critical temperature, ξ_F – ferromagnetic coherence length, γ_{BF} – transparency parameter of SF interface and temperature $T \to 0$. Also we took into account the FN-interface impact which terminates scalability of φ-junction and determines minimal thickness

$$d_N > \frac{\xi_F}{\gamma_{BFN}}\frac{\pi T_C}{H}\left(1+\frac{\rho_N}{\rho_F}\frac{1}{\gamma_{BFN}}\sqrt{\frac{\pi T_C}{H}}\right). \qquad (3)$$

The SN-FN-NS structure (Fig1.b) is founded to have significant advantages, including wider φ-state area and effective independence from N-layer thickness.
Furthermore we numerically estimated and showed φ-junction with scale in order of 100 *nm* and critical current reaching 1 *mA*.

1. A. Buzdin and A.E. Koshelev, Phys. Rev. B, **67**, 220504, 2003.
2. N.G. Pugach, E. Goldobin, R. Kleiner, D. Koelle, Phys. Rev. B, **81**, 104513, 2010.

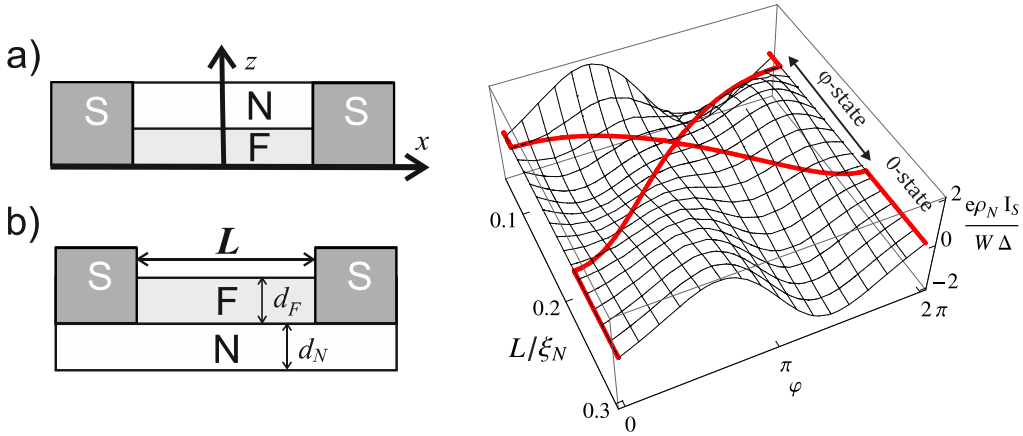

Figure 1: Different geometries of Josephson junctions: a) S-FN-S structure b) SN-FN-NS structure.
Figure 2: Supercurrent I_S versus Josephson phase φ and electrode spacing L in SN-FN-NS structure ($d_N=0.64\xi_N$, $d_F=1.45\xi_N$). Each section at certain L is a CPR. The thick lines mark ground state phase φ_g.

Macroscopic quantum effects in transmission of signals along the superconducting microwave slotline. Towards quantum transmission lines

M.A. Dresvyannikov, A.L. Karuzskii, A.V. Perestoronin, A.M. Tshovrebov, N.A. Volchkov, L.N. Zherikhina

P.N. Lebedev Physical Institute of Russian Academy of Sciences, Moscow, Russia, E-mail address karuz@sci.lebedev.ru

High-speed signal transmission lines are of a great importance for recent electronics. Faster propagation, weaker dispersion and lower losses of an electromagnetic field are very desirable qualities of transmission lines intended for high-speed applications. Recent electronics is characterized by growing demands of an increase of transmitted frequencies, by a miniaturization of electronic devices and by employment of advanced materials, from which elements of a device are fabricated, such as superconductors or other materials with quantum structures of lower dimensionality. These attributes should result in an increased significance of quantum effects in electronic transport phenomena in conducting components of transmission lines. It may happen that a characteristic coherence length of the electronic wave functions becomes to be comparable with a length of a characteristic piece of the transmission line in a device. Such a situation can make it necessary to take into account quantum effects in the electronic transport and to consider the line as a "quantum" transmission line. Here we discuss a kind of such phenomena connected with quantum effects related to the Einstein-Podolsky-Rosen (EPR) paradox, which concerns the problems of locality and causality in quantum mechanics. We analyze an influence of such effects on the properties of transmission lines and a possibility to increase a speed of signal transmission by using these quantum properties.

Brief review of alternatives and phenomena related to the problem of Einstein-Podolsky-Rosen paradox is presented. The essence of the EPR paradox related to the problems of locality and causality is highlighted by one of alternatives, which supposes, following EPR, some hidden interaction between the parts of many-body system, which would have to be instantaneous. Such an immediate interaction between distant parts of system would not in general be consistent with the classical physical theories and might be extremely interesting for high-speed applications whether it would exist. An inherent property of all effects associated with the EPR paradox is a presence of the strict correlation between the measured results, even if the points of measurement are divided by the space-like intervals (i.e. $-c^2\Delta t^2+\Delta r^2>0$). According to the presently adopted point of view, an absence of the classical field, which would provide an interaction between the distant parts of the system, opens a possibility of implementation of the conditions for a perturbation to propagate over the total system with hyperrelativistic velocity by means of disturbing only a part of this macroscopic quantum system. Additional experimental verifications of such possibility would be very desirable in view of high-speed applications.

Macroscopic quantum behavior of the propagation of magnetic perturbation along the microwave slotline at $T<T_c$ (superconducting state) has been considered here with account of the phenomena related to the problem of EPR paradox and an experiment is suggested. The experiment is aimed at testing whether there really is a quantum correlation in magnetic field perturbations of different parts of the macroscopic hole confined by superconducting boundary contour. The slotline is a waveguide system used in a microwave technique for transmission of electromagnetic waves. A slot, which is cut through a metal plate, forms the transmission line, so the field of wave concentrates in the slot gap. When the temperature decreases below $T<T_c$, the metal becomes to be superconducting, the current carriers condense into the Cooper-pair condensate - the coherent quantum-mechanical state possessing a single common many-body wave function. One of the most important attributes of this coherent state is the invariability of the magnetic flux trapped by the closed superconducting circuit and the fluxoid quantization phenomena. Just that conclusion is a reason to expect a possibility for manifestation of the quantum properties specific for EPR paradox in the systems consisting of superconducting contour with a trapped magnetic flux such, for example, as the presented here superconducting microwave slotline. For easier description of the suggested experiment an equivalent circuit taking into account the macroscopic quantum effects in superconducting slotline is developed.

This research was supported by Ministry ES of RF (GK №16.513.11.3079), by RFBR (11-02-01182, 11-02-12133), by Presidium and OFN RAN (24, program SCESMSMM, IV.12 and III.7).

Manifestation of long-range triplet superconducting correlations in F1-SF1F2-F1 structures

T. Karminskaya[1], M. Kupriyanov[1], A. Golubov [2]
1. Lomonosov Moscow State University, Skobeltsyn Institute of Nuclear Physics, Moscow 119991, Russia, janaph@gmail.com
2. Faculty of Science and Technology and MESA+ Institute of Nanotechnology, University of Twente, 7500 AE Enschede, The Netherlands

Artificial SF structures (S-superconductor, F- ferromagnetic metal) are under great interest nowadays. This interest is due not only to bunch of effects corresponding to similar to FFLO [1] phenomenon that was for the first time observed experimentally in SFS artificial structures [2, 3], but also due to recent experimental observations [4, 5] of supercurrents in structures with thick ferromagnetic layers; these supercurrents are believed to be a manifestation of an odd-frequency equal spin triplet superconducting correlations predicted theoretically for bulk materials in [6].

We propose and theoretically explore other possible structures in which odd-frequency equal spin triplet superconducting correlations can be observed experimentally. We investigate correlations in F1-SF1F2-F1 structures that represent a long thin ferromagnetic wire F1 connected with thick superconducting film S on the top of wire and thin ferromagnetic film F2 on the bottom of the wire (the lengths of S and F films are identical). Magnetization vector of the long ferromagnetic wire is constant and directs along the F1F2 interface. Magnetization vector of the short ferromagnetic film F2 is declined from the first vector on an angle α thus providing conditions for realization of equal spin triplet superconducting correlations in the structure. Odd-frequency equal spin triplet superconducting correlations are insensitive to the value of exchange energy, so they can penetrate ferromagnetic material at longer distance. So, these correlations can be observed in the long ferromagnetic wire F where the other singlet and short-range triplet correlations are already suppressed due to exchange energy.

Here we present results for Dos and differential conductance along F1 film calculations in F1-SF1F2-F1 structure with noncollinear magnetizations of ferromagnetic layers that also differs with values of exchange energies. The calculations were done in the limit of 'dirty' metals in the framework of Usadel equations for both linear and nonlinear cases. We show how Dos depends on angle α in the vicinity of SF1F2 part of the structure and how Dos transforms to Dos corresponding to long-range triplet correlations part only in the F1 wire far from SF1F2 part. Also we present differential conductance dependence on angle α. We show that maximum value of differential conductance is achieved not at $\alpha = \pi/2$ but for some intermediate angle that depends on difference between values of exchange energies of F films. As it was shown in [7] there are interesting effects form suppression parameter γ_B at F1F2 interface due to phase slip. We also investigate influence of parameter γ_B on the shape of Dos and differential conductance.

This work is supported by RFBR grant 12-02-90010-Бел_а

1. P. Fulde and R.A. Ferrell, PRB, **135, p.**A550, 1964; A.I. Larkin and Y.N. Ovchinnikov, Zh. Eksp. Teor. Fiz., **47**, p.1136, 1964.
2. V.V. Ryazanov, V.A Oboznov, A.Yu. Rusanov, A.V. Veretennikov, A.A. Golubov, J. Aarts, Phys. Rev. Lett., **86**, p.2427, 2001.
3. T. Kontos, M. Aprili, J, Lesueur, F. Genet, B. Stephanidis, R. Boursier, Phys. Rev. Lett., **89,** p.137007, 2002.
4. J.W.A. Robinson, J. Witt, M. Blamire *et al.*, Science, **329** pp.59-61, 2010.
5. T.S. Khaire, M.A. Khasawneh, W.P. Pratt, Jr., and N.O. Brige, Phys. Rev. Lett., **104**, p.137002, 2010.
6. V.L. Berezinskii, JEPT Lett., **20**, p.287, 1974.
7. T.Yu. Karminskaya, A.A. Golubov, M. Yu. Kupriyanov, Phys. Rev. B, **84**, p.064531, 2011.

Jitter in ballistic read-out circuit based on Josephson transmission line

I.I. Soloviev[1,2], N.V. Klenov[1,3], A.L. Pankratov[1], E.V. Il'ichev[4], L.S. Kuzmin[1,5]

1. Laboratory of Cryogenic Nanoelectronics, NNSTU, Russia. 2. D.V. Skobeltsyn Institute of Nuclear Physics, Moscow State University, Moscow, Russia, isol@phys.msu.ru. 3. Physics Faculty, Moscow State University, Moscow, Russia. 4. Institute of Photonic Technology, Jena, Germany 5. Chalmers University of Technology, Sweden

In the last few years a variety of approaches based on rapid single flux quantum (RSFQ) electronic circuits have been proposed for read-out the weak magnetic and current signals from nano-sized objects such SPD (single photon detectors) sensors or quantum bits [1-3]. One of these approaches is an extremely fast ballistic read-out [1] which exploits a ballistic motion of individual fluxons in a Josephson transmission line (JTL). Time delay or transmission/reflection events associated with fluxon interaction with measurement system gives information about the state of the studied object. Such detector allows achieving the read-out time of 30 ps [3].

Performance of the read-out circuit operating with SFQ pulses is limited by spontaneous changes in the speed of the pulses caused by thermal fluctuations, fluctuations of currents in power lines and technological spread in parameters of JTL elements. Obviously the time jitter has to be minimized for proper resolution of the states of the measured object.

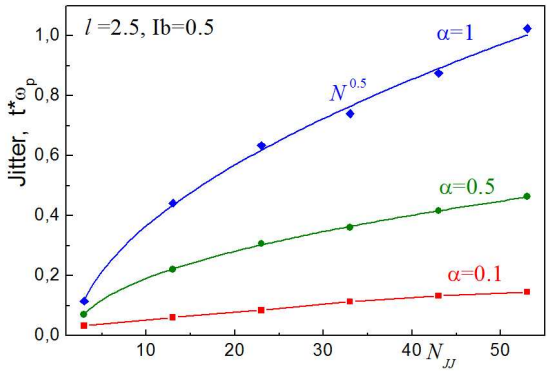

Fig. 1. Jitter in JTL for different values of damping parameter: α=1; 0.5; 0.1. Bias current $I_b = 0.5\, I_C$, coupling inductances $l = 2.5$, normalized intensity of fluctuations $\gamma = 10^{-3}$; N_{jj} – number of junctions in JTL, ω_p – plasma frequency.

Natural analog of JTL formed by unshunted Josephson junctions characterized by vanishing damping parameter α is a long Josephson junction (LJJ) if one considers the case of vanishing inductances coupling junctions in JTL. Analyses of the detector's JTL commonly based on study of LJJ as a model structure [4, 1, 3]. Analytical treatment in the frame of the model predicts that total jitter will increase with a number of junctions in JTL as N^{μ}, $\mu \geq 1/2$ [3]. However, recently it was shown by numerical calculations that in a long Josephson junction the rate of the jitter growth can be substantially reduced [5].

We developed special program that takes into account initially discreteness of Josephson transmission line and includes analysis of the noises. The program allows calculating the jitter in JTL for arbitrary parameters of Josephson junctions (damping and capacity) and finite values of inductances that couple junctions.

It is shown that imbalance of energy impact from current sources and dissipations leads to speeding-up or slowing-down of the fluxon motion with simultaneous sharpening or broadening of the SFQ pulse which is similar to soliton dynamics in a long Josephson junction [4, 5]. Using resistive shunted junction model of Josephson junction we have shown that for a typical case of relatively large velocity of fluxon the jitter of switching moment of a junction is inversely proportional to the rate of growth of the current i' flowing through the junction [6]. Thus, the pulse-sharpening leads to decrease of the jitter and therefore the fluxon acceleration is accompanied by significant reduction in rate of the jitter growth. For the same bias current and initial fluxon speed the imbalance increases with decrease of the damping parameter. Dependences illustrating according suppression of the jitter growth with number of junctions in JTL are shown in Fig. 1. Optimization of JTL with realistic parameters allows dramatically improvement of sensitivity of the ballistic detector.

The work was supported by the Act 220 of Russian Government (project 25), Dynasty Foundation, RFBR project 11-02-12065-ofi_m and Russian Ministry of Science.

1. D.V. Averin, K. Rabenstein, V. K. Semenov, Phys. Rev. B, **73**, 094504, 2006.
2. T. Ortlepp, M. Hofherr, Fritzsch, et al., Optics Express **19**, 18593, 2011.
3. A. Herr, A. Fedorov, A. Shnirman, E. Il'ichev, G. Schon, Supercond. Sci. Technol. **20**, p.S450, 2007.
4. D.W. McLaughhlin, A.C. Scott, Phys. Rev. A, **18**, p.1652, 1978.
5. A.L. Pankratov, A.V. Gordeeva, and L.S. Kuzmin // arXiv:1112.2805v1
6. K.K. Likharev *Dynamics of Josephson junctions and circuits*, Gordon and Breach, 1986.

Noise in bi-SQUID

I. Soloviev[1], N. Klenov[2], A. Sharafiev[2], V. Kornev[2]
1. Scobeltsyn Institute of Nuclear Physics, Moscow, Russia, igor.soloviev@gmail.com 2. Moscow State University, Physics Department, kornev@phys.msu.ru

We present analysis of thermal noise in bi-SQUID which has been recently suggested [1] to improve linearity of magnetic flux to voltage transfer function of the well-known dc SQUID. In low frequency SQUID-system, linearization of the transfer function can be achieved by implementation of an external following feedback loop. However this approach is infeasible in case of broadband system. The problem can be solved with implementation of bi-SQUIDs and arrays of bi-SQUIDs [2].

Despite the fact that the bi-SQUID is just a modification of dc SQUID, noise characteristics of bi-SQUID differ from the ones for dc SQUID due to difference of both the nonlinear dynamics and the phase transformation. Analytical theory has been developed and proved by numerical simulation with use of the noise-build software. The obtained noise characteristics are discussed in detail and compared with the ones for dc SQUID.

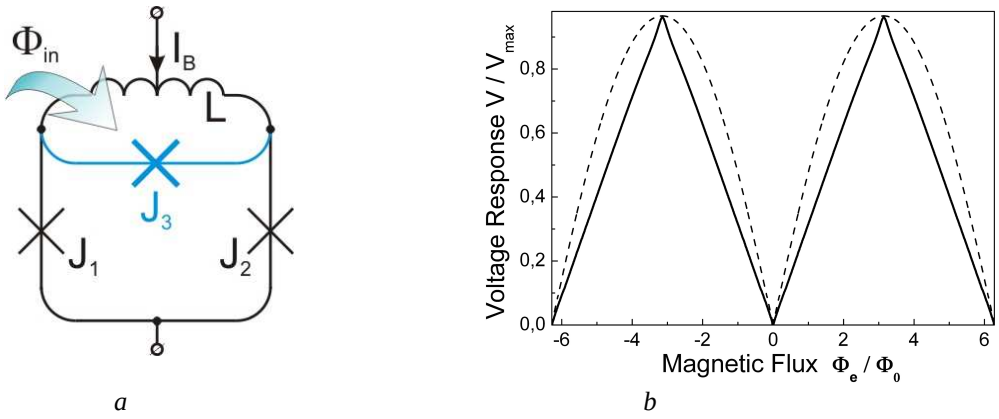

a *b*

Fig. 1. Schematic of bi-SQUID (a) and voltage responses of bi-SQUID (solid line) and dc SQUID (dashed line) at critical current biasing $I_B = 2I_C$, where I_C –critical current of Josephson junction.

1. V.K. Kornev, I.I. Soloviev, N.V. Klenov and O.A. Mukhanov, “Bi-SQUID - Novel Linearization Method for dc SQUID Voltage Response,” Superconductor Science and Technology (SUST), **22**, pp.114011-1-6, 2009.
2. V.K. Kornev, I.I. Soloviev, N.V. Klenov, A.V. Sharafiev, O.A. Mukhanov, “Linear Bi-SQUID Arrays for Electrically Small Antennas,” IEEE Transactions on Applied Superconductivity, **21**, pp.713-716, 2011.

Adequacy, completeness, and accuracy of quantum measurement protocols

Yu.I. Bogdanov, A.K. Gavrichenko
Institute of Physics and Technology, Russian Academy of Sciences, Moscow, 141700 Russia
e-mail: bogdanov@ftian.ru, gavrichen@mail.ru

A new methodology of statistical estimation of the quality of quantum measurement protocols is considered [1].The method is based on studying the completeness, adequacy, and accuracy of quantum measurement protocols. The completeness is estimated on the basis of considering a singular decomposition of a special matrix, which is constructed based on the measurement operators. The estimate of protocol adequacy supposes the presence of redundancy in the measurement protocol as compared to the minimally possible number of measurements that are necessary for full reconstruction of a quantum state. The adequacy of quantum measurements is estimated as the degree of how much the redundant statistical data agree with the laws of quantum theory.

The accuracy characteristics of the statistical reconstruction of arbitrary quantum states are studied based on the universal statistical distribution for accuracy losses. The quantitative characteristic of the accuracy of statistical reconstruction of an unknown quantum state is the so-called fidelity *F*. In the general case, the considered quantity is presented by the following formula [2]:

$$F = \left(Tr\sqrt{\rho_0^{1/2}\rho\rho_0^{1/2}}\right)^2, \quad (1)$$

where ρ_0 and ρ are the theoretical and reconstructed density matrices, respectively.

It is natural to call the quantity a loss of accuracy. A loss of accuracy is a random value the asymptotical distribution of which can be represented in the form [3],

$$1-F = \sum_{j=1}^{\nu} d_j \xi_j^2, \quad (2)$$

where $d_j \geq 0$ are nonnegative coefficients; $\xi_j \sim N(0,1)$, $j = 1,...,\nu$ are independent normally distributed random values with zero mean and unit variance; and $\nu = (2s-r)r-1$, where *r* is the rank of the mixture, *s* – dimension of the Hilbert space. The considered distribution is a natural generalization of the chi-square distribution.

For the parameter that characterizes the quality of a quantum measurement protocol, it is convenient to introduce a parameter (function of losses) that does not depend on the sample volume *n*,

$$L = n<1-F>= n\sum_{j=1}^{\nu} d_j. \quad (3)$$

The minimally possible (optimal) losses are given by the formula

$$L_{\min}^{opt} = \frac{\nu^2}{4(s-1)}. \quad (4)$$

Examples of applying the developed methods are presented for seven quantum protocols based on the geometry of polyhedra with a high degree of symmetry. Thus, the number of polyhedron faces defines the number of rows of the quantum measurement protocol and equals 4, 6, 8, 12, and 20 for the tetrahedron, cube, octahedron, dodecahedron, and icosahedron, respectively. For such polyhedra we chose a truncated icosahedron (that is form of fullerene) specifying a quantum measurement protocol of 32 rows and a polyhedron that is dual to a fullerene (that is pentakis dodecahedron) and specifies a quantum measurement protocol of 60 rows.

1. Yu.I. Bogdanov, I.D. Bukeev, and A K. Gavrichenko, “Studying Adequacy, Completeness, and Accuracy of Quantum Measurement Protocols”, Optics and Spectroscopy, **111**, pp.647–655, 2011.
2. M.A. Nielsen and I.L. Chuang. *Quantum Computation and Quantum Information.* Cambridge Univ. Press, Cambridge, 2000; Mir, Moscow, 2006.
3. Yu.I. Bogdanov, “Unified statistical method for reconstructing quantum states by purification”, JETP, **108**, p.928, 2009.

Polarization quantum operations in an anisotropic medium with dispersion

Yu.I. Bogdanov[1], A.A. Kalinkin[2,3], S.P. Kulik[4], E.V. Moreva[2,5], V.A. Shershulin[1,2,6]

1. Institute of Physics and Technology, Russian Academy of Sciences, 117218, Moscow, Russia
2. International Laser Center of Moscow State University, 119992, Moscow, Russia
3. Zavoisky Physical-Technical Institute, Russian Academy of Sciences, 420029, Kazan, Russia
4. Faculty of Physics, Moscow State University, 119992, Moscow, Russia
5. National Research Nuclear University "MEPHI", 115409, Moscow, Russia
6. National Research University of Electronic Technology MIET, 124498, Moscow, Russia

Based on the concept of χ-matrix and Choi-Jamiolkowski states we develop the approach of quantum process reconstruction. Special attention is paid to the adequacy of applied reconstruction models. The approach is applied to the statistical reconstruction of the polarization transformations in anisotropic and dispersive media realized by means of quartz plates and taking into account spectral shape of input states.

Experimental study of echo effect in polarization transformations of qubits

Yu. Bogdanov[1], A. Kalinkin[2,3], S. Kulik[4], E. Moreva[2,5], V. Shershulin[1,2,6]

1. Institute of Physics and Technology, Russian Academy of Sciences, Moscow, Russia. 2. International Laser Center of Moscow State University, Moscow, Russia. 3. Zavoisky Physical-Technical Institute, Russian Academy of Sciences, Kazan, Russia. 4. Faculty of Physics, Moscow State University, Moscow, Russia. 5. National Research Nuclear University "MEPHI", Moscow, Russia. 6. National Research University of Electronic Technology MIET, 124498, Moscow, Russia

The effect of light propagation in an anisotropic medium with dispersion is a close analog of the well-known effect of photon echo in optics, as well as the spin echo in nuclear magnetic resonance. This analogy is due to the coincidence between the evolution equations of the quasi-spin vectors of electromagnetic waves in an anisotropic medium with the Bloch equation for a spin in a magnetic field. In present work, we experimentally demonstrate the echo effect for polarization transformations qubits.

Mathematical modeling of polarization echo in optically anisotropic media

Yu.I. Bogdanov[1], A.A.Kalinkin[2,3], S.P.Kulik[4], E.V. Moreva[2,5], V.A.Shershulin[1,2,6], L.V. Belinsky[1,6]

1. Institute of Physics and Technology, Russian Academy of Sciences, 117218, Moscow, Russia. 2. International Laser Center of Moscow State University, 119992, Moscow, Russia. 3. Kazan Physical-Technical Institute, Russian Academy of Sciences, 420029, Kazan, Russia. 4. Faculty of Physics, Moscow State University, 119992, Moscow, Russia. 5. National Research Nuclear University "MEPHI", 115409, Moscow, Russia. 6. National Research University of Electronic Technology MIET, 124498, Moscow, Russia.

As optical systems are one of the candidates for implementation of a scalable quantum computer, it is important to develop an adequate method of description of both quantum states of light and operations performed by optical elements. Using the concept of chi-matrix representation of quantum operations and Choi-Jamiolkowski isomorphism we expand Jones calculus to allow description of evolution of mixed polarization states in linear optical systems. The developed method is then used to give a full description of polarization echo effect, which was described in [1] based on an analogy between the effects of polarization optics and spin dynamics. Theoretical predictions are confirmed by reconstructing operations performed by a series of quartz waveplates using quantum process tomography protocols. Potential use of polarization echo effect to strengthen BB84 quantum cryptography protocol is discussed.

1. V.S Zapasskii, G.G. Kozlov, “Bloch model of light polarization evolution in an anisotropic medium and polarization echo in optical waveguides”, Optics and Spectroscopy, **78**, pp.88-92, 1995.

Quantum interferometer with compressed coherent states

A. Karuzskii[1], A. Tskhovrebov[1], V. Prijmachenko[2], L. Zherikhina[1]
1. P.N. Lebedev Physical Institute of the RAS, Moscow 119991, Russia
2. Student of the Moscow Institute of Physical Engineering

The effect of quantum compression [1] is caused by a periodic change of nondissipative parameters of an oscillating system (modulation of capacity or inductivity of an electric *LC*-contour and correspondingly mass *M* or stiffness *K* of mechanical oscillator). The results of such influence happen to be periodic oscillations of middle square root deviations $\Delta X = \Delta X(t)$ and $\Delta P = \Delta P(t)$ of mutually complementary quantum mechanical variables ensuring the full description of the system. The middle square root deviations usually oscillate with double self frequency of the undisturbed system $\Omega_{mod} = 2\omega_0$ (where $\omega_0 = \sqrt{(L/C)}$ or $\omega_0 = \sqrt{(K/M)}$). It means that minimum values of quantum mechanical fluctuations amplitude $\Delta X(t_x) = \min\{\Delta X(t)\}$, $\Delta P(t_p) = min\{\Delta P(t)\}$ could not satisfy Heisenberg relationship $\Delta X \Delta P \geq \hbar/2$. It happens so that if one fixes variables at definite moments t_x, t_p, corresponding to the minimum of fluctuations amplitude $\Delta X(t_x)$ and $\Delta P(t_p)$, then precision of such strobe measuring can sufficiently exceed quantum restrictions $\Delta X(t_x) < \Delta X_{min} = \sqrt{(\hbar/(2M\omega_0))}$, $\Delta P(t_p) < \Delta P_{min} = \sqrt{(\hbar\omega_0 M/2)}$, where ΔX_{min} and ΔP_{min} are minimum indeterminatenesses in the absence of the compressing effect [2].

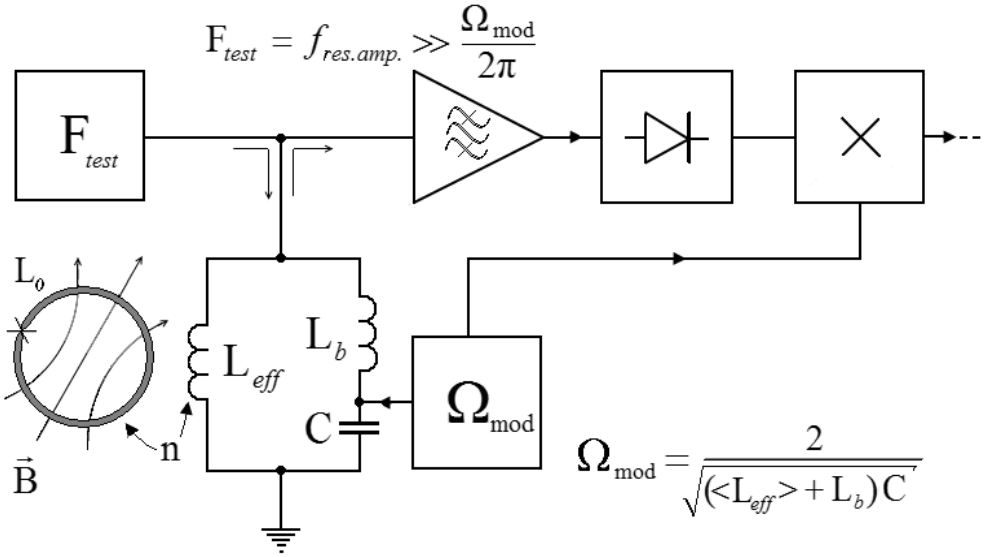

In the figure the block scheme of superconducting quantum interferometer is present where the regime of compressed coherent states could be realized. The cross on the circle defines Josephson junction included in the turn of nonhysteresis RF-SQUID [3]. The last is connected through the step-up transformer to the oscillatory contour consisted of inductivities ($L_{eff} + L_b$) and capacity *C*. The superconducting turn receiving measured magnetic flux serves as the primary winding of the transformer with the step-up coefficient equal to *n*. The generator (the square Ω_{mod}), providing the parametric pumping necessary to realize quantum compression, is adjusted to the frequency approximately equal to the doubled middle resonance frequency of the contour $\Omega_{mod} = 2\sqrt{(C(<L_{eff}> + L_b))}$. The blocking inductivity L_b is inserted in the contour to avoid a short circuit «to the ground» of the test signal $F_{test} >> \Omega_{mod}/2\pi$ through the capacity *C*. The measuring of the transformed value of Josephson inductivity $L_{eff} = n^2 L(\Phi_{ext})$ is performed through fixing the amplitude of F_{test} signal on the secondary winding of the transformer (square F_{test} is the generator of the test signal, triangle – the resonance amplifier, adjusted to F_{test}). After amplifying the F_{test} signal is detected and then with the help of synchronous detector the selection is made at the moments when the amplitudes of quantum fluctuations of the system are minimized due to quantum compression effect.

1. A. Pippard. *The Physics of Vibration*. Cambridge University Press, 2007.
2. Yu.I. Vorocov. Theory and methods of macroscopic measurements. Science, Moscow, 1989 (in Russian).
3. K.K. Likhirev, B.T. Ulrikh. The systems with Josephson contacts. Theory Basis. MGU, Moscow, 1978 (in Russian).

Tradeoff analysis of ballistic detector for Josephson qubits

N.V. Klenov, A.V. Sharafiev, V.K. Kornev
Physics Faculty, Moscow State University, Moscow, Russia, nvklenov@nm.ru

Ballistic detectors based on implementation of a pair of identical Josephson Transmission Lines (JTL) have been recently proposed to read out states of a superconducting quantum bit [1, 2]. One of the two JTLs is magnetically coupled with qubit and the other one is uncoupled. The detector and the JTL coupled with qubit are shown schematically in Fig. 1. In this circuit, driver of single flux quanta (SFQ) simultaneously triggers the quanta into each of the JTLs. The fluxon moving through the lines manifests itself by successive appearance of SFQ voltage pulses ($\int V dt = \Phi_0$, $\Phi_0 = h/2e$, h – the Planck's constant, e – the elementary charge) across Josephson junctions. When fluxon crosses the JTL cell coupled with qubit, it gains either

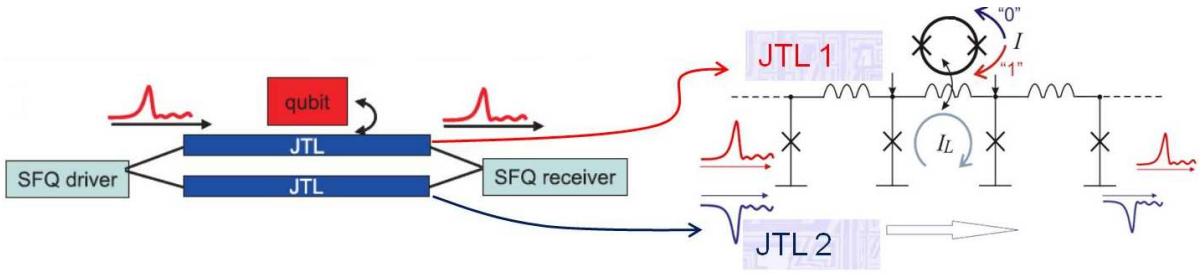

a *b*

Fig 1. (*a*) Principal scheme of a ballistic detector based on implementation of a pair of Josephson Transmission Lines (JTL) and (b) coupling between qubit and JTL.

acceleration or a delay in comparison to the fluxon in the reference JTL which is subject to the qubit state.

Informational approach considering decay of coherent state as an information flowing-out and the corresponding increase of Von Neumann entropy, is implemented to describe decoherence process during the read-out procedure [3]. One can express the entropy through a density matrix, and its evolution can be described by Lindblad equation. To simplify the problem solution and to get possibility of an analytical consideration, we use a reduced Lindblad equation taking into account only one-dimensional coupling to environment including readout device. Schematic illustration of the readout procedure is given in Fig. 2. Contradictory requirements to the procedure taking into account both the readout device influence on the coherent state decay and the desired increase in sensitivity of the ballistic detector, are discussed in detail.

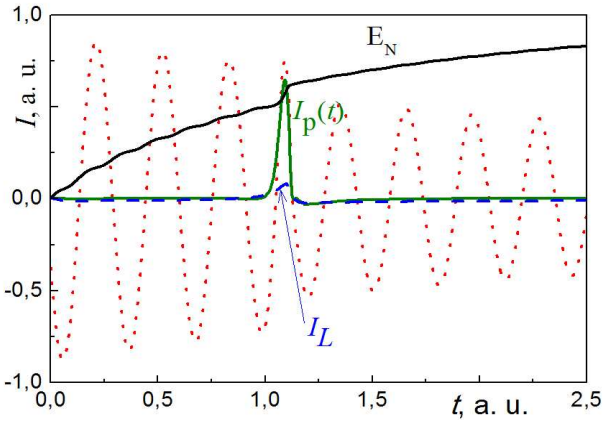

Fig 2. Illustration of the readout procedure: I_L is current in the JTL cell coupled with qubit, Ip is current induced in qubit, E_N is Von Neumann entropy; the dotted line shows Rabbi oscillations.

This work was supported in part by Russian Ministry of Science, Dynasty Foundation and RFBR grants 11-02-12065-ofi-m, 10-02-00870-a.

1. D.V. Averin, K. Rabenstein, V. K. Semenov, Phys. Rev. B, **73**, 094504, 2006.
2. A. Herr, A. Fedorov, A. Shnirman, E. Il'ichev, G. Schon, Supercond. Sci. Technol., **20**, S450–S454, 2007.
3. G. Lindblad, Commun. Math. Phys., **48**, pp.119-130, 1976.

Quantum error correction in Si double dot charge qubits

A. Melnikov[1,2], L. Fedichkin[1,2,3]

1. Institute of Physics and Technology, Russian Academy of Sciences, Moscow, Russia.

2. Moscow Institute of Physics and Technology, Dolgoprudny, Russia, leonid@phystech.edu.

3. NIX, Moscow, Russia, leonid@nix.ru.

We considered the interaction of semiconductor quantum register with noisy environment leading to various types of qubit errors [1]. In particular, we analyzed both phase and amplitude decays during the process of electron-phonon interaction. The performance of quantum error correction codes whose will be inevitably used in full scale quantum information processors was studied in realistic conditions in semiconductor nanostructures. As a hardware basis for quantum bit we chose the quantum spatial states of single electron in semiconductor coupled double quantum dot system [2]. The modified quantum error correction algorithms by Shor and Di Vincenzo without error syndrome extraction [3] were applied to quantum register composed of Si charge double dot qubits. 5- and 9-qubit error correction procedures were implemented for double dot qubits in the presence acoustic phonon environment.

Our results showed that the introduction of above quantum error correction techniques at small phonon noise levels provided quadratic improvement of output error rates. The efficiency of 5-qubits quantum error correction algorithm in semiconductor quantum information processors was demonstrated.

1. A.S. Holevo, *Probabilistic and Statistical Aspects of Quantum Theory*. North Holland, Amsterdam, 1982.

2. L. Fedichkin and A. Fedorov, Phys. Rev. A, **69**, 032311, 2004.

3. M.A. Nielsen and I.L. Chuang, *Quantum Computation and Quantum Information*. Cambridge University Press, Cambridge, 2004.

Could we believe that the moon is there?

A.V. Nikulov
Institute of Microelectronics Technology, Russian Academy of Sciences, 142432 Chernogolovka, Moscow District, Russia. E-mail: nikulov@iptm.ru

Most physicists believe that "*Quantum mechanics is the most accurate theory of modern physics*" [1] because of the progress connected with it. But as John Bell noted in his talk presented in 1984: "*This progress is made in spite of the fundamental obscurity in quantum mechanics*", see p. 169 in [2]. The fundamental obscurity is connected first of all with a vague concept of 'measurement' in quantum mechanics and the role of the mind of the observer in its description, see the Bell's paper "Against measurement", p. 213 in [2]. Because of the difficulties of realistic description of some quantum phenomena "*and influenced by positivistic and instrumentalist philosophies*" the creators of the orthodox quantum mechanics have admitted "*that atomic and subatomic particles do not have any definite properties in advance of observation*" p. 142 in [2]. Recently this scepticism about realism was expanded to macroscopic level [3]. The authors [3] quoting the known remark by Albert Einstein "*I like to think that the moon is there even if I don't look at it*" claims that some experimental results obtained on superconducting circuit [4] could refute this trust by Einstein in objective reality even on the macroscopic level. This scandalized claim bears a direct relation to the problem of a possibility of superconducting quantum bits. A small moon, which is not there according to [3], is a magnetic flux inside a superconducting loop [5] which is considered as flux qubit in numerous publications [6] including the one [7] of the author of the scandalized claim [3].

J.E. Mooij believes paradoxically that quantum mechanics can prove that nothing is there [3] but it is possible to create anything, superconducting quantum bits [7] for example, using this nothing. Ironically, quantum bits can be created indeed only if quantum systems *do not have any definite properties in advance of observation.* In this case definite properties should appear under influence of the mind of the observer. Therefore the creators of quantum mechanics, Heisenberg, Dirac, Pauli, von Neumann and other admitted that 'measurement' might be complete only in the mind of the observer. If definite properties, described any variables even hidden, exist in advance of observation than quantum bits are not possible. Thus, quantum bits can not be possible outside the mind of the observer, according to the orthodox quantum mechanics.

Only basis both of the doubt in macroscopic reality [3] and superconducting quantum bits [1,6,7] is the Leggett–Garg inequality referred to as a Bell's inequality in time [3,4]. It will be shown in the present work that the no-go theorem [8] by A.J. Leggett and A. Garg [5] is false at least because of three reasons: 1) there is not a well-grounded motive to call macroscopic realism in question; 2) the authors [5] repeat virtually the mistake [8] of the von Neumann's no-hidden-variables proof; 3) the assumption on superposition [5] contradicts to the fundamental law of angular momentum conservation. Therefore we can believe for the time being in reality of the moon, even small, and can not believe in a possibility of superconducting quantum bits.

1. A. Bezryadin, "Tunnelling across a nanowire", Nature, **484**, pp.324-325, 2012.
2. J.S. Bell, *Speakable and Unspeakable in Quantum Mechanics. Collected Papers on Quantum Philosophy*. Cambridge University Press, Cambridge, 2004.
3. J.E. Mooij, "Quantum Mechanics. No Moon there", Nature Physics **6**, pp.401-402, 2010.
4. A. Palacios-Laloy, F. Mallet, F. Nguyen, P. Bertet, D. Vion, D. Esteve, and A.N. Korotkov, "Experimental violation of a Bell's inequality in time with weak measurement", Nature Physics **6**, pp.442–447, 2010.
5. A.J. Leggett and A. Garg, "Quantum mechanics versus macroscopic realism: Is the flux there when nobody looks?" Phys. Rev. Lett. **54**, pp.857-860, 1985.
6. J. Clarke and F.K. Wilhelm, "Superconducting quantum bits", Nature **453**, pp.1031–1042, 2008.
7. I. Chiorescu, Y. Nakamura, C.J.P.M. Harmans, J.E. Mooij, "Coherent Quantum Dynamics of a Superconducting Flux Qubit", Science **299**, pp.1869–1871, 2003.
8. N.D. Mermin, "Hidden variables and the two theorems of John Bell," Rev. Mod. Phys. **65**, pp.803-815, 1993.

Measurement of charge and spin qubits in a transistor channel

M. Rudenko, V. Vyurkov, S. Filippov, A. Orlikovsky
Institute of Physics and Technology, Russian Academy of Sciences, Moscow, Russia, vyurkov@ftian.ru

Recently, a novel implementation of a solid-state quantum computer based on field-defined quantum dots in an ultrathin silicon bar was proposed [1] (Fig. 1). The quantum information can be encoded and processed in either spin or space degrees of freedom. The construction follows a natural way of nanoelectronics. Scalability is audible and it opens up a possibility of large-scale quantum computer.

Quantum algorithms could be effectuated via manipulation with gate potentials. After that the read-out could be performed via a transmission of current through the channel also operated by gate potentials. Worth noting during quantum computation the current is switched off and has no influence on a qubit evolution.

We propose a regime of Coulomb blockade for measurement of charge qubits and, respectively, a regime of spin blockade for measurement of spin qubits. In the present communication the most attention is paid to charge states, since they can be controlled by electrical pulses solely: initialization, one- and two-qubit operations, read-out. Charge qubits are based on double quantum dots (DQDs) with a single electron and the measurement must reveal which quantum dot is occupied by the electron. All quantum dots in the chain, but the measured one, are 'deepened' by positive potentials applied to corresponding gates. Those dots create potential wells for electrons moving through the channel. When the measured dot is empty there is a well (Fig. 2A); when an electron inhabits the dot there is a barrier (Fig. 2B). From classical point of view that kind of measurement is absolutely exact. The quantum situation is different. The quantum reflection from potential wells much matters. The potential profile in the channel should be fairly smooth to diminish quantum reflection. The thorough optimization of the structure based on simulation is required to make it possible to measure lots of qubits in the channel. The simulation is guided by the quantum ballistic approach of Landauer-Buttiker to calculate a current in field-effect transistors.

It is important that the measurements are necessary not only on the stage of read-out. They are also required before a quantum computer is run. One needs to adjust qubits because of their indispensable technological variability and stray charges in the structure.

A measurement of spin states of electrons in quantum dots (or impurity atoms) seems also plausible. In the case the spin-polarized current should be transmitted through the channel. The exchange interaction of moving electrons with the electron in a dot ensures sensitivity to its spin state. It turned out that quantum dots could be specially designed to make the strength of exchange interaction comparable with that of direct Coulomb interaction. Spin blockade of current turns thus feasible.

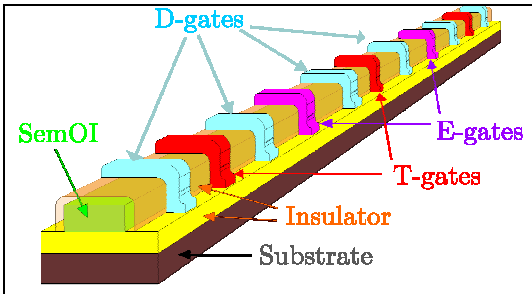

Fig. 1. Qubits in a transistor channel.

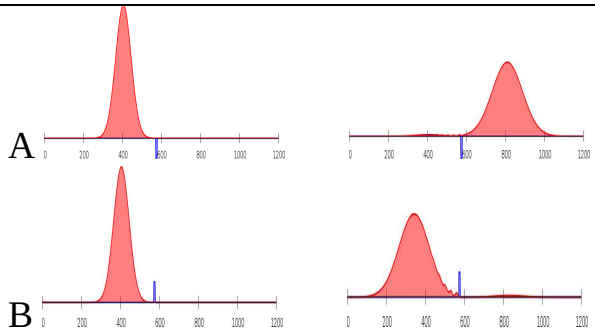

Fig.2. A: transmission of the wave packet through the empty QD; B: reflection from the occupied QD.

The work was supported via the grant # 07.524.12.4019 of the Ministry of Education and Science of the Russian Federation

1. S. Filippov, V. Vyurkov, and A. Orlikovsky, Proc. EUROSOI-2011, Granada, Spain, pp.101-102, 2011.

Atomic force microscopy studies of ferroelectric and electrical properties in epitaxial $BaTiO_3$/Pt heterostructures

A. Baturin[1], A. Chouprik[1], K. Bulakh[1], A. Kuzin[1], A. Zenkevich[2], M. Minnekaev[2]

1. Moscow Institute of Physics and Technology, Dolgoprudny, Russia, kvant755@gmail.com 2. National Research Nuclear University "Moscow Engineering Physiics Institute", Moscow, Russia, avzenkevich@mephi.ru

Using ultrathin ferroelectric (FE) films separating two different metal (Me) electrodes opens up new vistas for creating new type of non-volatile memory based on tunneling electroresistance effect (TER), when electrical resistance strongly depends on the orientation of the electric polarization in FE thin film [1,2]. In this work, epitaxial $BaTiO_3$ (4 nm)/Pt (10 nm) heterostructure grown on MgO (100) substrate by pulsed laser deposition [3] with top Cr electrodes is investigated. Top Cr electrodes are deposited by electron beam physical vapor deposition (EBPVD) through shadow mask of thickness 100 nm with 800 nm diameter holes. The ferroelectricity of ultrathin epitaxial $BaTiO_3$ film is confirmed by hysteresis and butterfly loop measurements. The coercive field $E_{coer} \approx -8400\,\mathrm{kV/cm}$ and $E_{coer} \approx 4000\,\mathrm{kV/cm}$ is calculated from hysteresis loop. TER effect reaching 10 for 4 nm $BaTiO_3$ barrier is obtained from *I-V* characteristics for generated antiparallel domains. Current density for low resistance state is $j \approx 2.5\,\mathrm{mA/cm^2}$.

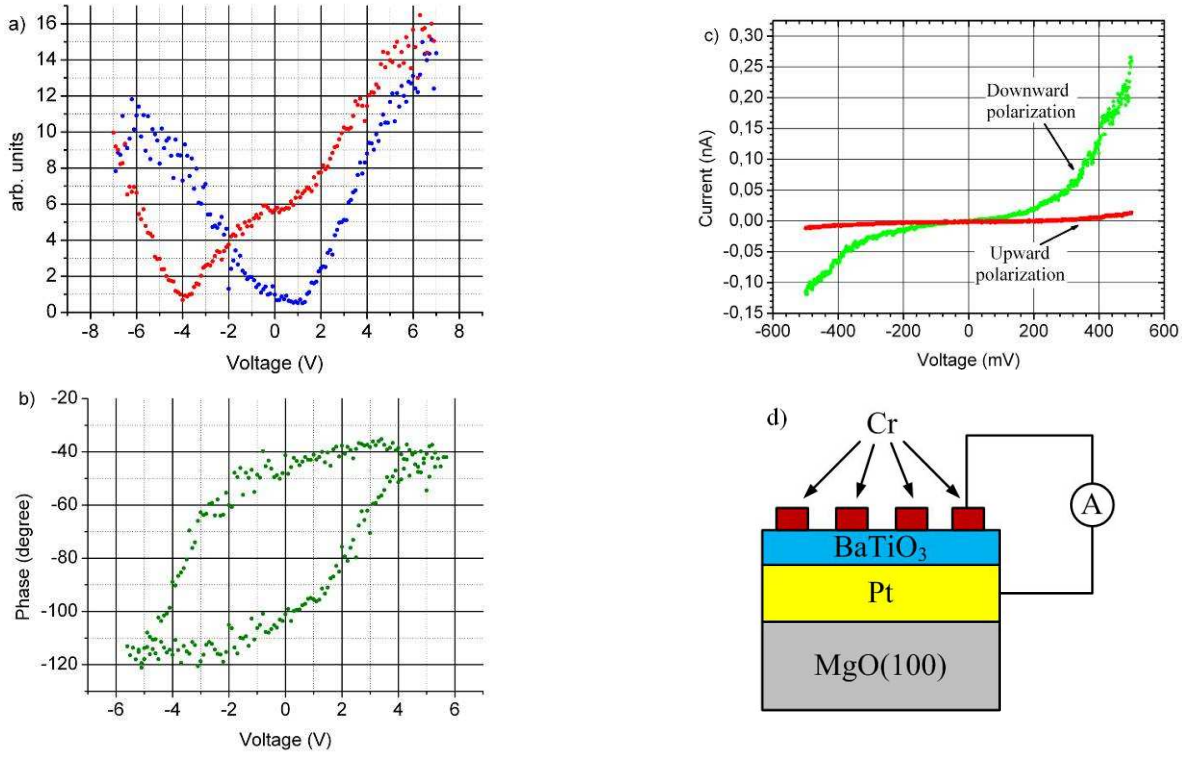

Fig. 1. a) Experimental local butterfly loop measured in 4 nm thick $BaTiO_3$ film; b) Experimental local hysteresis loop measured in 4 nm thick $BaTiO_3$ film; c) Experimental *I-V* characteristics recorded on the Au/Cr/$BaTiO_3$ (4 nm)/Pt tunnel junctions for opposite polarization orientations; d) Sketch illustrating the geometry of the experiment for AFM studies of ultrathin $BaTiO_3$ film.

1. M.Ye. Zhuravlev et al., "Giant Electroresistance in Ferroelectric Tunnel Junctions", Phys. Rev. Lett., **94**, 246802, 2005.

2. A. Gruverman et al., "Tunneling Electroresistance Effect in Ferroelectric Tunnel Junctions at the Nanoscale", Nano Lett., **9**, pp.3539-3543, 2009.

3. A. Zenkevich et al., "Pulsed laser deposition of ultrathin $BaTiO_3$/Fe bi-layers: structural characterization and piezoelectric response", Thin Solid Films, **520**, pp.4586-4589, 2012.

Formation of Ag clusters for resistive memory cells from thin film

A. Belov[1], D. Gromov[1], O. Pyatilova[1], O. Sakharov[2], A. Trifonov[2]
1. National Research University of Electronic Technology MIET, Moscow, Russia; e-mail: netadm@miee.ru
2. Scientific Research Institute of Physical Problems named after F.V.Lukin, Moscow, Russia; e-mail: admin@niifp.ru

In recent years, development of nanodevices based on separate molecules and atoms is of great interest. Much attention is given to nonvolatile memory cells with low power consumption and high memory volumes which will enable the replacement of known memory types. Development of periodical nanoparticles metal/Ag chalcogenide/Ag formation methods is a topical problem, because it forms a basis of nonvolatile memory cell creation. This structure includes silver cluster and chalcogenide glass which works as an electrolyte and is able to conduct silver ions. Resistive memory is characterized by high-speed performance, can be realized with very high density, has long life time and is easy to produce.

The aim of this work is to create an array of Ag nanoclusters which could be a basis of resistive memory cell creation. Heating of the thin films up to disintegration temperature is known as one of Ag clusters creation methods. Therefore, in order to develop the idea of nanocluster array creation process as a result of film disintegration to drops, the evolution of thin Ag films with various thicknesses deposited on SiO_2 surface during heating in vacuum was investigated. The samples were studied using FEI Tecnai 20 S-Twin transmission electron microscope (TEM).

Investigation of cluster size distribution has shown that for film thickness range from 12 to 130 nm there are two most preferable cluster sizes. The first one corresponds to diameter value from 40 to 80 nm, and the second is around 400 nm in diameter. For films in that thickness range the duration of the annealing has a remarkable influence on the evolution of cluster array due to the presence of two simultaneously ongoing processes:

- **Coalescence**: enlargement of the cluster size takes place (in some cases up to several micrometers) and the distance between them increases.
- **Evaporation**: the film is almost completely evaporated within 120 minutes of annealing.

The behavior in the disintegration process of the film with a thickness of 6 nm is quite different. The study of samples with different duration of annealing has demonstrated that practically no changing of cluster array was observed, and there was only one predominant size of 15 nm. One of such a film was annealed in hydrogen sulfide atmosphere during 12 hours. As a consequence the electron diffraction pattern of clusters has changed.

As a result the correlation of clusters parameters with the parameters of the process (temperature, annealing time) and initial film thickness have been identified. It is shown that during the disintegration of the films with a thickness from 20 to 130 nm two processes predominate: evaporation and coalescence. These processes are the cause of the presence of two preferred cluster sizes:

- Small-sized clusters. They can be called **mono-clusters**, that is, composed of a single nanocrystal.
- Large size clusters are **globular**, that is, consisting of the union of nanocrystals.

In the process of disintegration of the film 6 nm thick, these processes are hardly noticeable, therefore only mono-clusters are formed on the surface.

Memory cells on the basis of metal-insulator-semiconductor of structure with multilayer dielectric with same nanometer layers

A.E. Berdnikov, A.A. Popov, A.A. Mironenko, V.D. Chernomordick, A.V. Perminov
Yaroslavl Branch of Institute of Physics & Technology of Russian Academy of Sciences, 150007, Russia
e-mail: imiraslab4@yandex.ru

In multilayer dielectrics with nanometre layers tunnelling of a charge carriers on the built-in layers and preservation of this charge are possible. It allows creating various types of cells of non-volatile memory. The classical technology provides formation of MIS transistor with such dielectric. That (flash memory) is widely used in practice. The big relative square (7-8 of square of minimal topology size) at one memory cell is a main negative feature of such cell design. However other options of a memory cell design, allowing receiving a cross-bar topology of a memory device are possible also. The smaller area (approx. 5 of square of minimal topology size) needed from one bit of memory is a main advantages of such topology.

Properties of silicon oxide films with incorporated layers of silicon nitride with total thickness of 40-90 nanometers were studied. For this purpose metal – insulator – semiconductor (MIS) structures were made. All dielectric materials were produced by low frequency plasma enhanced chemical vapor deposition (LF PECVD). This method provides existence of silicon clusters in dielectric. Clusters appear as a result of gas phase polymerisation of silane radicals, and build-in deposited material. Materials differed also non-stoichiometric degree in various experimental samples. Surplus of silicon agglomerates in a separate phase as a nanosize clusters.

The research of current-voltage plot showed that such samples have effect of bipolar switching of conductivity. It is possible to assume that as a result of soft breakdown the conductivity channel between metal and the semiconductor formed. Conductivity in which controlled by charges deposited in nitride layers. It allows using MIS structure for creation of a cell of memory and a memory device on its basis. Technological parameters of layers deposition and a design of a memory cell were optimised. The memory design with cross-bar topology was developed. The prototype was made.

Research of such structures voltage-capacitance characteristic showed anti-hysteresis existence, see.fig.1. The word "hysteresis" means a delay, in our case we observe an advancing. Because it we use a word an "anti-hysteresis". The anti-hysteresis can deposit at zero bias voltage in case of correct MIS material combination. Thus MIS capacity will depend on background of voltage submitted on structure. It means that such structure can be used as a memory cell which conditions differ in capacity. The memory on their basis can have topology a cross-bar. Conductivity of such structures at direct voltage is equal to zero. Therefore reading of a condition is possible without snake-effect.

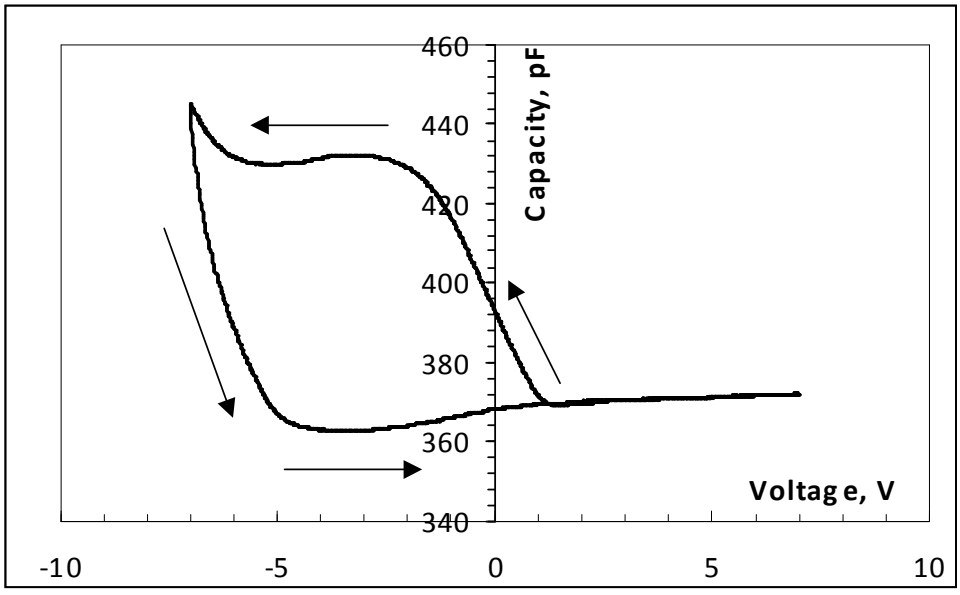

Fig.1. Voltage – capacitance plot of MIS structure with 5-layer insulator, aluminum metal and p-type of silicon semiconductor.

A resistive switching effect with memristive behavior in $Hf_xAl_{1-x}O_y$ layers grown by atomic layer deposition

A.A. Chouprik[1], K.V. Egorov[1], I.P. Grigal[1], Yu.Yu. Lebedinskii[2], A.M. Markeev[1], A.V. Zenkevich[2]

1. *Moscow Institute of Physics and Technology, Dolgoprudny, Russia, chouprik@mail.ru*
2. *NRNU Moscow Engineering Physics Institute, Moscow, Russia*

The phenomenon of memristive resistance switching (RS) in thin film devices is currently a focus of research for developing a high density non-volatile universal memory as well as computational functionality beyond CMOS technology (programmable logic, signal processing, neural networks). The simple structure of thin film memristor and the implementation of hafnium oxide in contemporary CMOS technology both facilitate the successful integration of hafnium oxide based memristors in the future technology. It is known that the resistivity in transition metal oxide layers embedded between metal layers in metal-insulator-metal stack changes following the drift of oxygen ions/vacancies in the sufficiently large electrical field. Therefore, the key to increase the memristive RS effect is to find methods enabling to change reproducibly and reversibly the concentration of oxygen vacancies in a dielectric layer. The formation energy of oxygen vacancies in HfO_2 is known to decrease once the 3^+ dopant is added (e.g. Al) [1]. In this work, we study the RS effect in $Hf_xAl_{1-x}O_y$ dielectrics with Al content in the wide range.

Single HfO_2 layer, $HfO_2/Hf_xAl_{1-x}O_y$ bilayer with the selected Al content in $Hf_xAl_{1-x}O_y$ layer and the "graded" $Hf_xAl_{1-x}O_y$ layers with the wedge Al depth profile varying in the range x=0.2-0.9 were grown by atomic layer deposition (ALD). The overall thickness of all dielectric films was ~ 6 nm. ALD was carried out at T=240°C using $Hf[N(CH_3)(C_2H_5)]_4$, $Al(CH_3)_3$ and H_2O precursors for Hf, Al and O constituents, respectively. Pd, TiN, Ti, Pt were used as electrodes. The composition, chemical, structural and electrical properties of as-grown films were studied using Rutherford backscattering spectrometry, X-ray photoelectron spectroscopy (XPS), X-ray diffractometry and *I-V* measurements, respectively.

According to the electrical measurements, unstable RS effect was found in $TiN/HfO_2/Pt$ structure. Instead, $HfO_2/Hf_xAl_{1-x}O_y$ bilayered structure and "graded" $Hf_xAl_{1-x}O_y$ exhibited the memristive (multilevel) RS behavior. "Graded" $Hf_xAl_{1-x}O_y$ based structure demonstrated the most stable RS effect with more than 8 resistance states and the highest/lowest resistance state ratio R_{OFF}/R_{ON} ~ 15 (Figs. 1-2). XPS analysis revealed the generation of the dipole at the Pt^-/HfO_2^+ interface caused by the drift of oxygen vacancies in HfO_2 towards the interface.

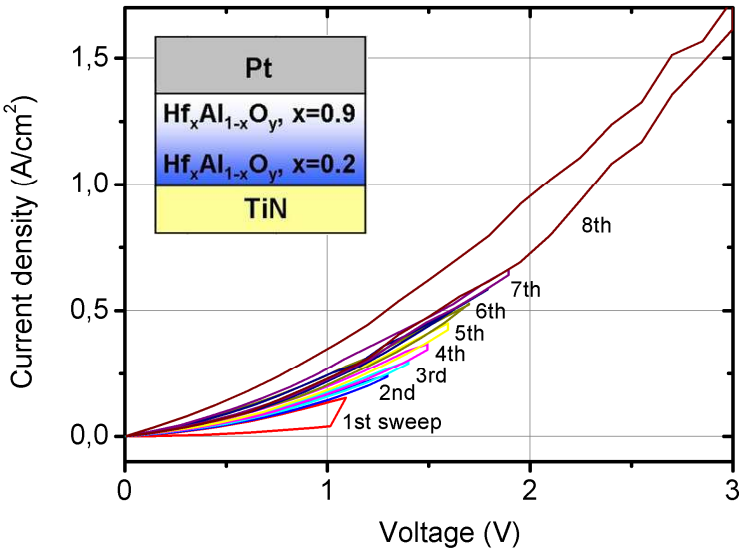

Fig. 1. Typical J-V characteristics of the structure $TiN/Hf_xAl_{1-x}O_y/Pt$ (x = 0.2-0.9), that reveals RS effect with memristive behavior

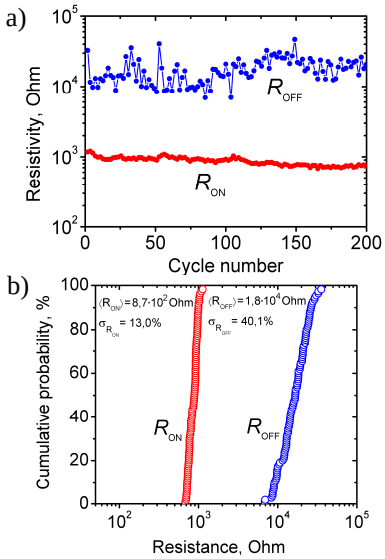

Fig. 2. Endurance properties (a) and statistical distribution of resistances (b) for the "graded" $TiN/Hf_xAl_{1-x}O_y/Pt$ (x = 0.2-0.9) structure

1. H.W. Zhang, B. Gao, S. Yu et al., "Effect of ionic doping on the behaviors of oxygen vacancies in HfO_2 and ZrO_2: A first principles study", IEEE, p.155, 2009.

Atomic layer deposition of $Hf_xAl_{1-x}O_y$ dielectric layers for memory devices

I.P. Grigal[1], A.A. Chouprik[1], K.V. Egorov[1], Yu.Yu. Lebedinskii[2], A.M. Markeev[1]

1. *Moscow Institute of Physics and Technology, Dolgoprudny, Russia, irina.grigal@gmail.com*
2. *NRNU Moscow Engineering Physics Institute, Moscow, Russia*

Transition metal oxides like Hf-based oxide attract much attention as a promising dielectric for logic and memory devices. Moreover Hf-oxide based resistive random access memory is one of the most promising candidates for future universal information storage applications due to its nonvolatility, simple structure, scalability, high speed (~1 ns) and low energy consumption (< 1 pJ) [1]. Defects like oxygen vacancies influence on dielectric properties. Meanwhile DFT calculation showed Al doping of HfO_2 decreases the oxygen vacancy formation energy [2]. However the mechanisms of resistive switching (RS) are not clear enough. Thermochemical processes during switching between low resistance and high resistance states can play an important role. In this study the influence of the mentioned processes are modeled by rapid thermal annealing. Thus this work is aimed at the structural and electrical properties investigations of as deposited and annealed $Hf_xAl_{1-x}O_y$ thin films grown by atomic layer deposition.

$Hf_xAl_{1-x}O_y$ thin films were deposited by atomic layer deposition using $Al(CH_3)_3$, $Hf[N(CH_3)_3(C_2H_5)]_4$ and H_2O at 240 °C on Si, TiN/Si and Pt/Si substrates. The composition of the Hf-aluminate was controlled by varying the ratio of cycles between the HfO_2 and Al_2O_3 reactants. The films thicknesses were varied from 4 to 25 nm. Part of the samples were annealed in N_2 atmosphere at T=700 °C for 5s.

The chemical, structural and electrical properties were studied using X-ray photoelectron spectrometry (XPS), Rutherford backscattering spectrometry (RBS), grazing incidence X-ray diffractometry (XRD), X-ray reflectometry, C-V and I-V measurements.

According to RBS and XPS measurements $Hf_xAl_{1-x}O_y$ films exhibit Hf-Al compositions in a wide range of x=0.2-1 depending on HfO_2/Al_2O_3 cycles ratio. The rapid thermal annealing led to $Hf_xAl_{1-x}O_y$ crystallized in metastable orthorhombic structure instead of monoclinic structure in pure HfO_2 (Fig. 1). The appearance of orthorhombic phase during annealing can be related to an oxygen deficit in $Hf_xAl_{1-x}O_y$ films [3]. Moreover electrical measurements of MIM-stack showed that $Hf_xAl_{1-x}O_y$ revealed more stable resistive switching effect in comparing with HfO_2. According to XPS investigations Hf3d and O1s lines in low resistance state shifted on 0.9eV compared with Pt4f line (Fig. 2). The shift can be due to the oxygen vacancies level increase in $Hf_xAl_{1-x}O_y$ dielectric what can confirm formation of oxygen deficient orthorhombic phase during RS.

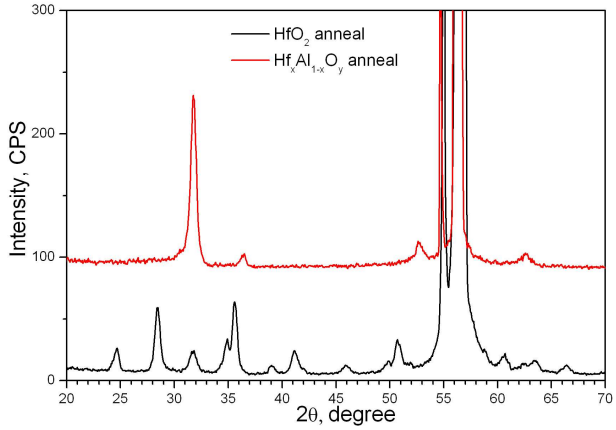

Fig. 1. XRD of HfO_2 (black line) and $Hf_{0.7}Al_{0.3}O_y$ (red line) annealed thin films.

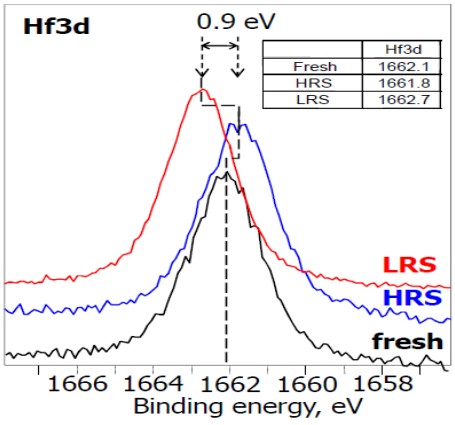

Fig. 2. XPS of $Pt/HfO_2/Hf_{0.7}Al_{0.3}O_y/TiN$ structure in different states: red – low resistance, blue – high resistance, black – fresh structure.

1. F.T.Chen et al., "Resistance switching for RRAM applications", Sci China Inf Sci, **54**, pp.1073-1086, 2011.

2. H.W. Zhang et al., "Effect of ionic doping on the behaviors of oxygen vacancies in HfO_2 and ZrO_2: A first principles study", IEEE, p.155, 2009.

3. C. Weimer et al., "Evolution of crystallographic ordering in $Hf_{1-x}Al_xO_y$ high-k dielectric deposited by atomic layer deposition", Appl. Phys. Lett., **83**, pp.5271-5273, 2003.

Influence of heating on electrical properties and morphology of indium-doped $Ge_2Sb_2Te_5$ thin films for phase change memory devices

P. Lazarenko[1], S. Kozuykhin[2], A. Sherchenkov[1], A. Babich[1], A. Vargunin[2], O. Pyatilova[1]
1. National Research University of Electronic Technology, Moscow, Russia, netadm@miee.ru. 2. Kurnakov Institute of General and Inorganic Chemistry, Russian Academy of Sciences, Moscow, Russia info@igic.ras.ru

In the last decade, thin films of $Ge_2Sb_2Te_5$ (GST225) are intensively studied due to their possible applications in devices of phase change memory (PCM), particularly in nonvolatile memory cells of PCRAM type. Variation and optimization of the properties of materials used in phase-change memory cells are possible by doping and modification of the structural matrix. It was reported that In-doping effectively influences the kinetics of crystallization of $Ge_2Sb_2Te_5$, which determine operation speed, and can be useful in solving a problem of compromise between crystallization rate and archival lifetime of the recording materials [1]. However, questions of the influence of In-doping on the properties and stability of $Ge_2Sb_2Te_5$ are not well understood yet. The principle of phase-change memory devices is based on thermally induced reversible transformation between amorphous and crystalline phases. It is well known that the crystallization of PCM is accompanied by a large density change [1]. In this case, volume change of the PCM material can lead to the degradation of contacts between GST225 and the electrodes, which will initiate reliability issue of PCRAM devices. So, in this study we investigated the influence of heating on electrical properties and morphology of In-doped $Ge_2Sb_2Te_5$ thin films.

The initially doped $Ge_2Sb_2Te_5$ alloys with different amounts of In (0, 0.5, 1 and 3 wt.%) were prepared using quenching technique. The amorphous thin films were deposited by the thermal evaporation in vacuum. Planar structures containing Al electrodes with fixed inter electrode distances (1, 5, 10 μm), and deposited upon them GST thin film were fabricated on oxidized c-Si substrates. The temperature of the samples during the measurements was varied from room temperature to 350 °C with the heating rate of 1 °C/min. The thicknesses of the films were determined with using of AFM (NT-MDT SolverPro), which were in the range from 50 to 80 nm. The morphology of the thin films was studied by SEM (Carl-Zeiss NVision 40) and AFM. The chemical compositions of the films were determined by X-ray fluorescence analysis (XRF).

The temperature dependences of resistivity were measured for $Ge_2Sb_2Te_5$ and In-doped $Ge_2Sb_2Te_5$. Exponential temperature dependences of resistivity were established for the investigated thin films in the range from room temperature to 120 °C, which are typical for the amorphous chalcogenide glassy semiconductors (CGS).The obtained data showed that incorporation of a small amount of indium into GST225 material (up to 1 wt. %) led to the increase of the activation energies conductivity and resistivity of amorphous thin films (0,29 eV, $1{,}5\cdot10^4$ Ω·cm for undoped GST225, and 0.35 eV, $2{,}4\cdot10^5$ Ω·cm for GST225 with 1 wt. %, respectively). At the same time the addition of 3 wt. % In is accompanied by the decrease of the activation energy and resistivity (0,31 eV, $9{,}3\cdot10^4$·cm, respectively, for GST225 with 3 wt. %). The deviation from the trends for the dependencies of electrical properties on the dopant concentration with the high dopant content might be associated with phase separation.

Sharp drops in resistivity for all investigated material were observed in the range from 130 to 170 °C, which corresponded to a phase transformation from amorphous to crystalline state. The value of resistivity drop $\rho_{аморф}/\rho_{крист}$ increased with the increase of In content. In addition, incorporation of In in $Ge_2Sb_2Te_5$ shifts the phase transition temperature range from amorphous to crystalline state to the higher values (132-141 °C for undoped GST225, and 140-166 °C for GST225 with 3 wt. % In), which can be attributed to the change in the energy bonding and local chemical order.

Further heating above the transformation temperature revealed increased resistivity values with unsystematic changes within the orders of magnitude for all measured samples. According to SEM heat treatment up to the temperature of 350 °C leads to the formation of large number of cracks, discontinuity areas, as well as the flaking of the CGS film away from the electrode contact boundaries. This effect was eliminated with the help of a SiO_2 covering thin films with 0.5 μm thickness deposition by electron-beam evaporation on the top of CGS film.

This work was supported by Ministry of Education and Science of RF (projects P847 from 25/05/2010 and № 16.552.11.7033 from 29/04/2011), RFBR (11-03-00269) and FASIE (project № 169867).

1. Ting Zhang, Zhitang Song, Bo Liu and Songlin Feng, Semicond. Sci. Technol. **23,** 055010, 2008.

Effect of the moist porous silicon oxide layer on the electrical characteristics of memory cells

V. Levin, V. Mordvintsev, S. Kudryavtsev
Yaroslavl Branch of the Institute of Physics and Technology, Russian Academy of Sciences, Yaroslavl, Russia, E-mail: el-bek@yandex.ru

Usually the washing operations in deionized water can solve the contamination problem, but the water molecules can be contaminating impurity, as it happened in our case. The memory element on self-forming nanostructures (MESN) [1], in a simplified design fig.1, is a plane-parallel capacitor system - "sandwich" structure consisting of two electrodes separated by a dielectric. The dielectric film is thin (tens of nanometers) to provide sufficient intensity for field emission in the insulating slit at low supplied voltages (5÷15V). In MESN the silicon dioxide (SiO_2) as a dielectric is used, which is a good insulator and has convenient functional properties as a storage medium, it is effortless to electroforming [1]. In our experiments, we used thermal oxidation of silicon and plasma-chemical deposition of SiO_2. In forming the butt-end of a thin dielectric insulating slit is particularly important etching operation, as the butt-end surface state effects significantly to the reliability of the MESN. Therefore, before the electroforming operation and after the removal of the protective film of photoresist, it was decided to subject the open housings with chips to boiling in deionized water for further cleaning of the open butt-ends of the dielectric from the possible ionic contamination. The quality of the obtained structures of the dielectric and electrical properties of the insulating slit has been tested.

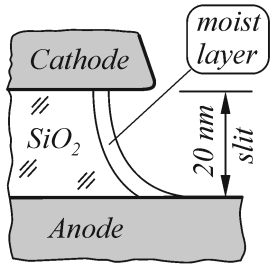

fig. 1

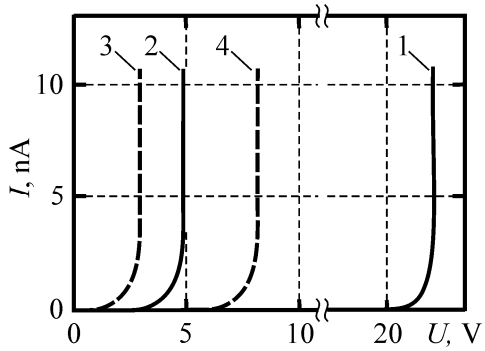

fig. 2

The experimental current-voltage characteristics (*I-U*) of structures with a thickness of silicon dioxide about 20 nm are shown in fig.2. For the closed structure, i.e. capacitor with a continuous film of SiO_2, the typical form of *I-U* are presented by curve 1 where a visible current appear when the voltage applied to the structure is more than 21 V only, which is typical for high-quality films of SiO_2. The curve 2 represents *I-U* of the opened structure, i.e. in which the butt-end of SiO_2 is formed by wet etching in the film of the same quality. After treatment in boiling water, it was found that for the structure with thermal silicon dioxide *I-U* shifted toward lower values - curve 3 and for the structure with the plasma-chemical silicon dioxide *I-U* shifted toward higher values - curve 4.

To explain this behavior of *I-U*, we used the effective medium theory formulas [2] and the numerical simulation of electric fields in MESN. The plasma-chemical oxide has a higher porosity that is indirectly confirmed by a comparatively higher rate of its etching due to rapid penetration of etchant into the pores. The increased porosity leads to the water penetration after boiling deep into the pores and can persist long in them. As the basis of the simulation model the assumption is taken that the thin surface layer of the *butt-end* of the oxide in the slit can be represented as a matrix mix - nanoparticles of water with the relative permittivity $\varepsilon = 81$ in SiO_2 - matrix with $\varepsilon = 3.8$.

The results of numerical simulations show that the increasing of the effective dielectric constant of the layer leads to a redistribution of the field in the slit, so the conditions for emission of electrons from the cathode is impaired, the breakdown probability of the dielectric near the anode increases and in consequence of this the stability of the electroforming process is reduced. In addition, it is founded that the deviations of the field intensity calculated for our model have extremes depending on the depth of moist layer.

1. V.M. Mordvintsev, S.E. Kudryavtsev, V.L. Levin, Nanotechnologies in Russia, Vol. 4, N 1-2, p.121, 2009.
2. Z. Hashin, S. Shtrikman, J. Appl. Phys., Vol. 33, p.3125, 1962.

Influence of thermocycling on the properties of Ge-Te system materials for application in nanoscale phase change memory cells

A. Sherchenkov[1], S. Kozyukhin[2], M. Michailova[1], A. Babich[1], P. Lazarenko[1]
1. National Research University of Electronic Technology. 2. Kurnakov Institute of General and Inorganic Chemistry of the Russian Academy of Sciences

Phase-change memory devices are actively developed now. Promising materials for this type of memory are compositions in ternary system Ge-Sb-Te. The most perspective is considered to be $Ge_2Sb_2Te_5$. However, some aspects of these materials are not yet studied, which does not allow fully realize the potential of phase change memory devices. We have previously shown that during repeated heat treatment of such materials the endothermic peak in the temperature range from 390 to 415°C may appear [1]. The study of the processes, which leads to the appearance of this peak, is very important because they may initiate reliability issue of the phase change memory cells. The origin of this peak may be caused by the phase separation during repeated heat treatments due to the diffusion of mobile Te atoms to the grain boundaries leading to strong heterogeneity of the composition. This is confirmed by X-ray diffraction analysis. The analysis of phase diagram showed that the most probable reason for the appearance of this endopeak is a local melting of the eutectic composition (Te+GeTe) in the system Ge-Te. However, referred data on the composition and melting temperature of the eutectic are contradictory. In addition, there is almost no information on its behavior during repeated heat treatments, which accompanies the processes of recording/erasure in phase change memory cells. Therefore, the aim of this work was to investigate thermal characteristics and behavior of the compositions close to the eutectic in the system Ge-Te by the multiple DSC measurements.

The synthesis of materials was carried out in evacuated sealed quartz ampoules at 850°C for 10 h, and 5 different compositions ($Ge_{13}Te_{87}$, $Ge_{14}Te_{86}$, $Ge_{15}Te_{85}$, $Ge_{16}Te_{84}$, $Ge_{17}Te_{83}$) were obtained.

The thermal behavior was investigated with using of differential scanning calorimeter DSC-50 (Shimadzu). Samples were heated with the rate of 10 K/min in the nitrogen atmosphere from room temperature to 470°C. Empty Al pans were used as references. The phase composition of the materials was investigated with using of X-ray diffraction diffractometer Rigacu D/max 2500. Processing of the results was performed with using of FindIt and Mercury programs.

For all investigated compositions endopeak in temperature range of 390-415°C was observed already after the first DSC measurement. This peak is associated with the melting of the eutectic in the system Ge-Te. In addition, for the two compositions with a high Te concentration ($Ge_{13}Te_{87}$ and $Ge_{14}Te_{86}$) there appeared another endothermic peak with the higher temperature. The repeated heat treatments of all investigated compounds leads to phase separation and the appearance of two additional peaks: a low temperature peak (370-385°C), and a high temperature peak (410-465°C). Moreover, the value of the eutectic melting peak decreased. With increasing the number of measurements, high-temperature peak increases and shifts towards higher temperatures with a saturation at 460 °C. This temperature is close to the melting point of tellurium, which indicates on a change in the composition of one of the phases towards the increase of the tellurium content. The position of low-temperature peak is close for all compositions, and during multiple heat treatments varies slightly (within 4 degrees). Thermodynamic calculations of the possible reactions in the solid phase were carried out. Presumably, this peak is due to the solid-phase reaction of formation of γ-GeTe from α-GeTe and Te. So, the decrease of the Te+GeTe eutectic melting peak is associated with a decrease of its concentration during heat treatment and the appearance of a high temperature eutectic Ge+GeTe.

X-ray analysis showed the presence of crystalline phases of tellurium in the initial materials, with increasing content after the heat treatments. The phases of Ge and GeTe were absent in the initial materials and appeared after the heat treatments. Thus, repeated heat treatments leads to the phase separation of compositions close to the eutectic, and appearance of crystalline phases of Te, Ge, GeTe.

This work was supported by Ministry of Education and Science of RF (projects P847 from 25/05/2010 and № 16.552.11.7033 from 29/04/2011) and RFBR (11-03-00269).

1. A.A. Sherchenkov, S.A. Kozyukhin, E.V. Gorhskova. “Transformations in phase-change memory material during thermal cycling”, Journal of Optoelectronics and Advanced Materials, **11**, pp.26-33, 2009.

Formation of nanomask with 10-20 nm elements using self-organizing processes in diblock-copolymers films

M.A. Bruk[1], E.N. Zhikharev[2], V.A. Kalnov[2], A.V. Spirin[1], I.I. Amirov[2]
1. Karpov Institute of Physical Chemistry, Moscow, Russia. 2. Institute of Physics and Technology, Russian Academy of Sciences, Moscow, Russia. E-mail: bruk@cc.nifhi.ac.ru

One of the ways of formation of the nanomask with small elements (5-10 nm) is the use of self-organization phenomena of diblock-copolymers thin films deposited on the substrate surface [1]. Each diblock-copolymer molecule consists of two polymer chains of different chemical nature, connected by a covalent bond. When you create certain conditions (an energy neutral surface of the substrate with respect to each of the blocks, a sufficiently high mobility of the blocks, a small 30-40 nm film thickness, etc.) the self-organization takes place in these films. In this process the blocks of one component (with the small volume fraction in the copolymer) may form a cylindrical nanodomains oriented perpendicular to the substrate surface, while blocks of the other component form the continuous matrix in which the nanodomains are evenly distributed. After the selective removal of cylindrical domains the nanomask is formed with the cells (diameter of 15-20 nm), separated by the matrix polymer walls with the width of 15-20 nm.
This report presents the preliminary results on the formation of nanomask on the basis of self-organizing films of diblok-copolymer of styrene (St) with methylmethacrylate (MMA) on silicon wafers with a thin natural oxide layer. The molecular weight of diblok-copolymer was 77,000 at volume content of poly(methylmethacrylate) blocks about 30%. To make the energy neutral substrate surface the random copolymer of St with MMA thin layer grafted to the silanol groups of the silicon oxide surface layer was deposited. It is shown that the method used allows to form the polystyrene nanomask with the sell diameter of 15-17 nm (see the figure). The observed irregularity of cell distribution in the mask is apparently due to discontinuous layer of the random copolymer grafted. This effect is apparently due to the discontinuous silanol layer on the thin natural oxide layer. Through the obtained mask the plasma etching of the silicon substrate was carried out.

This work was supported by the Russian Foundation for Basic Research, projects 10-03-00422 and 10-07-00581.

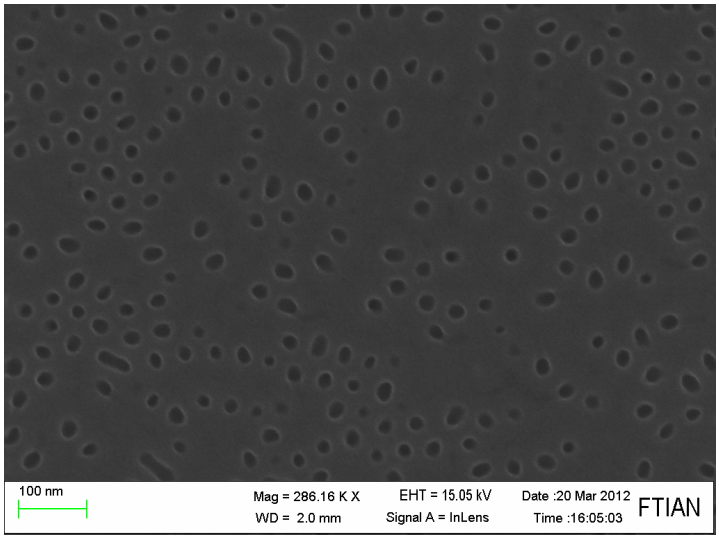

1. I.A. Zucchi, E. Poliani, and M. Perego, "Microdomain orientation dependence on thickness in thin films of cylinder-forming PS-*b*-PMMA". Nanotechnology, **21**, 185304 (5pp), 2010.

The new method of image formation by direct electron-beam etching of polymer resist

M.A. Bruk[1], E.N. Zhikharev[2], D.R. Streltsov[1], V.A. Kalnov[2], A.V. Spirin[1]
1. Karpov Institute of Physical Chemistry, Moscow, Russia. 2. Institute of Physics and Technology, Russian Academy of Sciences, Moscow, Russia, E-mail: bruk@cc.nifhi.ac.ru

This report presents the results associated with the development of the new "dry" technology of electron-beam lithography based on the direct etching of the some positive resists directly during exposure. The basis of the new technology is the electron-induced chain reaction of etching of the polymer resist to the volatile low molecular weight products. The method allows, in particular, to carry out the etching of the poly(methylmethacrylate) resist layer with the rates of 10-100 times greater than in the traditional "wet" technology. The main advantages of the method proposed are realized in the formation of spatial 3D-micro- and nanostructures. The three-dimensional structures in form of "steps" with the width of the step from 0.2 to 10 μm and the height from 5 to 50 nm are obtained in the PMMA resist films. The roughness of these structures on the Z-axis does not exceed 1-2 nm, which is about 5 times better than in "wet" 3D-lithography. The three-dimensional image in an atomic force microscope of the one of the spatial patterns produced by the new technology is presented below.

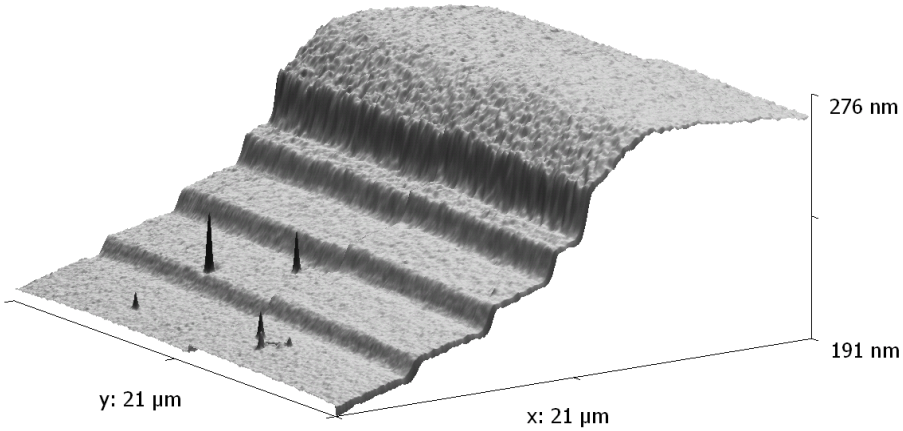

Technological advantages of the proposed method can be summarized as follows: 1) reducing the number of the lithographic process stages; 2) eliminating the need for organic developers; 3) significantly increasing the productivity of the lithographic process and reducing its cost; 4) in the formation of 3D-dimensional micro- and nanostructures the quality of derived structures is improved; 5) the method allows to form on the same sample the structures of various types without any limitation: the wet technology is limited to the structures with identical conditions of development.

At present the new field of technology, based on the use of electronic 3D-lithography for the production of micro- and nano-electromechanical devices, elements of optical systems (gratings, waveguides, lenses, etc.), stamps for nanoimprint lithography, etc. is actively formed. The proposed method can make the significant contribution to the development of this new field of technology.

This work was supported by the Russian Foundation for Basic Research, projects 10-03-00422 and 10-07-00581

The charging of PMMA-film resist in electron beam lithography

Evstafjeva E.N., Knjazev M.A., Rau E.I., Svintsov A.A., Tatarintsev A.A., Zaitsev S.I.
Institute of microelectronic technology and high purity materials RAS, Chernogolovka, Russia, E-mail: rau@phys.msu.ru.

A scanning electron microscope (SEM) is used in investigation of charging polymethylmethacrylate (PMMA) films on Si-substrate. The PMMA is an important insulating material and widely used in electron beam lithography, for photomask fabrication and direct pattern writing. But charges trapped in the photoresist cause a positive or negative surface potential V_S depending on the PMMA thickness d and primary electron energy E_0. The arising electric field will deflect incoming electrons and lead to pattern placement error.

We report the results of potential V_S measurements on PMMA coated silicon substrate with different values of PMMA thickness and beam energy. The estimation of V_S is based on the measurement of the shift secondary electrons spectra in the SEM with toroidal electrostatic spectrometer [1].

The resulting experimental surface potentials are shown in Fig.1 and 2. The electron energy was varied between 0.2 and 20 keV and the PMMA resist thickness values were 0.4, 1.4, 2.7, 4.0 μm. For comparison we have measured V_S on bulk PMMA crystal with thickness 1 mm. The electron beam current was 1 nA onto irradiated area 100x100 μm^2 (TV-scan mode) for 60 second corresponding to a total dose of 600 $\mu C/cm^2$.

The present results are important in low-voltage and high-voltage electron lithography and nanometrology, because of significant electron beam deflection effect by charged insulators. The pattern distortion due to electron beam deflection can reach unity nm in high-voltage and tens nm in low-voltage lithography.

The principal conclusion of the experiments is following. For different film thickness two cardinal energy points exist, where $V_S=0$. These cardinal energies can be used in the low-voltage and the high voltage lithography (and metrology) to minimize pattern placement error. These energies however do not coincide with well-known crossover energies for bulk insulators, which are usually estimated at exposure by primary electrons measuring a total yield of emitted electrons.

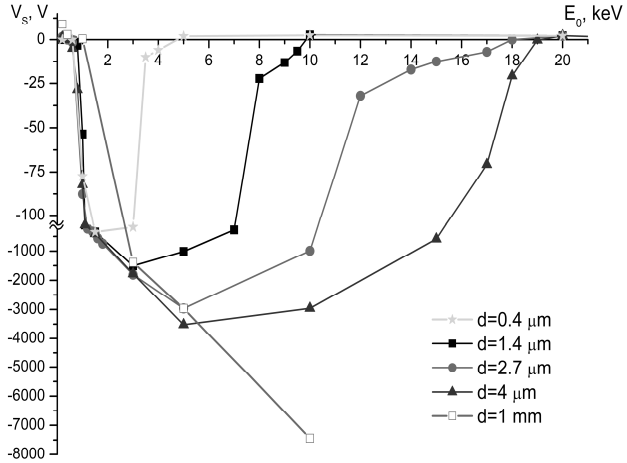

Fig. 1. Depending of surface potential V_S on electron energy E_0 for different PMMA film thickness d.

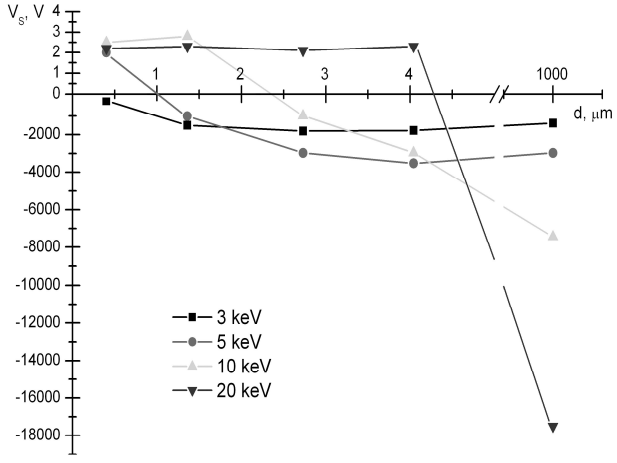

Fig. 2. Surface potential on PMMA as a function of film thickness for different electron beam energy E_0.

1. Rau E.I., Fakhfakh S., Andrianov M.V., Evstafjeva E.N., Jbara O., Rondot S. "Second crossover energy of insulating materials using stationary electron beam under normal incidence". Nuclear Instruments and Methods in Physics Research (B). **266**. pp.719-729, 2008.

Micropattern formation of diamond films

E.A. Il'ichev, A.E. Kuleshov, N.K. Matveeva, G.N. Petrukhin, R.M. Nabiev, and G.S. Rychkov
F.V. Lukin State Research Institute of Physical Problems, Zelenograd, Moscow, 124460 Russia
E-mail: polt@niifp.ru

We present a technology that makes possible high-precision lithography on diamond films with areas up to 10^4 mm^2. A minimum element size that can be achieved is only determined by the level of lithography accessible for silicon-based integrated circuits. A distinguishing feature of the proposed technology is that the mask for etching is created prior to the growth of a diamond film. The sequence of operations is as follows (see Fig. 1):

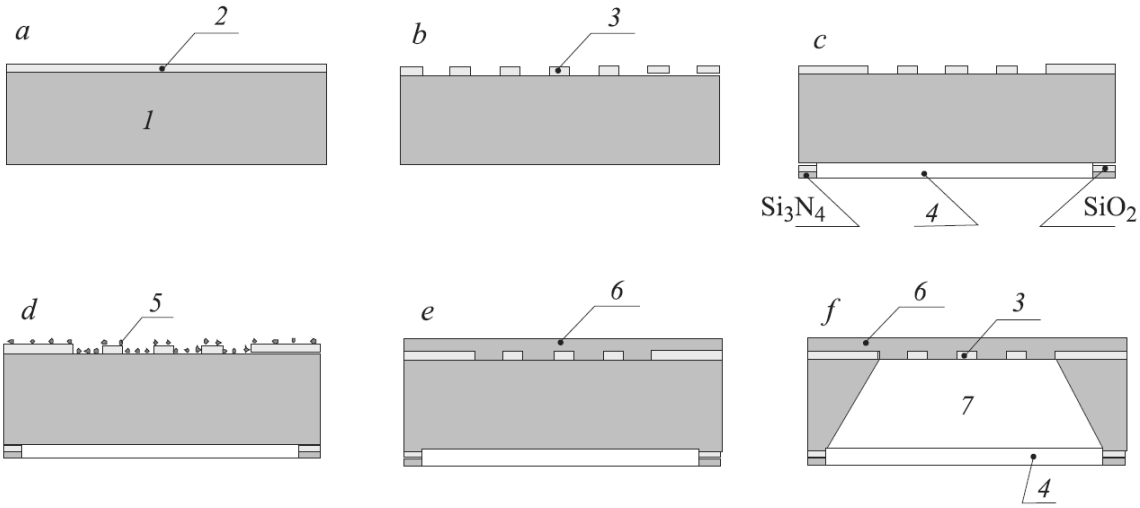

Fig. 1.

1. The surface of silicon wafer *1* is covered by deposited or grown film *2* of a material suited for making a mask for the etching of diamond (Fig. 1a). Possible materials are, e.g., silicon dioxide (SiO_2), silicon nitride (Si_3N_4), and titanium (Ti). Masks of these materials are not decomposed and deteriorated at the temperature of diamond film growth. The thickness of film *2* is determined by the depth of etching required for the diamond film. If the etching is to be performed in electron cyclotron resonance (ECR) plasma in argon–oxygen ($Ar:O_2$, 6:20 cm^2) mixture, the mask thickness can be determined using data on the etching rates of mask and diamond, which have been reported by Tran et al. [1] and are presented in the table together with data for etching in the presence of elegas (SF_6).
2. Mask *3* for the etching of a diamond film is formed from film *2* by the usual photolithography or electron lithography techniques (Fig. 1b).
3. Silicon dioxide (SiO_2) and silicon nitride (Si_3N_4) layers with thicknesses 0.3 and 0.1 μm, respectively, are deposited onto the rear side of the silicon wafer and then window *4* is opened for the subsequent etching of silicon (Fig. 1c).
4. A suspension of diamond nanocrystals is applied by centrifuging onto the prepared mask. After drying, nanocrystals *5* necessary for the stimulation of diamond film growth are retained on the surface of mask *3* and on the exposed surface of silicon (Fig. 1d).
5. An appropriate chemical vapor deposition (CVD) technique is used to grow a poly- or nanocrtystalline diamond film *6* on the upper surface of the silicon wafer (Fig. 1e).
6. Silicon substrate is etched in a 40% aqueous KOH solution at 85°C via window *4*. the process automatically terminated when the etching front reaches mask *3*. As a result, cavity *7* with a shape of truncated pyramid or cone is formed in the silicon wafer. The cavity base coincides with window *4* and its top is covered by mask *3* with diamond film *6* (Fig. 1f).

1. D.T. Tran, C. Fanster, T.A. Grotjohn, et al., "Investigation of mask selectivities and diamond etching using microwave plasma-assisted etching", Diamond and Related Materials, **19**, pp.778-782, 2010.

Formation of buried Ge nanocrystals and Cr (Mn) disilicides in Si by combination of ion implantation and MBE methods

N.G.Galkin[1], E.A. Chusovitin[1], K.N. Galkin[1], S.A. Dotsenko[1], S.V. Vavanova[1], R.I. Batalov[2], R.M. Bayazitov[2]

1. Institute of Automation and Control Processes, Far Eastern Branch, Russian Academy of Sciences, Vladivostok, Russia, ngalk@iacp.dvo.ru. 2. Kazan Physical-Technical Institute, Kazan Scientific Center, Russian Academy of Sciences, Kazan, Russia

Nanocrystallites (nc) of semiconducting chromium disilicide ($CrSi_2$), manganese disilicide ($MnSi_{1.74}$) and Ge formed in Si matrix is of great interest for optoelectronics as photodetectors of near infrared radiation (λ = 1-3 μm) and thermoelectrical converters [1]. The main method for the formation of buried $CrSi_2$ nanocrystals is the reactive deposition of thin Cr layers followed by Si epitaxial overgrowth by molecular-beam epitaxy (MBE) [2]. Alternative method of ion-beam synthesis of $Si/CrSi_2/Si$ heterostructures has been studied in [3], where high Cr^+ doses (Φ= (1-10)×10^{16} cm^{-2}) and pulsed ion beam treatment (PIBT) were applied. However, Mn silicide and Ge nanocrystallites in silicon matrix are not formed by this method as we know. In this paper Si/nc-$CrSi_2$/Si, Si/nc-$MnSi_{1.74}$/Si and Si/nc-Ge/Si heterostructures were fabricated by means of ion implantation, PIBT and MBE. The comparison of its morphology and properties was done.

Silicon wafers of *n*- and *p*-type conductivity (4.5-10 Ω×cm) with (100) and (111) orientations were implanted by Cr^+, Mn^+ or Ge^+ ions with energy E = 40 keV at room temperature with doses Φ = (1-6)×10^{16} cm^{-2}. After the implantation Si samples were subjected to PIBT by high-power carbon ion beam (E = 300 keV, τ = 50 ns, W = 1.0-1.5 J/cm^2). The dose of carbon ions implanted into Si during PIBT did not exceed Φ ~ 10^{14} cm^{-2}. After the implantation and pulsed annealing the surface of Si samples was subjected to UHV cleaning procedure which is slow deposition (v_{Si} = 0.05 nm/min) of thin Si layer (0.1-0.2 nm) onto heated Si substrate (T = 850 ^{0}C) for 20 min. After the cleaning procedure 100 nm thick Si layers were grown by MBE at the surface of the implanted samples at T = 700 ^{0}C with 7.5 nm/min deposition rate. The surface morphology of samples was studied by atomic force microscopy method in tapping mode. The optical transmittance and reflectance spectra of grown samples were registered at room temperature on Hitachi U-3010 spectrometer with an integrated sphere and Fourier spectrometer Bruker Vertex 80v.

Morphology investigations of samples with equal ion dose and after PIBT have shown that after UHV cleaning the root mean square (*rms*) roughness increases in line of ions: Mn^+,Ge^+ and Cr^+ from 2.88 nm to 4.88 nm. These none atomically flat surfaces were used for MBE growth of silicon top layer. The roughness of grown samples for all ions is in range of 16 – 26 nm. By low energy electron diffraction data only Si/nc-$CrSi_2$/Si heterostructures had silicon epitaxial continuous layer and minimum *rms* value (16 nm). The near continuous Si epitaxial layer was formed in Ge-implanted samples; it has *rms* value about 24.6 nm. Silicon layer grown atop Mn-implanted sample had a labyrinth structure without epitaxial orientation of silicon islands. Investigations of optical spectra have confirmed that MBE grown silicon top layer covers Cr (Mn) disilicides or Ge precipitates. It has monocrystalline structure for the case of Cr and Ge ions implanted in silicon and polycrystalline – for Mn implanted samples. Such difference is probably due to a large crystal mismatch of Si and $MnSi_{1.74}$. Thermoelectric measurements have shown that maximum value of Seebeck coefficient (200-300 μV/K) is observed for Cr- and Mn-implanted samples. Carrier scattering mechanism was studied from Hall temperature measurements in the range of 100-500 K. Photosensitivity of grown heterostructures in photon range of 0.8-1.0 eV was confirmed by photoconductivity measurements.

1. V.Borisenko, *Semiconducting Silicides*, Berlin, Springer Verlag, 2000
2. N.G. Galkin, L. Dozsa, et al.,"Properties of $CrSi_2$ nanocrystallites grown in silicon matrix", J. Phys.C: Condens. Matter, **19**, pp. 506204(1-11), 2007
3. N.G. Galkin, D.L. Goroshko, K.N. Galkin, S.V. Vavanova, a.o., "Influence of Cr+ ion implantation and pulsed ion-beam annealing on the formation and optical properties of $Si/CrSi_2/Si(111)$ heterostructures", Technical Physics, **55**, pp. 1036-1044, 2010

Electroluminescence and photovoltage properties of Si-p/β-$FeSi_2$ NC/Si-p/Si(100)-n mesa-diodes

N.G. Galkin[1], E.A. Chusovitin[1], D.L. Goroshko[1], A.V. Shevlyagin[1], T.S. Shamirzaev[2]

1. Institute of Automation and Control Processes, Far Eastern Branch, Russian Academy of Sciences, Vladivostok, Russia, galkin@iacp.dvo.ru. 2. Rzhanov Institute of Semiconductor Physics, Siberian Branch, Russian Academy of Sciences, Novosibirsk

Nowadays, two common ways to form silicon structures emitting light in wavelength range 1.5 – 1.6 μm are silicon ion implantation with Er^+ [1] and thin layers or nanocrystallite (NC) arrays of semiconducting iron disilicide (β-$FeSi_2$) formation on a silicon substrate by means of reactive deposition or molecular beam epitaxy [2]. Significant drawback of the both formation methods is a high density of point and linear defects arising in the silicon layers with embedded NC. Decrease of point defect density demands a long time high temperature annealing (900 ºC, up to 20 hours) [2]. However, such temperature treatment results in intense impurity diffusion which makes impossible integration silicon light emitters with a silicon integrated circuit. Recently we show that solid phase epitaxy allows of obtaining defect free epitaxial Si/NC-β-$FeSi_2$/Si heterostructures without additional high temperature annealing [3]. Thus, such heterostructures can be promising for light emitting diode fabrication, operating at room temperature.

In this work an electroluminescence (EL) of silicon diode structures with several β-$FeSi_2$ NC layers embedded in the *p*-*n* junction area was studied. The β-$FeSi_2$ NC's were formed by solid phase epitaxy (SPE) and the combination of reactive deposition and solid phase epitaxy (RDE + SPE) [3]. The diode structures were grown in ultrahigh vacuum chambers (UHV) on the substrates cut out from *n*-type silicon wafer with (100) orientation. Semiconducting iron disilicide NC's were formed on the atomically clean surface by two methods: SPE – using Fe layer deposition with initial thickness of 0.2 – 0.4 nm, at room temperature, followed by annealing at 630 °C during 20 minutes; RDE + SPE – by Fe layer deposition with initial thickness of 0.2 – 0.4 nm, at 375 °C followed by cooling down to room temperature, silicon deposition, and annealing at 475 °C for 2 minutes. Formed β-$FeSi_2$ NC's were covered by a *p*-type silicon layer at 700 °C. According to LEED data the silicon layer have grown epitaxially. Multilayer heterostructures were grown by repetition of two steps: NC's formation and the *p*-type capping silicon layer growth with thickness of 100 nm. To study EL of the heterostructures, mesa diodes with area of 1-7 mm^2 were made by chemical etching. Electrical contacts from the substrate and the film sides were fabricated by Al deposition and 10 minutes annealing at 450 °C. EL spectra were analyzed by double grating monochromator SDL-1 and recorded by Ge photodiode "Edinburgh Instruments" with liquid nitrogen cooling. All the measurements were taken in temperature range 5 – 300 K.

From analysis of EL spectra was found that β-$FeSi_2$ NC's grown by the combined method (RDE+SPE) results in the formation of high density of dislocations, which are the main radiative recombination channel of the non-equilibrium charge carriers at low temperatures, and of the defects that lead to the quenching of the radiative recombination at higher temperatures. In the structures where β-$FeSi_2$ NC's have been formed by SPE method the defect concentration is small therefore such structures show intense EL in the wavelength range 1.4 – 1.6 μm even at room temperatures. Photo voltage dependences of mesa diodes grown by SPE method have shown spectral sensitivity in the wavelength of 0.4 – 1.7 mm at low temperatures (10-100 K).

The work has been done under financial support from RFBR (grant No. 11-02-12075_ofi_m).

1. V. P. Kuznetsov, M. V. Kuznetsov, and Z. F. Krasil'nik, "Si:Er/Si diode structures for electroluminescence observation on the wavelength 1.5 μm at 300 K", Semiconductors, **44**, pp. 385-390, 2010

2. T. Suemasu, Y. Negishi, K. Takarura, F. Hasegawa, "Room temperature 1.6 μm electroluminescence from a Si-based light emitting diode with β-$FeSi_2$ active region", Jpn. J. Appl. Phys., **39**, pp. L1013-L1015, 2000

3. N. G. Galkin, E. A. Chusovitin, T. S. Shamirzaev, A. K. Gutakovski, and A. V. Latyshev, "Growth, structure and luminescence properties of multilayer Si/β-$FeSi_2$ NCs/Si/…/Si nanoheterostructures", Thin Solid Films **519,** pp. 8480-8488, 2011

Formation and properties of Ca silicide films and Si-Ca silicide-Si double heterostructures on Si(111) substrate

N.G. Galkin[1], S.A. Dotsenko[1], D.V. Bezbabny[2], K.N. Galkin[1], D.L. Goroshko[1], R. Kudrawiec[3], E. Zielony[3], J. Misiewicz[3]

1. Institute of Automation and Control Processes, Far Eastern Branch, Russian Academy of Sciences, Vladivostok, Russia, galkin@iacp.dvo.ru. 2. Amur State University, Blagoveshchensk, Russia. 3. Institute of Physics, Wroclaw University of Technology, Wroclaw, Poland.

Calcium silicide (Ca_2Si) is known as semiconductor material with direct energy band gap (0.3-0.35 eV) by data of theoretical calculations [1] in the framework of density functional theory in the local-density approximation. The recent results of Ca_2Si quasiparticle band structure calculations [2] in the frame of GW approximation shown that a direct energy band gaps are appeared for orthorhombic Ca_2Si (1.02 eV) and cubic Ca_2Si (1.16 eV) crystal structures. *In situ* temperature Hall measurements data [3] have shown that thin Ca_2Si layer grown on 2D Mg_2Si template on Si(111) substrate at 120-130 ^oC is characterized by 1.02 eV of energy band gap value which precisely corresponds to Ca_2Si quasiparticle band structure calculations [2]. But the formation of Ca_3Si_4 film has been observed at Ca deposition on Si(111)7x7 substrate at 500 ^oC with indirect band gap of 0.63 eV [4]. Both Ca silicide films are interesting for silicon planar technology as narrow-band-gap semiconductors for silicon-silicide-silicon optoelectronic devices, so methods of its growth, optical properties and burying in silicon matrix must be studied and optimized.

In this work we present morphology and optical data of Ca silicide nanostructured films grown on Si(111) substrate grown in the UHV chamber with base pressure $2x10^{-10}$ Torr. Ca, Mg and Si deposition rates calibrated by quartz microbalance were 0.38, 0.35 and 1.6 nm/min, respectively. N-type Si strip with resistivity 7.5 Ω·cm was used as a Si source for silicon cap layer growth. Compositions of calcium silicide and Mg_2Si films were investigated with Auger electron spectroscopy and electron energy losses spectroscopy after the finishing of corresponding growth procedures.

First series of samples was grown by deposition of Ca at 130 ^oC on preliminary formed amorphous silicon layer and nanocrystalline Mg_2Si template. The second series of samples was formed by different thickness Ca deposition at 500 ^oC on Si(111)7x7 and covered by Si layer at 500 ^oC. For all samples stages of Ca and Mg or Si depositions were repeated three or four times for the film thickness increase. It was shown by AFM data that all grown films consists from nanograins (20-50 nm), which are sometimes packed in larger granules (150-300 nm) and have crystalline planes for samples grown at 500 ^oC. Grown silicide layers have different structure by Raman and optical spectroscopy data. Calculations of optical properties of Ca silicide films and its modeling were performed. Only 2-nd series sample had strong Raman peaks at 333, 344, 382, 412 and 438 cm^{-1}, which corresponds to polycrystalline silicide closed to Ca_3Si_4 composition and correlated with first data [4]. By photoreflectance data only a sample grown at 500 ^oC had transitions at 0.89 and 0.91 eV that confirms its direct nature. Part of samples for double heterosrtucture formation was covered by thick polycrystalline silicon layers that were confirmed by Raman spectroscopy data. Sensitivity of double heterostructures in near infrared region (0.8-1.0 eV) was confirmed by photoconductivity measurements.

The work has been done under financial support from RFBR (grant No. 10-02-00284_a).

1. D.B. Migas, L. Miglio, V.L. Shaposhnikov and V.E. Borisenko, “Comparative study of structure, electronic and optical properties of Ca_2Si, Ca_2Ge, Ca_2Sn and Ca_2Pb”, Phys. Rev. B, **67**, pp. 205203 (1-7), 2003

2. S. Lebegue, B. Arnaud, and A. Alouani, “Calculated quasiparticle and optical properties of orthorhombic and cubic Ca_2Si”, Phys. Rev. B, **72**, pp. 085103 (1-8), 2005

3. S.A. Dotsenko, D.V. Fomin, K.N. Galkin, D.L. Goroshko, N.G. Galkin, “Growth, optical and electrical properties of Ca_2Si film growth on Si(111) and Mg_2Si/Si(111) substrates”, Physics Procedia, **11**, pp. 95-98, 2011

4. S.A. Dotsenko, K.N. Galkin, D.A. Bezbabny, D.L. Goroshko, N.G. Galkin “Formation, optical and electrical properties of a new semiconductor phase of calcium silicide on Si(111)”, Physics Procedia, **23**, pp. 41-44, 2012

Hydro chemical deposition method nanofilms $ZnS_{1-x}Se_x$

M.A. Jafarov, E.F. Nasirov, S.A. Jahangirova
Baku State University, Z.Xalilov-23, Baku, Azerbaijan, E-mail: maarif.jafarov@mail.ru

The use of a hydrochemical deposition method produces metal sulfide films with a wide variety of properties, as well as allows to synthesize thin films of supersaturated solid solutions of substitution. The use of chemically deposited thin films of metal chalcogenides as materials of chemical sensors is of great interest for sensor technology. The starting reagents for preparation of complexes of zinc and sulphoselenides on the surface of porous glass and in solution the following reagents were used: zinc nitrate $Zn(NO_3)_2 \cdot 4H_2O$ (analytical grade), selenouera $SeC(NH_2)_2$ (highly pure) water ammonia $NH_3 \cdot H_2O$ (analytical grade). Stock solutions were prepared with concentrations of 0.1 and 0.5 m in distilled water. pH of the solutions was measured on a pH-meter pH-340 mark with accuracy ± 0.01 units. For the synthesis of zinc sulfide semiconductor films including iodine-doped ammonium substitutional solid solution $ZnS_{1-x}Se_x$ (SSS). The porous glass marks a DV-sized 20h15 and 1 mm thick was used as a substrate material. To obtain films of the substrate was degreased at room temperature a solution of 0.1 m hydrochloric acid, hot during the day, and then repeatedly washed with distilled water. In order to obtain reproducible results in the preparation of reaction mixtures were of a strictly defined order of merging reagents. The solutions of complexes of lead and replacement of metal were prepared separately and blended together before adding to the reactor selenouera.

The rate of change in thickness of nanosize on time is important both for building of the quantitative theory of chemical vapor deposition, and for practice. Knowing the chemical reaction rate of deposition by varying the depth of its occurrence and mechanism of setting the film on a solid surface, can be influenced by the thickness of the resulting film. In turn, the thermal stability of nanocrystalline films determines the working temperature range of devices that run on them. In connection with this a study of the growth kinetics of nanocrystalline films and determination of their thermal stability was carried out. The selected material was a nanosize zinc sulfide. Films ZnS1-xSex were obtained by chemical precipitation from aqueous solutions at 325 K. Deposition of films was performed on silica glass. The kinetics of growth of nanosize $ZnS_{1-x}Se_x$ were investigated in detail by structural and optical methods. Thus, the method of interferometer shows that the film thickness of 30 nm is achieved by the deposition of about 45 minutes. The transparency derived nanosize has been studied spectrophotometrically in the wavelength range from 320 to 3100 nm. According to the optical transmission spectra in the initial stages of deposition some bleaching of the glass - the nanocrystalline film $ZnS_{1-x}Se_x$ was observed at wavelengths over 3700 nm. However, after 70 minutes of deposition absorption of $ZnS_{1-x}Se_x$ in the range 3700-4100 nm increases sharply, leading to a decrease in the intensity of transmission. According to the optical transmission spectra, annealing of the film edge region of absorption of the film is shifted to shorter wavelengths, due to, apparently, by the oxidation film on the air. X-ray diffraction shows that the film $ZnS_{1-x}Se_x$ is thermally stable up to temperature 620 K. Upon annealing at a temperature of 620K nanosize in the air is recrystallization, which remains stable in the temperature range studied up to 770 K. After annealing, the film $ZnS_{1-x}Se_x$ at 770 K, close to the glass transition point of silica glass, some of the particles $ZnS_{1-x}Se_x$ goes into the glass matrix near the surface. It is known that glasses with semiconductor quantum dots are of interest to study the fundamental properties of low dimensional structures. The observed phenomenon can be used as a basis for developing an alternative method for doping silicate glasses based on nanoparticles $ZnS_{1-x}Se_x$. In all cases, the films of solid solutions on porous glass are distinguished by a large content of zinc sulfide in the crystal lattice. The maximum content in the deposited ZnSe solid solution for both types of substrates is achieved. The results can be explained by more stable thiourea complexes of zinc compared to zinc.

Solar sell on the bazis heterojunctions p-CdS/p-CdTe/CdZnS, obtained by chemical deposition

M.A. Jafarov, E.F. Nasirov, S.A. Jahangirova
Baku State University, Z.Xalilov-23, Baku, Azerbaijan; E-mail: maarif.jafarov@mail.ru

Investigation of p-CdS/p-CdTe/CdZnS heterojunctions in order to use their in photovoltaic converters of solar energy began in the second half of XX century, and the best to create a photovoltaic structure were CdTe/CdZnS. This study focuses on the development of new technology of CdTeSe thin film deposition on the CdZnS substrate and the photovoltaic properties of p-CdS/p-CdTe/CdZnS heterostructures [1,2]. Particle size of cadmium selenide prepared during reaction process has been defined by spectrophotometrical method. Dependence of optical density on wavelength was measured by spectrophotometer in cuvette in the range of wavelength 320-500 nm.

Electrodeposition of the p-CdS films onto the Al substrates was carried out at room temperature from aqueous solution containing 50 mM each of $CdCl_2$ and $Na_2S_2O_3$. Polycrystalline films of p-CdTe were prepared by using a threeelectrode system with the saturated calomel electrode from aqueous solution containing $CdSO_4$ (1.0 M), TeO_2 (0.15 mM), 30 mM citric acid, and 10% ethanol by volume. The deposition potential was – 0.75 V and the current amplitude was 10 to 12 mA/cm^2. Nanocrystalline ZnCdS and CdTe thin films were deposited by electrodeposition from single source onto ITO covered optical glass and Al-pCdS substrates.

These films were analyzed by scanning electron microscopy (SEM) and spectroscopic ellipsometry in the range of 300 – 1500 nm. The optical constants as well as the films thicknesses and the optical band gaps were obtained by fitting the experimental spectra from ellipsometric measurements. The recorded data were analyzed using a dedicated software package specially designed for optical modeling. The ellipsometrical parameters were acquired at three incidence angles for a high number of wavelengths in the mentioned wavelength range. In order to determine the refractive index, the thickness and the surface roughness of p-CdS thin films, as well as for obtaining a smooth control for the experimental data fitting processes, the identification of the spectral regions in which the films showed good transparency is required. This working procedure generates a significantly increased number of optical models with a slightly reduced number of fitting parameters. A study of the function of p-CdS thin films and of its dependence on the substrate temperature during deposition processes was also carried.

The structural variations and photovoltaic performance of the p-CdS/p-CdTe and p-CdTe/n -ZnCdS thin film structures were investigated. Electrodeposition of has been used in order to prepare thin film structures on Al and ITO coated glass substrates. The deposition conditions and layer thicknesses of the films were systematically varied in order to create structural variations. The local structures of the thin films were probed by x-ray diffraction and x-ray absorption spectroscopy (XAS). XAS simulations and fits determined the process induced structural variations. This determined structural modification was correlated by photovoltaic efficiency of the thin films.

Thus, the advanced technology in the chemical surface deposition of CdTe thin films on the surface of CdZnS allowed for the first time to get photoconverting p-CdS/p-CdTe/CdZnS heterojunctions, showing the possibility to realize high conversion efficiency of solar radiation on the substrates CdZnS of large areas.

1. A.Sh. Abdinov, M.A. Jafarov, "Functionalities of the CdSe1-xTex, films in IR region of spectrum", Proc. SPIE, **6636**, pp.68-71, 2007.
2. A.Sh. Abdinov, M.A. Jafarov, E.F. Nasirov, "Negative infrared photoconductivity in CdS1-xSex films", Proc. SPIE, **4467**, pp.186-194, 2003.

STM study of single tetrapod-shaped CdTe and CdTe/CdSe nanocrystal

A.S. Trifonov[1], R.B. Vasiliev[2], I.S. Ezubchenko[3], M.S. Sokolikova[2], D.R. Britov[4], D.E. Presnov[1], O.V. Snigirev[4]

1. Lomonosov Moscow State University, Skobeltsyn Institute of Nuclear Physics, 1(2), Leninskie Gory, GSP-1, Moscow 119991, Russia, trifonov.artem@phys.msu.ru. 2. Department of Materials Science, Moscow State University, Leninskie Gory, Moscow 119991, Russia. 3. National Research Centre «Kurchatov institute», 1, Akademika Kurchatova pl., Moscow, 123182, Russia. 4. Faculty of Physics, M.V.Lomonosov Moscow State University, Leninskie Gory, Moscow 119991, Russia.

Size-dependent electronic properties of semiconductor nanocrystals have been intensively studied over the last decade. Branched nanocrystals for example tetrapods [1] provide a new class of nanostructures. A tetrapod-shaped nanocrystal is formed by four arms that branch out at tetrahedral angles from a central region. Due to their shape, tetrapods are attractive for electronic and opto-electronic devices, for example solar cell [2] and single-electron transistor [3]. Although charge transport phenomena through a single nanocrystal are of significant fundamental and practical interest, a few experimental works were reported [3]. In present work we have studied by scanning tunneling microscopy a monolayer of tetrapod-shaped nanocrystals immobilized on gold surface. We use a CdTe/CdSe heterostructured tetrapods with heterojunction formed within single nanocrystal.

CdTe and CdTe/CdSe tetrapods were synthesized analogously to [4]. According to TEM measurements, the average length of tetrapod arms was found to be 21 nm and arm width was about 3 nm with size distribution of about 10–20% and high homogeneity of shape. Each arm consists from two domains: CdTe part with length of 12 nm and CdSe tip with length of 9 nm selectively grown at the end CdTe arm along [0001] direction. Due to small cross-sectional size (3 nm) tetrapods clearly show size-dependent absorbance and luminescent bands with spectral position near 670 nm. Monolayer of CdTe and CdTe/CdSe tetrapods was immobilized on gold surface with use of mercaptoundecanoic acid employed as linker molecule. Silicon substrate coated with gold film was immersed in acetone solution of mercaptoundecanoic acid for 24 hours and then in toluene solution of tetrapods for 24 hours, washed with toluene and then dried.

We investigated electronic transport through single CdTe tetrapods and CdTe/CdSe heterostructured tetrapod using scanning tunneling microscope (STM). In particular, we measured and analyzed statistics of current-voltage characteristics (CVC) recorded in random place of the CdTe, CdTe/CdSe and pure gold sample (~ 3000 CVC were recorded). It was 3 different types of CVC shapes detected. The first shape is CVC which well fitted by Simmons formula [5]. Such shape of CVC is typical for metal-dielectric-metal (MDM) systems [6]. The second shape is symmetrical CVC, which do not fit by Simmons. The third shape is asymmetrical. CdTe tetrapods have 88.8% CVC of the second type. CdTe/CdSe tetrapods have 69.5% CVC of the second type and 26.6 % CVC of the third type. Different CVC for CdTe/CdSe tetrapods we explain by different possible electrical current channels in STM: “top CdSe-CdTe-bottom CdSe”, “CdTe-bottom CdSe” or “bottom CdSe”. Observation of asymmetrical CVC may indicate current rectification within single nanocrystal heterojunction.

1. D.J. Milliron, et al., “Colloidal nanocrystal heterostructures with linear and branched topology”, Nature, **430**, pp.190-195, 2004.
2. I. Gur, N.A. Fromer, A.P. Alivisatos, “Controlled assembly of hybrid bulk-heterojunction solar cells by sequential deposition”, J. Phys. Chem. B, **110**, pp.25543-25546, 2006.
3. Y. Cui, U. Banin, M.T. Bjork, A.P. Alivisatos, “Electrical transport through a single nanoscale semiconductor branch point”, Nano Lett., **5**, pp.1519-1523, 2005.
4. R.B. Vasiliev, et al., “Facet-selective growth and optical properties of CdTe/CdSe tetrapod-shaped nanocrystal heterostructures”, J. Mater. Res., **26**, pp.1621-1626, 2011.
5. J.G. Simmons, “Generalized Formula for the Electric Tunnel Effect between Similar Electrodes Separated by a Thin Insulating Film”, J. Appl. Phys., **34**, pp.1793-1803, 1963.
6. J.H. Scott, H.S. White, “Electric Field Induced Phenomena in Scanning Tunneling Microscopy:Tip Deformations and Au(111) Surface Phase Transitions during Tunneling Spectroscopy Experiments”, Langmuir, **9**, pp.3471-3477, 1993.

Luminescent properties of carbon incorporated porous silicon oxide

A. Vasin[1], S. Gordienko[1], A. Rusavsky[1], A. Nazarov[1], V.S. Lysenko[1], Yu. Piryatinski[2], I. Blonsky[2], E. Makila[3], J.Salonen[3], S. Prucnal[4], L. Rebohle[4], W. Skorupa[4]

1. Lashkaryov Institute of Semiconductor Physics, pr. Nauki 41, Kiev 03028, Ukraine. 2. Institute of Physics, pr. Nauki 46, Kiev 03028, Ukraine. 3. Department of Physics, University of Turku, Turku FI-20014, Finland. 4. Institut fur Ionenstrahlphysik und Materialforschung, Helmgolz-Zentrum Dresden Rossendorf e.V., Dresden, Germany

White light emitting carbon incorporated nanostructured silicon oxide composite material (SiO_2:C) is a promising material for artificial lighting and light indication devices (for converting ultraviolet radiation into white light) as well as luminescent labels in biomedicine. It is interesting that spectral properties of the photoluminescence (PL) of por-SiO2:C can be tuned almost ideally to that of natural white light of the scattered day sun irradiation opening a new application prospective for this material as a single-component environment and human health friendly white luminophore free of heavy metal activators. Despite increasing number of publications on the topic recent years the physical mechanism of visible photoluminescence in such kind of materials is still unclear. In present report the light-emitting carbon incorporated porous silicon oxide layers (por-SiO_2:C) were fabricated by successive procedure of thermal treatment of porous silicon in flow of acetylene (in temperature range of 1100-1300 K) followed by oxidation in flow of wet argon (in temperature range of 900-1000 K). Time-resolved PL measurements were performed using stroboscopic registration system allowing PL registration with given delay times. Excitation PL spectroscopy measurements were performed using excitation radiation in range of 250-400 nm. Luminescent properties were studied in temperature range of 20-420 K.

Por-SiO_2:C layers exhibited strong white photoluminescence (PL) with broad spectrum covering all visible range. PL spectra were shown to be composed of two bands with different decay time: (1) blue band centered at about 400 nm with long decay time (about 100 ns), and (2) broad band with maximum at about 540 nm. Green component is significantly faster with decay time in order of several nanoseconds. Maximum of PL intensity was shifted from green to orange spectral region with increasing of carbonization temperature from 1100 to 1300 K due to decrease of the relative intensity of the blue component and red shift of the green component.

Under intense ultra-violet irradiation under atmospheric conditions light emission efficiency of the material dropped while in experiments performed in high vacuum PL intensity increased by UV laser radiation. It is shown that degradation of PL efficiency under ultraviolet radiation is associated with photo-induced interaction (probably oxidation) of carbon material with atmospheric oxygen and can be avoided by encapsulation of the material.

Luminescent properties of por-SiO_2:C layers were studied at temperature range of 20-420 K. It is shown that in temperature range of 20-300 K the PL intensity is almost constant indicating a strong localization of photo exited carriers. Farther increase of the temperature up to 420 K resulted in drastic increase of the light emission efficiency. Physical mechanisms of temperature dependent PL evolution as well as origin of light emitting centers will be discussed.

Germanium substrates for molecular-beam epitaxy

I.D. Burlakov, A.L.Sizov, N.I. Iakovleva, E.D. Korotaev, A.E. Mirofianchenko
State Scientific Center of Russian Federation "RD&P Center ORION", Moscow, Russia, orion@orion-ir.ru

HgCdTe epitaxial heterostructures grown on Ge (112) substrates by molecular beam epitaxy (MBE) are the most perspective materials for high performance infrared focal plane arrays (IRFPA) in the field of defense industry production [1, 2]. An atomic smooth surface of Ge substrates with <1-nm root-mean-square surface roughness, a good surface morphology, high crystalline quality, optical transmittance in the LWIR range, electrophysics properties are need to obtain structural perfect epitaxial layers.

Advanced photodiode arrays using the new architectures and technologies were produced in high-quality surfaces "epiready" substrates, including combinations of different basic polishing techniques, several methods such as cleaning, etching, and preparing to epitaxy. Before epitaxy the substrate surface would be delivering from by-product of preliminary technological operations. A three-part procedure for preparing atomically flat Ge surfaces was included cleaning, wet chemical treatment, and surface stabilization with further washing in deionized water. The sample was initially degreased by boiling in isopropyl alcohol followed cleaning in HF:S_2OH_4 solution during 2-4 minutes at room temperature and washing in special clean deionized water.

The etching part of the procedure was included a wet chemical treatment at room temperature. A chemical etching process based on HF and H_2O_2 solution was dependent on temperature and concentration of using components. Etching substrates followed by a deionized water rinse and UV/ozone oxidationare or drying. It was estimated, that approximately 0.02–0.03 monolayers of carbon was present after oxide removal.

Under atmospheric influence the surface is covered with the oxide layer, which also contaminate Ge/GeO_2 interface. Special attention goes to Ge substrate of how to remove the GeO_x oxide from the substrate. The most commonly used method to prepare clean surface and remove oxides has been ion sputtering with etching of damage layer followed storage in N_2 atmosphere to protect from repeated oxidizing.

We have investigated combinations of different basic cleaning and etching techniques and measured the resultant substrate surface quality using several advanced characterization methods, including optical analysis, atomic force microscopy (AFM), as well as scanning (SEM) and transmission (TEM) electron microscopy. Scanning tunneling microscopy showed that the surfaces were flat on the >50 nm length scale and that atomic resolution was achieved. X-ray photoelectron spectroscopy showed the formation and removal of an oxide layer. The investigations of Ge (211) high-alloy transparent substrates with of 600±20 μm intended for epitaxy showed high parameters, namely 0,2-0,6-nm root-mean-square surface roughness, a good surface morphology, high crystalline quality, optical transmittance 40 % in the LWIR range, that confirms a possibility of producing high-quality "epiready" substrates. Substrate after treatment is shown in the Fig. 1.

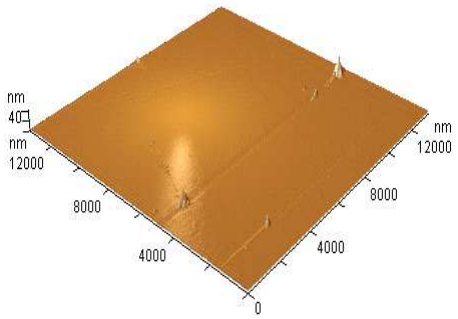

Fig. 1. Ge substrate after treatment

1. J.P. Zanatta, P. Ferret, G. Theret, A. Million, M. Wolny, J.P. Chamonal, and G. Destefanis, "Heteroepitaxy of HgCdTe (211)B on Ge substrates by molecular beam epitaxy for infrared detectors", Journal of Electronic Materials, **27**, pp.542–545, 1998.
2. M.F. Vilela, D.D. Lofgreen, E.P.G. Smith, M.D. Newton, G.M. Venzor, J.M. Peterson, J.J. Franklin, M. Reddy, Y. Thai, E.A. Patten, S.M. Jonhnson, and M.Z. Tidrow, "LWIR HgCdTe Detectors Grown on Ge Substrates", Journal of Electronic Materials, **37**, pp.1465-1470, 2008.

Direct wafer bonding of SiGe and Si crystalline wafers for high-power bipolar devices and SGOI

I.V. Grekhov[1], L.S. Kostina[1], T.S. Argunova[1,2], E.I. Belyakova[1], N.M. Shmidt[1], J.H. Je[2]
1. Ioffe Physical Technical Institute, Russian Academy of Sciences Petersburg, Russia, konst@mail.ioffe.ru
2. Pohang University of Science and Technology, Pohang, Republic of Korea, argunova2002@mail.ru

$Si_{1-x}Ge_x$ (SiGe) solid solutions are presently used to fabricate high-power high-speed bipolar transistors (HBTs), p-i-n diodes, field-effect transistors (FETs). SiGe layers are grown on silicon substrates by epitaxial growth technologies. In bipolar transistors, misfit and threading dislocations affect device performance and production yield. In FET structures, SiGe buffer layer is prepared on Si wafer for the epitaxial growth of a tensile strained silicon channel on top. The foremost critical challenge in the FET technology is the control of dislocation defects in the epitaxial layers.
As a second approach for FET structures, $SiGe/SiO_2/Si$ (SiGe-on-insulator, SGOI) substrates were used to attain high degree of strain relaxation at a low density of threading dislocations. SGOI substrates contain an inner SiO_2 layer that is formed, as a rule, by oxygen ion implantation (separation by implanted oxygen, SIMOX). Another way of the SGOI formation is direct wafer bonding (DWB) of oxidized silicon with SiGe/Si virtual substrate.
In this communication we suggest an alternative approach. As reported previously, the relaxed $Si_{1-x}Ge_x/Si$ and SGOI compositions with satisfactory structural and electrical characteristics can be formed by direct bonding of SiGe and Si single-crystal wafers [1, 2]. Misfit dislocations in such structures are localized in a thin layer near the interface where strain relaxation mostly occurred without threading dislocations. Structural defects in SiGe bulk affect the electrical properties of the bonded structures. We have studied the evolution of dislocations in SiGe single crystals with Ge concentration. Good quality crystals up to 50 mm in diameter with Ge concentrations of up to 15 at. % were produced with the Czochralski technique [3]. We compare the structural quality with the electrical resistance, the Hall carrier mobility, and the carrier lifetime measured in the pre-studied samples. We analyze current-voltage *I-V* characteristics and reverse recovery processes from the bonded diodes *p*-$Si_{1-x}Ge_x$/*n*-Si. We introduce the fabrication of SGOI substrates by a modified surface grooved DWB technology.
To fabricate *p*-SiGe/*n*-Si heterostructures, mirror-polished SiGe wafers were bonded to *n*-type Si wafers of the same orientation. Prior to bonding, an artificial relief in the form of an orthogonal net of grooves was photolithographically prepared on the Si wafer surfaces. To fabricate SGOI structures, mirror-polished *n*-type SiGe (111) wafers with 2-15% of Ge were bonded to preliminary oxidized *n*-Si (111) wafers. The bonded SiGe was then thinned down to below 10 μm. To increase the germanium content, bonding was complemented by the sequential thermal oxidations and oxide etching from the surface of thinned SiGe layer in $SiGe/SiO_2/Si$ structures. Structural defects were investigated by x-ray topography combined with phase contrast imaging at the 7B2 X-ray microscopy beamline of the Pohang Light Source in Pohang, Korea.
For all samples with $N_{Ge} \leq 15$ at. %, the *I-V* curves of $Si_{1-x}Ge_x/Si$ heterodiodes are satisfactory in the entire range of current densities (1 mA/cm^2 — 200 A/cm^2), which shows good prospects for using DWB technology in the formation of $Si_{1-x}Ge_x/Si$ heterostructures. The use of $Si_{1-x}Ge_x$ single crystals instead of $Si_{1-x}Ge_x/Si$ epitaxial structures significantly simplifies the fabrication technology of SGOI substrates.

1. I.V. Grekhov, E.I. Belyakova, L.S. Kostina, et al., "Current-voltage characteristics of $Si/Si_{1-x}Ge_x$ heterodiodes fabricated by direct bonding", Tech. Phys. Lett., **34**, pp.1027-1029, 2008.
2. I.V. Grekhov; L.S. Kostina; T.S. Argunova, et al., "Structural and electrical properties of SGOI substrates fabricated by direct bonding", Semiconductors, **44**, pp.1101-1105, 2010.
3. N.V. Abrosimov, S.N Rossolenko, V. Alex, et al., "Single crystal growth of $Si_{1-x}Ge_x$ by the Czochralski technique", J. Cryst. Growth, **166**, pp.657-662, 1996.

Copper germanium alloys formation by the low temperature atomic hydrogen treatment

A. Kazimirov[1], E. Erofeev[2], V. Kagadei[2]
1. Scientific Research Institute of Electrical Communication Systems, Tomsk, Russia, smart300389@mail.ru
2. Research and production company "Micran", Tomsk, Russia, erofeev@micran.ru

The thin films of stoichiometric copper germanide compounds (Cu_3Ge) are perspective material for metallization in micro- and nanoelectronics devices. It is known [1] that Cu_3Ge compounds are achieved room-temperature resistivity comparable to that of elemental Cu, with superior thermal and chemical stability upon exposure to air or oxygen at room temperatures. However there are no studies where Cu_3Ge alloys were used as transistor's metallization material. Because, traditionally Cu_3Ge alloys are formed using heat treatment (T = 400 ºC) for a long time (t = 20–30 min) in a high vacuum environment. It is difficult to introduce into resist lift-off technique at manufacturing GaAs RF semiconductor devices and monolithic integrated circuits. It is known [2], that the low-temperature atomic hydrogen treatment can stimulate diffusion of Au, Ni, Cu, and In into a Ge crystalline substrate. The activation of the solid state diffusion can be caused by the surface recombination of hydrogen atoms into molecules. It is possible to assume that the atomic hydrogen treatment of Cu/Ge thin-film system can solve the above-mentioned problem and create a Cu_3Ge compound at the lowered temperatures.

The purpose of the present work is investigation the opportunity of the formation of Cu_3Ge compounds by atomic hydrogen treatment at room temperature.

In experiments for the Cu_3Ge compound formation with low temperature atomic hydrogen treatment *i*-GaAs (100) substrate was used. To remove the oxides of GaAs surface before deposition, the substrate was treated in HCl : H_2O (1 : 10) solution, followed by rinsing in de-ionized water and drying in a flow of pure nitrogen. The Ge (d = 78 nm) and Cu (d = 122 nm) thin films were deposited by the vacuum e-beam evaporation. The samples were treated in a flow of atomic hydrogen with a flow density of $j = 10^{15}$ at.·cm^2·s^{-1} during t = 5–30 min at room temperature for Cu_3Ge compound formation. The surface morphology of treated samples was investigated with scanning electron microscopy (SEM), the distribution of Cu and Ge elements in the depth of the samples was investigated by Auger electron spectroscopy (AES) and the electrical resistivity of Cu_3Ge thin films was measured by the four probe method.

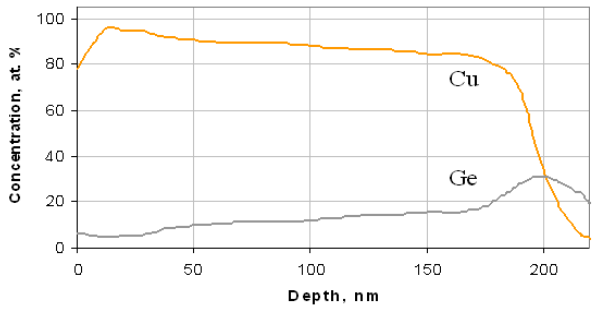

Fig. 1. Distributions of Cu and Ge elements in the depth of the samples treated in the flow of atomic hydrogen for t = 5 min at room temperature

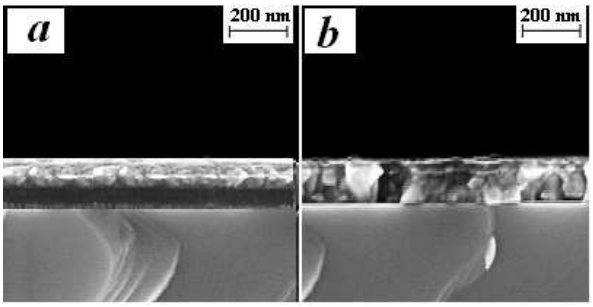

Fig. 2. Cross sectional SEM images of the as-deposited (*a*) and Ge/Cu films treated in atomic hydrogen flow for 5 min at room temperature (*b*)

There was found, that the treatment of Cu/Ge/GaAs samples in the atomic hydrogen flow with density $j = 10^{15}$ at.·cm^2·s^{-1} during t = 5 min at room temperature leads to interdiffusion Cu and Ge thin films (fig.1) with the formation of the polycrystalline Cu_3Ge compound with vertically oriented grains (d = 100–150 nm) (fig. 2) and low electrical resistance (4,5 μOhm·cm). Increasing the treatment time in atomic hydrogen flow lets to improve interdiffusion of Cu and Ge elements. The mechanisms responsible for the discovered phenomenon have been discussed.

1. M.O. Aboelfotoh, M.J. Brady, Lia Krusin-embaum, "Compound with room temperature electrical resistivity comparable to that of elemental copper", United States Patent №5288456 at 22.02.1994.
2. V.M. Matyushin, R.V. Martynyuk, "Influence of defect generation on low-temperature diffusion of Au in Ge under influence of atomic hydrogen", Journ. Functional Materials, **8**, pp.401–404, 2001.

Fabrication and structural study of $In_xGa_{1-x}As$ layers on porous GaAs(001) substrates

A. Lomov[1], J. Grym[2], D. Nohavica[2], E. Hulicius[3], J. Pangrác[3], A. Orehov[4], A. Vasiliev[4]

1. Institute of Physics and Technology of Russian Academy of Sciences, Moscow, Russia, E-mail lomov@ftian.ru. 2. Institute of Photonics and Electronics of Academy of Science of Czeh Republic, Prague, Czech Republic, E-mail grym@ufe.cz . 3. Institute of Physics of Academy of Science of Czeh Republic, Prague, Czech Republic. 4.-National Research Centre "Kurchatov Institute", Moscow, Russia, E-mail: a.vasiliev56@gmail.com

The growth of perfect InGaA/GaAs heterostructures with high In content is a fundamental task for the fabrication of modern optoelectronics devices, high-frequency and lower-noise electronic equipment. But the remarkable lattice mismatch between the GaAs substrate and an InGaAs layer stimulates forming a lot of misfit and threading dislocations. This process is a barrier for increasing the critical layer thickness. The growth of strained InGaAs layers does not solve completely the problem of fabrication of fault-free layers because residual stresses lead to degradation of the electronic and optical properties subsequently. In [1] the possibility to reduce elastic stresses at the interface by forming a porous buffer layer between InGaAs and GaAs substrate. But the growth on porous substrates has a weak point: it is difficult to have sharp In concentration profile at the interface because of the porous substrate surface roughness.

In the present study we show the influence of different types of porous buffers on crystalline perfection and content of In in InGaAs/por-GaAs/GaAs:Si(001) (carrier concentration of $2*10^{18}$ cm^{-3}) heterostructure. The task was to prepare porous subsurface (buffer) layer on substrate with a high degree of porosity and uniformity while leaving minimum damage to the substrate surface. This was achieved by a two-steps anodization process. In the first step, a short high current density pulse was applied to create a number of nucleation sites while in the second step a low current density regime was used to get a highly porous layer under "smooth" surface with small pore diameters. The pore etching was carried out in an electrochemical cell containing a fluoride-iodide aqueous electrolyte (H_2O-HF-KI) using a three-electrode configuration. In(x)Ga(1-x)As layers were prepared in an EpiRAS 200 TT equipped AIXTRON 200 machine by low pressure metalorganic vapor phase epitaxy (MOVPE). TMGa, TMIn and arsine were used as precursors. The following technological parameters were used: total growth pressure 70 hPa, H_2 total flow 8 slpm and the V/III ratio was 334. Prior to growth, the substrate temperature was increased to 560°C for 10 minutes under arsine flow and the same temperature was used for the growth.

The structural properties of the samples were investigated by high resolution triple axis diffraction, electron microscopy (SEM, TEM, STEM), and energy dispersive X-ray spectroscopy (EDXS). The X-ray diffraction curves (scans around 004 GaAs reflection in $\vartheta/2\vartheta$ and ω modes, CuKα rad.) were taken with using Ge(004) 3-fold crystal as a monochromator and 2arc min slit in front of a counter. Figure shows the experimental $\vartheta/2\vartheta$ scans from InGaAs ~25nm layers on GaAs with one-step (*1*) and two-steps (*2*) anodized porous buffer.

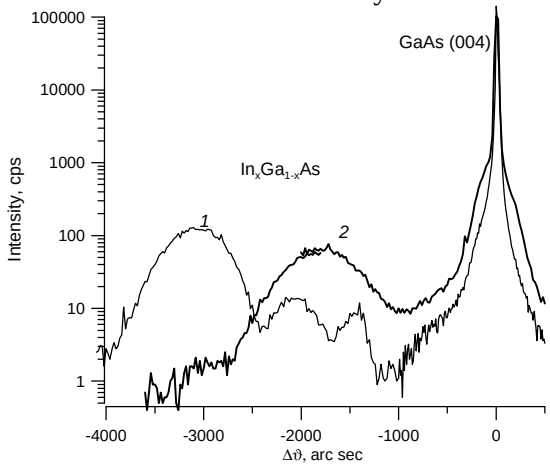

Fig. Rocking curves from InGaAs layers on por-GaAs

The measured curves demonstrate a good structural quality of epilayers with different values and depth profiles of In. It has to be pointed out that both samples were fabricated in one growth process with x~0.15. The shape of the curve (*2)* proves that there is In diffusion into the substrate across the pores. The reconstructed parameters (thickness, strain, In content) are in satisfactory agreement with the scanning electron microscopy data.

This study was supported in part by the Russian Foundation for Basic Research, project no. 10-02-00527 and the project P108/10/0253 of the Czech Science Foundation.

1. F.Yu. Soldatenkov, V.P. Ulin, A.A. Yakovenko et al., "Unstrained epitaxial InxGa12xAs films obtained on porous GaAs", Tech. Phys. Lett., **25**, pp.852-854, 1999.

Conductive Langmuir-Blodgett films based on poly (p-phenylenevinylene) derivates

N.K. Matveeva, E.A. Il'ichev

Federal State Unitary Enterprise "Research Institute of Physical Problems named after F.V.Lukin", Zelenograd, Russia, E-mail: Nadezhda.Matveeva.41@mail.ru address: Bld. 6, Pas. 4806, Zelenograd, Moscow, Russia, 124460

Highly oriented electroluminescence films on the basis of charge-transfer complexes (CTC) were prepared by the Langmuir-Schaefer (LS) technique Poly (p-phenylenevinylene (PPV)) modificated with alkyl-chains was used. Stable monomolecular layers of PPV were prepared and studied at the air-water interface. The surface pressure-area isotherms of PPV monolayers were measured. The collapse pressure value and the area molecule of PPV monolayers are equal to about 40 mN/m and 0.25 nm^2 correspondingly. Thin films containing from 1 to 100 and more monolayers were deposited for investigating. Nonamphiphilic acceptors were used for CTC obtaining. It was found, that PPV monolayers areas per decrease with contents of acceptors. Such a behavior can have the following explanation. Donor-acceptor complex arising during monolayers formation have more dense packing at the air-water interface.

Absorption spectra of PPV and CTC Langmuir-Blodgett (LB) films were measured. Absorption was observed at 470 and 540 nm correspondingly (Fig. l).

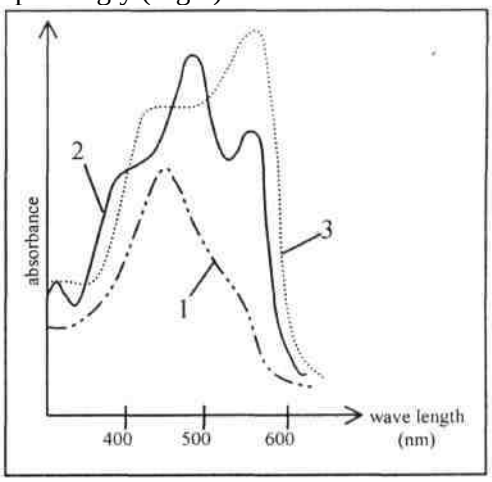

FIG. 1. Absorption spectra of PPV and CTC LB films: 1 – PPV, 2 – PPV + acceptor 1, 3 – PPV + acceptor 2.

The longitudinal conductivity have appeared I = 10^{-8} A for PPV and I = 3 10^{-6} for PPV+ acceptor (without doping), U = 10 V (Fig. 2). The electroluminescence of PPV LB films was detected in present of acceptor by using SnC_2 and Al electrode par.

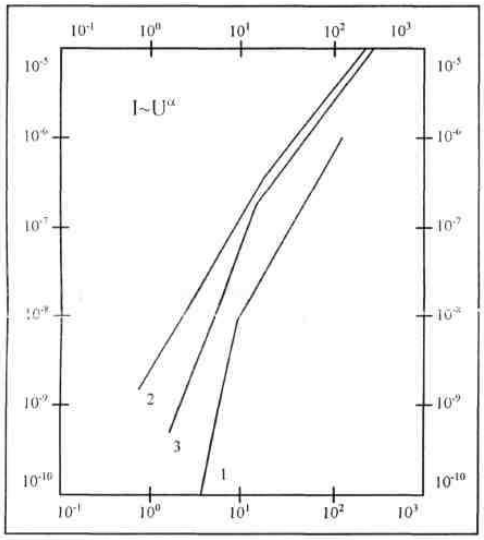

FIG. 2. The longitudinal conductivity of PPV and CTC LB films: 1 – PPV, 2 – PPV + acceptor 1, 3 – PPV + acceptor 2.

Features of formation of high-*k* dielectric layer in the W/ultrathin HfO_2/Si (100) structures under annealing

V. Rudakov, E. Bogoyavlenskaya, Yu. Denisenko, V. Naumov
Yaroslavl Branch of the Institute of Physics and Technology, Institution of Russian Academy of Sciences,
E-mail: valeryrudakov@rambler.ru

The dimensional scaling of MOS transistor elements requires the replacement of the conventional SiO_2 gate with a higher dielectric constant (high-*k*) material. The main purpose of this change is to reduce the parameter of "equivalent oxide thickness." It objective is to increase the physical thickness of the dielectric by the use of a high-*k* material. This will keep the same or even increase the capacitance of the dielectric, simultaneously solving the problem of leakage current resulting from direct tunneling. HfO_2 and Hf-based dielectrics ($k \approx 15 – 30$) are the most promising candidates for it. However, the sputtering of HfO_2 directly on Si-substrate results the formation of an interfacial layer. Its composition (SiO_2, $HfSi_x$, $HfSi_xO_y$) strongly depends on the methods of formation of the HfO_2 film. Moreover, the replacement of SiO_2 with HfO_2 involves the replacement of the doped *poly*-Si gate with an alternative one. In the case of HfO_2, tungsten W is the most frequent material for a metal gate. Obviously, the electrical properties of the W/HfO_2/Si (100) structures will depend on the chemical state and the structure of the interfacial layers at the bottom HfO_2/Si (100) and the upper W/HfO_2 interfaces. Therefore, the study of features of formation of these layers and their composition are important. In this work, the investigation of the relationship between the change in the electrical parameters (maximum capacitance per unit area in the accumulation (that is the capacitance per unit area of high-*k* dielectric) C_{max} and *k* parameter) and the change in the chemical composition of the bottom and upper interfaces of the W/ultrathin HfO_2/Si (100) structures during annealing are presented.

The initial W(150 nm)/HfO_2(5 nm)/Si (100) structures were fabricated by rf magnetron sputtering (high-purity HfO_2 target, Ar^+-plasma [1]). Then the annealing either at 500 °C in vacuum for 30 min, either RTA at 950 °C in Ar_2 atmosphere for 12 s were held. After the annealing, W-pads were plasma-chemically etched through a photomask. With the help of SIMS using the TOF.SIMS^5, two types of SIMS profiles were taken: 1) in the W-pads free places, i.e. on the HfO_2 film surface, 2) over a depth of metallization during the ion milling of the W/HfO_2/Si (100) structures. On the basis of the first type measurements it was established that the physical thickness of the dielectric layer after RTA was ~ 6.5 nm, which is 30 % greater than that of the as-deposited HfO_2 film (5 nm). According to the SIMS profiles, the following transitions at the HfO_2/Si (100) interface could take place: $HfO_2 \rightarrow HfSi_xO_y \rightarrow (HfSi_x + SiO_x + Si) \rightarrow Si$ (substrate). The results of the second type measurements also indicated the presence of the $HfSi_xO_y$ interfacial layer. The SIMS profiles simultaneously evidenced the relationship dynamics between the W-, Hf- and Si- oxide phases. It was found that with the increasing of the annealing temperature, the penetration of the substrate atoms into the interfacial layer at the HfO_2/Si (100) interface was intensified as well. It should be noted that an increase in the intensity of the HfO_3^- (HfO_2^-) and SiO_2^- (SiO^-) ions from the corresponding oxide phases was observed in the evident absence of an external source of oxygen in the structures. The electrical parameters of the samples before and after RTA were determined by high-frequency (0.9 and 1.0 MHz) *C-V* measurements performed with the Keithley 4200-SCS. The *C-V* curves were plotted in accordance with the approach taken for the measurements for ultrathin dielectrics [2]. It was determined that C_{max} for the W/HfO_2/Si (100) structures before RTA was 4.8×10^{-6} F/cm^2 and after RTA – 3.2×10^{-6} F/cm^2. The estimation of the average *k* value (taking into account the complex structure of the interfacial layer) showed that such a behavior of C_{max} was in conjunction with a decrease in *k* from 27 to 23. Besides, a shift of the *C-V* characteristics towards positive values of the applied voltage was observed. Thus, the reducing of the C_{max} and *k* values during the annealing of the initial W/ultrathin HfO_2/Si (100) structures was closely connected with the formation of the new phases under the temperature treatment. These effects were accompanied by an increase in the total physical thickness of the oxide layer and an increase of the Hf-silicate phase in its fraction formed at the bottom interface of the investigated structures. The reason of the formation of the WO_x phase type at the upper interface is probably the residual oxygen initially presented in the structures.

1. V.I. Rudakov, E.A. Bogoyavlenskaya, Yu.I. Denisenko, V.V. Naumov, “Formation of thin-film HfO_2/Si (100) structures by high-frequency magnetron sputtering”, Russian Microelec., **40**, pp.383-388, 2011.
2. K.J. Yang and C. Hu, “MOS capacitance measurements for high-leakage thin dielectrics”, IEEE Trans. on Elec. Dev., **46**, pp.1500-1501, 1999.

Temperature oscillations in a silicon wafer under constant power of incoherent irradiation by heating lamps in a thermal chamber of RTP set up

V. Rudakov, A. Kurenya, V. Ovcharov, V. Prigara
Institute of Physics and Technology, Yaroslavl branch, Russian Academy of Science, Yaroslavl, Russia,
E-mail: valeryrudakov@rambler.ru

The technology evolution of microelectronics calls for new effects involving temperature behavior and variation of optical properties of semiconductor wafers under technological processing. In recent publication the observation of optical and temperature bistability in a silicon wafer at radiation heat exchange between the wafer and thermal chamber elements of a rapid thermal processing (RTP) set up is reported [1]. It is assumed, that this effect can be utilized for supplementary controlling in the technology of the rapid thermal processes in the elevated temperature range (300-900 K), wherein the constituent elements of semiconductor devices, such as contact systems, gate structures and metallization are formed in manufacturing process of microelectronics and nanoelectronics.

Among the effects connected with optical bistability there is such effect as periodic temperature oscillations which is observed at interaction of laser radiation with non-linear media. In this paper we report about the observation of temperature periodic oscillations in the silicon wafer which is heated and cooled in the mode of constant power incoherent radiation of heating lamps in the thermal chamber of the RTP setup. Oscillations are observed at temperatures corresponding to instable steady state solutions to the heat balance equation for the silicon wafer. Figure shows the temperature time diagram (TTD) of heating and cooling of the silicon wafers p-Si:B (100) ρ =12 Ω. The solid line represents readings of a thermocouple attached to the wafer; the broken line represents readings of a pyrometer responsive to the optical variations of the wafer [1]. The temperature oscillations are corresponded the TTD interval from 1400 to 6100 s at the process of heating of the wafer and from 7600 to 10600 s at the cooling.

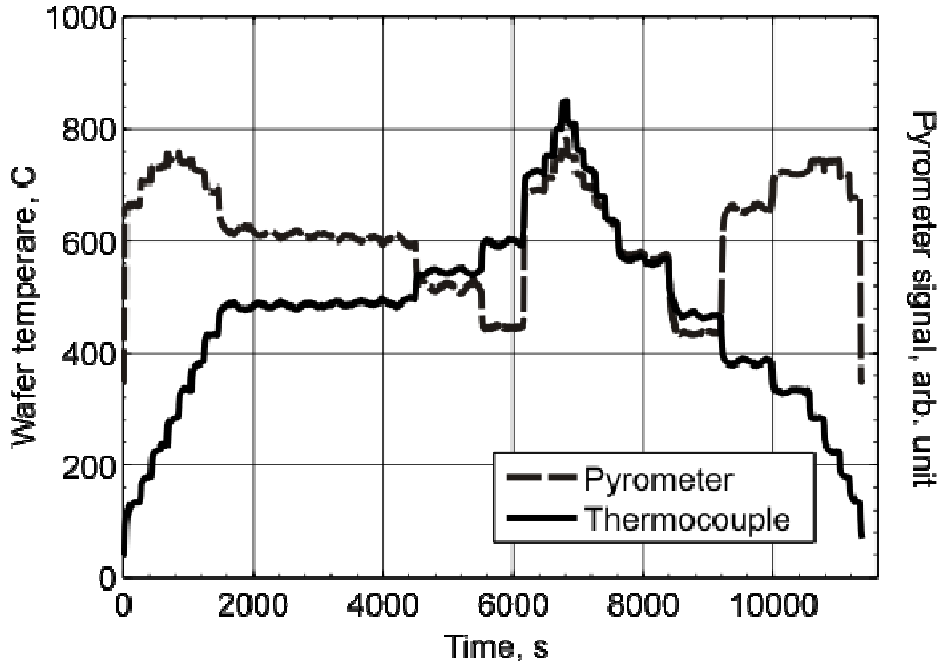

The revealed effect can be used in epitaxial growth of superlattices.

This study was supported by the Russian Foundation for Basic Research, Project No. 11-07-00521-a.

1. V.I. Rudakov, V.V. Ovcharov, A.L. Kurenya, V.P. Prigara, "Bistable behavior of silicon wafer in rapid thermal processing setup", Microelectronic Engineering, **93**, pp.67–73, 2012.
2. H.M. Gibbs. *Optical Bistability: Controlling Light with Light*. Academic Press, Inc., New York, 1985.

Hopping conductivity in Ge-SiO_x-Si structures with Ge nanoclusters

S.V. Kondratenko[1], Y.N Kozyrev[2], M.Y. Rubezhanska[2], V.S. Lysenko[3], Y.V. Gomeniuk[3,*]

1. National Taras Shevchenko University, Physics Department, Kyiv, Ukraine.

2. Chuiko Institute of Surface Chemistry, Kyiv, Ukraine.

3. Lashkaryov Institute of Semiconductor Physics, NAS of Ukraine, Kyiv, Ukraine, * *yurigom@lab15.kiev.ua*

The Ge nanocluster structures were grown using a molecular beam epitaxy (MBE) technique on boron-doped ($N_a \sim 10^{17}$ cm^{-3}) *p*-Si(100) substrates. A standard chemical pre-epitaxial treatment resulted in formation of a 2 nm thick SiO_x layer on the substrate. The presence of a silicon oxide layer at the surface was checked using high-energy electron diffraction technique. Then the oxidized silicon surface was annealed in vacuum at the temperature of about 800°C for an hour. The diffraction pattern allows us to conclude, that the film can be considered as a silicon suboxide SiO_x ($0<x<2$). Then the temperature was lowered to 700–730 °C, and the deposition of germanium from electron beam evaporators was performed, leading to the formation of Ge nanoclusters on the SiO_x layer. After deposition of Ge nanoclusters, half of the wafer was covered by a mask, and the system was exposed to a weak flow ($2\text{-}3\times10^{14}$ cm^2/s) of Si ions. As a result, on the uncovered part of the wafer Si/Ge nanoclusters were formed due to additional deposition of silicon.

AFM image shows that deposition of germanium onto the SiO_x film results in formation of nanoislands with the semispherical top surface and the surface density of $\sim 5\times10^{11}$ cm^{-2}. The height distribution of Ge nanoclusters is approximated by Gaussian function with a maximum at 1.7 nm and a full width at half maximum (FWHM) of 1.1 nm. After deposition of Si atoms onto the surface with Ge nanoclusters, the surface morphology changes: the mean size of the formed Si/Ge nanoclusters increases and their surface density decreases to $\sim 10^{10}$ cm^{-2}. The height distribution of Si/Ge nanoclusters is approximated by Gaussian function with a maximum at 7 nm and an essentially larger FWHM of 7 nm. Measurements of a.c. and d.c. conductivity were carried out in a coplanar geometry. The distance between two Au-Si contacts was 5 mm.

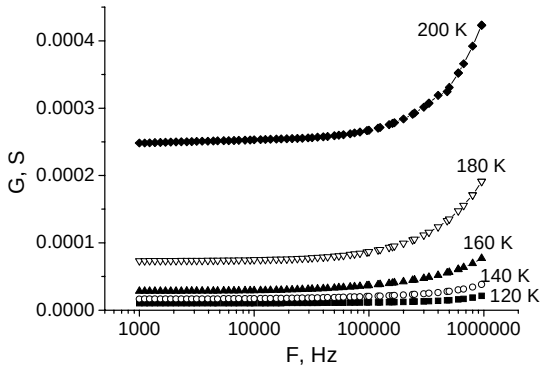

Fig. 1. Dependence of a.c. conductivity on frequency at different temperatures.

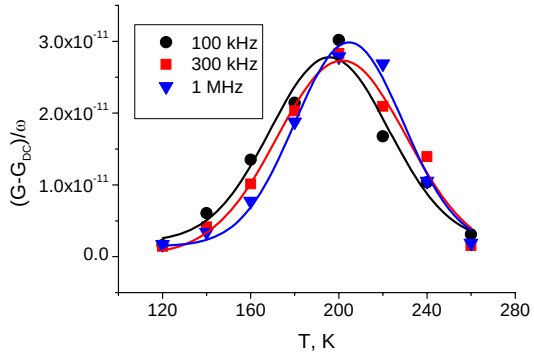

Fig. 2. Dependence of pairwise hopping component of a.c. conductivity on temperature for different frequencies.

Figure 1 shows frequency dependences of conductivity of the as-grown sample measured in the temperature range 120–200 K. It can be seen that conductivity increases with increasing frequency as $\sigma = \sigma_{dc}+A\omega^s$ [1]. Low-frequency part of conductivity represents the d.c. conductivity, the temperature dependence of which can also be fitted by Mott's law for variable range hopping conductivity. Subtraction of d.c. conductivity from the measured conductivity σ gives us the a.c. fraction of conductivity related purely to hopping between two states in frame of pair approximation theory [2]. The temperature dependences of reduced conductivity at different temperatures are shown in Figure 2. Such a behaviour of conductivity is explained in terms of electron hopping transport through the system of states in the quasi-impurity band in the near-surface silicon layer. This band is induced by the holes trapped in the Ge or Si/Ge nanoclusters.

1. M. Pollak and T.H. Geballe, "Low-frequency conductivity due to hopping processes in silicon", Phys. Rev., 122, pp.1742-1753, 1961

2. A.R. Long, "Frequency dependent loss in amorphous semiconductors", Advances in Physics, 31, pp.553-637, 1982

Modeling the influence of internal mechanical stresses on spatial distribution of oxygen during its precipitation in silicon

R. Goldstein[1], T. Makhviladze[2], M. Sarychev[2]

1. Institute for Problems in Mechanics, Russian Academy of Sciences, Russia, goldst@ipmnet.ru 2. Institute of Physics and Technology, Russian Academy of Sciences, Russia, tarielmakh@mail.ru

In the given work we continue to develop the new model for kinetics of formation and growth of oxygen precipitates in crystalline silicon plates used in microelectronics [1,2]. The model earlier suggested in [1,2] takes into account the influence of the internal mechanical stresses caused by the difference of the specific volumes per one silicon atom in a precipitate particle (SiO_2) and in the silicon matrix on the rate constants of atomic oxygen transport and the chemical reaction of oxidation of silicon on the precipitate particle surface. In [1,2] the dependences of activation energies of the referred above processes on the internal mechanical stresses were obtained. The estimations performed in these works showed that the influence of the given factor on the rate of growth of precipitate particle sizes and the rate of oxygen accumulation in precipitates can be sufficiently considerable.

In the present work the model is applied to the description of precipitation kinetics in the case when an inhomogeneous distribution of atomic oxygen concentration over a silicon wafer is taken into account. In the framework of the 1D diffusion-kinetics description [3] the equations determining the distribution of interstitial atomic oxygen over the silicon plate volume are reformulated and analyzed. These equations take into account the diffusion of oxygen and its participation in the processes of growth of precipitate particles. The diffusion and kinetic regimes are two practically important limiting ones of the growth kinetics which have been analyzed in the work.

It is shown in the work that the diffusion regime is the most realistic one for the oxygen precipitation in silicon. For this regime the comparison between the results of the calculations of the dependence of the defect-free zone width on a annealing time obtained with the help of the new model equations and the results of the analogous calculations in the work [3], where the presence of the internal mechanical stresses was not taken into account. The comparison is performed for different annealing temperatures. It is obtained that the differences obtained in the results can be formally reduced or to a change of the time scale or to a change of the annealing temperature values for which the calculations are performed. Thus including the internal mechanical stresses in the model we have that the form of the calculated curves is the same as earlier but their slopes decrease in some manner. In our opinion this result is in the better agreement with the available experimental data [3]. On the base of the obtained results one can draw a conclusion that simultaneous consideration of an inhomogeneous oxygen distribution and action of internal mechanical stresses is needed for a correct description of oxygen precipitation in massive silicon plates.

1. R.V. Goldstein, T.M. Makhviladze, M.E. Sarychev, “Modeling the influence of mechanical stresses on the growth kinetics of oxygen precipitates in silicon”, Vestnik PGTU, Mekhanika, № 1, pp.35-43, 2010 (in Russian).

2. R.V. Goldstein, T.M. Makhviladze, M.E. Sarychev, “Modeling the influence of internal mechanical stresses on the rate of growth of oxygen precipitates in silicon”, Izvestia VUZ, № 2, pp.37-42, 2012 (in Russian).

3. S.V. Buliarsky, V.V. Svetukhin, O.V. Prihodko, “Modeling inomogeneous oxygen precipitation in silicon“, Phys. Techn. Semicond., **33**, pp.1281-1286, 1999 (in Russian).

Modeling the electromigration and mechanical stresses in conductor lines containing impurities

T. Makhviladze, M. Sarychev
Institute of Physics and Technology, Russian Academy of Sciences, Russia, tarielmakh@mail.ru

To evaluate the reliability and lifetime of nano- and microelectronic structures of IC it is necessary to model their electrical and mechanical properties determined by microstructure and evolution of the IC elements. One of the main failures in integrated circuit performance occurs due to electromigration of vacancies (ions) in thin film conducting lines, which causes their damage. Last years we have developed a full 3D model of electromigration and generation of electromigration-induced mechanical stresses in IC metallization lines [1-4]. It considers the electromigration failures as a set of processes occurring at the nano-, micro- and mesoscale. These processes determine operational reliability of IC metallization system. The physical foundations of degradation and lifetime of conducting elements of micro- and submicroelectronics products are analyzed. By now the various mechanisms of their deformations and failures that are of practical importance for different types of multilevel arrangement and microstructure of conductors were studied [1-4].

In the framework of the theory above, now we put forward an approach to modeling the electromigration and mechanical stresses in conductors containing impurities. We investigate the influence of impurities on vacancy transfer in the metallization under a simultaneous action of electric current, mechanical stress gradients and temperature fields. This clarifies how the metallization lifetime can be controlled by introducing various impurities. For the first time an *ab initio* model for calculating the effective charge of vacancies (ions) in grain boundaries of polycrystalline conductor structure is proposed, this charge being the major electromigration parameter. The model developed adequately describes the influence of grain boundary characteristics on the effective charge of proper and impurity ions. These quantities strongly effect on the reliability of microcircuit performance. The main factor that results in distinction between values of effective ion charges in a grain boundary and in a monocrystal of the same metal is a difference of their atomic densities. The effective charges of ions of Al and Cu in an Al grain boundary are calculated as a function of the grain boundary misorientation angle, the grain boundary texture, and the temperature. We give also the modeling results for some other metallization systems. In particular, these simulation results demonstrate that the effective charge value in the grain boundary can differ greatly from that in the crystal bulk and strongly depend on the boundary texture and temperature**.** The ways of the interconnect lifetime increasing are discussed.

1. T. Makhviladze, M. Sarychev. “Electromigration theory and its applications to integrated circuit metallization”, Proc. SPIE, **7521,** 752117 (pp.1-15), 2010.
2. T.M. Makhviladze, M.E. Sarychev. “The theory of elecrtomigration failufe of thin-film conluctors and its application”, Proc. of the Phys.-Techn. Inst., *Quantum computers, micro- and nanoelectronics: physics, technology, diagnostics and modeling,* ed.by A.A. Orlikovsky, Vol.20, pp.85-110, Moscow, 2009 (in Russian).
3. K.A. Valiev, R.V. Goldstein, Yu.V. Zhitnikov, N.M. Makhviladze, M.E. Sarychev, “Nano- and micrometer-scale thin-film-interconnection failure theory and simulation and metallization lifetime prediction, Part 2: polycrystalline-line degradation and bulk failure”, Russian Microelectronics, **39**, pp.145-157, 2010.

The numerical model of simplest FIB on ions of rare gases for nano diagnostics and nano patterning

VA. Zhukov[1], N. V. Badenko[2], P. V. Shpartko[2]

1 St. Petersburg Institute of Information Science and Automation, Russian Academy of Sciences, St. Petersburg, Russia, E-mail address: valery.zhukov2@gmail.com 2. St. Petersburg State Polytechnic University, St. Petersburg, Russia

The so-called "ion guiding effect" [1-3] has been discovered in the past decade. It consists in elastic passing of singly and multiply charged ions of noble gases (He^{1+}, Ne^{7+}, Ar^{8+}) with medium energy (7 keV ÷ 2 MeV) through a conical glass capillary without kinetic energy and charge losses. In the experiments [1-3] capillary was 50 mm in length and had an output diameter of 1 ÷ 25 microns.

There are the two most important characteristic features of "ion guiding effect" observed experimentally:

1) The ion current, coming from the end of the tube, increases monotonically with time and goes to its saturation level which is equal to the level of the input current;

2) The ion beam, passing through the conical capillary tube, is concentrated in axisymmetric spot of much smaller area (10^4 ÷ 10^6 times) than the area of the tube inlet (~ 1 mm^2).

In the present work a numerical-analytical model of electric charging of short (1 ÷ 3 mm) tapered dielectric rings by the beam of inert gases ions was developed. It is proposed that the beam passes parallel to the axis of the ring and has constant bulk density. In contrast to our previous work [4] we took into account the presence of a metal screen with a circular hole in it, placed in front of the inlet hole of the tapered dielectric ring. It is shown that in the charged stationary state the ring can be used as a lens. It is calculated that such a lens of 1mm has a focal length of 3.4 mm (calculated using parameters from experiments [1-3] where an input diameter was 0.8 mm, the angle between the generatrix of the cone and the axis was equal to 10^{-2} rad). Spherical aberration coefficient and chromatic aberration coefficient of the lens are 760mm and 14 mm respectively. The resolution of a scanning ion microscope with such lens would be comparable to the resolution of the best modern scanning helium ion microscope [5]. At the same time production of such devices would be much easier and cheaper.

This work was supported by the program of basic research of RAS, the direction of "The organization of calculations on the basis of new physical principles".

T. Nebiki, T.Yamamoto, T. Narusava, “Focusing of MeV ion beams by means of tapered glass capillary optics” J.Vac. Sci. Technol. A., **21,** No**.** 5, pp.1671-1674, 2003.

T. Ikeda, Y. Y. Kanai, T.M. Kojima, Y. Iwai, T. Kambara, Y.Yamazaki, M.Hoshimo, T. Nebiki, T.Narusawa, “Production of a microbeam of slow highly charged ions with a tapered glass capillary” Applied Physics letters.. **89,**.163502, pp. 1-3, 2006

T.Ikeda, Y.Kanai, T. M.Kojima, Y.Iwai, Y.Kanazawa, M.Hoshino, T.Kobayashi, G. P.Pokhil, Y.Yamazaki, “Focusing of charged particle beams with various glass-made optics”, Journal of Physics: Conference Series, **88**, 012031, pp**.** 1-9, 2007.

4. V. A.. Zhukov, P.V. Shpartko “Electron-optical properties of a charged conical dielectric rings”, Russian Microelectronics, **41,** No. 5, 2012 (in print).

5. Essential Specification data of “ORION” helium ion microscope. Available on http://www.smt.zeiss.com/nts.

Molecular dynamics simulations of the low energy Ar ion-plasma sputtering of copper nanostuctures

A. Kupriyanov, O. Trushin, I. Amirov
Yaroslavl Branch of the Institute of Physics and Technology of Russian Academy of Science, Yaroslavl, Russia.
ildamirov@yandex.ru

The processes of ion sputtering and surface modification are increasingly used in the technology of nanoelectronics [1]. Low energy ion treatment of solid surfaces can cause ultra-smoothening or self-organized nanoscale surface pattern formation, depending on control parameters such as ion and target species, ion energy and incidence angle. In contrast to traditional monoenergetic ion beam sputtering an ion-plasma sputtering is characterized by wide distribution of energies of the incident ions. In addition, the ion flow is characterized by a certain angular distribution.

In this paper molecular dynamics (MD) simulation was used to study the sputtering of copper rectangular groove (Fig 1a) by low energy argon ions (E_i <200 eV). MD simulation was done using home made computer code (IMPACT) implementing numerical algorithm Leap-Frog [2] with a time step of 10^{-15} s. The substrate is modeled by a single crystal of copper with orientation of surface FCC (100) consisting of 6000 atoms. Interatomic forces were modeled by generalized form of the Lennard-Jones potentials [2].

The simulation showed that the dependences of the yield of Cu atoms sputtering per ion on impact energy (Y) and the angle of incidence of the ions are in satisfactory agreement with experimental data [3]. A small angular deviation of the ion flux is not affected by this dependence. The yield Y has maximum at an angle of incidence of the ions equal to 40-60 degrees, depending on the energy of the incident ions.

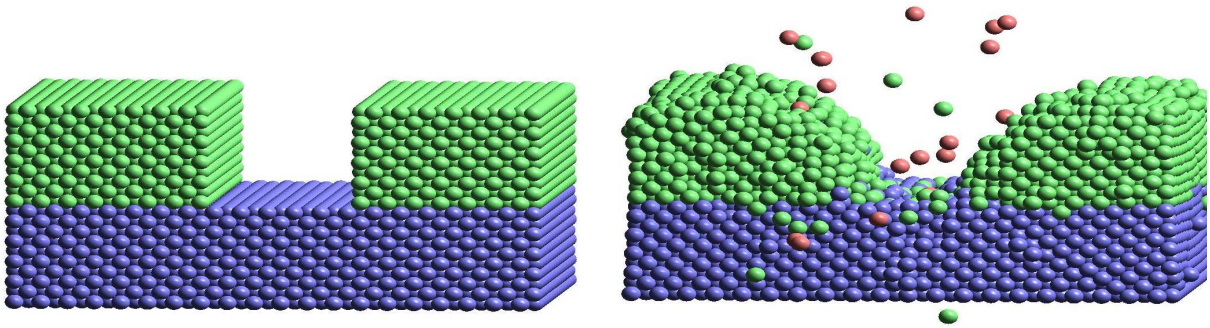

Fig.1. a) Cu rectangular grooves and b) Cu grooves after the fall of 500 Ar^+ with energy 50 eV.

Simulation of sputtering copper rectangular groove width of 5 nm with an energy of 50-150 eV (Y = 0.22-0.65) showed that the preferential sputtering of copper atoms occurs at sharp corners (Fig 1b). The effect of smoothing of sharp corners of the groove was also observed in the experiments. Results of modeling and dependence Y on the parameters stated above was analyzed.

1. K. Sugiura, S. Takahashi, M. Amano, T. Kajiyama, M. Iwayama, Y. Asao, N. Shimomura, T. Kishi, S. Ikegawa, H. Yoda, A. Nitayama, “Ion Beam Etching Technology for High-Density Spin Transfer Torque Magnetic Random Access Memory”, Jap. J. Appl. Phys, **48**, pp.08HD02, 2009.
2. W. Eckstein. *Computer Simulation in Ion-Solid Interactions.* Springer-Verlag, Berlin, 1991.
3. D. Kress, D.E. Hanson, A.F. Voter, C.L. Liu, X.-Y. Liu, and D.G. Coronell, “Molecular dynamics simulation of Cu and Ar ion sputtering of Cu (111) surfaces”, J. Vac. Sci. Technol. A, **17**, pp.2819-2827, 1999.

Mechanisms of strain relief in Cu/Ni(100) heteroepitaxy

O. Trushin[1], T. Ala-Nissila[2], S-C. Ying[3], E. Granato[4]

1. Yaroslavl Branch of the Institute of Physics and Technology, Russian Academy of Sciences, Yaroslavl, Russia, otrushin@gmail.com; 2. Aalto University, Helsinki, Finland; 3. Brown University, Providence, USA; 4. Instituto National de Pesquisas Espaciais, Sao Jose dos Campos, SP Brasil.

Heteroepitaxial systems play an important role in modern microelectronics technology [1]. Due to the lattice mismatch between the film and the substrate, considerable elastic strain energy is accumulated in epitaxy. For sufficiently thick films, defects will form leading to the relaxation of strain energy and to the loss of coherent epitaxy [2]. Controlling the film-substrate interface quality and preventing defect formation is an important problem of modern technology. Experimental methods at present do not allow either a detailed study of the defect core at the atomic level or the time evolution of the system during defect nucleation process. Therefore, theoretical modeling plays an important role in the studies of defect core structures and the mechanisms of their formation.

Typical example of heteroepitaxial system is of Cu/Ni(100) system having compressive strain (+2.6%) and FCC(100) surface geometry. Experimental studies of this system showed presence of rectangular shape defects on the surface [3] for film thickness up to 20 ML. Simple geometrical interpretation of the defect has been given (internal (111) faceting model), however no atomistic simulations supporting this idea is available in literature up to now according to our knowledge.

In this work we made an attempt to explore nature of those defects using atomistic simulations with semiempirical potential of Embedded Atom Model [4]. In all cases we use a universal molecular static method for generating Minimum Energy Paths for transitions from the coherent epitaxial (defect free) state to the state containing an isolated defect (localized or extended) [5,6]. In this way we are able to generate isolated defects in this system and explore its geometry and energetics.

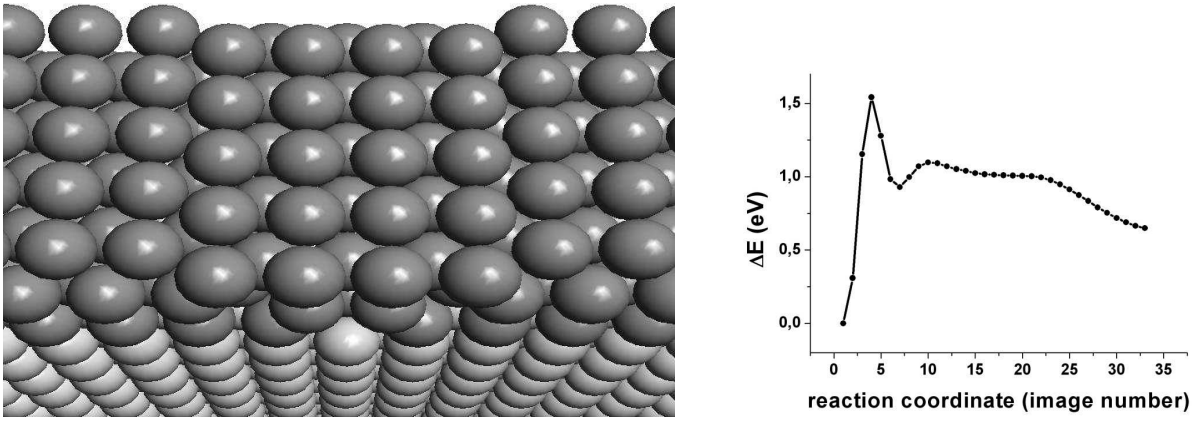

Fig.1 Top view on atomistic model showing wedge shape defect (Cu atoms shown in dark, Ni atoms in light) and corresponding energy profile along Minimal Energy Path obtained in simulation.

Our simulations showed (Fig.1) that wedge type defect observed in experiment [3] is indeed local energy minimum for the system. However, according to our simulation, it should be metastable state (defect state has higher energy than initial coherent state) and could be induced by the kinetics of the growth mode.

1. S.A. Campbell. *The Science and Engineering of Microelctronic Fabrication*, Oxford University Press, New York, 2001.
2. H. Luth. *Surfaces and Interfaces of Solid Materials*, Springer 1998.
3. B. Muller, et a.l, Phys. Rev. Lett., **76**, pp.2358-2361, 1996.
4. S.M. Foiles, M.I. Baskes, and M.S. Daw, Phys. Rev. B, **33**, p.7983, 1986.
5. O. Trushin, P. Salo, T. Ala-Nissila, and S.C. Ying, Phys. Rev. B, **69**, p.033405, 2004.
6. H. Jonsson, G. Mills and K.W. Jacobsen, in *Classical and Quantum Dynamics in Condensed Phase Simulations*, ed. by B.J. Berne ,World Scientific, Singapore, 1998.

Modeling of profile evolution at the low-energy ion sputtering in Ar plasma

A.S. Shumilov, I.I. Amirov
Yaroslavl Branch of the Institute of Physics and Technology of Russian Academy of Sciences, Yaroslavl, Russia.
ashumilov@inbox.ru

The control of feature profiles in directional plasma etching processes is crucial as critical a formation of nanostructures, line-edge roughening, dimension and other artifacts affect device performance and process yields. The developed dynamic Monte Carlo methods [1, 2] explore the atomic scale mechanisms of nucleation of nanostructures, provide pertinent information and physical insights. However, in the framework of this method is impossible to simulate the processes of formation of high aspect ratio nanostructures in real time intervals. That's why the predictable modeling of this process is necessary to understand the surface processes responsible for changes in profile morphology. The purpose of this work was to develop a modeling method for simulating materials at low-energy ion sputtering processes, taking into account ion reflections and material redeposition. The method was incorporated into the 2-DimensionaI Monte Carlo profile simulator EDPS with a cell-based representation. Method uses special algorithms to calculate the surface normal for accurate determination of the ion's incidence angle and the emission angle of sputtered atoms. The simplified set of particle-surface interactions was carefully chosen to reflect the overall etching characteristics and the rate coefficients were fitted to experimental data. A single-layer surface kinetic model with 6Å cell width was used to account for plasma-surface interactions.

Model was tested for accuracy using Si and Cu wave-like structures sputtering in Ar gas plasma. We approximate the sputtering yield dependence with the incident energy by linear function [1-3]. The sputtering energy threshold and the linear yield coefficient were calculated using formulas obtained in article [3]. In lack of precise experimental results we use specula reflection of ions in all angle range. Sputtering of surface Ar atoms was not considered because of its low emitted energy. We use an analytical formula of angular dependence of sputtering yields which was developed in work [4] with the peak in 50-65°. We have found that the angular distribution of sputtered particles with low-energy ions is greatly different of well known Sigmund cosines distribution [4], but can be described by a simple Gaussian-like formula [1, 5]. Our experiments show that the sputtered atoms fly out at the semi-specula direction of reflected ions at off-normal ion angles and along the surface at direct strikes. Sputtered material atoms redeposited on the surface with a constant sticking probability.

We examined the dependence of smoothing or roughening behavior on the initial surface of Si. Result shows that the rough surface becomes smooth and the smooth surface becomes rough due to low energy Ar^+ vertical ion beam sputtering process and both finally saturates at concrete RMS value. With the none-vertical ion directions we observe the periodic structures known as sputter ripples [2]. We compare the modeling results with experiments of sputtering of pyramidal nanostructures on Si surface by low energy argon ions (E_i < 200 eV). The resulting profile depends of the ion's energy, angular dependence of sputtering yields and redeposition of sputtered atoms. The simulation results agree well with the experimental data.

1. X.-Y. Liu, M.S. Daw, J.D. Kress, D.E. Hanson, V. Arunachalam, D.G. Coronell, C.-L. Liu, A.F. Voter, "Ion solid surface interactions in ionized copper physical vapor deposition", Thin Solid Films **422**, pp.141–149, 2002.
2. Y. Ishii, W.L. Chan, E. Chason, "Kinetic Monte Carlo simulation of ripple formation by sputtering: Effects of multiple defects and Ehrlich–Schwoebel barriers", Nuclear Instruments Methods in Phys. Res. B, **272**, pp.188–192, 2012.
3. W. Guo, Bo Bai, H.H. Sawin, "Mixing-layer kinetics model for plasma etching and the cellular realization in three-dimensional profile simulator", J. Vac. Sci. Technol. A, **27**, pp.388-403, 2009.
4. Q. Wei, K.-D. Li, J. Lian, L. Wang, "Angular dependence of sputtering yield of amorphous and polycrystalline materials", J. Phys. D: Appl. Phys, **41**, pp.172002 -172006, 2008.
5. Yu V. Martynenko, A.V. Rogov, and V.I. Shul'ga, "Angular distribution of atoms during the magnetron sputtering of polycrystalline targets", Technical Physics, **57**, pp.439-444, 2012.

Numerical calculations of the concentration profile for InGaAs/GaAs heterostructures with δ-doping layers

S.V. Khazanova, V.E. Degtyarev
Lobachevskiy Nizhnii Novgorod University, Nizhni Novgorod, Russia, khazanova@phys.unn.ru

Semiconductor heterostructures with quantum wells is great interest due to wide implications for electronic and optoelectronic devices. In particular, InGaAs/GaAs heterostructure is applied for construction of PHEMT structures. Because growth of high-quality heterostructures is the expensive processes, previous analyzing of these structures is needed. It is known the analytical solution of the same systems is possible only for limited cases, therefore numerical method is used. This is a powerfull method for determination of parameters of semiconductor heterostructures including energy positions of subband levels, wave functions. One of the main problems is determination of the electron density distribution in the obtained structures. Unfortunately known methods from the literature are not sufficiently exactly for structure with δ-doping layers ore require large time of computation [1-3].

In this work we prepare modified numerical method concentration calculation in the nanostructure containing of quantum well and δ -layer (рис. 1). The width of quantum well is about 10 нм and distance between well and δ-layer is 8-12 нм. The numerical self-consistent solution of coupled Shredinger and Poisson equations is used to solve this problem. A conventional approach to the solution of equations has been the finite difference method. Real space is divided into discrete mesh points and wave functions are solved within discrete spacing. As known in the quantum system spectrum energy have both continuous and discrete component. But if we put our system the box with infinity potential walls the problem is reducing to concentration calculation for system with discrete spectrum [2]. It should be noted levels density and their number will be determined by box size. According our investigations, number of levels used for correct calculation should be N/4, N – spacing discretization number. By the way, spacing discretization result in to energy nonparabolicity and this fact should be account in the calculations. Our testing shows that the approach is valid for large range of Fermi level position and coordinate variation.

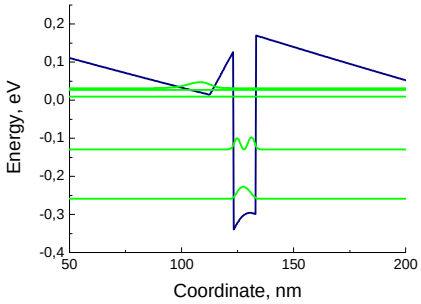

Рис.1.Calculated band conduction profile and quantum level energy.

Iterative procedure was used to obtain the self-consistent solution. Starting with a trial potential, we find eigenvalues of the quantum states and wave functions in the structure. The iteration procedure was repeated until maximum difference between the present and previous effective potential was 10^{-7}eV.

Effect of structure geometrical parameters and the doping degree on the concentration profile are investigated. It is shown concentration dependence on the distance between the doping layer and the quantum well. Our results show that at the certain parameters we can see double concentration peak, carriers is distributed between well and δ-layer. The same profile has been observed in the experimental work [4].

We demonstrated modified numerical model for calculation of carrier concentration of the complex InGaAs/GaAs heterostructure. The results of the calculation are compared with experimental work, good agreement is observed.

1. P.N. Brounkov, T. Benyattou, G. Guillot, J.Appl.Phys., **80**, p.864, 1996.
2. V.I. Zubkov, M.A. Melnik, A.V. Solomonov, and E.O. Tsvelev, Phys.Rev. B, **70**, 075312 (2004).
3. M.P. Anantram, M.S. Lundstrom, D.E. Nikonov, Proceedings of the IEEE, **96**, pp.1511-1550, 2008.
4. Proc. of XVI Int. Symp. «Nanophysics and Nanoelectronics», pp.406-407, 2012.

Formation of silicon oxide layer on the surface of mono-Si wafer by means of ion beam irradiation

B. Gurovich, K. Prikhodko, A. Taldenkov, D. Komarov, L. Kutuzov
National Research Center "Kurchatov Institute", Kurchatov sq.1, Moscow, Russia, E-mail: kirill@irmrnt.kiae.ru

This work is dedicated to the formation of the silicon oxide on the surface of the mono-crystal wafer using two types of ion beam irradiation. First technique is utilized the irradiation by the 1 keV composite ion beam containing protons and oxygen ions at room temperature up to the fluence of $3\cdot10^{20}$cm^{-2}. The second one is using low energy (40 eV) oxygen ions irradiation at temperature 400°C up the fluence of $7.7\cdot10^{19}$ cm^{-2}.
Industrial *n*-type P doped 0.006 Ohm·cm (carrier concentration 10^{19} cm^{-3}) and *p*-type B doped 0.03 Ohm·cm (carrier concentration $4\cdot10^{18}$ cm^{-3}) [001] silicon wafers were chosen for ion beam irradiation. Ions were extracted from the RF plasma discharge by applying the negative bias to the substrate. Ions content at the composite beams was controlled by the partial pressures of the gases injected to the discharge chamber. Typical value of P_{O2}/P_{H2} ratio was $3.2\cdot10^{-5}$. The thickness of the silicon oxide layer after irradiation was measured by XPS depth profiling using "Quantera" scanning x-ray spectrometer (PHI). The microstructure was investigated by EFTEM/STEM techniques using "Titan" transmission microscope (FEI) equipped with GIF2001 EELS spectrometer (Gatan) on a cross-sectional samples produced by Ar ion milling using PIPS (Gatan). Irradiation induced oxide electrical properties were studied on MOS (metal-oxide-semiconductor) structures which were formed by the sputtering of 100 nm Au layer on the surface of the samples after ion irradiation. These MOS structures were investigated using Keithley 4200-SCS semiconductor measuring station and Agilent 4980A LCR-meter. Frequency range was 10^{-3} Hz – 2 MHz and voltage range was ±10 V.

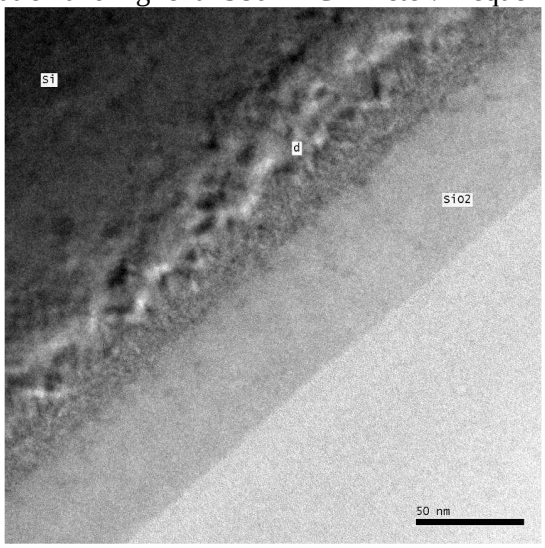

Fig.1 Bright field TEM cross section image of the wafer after ion irradiation (d- damage layer).

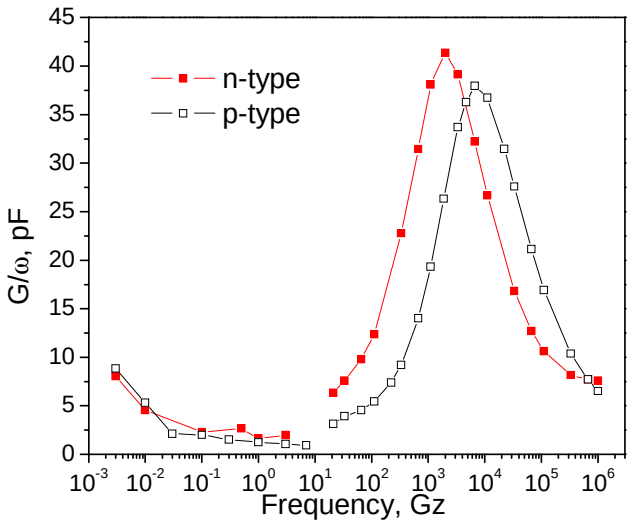

Fig.2 Frequency dependence of *n*- and *p*-MOS structure conductivity at zero bias.

TEM structure investigations of irradiates samples showed uniform distribution of the silicon oxide layer at the surface of the silicon wafer and the presence of a silicon damage layer between the oxide and bulk wafer (fig.1). The position of the plasmon energy loss peak within the radiation-induced oxide layer was 24 eV that corresponds to the value of bulk SiO_2. It was found the presence of a transition SiO_x layer close to the SiO_2/Si interface with the thickness ~10 nm. It had been found that the electrical field working range of the irradiation-induced silicon oxide was above $3\cdot10^6$ V/cm and the resistivity ~10^{15} Ohm·cm. One of the features of irradiation-induced insulation layers was the formation of electrical traps that reveals in the presence of maximum at the G/ω frequency dependence curve (fig.2).
The perfect structure and low level of leakage current proves that this radiation induced silicon oxide can be used as an insulator during nanostructures formation under ion irradiation for various applications [1].
This work is supported by the Russian Ministry of Science and Education (contract № 16.513.12.3004).

1. B.A. Gurovich, K.E. Prikhod'ko, A.N. Taldenkov, A.Yu. Yakubovskii, K.I. Maslakov, D.A. Komarov, L.V. Kutuzov, G.E. Fedorov, "Development of IonBeam Technique for Manufacturing Silicon Nanowires", Nanotechnologies in Russia, **7**, Nos.1–2, pp.93–97, 2012.

The quantum-size Si dots formed in PECVD Si/SiO_2 multilayers by irradiation with swift heavy ions

G. Kamaev[1,2], S. Cherkova[1,2], A. Antonenko[1,2], G. Kachurin[1], A. Gismatulin[1], D. Marin[1,2], V. Volodin[1,2], A. Cherkov[1,2], and V. Skuratov[3]

[1]*A.V. Rzhanov Institute of Semiconductor Physics SB RAS, 630090 Novosibirsk, Russia;*
[2]*Novosibirsk State University, 630090 Novosibirsk, Russia;*
[3]*Joint Institute for Nuclear Research, 141980 Dubna, Russia; e-mail: kamaev@isp.nsc.ru*

The ability of the quantum-size Si nanocrystals (Si-ncs) to emit light stimulates research into the processes of their formation and modification. Usually Si-ncs are formed via self-organization in the Si-rich SiO_2 layers during furnace annealing. However, this way of formation results in a relatively broad size distribution of the synthesized Si-ncs. Moreover, the size and density of the quantum dots cannot be controlled independently. To make the Si-ncs formation more predictable the layer-by-layer gas phase deposition of the nanometer-thick amorphous Si and SiO_2 followed by a high temperature annealing was proposed. Unfortunately, the thinner is a nanolayer, the higher temperatures are needed for its crystallization; therefore the methods which allow a local stimulation of the structural transformations would be of great interest.

We studied the influence of swift heavy ions (SHI) on synthesis of the silicon quantum dots in stacks of the gas phase deposited ultrathin Si/SiO_2 multilayers. Si/SiO_2 multilayer nanoscale structures were obtained using a procedure of amorphous silicon (α-Si:H) thin film PECVD and subsequent partial plasma enhanced oxidation in the plasma-chemical reactor with a wide aperture source. Such sources provide high density of the active ions (up to $10^{11}\div10^{12}$ cm^{-3}) with low energies (less than 4÷6 eV), as well as good uniformity of the film thickness within the large spatial area. Six pairs of the 7÷8 nm-thick α-Si:H and 10÷12 nm-thick SiO_2 layers have been prepared on the crystalline Si substrates. The quantum-size Si dots were formed in PECVD Si/SiO_2 heterostructures by irradiation with 167 MeV Xe ions in the dose range of $10^{12}\div10^{14}$ cm^{-2}. Some samples were annealed in the temperature region of 500÷1100 ^{0}C for 30 min in N_2 ambient.

Photoluminescence (PL), optical FTIR absorption, Raman scattering and cross-sectional high resolution electron microscopy (HREM) were used for the characterizations. The electrical properties of multilayer nanostructures were studied by the measurements of their capacitance-voltage (C-V), conductance-voltage (G-V), and current–voltage (I–V) characteristics. The C–V and G-V characteristics were studied in the frequency range 1 kHz – 1 MHz by using an automated Agilent E4980A multifrequency LCR-Meter.

According to the electron microscopy data the irradiation broke the layers integrity (see inset in Fig.1). Raman spectroscopy evidenced an increase in the scattering by amorphous silicon, and in the photoluminescence (PL) spectra the yellow-orange band appeared, usually ascribed to the tiny inclusions of Si in SiO_2. The annealing at 800^{o}C restored the SiO_2 net, pushing the excess Si atoms out. The annealing at 1100^{o}C led to an appearance of more intensive PL peak at about 780 nm, typical of the Si nanocrystals, and its intensity was growing with the dose. It is concluded, that the irradiation creates the nucleation sites, which facilitate formation of the Si nanocrystals under the subsequent annealing. The processes proceed inside the tracks due to the high temperatures resulting from the heavy ionization losses of the ions.

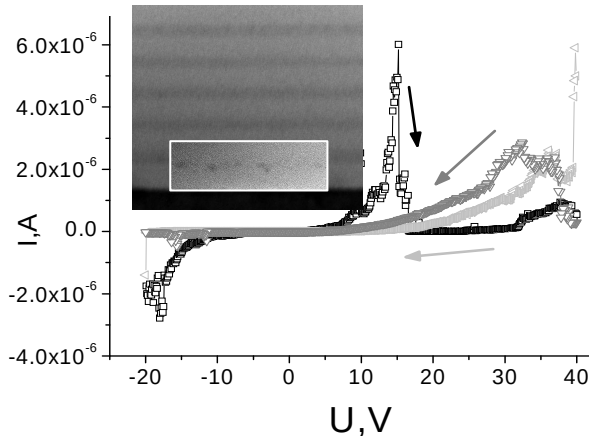

Fig. 1

The electrical properties of the structures were investigated by the measurements of MOS capacitors the characteristics. Electrical measurements revealed the significant peculiarities connected with charge transport through the prepared nanoscale multilayer structures. It is seen in Fig.1 that the I-V curves have the steps and the negative differential resistance regions, which can be caused by the resonant tunneling through the Si clusters.

The study of nanostructures formation on AlSi thin film surface under ion-plasma sputtering

V. Bachurin, I. Amirov, M. Izyumov, V. Naumov, S. Simakin
Yaroslavl branch of the Institute за Physics and Technology of Russian Academy of Science, Yaroslavl, Russia, vibachurin@mail.ru

Ion bombardment is widely used method in the last time for formation on the solid surfaces such nanostructures as ripples, quantum wires and dots and etc. The sizes of such structures depend on the conditions of ion bombardment (ion energy, angle of ion incidence, fluence) which can be easy changed. The goal of the present work was to study the possibilities to obtain nanostructures on the surface of two components thin films under low energy ion-plasma sputtering. It was supposed that the same structures may be formed due the preferential or selective sputtering if one of the components of thin film has a small concentration and lower partial sputtering yield.

AlSi thin films on the SiO_2 substrate were used as the samples. The ratio of partial sputtering yields (Y_i) in this case is defined mainly by the ratio of surface binding energies which is U_{Al}/U_{Si} =0.71 and sputtering yield of Al is almost two times more then of Si [1]. The samples were prepared by magnetron sputtering of $Al_{0.99}Si_{0.01}$ target. The content of Si in the film measured with AES was less then 1%. The sputtering of samples was carried out in the reactor of high density Ar plasma of RF inductive discharge [2]. The average energy E_i of the Ar^+ ions (25-400 eV) bombarding the substrate surface was determined by the applied RF bias power P_{sb} (0-400 W, 13.56 MHz). The morphology of the surfaces was studied with SEM Supra 40. The chemical composition of surface was investigated using SIMS IONTOF[5]. It permitted to measure the relative concentration and distribution of Si on the surfaces of initial and irradiated samples.

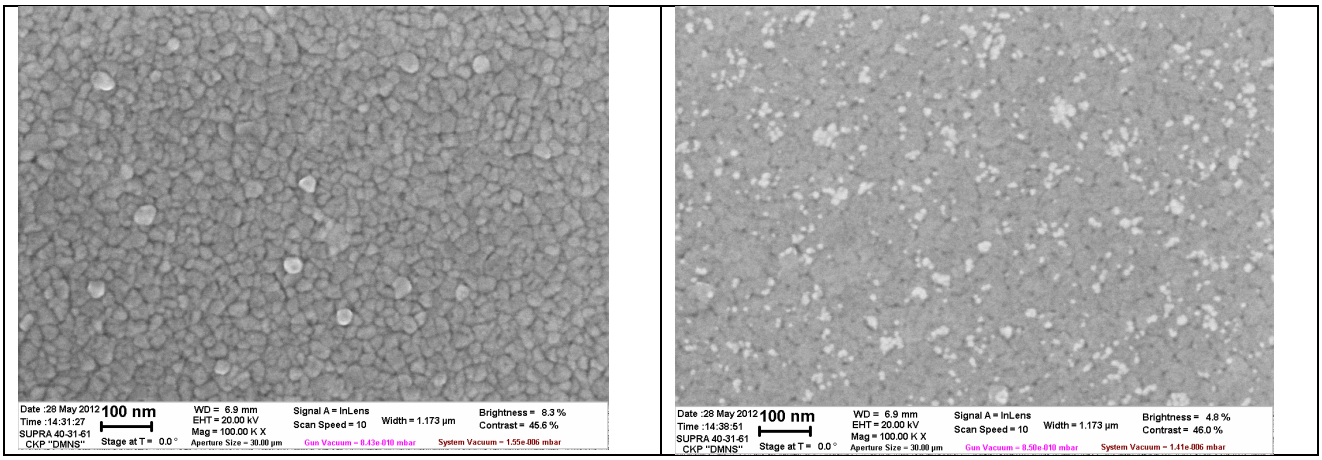

Fig. 1. SEM image of initial (left) and irradiated (right) AlSi thin film surfaces.

One can see that initial thin films have a grain structure with the average size of grain about 20 nm. The small parts of grains are brighter. The data of SIMS analysis show that they belong to Si. Usually the AlSi is one phase compound at Si concentration more than 5%. Possibly the thin film is the mixture of homogeneous AlSi with inclusions of Si grains. Irradiation of the surface with 60 ev Ar^+ ions leads to the decreasing average sizes of grain (about 10 nm), increasing on one order the content of Si on the surface and the formation of a lot of Si grains (see Fig. 1, right). The possible mechanisms of the formation nanostructures including the preferential and selective sputtering ion induced diffusion and segregation will be considered in the report.

1. *Sputtering by Particle Bombardment II*. Edited by R. Behrisch. Springer-Verlag, Berlin, 1983.

Efficiency of fast neutral particle beam sources based on gas-phase charge exchange processes

V.P. Kudrya
Institute of Physics and Technology, RAS, Moscow, Russia, E-mail address: kvp@ftian.ru

Gas-phase charge exchange processes are one of the mechanisms to produce beams of fast neutral particles from ion beams. Fast atom beam (FAB) sources based on this mechanism have been used for sputtering, etching, and neutral beam lithography [1-4]. A specific feature of this mechanism is an inevitable influence of the elastic neutral-neutral and ion-neutral scattering that results in removal of fast particles (neutral and ion) from the beam. Therefore, passing through a gas the fast ion beam is neutralized but its intensity decreases due to scattering. Thus, efficiency of the FAB sources considered depends on the gas thickness (product of the pressure and the length) of the neutralizing system used.

An analytical model in which the elastic scattering of ions and neutrals are equal was used in [2, 5]. We present a model in which different elastic cross sections for ions and neutrals can be used. In this case the neutrality coefficient (fraction of neutrals in the beam that characterizes the charge quality of the output beam) is given by

$$K_{\text{neutr}}(l) = \frac{N_{\text{n}}(l)}{N_{\text{i}}(l) + N_{\text{n}}(l)} = \frac{1 - \exp\left[-\left(\lambda_{\text{exch}}^{-1} + \lambda_{\text{i elast}}^{-1} - \lambda_{\text{n elast}}^{-1}\right)l\right]}{1 + \lambda_{\text{exch}}\left(\lambda_{\text{i elast}}^{-1} - \lambda_{\text{n elast}}^{-1}\right)\exp\left[-\left(\lambda_{\text{exch}}^{-1} + \lambda_{\text{i elast}}^{-1} - \lambda_{\text{n elast}}^{-1}\right)l\right]},$$

where l is the length of the neutralizing system, $N_{\text{n}}(l)$ and $N_{\text{i}}(l)$ are the numbers of neutrals and ions in the output beam, λ_{exch}, $\lambda_{\text{n elast}}$, and $\lambda_{\text{i elast}}$ are the mean free lengths for ion-neutral charge exchange, neutral-neutral elastic, and ion-neutral elastic scattering, respectively. Due to the inequality $\lambda_{\text{n elast}} \geq \lambda_{\text{i elast}}$ the dependency $K_{\text{neutr}}(l)$ is monotone increasing.

The second important value is the neutralization coefficient (efficiency of converting the primary ion beam into the neutral beam) is given by

$$K_{\text{eff}}(l) = \frac{N_{\text{n}}(l)}{N_{\text{i}}(0)} = \frac{\exp\left(-\lambda_{\text{n elast}}^{-1} l\right)}{1 + \lambda_{\text{exch}}\left(\lambda_{\text{i elast}}^{-1} - \lambda_{\text{n elast}}^{-1}\right)}\left\{1 - \exp\left[-\left(\lambda_{\text{exch}}^{-1} + \lambda_{\text{i elast}}^{-1} - \lambda_{\text{n elast}}^{-1}\right)l\right]\right\}.$$

The maximum value of $K_{\text{eff}}(l)$ is given by

$$K_{\text{eff max}} = \frac{\left[\lambda_{\text{n elast}}\left(\lambda_{\text{exch}}^{-1} + \lambda_{\text{i elast}}^{-1}\right)\right]^{-\lambda_{\text{n elast}}^{-1}/\left(\lambda_{\text{exch}}^{-1} + \lambda_{\text{i elast}}^{-1} - \lambda_{\text{n elast}}^{-1}\right)}}{1 + \lambda_{\text{exch}} / \lambda_{\text{i elast}}}.$$

In the approximation of $\lambda_{\text{n elast}} = \lambda_{\text{i elast}} = \lambda_{\text{elast}}$ one can obtain that

$$K_{\text{eff max}} = \frac{\xi}{(1+\xi)^{1+1/\xi}},$$

where $\xi = \lambda_{\text{elast}}/\lambda_{\text{exch}} = \sigma_{\text{exch}}/\sigma_{\text{elast}}$, σ is the cross section. The dependency $K_{\text{eff max}}(\xi)$ is monotone increasing.

1. Mizutani T., Nishimatsu S., "Sputtering yield and radiation damage by neutral beam bombardment", J. Vac. Sci. & Technol. A, **6**, pp.1417-1420, 1988.
2. Tsuchizawa T., Jin Y., Matsuo S., "Generation of Electron Cyclotron Resonance Neutral Stream and Its Application to Si Etching", Jap. J. Appl. Phys., **33**, pp.2200-2206, 1994.
3. Iijima Y., Yamada T., Matsumoto S., Hiraoka K., "Low-energy Ar Neutral Beam Etching Method for X-ray Photoelectron Spectroscopy", Surf. Interface Anal., **21**, pp.778-784, 1994.
4. Wolfe J.C., Craver B.P., "Neutral particle lithography: a simple solution to charge-related artefacts in ion beam proximity printing", J. Phys. D, **41**, 024007, pp.1-12, 2008.
5. Hara Y., Takashima S., Yamakawa K., Den S., Toyoda H., Hori M., "Tunable low-energy Ar fast atom source with large diameter", Appl. Phys. Lett., **91**, 231502 (pp.1-3), 2007.

Piezoelectric generator with filled space between the ZnO nanowires

D.G. Gromov[1], A.M. Kozmin[1], M.U.Nazarkin[1], S.P.Timoshenkov[1], S.A.Gavrilov[1], A.I.Kozlitin[2]
[1]*National Research University of Electronic Technology, Moscow, Russia, e-mail: nodanceak@mail.ru.*
[2]*Joint research center "Synchrotron", Moscow, Russian, e-mail: info@ckp.su*

In the world scientific community over the past few years the idea of converters any to electrical energy successfully developed. Already known devices that convert most powerful solar, wind and ocean waves energy into electricity, but along with it humanity surrounds a lot of sources of dissipated energy - the vibrations, mechanical and sound fluctuations. One of such converter type is energy “harvester” that collects electrical energy from array of nanotransducer elements. Such energy harvester is the nanogenerator using piezoelectric ZnO nanowires array for converting mechanical ultrasonic energy into electricity [1]. However the nanogenerator has the deficiency: low voltage (hundreds of mV) and low current (tens of nA) values. The main problem of piezoelectric nanowires array device is to take off signals simultaneously from tip of every nanowire. It is considered that when piezoelectric nanowire is bent at the top tip its polarization results in appearance of positive and negative charges [1]. The region of the nanowire where the crystal lattice extends becomes positively charged, and the one where the lattice shrinks charges negatively. In this connection the top electrode should commutate only with that part of the top tip of each piezoelectric wire which has a charge of one type. For this purpose different top electrode structures were used such as an array of metalized V-shaped trenches or an array of metalized spikes as a top electrode in the nanogenerator structure [2].

According to the classical theory of the piezoelectric effect [3], for higher piezoelectric effect it is necessary to apply pressure on lateral edges or lateral faces of the hexagonal ZnO crystal. To achieve this aim, we have filled the free space between the ZnO nanowires with solid material. We have used a flat movable top electrode to gather the electric charge at the top contact with the array of ZnO nanowires.

The first oxidized silicon substrate using magnetron sputtering method was covered with 300 nm Ni layer, which was playing the role of the bottom electrode. Then using the same method of magnetron sputtering of ZnO:Al target the bottom electrode was covered with 20 nm ZnO:Al seeding layer. ZnO nanowires array was formed on the structure by chemical deposition from water solution 0,4M NaOH and 0,01M $(Zn(NO_3)_2)\cdot 6H_2O$. Further 300 nm ZnO layer was deposited on ZnO nanowires array. At the final stage ZnO nanowires array has grown additionally. The second oxidized silicon substrate was covered with a 400 nm Cu layer playing the role of the top electrode using magnetron sputtering. The second substrate with its Cu layer down was placed on the ZnO nanowires array of the first substrate. And finally an elastic adhesive sealant was applied along the perimeter of the structure to guarantee the moving of the second substrate relative to the first one.

To study electrophysical properties of the assembled piezoelectric device a vibration machine LDS V455 PA1000L was used, having the following characteristics: from 10 to 1000 Hz vibration frequency range and acceleration amplitude up to 1147 m/s^2. Piezoelectric device was exposed to sinusoidal vibrations by the vibration machine. The piezoelectric device output signal was recorded by oscilloscope and nanoammeter.

It was found that the ZnO nanowire piezoelectric generator is sensitive to low-frequency vibration range (from tens of Hertz to hundreds of Hertz). It is important to mention that the voltage and current device signal change in time repeats the sinusoid of the vibration machine. The maximum response of 7 V and 156 nA for an acceleration of 1g was achieved with a vibration frequency of 300 Hz.
References:

1. Y. Gao, Z.L. Wang, "Electrostatic Potential in a Bent Piezoelectric Nanowire. The Fundamental Theory of Nanogenerator and Nanopiezotronics", Nano Lett., **7**, pp.2499-2505, 2007.
2. Z.L. Wang, "Nanogenerators for Self-powered Devices and Systems", School of Materials Science and Engineering Georgia Institute of Technology, Atlanta GA USA, 2011.
3. S.G. Kalashnikov, *Electricity*, FIZMATLIT, Moscow, 2003 (in Russian).

Simulation of ZnO piezocantilever deflection for a contact AFM

E. Gusev, Yu. Eroshina
Taganrog Institute of Technology – Southern Federal University, Taganrog, Russia, eyugusev@gmail.com

Obtaining a qualitative conception of the sample surface is challenging for materials technology and related application. Traditional technique for surface study is atomic force microscopy (AFM). The developing of design and fabrication technology of cantilever probe determines the AFM advancement [1]. Appearance of new constructions of cantilevers is conditioned by tendency to increase spatial resolution and threshold of minimum measureable force of interaction. The former depends on tip shape, and the latter – on design of cantilever and deflection registration system. The registration system based on external (optical) and internal (e.g. piezo) electronic are known. The latter represents integrated strain-sensitive element in the form of a piezoresistive or piezoelectric layer. Today piezoelectric cantilever is used as a basic element in sensing and actuation [1].

In this work we performed numerical simulation of beam deflection of piezocantilevers based on zinc oxide as sensitive layer. Planar cantilever beam bending dependence on electrodes shape under DC voltage applying was investigated early [2].

Two type of electrode pattern were investigated: planar and sandwich. The first shape was presented as a structure of Si – ZnO – Al having silicon tip: bulk silicon base of 3,4×1,6×0,3 mm with rectangular beam of 400×240×2 μm and extension of 150×50×2 μm, piezoelectric ZnO film of 400×240×0,7 μm and aluminum interdigital electrodes, tip basis radius of 4 μm and tip height of 12 μm. Geometry of multi-layered model of cantilever was presented as a structure of Si – Al – ZnO – Al: same bulk silicon base with rectangular the cantilever of 400×240×2 μm and extension of 150×50×2 μm; first aluminum layer as a bottom electrode, piezoelectric ZnO film of 380×230×0,6 μm, and second aluminum layer as a top electrode.

Total displacement and deformation of the piezocantilevers were developed by finite element method (FEM). Cantilever deflection and sensitivities was determined. Physicochemical properties of the materials (density, Young modulus, Poisson ratio, piezoelectric strain tensor, etc.) were taken into consideration.

The value of beam deflection was 49.9 nm for planar cantilever (fig. 1) and 62.7 nm for multilayer cantilever. The sensitivities were 7 mV/nN (fig. 2),10 nm/V and 80 nm/nN for of planar cantilever, and 8.8 mV/nN, 12.6 nm/nN and 110 nm/nN for multilayer cantilever.

These results correlate with well-known in the literature estimates made by analytical models and FEMs [1]. The results will be checked after cantilevers fabricated and tested.

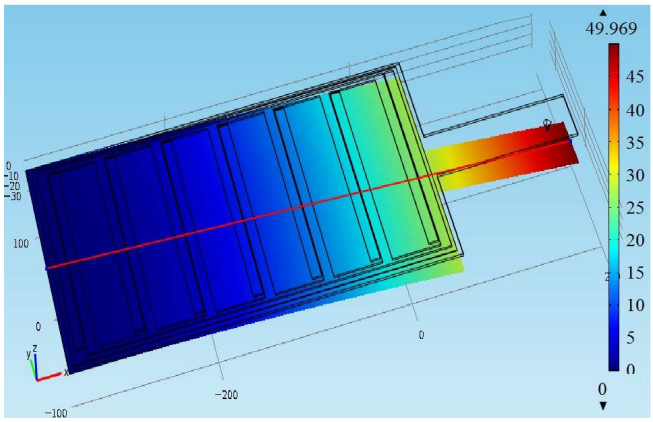

Figure 1. Total displacement and deformation (nm) of the “planar” piezocantilever

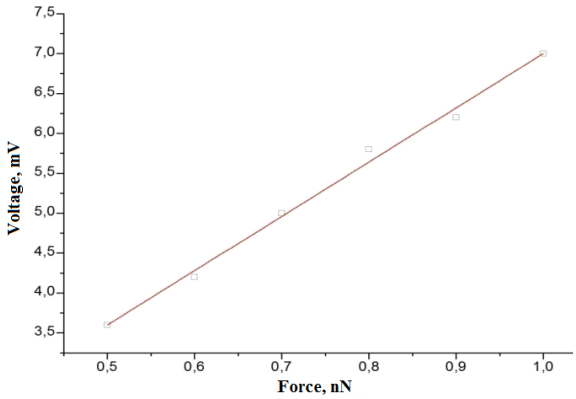

Figure 2. Induced voltage dependence on effective force to cantilever tip

1. D. Sarid. *Exploring Scanning Probe Microscopy with MATHEMATICA.* Wiley-VCH, Weinheim, 2007.
2. Yu.Yu. Eroshina, R.V. Velichko, “Bending model and investigation of piezocantilever beam”, V.V. Titov ed., pp.182–183, SSC RAS Publishers, Rostov-on-Don, 2012 (in Russian).

NO_2, CO and CO_2 gas sensor based on magnetron deposited n- and p-type ZnO films

E. Gusev, A. Mikhno, V. Gamaleev, O. Mironenko
Taganrog Institute of Technology – Southern Federal University, Taganrog, Russia, eyugusev@gmail.com

Thin metal oxide films are widely used in sensing devices, micro-mechanics, gas-sensitive sensors, solar cells, etc. One of materials, whose properties determine its applicability in these applications, is zinc oxide (ZnO) [1]. For formation of ZnO films and other metal oxides, magnetron sputtering, pulsed laser deposition, vapor deposition methods are used. Magnetron reactive sputtering allows to obtain high-quality pure films of metal oxides at high speed [1, 2].

We investigated the deposition conditions of thin ZnO films by magnetron reactive sputtering at radio-frequency currents and its sensitivity to NO_2, CO and CO_2 gases was detected.

Zinc oxide films were deposited by BOC Edwards Auto 500 vacuum coating system [3]. Morphology of the surface, thickness, refractive index and sensitivity of the films were analyzed by scanning probe nanolaboratory NTEGRA Vita, scanning electron microscope Nova Nanolab 600, Linnik interferometer and gas-sensitive bench.

Deposition of ZnO films was carried out by sputtering of zinc in the gas mixture of argon and oxygen [3]. The effect of conditions on quality and characteristics of the films, in the range of operating pressures in the chamber from 0.2 to 0.8 Pa, the percentage of oxygen in the gas mixture from 10% to 80%, power from 35 to 150 Watts, pre-heating phase up to 250ºC was studied. Refractive index and RMS roughness of the films were 2.157 to 2.224 and 2.11 to 4.86, respectively.

The sensors based on the films were created. It was found, that the average response time of the gas sensors was about 5-10 seconds to NO_2, CO and CO_2 gases (Fig. 1). At various concentrations of the gas (from 20 ppm to 100 ppm for NO_2, from 50 to 100 ppm for CO and CO_2) sensitivity was 30-67%. At various concentrations of the gas (from 200 ppm to 1000 ppm) sensitivity was 80-97%. Average response time of gas sensors based on p-type zinc oxide was about 5-10 seconds on NO_2. Figure 1 shows that the films of n- and p-type conduction were obtained as confirmed by [1].

Thus, optimal conditions of n- and p-type ZnO films deposition by magnetron reactive sputtering, suitable for the manufacture of gas sensors were obtained.

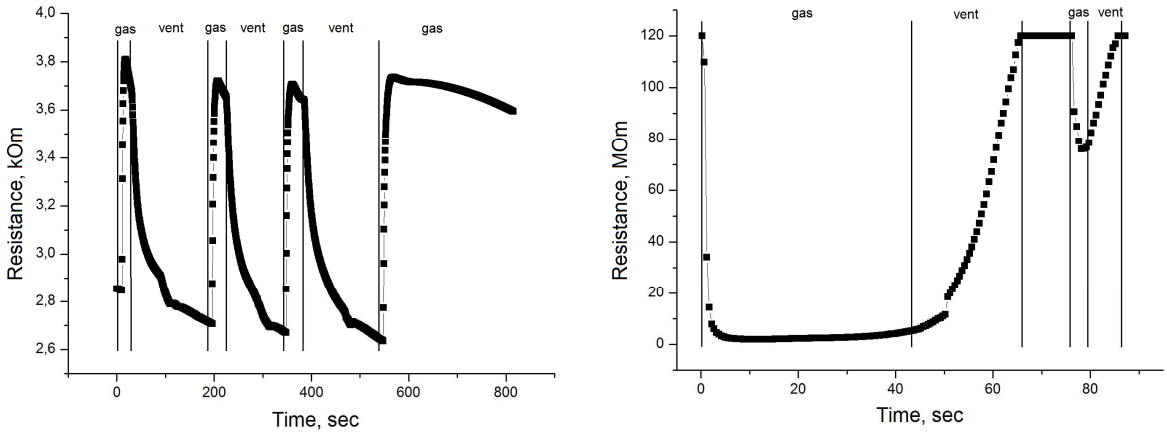

Figure 1 – Sensitivity of the ZnO films to NO_2 at room temperature: n-type (left, 50 ppm) and p-type (right,200 ppm)

1. V. Kobrinsky, E. Fradkin, V. Lumelsky, A. Rothchild, Y. Komem, Y. Lifshitz, "Tunable gas sensing properties of p- and n-doped ZnO thin films", Sensors and actuators B, **148**, pp.379-387, 2010.
2. H. Czternastec, "ZnO thin films prepared by magnetron high pressure sputtering", Opto-Electronics Review, **12**, pp.49-52, 2004.
3. A.S. Mikhno, V.A. Gamaleev, R.V. Velichko, "The investigation of magnetron sputtering conditions for thon zinc oxide films formation for sensor devices", V.V. Titov ed., pp.200-201, SSC RAS Publishers, Rostov-on-Don, 2012 (in Russian).

The mode matching technology for MEMS gyroscope with mutually spaced eigenfrequences

O. Morozov[1], A. Postnikov [1], I. Kozin[1], A. Soloviev[2], A. Tarasov[2]

1. Yaroslavl Branch of the Institute of Physics and Technology, Russian Academy of Sciences, Yaroslavl, Russia, laser_lab@bk.ru. 2. Federal state Unitary Enterprise "Center for Ground-Based Space Infrastructure Facilities Operation", Moscow, Russia, gyros@inbox.ru

The operation principle of the micromachined vibratory gyroscopes relies on the generation of a sinusoidal Coriolis force due to the combination of vibration of a proof-mass and an orthogonal angular-rate input. The proof mass is generally suspended above the substrate by a suspension system consisting of flexible beams (torsions). The overall dynamical system is typically a two degrees-of-freedom (2-DOF) mass-spring-damper system, where the rotation-induced Coriolis force causes energy transfer to the sense-mode proportional to the angular rate input. Ideally, it is desired to utilize resonance in both the drive and the sense modes in order to attain the maximum possible response gain, and hence sensitivity. This is typically achieved by designing and electrostatically tuning the drive and sense resonant frequencies to match. However, the limitations of the micromachining technologies define the upper-bound on the performance and robustness of micromachined gyroscopes[1]. Inevitable fabrication imperfections affect both the geometry and the material properties of MEMS devices and shift the drive and sense-mode resonant frequencies [1]. Paper presents a new technology for silicon micromachined gyroscope mode matching with mutually spaced eigenfrequencies by repeated oxidation-wet etching cycles. This technique leads to simultaneous thinning of the torsions which comprise 2-DOF dynamic system. The torsions have a hourglass section so the values of widths $W(\beta,\gamma)$ at the base and waist size contribute significantly to frequency shift. A peculiarity of considered gyro is that drive frequency $F(\gamma)$ is half of sense mode natural frequency $F(\beta)$. The device design limits mismatch frequencies values within ΔF =0…+150 Hz

$$\Delta F = F(\beta)\text{-}2^* F(\gamma) \quad (1)$$

On the basis of FEM (finite element method) modeling crucial geometry parameters responsible for resonant frequency shift were determined. Torsions width random divergence (from chip to chip within one wafer) was ±0,15 um. It was found by comparison natural frequencies measurements and computer simulations. Frequency mismatch distribution measured through a wafer presented in Fig. 1 A. The frequency shift could gain 73.4 Hz. This quantity defines the requirements for resulting inherent imperfections of micro-fabrication techniques. It is worth noting that mismatch values could be both positive and negative. Taking into account wafer thickness variations total mismatch overrides design limit. To meet this condition for all chips on wafer and a mode match technology was developed. The repeated silicon oxidation-wet etching in HF solution procedure based on reliable FEM calculations solves the problem. Frequency mismatch distribution has undergone desired change to positive values as one could see in figure 1B after tuning procedure. Technology could be applied for fine tuning of silicon fabricated resonators.

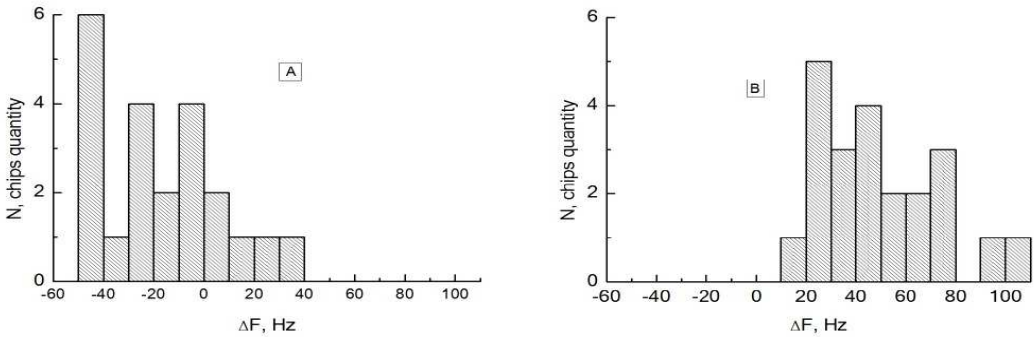

Fig. 1. Frequency mismatch distribution ΔF before A), and after B) treatment oxidation/wet etching depth 0.95 um.

1. C. Acar, A. Shkel *MEMS Vibratory Gyroscopes: Structural Approaches to Improve Robustness.* Springer, 2008.

2. A. Soloviev, Y. Malkov, "Alternative designs of MEMS gyroscope with mutually spaced eigenfrequencies silicon sensor", Digest of "New materials and technologies in rocket and space technics" conference, Zvezdniy Gorodok, 2011.

Principal Physical and Technological Problems and Technical Solutions for Creating a New Generation of High-Temperature Microelectromechanical SOIMT Strain Sensors

L. Sokolov[1], N. Parfenov[2], S. Igochin[3]

1. Branch of MAI (TU) "Strela", Zhukovsky, Moscow Region, Russia, E-mail: sokol@niiao.com. 2. MAI (TU), Moscow, Russia, E-mail: sedennik@mail.ru. 3. JSC "Interlab", Moscow, Russia, E-mail: igochin@interlab.ru

Under severe operational conditions for electronic systems of aerospace equipment there is an acute problem of creating high-temperature, high-reliability and also competitive sensors of mechanical quantities [1]. This problem can be resolved on the basis of innovative microelectronics and micromechanics technologies, which allow integral strain sensors without isolation p-n-junctions to be produced in batches [2].

The analysis of physical and technological problems, as well as some basic technical solutions are given for manufacturing an experimental batch of strain sensor modules and integral MEMS-SOI membrane-type pressure sensors with a monolithic tensoframe (SOIMT) based on a "monosilicon-glass-monosilicon" heterostructure by a group method.

VEECO, TM-3000, as well as Quanta 200 3D FEI electronic scanning microscopes, that include an EDAX detector for the X-ray microanalysis, are used to analyze the physical and technological problems of precision microprofiling of a 3D micromechanical structure for MEMS-SOIMT sensors, which are caused by the contact photolithography process on a relief surface, and the problem of jointing a MEMS-SOIMT sensor chip, which contains glass nanocluster fragments on its contact surface, with a Pyrex glass support element, in the electrostatic field.

1. L.V. Sokolov, A.A. Zhukov, A.V. Kapustian, "Physical and Technological Problems of Producing New Generation High-Precision Semiconductor Pressure Sensors with Digitized Output for Information Measuring, Control and Diagnostics Systems". Proceedings of the All-Russian Scientific&Technical Conference "Actual Problems of Space Rocket Instrument Engineering and Information Technologies", Moscow, 28-30 April, 2008, Fizmatlit, 2009, pp.364-367 (in Russian).

2. L.V. Sokolov, "Conceptual Basis for Creating New-Generation High-Stable High-Temperature Microelectromechanical Sensors Based on a Silicon-On-Isolator Heterostructure with a Monolithic Integral Tensoframe for Intelligent Transducers". Proceedings of the 9th International Symposium on Measurement Technology and Intelligent Instruments (ISMTII-2009), Volume 3, St.-Petersburg, 29 June – 2 July 2009, pp.248-251.

MEMS angular rate sensors and roll sensors

A. Timoshenkov, S.M. Naing, D. Daniltsev, V. Kalugin
National Research University of Electronic Technology, Department of Microelectronics, Moscow, Russia,
E-mail: spt@miee.ru, sanminnaing@gmail.com

MEMS in particular micromechanical gyroscope (MMG) are now widely used in civilian and military industries [1.] A gyroscope is a rapidly rotating rigid body which axis of rotation can change its direction in space. It has some interesting properties observed in rotating celestial bodies, artillery shells, turbine rotors installed on ships, etc. The gyroscope is most often used as: (a) sensing element indicating gyroscopic instruments; (b) how to gauge the angle of rotation; (c) or angular velocity for the automatic control. In some cases, such as gyrostabilizer, gyroscopes are used as generators of force or energy moment.

Sensors and micro systems can independently perform the functions of measurement, evaluation of their results, the adoption and implementation of management decisions. They are compatible with the technologically advanced systems of information processing. In general case MEMS consist of a sensing element (SE) that responds to external perturbations, and electronics to process the incoming signal [2].

The developed design is in demand in practical problems. Some of them are basically new to the micro-mechanical ARS, in particular, their application for the sensor roll, which must measure the angle of rotation around the longitudinal axis of the object. Rotational speed can reach 20 Hz. Acceleration acting along the longitudinal axis of the object (acceleration or braking) can reach 200 g, and also perpendicular to them (due to taxiing or maneuvering) as high as 20 g. The flight time of ammunition was less than 60 seconds. Error in determining the roll angle of the flight should not exceed 20 degrees in order to implement the control system could taxi plumage object. Such high dynamic requirements for the measuring system, based on the dynamic characteristics of the object would require not only the development of special ARS, but the corrections for the vector acceleration of gravity, if not the vertical flight of the object, or magnetic fields of the earth. With the help of accelerometers and magnetometers can track the frequency of rotation, and reduce calculation errors. In dynamic conditions, this problem will make the adjustment to an accelerometer is quite difficult, since the congestion during taxiing as high as 20 g.

In researching the problem of measuring the roll angle by the direct transformation of the angular velocity, where the axis of the measuring sensor is almost identical with the axis of rotation, we obtained the following results. Standard deviation or SKO (error for 25 seconds at the rotation speed of 3000 degrees per second was 4.88 degrees. Indeed, in practice, the systematic error components cannot always be reduced to a level much lower than random. For the successful solution of such problems requires individual calibration of each sample in a two-level approximation to reality. Nevertheless, the use of ARS series production MMGK MIET to resolve this problem is justified and timely.

As a result, we can conclude that the use of angular velocity sensor series MMGK MIET production allows us to solve the problem of constructing roll sensor for rapidly rotating body (20 Hz) along the longitudinal axis of which are speed reaching 200 g, and also perpendicular speed up 20g. Creating such a sensor on the basis of domestic MMG has real prospects of implementation in the military and civil industries, and relatively low cost makes it possible to compete with foreign manufacturers.

1. A.S. Timoshenkov, S.M. Naing, “Vibrating Ring Gyroscope micro-electromechanical: study characteristics, methods, variations and signal processing schemes”. Proceedings of the 4th All-Russian Inter-University Scientific Conference on "Actual problems of information in science, education and the economy." MIET, p.105, October 2011.
2. S.P. Timoshenko, V.V. Kalugin, S.A. Anchutin, Y.S. Morozov. *Micro - electromechanical Systems*. Moscow: MIET, pp.3-22, 2009.

Technology development for the creation of conformal multilayer wiring boards based on polymers

A. Titov, Yu. Dolgovykh, K. Tikhonov, S. Timoshenkov
National Research University of Electronic Technology, Department of Microelectronics, Moscow, Russia, E-mail address: mg@miee.ru

Development of micro-mechanical sensors and systems based on them is one of the development branches in microelectronic technology and labeled as one of the technologies of the 21-st century. In recent years, this industry is one of the fastest growing. Applications include micro computing and telecommunications, biology, medicine, chemistry, environmental monitoring, automotive, space exploration, aviation and other technologies.

Manufacturing techniques of conformal multilayer wiring boards (CMWB) is constantly evolving. It is necessary to create new manufacturing technologies of the CMWB following the increasing integration of components, the functionality of the equipment, reducing its size and weight.

The use of flexible dielectric material for the manufacture of printed circuit boards allows developers and users of electronic devices, a number of unique features. We can say, that this, above all, reducing the construction size and weight, assembly efficiency, improving the electrical characteristics, heat transfer and, in general, reliable.

Three technological routes through the creation of the CMWB: polyimide film, liquid crystal polymer (LCP), as well as the version of the sequential deposition of dielectric layers of the metal soared to an insulating substrate have been developed and investigated.

The process of making test structures starts with the initial laser cutting of sheet materials Ultralam 3850 and 3908 Ultralam for the formation of the external circuit fibre wise blanks format 200 x 200 mm. Also, laser cutting is used to create cross-cutting core holes for the mechanical alignment of the layers, and structural holes in the intermediate layer Ultralam 3850 and in two layers of connective Ultralam 3908, serving for the formation of internal cavities of the built-in semiconductor chips and MEMS switches.

One promising technology to create multi-layer board is conformal, so-called vacuum brazing technique, which avoids the high pressure during compaction of individual layer.

The analysis showed that the LCP material has a number of enhanced features compared to the polyimide film, such as stable electrical properties ($\varepsilon = 2.9$; polyimide $\varepsilon = 3.5$); uniform thickness ($\Delta = \pm 0.05\%$), extremely low moisture absorption (<0.04% for 24 hours at 23 ºC), maintaining a stable electrical, mechanical and dimensional properties in humid environments.

Prospects for the use of LCP as a material for switching boards provide the possibility of using unpackaged LSI-s mounted inside, which provides protection from external influences have been showed. The relevance and significance of the paper related to the methodology creation for the development and manufacture of silicon sensors with capacitive signal pickup system. Methodology was based on an integrated approach to solving such problems as the processes of surface preparation, etching of the complex profile surfaces, matching the silicon structures, etc. which allows to create MEMS elements.

Author Index

Author Index

Author Index

Author Index

Author Index

Author Index

Author Index

Author Index

Author Index

Author Index

Author Index